

AD-A197 314

UNITED STATES DEPARTMENT OF THE INTERIOR
GEOLOGICAL SURVEY

Pacific Enewetak Atoll Crater Exploration (PEACE) Program
Enewetak Atoll, Republic of the Marshall Islands

Part 4: Analysis of borehole gravity surveys and other geologic
and bathymetric studies in vicinity of OAK and KOA craters

edited by

Thomas W. Henry¹ and Bruce R. Wardlaw²

U.S. Geological Survey

Open File Report 87-665

Prepared in cooperation with the Defense Nuclear Agency

and funded

This document has been approved
for public release and sale; its
distribution is unlimited.

This report is preliminary and has not been reviewed for conformity with
U.S. Geological Survey editorial standards and stratigraphic nomenclature

¹Branch of Paleontology and Stratigraphy, Denver, CO 80225-0046

²Branch of Paleontology and Stratigraphy, Reston, VA 22092

TABLE OF CONTENTS

Page No.

CHAPTER 1: INTRODUCTION TO PART 4 OPEN-FILE REPORT 1- 1

 GENERAL REMARKS 1- 1

 PEACE PROGRAM REPORTS 1- 3

 DATA ACQUISITION AND BASES 1- 3

 SYNOPSIS OF CHAPTERS 1- 7

 Borehole Gravity 1- 7

 Paleontologic Evidence for Mixing 1- 8

 Electron Paramagnetic Resonance Studies 1- 8

 Bathymetric Studies of OAK Crater 1- 9

 Constraints on Densification and Piping for OAK 1-10

 Additional Studies of Geologic Crater Models 1-11

 ACKNOWLEDGEMENTS 1-11

 REFERENCES CITED 1-12

CHAPTER 2: BOREHOLE GRAVIMETRY, OAK CRATER 2- 1

 INTRODUCTION 2- 1

 BOREHOLE GRAVITY ANALYSIS 2- 4

 LATERAL DENSITY CHANGES 2- 6

 CORRECTION FOR LATERAL DENSITY CHANGES 2- 6

 CORRECTED BOREHOLE DENSITY AND POROSITY 2-14

 NATURAL DENSITY AND POROSITY VARIATIONS 2-22

 CHANGES RELATED TO CRATERING 2-28

 SUMMARY 2-33

 ACKNOWLEDGEMENTS 2-36

 REFERENCES CITED 2-36

 APPENDIX 2-1; Gravity Survey, Borehole E-1, Medren Island 2-54

 APPENDIX 2-2; Determination of Interval Grain Density 2-56

(continued on next page)



Accession For	
NTIS GRA&I	<input checked="" type="checkbox"/>
DTIC TAB	<input type="checkbox"/>
Unannounced	<input type="checkbox"/>
Justification	
By	<i>per Statement on Title Page</i>
Distribution/	
Availability Codes	
Dist	Avail and/or Special
<i>A-1</i>	

TABLE OF CONTENTS (continued)

	Page No.
CHAPTER 3: PALEONTOLOGIC EVIDENCE FOR SEDIMENTARY MIXING	3- 1
INTRODUCTION	3- 1
MATERIALS AND METHODS	3- 1
STANDARD MICROFAUNAL SEQUENCE	3- 2
RESULTS	3- 7
Central Crater Boreholes	3- 8
Homogenized Zone	3- 8
Upwardly Mixed Zone	3- 8
Maximum Piping Zone	3- 8
Basal Mixed Zone	3-11
Statistical Analysis	3-11
Injection Dikes	3-11
Transition Boreholes	3-11
OCT-5	3-11
OFT-8	3-13
OKT-18	3-13
SUMMARY AND CONCLUSIONS	3-14
REFERENCES CITED	3-15
APPENDIX 3-1; Occurrence of Species, OAR-2/2A	3-21
APPENDIX 3-2; Occurrence of Species, OOR-17	3-23
APPENDIX 3-3; Occurrence of Species, OBZ-4	3-25
APPENDIX 3-4; Occurrence of Species, OPZ-18	3-27
APPENDIX 3-5; Occurrence of Species, OCT-5	3-28
APPENDIX 3-6; Occurrence of Species, OFT-8	3-29
APPENDIX 3-7; Occurrence of Species, OKT-13	3-30
CHAPTER 4: ELECTRON PARAMAGNETIC RESONANCE STUDIES, OAK CRATER	4- 1
INTRODUCTION	4- 1
ELECTRON PARAMAGNETIC RESONANCE ANALYSIS	4- 1
Sample Preparation and Spectrometer Settings	4- 1
SHOCK-PRESSURE CALIBRATION OF EPR SPECTRA	4- 3
Shock-Wave Calibration Experiments	4- 3
Description of Shocked Spectra	4- 4
Pressure Calibration by Differencing Spectra	4- 7
OAK DATA	4-11
Borehole Sample Selection	4-11
Results of Borehole-Sample Analysis	4-12
Results from Debris Samples	4-14
DISCUSSION	4-19
ACKNOWLEDGEMENTS	4-20
REFERENCES CITED	4-20

(continued on next page)

TABLE OF CONTENTS (continued)

	Page No.
CHAPTER 5: BATHYMETRIC STUDIES OF OAK CRATER	5- 1
INTRODUCTION	5- 1
Objectives and General Procedures	5- 1
Terminology	5- 1
DATA BASE	5- 3
Holmes & Narver Preshot Bathymetric Map	5- 3
Holmes & Narver Postshot Bathymetric Map	5- 4
USGS 1984 Bathymetric Map	5- 4
DATA PROCESSING	5- 6
Digitized Base Contour Maps	5- 6
Derived Isopach Maps	5- 6
Map Products	5- 7
ANALYSIS	5-10
Map Derived Quantities	5-10
Water Depths	5-10
Cross Sections	5-12
Areas and Volumes	5-12
MAP CHARACTERISTICS	5-14
Holmes & Narver Preshot Contour Map	5-14
Holmes & Narver Postshot Contour Map	5-15
USGS 1984 Contour Map	5-15
H&N Postshot - H&N Preshot Isopach Map (Δ -Relief)	5-16
USGS 1984 - H&N Preshot Isopach Map (Δ -Relief)	5-17
USGS 1984 - H&N Postshot Isopach Map (Δ -Relief)	5-18
CONCLUSIONS	5-18
ACKNOWLEDGEMENTS	5-19
REFERENCES CITED	5-20
CHAPTER 6: CONSTRAINTS ON DENSIFICATION AND PIPING, OAK CRATER	6- 1
BACKGROUND AND SUMMARY	6- 1
BASIC FACTS AND PARAMETERS	6- 2
SHORTENING OF "CORAL" COLUMNS BY DENSIFICATION	6- 7
DENSITY PROFILES, TREATMENT, AND DOWNWARD DISPLACEMENTS	6- 8
CONTRIBUTION OF SIMPLE SUBSIDENCE TO THE OAK CRATER	6-10
CONFIDENCE ASSESSMENT	6-18
LONG-TERM SETTLING	6-23
PIPING	6-26
OTHER CONSTRAINTS; HORIZONTAL PIPING	6-29
DENSIFICATION: SUMMARY AND CRITIQUE	6-32
CONCLUSIONS	6-34
ACKNOWLEDGEMENTS	6-36
REFERENCES CITED	6-37
APPENDIX 6-1 -- PEACE Program Density Profiles	6-39
APPENDIX 6-2 -- Densities as Continuous Depth Function	6-74
Mass as Continuous Depth Function	6-75
Thickness Change as Continuous Depth Function	6-76
References Cited	6-78

(continued on next page)

TABLE OF CONTENTS (continued)

	Page No.
CHAPTER 7: INTEGRATION OF MATERIAL-PROPERTY UNITS, GRAVIMETRY,	7- 1
AND ADDITIONAL STUDIES OF OAK AND KOA CRATERS	
INTRODUCTION	7- 1
PRE-EVENT GEOLOGY OF OAK AND KOA CRATERS	7- 1
POST-EVENT GEOLOGY OF OAK AND KOA CRATERS	7- 7
Crater Zones	7- 7
Geologic Crater Zones	7- 7
Paleontologic Crater Zones	7-10
Seismic Crater Zones	7-15
CRATER FEATURES	7-16
Crater Material in the Lagoon	7-16
Breach Deposit in the Lagoon	7-16
Piping	7-24
Paleontologic Mixing	7-24
OAK Crater	7-29
KOA Crater	7-29
Estimates of Volume of Piped Material	7-30
Paleontologic Model of Crater Fill	7-31
Injection	7-31
Gamma Activity	7-31
Distribution of Radionuclides	7-34
Distribution of Shocked Calcite	7-37
Depression and Uplift of Structural Surfaces	7-37
COMPARISON OF OAK AND KOA CRATERS	7-37
GEOLOGIC CRATER MODEL FOR OAK AND KOA	7-42
Thinning Analysis	7-43
Stratigraphic Density Profile	7-43
General Densification and Flow Patterns	7-58
OAK Crater	7-58
KOA Crater	7-59
Relative Timing of Depositional Events	7-59
VOLUME PROBLEMS	7-61
Evidence for Piping and Lateral Flow	7-62
Surface	7-62
Crater-Fill	7-62
Subsurface	7-62
Loss of Material from Crater	7-63
SUMMARY	7-63
REFERENCES CITED	7-64

FIGURE INDEX

Figure No.	Description	Page No.
CHAPTER 1: INTRODUCTION		
1- 1	Location Map of Enewetak	1- 2
1- 2	Location map of KOA crater	1- 5
1- 3	Location map of OAK crater	1- 6
CHAPTER 2: BOREHOLE GRAVIMETRY, OAK CRATER		
2- 1	Map of Enewetak showing OAK and KOA craters and Medren Island borehole E-1 site.	2- 2
2- 2	Map of OAK crater area and gravity survey boreholes	2- 3
2- 3	Distribution of repeated gravity measurements	2- 5
2- 4	Density model of natural atoll facies changes	2- 7
2- 5	Cross section, southwest transect	2- 9
2- 6	Cross section, southeast transect	2-11
2- 7	Density model, southwest transect	2-13
2- 8	Well logs, densities, and porosity, OOR-17	2-15
2- 9	Well logs, densities, and porosity, OPZ-18	2-16
2-10	Well logs, densities, and porosity, OQT-19	2-17
2-11	Well logs, densities, and porosity, ORT-20	2-18
2-12	Well logs, densities, and porosity, OSR-21	2-19
2-13	Densities and porosity, OTG-23	2-20
2-14	Variability of BHG and gamma-gamma density	2-21
2-15	Porosity cross plots	2-23
2-16	Interval densities and porosities, southwest transect ...	2-25
2-17	Cross plot of interval grain density vs BHG porosity	2-27
2-18	Density and porosity model, southwest transect	2-29
2-19	Interval densities and porosities, southwest transect ...	2-31
2-20	Density profile, borehole E-1 (Medren Island)	2-55
CHAPTER 3: PALEONTOLOGIC EVIDENCE FOR SEDIMENTARY MIXING		
3- 1	Plot of ostracode species versus depth, OAR-2/2A	3- 5
3- 2	Plot of ostracode species versus depth, OOR-17	3- 6
3- 3	Plot of ostracode species versus depth, OBZ-4	3- 9
3- 4	Plot of ostracode species versus depth, OPZ-18	3-10
3- 5	Plot of piped specimens versus depth	3-12

(continued on next page)

FIGURE INDEX (continued)

Figure No.	Description	Page No.
CHAPTER 4: ELECTRON PARAMAGNETIC RESONANCE STUDIES		
4- 1	EPR spectrum of powdered single crystal calcite	4- 2
4- 2	Comparison of laboratory-shocked limestone spectra	4- 5
4- 3	Comparison of "coral" spectra shocked in laboratory	4- 6
4- 4	Differencing technique, overlay of standard vs	4- 8
	unshocked limestone spectra.	
4- 5	Plot of summed differences, low- and high-field	4- 9
	components vs shock pressure.	
4- 6	Map of OAK crater showing boreholes sampled	4-13
4- 7	Sample analysis showing calculated shock pressures	4-15
	vs sample depth for OAK boreholes.	
4- 8	Depth and thickness of regions of highly shocked	4-16
	carbonates from boreholes.	
4- 9	Map of OAK crater showing debris-sample sites	4-17
4-10	Shock pressure versus range from GZ and versus	4-18
	estimated pre-event depth below sea level.	
CHAPTER 5: BATHYMETRIC STUDIES OF OAK CRATER		
5- 1	Map of area included in Holmes & Narver and	5- 2
	USGS surveys.	
5- 2	Fathometer lines in 1984 USGS study	5- 5
5- 3	Isopach computational grid	5- 8
5- 4	Cross sections through OAK ground zero	5-13
CHAPTER 6: CONSTRAINTS ON DENSIFICATION AND PIPING		
6- 1	Cross sections at OAK	6- 3
6- 2	Density profiles from gravimetry	6-11
6- 3	Density profiles from gamma-gamma logging	6-12
6- 4	Change in rock thickness from BHG densities, simple	6-13
	subsidence, OPZ-18 vs OSR-21, OPZ-18 vs OOR-17.	
6- 5	Change in rock thickness from BHG densities, simple	6-14
	subsidence, OTG-23 vs OSR-21, OTG-23 vs OOR-17.	
6- 6	Change in rock thickness from BHG densities, simple	6-15
	subsidence, OQT-19 vs OSR-21, OQT-19 vs OOR-17.	
6- 7	Change in rock thickness from BHG densities, simple	6-16
	subsidence, ORT-20 vs OSR-21, ORT-20 vs OOR-17.	
6- 8	Change in rock thickness form BHG densities, simple	6-19
	subsidence, OSR-21 vs OOR-17.	
6- 9	Change in rock thickness from BHG densities, simple	6-20
	subsidence, OOR-17 vs OSR-21.	
6-10	High, low, and best estimates of fraction contributed ...	6-35
	by densification to seafloor drop, OQT-19 and ORT-20.	

(continued on next page)

FIGURE INDEX (continued)

Figure No.	Description	Page No.
6-11	BHG Profile, OOR-17	6- 40
6-12	BHG Profile, OSR-21	6- 41
6-13	BHG Profile, ORT-20	6- 42
6-14	BHG Profile, OQT-19	6- 43
6-15	BHG Profile, OTG-23	6- 44
6-16	BHG Profile, OPZ-18	6- 45
6-17	Y-Y Profile, OOR-17	6- 46
6-18	Y-Y Profile, OSR-21	6- 47
6-19	Y-Y Profile, ORT-20	6- 48
6-20	Y-Y Profile, OQT-19	6- 49
6-21	Y-Y Profile, OBZ-04	6- 50
6-22	Y-Y Profile, OCT-05	6- 51
6-23	Y-Y Profile, OAR-2A	6- 52
6-24	Y-Y Profile, OIT-11	6- 53
6-25	Y-Y Profile, OKT-13	6- 54
6-26	Y-Y Profile, OPZ-18	6- 55
6-27	Thickness changes, Y-Y densities, ORT-20 & OOR-17	6-102
6-28	Thickness changes, Y-Y densities, ORT-20 & OSR-21	6-103
6-29	Thickness changes, Y-Y densities, ORT-20 & OAR-2A	6-104
6-30	Thickness changes, Y-Y densities, OQT-19 & OOR-17	6-105
6-31	Thickness changes, Y-Y densities, OQT-19 & OSR-21	6-106
6-32	Thickness changes, Y-Y densities, OQT-19 & OAR-2A	6-107
6-33	Thickness changes, Y-Y densities, OBZ-04 & OOR-17	6-108
6-34	Thickness changes, Y-Y densities, OBZ-04 & OSR-21	6-109
6-35	Thickness changes, Y-Y densities, OBZ-04 & OAR-2A	6-110
6-36	Thickness changes, Y-Y densities, OCT-05 & OOR-17	6-111
6-37	Thickness changes, Y-Y densities, OCT-05 & OSR-21	6-112
6-38	Thickness changes, Y-Y densities, OCT-05 & OAR-2A	6-113
6-39	Thickness changes, Y-Y densities, OIT-11 & OOR-17	6-114
6-40	Thickness changes, Y-Y densities, OIT-11 & OSR-21	6-115
6-41	Thickness changes, Y-Y densities, OIT-11 & OAR-2A	6-116
6-42	Thickness changes, Y-Y densities, OKT-13 & OOR-17	6-117
6-43	Thickness changes, Y-Y densities, OKT-13 & OSR-21	6-118
6-44	Thickness changes, Y-Y densities, OKT-13 & OAR-2A	6-119
6-45	Thickness changes, Y-Y densities, OPZ-18 & OOR-17	6-120
6-46	Thickness changes, Y-Y densities, OPZ-18 & OSR-21	6-121
6-47	Thickness changes, Y-Y densities, OPZ-18 & OAR-2A	6-122
6-48	Thickness changes, Y-Y densities, OOR-17 & OSR-21	6-123
6-49	Thickness changes, Y-Y densities, OSR-21 & OOR-17	6-124
6-50	Thickness changes, Y-Y densities, OOR-17 & OAR-2A	6-125
6-51	Thickness changes, Y-Y densities, OAR-2A & OOR-17	6-126
6-52	Thickness changes, Y-Y densities, OSR-21 & OAR-2A	6-127
6-53	Thickness changes, Y-Y densities, OAR-2A & OSR-21	6-128

(continued on next page)

FIGURE INDEX (continued)

Figure No.	Description	Page No.
CHAPTER 7: INTEGRATION OF MATERIAL-PROPERTY UNITS, GRAVIMETRY, AND ADDITIONAL STUDIES OF GEOLOGIC MODELS, OAK AND KOA CRATERS		
7- 1	Distribution of shallow cemented zones on Enjebi Island, EXPOE cores.	7- 2
7- 2	Relationship of discontinuities, major discontinuities, biostratigraphic zones, material-property units, and sedimentary packages in reference boreholes.	7- 3
7- 3	Cementation and sediment types, relationships to material-property units, reference boreholes.	7- 5
7- 4	Probable pre-shot surfaces for tops of Pleistocene and Pliocene in OAK and KOA areas.	7- 6
7- 5	Comparison of pre-shot ground surface and subsurface geology, OAK and KOA areas.	7- 8
7- 6	Geologic crater model	7-11
7- 7	Fence diagram of KOA crater showing relationship of crater zones and geologic horizons.	7-17
7- 8	Fence diagram of OAK boreholes OOR-17 to OPZ-18, relationship of crater and geologic horizons.	7-18
7- 9	Fence diagram of OAK boreholes OBZ-4 to OAR-2/2A, relationship of crater and geologic horizons.	7-19
7-10	Fence diagram, OAK boreholes, reef tract to OLT-14 relationship of crater and geologic horizons.	7-20
7-11	Geologic interpretation of multichannel seismic lines 101 and 103, OAK crater area.	7-21
7-12	Geologic interpretation of multichannel seismic lines 303 and 306, KOA crater area.	7-22
7-13	Isopach map showing distribution of muddy sediments, Enewetok lagoon.	7-23
7-14	Distribution of sand volcanoes on enhanced sea-floor image of OAK crater.	7-25
7-15	Comparison of number of specimens from MP-4 and -5 to percent ostracodes from crater zones in OBZ-4 and OPZ-18.	7-26
7-16	Paleontologic mixing in mixed zone of OAK crater	7-27
7-17	Paleontologic mixing in mixed zone of KOA crater	7-28
7-18	Paleontologic model of crater-fill and paleontologic mixed zones.	7-32
7-19	Borehole lithology, geologic and paleontologic crater zones, and gamma-ray logs, OAK crater.	7-33
7-20	Borehole lithology, geologic and paleontologic crater zones, and gamma-ray logs, KOA crater.	7-35
7-21	Distribution of shocked calcite and Cesium-137 and relationship to crater zones, OAK crater.	7-36
7-22	Maximum depression/uplift of Pleistocene and Pliocene surfaces, OAK crater.	7-38
7-23	Maximum depression of Pleistocene and Pliocene surfaces, KOA crater.	7-39

(continued on next page)

FIGURE INDEX (continued)

Figure No.	Description	Page No.
------------	-------------	----------

CHAPTER 7: (Continued from preceding page).

7-24	Present-day (post-shot) location of Pleistocene and Pliocene surfaces, KOA and OAK craters.	7-40
7-25	Idealized model of geologic crater for symmetric crater and asymmetric crater on significant slope.	7-44
7-26	Horizon locations, fence diagram, OOR-17 to OPZ-18	7-47
7-27	Horizon locations, fence diagram, OBZ-4 to OAR-2/2A	7-48
7-28	Horizon locations, fence diagram, OUT-24 to OLT-14	7-49
7-29	Horizon locations, fence diagram, XBK-1 to KET-7	7-50
7-30	Graphic thinning analysis, OAK crater	7-53
7-31	Graphic thinning analysis, KOA crater	7-54
7-32	Stratigraphic density profile, borehole gravimetry	7-56
7-33	Idealized succession of major depositional events to form geologic crater.	7-57

PLATE INDEX

(All plates in map pocket)

Plate No.	Description
CHAPTER 5: BATHYMETRIC STUDIES OF OAK CRATER	
5- 1	Digitized Holmes and Narver (1958a) Preshot Topographic and Hydrographic Map.
5- 2	Digitized Holmes and Narver (1958b) Postshot Topographic and Hydrographic Map.
5- 3	Digitized U.S. Geological Survey (1984) Postshot Bathymetric Map.
5- 4	Negative Δ -Relief Map, H&N Preshot and H&N Postshot Map Pair.
5- 5	Positive Δ -Relief Map, H&N Preshot and H&N Postshot Map Pair.
5- 6	Negative Δ -Relief Map, H&N Preshot and USGS Postshot Map Pair.
5- 7	Positive Δ -Relief Map, H&N Preshot and USGS Postshot Map Pair.
5- 8	Negative Δ -Relief Map, H&N Postshot and USGS Postshot Map Pair.
5- 9	Positive Δ -Relief Map, H&N Postshot and USGS Postshot Map Pair.

TABLE INDEX

Table No.	Description	Page No.
CHAPTER 1: INTRODUCTION TO PART 4 OPEN-FILE REPORT		
1- 1	Matrix of data bases and analyses	1- 4
CHAPTER 2: BOREHOLE GRAVIMETRY, OAK CRATER		
2- 1	Corrections for lateral density changes	2-39
2- 2	Density and porosity values, OOR-17	2-41
2- 3	Density and porosity values, OPZ-18	2-43
2- 4	Density and porosity values, OQT-19	2-45
2- 5	Density and porosity values, ORT-20	2-47
2- 6	Density and porosity values, OSR-21	2-49
2- 7	Density and porosity values, OTG-23	2-51
2- 8	Density of atoll material surrounding OAK	2-52
CHAPTER 3: PALEONTOLOGIC EVIDENCE FOR SEDIMENTARY MIXING		
3- 1	Borehole depth of examined samples	3- 3
3- 2	Foraminifer occurrences, OBZ-4	3-16
3- 3	Foraminifer occurrences, OCT-5	3-17
3- 4	Foraminifer occurrences, OFT-8	3-18
3- 5	Foraminifer occurrences, OKT-13	3-19
3- 6	Foraminifer occurrences, OPZ-18	3-20
CHAPTER 4: ELECTRON PARAMAGNETIC RESONANCE STUDIES		
4- 1	Pressure and integrated difference data for high- resolution spectra, laboratory samples.	4-10
4- 2	Results for OAR-2A samples	4-22
4- 3	Results for OBZ-4 samples	4-23
4- 4	Results for OCT-5 samples	4-24
4- 5	Results for OET-7 samples	4-25
4- 6	Results for OFT-8 samples	4-26
4- 7	Results for OPZ-18 samples	4-27
4- 8	Results for OAK debris samples	4-28
CHAPTER 5: BATHYMETRIC STUDIES OF OAK CRATER		
5- 1	Summary of digitized bathymetric map products	5- 9
5- 2	Water depths and vertical differences	5-11
5- 3	Summary of areas and volumes from derivative map from H&N preshot vs H&N postshot maps.	5-21
5- 4	Summary of areas and volumes from derivative map from H&N preshot and USGS postshot maps.	5-22
5- 5	Summary of areas and volumes from derivative map from H&N postshot and USGS postshot maps.	5-23
5- 6	Grand summary of areas and volumes of negative, zero, and positive Δ -relief, OAK crater.	5-24

(continued on next page)

TABLE INDEX (continued)

Table No.	Description	Page No.
CHAPTER 6: CONSTRAINTS ON DENSIFICATION AND PIPING, OAK CRATER		
6- 1	Column-height changes down OAK boreholes	6- 5
6- 2	Uniformity of horizons in OAK area	6- 6
6- 3	Column-height changes due to densification	6-17
6- 4	Probability estimates	6-22
6- 5	Column-height changes due to densification 48 to 67 days after burst and probability estimates.	6-25
6- 6	Piping hypothesis analysis	6-30
6- 7	Endpoints of segments of piecewise linear fits to density profiles from BHG.	6-56
6- 8	Endpoints of segments of piecewise linear fits to density profiles from γ - γ logging.	6-57-73
6- 9	Mass of solid in vertical columns of unit cross- section, from BHG survey data.	6-79-81
6-10	Mass of solid in vertical columns of unit cross- section, from γ - γ survey data.	6-82-101
 CHAPTER 7: INTEGRATION OF MATERIAL-PROPERTY UNITS, GRAVIMETRY, AND ADDITIONAL STUDIES OF OAK AND KOA CRATERS		
7- 1	Relationship of geologic and paleontologic zones in crater and debris blanket.	7-12
7- 2	Depth to tops of crater zones, OAK and KOA	7-13
7- 3	Paleontologic crater zones, transition sand, KOA and OAK craters.	7-14
7-4	Correlation of geologic crater zones and multi- channel seismic zones.	7-15
7- 5	Depths to material-property unit boundaries, pre- and post-shot, OAK crater.	7-45-46
7- 6	Thinning analysis of material-property units, OAK	7-51
7- 7	Depths to material-property units, pre- and post- shot, KOA crater.	7-52
7- 8	Thinning analysis of material-property units, KOA	7-52
7- 9	Stratigraphic bulk-density analysis, OAK crater	7-55

**PACIFIC ENEWETAK ATOLL CRATER EXPLORATION (PEACE) PROGRAM
ENEWETAK ATOLL, REPUBLIC OF THE MARSHALL ISLANDS**

**Part 4: Analysis of borehole gravity survey and other
geologic and bathymetric studies in vicinity of
OAK and KOA craters**

CHAPTER 1:

INTRODUCTION TO PART 4 OPEN-FILE REPORT

By

Thomas W. Henry^{1/2} and Bruce R. Wardlaw^{1/3}

GENERAL REMARKS

The Pacific Enewetak Atoll Crater Exploration (PEACE) Program was established and funded by the Defense Nuclear Agency (DNA) to resolve a number of questions for the Department of Defense (DOD) about the geologic and material-properties parameters of two craters (KOA and OAK), formed by near-surface bursts of high-yield thermonuclear devices on the northern margin of Enewetak Atoll, (fig. 1-1), Marshall Islands, in 1958. The multidisciplinary studies conducted by the USGS in collaboration with the DNA, the Department of Energy (DOE), and other organizations during 1984 through 1987 were part of a much larger research initiative by the DNA to better understand the dynamic properties of strategic-scale nuclear bursts and the relevance of the Pacific Proving Grounds (PPG) craters to issues of strategic basing and targeting of nuclear weapons.

The reader is referred to the reports cited in the succeeding section for a detailed explanation of the events leading up to the PEACE Program and the collaborative roles of the USGS, other Federal agencies, and scientists and engineers from universities and private research laboratories.

¹ Branch of Paleontology and Stratigraphy, U.S. Geological Survey.

² Denver, CO 80225-0046.

³ Reston, VA 22092.

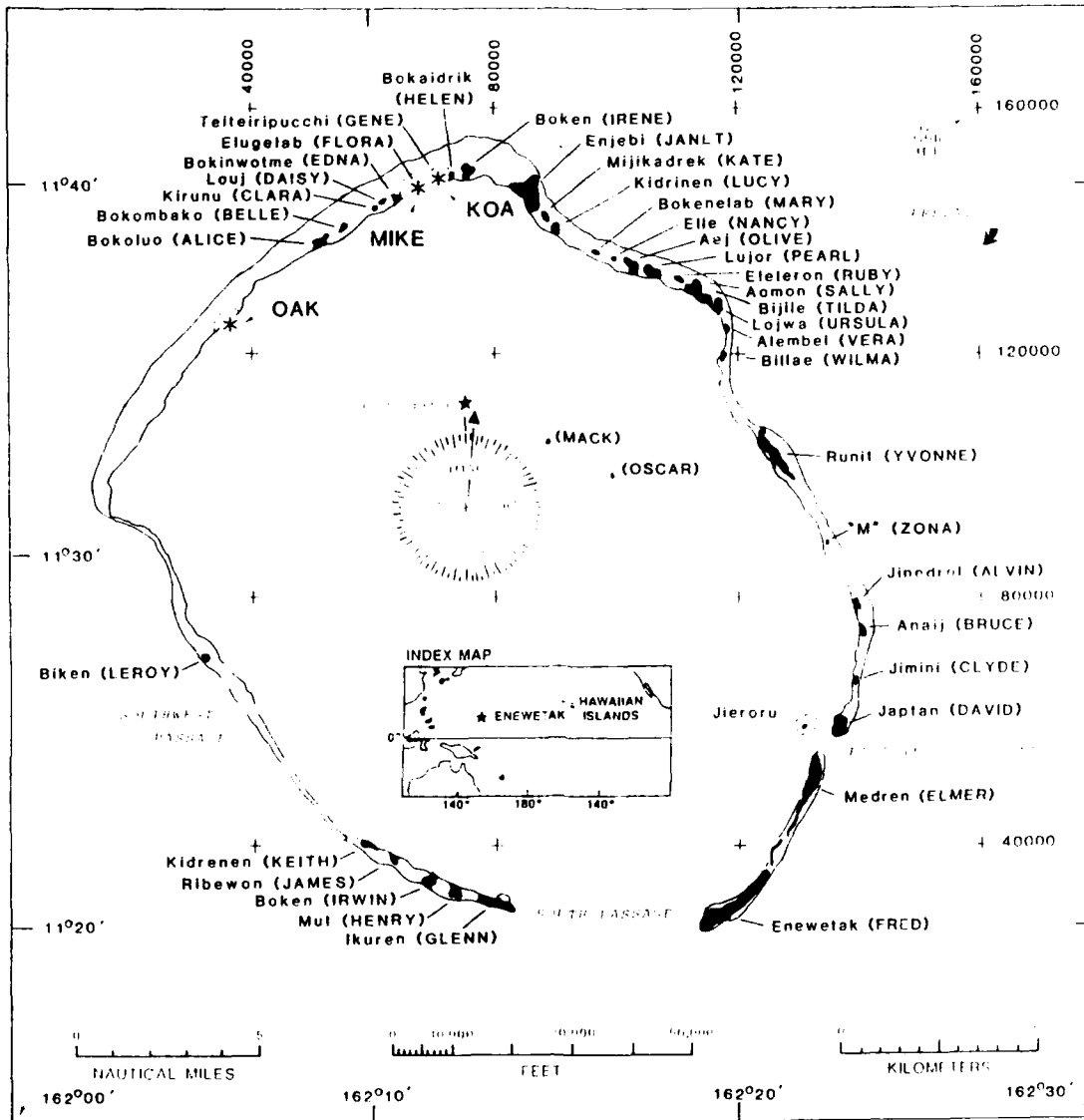


FIGURE 1-1. -- Map of Enewetak Atoll, Republic of the Marshall Islands (RMI), showing native names of principal islands and other features (military site name in parenthesis), and location of OAK, KOA, and MIKE craters. Inset map shows location of Enewetak within Pacific Ocean. Map from Henry, Wardlaw, and others (1986, p. 12, fig. 3).

PEACE PROGRAM REPORTS

This volume is the fifth and final volume of a series of four U.S. Geological Survey (USGS) Open-File Reports (Henry, Wardlaw, and others, 1986; Cronin, Brouwers, and others, 1986; and Henry and Wardlaw, 1986a) and one USGS Bulletin (Folger, 1986a) documenting geologic and geophysical data, analyses, and interpretations for the PEACE Program. Syntheses for the geologic and material-properties models for the craters are found in Wardlaw and Henry (1986, Ch. 14) and Wardlaw (1987, Ch. 7, this Report). The material-properties studies themselves, which provide quantitative parameters for computational modeling, for the most part were not conducted by USGS personnel and are published elsewhere for the DNA (e.g., Blouin and Timian, 1986a, 1986b; Borschel, Klauber, and Earley, 1986; McClelland Engineers, 1986; Mueller, 1987; Patti and Schatz, 1987 [1988], in preparation, Schatz, Patti, and Melzer, 1987 [1988], in preparation, and Simons and others, 1984).

DATA ACQUISITION AND BASES

The PEACE Program was truly a multidisciplinary endeavor. Field work for the program on Enewetak Atoll was done in two parts, the Marine Phase (mid- to late summer, 1984) and the Drilling Phase (late winter through mid-summer, 1985). The primary and derivative PEACE Program data bases and framework groups consist of the elements shown in Table 1-1. For general discussion of the fieldwork and data-acquisition procedures for the Marine Phase, the reader is referred to Folger (1986b), and, for the Drilling Phase, to Henry, Wardlaw, and others (1986, p. 29-97). For more detailed information about the field and laboratory procedures employed for a specific data set, refer to the individual Chapters or volumes (see tbl. 1-1). Many of the derivative data sets and framework groups from the Drilling Phase utilized samples from the 32 deep and intermediate boreholes drilled from the M/V Knut Constructor in the Enewetak lagoon. These boreholes (figs. 1-2 and 1-3) provide a data base upon which the subsurface geologic framework is grounded and upon which interpretations made from the geophysical and material-properties studies must be validated.

A wide array of pre-PEACE Program data from the PPG was re-examined, including (but not limited to) the following:

- (1). Published accounts in USGS Professional Paper 260 series (see Emery, Tracey, and Ladd, 1954) from the initial geologic, geophysical, and oceanographic investigations in the Marshall Islands associated with the early phases of nuclear testing.
- (2). Published reports and raw data from the geologic and geophysical studies of the PACE, EXPOE, and EASI Projects, sponsored by the DNA and conducted on Enewetak by the Air Force Weapons Laboratory (AFWL) (Couch, Fetzer, and others, 1975; Henny, Mercer, and Zbur, 1974; Ristvet, Tremba and others, 1978; Tremba, Jones, and Henny, 1981; Tremba, Couch, and Ristvet, 1982; and Tremba, 1987). For example, some of the multichannel-seismic lines from EASI were reprocessed by Grow, Lee, and others (1986), and selected PACE/EXPOE boreholes were redescribed and analyzed stratigraphically and isotopically before the Drilling Phase actually got underway (Henry, Wardlaw, and others, 1986;

TABLE 1-1. -- Matrix of data bases and analyses from PEACE Program. In heading, CH = Chapter; under heading PHASE, Marine or Drilling connotes which phase the samples were obtained originally. The pilot gravity survey in the old borehole on Medren (ELMER) Island was conducted in April 1984, hence the asterisk (*) in the appropriate column. The geologic and material-properties models for the craters are presented in Wardlaw and Henry (1986, Ch. 14) and in Wardlaw (1987, Ch. 8, this Report). U.S. Geological Survey Open-File Report 87-665 is the current volume.

DATA GROUP	PHASE	PUBLICATION	CH.	REFERENCE CITATION
Bathymetric Maps	Marine	Bull. 1678 OF-87- 665	A 5	Folger, Hampton, and others (1986); Peterson and Henry (1987*).
Side-Scan Sonar Imagery	Marine	Bull. 1678	B	Folger, Robb, and others (1986).
Single-Channel Seismic Reflection	Marine	Bull. 1678	C	Robb, Foster, and others (1986).
Multichannel-Seismic Reflection	Marine	Bull. 1678	D	Grow, Lee, and others (1986).
Seismic-Refraction	Marine	Bull. 1678	E	Ackermann, Grow, and Williams (1986).
Submersible Observations	Marine Both	Bull. 1678 OF-86- 555	F 11	Halley, Slater, and others (1986); Slater, Roddy, and others (1986).
Debris/Ejecta	Marine Marine Drilling	Bull. 1678 OF-86- 555 OF-87- 665*	G 3 4	Halley, Major, and others (1986); Ludwig, Halley, and others (1986); Polanskey and Ahrens (1987*).
Scuba Observations	Marine	Bull. 1678	H	Shinn, Kindinger, and others (1986).
Bottom Samples	Marine Mainly	OF-86- 555	10	Wardlaw, Henry, and Martin (1986).
Boreholes	Drilling	OF-86- 555	-	Henry, Wardlaw, and others (1986).
Lithostratigraphic Framework	Drilling	OF-86- 555	2	Wardlaw and Henry (1986a).
Biostratigraphic Framework & Mixing Studies	Drilling	OF-86- 159 OF-86- 555 OF-87- 665*	- 11 3	Cronin, Brouwers, and others (1986); Brouwers, Cronin, and Gibson (1986); Cronin and Gibson (1987*).
Geophysical Logs	Drilling	OF-86- 555 OF-87- 665*	7 6	Melzer (1986). Trullo (1987*).
Seismic Reference Survey	Drilling	OF-86- 555	9	Tremba and Ristvet (1986b).
Borehole Gravimetry	Drilling	OF-86- 555 OF-87- 665* OF-87- 665*	8 2 6	Beyer, Ristvet, and Oberate-Lehn (1986); Beyer (1987*); Trullo (1987*).
Stratotype Framework	Marine Drilling	Bull. 1678 OF-86- 555	G 3	Halley, Ludwig, and others (1986). Ludwig, Halley, and Simmons (1986).
X-Ray Mineralogy	Drilling	OF-86- 555	4	Tremba and Ristvet (1986).
Organic Geochemistry	Drilling	OF-86- 555	5	Ristvet and Tremba (1986).
Insoluble Residues	Drilling	OF-86- 555	6	Ristvet and Tremba (1986).
Radiation Chemistry	Drilling	OF-86- 555	12	Ristvet and Tremba (1986).
Electron-Spin Resonance	Drilling Mainly	OF-87- 665*	4	Polanskey and Ahrens (1987*).
Crater-Area Bottom Samples	Drilling	OF-86- 555 OF-86-555 ---	4 10 -	Tremba and Ristvet (1986). Wardlaw, Henry, and Martin (1986). Patti and Schatz (1987) [1988?].
Crater Synthesis	Marine Both Both	Bull. 1678 OF-86- 555 OF-87- 665*	A 14 7	Folger (1986b); Wardlaw and Henry (1986b); Wardlaw (1987*).

* OF-87-665 is the current report.

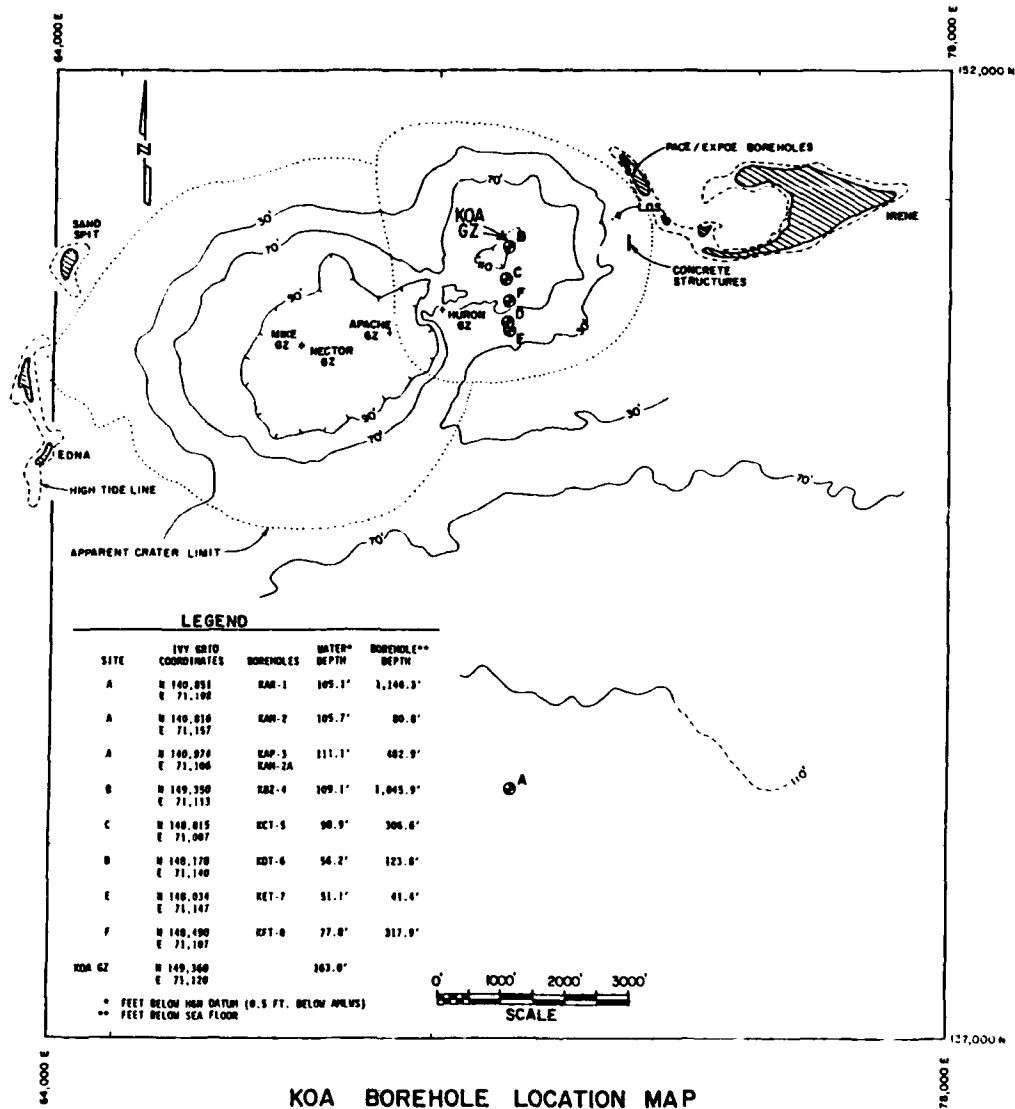


FIGURE 1-2. -- Map of KOA crater area showing borehole sites (depicted by letters) and general bathymetric contours (contour interval in feet). Map modified from Henry and Wardlaw (1986b, fig. 1-2).

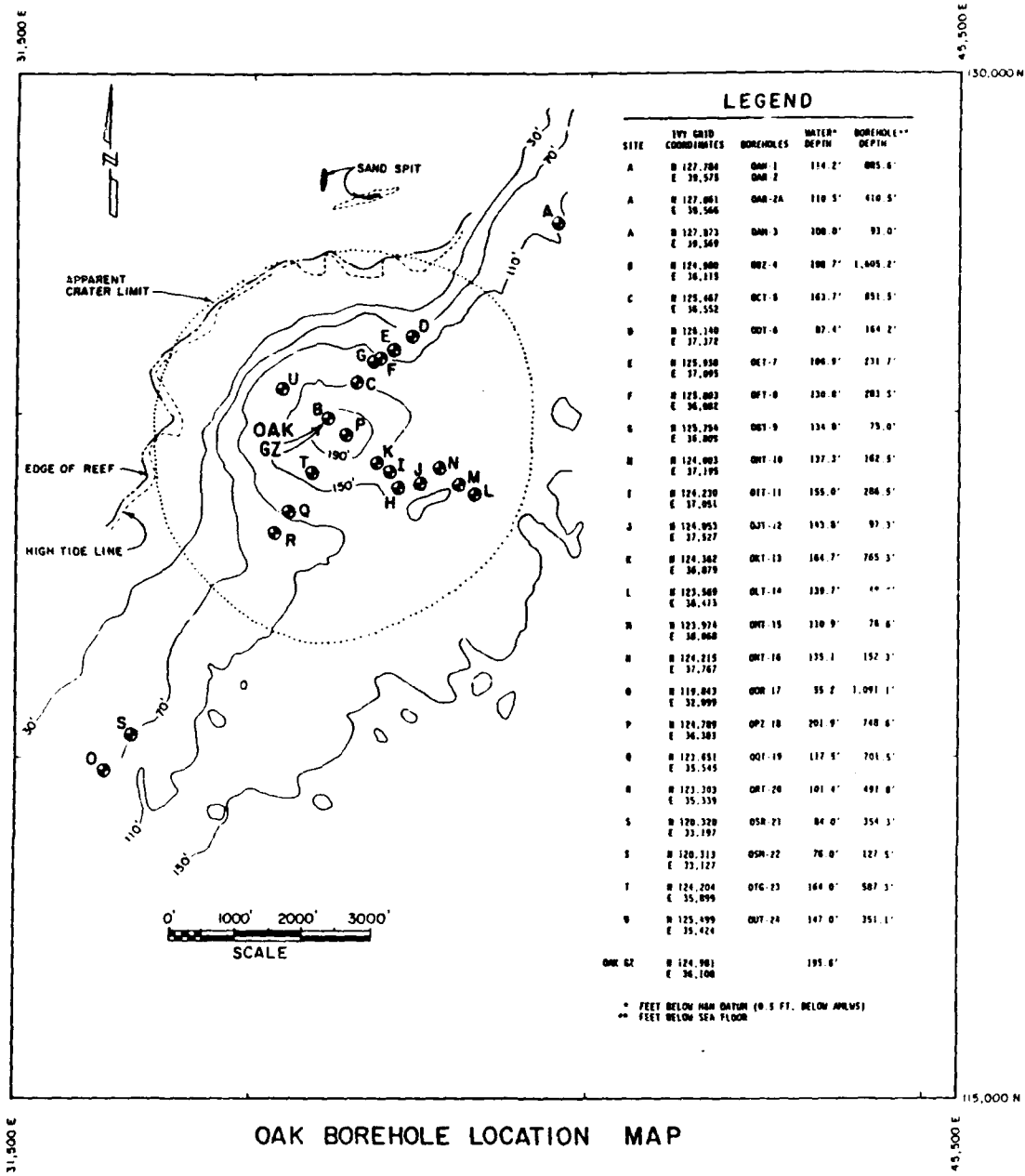


FIGURE 1-3. -- Map of OAK crater area showing borehole sites (depicted by letters) and general bathymetric contours (contour interval 10 feet). Map modified from Henry and Wardlaw (1986b, fig. 1-3).

Cronin, Brouwers, and others, 1986; Halley, Major, Ludwig, and others, 1986).

- (3). A broad spectrum of unpublished archival material from the PPG made freely available to us by the DNA and the DOE. These data include pre- and post-shot survey maps of the OAK and KOA crater areas, both black-and-white and color, stereographic aerial photographs, other kinds of aerial photographs, and pictures made (both pre- and post-testing) from ground-level of various crater features and man-made structures. The pre- and post-shot Holmes and Narver maps of OAK crater were digitized and form an essential part of the volumetric studies for the PEACE Program (Peterson and Henny, 1987, Chapter 5 of the current Report).
- (4). Other published reports, too numerous to cite here.

SYNOPSIS OF CHAPTERS OF CURRENT VOLUME

This Open-File Report consists of seven Chapters. The interrelationship of each Chapter to the overall data base is depicted in Table 1-1. Salient points of each Chapter are summarized below.

Borehole Gravity (Ch. 2; Beyer)

The borehole gravity measurements from the southwest transect of OAK crater and in the Medren (ELMER) Island borehole provide a critical set of data for bulk density and porosity of both the undisturbed stratigraphic sequence and the sediments and rock that were affected by the OAK event.

Significant densification, porosity diminution, and mass removal are indicated for discrete intervals within the boreholes in the central-crater region of OAK. Zones in which these phenomena are indicated correspond closely to the geologic crater zones and provide strong corroborative evidence for their integrity.

One of the primary goals of the gravimetry was to determine whether densification of the shallow substrate in the crater-flank region (or "wings") could account for the measured lowering of the sea floor. This is particularly critical because the bulk of the volume of the apparent crater lies within its flank region. Gravity analysis conducted in the upper parts of transition-zone boreholes (OQT-19 and ORT-20, see fig. 1-3) demonstrates conclusively that the materials (sediment, rock, and rock debris) are only slightly denser than comparable intervals of materials in reference boreholes OOR-17 and OSR-21. In fact, only perhaps about 15 percent of the documented lowering of the sea floor in the crater wings region can be explained by densification alone. Thus, for the wings region, processes other than densification clearly are also involved.

Paleontologic Evidence for Mixing (Ch. 3; Cronin, Gibson)

Paleontologic analysis of the upper 1,200 ft of strata on Enewetak established the division of the upper part of the carbonate cap into twelve discrete biostratigraphic zones (named zones AA, the youngest, through LL, the oldest -- see also Cronin, Brouwers, and others, 1986, and Brouwers, Cronin, and Gibson, 1986). For the current study, additional samples from stratigraphically undisturbed boreholes from the OAK crater area (i.e., from the reference boreholes) were examined to refine the local zonation and to more closely resolve key biostratigraphic boundaries. Several of these boundaries, combined with physical stratigraphic datums, form surfaces or marker horizons that are Lagrangian (see Chapter 6), permitting employment of a powerful tool in the analysis of crater evolution.

The microfossil studies of OAK reference-borehole plus crater samples provides significant new information about the timing and methods of emplacement¹ of materials from various biostratigraphic zones within the materials that partially infill the crater itself. This includes for the first time identification of sediments that were either at or within a few centimeters of the pre-event lagoon floor. These new data have furnished quantitative estimates of material from each zone (or group of zones) admixed in the crater fill. These estimates include volumes and percentages of materials originating from the deeper stratigraphic zones not involved in the excavation of the initial crater itself and from shallower geologic units as well. The editors emphasize that materials from stratigraphically shallower zones pose a real problem of differentiation. For example, how does one separate material that may have been emplaced from, say, zone CC from material within CC that has not moved? *Therefore, estimated volumes or percentages of material that may have been piped or otherwise moved from these shallow zones may be underestimated, perhaps grossly.*

Electron Paramagnetic Resonance Studies (Ch. 4; Polansky, Ahrens)

EPR spectrometry was applied to measure the peak-shock stress to which calcitic materials were subjected during the OAK event. Most of the samples analyzed can be characterized as either unshocked or very heavily shocked, with few samples showing intermediate states. Samples of the "transition sand" from OPZ-18 show the greatest concentration of very highly shocked material, interpreted as originating in the proximity of ground zero and plastered onto the walls of the excavational crater. Because of subsequent collapse of the excavational crater walls and dilution by mixing with less-shocked or unshocked materials, this lining, as a discrete stratigraphic unit, is identifiable only in the OPZ-18 borehole. Surprisingly, none of the 26 samples from the ground-zero borehole OBZ-4 showed significant shock damage. However, a zone containing less concentrated, very highly shocked material can be recognized in the three transition-zone boreholes studied (OCT-5, OET-7, and OFT-8), and its base occurs at progressively shallower depths away from ground zero.

¹ The term emplacement is used as a generic term to describe the deposition of material transported from one point to another without reference to the mechanism involved.

Bathymetric Studies of OAK Crater (Ch. 5; Peterson, Henny)

Three pertinent base maps were digitized and processed with a computer to facilitate analysis of the changes in the sea-floor bottom topography (bathymetry) and corresponding volumes in the area affected by the detonation of the OAK device (June 29, 1958) and by subsequent, longer term geologic processes. These maps are: (1) the pre-shot Holmes and Narver (H&N) survey, completed three days prior to the burst; (2) the post-shot H&N map, surveyed 47 to 67 days after the burst; and (3) the USGS map, made during the Marine Phase of the PEACE Program, 26 years after the burst.

The USGS map, in the format presented by Folger, Hampson, and others (1986), was not amenable for comparison with the two H&N maps (even undigitized) primarily because the USGS depth contours are given in meters rather than feet. The irregular area common to all three base maps is shown in Figure 5-1.

OAK is a strongly asymmetric crater; part of the asymmetry is a geologic function of the reef being on one side of surface ground zero and the atoll lagoon on the other. Many independent lines of evidence demonstrate that the excavational crater was appreciably smaller and more nearly circular than the current (or apparent) crater. Using the standardized digitized data for the common area of the base maps, three pairs² of vertical-difference contour maps were prepared. These maps show that: (1) the pre-shot topographic (geologic) features significantly influenced not only the evolution and final size/shape of the crater but also the initial distribution and subsequent reworking of debris from the OAK event; (2) the area of greatest downward displacement of the sea floor between the two post-shot base maps is that of the inner crater; and (3) the entire map area was lowered (and not uniformly) an average of 23 ft by 67 days after the burst and by another 12 ft during the next 26 years. As the surface of the lagoon and crater floor in this area was lowered, areas of positive-difference in relief (i.e., those areas that were higher post-shot than pre-shot) also decreased from about 27 percent by 67 days to about 14 percent 26 years later.

Two notes of caution must be clearly understood in using these maps for quantitative estimates for cratering calculations. The first is that there is no Lagrangian marker for the pre-event lagoon floor. The second is that the debris volumes estimated from these maps are understated simply because the apparent crater of OAK extends beyond the areas mapped, including the USGS map, which encompasses the largest area.

¹ Following the glossary presented in Henry and Wardlaw (1986a), the apparent crater is defined as the locus of the zero-difference contour line surrounding a crater -- viz, the locus of points where the effects of an explosion can no longer be detected when the pre-event contours are compared with the post-event contours (fide, B.L. Ristvet.)

² A negative- and a positive-relief-difference (called Δ -relief) isopachous map was constructed for each combination of two base maps.

Constraints on Densification and Piping for OAK (Ch. 6; Trulio)

As mentioned previously, it is established from a wide array of data that the excavational crater of OAK had an appreciably smaller radius than that of the apparent crater. Because crater volume is a radius-squared function, it is evident that most of the volume of OAK is contained within its flank or "wing" area. What is (are) the significant mechanism(s) responsible for forming the wings of the large apparent craters in the PPG? Trulio presents a number of different models dealing with the PEACE Program data bases and makes a number of inferences about these mechanisms based on these models.

Using the data base from the gravimetry (Chapter 2), Trulio applies mathematical analyses to the data, from a purely physical viewpoint, and verifies Beyer's conclusion that densification (or, in Trulio's terminology, "simple subsidence") accounts for just a small part of the formation of the wings of OAK crater. As a best estimate, only about 8 percent of the sea-floor drop on the wings can be attributed to density increases caused by the burst.

Another explanation for part of the observed sea-floor lowering phenomenon is piping, or movement (driven by gravity and density differences) of a sediment/water slurry through conduits (cracks, fissures, etc.) to generally shallower depths or to the surface through vents to form "sand volcanoes". That piping occurred associated with the OAK and KOA bursts, particularly in the central crater region, is supported by independent lines of evidence (see Chapter 7 for discussion). However, at issue are: (1) the role of piping relative to other mechanisms to account for the drop in the sea floor; and (2) the amount of material transported by this mechanism. Mean values for the density of material piped up to the sea floor from beneath OAK can be derived from the combination of sea-floor base maps and gravimetry profiles. If correct, this model poses limitations on the amount of material transported out of the crater by piping. The best estimate based on this model is that the piped and residual materials differed by only about 0.2 g/cc, a density difference that can drive piping, in Trulio's words, "but weakly". Trulio cautions that the sequence of events leading to the transport of piped material out of the crater is subject to interference at many points.¹

It is suggested that plastic flow also should be considered as a plausible mechanism to account for most of the phenomenon of sea-floor lowering. Trulio points out, however, that little is known about the displacement field around a flow crater.

¹ See caveat in italics on page 1-8. The editors also emphasize that the observed "subsidence" or sea-floor lowering on the wings of the Enewetak craters studied is not reasonably attributable to one mechanism operating alone. The lowering was caused in part by densification, in part by piping (certainly upwardly and probably laterally as well), probably in part to plastic flow, and possibly to other mechanisms that may not have even been thought of yet.

Additional Studies of Geologic Crater Models (Ch. 7, Wardlaw)

The final Chapter provides an integration of the new information from the various studies presented in the current Open-File Report with the previously developed analyses of PEACE Program data. Of particular interest to the material-properties community is the formulation of a set of material-properties units for the normal stratigraphic (geologic) sequence and a discussion of the relationship of these units to the sedimentary packages presented in Wardlaw and Henry (1986a, 1986b).

Using available evidence, the pre-event geology beneath the OAK and KOA crater areas is reconstructed, including paleotopographic contour maps of several of the more significant subsurface datums. Wardlaw points out that topographic differences of the pre-event Holocene ground surfaces (i.e., the pre-1958 lagoon, reef, and island surface) between the KOA and OAK area produced differences in the surface configurations of the two craters. Differences in cementation and structural competency of key stratigraphic intervals beneath the surface ground zeros of KOA and OAK and the effects of these differences on the development of the two craters are summarized.

A study of the thinning of the stratigraphic units influenced by OAK and KOA is presented. A more comprehensive interpretation of the models for these two craters given in Wardlaw and Henry (1986b) is developed based primarily on the inferred pre-shot elevation of certain datums and thicknesses of stratigraphic intervals in contrast to their post-shot attributes. The case is made that movement of material laterally ("lateral flow") may account for much of the "subsidence" and formation of the wings.

An idealized succession of cratering and depositional events is presented.

ACKNOWLEDGEMENTS

We, the editors, extend a special note of appreciation to the following people, without whom this program would have not been possible. Lt. Col. Robert F. Couch, Jr. (U.S. Air Force and DNA Program Manager for the PEACE Program) and Byron L. Ristvet and Edward L. Tremba (both of S-Cubed Division of Maxwell Laboratories), and Robert W. Henny (Air Force Weapons Laboratory) were full scientific collaborators with us during the PEACE Program. All four of these geologists logged extensive on-site experience in the PPG prior to the current program and were principal investigators in all of various phases of the earlier AFWL investigations on Enewetak. And, in a real sense, they represent a vital component of the record of cratering studies on Enewetak. Their expertise and geotechnical knowledge were invaluable to the current program, and we owe them a profound debt of gratitude. Couch, Ristvet, and Tremba served (alternatively) as Chief Scientists aboard the Knut Constructor during the Drilling Phase of the program, and all three were on-site during parts of the earlier Marine Phase.

We would like to thank also the authors of the Chapters of the current Open-File Report for their timely response to our needs in editing, compiling,

and finalizing this volume and for their input for synthesizing the diverse data bases.

We are indebted also to John F. Schatz and L. Stephen Melzer of SAIC for constructive exchange of scientific and technical information for this volume. Melzer was on-site with us as Chief Scientist during part of the Drilling Phase field work, and it was his observations along with that of the geologists and paleontologists studying the OAK ground-zero borehole aboard the drill ship that demonstrated the reality of piping of materials from zones from far below the excavational crater into the sediment forming part of the crater fill.

The plates for Chapter 2 were laid out by James MacCornack, S-Cubed, Albuquerque, and printed by the Defense Nuclear Agency Printing Plant, Kirtland AFB, New Mexico. We thank Leonard MacDonald, head printer, for his assistance.

REFERENCES CITED

- Ackermann, H.D., Grow, J.A., and Williams, J.M., 1986, Chapter E: Seismic-refraction survey of OAK crater; 18 p., 19 figs., 1 tbl.; in Folger, D.W., editor, Sea-floor observations and subbottom seismic characteristics of OAK and KOA craters, Enewetak Atoll, Marshall Islands: U.S. Geological Survey Bulletin 1678.
- Beyer, L.A., Ristvet, B.L., and Oberste-Lehn, D., 1986, Chapter 8: preliminary density and porosity data and field techniques of borehole gravity surveys, OAK crater; 28 p., 4 figs., 10 tbls., 2 appendices; in Henry, T.W., and Wardlaw, B.R., editors, Pacific Enewetak Atoll Crater Exploration (PEACE) Program, Enewetak Atoll, Republic of the Marshall Islands; Part 3: Stratigraphic analysis and other geologic and geophysical studies in vicinity of KOA and OAK craters: U.S. Geological Survey Open-File Report 86-555.
- Blouin, S.E., and Timian, D.A., 1986a, Core description and ultrasonic logs from Enewetak Atoll: Defense Nuclear Agency, Washington, DC., Technical Report TR-86-198, 98 p., [released 3 February 1986, unclassified document].
- Blouin, S.E., and Timian, D.A., 1986b, Material properties testing in support of PEACE Program, Enewetak Atoll: Defense Nuclear Agency, Washington, DC., Technical Report TR-86-197, 458 p., [released 4 June 1986, unclassified document].
- Borshel, T.F., Klauber, W.P., and Earley, K.H., 1986, Lithological, physical, and mechanical characterization of geologic samples from Enewetak Atoll: TerraTek Research, Inc., Report TR-87-25, prepared for the Defense Nuclear Agency.

- Brouwers, E.M., Cronin, T.M., and Gibson, T.G., 1986, Chapter 11: Additional paleontologic studies, OAK and KOA craters; 18 p., 5 figs., 5 tpls., 1 pl.; in Henry, T.W., and Wardlaw, B.R., editors, Pacific Enewetak Atoll Crater Exploration (PEACE) Program, Enewetak Atoll, Republic of the Marshall Islands; Part 3: Stratigraphic analysis and other geologic and geophysical studies in vicinity of KOA and OAK craters: U.S. Geological Survey Open-File Report 86-555.
- Couch, R.F., Jr., Fetzer, J.A., Goter, E.R., Ristvet, B.L., Tremba, E.L., Walter, D.R., and Wendland, V.P., 1975, Drilling operations of Enewetak Atoll during Project EXPOE: Air Force Weapons Laboratory Technical Report AFWL-TR-75-216, Kirtland Air Force Base, New Mexico, 270 p., 17 figs., 4 tpls. [unclassified document].
- Cronin, T.M., Brouwers, E.M., Bybell, L.M., Edwards, E.E., Gibson, T.G., Margerum, R., and Poore, R.Z., 1986, Pacific Enewetak Atoll Crater Exploration (PEACE) Program, Enewetak Atoll, Republic of the Marshall Islands; Part 2: Paleontology and biostratigraphy, application to OAK and KOA Craters: U.S. Geological Survey Open-File Report 86-159, 39 p., 20 figs., 12 tpls., 3 appendices.
- Emery, K.O., Tracey, J.I., Jr., and Ladd, H.S., 1954, Geology of Bikini and nearby atolls: U.S. Geological Survey Professional Paper 260-A, 265 p., 73 pls., 84 figs., 11 charts, 27 tpls.
- Folger, D.W., editor, 1986a, Sea-floor observations and subbottom seismic characteristics of OAK and KOA craters, Enewetak Atoll, Marshall Islands: U.S. Geological Survey Bulletin 1678, 301 p., 112 figs., glossary, 2 appendices. [Chapters A - H, plus Introduction.]
- Folger, D.W., 1986b, Introduction to the volume; 7 p., 2 figs., 2 tpls.; in Folger, D.W., editor, Sea-floor observations and subbottom seismic characteristics of OAK and KOA craters, Enewetak Atoll, Marshall Islands: U.S. Geological Survey Bulletin 1678.
- Folger, D.W., Hampson, J.C., Robb, J.M., Woellner, R.A., Foster, D.S., and Tavares, L.A., 1986, Chapter A: Bathymetry of OAK and KOA craters; 35 p., 12 figs., 2 appendices; in Folger, D.W., editor, Sea-floor observations and subbottom seismic characteristics of OAK and KOA craters, Enewetak Atoll, Marshall Islands: U.S. Geological Survey Bulletin 1678.
- Folger, D.W., Robb, J.M., Hampson, J.C., Davis, P.A., Bridges, P.M., and Roddy, D.J., 1986, Chapter B: Sidescan-sonar survey of OAK and KOA craters; 18 p., 6 figs.; in Folger, D.W., editor, Sea-floor observations and subbottom seismic characteristics of OAK and KOA craters, Enewetak Atoll, Marshall Islands: U.S. Geological Survey Bulletin 1678.
- Grow, J.A., Lee, M.W., Miller, J.J., Agena, W.F., Hampson, J.C., Foster, D.S., and Woellner, R.A., 1986, Chapter D: Multichannel seismic-reflection survey of KOA and OAK craters; 46 p., 39 figs.; in Folger, D.W., editor, Sea-floor observations and subbottom seismic characteristics of OAK and KOA craters, Enewetak Atoll, Marshall Islands: U.S. Geological Survey Bulletin 1678.

- Halley, R.B., Major, R.P., Ludwig, K.R., Peterman, Z.L., and Matthews, R.K., 1986, Chapter G: Preliminary analyses of OAK debris samples; 11 p., 6 figs., 4 tbls.; in Folger, D.W., editor, Sea-floor observations and subbottom seismic characteristics of OAK and KOA craters, Enewetak Atoll, Marshall Islands: U.S. Geological Survey Bulletin 1678.
- Halley, R.B., Slater, R.A., Shinn, E.A., Folger, D.W., Hudson, J.H., Kindinger, J.L., and Roddy, D.J., 1986, Chapter F: Observations of OAK and KOA craters from the submersible; 32 p., 13 figs., 1 appendix; in Folger, D.W., editor, Sea-floor observations and subbottom seismic characteristics of OAK and KOA craters, Enewetak Atoll, Marshall Islands: U.S. Geological Survey Bulletin 1678.
- Henny, R.W., Mercer, J.W., and Zbur, R.T., 1974, Near-surface geologic Investigations at Eniwetok Atoll: Air Force Weapons Laboratory Technical Report AFWL-TR-74-257, Kirtland Air Force Base, New Mexico, 367 p. [unclassified document].
- Henry, T.W., and Wardlaw, B.R., editors, 1986a, Pacific Enewetak Atoll Crater Exploration (PEACE) Program, Enewetak Atoll, Republic of the Marshall Islands; Part 3: Stratigraphic analysis and other geologic and geophysical studies in vicinity of KOA and OAK craters: U.S. Geological Survey Open-File Report 86-555, 486 p., 92 figs., 90 tbls, 34 pls. [14 Chapters.]
- Henry, T.W., and Wardlaw, B.R., 1986b, Chapter 1: Introduction: 13 p., 3 figs., 1 tbl., in Henry, T.W., and Wardlaw, B.R., editors, Pacific Enewetak Atoll Crater Exploration (PEACE) Program, Enewetak Atoll, Republic of the Marshall Islands; Part 3: Stratigraphic analysis and other geologic and geophysical studies in vicinity of KOA and OAK craters: U.S. Geological Survey Open-File Report 86-555.
- Henry, T.W., Wardlaw, B.R., Skipp, B.A., Major, R.P., and Tracey, J.I., Jr., 1986, Pacific Enewetak Atoll Crater Exploration (PEACE) Program, Enewetak Atoll, Republic of the Marshall Islands; Part 1: Drilling operations and descriptions of boreholes in vicinity of KOA and OAK craters: U.S. Geological Survey Open-File Report 86-419, 497 p., 32 figs., 29 pls., 13 tbls., 3 appendices.
- Ludwig, K.R., Halley, R.B., Simmons, K.R., and Peterman, Z.E., 1986, Chapter 3: Sr-isotope stratigraphy of disturbed and undisturbed carbonates; 23 p., 8 figs., 6 tbls.; in Henry, T.W., and Wardlaw, B.R., editors, Pacific Enewetak Atoll Crater Exploration (PEACE) Program, Enewetak Atoll, Republic of the Marshall Islands; Part 3: Stratigraphic analysis and other geologic and geophysical studies in vicinity of KOA and OAK craters: U.S. Geological Survey Open-File Report 86-555.
- McClelland Engineers, Inc., 1986, Relative liquefaction for potential study for carbonate versus noncarbonate materials: Report No. 0186-1069, to Holmes and Narver, Inc., Honolulu, Hawaii; dated December 19, 1986; 37 p., 13 pls. [Signed by Ronald J. Ebehar, Project Supervisor, and Alan G. Young, Vice President, Marine Geosciences.]

- Melzer, L.S., 1986, Chapter 7: Downhole geophysical logs; 32 p., 16 figs., 7 tbls.; in Henry, T.W., and Wardlaw, B.R., editors, Pacific Enewetak Atoll Crater Exploration (PEACE) Program, Enewetak Atoll, Republic of the Marshall Islands; Part 3: Stratigraphic analysis and other geologic and geophysical studies in vicinity of KOA and OAK craters: U.S. Geological Survey Open-File Report 86-555.
- Mueller, C.M., 1987, Mechanical response of undisturbed cores and remolded coral sand from Enewetak Atoll: Department of the Army, Corps of Engineers, Waterways Experiment Station, Technical Report SL-87-14, Vicksburg, Mississippi, 361 p., 274 pls., 56 figs., 5 tbls. [unclassified document].
- Patti, N., and Schatz, J.F., 1987 [1988?], in preparation, Material properties tests, material compaction on shot-similar stress/strain paths, and grain size distribution on Enewetak Atoll coral specimens: Science Applications International Corporation, Report SAIC-87/1158, prepared for the Defense Nuclear Agency.
- Ristvet, B.L., and Tremba, E.L., 1986a, Chapter 5: Total organic content of lagoon benthic sediments and of subsurface samples from the PEACE drilling program; 9 p., 2 figs., 2 tbls.; in Henry, T.W., and Wardlaw, B.R., editors, Pacific Enewetak Atoll Crater Exploration (PEACE) Program, Enewetak Atoll, Republic of the Marshall Islands; Part 3: Stratigraphic analysis and other geologic and geophysical studies in vicinity of KOA and OAK craters: U.S. Geological Survey Open-File Report 86-555.
- Ristvet, B.L., and Tremba, E.L., 1986b, Chapter 6: Insoluble residue analysis of carbonate sediments from the subsurface of Enewetak Atoll; 5 p., 1 tbl., ; in Henry, T.W., and Wardlaw, B.R., editors, Pacific Enewetak Atoll Crater Exploration (PEACE) Program, Enewetak Atoll, Republic of the Marshall Islands; Part 3: Stratigraphic analysis and other geologic and geophysical studies in vicinity of KOA and OAK craters: U.S. Geological Survey Open-File Report 86-555.
- Ristvet, B.L., and Tremba, E.L., 1986c, Chapter 12: Radiation chemistry of the subsurface of OAK and KOA craters; 15 p., 5 figs., 5 tbls; in Henry, T.W., and Wardlaw, B.R., editors, Pacific Enewetak Atoll Crater Exploration (PEACE) Program, Enewetak Atoll, Republic of the Marshall Islands; Part 3: Stratigraphic analysis and other geologic and geophysical studies in vicinity of KOA and OAK craters: U.S. Geological Survey Open-File Report 86-555.
- Ristvet, B.L., Tremba, E.L., Couch, R.F., Jr., Fetzer, J.A., Goter, E.R., Walter, D.R., and Wendland, V.P., 1978, Geologic and geophysical investigations of the Enewetak nuclear craters; Final reports: Air Force Weapons Laboratory Technical Report AFWL-TR-77-242, Kirtland Air Force Base, New Mexico, 298 p. [unclassified document].
- Robb, J.M., Foster, D.S., Folger, D.W., Hampson, J.C., and Woellner, R.A., 1986, Chapter C: Single-channel seismic survey of OAK and KOA craters: 51 p., 24 figs.; in Folger, D.W., editor, Sea-floor observations and subbottom seismic characteristics of OAK and KOA craters, Enewetak Atoll, Marshall Islands: U.S. Geological Survey Bulletin 1678.

- Schatz, J.F., Patti, N., and Melzer, L.S., 1987 [1988?], in preparation, Material properties at OAK/KOA -- Summary Report: Science Applications International Corporation, Report SAIC-87/1159, prepared for the Defense Nuclear Agency.
- Simons, D., and others, 1984, Recommendations for laboratory material properties testing of core materials from the Pacific Proving Grounds: Research and Development Associates, Los Angeles, California; unnumbered report submitted to Defense Nuclear Agency.
- Shinn, E.A., Kindinger, J.L., Halley, R.B., and Hudson, J.H., 1986, Chapter H: Scuba observations of OAK and KOA craters, 39 p., 38 figs., 1 tbl.; in Folger, D.W., editor, Sea-floor observations and subbottom seismic characteristics of OAK and KOA craters, Enewetak Atoll, Marshall Islands: U.S. Geological Survey Bulletin 1678.
- Slater, R.A., Roddy, D.J., Folger, D.W., Halley, R.B., and Shinn, E.A., 1986, Chapter 13: Additional submersible studies; detailed observations of the seafloor of OAK, KOA, and MIKE craters; 153 p., 2 tbls., 4 pls.; in Henry, T.W., and Wardlaw, B.R., editors, Pacific Enewetak Atoll Crater Exploration (PEACE) Program, Enewetak Atoll, Republic of the Marshall Islands; Part 3: Stratigraphic analysis and other geologic and geophysical studies in vicinity of KOA and OAK craters: U.S. Geological Survey Open-File Report 86-555.
- Tremba, E.L., 1987 [1984], Enewetak Atoll Seismic Investigation (EASI): Phase III; Final Report: Air Force Weapons Laboratory Technical Report 84-105, Air Force Systems Command, Kirtland Air Force Base, New Mexico, 87117-6008, 122 p., 36 figs., 11 tbls. [unclassified document].
- Tremba, E.L., Couch, R.F., Jr., and Ristvet, B.L., 1982, Enewetak Atoll Seismic Investigation (EASI) Project; Phases I and II: Air Force Weapons Laboratory Technical Report AFWL-TR-82-20, Kirtland Air Force Base, New Mexico, 124 p., 38 figs., 3 tbls., 3 appendices [unclassified document].
- Tremba, E.L., Jones, G.L., and Henny, R.W., 1981, Pacific atoll cratering experiments (Project PACE 2); Results and analysis of cratering and related effects: Air Force Weapons Laboratory Technical Report AFWL-TR-81-167, Air Force Systems Command, Kirtland Air Force Base, New Mexico, 334 p., 32 figs., 8 tbls., 8 appendices [unclassified document].
- Tremba, E.L., and Ristvet, B.L., 1986a, Chapter 4: X-ray diffraction mineralogy; 49 p., 11 figs., 35 tbls., in Henry, T.W., and Wardlaw, B.R., editors, Pacific Enewetak Atoll Crater Exploration (PEACE) Program, Enewetak Atoll, Republic of the Marshall Islands; Part 3: Stratigraphic analysis and other geologic and geophysical studies in vicinity of KOA and OAK craters: U.S. Geological Survey Open-File Report 86-555.
- Tremba, E.L., and Ristvet, B.L., 1986b, Chapter 9: Seismic reference surveys; 16 p., 1 fig., 12 tbls.; in Henry, T.W., and Wardlaw, B.R., editors, Pacific Enewetak Atoll Crater Exploration (PEACE) Program, Enewetak Atoll, Republic of the Marshall Islands; Part 3: Stratigraphic analysis and other geologic and geophysical studies in vicinity of KOA and OAK craters: U.S. Geological Survey Open-File Report 86-555.

Wardlaw, B.R., and Henry, T.W., 1986a, Chapter 2: Physical stratigraphic framework; 36 p., 10 figs., 2 tpls.; in Henry, T.W., and Wardlaw, B.R., editors, Pacific Enewetak Atoll Crater Exploration (PEACE) Program, Enewetak Atoll, Republic of the Marshall Islands; Part 3: Stratigraphic analysis and other geologic and geophysical studies in vicinity of KOA and OAK craters: U.S. Geological Survey Open-File Report 86-555.

Wardlaw, B.R., and Henry, T.W., 1986b, Chapter 14: Geologic interpretation of OAK and KOA craters; 39 p., 21 figs., 2 tpls.; in Henry, T.W., and Wardlaw, B.R., editors, Pacific Enewetak Atoll Crater Exploration (PEACE) Program, Enewetak Atoll, Republic of the Marshall Islands; Part 3: Stratigraphic analysis and other geologic and geophysical studies in vicinity of KOA and OAK craters: U.S. Geological Survey Open-File Report 86-555.

Wardlaw, B.R., Henry, T.W., and Martin, W.E., 1986, Chapter 10: Benthic samples from Enewetak Atoll; 50 p., 6 figs., 12 tpls., 29 pls.; in Henry, T.W., and Wardlaw, B.R., editors, Pacific Enewetak Atoll Crater Exploration (PEACE) Program, Enewetak Atoll, Republic of the Marshall Islands; Part 3: Stratigraphic analysis and other geologic and geophysical studies in vicinity of KOA and OAK craters: U.S. Geological Survey Open-File Report 86-555.

CHAPTER 2:

ANALYSIS OF BOREHOLE GRAVITY SURVEYS AT OAK CRATER

by

L. A. Beyerl

INTRODUCTION

Borehole gravity (BHG) surveys were made in selected PEACE Program boreholes at OAK crater on Enewetak Atoll because they provide the only means to directly and accurately measure in situ bulk density of large volumes of rock and sediment that surround the boreholes and to provide data to calculate the total porosity of these materials². The differences between the density and porosity of undisturbed atoll materials and the sediment and rock involved in the excavational and apparent craters are crucial to understanding various cratering phenomena. In addition, accurate and representative density and porosity measurements of undisturbed atoll materials are important for nuclear-event calculations. The nature of BHG measurements, rationale for siting BHG boreholes, field techniques, and preliminary (apparent) BHG density data and calculated porosity values are given in Beyer, Ristvet, and Oberste-Lehn (1986).

This report presents the models used to correct the apparent (BHG) density and porosity data for large-scale lateral density changes across the reef margin (due to natural facies changes) and for smaller-scale lateral density changes due to cratering phenomena. Corrected BHG density data and calculated porosity values are described in terms of their modification due to cratering processes.

Ancillary topics include: (1) general results of the BHG survey in the E-1 borehole on Medren (ELMER) Island (Appendix 2-1), (2) brief comparison of estimates of density and porosity from BHG, gamma-gamma, and neutron logs, and (3) relationship between grain density and BHG porosity in undisturbed atoll materials. A short description of how average interval grain density was determined from the x-ray mineralogy and organic analyses studies of core samples is found in Appendix 2-2.

The locations of OAK crater and E-1 and F-1 deep boreholes referred to later in this chapter are shown in Figure 2-1. Locations of boreholes drilled at OAK crater during the PEACE Program are given in Figure 2-2, along with a table that summarizes pertinent information about the boreholes in which BHG surveys were made. Locations of two cross sections presented later in the chapter also are shown in Figure 2-2.

¹Branch of Sedimentary Processes, U.S. Geological Survey, Menlo Park, CA.

²Bulk density and total porosity are abbreviated as density and porosity in this Chapter. Porosity is calculated from a combination of in situ density and grain-density data derived from x-ray mineralogic analyses.

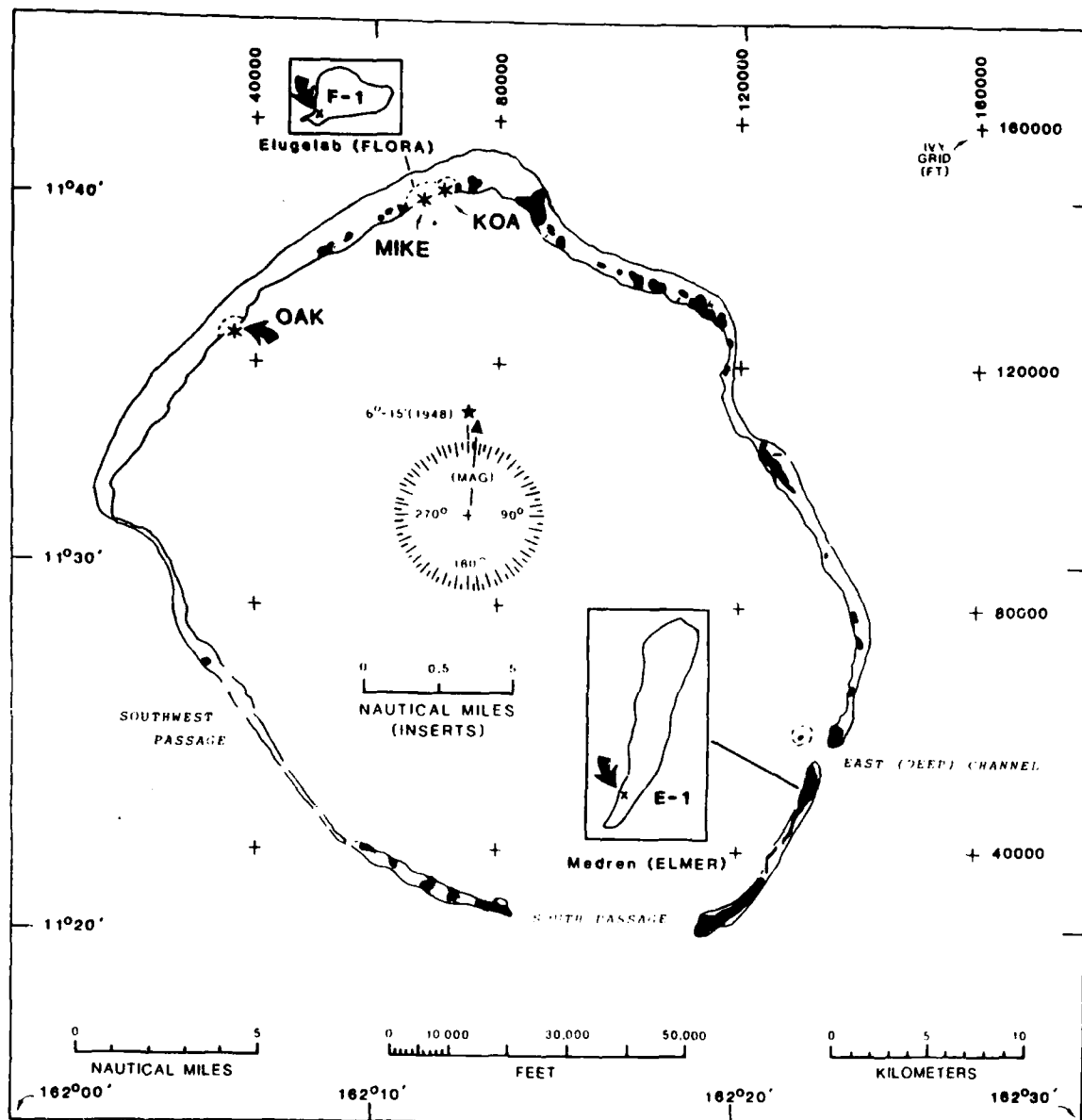


FIGURE 2-1. - Map of Enewetak Atoll showing locations of OAK, KOA, and MIKE craters and Medren (ELMER) Island. Deep boreholes E-1 and F-1 drilled in 1951 and 1952 by the USGS and AEC (Ladd and others, 1953; Ladd and Schlanger, 1960) and referred to in this paper are shown by "X"'s on the inset maps.

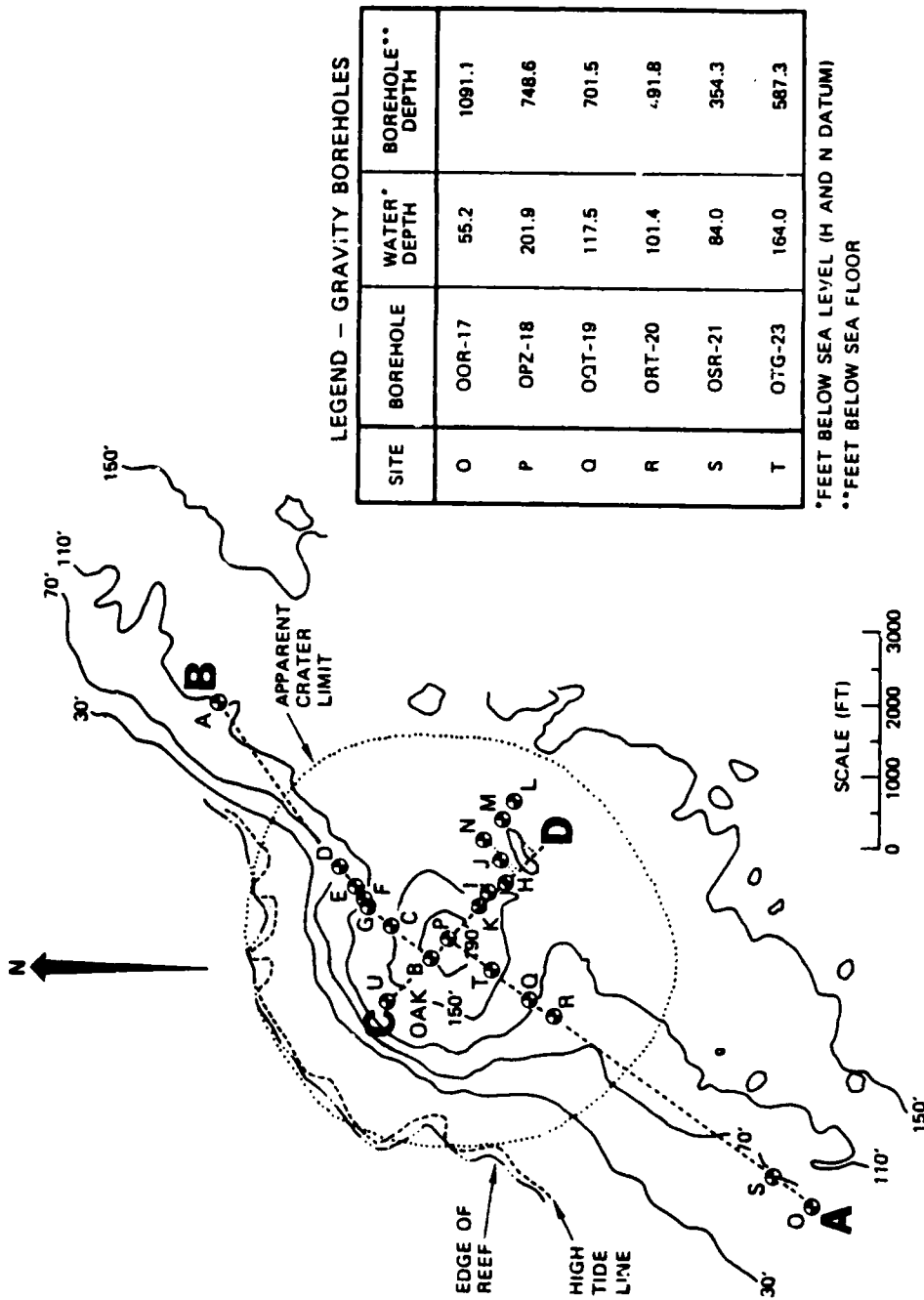


FIGURE 2-2. - Map of OAK crater and vicinity showing locations of PEACE Program boreholes and cross sections AB and CD. Inset shows designation, water depth and total subsea-floor depth of boreholes in which gravity surveys were made.

The efficacy of BHG surveys to determine subtle density differences at OAK crater depends in great part on the precision of the field measurements. This is determined by making repeated W_g/W_z measurements over the same depth interval. Of 98 intervals surveyed in six boreholes, 8 percent were repeated four or more times, 81 percent were repeated three times, 10 percent were repeated two times, and 1 percent were not repeated due to operational constraints. These repeated W_g/W_z measurements indicate that the precision of the surveys is quite high and fully adequate for the purposes of the OAK study (fig. 2-3). Standard deviations of repeated measurements are given in column 3 of Tables 2-2 through 2-7 (located at the end of the current Chapter), are illustrated graphically on BHG density and porosity profiles in subsequent figures, and are explained in Appendix 8-2 of Beyer, Ristvet, and Oberste-Lehn (1986).

BOREHOLE GRAVITY ANALYSIS

The analysis of BHG measurements at OAK crater follows the only logical path available in the absence of independent data such as a detailed surface gravity anomaly map and reliable density data from gamma-gamma and/or core measurements. BHG measurements are corrected for recognizable lateral density variations so that the corrected BHG densities are reasonably accurate measures of the atoll materials within a few tens to a few hundreds of feet of each surveyed borehole. Then, comparisons of density (and porosity) can be made between different boreholes in and near OAK crater.

Corrections can be made rationally for submarine topography (Beyer, Ristvet, and Oberste-Lehn, 1986), for large-scale lateral density charges across the reef margin that are caused by natural facies changes, and for smaller-scale lateral density changes related to cratering processes. A summary of the range of corrections calculated and applied to the BHG surveys is given in Table 2-1. Individual corrections are presented in Tables 2-2 through 2-7, located at the end of the Chapter.

Corrections cannot be made for even smaller-scale lateral density changes on the order of tens to about a hundred feet distant from each borehole, because data needed to model these very small density changes were beyond the scope of the PEACE Program. We will note where these very small-scale effects may be present. Neglect of them does not impair the objectives of the BHG phase of the PEACE Program.

Please note that these corrections are computed as vertical gravity gradients which, when multiplied by $0.25 k$, where k is the Newtonian gravitational constant, become density corrections in g/cm^3 . Lateral density variations that cause a downward positive vertical gravity gradient result in a positive density correction, whereas a downward negative gradient causes a negative density correction (see Appendix 8-2 of Beyer, Ristvet, and Oberste-Lehn, 1986).

1All tables are located at the end of the Chapter.

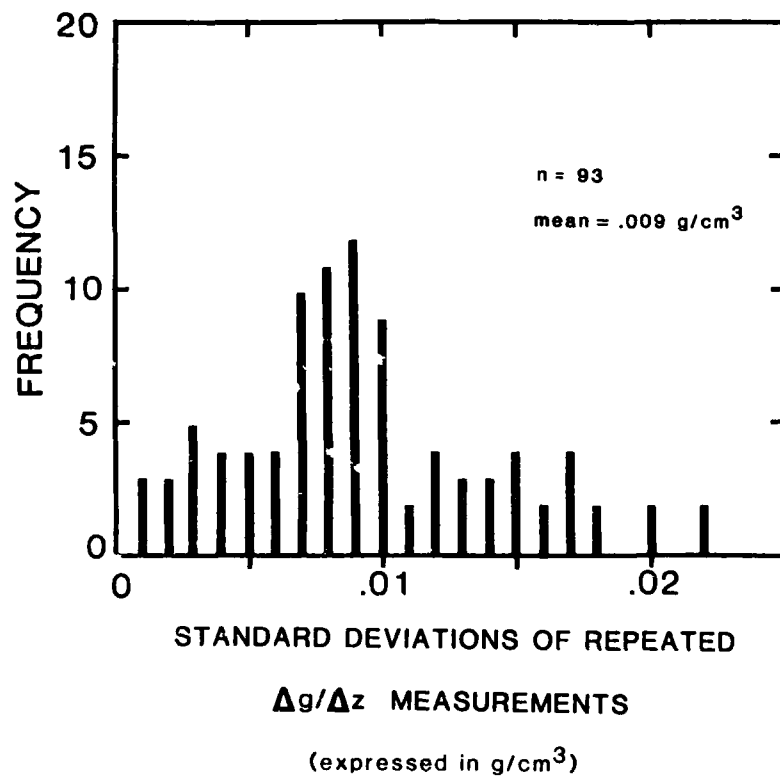


FIGURE 2-3. - Distribution of 93 sets of repeated $\Delta g/\Delta z$ measurements during borehole gravity surveys in OAK boreholes, expressed in g/cm³. Mean is .009 g/cm³ and is a measure of the high quality of the borehole gravity surveys (Beyer, 1968; Black and Herring, 1983).

LARGE-SCALE LATERAL DENSITY CHANGES ACROSS REEF MARGIN

A substantial body of work by many investigators at modern Pacific atolls has shown that forereef and reef core facies generally are more highly cemented (and therefore denser) than lagoon facies, and that atoll reefs generally prograde seaward (e.g., Buigues, 1985). These relationships are believed to be present along the northwest margin of Enewetak Atoll according to B. L. Ristvet, who provided the author with a sketch of the probable distribution of facies and densities across the reef margin at OAK crater. Other PEACE Program studies (Folger, 1986a) and earlier work at Enewetak, especially deep boreholes E-1 and F-1 and the XEN series of boreholes on Engebí Island (Ladd and others, 1953; Ladd and Schlanger, 1960; Couch and others, 1975), led to this assessment of atoll margin structure. Densities provided by Ristvet were modified slightly using the BHG densities from the E-1 borehole on Medren Island (see Appendix 2-1).

Deeper density contrasts (e.g., between the volcanic core and overlying carbonate rocks of the atoll) and possible incomplete isostatic compensation of the atoll also can affect the vertical gravity gradients (and BHG densities). Corrections for these possible effects are almost certainly negligibly small and, if determined, would cause only a very small, constant dc-type shift of all density data. The absence of even a rudimentary surface gravity anomaly map and more detailed deep borehole data prevent any attempt to examine these effects.

The two-dimensional density model prepared for the atoll margin at OAK crater is shown in Figure 2-4. Vertical gravity gradient corrections were calculated for the two-dimensional model with a well-established algorithm (Talwani and others, 1959) that has been modified for borehole gravity applications. These corrections are given in column 5 of Tables 2-2 to 2-7 and probably are unnecessary but their magnitudes needed to be evaluated.

CORRECTION FOR LATERAL DENSITY CHANGES DUE TO CRATERING PROCESSES

Lateral density variations due to cratering processes also can affect the BHG densities and, therefore, were evaluated. The model used to correct for these crater-related lateral density changes was developed along the southwest transect from OPZ-18 to OOR-17 by using BHG densities (corrected for submarine topography and large-scale density changes across the atoll margin) and a correlation cross section prepared by D. Oberste-Lehn and modified by B. R. Wardlaw (fig. 2-5; correlation cross section CD, fig. 2-6, also was prepared by Oberste-Lehn and Wardlaw). The density model is shown in Figure 2-7 and was assumed to have circular symmetry about OPZ-18. Trial gravity calculations taking into account the departure of OAK crater from circular symmetry about OPZ-18 (based only on correlation cross sections) showed that the assumption of circular symmetry is valid. The size of the corrections due to crater-related lateral density changes is so small that the question of true three-dimensionality versus circular symmetry about OPZ-18 is academic. The question of the actual crater density structure along cross section CD remains. A very careful sea floor gravity survey or more BHG drillholes and surveys would shed light on this question.

Generalized 2-D Density Model through OAK Crater

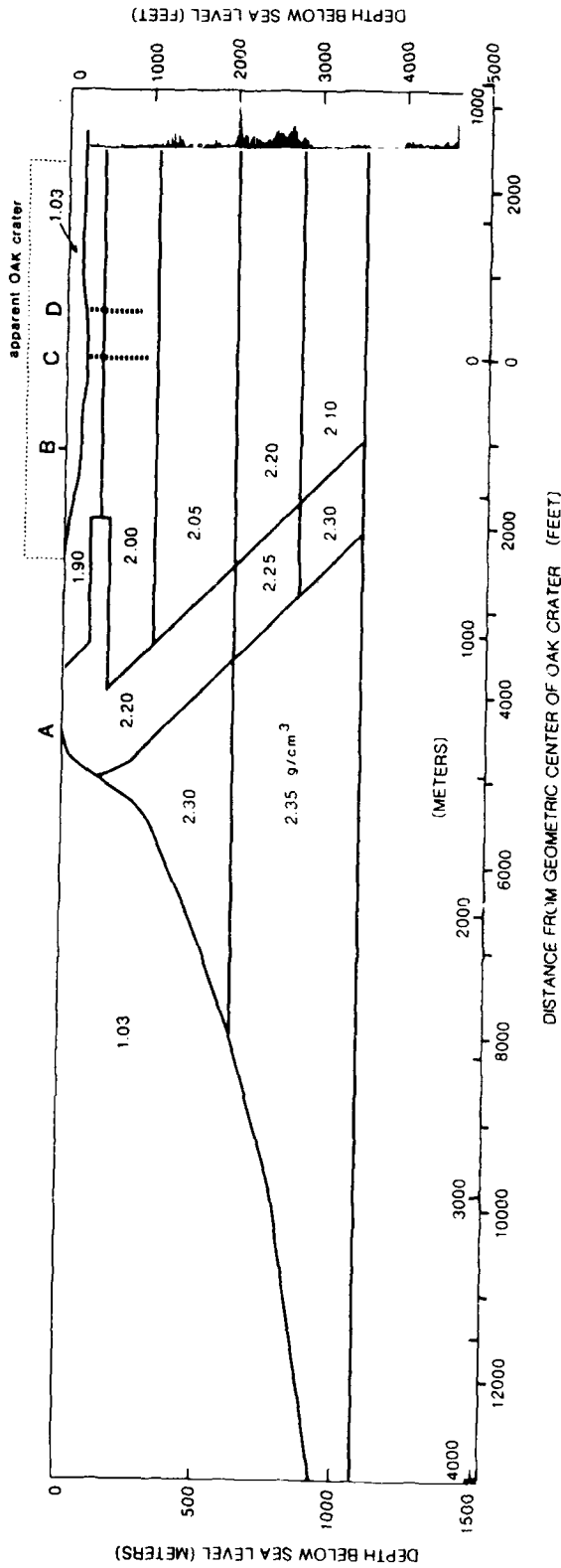


FIGURE 2-4. - Two-dimensional density model (assumed to extend as shown to great distances in directions perpendicular to page) of natural atoll facies changes in section orthogonal to reef. Labels include model element densities in g/cm³, outer reef edge ("A"), inner reef edge prior to OAK event ("B"), position of boreholes OPZ-18, OTG-23, OQT-19, and ORF-20 ("C") and position of boreholes OSR-21 and OOR-17 ("D"). Drilling time profile (near right of depth scale) is for borehole F-1 (see fig. 2-1 for location). Remember that submarine topography correction replaced seawater (1.03 g/cm³) with 1.90 g/cm³ (Beyer, Ristvet, and Oberste-Lehn, 1986). No vertical exaggeration.

BLANK PAGE

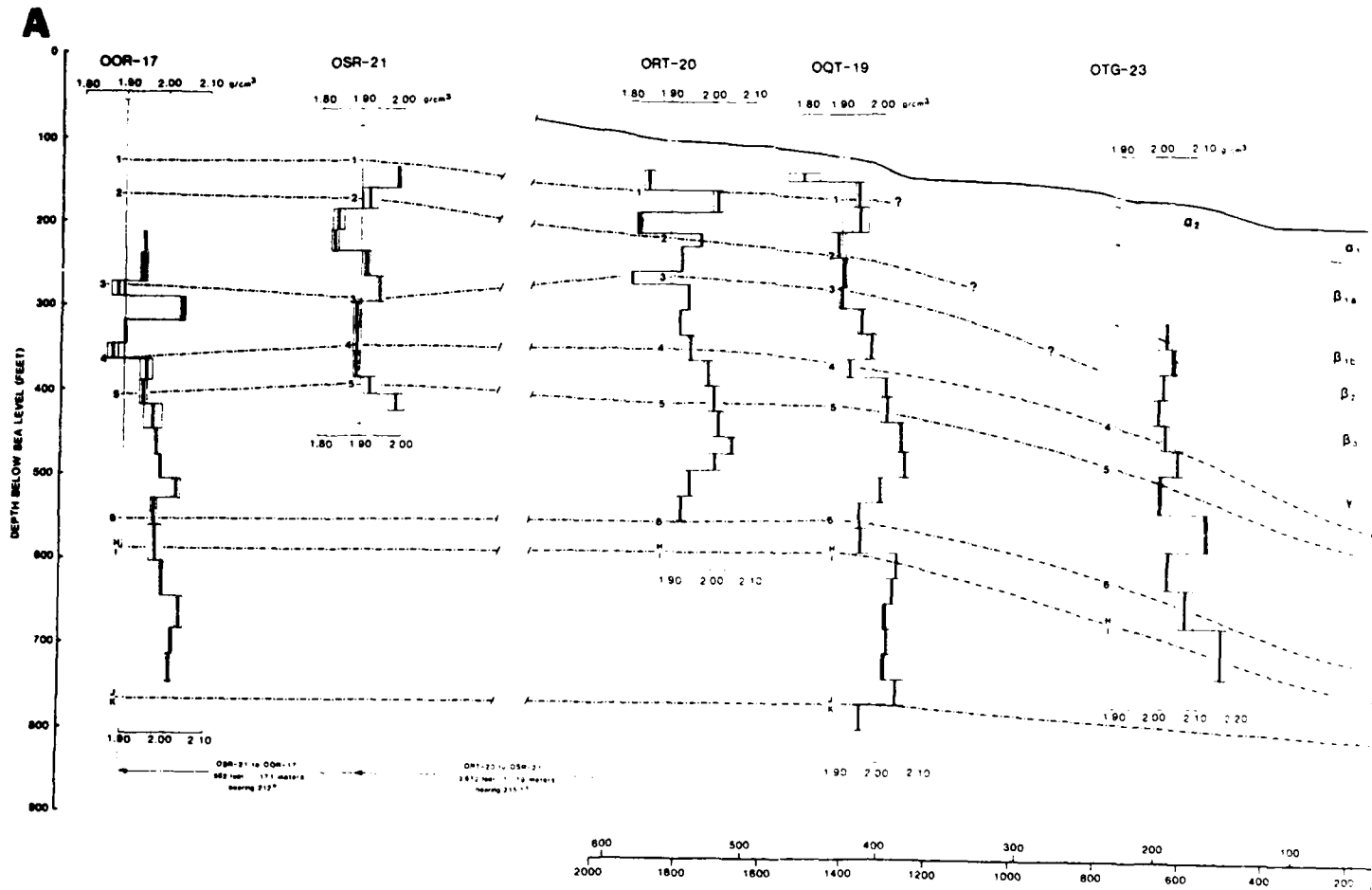
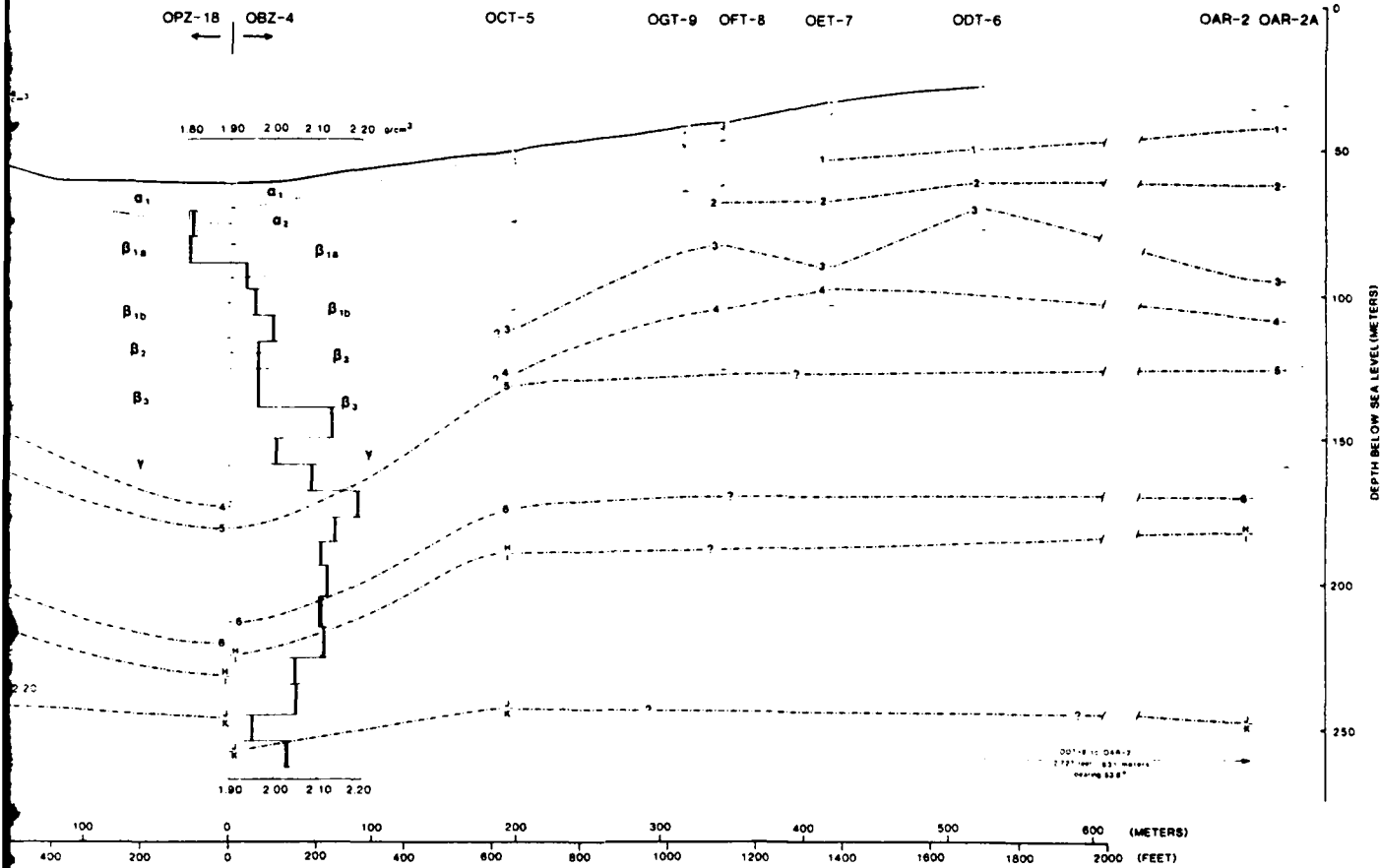


FIGURE 2-5. - Cross section AB extends from south-southwest to north-northeast through markers in OBZ-4 extending to the right and markers in OPZ-18 extending to the left zone boundaries H/I and J/K, and crater geologic zones α_1 through γ (see Wardlaw a by D. Oberste-Lehn and modified by B. R. Wardlaw. BHG density profiles are super scale labels "1.90" correspond to the positions of the surveyed boreholes in the c

B

ast through OAK crater (fig. 2-2). Section is broken at center with geologic to the left. Correlation lines tie disconformities 1 through 6, biostratigraphic Wardlaw and Henry, 1986a,b). This section and that of Figure 2-6 were prepared are superimposed on the section for the six surveyed boreholes. The density is in the cross section. Vertical exaggeration from ORT-20 to ODT-6 is 2X.

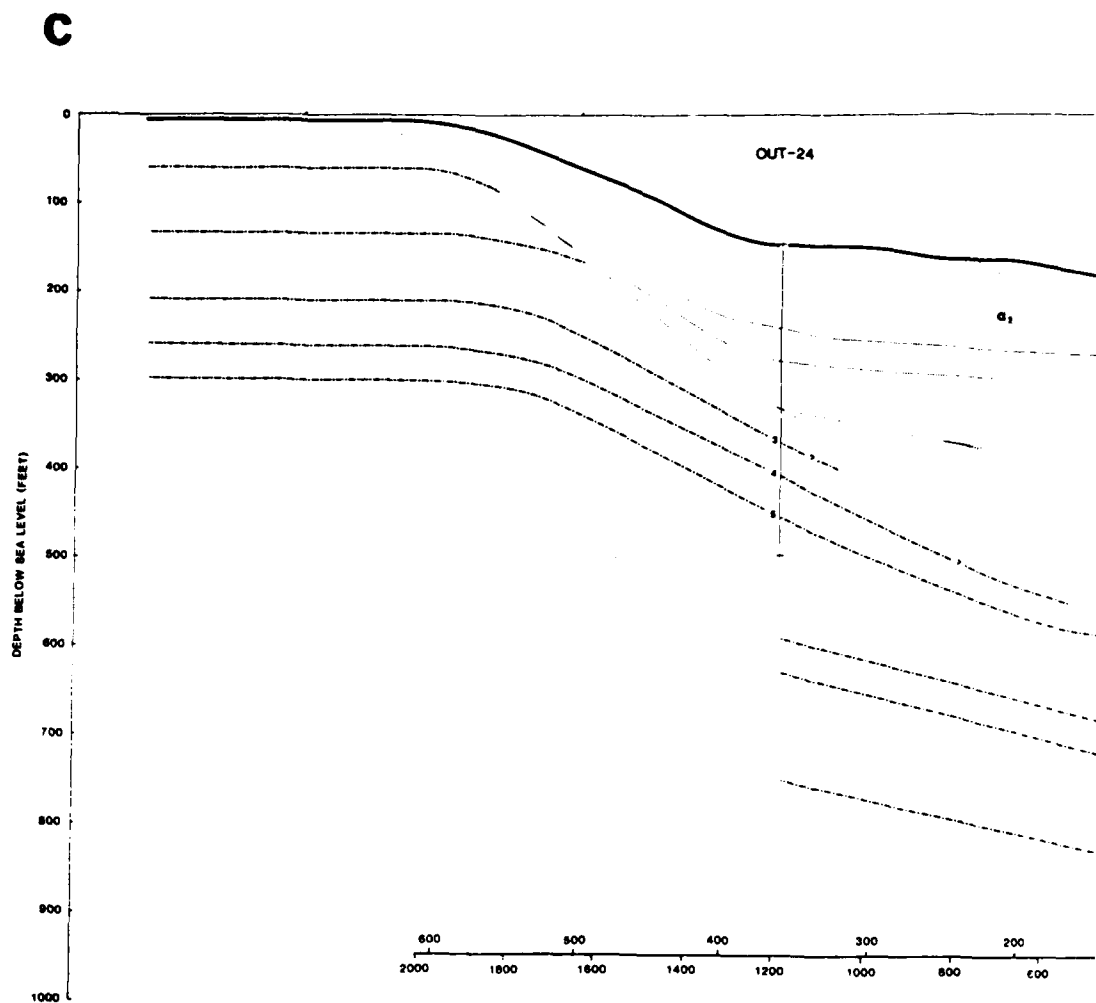
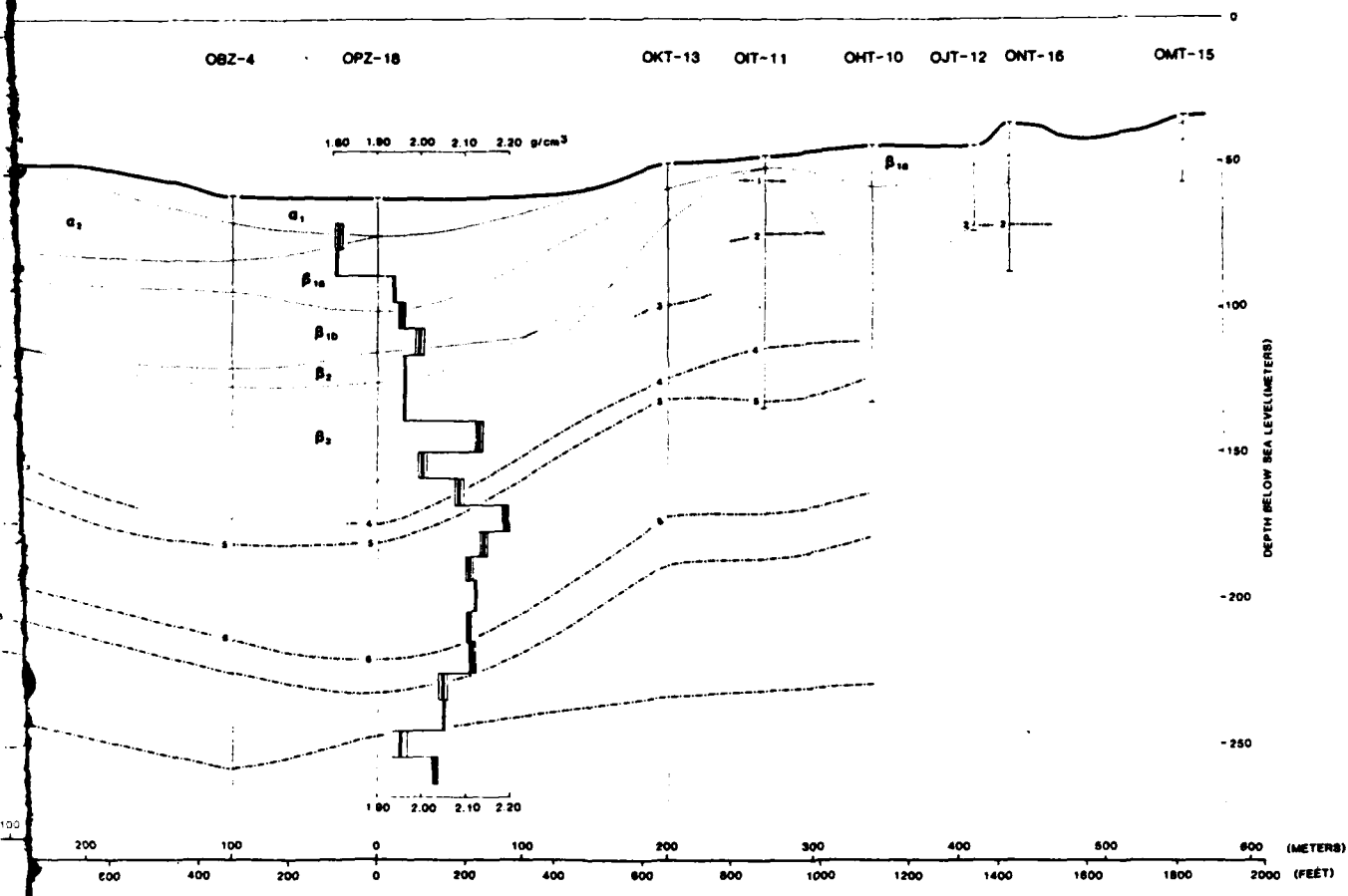


FIGURE 2-6. - Cross section CD extends from west-northwest to east-south
 Figure 2-5. Only the BHG density profile of OP2-18 lies in this sec
 in Figure 2-2. Vertical exaggeration is 2X.

D



East-southeast through OAK crater (fig. 2-2). Data are identical to those described for this section. Boreholes OJT-12, ONT-16, and OMT-15 are projected into section as shown

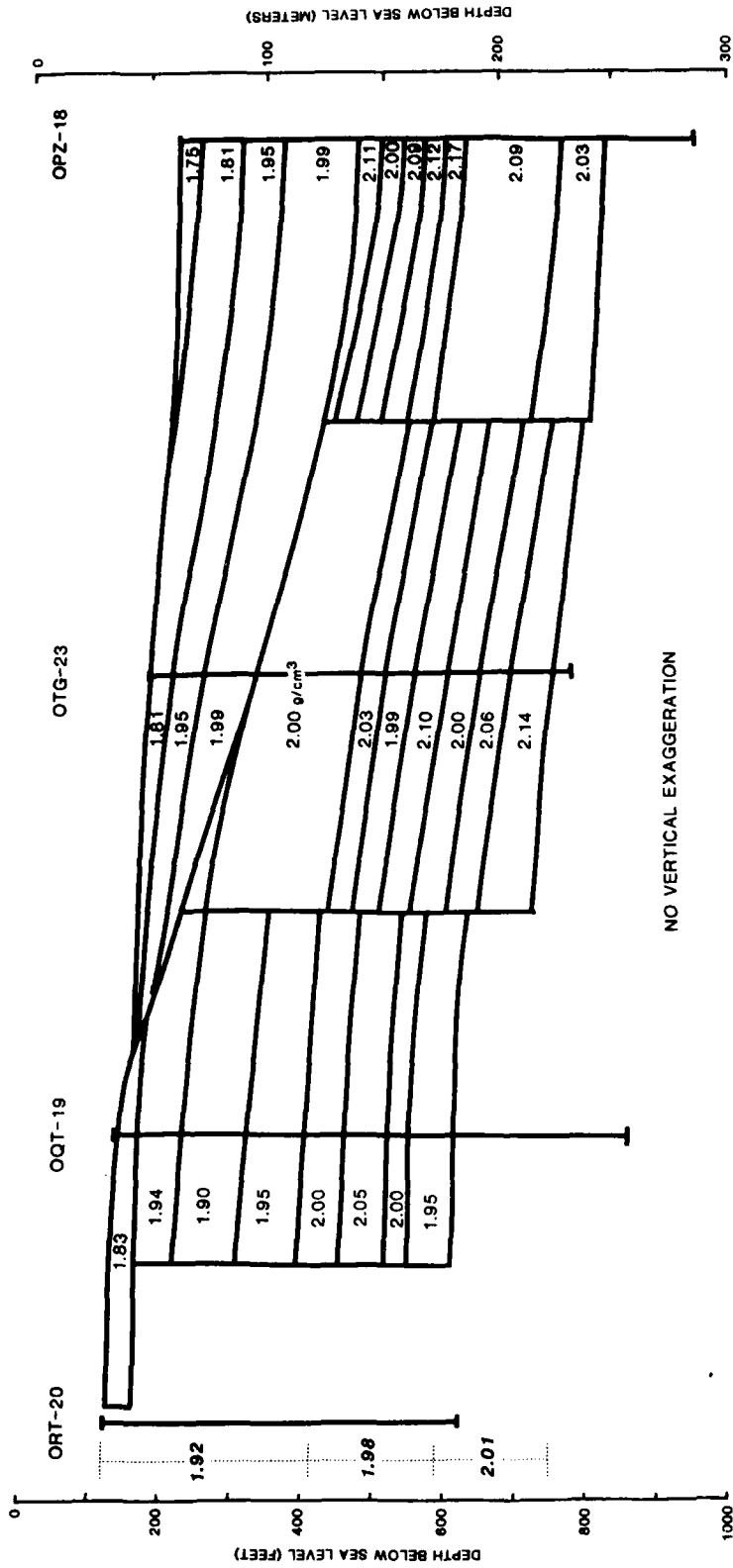


FIGURE 2-7. - Cross section along south-southwestern transect for lateral density variations caused by cratering processes. Density model is assumed to have circular symmetry about borehole OPZ-18. Densities of surrounding atoll materials as determined from BHG densities from reference boreholes OOR-17 and OSR-21 are shown next to left depth scale.

In order to perform density calculations using the model shown in Figure 2-7, the assigned densities must be recast as density contrasts relative to the surrounding medium. The density of the surrounding atoll material was determined from the BHG density profiles of reference boreholes OOR-17 and OSR-21 which were assumed to be unaltered by crater-related processes. The density model for the surrounding medium is summarized in Table 2-8, and values are shown along the left side of Figure 2-7. These reference density values were subtracted from laterally juxtaposed crater density model elements to arrive at a density contrast model.

Corrections to the BHG densities in OPZ-18, OTG-23, OQT-19, and ORT-20 were calculated from the density contrast model using a well-established algorithm for three-dimensional density elements (Plouff, 1976) modified for borehole gravity application. These corrections proved to be very small (column 6, tables 2-2 through 2-7), which could be predicted from the gentle dips of the density element boundaries as shown in Figure 2-7.

CORRECTED BOREHOLE GRAVITY DENSITY AND POROSITY AND COMPARISON WITH GAMMA-GAMMA AND NEUTRON DATA

Tabular and graphical summaries of BHG density and porosity with error estimates, grain densities with error estimates and interval-averaged density and porosity from gamma-gamma and neutron logs are presented in Tables 2-2 through 2-7 and Figures 2-8 through 2-13. Open-hole well log curves also are shown in Figures 2-8 through 2-12. Interval-averaged neutron porosity is not graphically displayed in Figures 2-8 through 2-12 because of a systematic error that has made all values too large. Interval grain density profiles are derived from individual grain density values, examination of open-hole well logs, and descriptions of cores and samples, sedimentary packages, and boreholes (Henry and Wardlaw, 1986; Wardlaw and Henry, 1986a; Holloway and Young, 1986). Errors in interval grain density are only estimates that may be increased or decreased with further information about the mineralogy of individual intervals, particularly intervals with both aragonite and calcite.

A number of questions about the reliability of the gamma-gamma density and neutron porosity logs run in OAK boreholes were raised during the analysis of the borehole data. Corrected BHG density and porosity provide a reliable standard against which gamma-gamma and neutron logs can be evaluated. In OAK boreholes, the differences between BHG density and interval-averaged gamma-gamma density decrease with increasing depth below the sea floor (fig. 2-14). This result agrees with the well-documented body of literature from the petroleum industry, which indicates that shallow-penetration radiation well logs, such as the gamma-gamma and neutron logs run in OAK boreholes, perform poorly in loosely consolidated, highly permeable sediments where formation damage caused by rotary drilling is almost always substantial.

Relatively good correspondence between BHG and gamma-gamma data is obtained for intervals deeper than 600 ft below sea level in OOR-17 and OQT-19, and deeper than 500 ft below sea level in ORT-20 where drill-induced borehole and formation damage is less because sediments are somewhat more consolidated than at shallower depths (figs. 2-8, 2-10, and 2-11). More specifically, Figure 2-14 suggests that gamma-gamma density departs

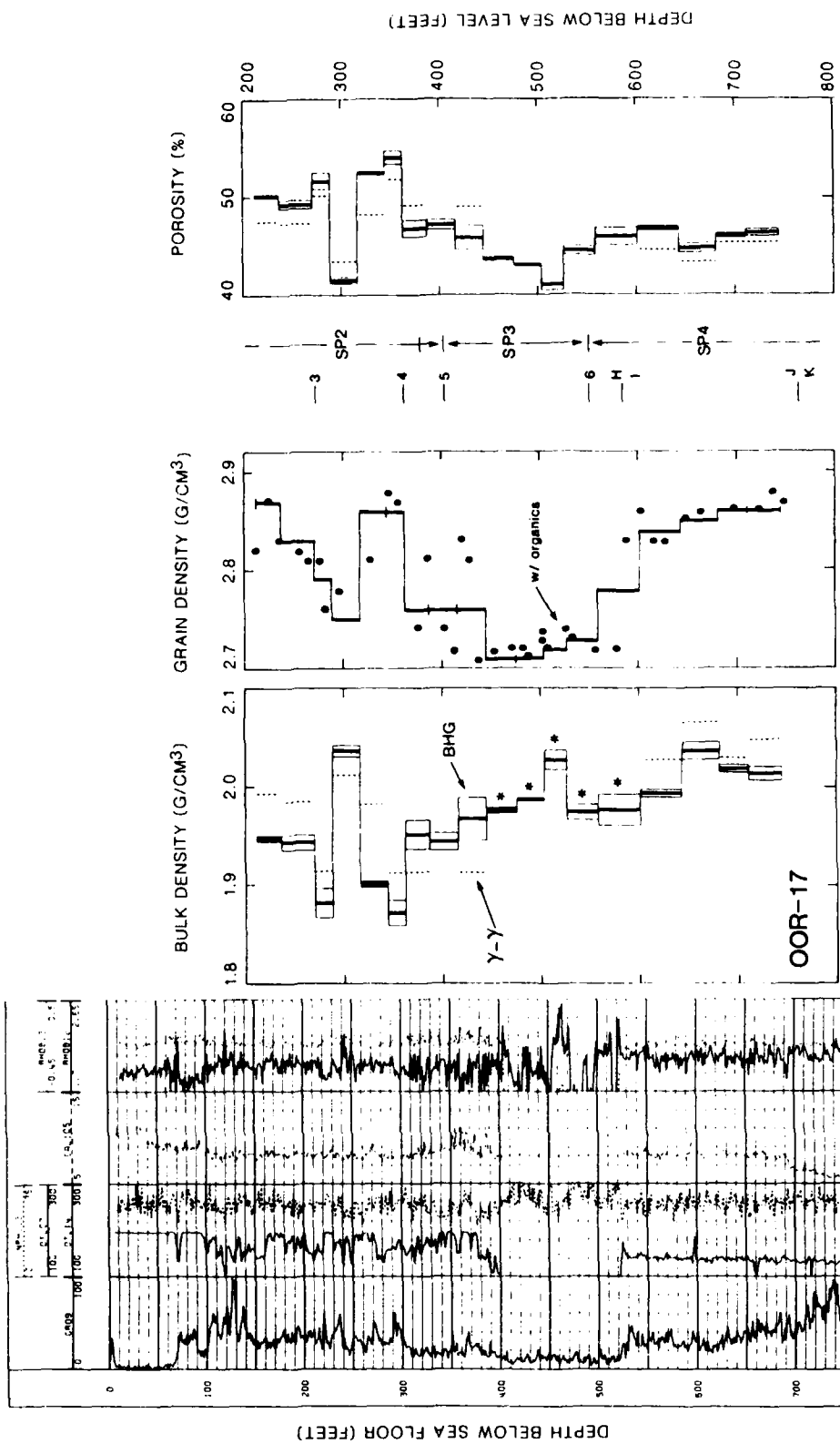


FIGURE 2-8. - Open-hole well logs, BHG and gamma-gamma density, core and interval grain density, disconformities and facies boundaries, sedimentary packages, and BHG and gamma-gamma porosity for borehole OOR-17 (left to right). Well logs from left to right are gamma-ray, multi-channel sonic, neutron porosity, caliper, gamma-gamma density, and gamma-gamma density correction. Asterisks indicate intervals where gamma-gamma log not available due to drillpipe. Interval averages of gamma-gamma density and porosity are plotted where values are outside error regions of BHG density and porosity.

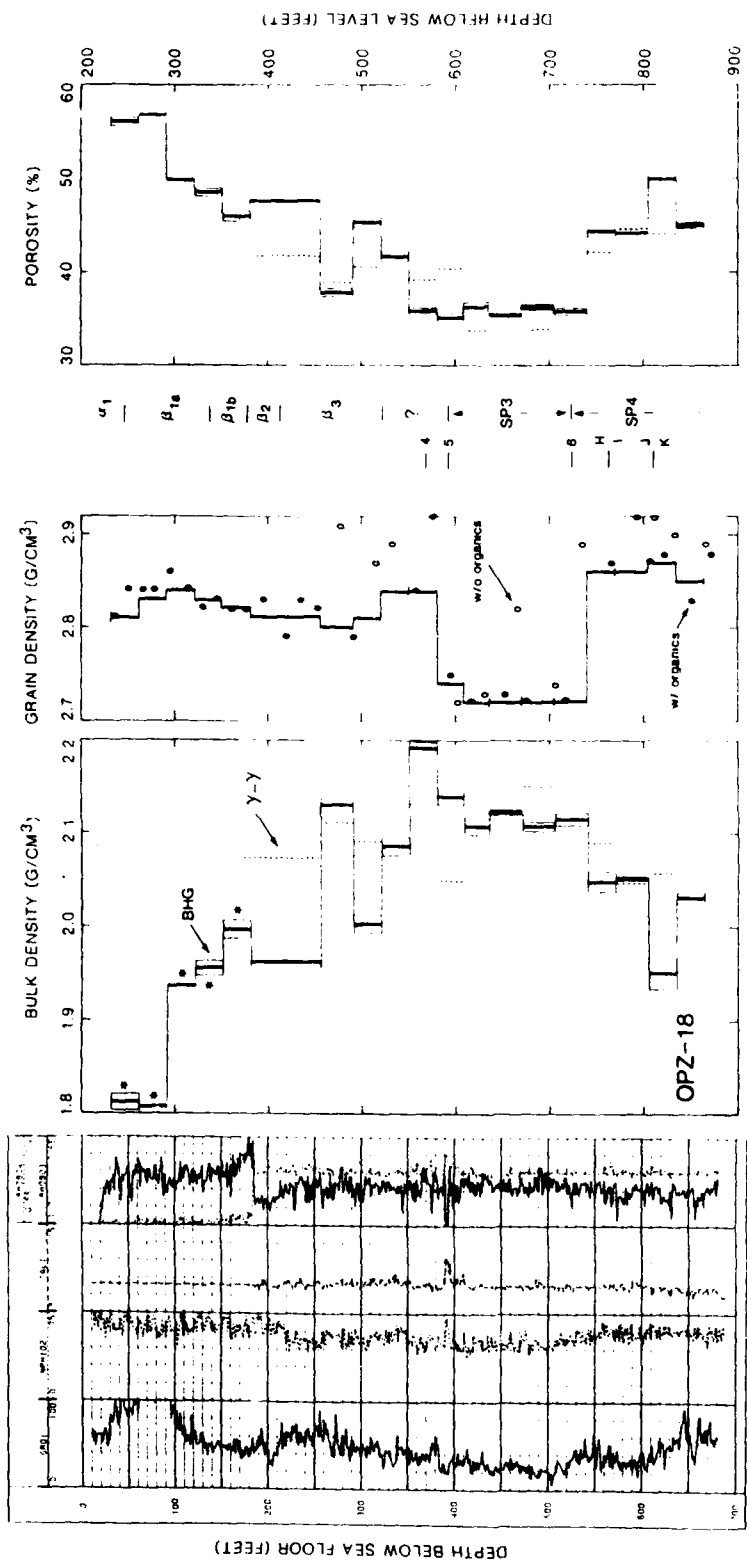


FIGURE 2-9. - Open-hole well logs, BHG and gamma-gamma density, core and interval grain density, disconformities and facies boundaries, sedimentary packages, and BHG and gamma-gamma porosity for borehole OPZ-18 (left to right). Well logs from left to right are gamma-ray, neutron porosity, caliper, gamma-gamma density, and gamma-gamma density correction. Asterisks indicate intervals where gamma-gamma log not available due to casing. Interval averages of gamma-gamma density and porosity are plotted where values are outside error regions of BHG density and porosity.

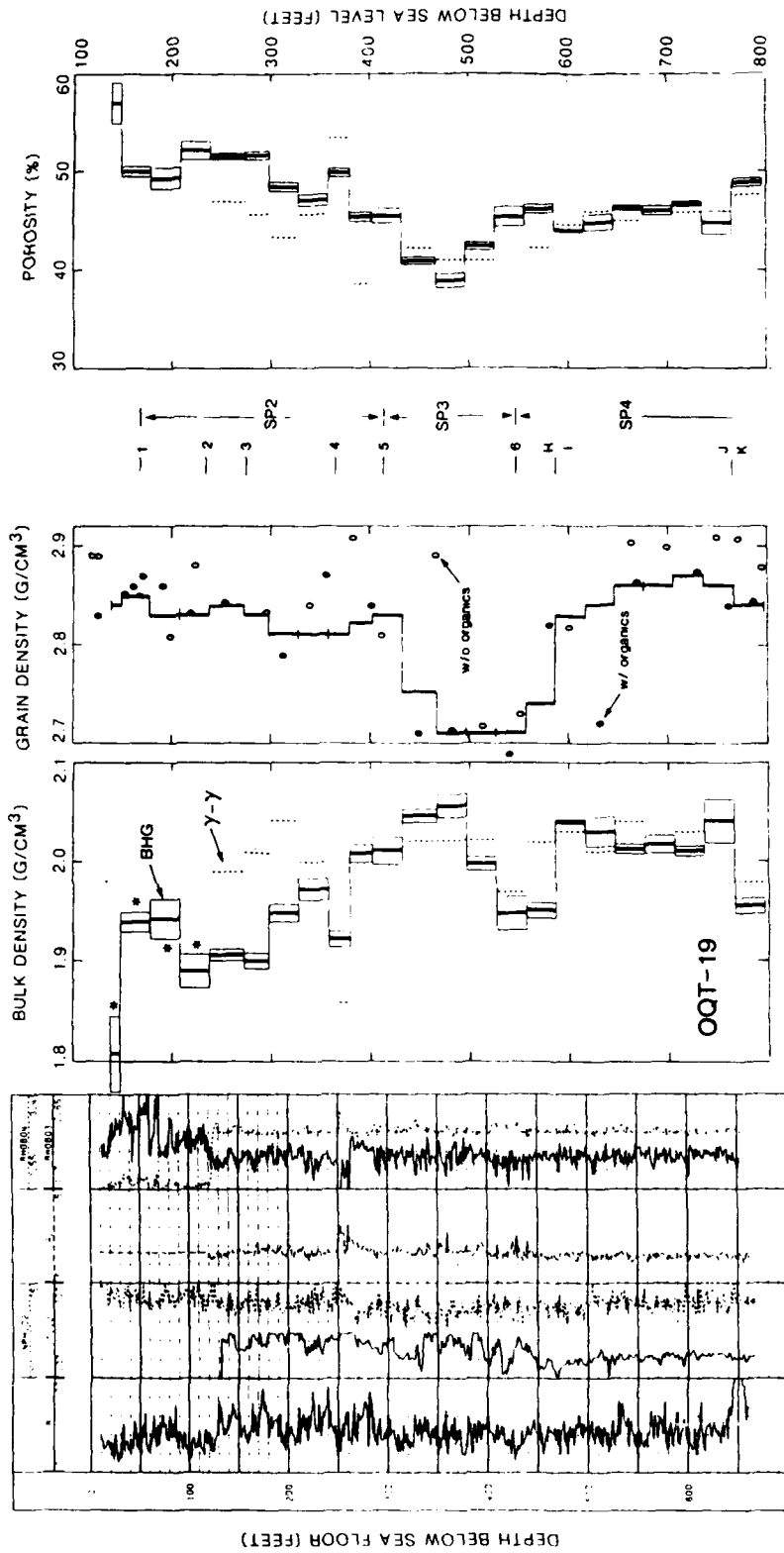


FIGURE 2-10. - Open-hole well logs, BHG and gamma-gamma density, core and interval grain density, disconformities and facies boundaries, sedimentary packages, and BHG and gamma-gamma porosity for borehole OQT-19 (left to right). Well logs from left to right are gamma ray, multi-channel sonic, neutron porosity, caliper, gamma-gamma density, and gamma-gamma density correction. Asterisks indicate intervals where gamma-gamma log not available due to casing. Interval averages of gamma-gamma density and porosity are plotted where values are outside error regions of BHG density and porosity.

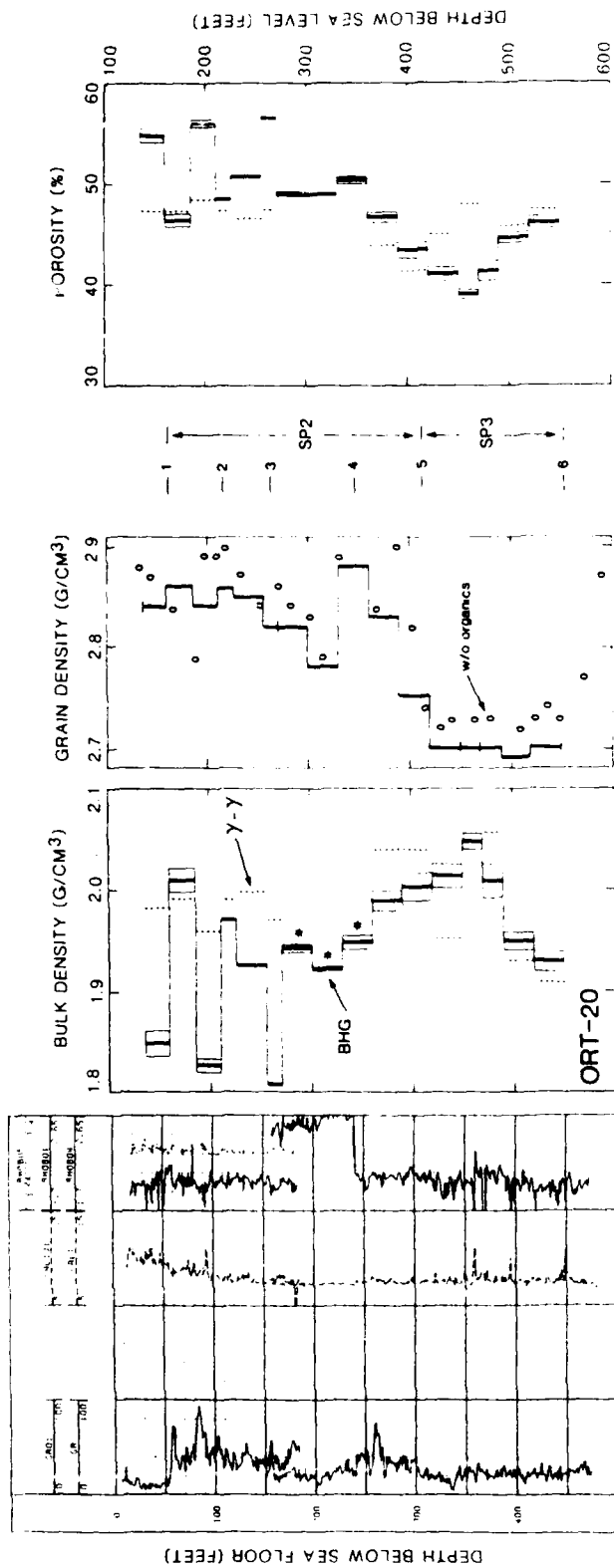


FIGURE 2-11. - Open-hole well logs, BHG and gamma-gamma density, core and interval grain density, discontinuities and facies boundaries, sedimentary packages, and BHG and gamma-gamma porosity for borehole ORT-20 (left to right). Well logs from left to right are gamma ray, caliper, gamma-gamma density, and gamma-gamma density correction (partial). Asterisks indicate intervals where gamma-gamma log not available due to casing. Interval averages of gamma-gamma density and porosity are plotted where values are outside error regions of BHG density and porosity.

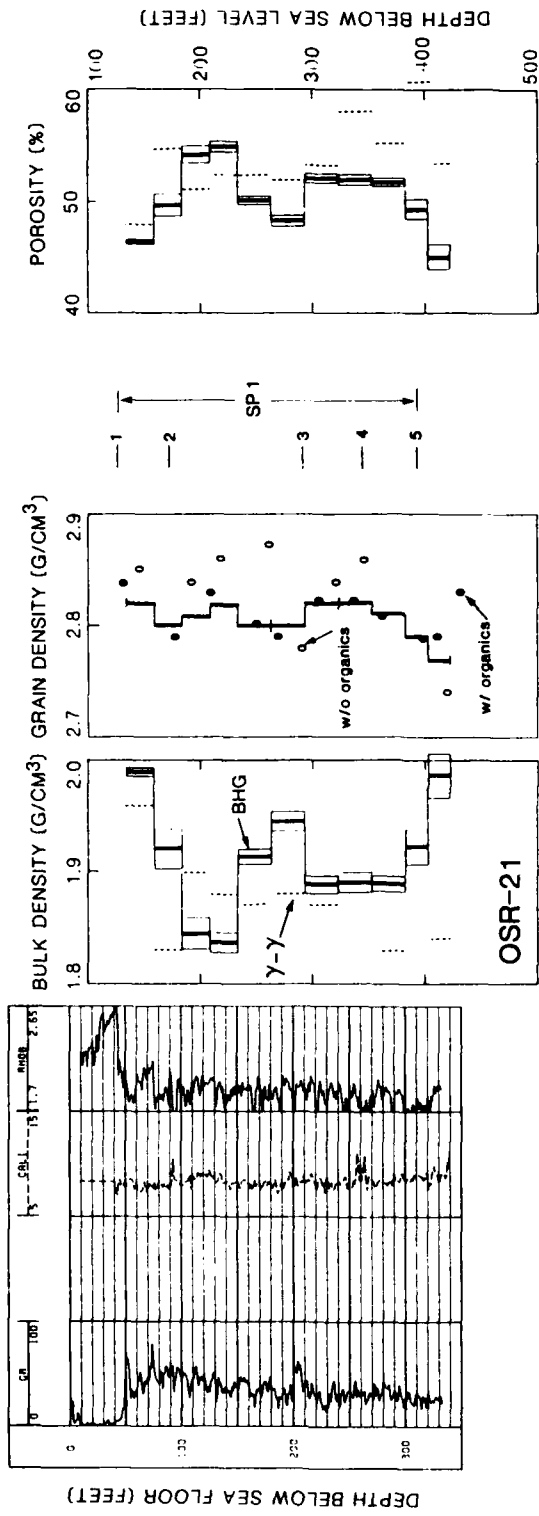


FIGURE 2-12. - Open-hole well logs, BHG and gamma-gamma density, core and interval grain density, disconformities and facies boundaries, sedimentary packages, and BHG and gamma-gamma porosity for borehole OSR-21 (left to right). Well logs from left to right are gamma ray, caliper, and gamma-gamma density. Interval averages of gamma-gamma density are plotted where values are outside error regions of BHG density and porosity.

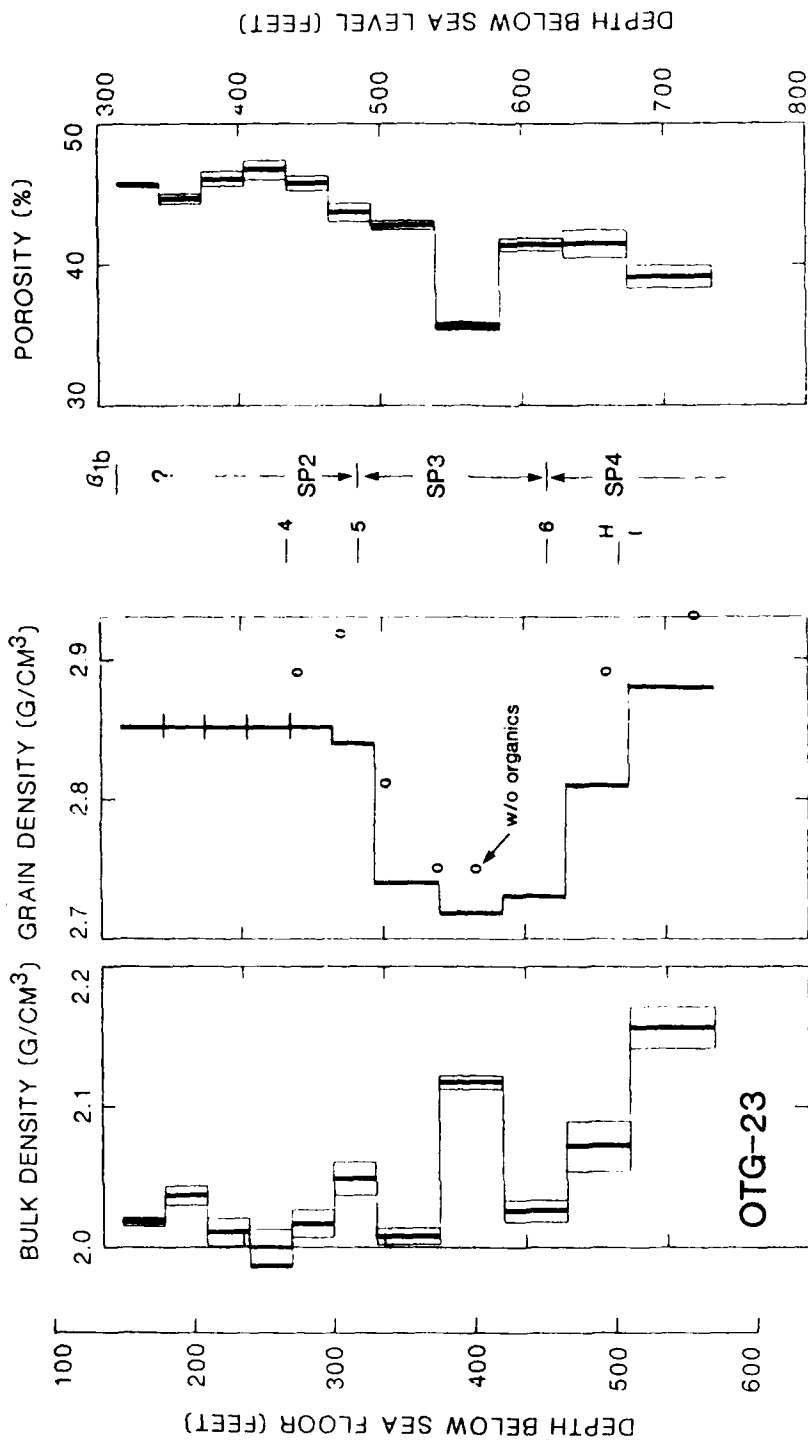


FIGURE 2-13. - BHG density, core and interval grain density, discontinuities and facies boundaries, sedimentary packages, and BHG porosity for borehole OTG-23 (left to right). No open-hole well logs were run.

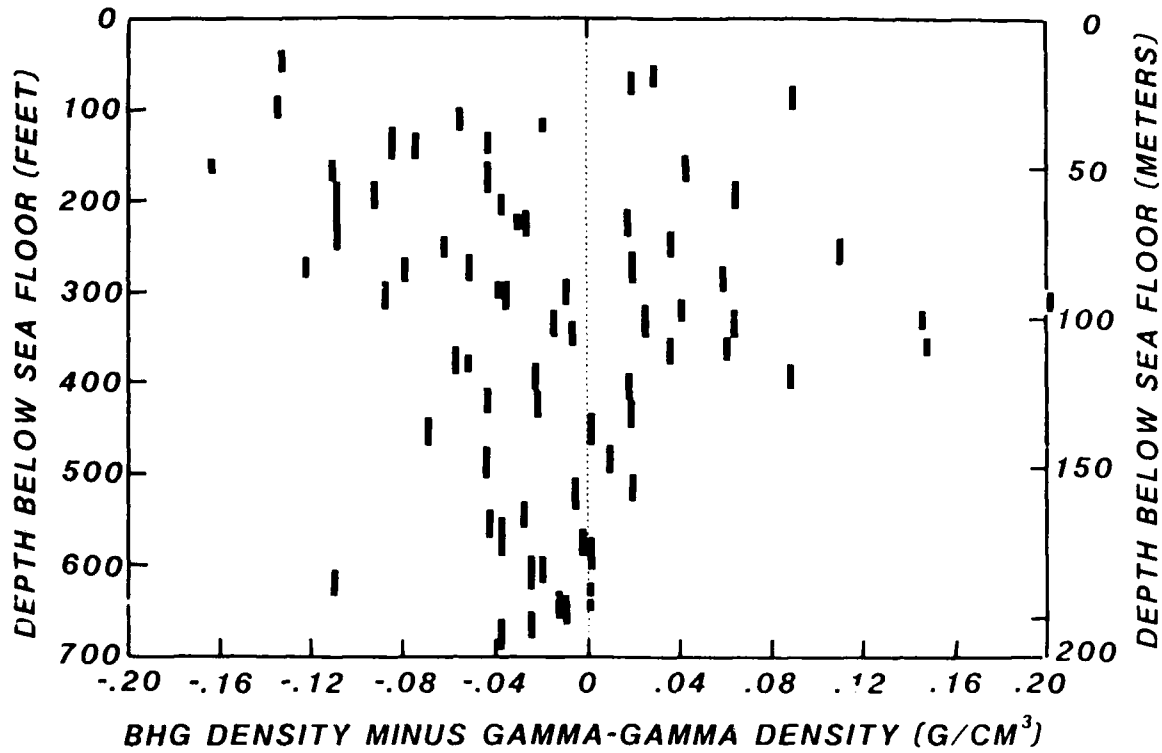


FIGURE 2-14. - Differences between BHG density and interval averages of gamma-gamma density versus depth below sea floor (bsf). Seventy differences are from boreholes OOR-17, OPZ-18, OQT-19, ORT-20 and OSR-21.

unsystematically from BHG density by as much as +10 percent at depths shallower than about 400 ft below the sea floor. At depths greater than about 500 ft below sea level, gamma-gamma density appears to vary from BHG density by about 2 percent or less.

Cross plots between BHG porosity and neutron porosity, gamma-gamma porosity and neutron porosity, and gamma-gamma porosity versus BHG porosity confirm that the neutron data are not adequate (fig. 2-15). These cross plots, along with Figure 2-14, emphasize the need for caution in the use of the gamma-gamma logs for quantitative density or porosity evaluation. Furthermore, bulk density and total porosity data derived from core measurements should be viewed skeptically if they differ significantly and systematically from corresponding BHG density and porosity.

NATURAL DENSITY AND POROSITY VARIATIONS OF ATOLL MATERIALS

Natural variations of density and porosity of atoll materials represent the background "noise" through which density and porosity changes caused by cratering phenomena must be determined. At the volume scale of core samples of several cubic feet, a broad range of values of densities and porosities from virtual sea-water-filled voids to dense crystalline carbonate is expected. At the volume scale of BHG studies (hundreds of thousands of cubic feet--an appropriate scale for studies of large craters), one expects the range of values of natural densities and porosities to narrow considerably because of the averaging effect. This is confirmed by the BHG surveys at OAK crater where the range of densities in reference boreholes OOR-17 and OSR-21 is not great.

At shallow depths in OOR-17, OSR-21, ORT-20 and OQT-19, density fluctuations are substantial but can be averaged to give nearly identical values (fig. 2-16). Based on the similarity of averaged BHG densities for OOR-17, OSR-21, ORT-20, and parts of OQT-19, the "noise" problem connected with natural density and porosity variations is believed to be small. However, close correspondence between individual BHG intervals from borehole to borehole can not be expected because of natural variations of density in porosity.

A general systematic relationship exists between BHG porosity and interval grain density based on data from reference boreholes OOR-17 and OSR-21 (fig. 2-17). Back reef sediments dominated by aragonite have higher porosities than sediments dominated by calcite. Effects on porosity caused by mechanical compaction and grain-size distribution and uncertainty about values of interval grain density may account for some or all of the scatter of points in Figure 2-17. Nevertheless, the rate of change of porosity with respect to aragonite content, as estimated by the dashed line, is almost identical to that found by Schmoker and Hester (1986) in a study of the late Pleistocene Miami Limestone. However, porosity values of the Miami Limestone are lower than Enewetak back-reef sediments by about 15 percent for equivalent aragonite content, emphasizing the different geologic settings of these two locations.

If bulk density is held constant, the mineral volume increase accompanying simple transformation of aragonite to calcite causes porosity to decrease by about 5 percent (line A in fig. 2-17). It is clear from Figure

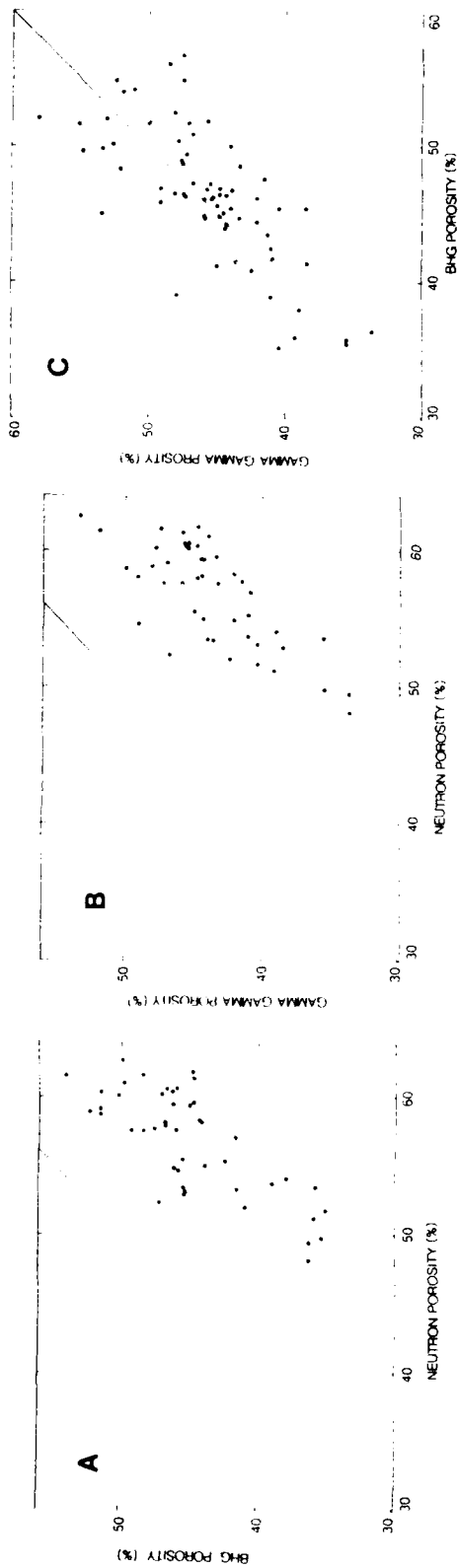


FIGURE 2-15. - Cross plot of BHG porosity and neutron porosity averaged over equivalent depth intervals
 (A). Cross plot of gamma-gamma porosity and neutron porosity, each averaged over BHG depth intervals
 (B). Cross plot of BHG porosity and gamma-gamma porosity averaged over equivalent depth intervals
 (C). Data are from columns 10, 13 and 14, Tables 2-2 through 2-7.

BLANK PAGE

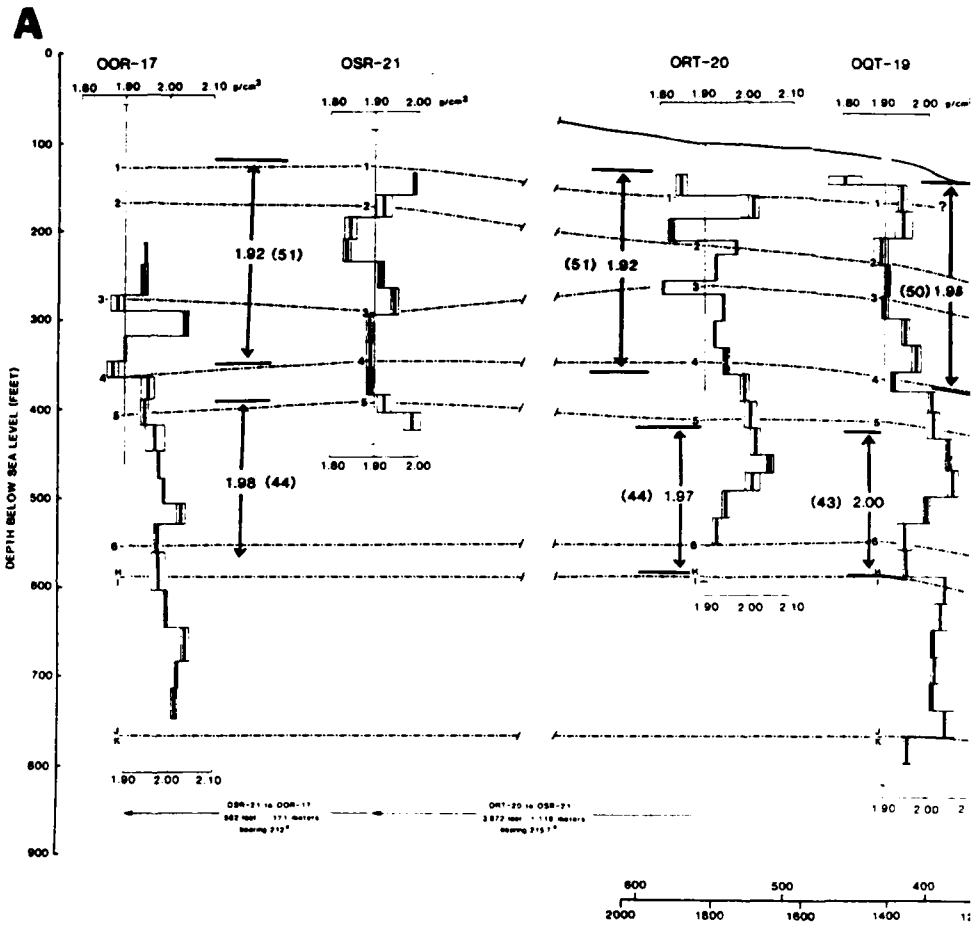
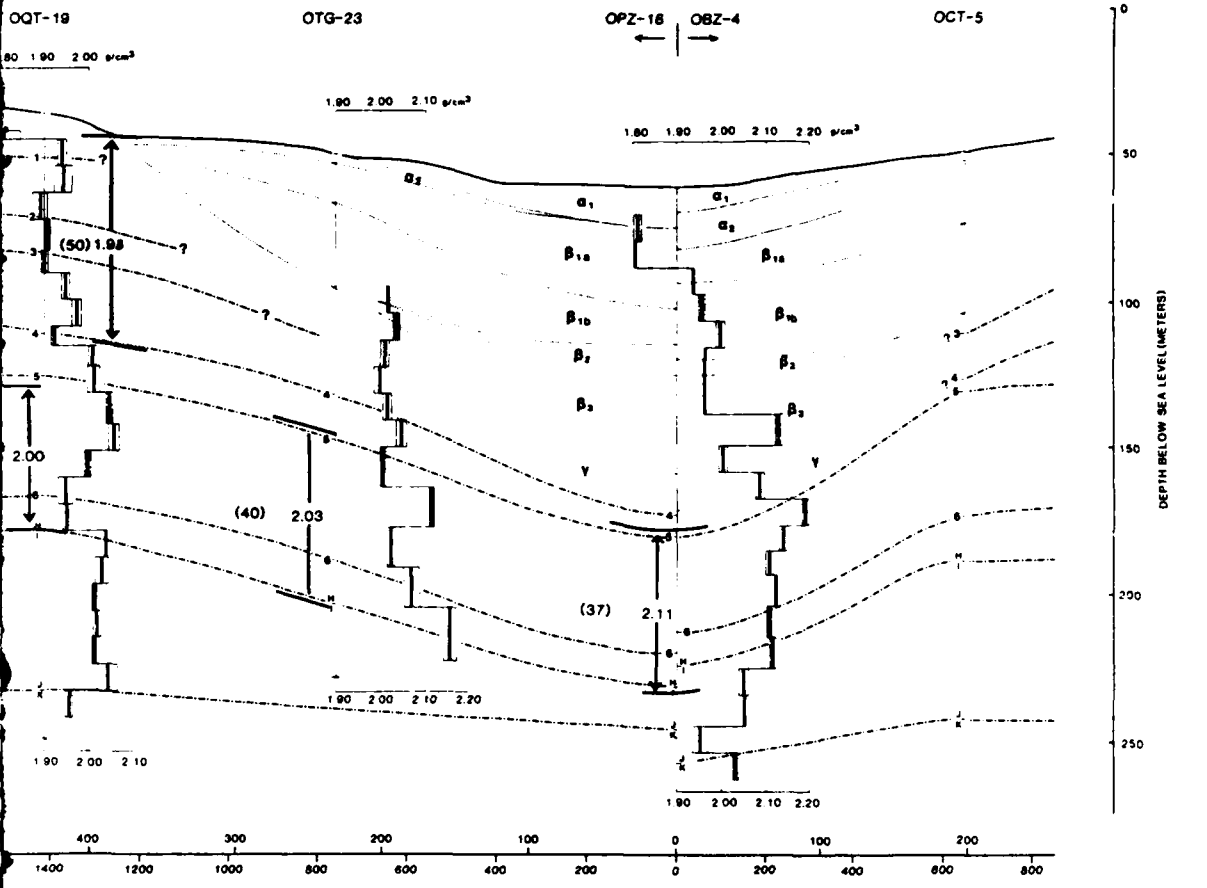


FIGURE 2-16. - Averages of BHG density and porosity for



Porosity for selected large interval. Porosities are in parentheses.

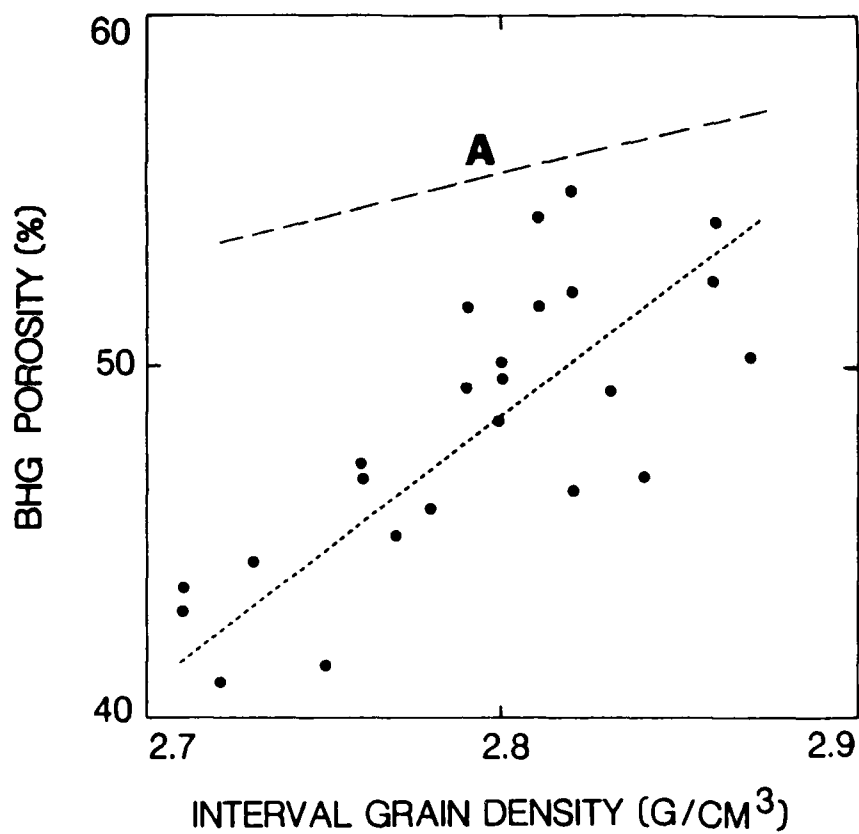


FIGURE 2-17. - Interval grain density versus BHG porosity. Data from reference boreholes OOR-17 and OSR-21. Line A shows decrease in porosity (due only to mineral volume increase) during transformation of an aragonite-bearing sediment to calcite-bearing sediment, assuming 100% aragonite sediment has porosity of 58.5%, and bulk-density is held constant.

2-17 that calcite solution and recrystallization, deposition of externally derived carbonate cement, some compaction, and other processes during well-documented cycles of atoll emergence and submergence (Ristvet and others, 1974; Tracey and Ladd, 1974) also have contributed to porosity loss in the back-reef sediments around OAK crater.

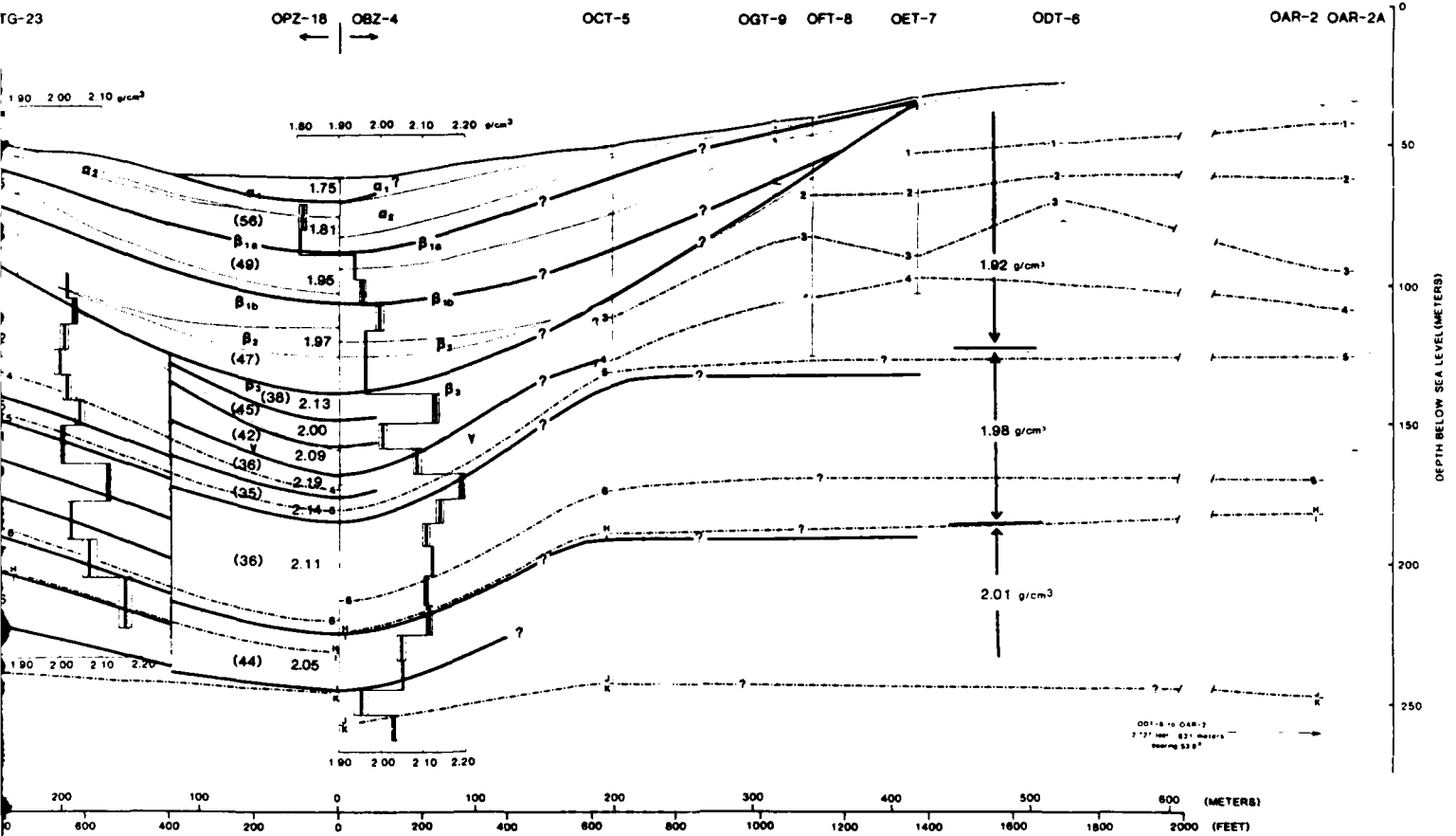
DENSITY, POROSITY, AND MASS CHANGES RELATED TO CRATERING PHENOMENA

A corrected BHG density and porosity model of the south-southwest transect of OAK crater is shown in Figure 2-18. This generalized model closely, but not exactly, follows the disconformity, facies changes, and geologic crater zone correlations defined by Wardlaw and Henry (1986a,b). The density elements of this model are based on the interval divisions of the BHG surveys that were selected during field work prior to knowledge of the exact downhole locations of the geologic boundaries. Intervals of BHG density and porosity have not been divided to correspond to the geologic boundaries because such divisions would be arbitrary in the absence of gravity station readings at the downhole locations of the geologic boundaries. Furthermore, BHG density and porosity are based on mass/volume characteristics that may or may not coincide with divisions based on the geologic characteristics of the sediments. This is clearly seen in Figure 2-5 where a significant number of major BHG density changes occur between, rather than at, the geologic boundaries defined by Wardlaw and Henry (1986a,b). Lack of exact depth correspondence of geologic and density/porosity models does not interfere with comparisons of geologically equivalent intervals between boreholes (figs. 2-16 and 2-19). (Application of the borehole gravity data to the geologic interpretation of OAK crater is expanded in Chapter 7 of the current Open-File report.)

A primary goal of the BHG phase of the PEACE Program was to determine if densification in crater-flank regions could account for observed sea-floor subsidence. BHG surveys were made in transition-zone boreholes OQT-19 and ORT-20 to investigate possible densification. There is considerable variation of BHG density and porosity in the upper parts of these boreholes but averages over larger intervals show that the sediments are not now appreciably denser than in the reference boreholes OOR-17 and OSR-21 (fig. 2-16).

Because documented subsidence of the sea floor at OQT-19 and ORT-20 cannot be explained by densification of the upper few hundred feet of underlying sediments alone, mass displacement from this region and densification of deeper materials probably occurred. Selective removal of finer fractions in this way could be investigated by comparing grain-size distributions of core samples from OQT-19 and the reference boreholes. Slight but definite densification and porosity decreases are present at greater depths in OQT-19 (figs. 2-16 and 2-19).

Unmistakable densification and porosity diminution are inferred in boreholes OTG-23 and beneath 292 ft below sea level in OPZ-18 (figs. 2-16 and 2-19). Independently documented mass transport (Wardlaw and Henry, 1986b) also can be quantified with the BHG density and porosity data. For example, the mass columns at OQT-19 and OPZ-18 are mass deficient by 3 to 5 percent and 6 to 8 percent, respectively, when compared to the mass column at reference

B

south-southwest transect at OAK crater. Porosities are in parentheses.

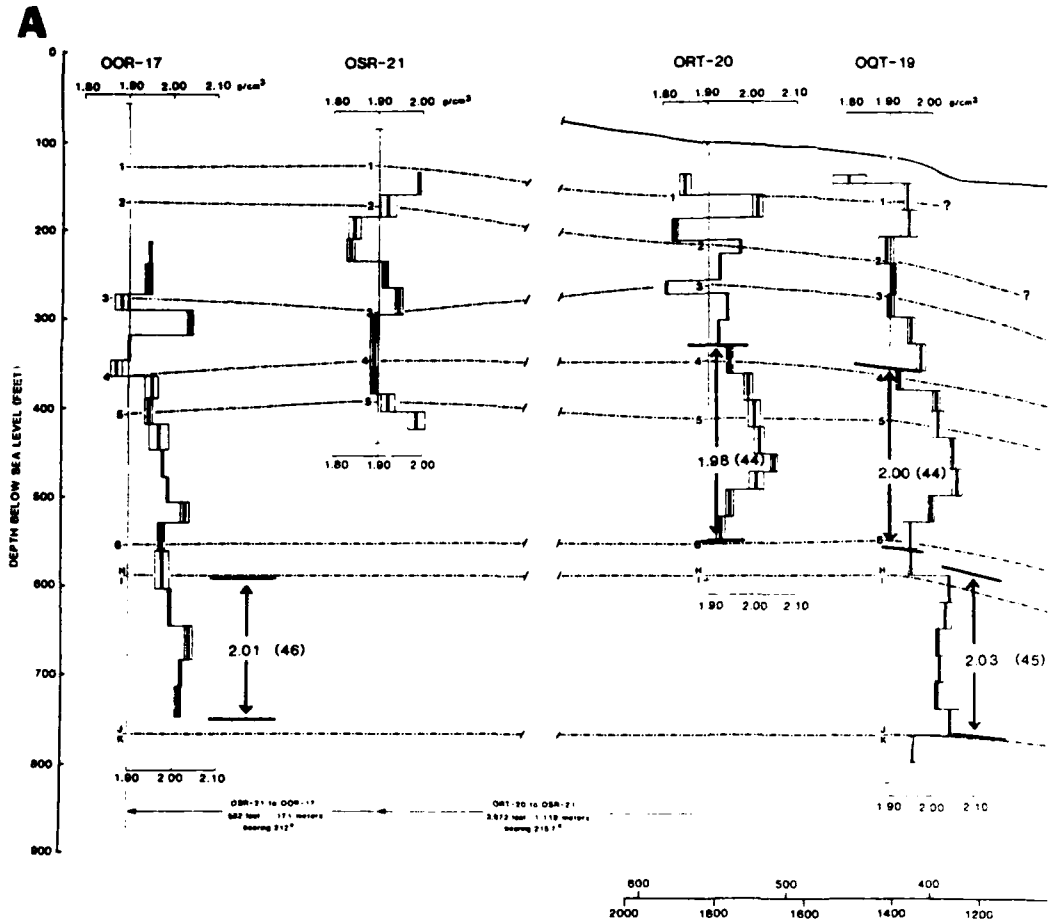
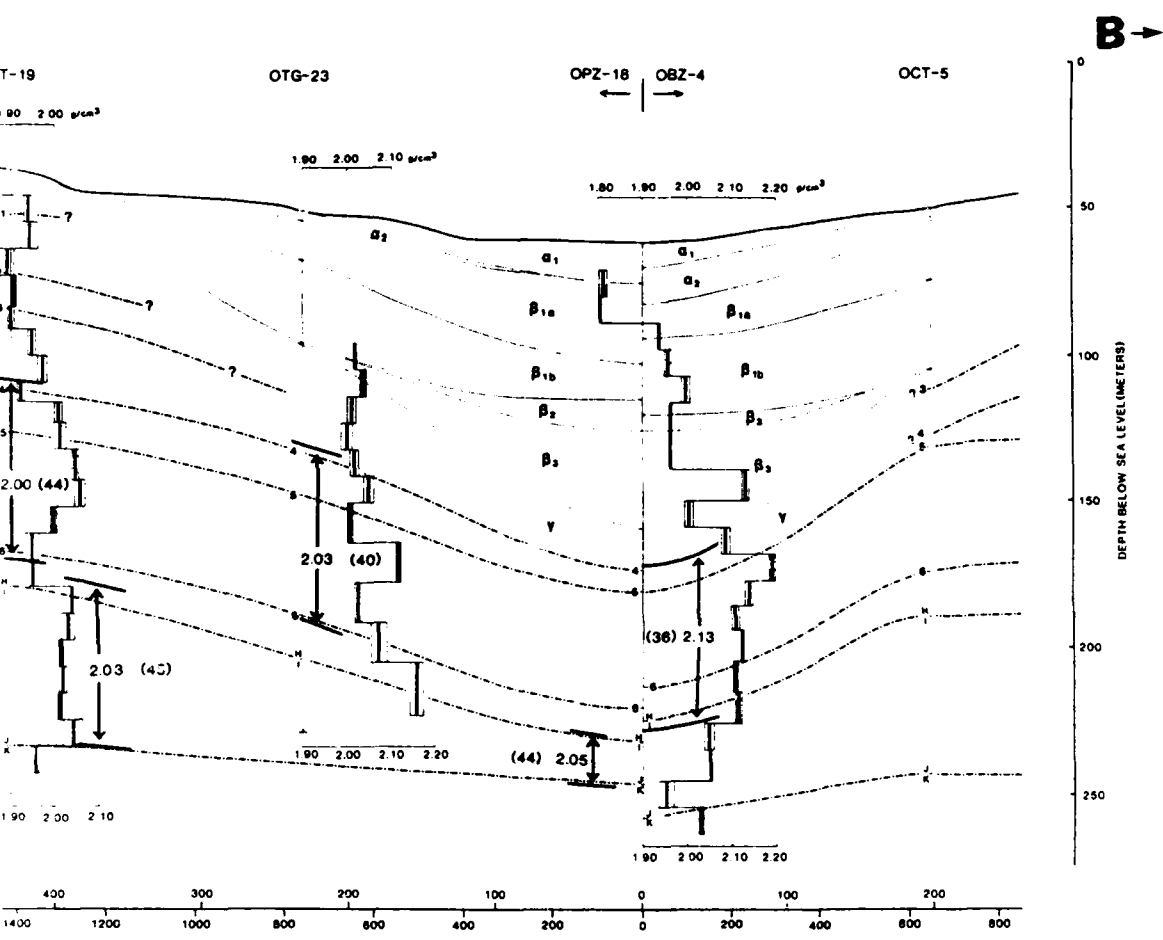


FIGURE 2-19 - Averages of BHG density and porosity for selected wells



ity for selected large intervals. Porosities are in parentheses.

boreholes OOR-17 and OSR-21. Density and porosity changes over the large intervals shown in Figures 2-16 and 2-19 are summarized in Table 2-9.

Many more types of comparisons are possible but are beyond the intent of this paper, which is to provide accurate representative density data and calculated porosity values for atoll materials at the six surveyed boreholes and to present a general density model of the crater.

SUMMARY

Borehole gravity surveys were conducted at OAK crater to obtain accurate large-volume estimates of in situ bulk-density and total porosity of atoll materials beneath and beyond the crater. Reliable density and porosity measurements of undisturbed atoll materials provide important geologic information about these young, loosely consolidated back-reef sediments, and predictions of pre-event material-property conditions for nuclear event calculations. Accurate measurements of differences between the density and porosity of undisturbed atoll materials and the sediment and rock involved in the excavational and apparent OAK craters are crucial to understanding the cratering phenomena at OAK and the mechanics of large crater formation.

Six boreholes were drilled and successfully logged with a borehole gravity meter along a 6,000-foot southwest transect from the bathymetric center of OAK crater (fig. 2-2). Gravity measurements were made in these cased boreholes, generally at spacings of 20 to 35 ft. To obtain reference values for the density and porosity of undisturbed reef-forming material for comparison with material disturbed by cratering processes, gravity surveys were conducted in boreholes OSR-21 and OOR-17, separated by 562 ft, and located approximately 5,500 and 6,050 ft south-southwest of the bathymetric center of OAK crater. Possible densification caused by suspected subsidence on the crater flank just outside the excavational crater was investigated by gravity surveys made in boreholes OQT-19 and ORT-20. These boreholes were separated laterally by 404 ft, and located approximately 1,400 and 1,800 ft south-southwest of the bathymetric center of OAK crater. Gravity surveys were made in borehole OPZ-18 at the bathymetric center of OAK crater, and in OTG-23 located 759 ft south-southwest of OPZ-18 to measure densification beneath the excavational crater and the density of fill within the excavational crater.

The ability of BHG surveys to determine subtle density differences between reef materials located at different locations inside and outside OAK crater depends crucially on the precision of field measurements. Consequently, great effort was devoted to insure that requisite precisions were achieved (Beyer, Ristvet, and Oberste-Lehn, 1986). Repeated measurements show that the precision of BHG densities averages about .01 g/cm³, which is fully adequate for the purposes of the OAK study (fig. 2-3).

BHG measurements permit examination of large volumes of material surrounding the borehole, which means that larger-scale, more distant, lateral density changes are sensed, along with smaller-scale, local density changes that occur within tens to a few hundred feet of the borehole. To obtain BHG density and porosity of atoll materials immediately surrounding each borehole, corrections were calculated and applied for: (1) submarine topography out to a distance of 103 statute miles using bathymetric charts of various scales

(Beyer, Ristvet, and Oberste-Lehn, 1986); (2) generalized two-dimensional density variations associated with large-scale facies changes and diagenesis across the reef margin (fig. 2-4); and (3) generalized three-dimensional density changes due to cratering processes (fig. 2-7). Corrections range from .067 to .156 g/cm³ for submarine topography, .018 to .025 g/cm³ for two-dimensional density variations across the atoll margin, and +.025 to -.021 g/cm³ for generalized three-dimensional density changes due to cratering (tables 2-1 through 2-7).

The following conclusions can be drawn from the corrected BHG densities (fig. 2-5), the derived crater density model (fig. 2-18), and comparisons of corrected BHG density and porosity of geologically equivalent intervals along the south-southwest transect from OOR-17 to OPZ-18 (figs. 2-16 and 2-19):

1. Large natural variations of density and porosity of atoll materials are well-known from numerous geological observations at scales of cubic inches to hundreds of cubic feet. Serious concern was expressed prior to this study that these natural variations of density and porosity would obscure those due to cratering phenomena. The shallow portions of the BHG density profiles from OOR-17, OSR-21, ORT-20, and OQT-19 suggest that this concern may be well-founded when attempting to compare shallow vertical intervals in different boreholes that are on the order of tens of feet thick (fig. 2-5). However, averages of BHG densities over larger vertical intervals show that natural variations of density and porosity tend to average out so that valid lateral comparisons of geologically equivalent intervals can be made (figs. 2-16 and 2-19). Also, over the depths surveyed in OAK boreholes, the range of natural variation of density and porosity appears to decrease slightly with depth, allowing valid comparisons of smaller vertical intervals with increasing depth (fig. 2-5). These results are based solely on BHG surveys made on a trend nearly parallel to the reef along which facies and density changes are believed to be minimal.
2. The shallow section beneath the crater-flank region penetrated by OQT-19 and ORT-20 is not appreciably denser than the equivalent section penetrated by the more distant reference boreholes OOR-17 and OSR-21 (fig. 2-16). Crater-flank subsidence in this area cannot be explained by densification of this shallow section, but probably involved mass removal and densification of a larger vertical interval. Slight densification is evident at greater depth in OQT-19 but cannot be confirmed at greater depth in ORT-20 (figs. 2-16 and 2-19).
3. Atoll material penetrated by OTG-23 within the excavational crater is significantly denser over the surveyed intervals than the geologically equivalent sections penetrated by reference boreholes OPR-17 and OSR-21 and crater flank boreholes ORT-20 and OQT-19 (figs. 2-16, 2-18, and 2-19). Porosity reduction also has occurred as a result of cratering processes.
4. At the bathymetric center of OAK crater, the section penetrated by OPZ-18 is dominated by cratering effects. Major discontinuities of BHG density and porosity occur midway through crater zones β_{1a} and β_3 . Beneath the second discontinuity midway through zone β_3 , and extending at least to the J/K biostratigraphic boundary, a large amount of densification and porosity reduction has resulted from cratering processes (figs. 2-16 and

2-19). In the lower part of this densified interval, the low BHG densities compared to the indicated thinning of geologic units means that major amounts of mass have been removed (fig. 2-19). Densification and/or mass removal appears to extend beneath the depth of the BHG survey in OPZ-18, and may be evaluated by careful study of the lower portions of the gamma-gamma density logs from OAM-1/OAR-2, OBZ-4, OCT-5, and OOR-17.

5. Mass deficiencies of about 3 to 5 percent at OQT-19, and 6 to 8 percent at OPZ-18 are indicated from mass column calculations that utilize BHG densities at OOR-17, OQT-19, and OPZ-18.

Other conclusions of this study are as follows:

1. In reference boreholes OOR-17 and OSR-21, back-reef sediments dominated by aragonite have higher porosities than materials dominated by calcite (fig. 2-17). The mineral volume increase that accompanies the transformation of aragonite to calcite is not sufficient to explain the observed decrease in porosity. Not surprisingly, other diagenetic processes, such as calcite solution and recrystallization and deposition of externally derived carbonate cement, must have contributed to (or dominated) the observed natural decrease of porosity that accompanies the transformation of aragonite to calcite in these back-reef materials.
2. The BHG survey in the E-1 borehole on Medrin (ELMER) Island provided BHG densities of the shallow section that differed only slightly from those measured across Enewetak Atoll at OAK crater (figs. 2-1 and 2-20). BHG densities of the deeper section in the E-1 borehole were important to the construction of the two-dimensional density model of the reef margin (fig. 2-4). The BHG survey in the E-1 borehole also revealed a cyclical pattern of density and porosity that may be due to diagenesis caused by repeated periods of atoll emergence and submergence since middle Miocene (fig. 2-20).
3. BHG measurements permit examination of volumes of materials measured in hundreds of thousands of cubic feet. Unlike conventional, shallow penetration gamma-gamma and neutron logging methods, the large volume of material examined by the BHG method makes it immune to formation damage or borehole rugosity that commonly occurs when drilling through loosely consolidated, highly permeable strata or alternating soft and hard beds. Not unexpectedly, BHG density and porosity in the OAK study are about an order of magnitude more reliable than the next most reliable density or porosity logging method, the gamma-gamma density log, at depths less than about 400 ft below the sea floor in the five OAK boreholes where comparisons were possible (figs. 2-8 through 2-12, 2-14, and 2-15).

This first BHG study of the carbonate deposits of an atoll island and of the materials beneath a large nuclear crater affirms the unique ability of borehole gravimetry to evaluate the density and porosity of heterogeneous and/or loosely consolidated geologic formations.

ACKNOWLEDGEMENTS

I am especially indebted to several key people. D. Oberste-Lehn, of R & D Associates, one of several people who initially recognized the potential value of borehole gravity surveys to the PEACE Program, solicited my involvement and worked closely with me during the past several years. Her persistent questions, stimulating ideas, and material support have been invaluable. Crucial leadership and considerable effort during the difficult field surveys were very ably provided by B. L. Ristvet of S-Cubed, Inc. Early recognition of the value of BHG surveys and strong backing from within the cratering community came from J. G. Trulio of Applied Theory, Inc. I also benefited greatly from information provided at various stages by J. J. Daniels, J. A. Grow, R. B. Halley, J. C. Hampson, T. W. Henry, L. S. Melzer, B. L. Ristvet, E. L. Tremba, J. G. Trulio, and B. R. Wardlaw.

REFERENCES

- Beyer, L. A., 1968, Recent tests of the United States Geological Survey -- La Coste and Romberg borehole gravimeter system (abs.): *Geophysics*, v. 33, no. 6, p. 1030.
- Beyer, L. A., and Corbato, C. E., 1972, A FORTRAN IV computer program for calculating borehole gravity terrain corrections: U.S. Geological Survey Open-File Report, 30 p.; available as report PB-208-679 from National Technical Information Service, Springfield, Virginia.
- Beyer, L. A., Ristvet, B. L., and Oberste-Lehn, D., 1986, Chapter 8: Preliminary density and porosity data and field techniques of borehole gravity surveys, OAK crater: 28 p., 4 figs., 10 tpls.; in Henry, T. W., and Wardlaw, B. R., eds., *Pacific Enewetak Atoll Crater Exploration (PEACE) Program. Enewetak Atoll, Republic of the Marshall Islands; Part 3: Stratigraphic analysis and other geologic and geophysical studies in vicinity of OAK and KOA craters*: U.S. Geological Survey Open-File Report 86-555.
- Black, A. J., and Herring, A. T., 1983, Borehole gravity: Expanded operating limits and performance: Expanded Abstracts with Bibliographies, 1983 Technical Program, 53rd Annual International Society of Economic Geologists Meeting, September 11-15, 1983, Las Vegas, Nevada, p. 21-33.
- Buigues, D., 1985, Principal facies and their distribution at Mururoa Atoll: *Proceedings of the Fifth International Coral Reef Congress*, v. 3, p. 249-255.
- Couch, R. F., Jr., Fetzer, J. A., Goter, E. K., Ristvet, B. L., Tremba, E. L., Walter, D. R., and Wendland, V. P., 1975, *Drilling operations on Enewetak Atoll during Project EXPOE*: Air Force Weapons Laboratory Technical Report AFWL-TR-75-216, Kirtland Air Force Base, New Mexico, 270 p., 17 figs., 4 tpls. [Unclassified].

- Folger, D. W., ed., 1986a, Sea-floor observations and subbottom seismic characteristics of OAK and KOA craters, Enewetak Atoll, Marshall Islands: U.S. Geological Survey Bulletin 1678, 301 p., 112 figs., glossary, 2 appendices.
- Henry, T. W., Wardlaw, B. R., Skipp, Betty, Major, R. P., and Tracey, J. I., Jr., 1986, Pacific Enewetak Atoll Crater Exploration (PEACE) Program; Part 1: Drilling operations and descriptions of boreholes in vicinity of KOA and OAK craters: U.S. Geological Survey Open-File Report 86-419, 497 p., 32 figs., 29 pls., 13 tbls., 3 appendices.
- Holloway, G. L., and Young, A. G., 1986, Appendix II: Geotechnical Investigations, Phase II of PEACE Program: 29 p., 16 figs., 36 pls.; in Henry, T. W., Wardlaw, B. R., Skipp, Betty, Major, R. P., and Tracey, J. I., Jr., 1986, Pacific Enewetak Atoll Crater Exploration (PEACE) Program; Part 1: Drilling operations and descriptions of boreholes in vicinity of KOA and OAK craters: U.S. Geological Survey Open-File Report 86-419.
- Ladd, H. S., Ingerson, E., Townsend, R. D., Russell M., and Stephenson, n. K., 1953, Drilling on Eniwetok Atoll, Marshall Islands: Bulletin of the American Association of Petroleum Geologists, v. 37, no. 10, p. 2257-2280.
- Ladd, H. S., and Schlanger, S. O., 1960, Drilling operations on Eniwetok Atoll: U.S. Geological Survey Professional Paper 260-Y, p. 863-903, pls. 255-256, figs. 260-287, 3 tbls.
- Plouff, D., 1976, Gravity and magnetic fields for polygonal prisms and application to magnetic terrain corrections: Geophysics, v. 41, no. 4, p. 727-741.
- Ristvet, B. L., Couch, R. F., Jr., Fetzer, J. D., Goter, E. R., Tremba, E. L., Walter, D. R., and Wendland, V. P., 1974, A Quaternary diagenetic history of Eniwetok Atoll: Geological Society of America Abstracts with Programs, v. 6, p. 928-929.
- Ristvet, B. L. and Tremba, E. L., 1986, Chapter 5: Total organic content of lagoon benthic sediments and of submarine samples from the PEACE drilling program: 9 p., 2 figs., 2 tbls.; in Henry, T. W., and Wardlaw, B. R., eds., Pacific Enewetak Atoll Crater Exploration (PEACE) Program, Enewetak Atoll, Republic of the Marshall Islands; Part 3: Stratigraphic analysis and other geologic and geophysical studies in vicinity of OAK and KOA craters: U.S. Geological Survey Open-File Report 86-555.
- Schmoker, J. W., and Hester, T. C., 1986, Porosity of the Miami Limestone (Late Pleistocene), Lower Florida Keys: Journal of Sedimentary Petrology, v. 56, no. 5, p. 629-634.
- Talwani, M., Worzel, J. L., and Landisman, M., 1959, Rapid gravity computations for two-dimensional bodies with application to the Mendocino submarine fracture zone: Journal of Geophysical Research, v. 64, no. 1, p. 49-59.

- Tracey, J. I., Jr., and Ladd, H. S., 1974, Quaternary History of Eniwetok and Bikini Atolls, Marshall Islands: Proceedings of the Second International Symposium on Coral Reefs, Great Barrier Reef Committee, Brisbane, Australia, p. 537-550, 15 figs., 3 tpls.
- Tremba, E. L. and Ristvet, B. L., 1986, Chapter 4: X-ray diffraction mineralogy: 49 p., 11 figs., 35 tpls.; in Henry, T. W., and Wardlaw, B. R., eds., Pacific Enewetak Atoll Crater Exploration (PEACE) Program, Enewetak Atoll, Republic of the Marshall Islands; Part 3: Stratigraphic analysis and other geologic and geophysical studies in vicinity of OAK and KOA craters: U.S. Geological Survey Open-File Report 86-555.
- Wardlaw, B. R. and Henry, T. W., 1986a, Chapter 2: Physical stratigraphic framework: 36 p., 10 figs., 2 tpls.; in Henry, T. W. and Wardlaw, B. R., eds., Pacific Enewetak Atoll Crater Exploration (PEACE) Program, Enewetak Atoll, Republic of the Marshall Islands; Part 3: Stratigraphic analysis and other geologic and geophysical studies in vicinity of OAK and KOA craters: U.S. Geological Survey Open-File Report 86-555.
- Wardlaw, B. R. and Henry, T. W., 1986b, Chapter 14: Geologic interpretation of OAK and KOA craters: 39 p., 21 figs., 2 tpls.; in Henry, T. W. and Wardlaw, B. R., eds., Pacific Enewetak Atoll Crater Exploration (PEACE) Program, Enewetak Atoll, Republic of the Marshall Islands; Part 3: Stratigraphic analysis and other geologic and geophysical studies in vicinity of OAK and KOA craters: U.S. Geological Survey Open-File Report 86-555.

TABLE 2-1. -- Range of corrections for lateral density changes calculated from submarine topography and density models for six BHG surveys at OAK Crater.

Borehole	Range of Corrections Expressed in g/cm^3 Due to		
	Submarine Topography	Large-Scale Lateral Density Changes Across Reef Margin	Smaller-Scale Lateral Density Changes Related to Cratering Processes
OOR-17	.156 to .144	.021 to .019	negligible
OPZ-18	.118 to .067	.025 to .021	.025 to -.021
OQT-19	.145 to .135	.024 to .020	.008 to -.004
ORT-20	.140 to .130	.023 to .020	.005 to -.005
OSR-21	.137 to .126	.020 to .018	negligible
OTG-23	.122 to .108	.022 to .024	.019 to .014

TABLE 2-2.--(on adjacent page) Bulk density, porosity, and grain density obtained from borehole gravity, gamma-gamma, and neutron measurements in borehole OOR-17 and from analysis of cores taken from OOR-17. Gamma-gamma and neutron data averages over depth intervals of BHG survey. Grain densities were calculated by the procedure described in Appendix 2-1 using data from Tremba and Ristvet (1986) and Ristvet and Tremba (1986).



TABLE 2-2.

	1	2	3	4	5	6	7	8	9	10	11	12	13	14
	212.-237.	1.772	.003	.156	.019	0.	1.947	2.87	.02	50.2	0.2	1.99	47.8	60.2
	237.-271.	1.769	.008	.155	.019	0.	1.943	2.83	.02	49.3	0.4	1.98	47.2	57.6
	271.-289.	1.709	.015	.154	.019	0.	1.882	2.79	.02	51.6	0.9	1.91	50.0	58.8
	289.-317.	1.864	.006	.153	.019	0.	2.036	2.75	.02	41.5	0.3	2.00	43.6	53.3
	317.-345.	1.730	.003	.152	.019	0.	1.901	2.86	.02	52.4	0.2	1.98	48.1	58.9
	345.-363.	1.700	.013	.152	.020	0.	1.872	2.86	.02	54.0	0.7	1.91	51.9	61.5
	363.-388.	1.780	.015	.151	.020	0.	1.951	2.76	.04	46.8	0.9	1.91	49.1	58.1
	388.-417.	1.774	.009	.150	.020	0.	1.944	2.76	.04	47.2	0.5	1.95	46.8	52.3
	417.-446.	1.798	.022	.149	.020	0.	1.967	2.76	.04	45.8	1.3	1.91	49.1	54.6
	446.-477.	1.807	.003	.149	.020	0.	1.976	2.71	.02	43.7	0.2	0.	0.	0.
	477.-505.	1.819	.001	.148	.020	0.	1.987	2.71	.02	43.0	0.1	0.	0.	0.
	505.-528.	1.860	.010	.147	.020	0.	2.027	2.72	.02	41.0	0.6	0.	0.	0.
	528.-560.	1.807	.008	.147	.020	0.	1.974	2.73	.02	44.5	0.5	0.	0.	0.
	560.-603.	1.809	.016	.146	.021	0.	1.976	2.78	.02	45.9	0.9	0.	0.	0.
	603.-645.	1.826	.004	.146	.021	0.	1.993	2.84	.02	46.8	0.2	2.03	44.8	58.0
	645.-683.	1.870	.009	.145	.021	0.	2.036	2.85	.02	44.7	0.5	2.06	43.4	59.6
	683.-713.	1.852	.004	.145	.021	0.	2.018	2.86	.02	46.0	0.2	2.03	45.4	60.6
	713.-747.	1.848	.007	.144	.021	0.	2.013	2.86	.02	46.3	0.4	2.05	44.3	59.4

Column 1 Depth interval in feet below sea level

Column 2 Apparent BHG density in g/cm³ (corrected for instrument calibration and drift and earth tides).

Column 3 Standard deviation of repeated $\Delta g/\Delta z$ measurements expressed in g/cm³.

Column 4 Vertical gravity gradient correction (expressed in g/cm³) for submarine topography out to a radial distance of 103.5 statute miles (166.7 kilometers). Correction calculated by replacing sea water with density of 1.90 g/cm³ (see Beyer and Corbato, 1972).

Column 5 Vertical gravity gradient correction expressed in g/cm³ for lateral density changes (assumed to be two-dimensional) caused by geologic facies changes across the reef (see Figure 2.4).

Column 6 Vertical gravity gradient correction (expressed in g/cm³) for lateral density changes caused by crater-related processes and assumed to be symmetrical about 0pg-18 (see Figure 2.7).

Column 7 BHG density in g/cm³ after correction for submarine topography and lateral density variations due to geologic facies changes and cratering processes.

Column 8 Mean grain density for depth interval in g/cm³ (calculated from mineral and organic content percentages estimated from x-ray diffraction and loss-on-ignition analyses (see Appendix 2.2)).

Column 9 Estimated uncertainty in mean grain density in g/cm³.

Column 10 BHG porosity in percent calculated from BHG density (column 7), grain density (column 8) and sea-water density of 1.03 g/cm³.

Column 11 Uncertainty in BHG porosity in percent calculated from standard deviation of BHG density (column 4) and uncertainty in mean grain density (column 9).

Column 12 Average gamma-gamma density for depth interval in g/cm³.

Column 13 Gamma-gamma porosity in percent calculated from gamma-gamma density (column 12), grain density (column 8) and sea-water density of 1.03 g/cm³.

Column 14 Average neutron porosity for depth interval in percent.

TABLE 2-3.--(on adjacent page) Bulk density, porosity, and grain density obtained from borehole gravity, gamma-gamma, and neutron measurements in borehole OPZ-18 and from analysis of cores taken from OPZ-18. Gamma-gamma and neutron data averages over depth intervals of BHG survey. Grain densities were calculated by the procedure described in Appendix 2-1 using data from Tremba and Ristvet (1986) and Ristvet and Tremba (1986).



TABLE 2-3.

	1	2	3	4	5	6	7	8	9	10	11	12	13	14
	232.-262.	1.729	.009	.067	.021	-.005	1.812	2.81	.02	56.1	0.5	0.	0.	0.
	262.-292.	1.719	.001	.073	.021	-.006	1.807	2.83	.02	56.8	0.1	0.	0.	0.
	292.-322.	1.844	.001	.077	.021	-.005	1.937	2.84	.02	49.9	0.1	0.	0.	0.
	322.-352.	1.861	.008	.080	.021	-.006	1.956	2.83	.02	48.6	0.4	0.	0.	0.
	352.-382.	1.892	.010	.084	.022	-.001	1.997	2.82	.02	46.0	0.6	0.	0.	0.
	382.-457.	1.871	.	.090	.022	-.021	1.962	2.81	.02	47.6	0.	2.07	41.6	57.8
	457.-492.	1.997	.008	.095	.022	0.016	2.130	2.80	.02	37.9	0.5	2.11	39.0	54.0
	492.-522.	1.881	.010	.098	.022	0.002	2.003	2.81	.02	45.3	0.6	2.09	40.4	53.1
	522.-552.	1.958	.010	.100	.023	0.005	2.086	2.84	.02	41.7	0.6	2.10	40.9	57.0
	552.-582.	2.046	.007	.103	.023	0.019	2.191	2.84	.02	35.9	0.4	2.13	39.2	51.2
	582.-610.	1.991	.009	.105	.023	0.020	2.139	2.74	.02	35.1	0.5	2.05	40.4	51.7
	610.-637.	1.957	.009	.107	.023	0.020	2.107	2.72	.02	36.3	0.5	2.15	33.7	48.1
	637.-672.	1.968	.003	.109	.024	0.021	2.122	2.72	.02	35.4	0.2	2.12	35.5	49.8
	672.-707.	1.950	.005	.111	.024	0.022	2.107	2.72	.02	36.3	0.3	2.15	33.7	49.5
	707.-742.	1.953	.007	.113	.024	0.025	2.115	2.72	.02	35.8	0.4	2.12	35.5	53.5
	742.-772.	1.889	.011	.114	.024	0.021	2.048	2.86	.02	44.4	0.6	2.09	42.1	58.3
	772.-807.	1.891	.002	.116	.024	0.021	2.052	2.86	.02	44.2	0.1	2.05	44.3	58.1
	807.-837.	1.789	.017	.117	.024	0.021	1.951	2.87	.02	49.9	0.9	2.06	44.0	61.1
	837.-867.	1.868	.006	.118	.025	0.020	2.031	2.85	.02	45.0	0.3	2.04	44.5	59.4

Column 1 Depth interval in feet below sea level

Column 2 Apparent BHG density in g/cm³ (corrected for instrument calibration, and drift and earth tides).

Column 3 Standard deviation of repeated $\Delta g/\Delta z$ measurements expressed in g/cm³.

Column 4 Vertical gravity gradient correction (expressed in g/cm³) for submarine topography out to a radial distance of 103.5 statute miles (166.7 kilometers). Correction calculated by replacing sea water with density of 1.90 g/cm³ (see Beyer and Corbato, 1972).

Column 5 Vertical gravity gradient correction expressed in g/cm³ for lateral density changes (assumed to be two-dimensional) caused by geologic facies changes across the reef (see Figure 2.4).

Column 6 Vertical gravity gradient correction (expressed in g/cm³) for lateral density changes caused by crater-related processes and assumed to be symmetrical about 082-18 (see Figure 2.7).

Column 7 BHG density in g/cm³ after correction for submarine topography and lateral density variations due to geologic facies changes and cratering processes.

Column 8 Mean grain density for depth interval in g/cm³ (calculated from mineral and organic content percentages estimated from x-ray diffraction and loss-on-ignition analyses (see Appendix 2.2)).

Column 9 Estimated uncertainty in mean grain density in g/cm³.

Column 10 BHG porosity in percent calculated from BHG density (column 7), grain density (column 8) and sea-water density of 1.03 g/cm³.

Column 11 Uncertainty in BHG porosity in percent calculated from standard deviation of BHG density (column 4) and uncertainty in mean grain density (column 8).

Column 12 Average gamma-gamma density for depth interval in g/cm³.

Column 13 Gamma-gamma porosity in percent calculated from gamma-gamma density (column 12), grain density (column 8) and sea-water density of 1.03 g/cm³.

Column 14 Average neutron porosity for depth interval in percent.

TABLE 2-4.--(on adjacent page) Bulk density, porosity, and grain density obtained from borehole gravity, gamma-gamma, and neutron measurements in borehole OQT-19 and from analysis of cores taken from OQT-19. Gamma-gamma and neutron data averages over depth intervals of BHG survey. Grain densities were calculated by the procedure described in Appendix 2-1 using data from Tremba and Ristvet (1986) and Ristvet and Tremba (1986).



TABLE 2-4.

	1	2	3	4	5	6	7	8	9	10	11	12	13	14
138.-148.		1.646	.038	.145	.020	-.004	1.807	2.84	.02	57.1	2.1	0.	0.	0.
148.-178.		1.777	.010	.140	.020	0.002	1.939	2.85	.02	50.1	0.5	0.	0.	0.
178.-208.		1.787	.020	.134	.021	0.	1.942	2.83	.02	49.3	1.1	0.	0.	0.
208.-238.		1.737	.017	.132	.021	0.	1.890	2.83	.02	52.2	0.9	0.	0.	0.
238.-273.		1.753	.006	.131	.021	0.001	1.906	2.84	.02	51.6	0.3	1.99	47.0	59.1
273.-298.		1.747	.008	.131	.021	0.001	1.900	2.83	.02	51.7	0.4	2.01	45.6	60.4
298.-328.		1.791	.009	.131	.021	0.005	1.948	2.81	.02	48.4	0.5	2.04	43.3	57.6
328.-358.		1.814	.011	.131	.022	0.005	1.972	2.81	.02	47.1	0.6	2.00	45.5	60.2
358.-380.		1.764	.008	.132	.022	0.004	1.922	2.81	.02	49.9	0.4	1.86	53.4	62.6
380.-403.		1.846	.009	.132	.022	0.008	2.008	2.82	.02	45.4	0.5	2.13	38.5	52.8
403.-433.		1.849	.014	.132	.022	0.008	2.011	2.83	.02	45.5	0.8	2.02	45.0	55.4
433.-468.		1.885	.007	.132	.022	0.007	2.046	2.75	.02	40.9	0.4	2.02	42.4	52.0
468.-498.		1.897	.012	.133	.022	0.004	2.056	2.71	.02	38.9	0.7	2.02	41.1	53.7
498.-528.		1.842	.007	.133	.022	0.001	1.998	2.71	.02	42.4	0.4	2.02	41.1	55.3
528.-558.		1.792	.017	.133	.023	0.	1.948	2.71	.02	45.4	1.0	1.97	44.0	53.5
558.-588.		1.793	.008	.134	.023	0.001	1.951	2.74	.02	46.1	0.5	2.02	42.1	54.8
588.-618.		1.882	.002	.134	.023	0.001	2.040	2.83	.02	43.9	0.1	2.03	44.4	54.9
618.-648.		1.874	.015	.134	.023	-.001	2.030	2.84	.02	44.8	0.8	2.01	45.9	61.4
648.-678.		1.858	.005	.134	.023	-.002	2.013	2.86	.02	46.3	0.3	2.04	44.8	60.4
678.-708.		1.861	.009	.135	.024	-.002	2.018	2.86	.02	46.0	0.5	2.02	45.9	57.6
708.-738.		1.854	.005	.135	.024	-.002	2.011	2.87	.02	46.7	0.3	2.03	45.7	60.5
738.-768.		1.884	.022	.135	.024	-.002	2.041	2.86	.02	44.8	1.2	2.04	44.8	61.8
768.-798.		1.799	.008	.135	.024	-.002	1.956	2.84	.02	48.8	0.4	1.98	47.5	61.7

Column 1 Depth interval in feet below sea level
 Column 2 Apparent BHG density in g/cm³ (corrected for instrument calibration and drift and earth tides).
 Column 3 Standard deviation of repeated $\Delta g/\Delta z$ measurements expressed in g/cm³.
 Column 4 Vertical gravity gradient correction (expressed in g/cm³) for submarine topography out to a radial distance of 103.5 statute miles (166.7 kilometers). Correction calculated by replacing sea water with density of 1.90 g/cm³ (see Beyer and Corbato, 1972).
 Column 5 Vertical gravity gradient correction expressed in g/cm³ for lateral density changes (assumed to be two-dimensional) caused by geologic facies changes across the reef (see Figure 2.4).
 Column 6 Vertical gravity gradient correction (expressed in g/cm³) for lateral density changes caused by crater-related processes and assumed to be symmetrical about Op2-18 (see Figure 2.7).
 Column 7 BHG density in g/cm³ after correction for submarine topography and lateral density variations due to geologic facies changes and cratering processes.
 Column 8 Mean grain density for depth interval in g/cm³ (calculated from mineral and organic content percentages estimated from x-ray diffraction and loss-on-ignition analyses (see Appendix 2.2)).
 Column 9 Estimated uncertainty in mean grain density in g/cm³.
 Column 10 BHG porosity in percent calculated from BHG density (column 7), grain density (column 8) and sea-water density of 1.03 g/cm³.
 Column 11 Uncertainty in BHG porosity in percent calculated from standard deviation of BHG density (column 4) and uncertainty in mean grain density (column 8).
 Column 12 Average gamma-gamma density for depth interval in g/cm³.
 Column 13 Gamma-gamma porosity in percent calculated from gamma-gamma density (column 12), grain density (column 8) and sea-water density of 1.03 g/cm³.
 Column 14 Average neutron porosity for depth interval in percent.

TABLE 2-5 (On opposite page). -- Bulk density, porosity, and grain density obtained from borehole gravity, gamma-gamma, and neutron measurements in borehole ORT-20 and from analysis of cores taken from ORT-20. Gamma-gamma and neutron data averages over depth intervals of BHG survey. Grain densities were calculated by the procedure described in Appendix 2-1 using data from Tremba and Ristvet (1986) and Ristvet and Tremba (1986).



TABLE 2-5.

	1	2	3	4	5	6	7	8	9	10	11	12	13	14
	136.-160.	1.693	.013	.130	.020	0.005	1.848	2.84	.02	54.8	0.7	1.98	47.5	0.
	160.-186.	1.857	.012	.133	.020	0.	2.010	2.86	.02	46.4	0.7	1.99	47.5	0.
	186.-211.	1.673	.007	.134	.021	-.002	1.826	2.84	.02	56.0	0.4	1.96	48.6	0.
	211.-226.	1.818	.	.135	.021	-.003	1.971	2.86	.02	48.6	0.	1.99	47.5	0.
	226.-256.	1.772	.	.136	.021	-.003	1.926	2.85	.02	50.8	0.	2.00	46.7	0.
	256.-271.	1.653	.	.137	.021	-.004	1.807	2.82	.02	56.6	0.	1.97	47.5	0.
	271.-301.	1.787	.004	.138	.021	-.004	1.942	2.82	.02	49.1	0.2	0.	0.	0.
	301.-331.	1.766	.002	.139	.021	-.004	1.922	2.78	.02	49.0	0.1	0.	0.	0.
	331.-361.	1.792	.007	.139	.022	-.005	1.948	2.88	.02	50.4	0.4	0.	0.	0.
	361.-391.	1.833	.010	.139	.022	-.005	1.989	2.83	.02	46.7	0.6	2.04	43.9	0.
	391.-421.	1.846	.014	.140	.022	-.005	2.003	2.75	.02	43.4	0.8	2.04	41.3	0.
	421.-451.	1.857	.012	.140	.022	-.005	2.014	2.70	.02	41.1	0.7	1.95	44.9	0.
	451.-471.	1.891	.008	.140	.022	-.005	2.048	2.70	.02	39.0	0.5	1.90	47.9	0.
	471.-491.	1.852	.017	.140	.022	-.005	2.009	2.70	.02	41.4	1.0	2.06	38.3	0.
	491.-521.	1.792	.009	.140	.022	-.005	1.949	2.69	.02	44.6	0.5	1.93	45.8	0.
	521.-551.	1.770	.010	.140	.023	-.004	1.929	2.70	.02	46.2	0.6	1.91	47.3	0.

Column 1 Depth interval in feet below sea level

Column 2 Apparent BHG density in g/cm³ (corrected for instrument calibration and drift and earth tides).

Column 3 Standard deviation of repeated $\Delta g/\Delta z$ measurements expressed in g/cm³.

Column 4 Vertical gravity gradient correction (expressed in g/cm³) for submarine topography out to a radial distance of 103.5 statute miles (166.7 kilometers). Correction calculated by replacing sea water with density of 1.90 g/cm³ (see Beyer and Corbato, 1972).

Column 5 Vertical gravity gradient correction expressed in g/cm³ for lateral density changes (assumed to be two-dimensional) caused by geologic facies changes across the reef (see Figure 2.4).

Column 6 Vertical gravity gradient correction (expressed in g/cm³) for lateral density changes caused by crater-related processes and assumed to be symmetrical about OP2-18 (see Figure 2.7).

Column 7 BHG density in g/cm³ after correction for submarine topography and lateral density variations due to geologic facies changes and cratering processes.

Column 8 Mean grain density for depth interval in g/cm³ (calculated from mineral and organic content percentages estimated from x-ray diffraction and loss-on-ignition analyses (see Appendix 2.2)).

Column 9 Estimated uncertainty in mean grain density in g/cm³.

Column 10 BHG porosity in percent calculated from BHG density (column 7), grain density (column 8) and sea-water density of 1.03 g/cm³.

Column 11 Uncertainty in BHG porosity in percent (calculated from standard deviation of BHG density (column 4) and uncertainty in mean grain density (column 8)).

Column 12 Average gamma-gamma density for depth interval in g/cm³.

Column 13 Gamma-gamma porosity in percent calculated from gamma-gamma density (column 12), grain density (column 8) and sea-water density of 1.03 g/cm³.

Column 14 Average neutron porosity for depth interval in percent.

TABLE 2-6 (On opposite page). -- Bulk density, porosity, and grain density obtained from borehole gravity, gamma-gamma, and neutron measurements in borehole OSR-21 and from analysis of cores taken from OSR-21. Gamma-gamma and neutron data averages over depth intervals of BHG survey. Grain densities were calculated by the procedure described in Appendix 2-1 using data from Tremba and Ristvet (1986) and Ristvet and Tremba (1986).



TABLE 2-6.

	1	2	3	4	5	6	7	8	9	10	11	12	13	14
	134.-159.	1.845	.004	.126	.018	0.	1.989	2.82	.02	46.4	0.2	1.96	48.0	0.
	159.-184.	1.776	.018	.126	.018	0.	1.920	2.80	.02	49.7	1.0	1.83	54.8	0.
	184.-209.	1.698	.014	.128	.019	0.	1.845	2.81	.02	54.2	0.8	1.90	51.1	0.
	209.-234.	1.689	.009	.129	.019	0.	1.837	2.82	.02	54.9	0.5	1.88	52.5	0.
	234.-264.	1.763	.007	.131	.019	0.	1.913	2.80	.02	50.1	0.4	1.87	52.5	0.
	264.-294.	1.794	.009	.132	.019	0.	1.945	2.80	.02	48.3	0.5	1.88	52.0	0.
	294.-324.	1.735	.008	.134	.019	0.	1.888	2.82	.02	52.1	0.4	1.87	53.1	0.
	324.-354.	1.736	.009	.135	.019	0.	1.890	2.82	.02	52.0	0.5	1.78	58.1	0.
	354.-384.	1.734	.007	.136	.019	0.	1.889	2.81	.02	51.7	0.4	1.83	55.1	0.
	384.-404.	1.765	.016	.137	.020	0.	1.922	2.79	.02	49.3	0.9	1.72	60.8	0.
	404.-424.	1.829	.020	.137	.020	0.	1.986	2.77	.02	45.1	1.1	1.84	53.4	0.

Column 1 Depth interval in feet below sea level

Column 2 Apparent BHG density in g/cm^3 (corrected for instrument calibration and drift and earth tides).

Column 3 Standard deviation of repeated $\Delta g/z$ measurements expressed in g/cm^3 .

Column 4 Vertical gravity gradient correction (expressed in g/cm^3) for submarine topography out to a radial distance of 103.5 statute miles (166.7 kilometers). Correction calculated by replacing sea water with density of $1.90 g/cm^3$ (see Beyer and Corbato, 1972).

Column 5 Vertical gravity gradient correction expressed in g/cm^3 for lateral density changes (assumed to be two-dimensional) caused by geologic facies changes across the reef (see Figure 2.4).

Column 6 Vertical gravity gradient correction (expressed in g/cm^3) for lateral density changes caused by crater-related processes and assumed to be symmetrical about Op2-18 (see Figure 2.7).

Column 7 BHG density in g/cm^3 after correction for submarine topography and lateral density variations due to geologic facies changes and cratering processes.

Column 8 Mean grain density for depth interval in g/cm^3 (calculated from mineral and organic content percentages estimated from x-ray diffraction and loss-on-ignition analyses (see Appendix 2.2)).

Column 9 Estimated uncertainty in mean grain density in g/cm^3 .

Column 10 BHG porosity in percent calculated from BHG density (column 7), grain density (column 8), and sea-water density of $1.03 g/cm^3$.

Column 11 Uncertainty in BHG porosity in percent calculated from standard deviation of BHG density (column 4) and uncertainty in mean grain density (column 8).

Column 12 Average gamma-gamma density for depth interval in g/cm^3 .

Column 13 Gamma-gamma porosity in percent calculated from gamma-gamma density (column 12), grain density (column 8) and sea-water density of $1.03 g/cm^3$.

Column 14 Average neutron porosity for depth interval in percent.

TABLE 2-7 (On opposite page). -- Bulk density, porosity, and grain density obtained from borehole gravity, gamma-gamma, and neutron measurements in borehole OTG-23 and from analysis of cores taken from OTG-23. Gamma-gamma and neutron data averages over depth intervals of BHG survey. Grain densities were calculated by the procedure described in Appendix 2-1 using data from Tremba and Ristvet (1986) and Ristvet and Tremba (1986).

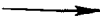


TABLE 2-7.

	1	2	3	4	5	6	7	8	9	10	11	12	13	14
314.-344.		1.869	.003	.108	.022	0.019	2.018	2.85	.04	45.7	0.2	0.	0.	0.
344.-374.		1.888	.007	.109	.022	0.018	2.037	2.85	.04	44.7	0.4	0.	0.	0.
374.-404.		1.860	.010	.111	.022	0.018	2.011	2.85	.04	46.1	0.5	0.	0.	0.
404.-434.		1.848	.013	.112	.022	0.018	2.000	2.85	.04	46.7	0.7	0.	0.	0.
434.-464.		1.864	.010	.113	.022	0.018	2.017	2.85	.02	45.8	0.5	0.	0.	0.
464.-494.		1.895	.012	.114	.022	0.018	2.049	2.84	.02	43.7	0.7	0.	0.	0.
494.-539.		1.855	.006	.116	.022	0.015	2.008	2.74	.02	42.8	0.4	0.	0.	0.
539.-584.		1.958	.005	.117	.023	0.019	2.117	2.72	.02	35.7	0.3	0.	0.	0.
584.-629.		1.867	.008	.119	.023	0.017	2.026	2.73	.02	41.4	0.5	0.	0.	0.
629.-674.		1.915	.018	.120	.023	0.014	2.072	2.81	.02	41.5	1.0	0.	0.	0.
674.-734.		1.991	.015	.122	.024	0.019	2.156	2.88	.02	39.1	0.8	0.	0.	0.

Column 1 Depth interval in feet below sea level
 Column 2 Apparent BHG density in g/cm^3 (corrected for instrument calibration and drift and earth tides).
 Column 3 Standard deviation of repeated $1g/2z$ measurements expressed in g/cm^3 .
 Column 4 Vertical gravity gradient correction (expressed in g/cm^3) for submarine topography out to a radial distance of 103.5 statute miles (166.7 kilometers). Correction calculated by replacing sea water with density of $1.90 g/cm^3$ (see Beyer and Corbato, 1972).
 Column 5 Vertical gravity gradient correction expressed in g/cm^3 for lateral density changes (assumed to be two-dimensional) caused by geologic facies changes across the reef (see Figure 2.4).
 Column 6 Vertical gravity gradient correction (expressed in g/cm^3) for lateral density changes caused by crater-related processes and assumed to be symmetrical about OPZ-18 (see Figure 2.7).
 Column 7 BHG density in g/cm^3 after correction for submarine topography and lateral density variations due to geologic facies changes and cratering processes.
 Column 8 Mean grain density for depth interval in g/cm^3 (calculated from mineral and organic content percentages estimated from x-ray diffraction and loss-on-ignition analyses (see Appendix 2.2)).
 Column 9 Estimated uncertainty in mean grain density in g/cm^3 .
 Column 10 BHG porosity in percent calculated from BHG density (column 7), grain density (column 8) and sea-water density of $1.03 g/cm^3$.
 Column 11 Uncertainty in BHG porosity in percent (calculated from standard deviation of BHG density (column 4) and uncertainty in mean grain density (column 8)).
 Column 12 Average gamma-gamma density for depth interval in g/cm^3 .
 Column 13 Gamma-gamma porosity in percent calculated from gamma-gamma density (column 12), grain density (column 8) and sea-water density of $1.03 g/cm^3$.
 Column 14 Average neutron porosity for depth interval in percent.

Table 2-8. -- Density model for atoll material surrounding OAK crater. Density layers are averages of BHG densities from OOR-17 and OSR-21 and are contrasted with the crater density model of Figure 2-7. Averaged grain densities and BHG porosities are also shown.

Approximate Depth Interval (feet below sea level)	Averaged BHG Density (g/cm ³)	Averaged Grain Density (g/cm ³)	Averaged BHG Porosity (%)
134 - 410	1.92	2.81	50
410 - 587	1.98	2.73	44
587 - 747	2.01	2.84	46
750 - 962	2.09 ± .03 (estimate from gamma-gamma log run in OOR-17)		

Table 2-9. -- BHG density and porosity values and their contrasts with respect to reference borehole values (Table 2-8) for the averaged large intervals shown in Figures 2-16 and 2-19.

	<u>OOR-17/OSR-21</u>	<u>OTG-20</u>	<u>OQT-19</u>	<u>OTG-23</u>	<u>OPZ-18</u>
<u>Interval approximately from discontinuity 1 to 4</u>					
Density(contrast) in g/cm ³	1.92	1.92(0)	1.93(+.01)	--	--
Porosity(contrast) in %	50	51(+1)	50(0)	--	--
<u>Interval approximately from discontinuity 4 to 6</u>					
Density(contrast) in g/cm ³	1.97	1.98(+.01)	2.00(+.03)	2.05(+.08)	2.13(+.16)
Porosity(contrast) in %	45	44(-1)	44(-1)	41(-4)	36(-9)
<u>Interval approximately from discontinuity 5 to facies change H/I</u>					
Density(contrast) in g/cm ³	1.98	1.97(-.01)	2.00(+.02)	2.03(+.05)	2.11(+.13)
Porosity(contrast) in %	44	44(0)	43(-1)	40(-4)	37(-7)
<u>Interval approximately from facies change H/I to J/K</u>					
Density(contrast) in g/cm ³	2.01	--	2.03(+.02)	--	2.05(+.04)
Porosity(contrast) in %	46	--	45(-1)	--	44(-2)
<u>Mass columns (%)</u>					
	100		95-97		92-94

APPENDIX 2-1

BOREHOLE GRAVITY SURVEY, BOREHOLE E-1, MEDREN ISLAND

The BHG survey in borehole E-1 on Medren (ELMER) Island (see fig. 2-20) was conducted in April, 1984, by the U.S. Geological Survey to determine if reliable BHG data could be gathered in the microseismic environment of an atoll and to evaluate the range of natural density variations of reef-forming materials. Near-surface vibrations caused by wave action were minimal and the repeatability of BHG measurements generally was excellent. The tabulated data for this survey are given in Beyer, Ristvet, and Oberste-Lehn (1986).

The borehole gravity survey in the E-1 borehole shows that the bulk density of atoll materials to a depth of 1,800 ft ranges from about 1.9 to about 2.3 g/cm³ and averages slightly more than 2.0 g/cm³ at the scale examined by the BHG survey. Several density patterns are evident.

1. Higher densities between 1,140 and about 1,290 ft correspond to harder rocks as indicated by slower drill rates (fig. 2-20).
2. The gravity station at 1,410 ft (point labeled "A" in fig. 2-20) probably is in close proximity to a sizable cavern that has caused measured gravity to be unexpectedly low. This one anomalous gravity reading incorporated into the overlying and underlying density calculations explains the generally high and low densities of the two adjacent intervals.
3. A repeated pattern of density variations (labeled "1" through "5" in fig. 2-20) may be due to facies changes and/or diagenesis associated with relative sea-level changes. These repeated patterns of downward decrease in density (increase in porosity) followed by more abrupt increase in density (decrease in porosity) should be examined for possible correlation with available geologic data.

Densities in the upper 600 ft are slightly higher than the densities over the same depth interval in PEACE Program reference boreholes OOR-17 and OSR-21 at OAK crater. Part of this may be due to the E-1 borehole being much closer to the ocean edge of the reef than are OOR-17 and OSR-21. Boreholes OOR-17 and OSR-21 are more likely to be in a less dense, more lagoonward facies. Corrections for submarine topography are more critical at the E-1 borehole because of its closer proximity to the outer reef slope than the PEACE Program boreholes. Unfortunately, bathymetry is less well known adjacent to the E-1 borehole, and some of the density differences between E-1 and OOR-17 and OSR-21 may be due to errors in corrections for submarine topography at E-1.

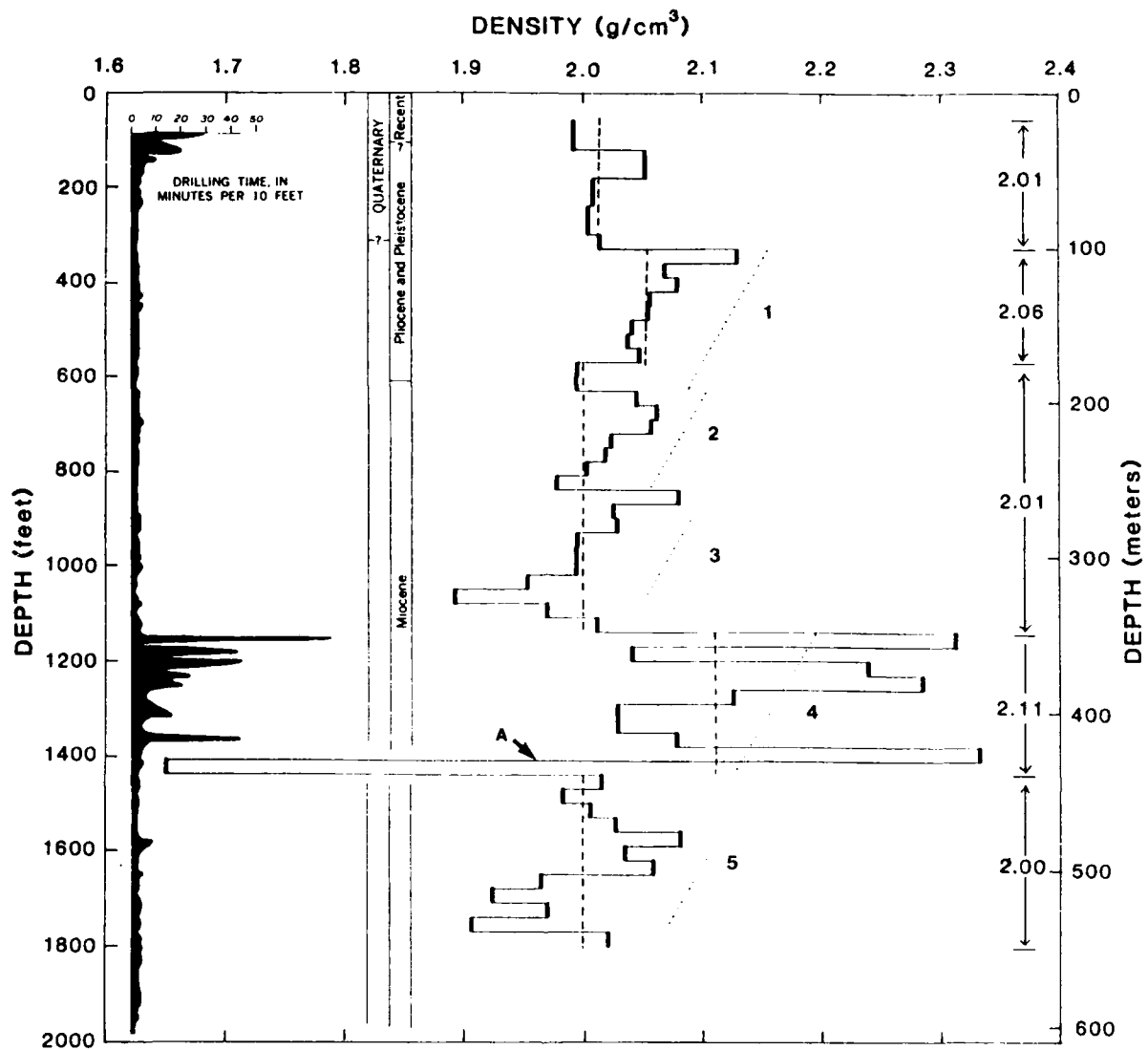


FIGURE 2-20 - BHG density profile for borehole E-1, Medren (ELMER) Island. Drilling time profile and geologic ages are from Ladd and Schlanger (1960). Large interval averages of density along righthand depth scale correspond to vertical dashed lines. Diagonal dotted lines labeled "1" through "5" designate suggested repeated density (porosity?) cycles.

APPENDIX 2-2

DETERMINATION OF INTERVAL GRAIN DENSITY

An estimate of interval grain density is needed before BHG porosity can be calculated from BHG density. Grain densities of individual core samples were estimated from x-ray mineralogy and organic analyses by Tremba and Ristvet (1986) and Ristvet and Tremba (1986) and are shown in Figures 2-8 through 2-13.

An example of how grain density was calculated from x-ray mineralogy and organic analyses follows. Calcite (and magnesium calcite), aragonite, and organic matter were assigned grain densities of 2.72, 2.93, and 1.00 g/cm³ respectively. If organic matter was present and measured in weight percent of dry solids (generally 3 percent or less), the remainder of the dry sample was assumed to consist of inorganic material (generally 97 percent or more). Thus, for a sample with the analysis

Calcite	Aragonite	Organic Matter
<u>(wt %)</u>	<u>(wt %)</u>	<u>(wt %)</u>
29	71	2.5

The grain density is

$$[(.29)(2.72) + (.71)(2.93)](1-.025) + .025 = 2.82 \text{ g/cm}^3$$

If the sample had no measurable organic matter, the grain density is

$$(.29)(2.72) + (.71)(2.93) = 2.87 \text{ g/cm}^3$$

The plots of grain densities of core samples were generalized to average grain densities for BHG intervals as shown in Figures 2-8 through 2-13. Grain densities averaged by sedimentary packages by Tremba and Ristvet (1986) were too generalized for the BHG data. Uncertainties of ± 0.02 or ± 0.04 g/cm³ were assigned in order to estimate errors in porosity calculations (columns 8, 9, 11 of Tables 2-2 through 2-7; also see Appendix 8-2, Beyer, Ristvet, and Oberste-Lehn, 1986).

CHAPTER 3:

PALEONTOLOGIC EVIDENCE FOR SEDIMENTARY MIXING IN OAK CRATER

by

Thomas M. Cronin and Thomas G. Gibson¹

INTRODUCTION

In 1985, during the course of paleontologic studies of OAK and KOA craters, Enewetak Atoll, it was discovered that the analysis of the distribution of microfossils aided the understanding of the dynamic processes involved in the formation and evolution of the nuclear craters (Cronin, Brouwers, and others, 1986; Brouwers, Cronin, and Gibson, 1986; Henry, Wardlaw, and others, 1986; Henry and Wardlaw, 1986; and Wardlaw and Henry, 1986). These paleontologic studies were particularly useful in determining the depth of origin (or provenance) and sedimentologic history of the disturbed and mobilized materials that partially infilled KOA crater after the initial excavation by the detonation of the nuclear device.

The primary purpose of the present study is to determine the composition and provenance of crater-fill materials and the nature of sediment mixing in OAK crater using micropaleontologic data. This study is an extension of the paleontologic component by the U.S. Geological Survey for the PEACE Program (Cronin, Brouwers, and others, 1986; Brouwers, Cronin, and Gibson, 1986). In this study of OAK, we intend to establish the depth limits of mixing of: (1) surficial material, (2) sediment from the uppermost 50 ft of the stratigraphic section, and (3) material from intermediate depths (50 to 300 ft). Furthermore, we intend to determine the pattern of "piping" of deep material emplaced in the crater-fill from horizons 500 to 900 ft below the lagoon bottom or sea floor. Our results are integrated with geologic and geophysical data to form a general model of crater formation in Chapter 7 of this Open-File Report.

MATERIAL AND METHODS

To accomplish our objectives, detailed restudy of samples from reference boreholes OAR-2A and OOR-17 was necessary to refine our zonation of the microfaunal sequence in the upper 400 ft of the stratigraphic section (for discussion of the succession of microfaunal zones used on Enewetak, see Cronin, Brouwers, and others, 1986, and Brouwers, Cronin, and Gibson, 1986). The laboratory and biostratigraphic procedures used herein are the same as those described in the reports cited above. Microfossils were extracted from sediment between 63 and 850 μm in grain size. Samples from two central-crater (ground-zero) boreholes (OBZ-4 and OPZ-18) and three transition boreholes

¹ Branch of Paleontology and Stratigraphy, U.S. Geological Survey,
Reston, VA 22092.

(OCT-5, OFT-8, and OKT-13) were examined in detail for the mixing study of OAK crater. Table 3-1 lists the depths of all 159 samples studied.

Throughout this report, depths of zonal boundaries are occasionally rounded off to whole numbers for convenience. Of course, the accuracy of any particular faunal zone is limited by the resolution of the sampling interval.

STANDARD MICROFAUNAL SEQUENCE

Quantitative data on the occurrence of diagnostic ostracode species (Appendices 3-1 and 3-2) and semiquantitative data on benthic foraminifers (Gibson and Hill, in preparation) from boreholes OAR-2/2A and OOR-17 were used to improve the standard zonation of Cronin, Brouwers, and others (1986) and Brouwers, Cronin, and Gibson (1986), in which 12 faunal zones, designated AA through MM, in descending order, were defined. In addition, the percent of specimens of the ostracode Neonesidea schulzi with preserved setae¹ was used as a new measure to quantify the amount of material mixed downward from the surface. Only living or recently dead specimens of this species found in surficial lagoon sediments have setae preserved (generally 70 to 80%). Ostracode setae normally are degraded and destroyed by natural processes soon after death of the organism and burial of the shell. Therefore, the occurrence of setae in specimens below the sediment surface in the crater-fill materials is taken to indicate mixing of specimens from the surface sediments.

The following zones were used in the quantitative analyses of ostracodes:

- Surface: The percent of Neonesidea schulzi with setae preserved.
- Zone AA: The combined percentages of Hermanites mooneyi and Loxoconchella sp. A.
- Zone BB-CC: The combined percentages of Cletocythereis sp. A and Loxoconcha heronislandensis.
- Zone EE-FF: The combined percentages of Caudites sp. A, Caudites sp. B, Cletocythereis rastromarginata, Loxonconcha labrynthica, and Loxoconchella sp. C.
- Zone FF-GG: The combined percentages of Australimoosella sp. A, Bythoceratina sp. A, Cletocythereis canaliculata, Procythereis sp. A, and Semicytherura sp. A.
- Zone II-MM: The combined percentages of all species restricted to zones II, JJ, KK, LL, and MM as determined by Cronin, Brouwers, and Gibson (1986). In Appendices 3-1 and 3-2 at the end of this Chapter, the totals for these species are given in row 41. Procythereis sp. B generally occurs in zones

¹ Setae are small hairs that occur on the exterior of the valves of some taxa of ostracodes.

TABLE 3-1. — Depth (ft bsf) in boreholes of samples examined during the study of the mixing of crater-fill materials from OAK.

OAR-2A	OBZ-4	OCT-5	OFT-8	OKT-13	OOR-17	OPZ-18
0.25	2.8	0.2	8.75	10.4	0.25	7.0
2.3	11.8	8.8	18.6	18.5	14.15	35.0
6.0	21.1	17.5	27.9	25.4	25.75	44.6
9.3	33.0	39.5	35.1	28.75	38.4	57.85
11.85	40.5	57.55	43.1	36.0	49.7	74.3
14.5	58.5	66.8	48.85	55.65	60.2	89.45
17.1	66.35	76.65	64.0	59.9	66.75	102.0
20.8	75.15	86.15	74.0	68.2	72.8	115.05
22.75	84.15	95.35	-	80.0	83.7	131.0
23.75	93.1	104.25	-	-	89.8	139.7
26.05	104.55	113.15	-	-	100.45	154.2
31.9	112.9	124.0	-	-	101.4	169.35
34.75	121.8	132.8	-	-	110.5	174.95
40.2	130.0	140.9	-	-	119.1	182.3
43.55	144.5	149.65	-	-	125.25	198.0
62.5	151.55	157.6	-	-	131.95	207.3
74.8	166.85	166.4	-	-	137.15	210.4
90.4	178.6	176.25	-	-	146.1	229.95
95.8	186.8	186.0	-	-	154.25	232.1
115.1	193.6	-	-	-	165.6	239.15
127.8	196.5	-	-	-	173.05	-
134.0	205.1	-	-	-	184.25	-
157.45	213.9	-	-	-	193.6	-
171.2	225.65	-	-	-	200.8	-
188.25	-	-	-	-	209.3	-
195.3	-	-	-	-	215.5	-
204.9	-	-	-	-	226.05	-
212.45	-	-	-	-	233.35	-
223.9	-	-	-	-	239.0	-
234.6	-	-	-	-	250.3	-
244.55	-	-	-	-	261.5	-
246.8	-	-	-	-	270.1	-
268.45	-	-	-	-	285.65	-
282.55	-	-	-	-	292.1	-
289.7	-	-	-	-	299.15	-
337.05	-	-	-	-	310.7	-
379.5	-	-	-	-	320.2	-
-	-	-	-	-	331.2	-
-	-	-	-	-	339.0	-
-	-	-	-	-	367.9	-

II-MM; however, it does occur higher in the section in single samples from OOR-17 (331.2 ft bsf) and in OAR-2A (223.9 ft). Specimens of Procythereis sp. B in crater boreholes are considered piped, so that the percent of II-MM species includes species groups 36 and 41 from the appendices.

For the companion analysis of the foraminifers, the zones used are characterized as follows:

- Surface: The presence of chitinous inner linings and original (natural) coloration in several species.
- Zone AA: The presence of Calcarina spengleri and C. hispida. Upper AA is characterized by coloration in specimens of C. spengleri that is not present in specimens in the lower part of this zone, as determined from the reference boreholes.
- Zone BB: The presence of Epistominella tubulosa and Anomolina sp. A.
- Zone CC: The presence of advanced forms of Calcarina rustica.
- Zone EE: The presence of Calcarina delicata and primitive forms of Calcarina rustica.
- Zone FF-GG: The presence of Calcarina calcar and Cibicides sp. A.

The percentages of ostracodes for each category (excluding the Surface¹ and II-MM categories) are plotted for boreholes OAR-2A and OOR-17 in Figures 3-1 and 3-2. These were used for comparison with the mixed faunal sequences in the central crater and transition boreholes. It is noteworthy that the two faunal sequences in OOR-17 and OAR-2A are very similar to each other, enhancing the accuracy of estimates of the original depths of mixed specimens.

A large proportion (generally about 40 to 60% of each sample) consists of long-ranging species not restricted to a particular zone. Some of these non-diagnostic species probably also were mixed during crater filling. Consequently, the percentage values for samples from crater boreholes are, in some cases, minimum values (i.e., if mixed specimens of non-diagnostic species could be identified, the true percentage of an assemblage from any particular zone would be slightly higher).

In many ways, the use in the mixing study of selected species that have acme zones (intervals of greatest abundance) is an exercise in probability. Those species chosen as diagnostic of zones AA, BB-CC, EE-FF, and FF-GG in the upper 400 ft of normal stratigraphic section have a high probability (generally about 80 to 90%) that they originated from within that interval.

¹ Sediments from the lagoon floor or the upper several inches of sediment below the lagoon floor itself are referred hereafter as Surface materials.

OAR-2/2A

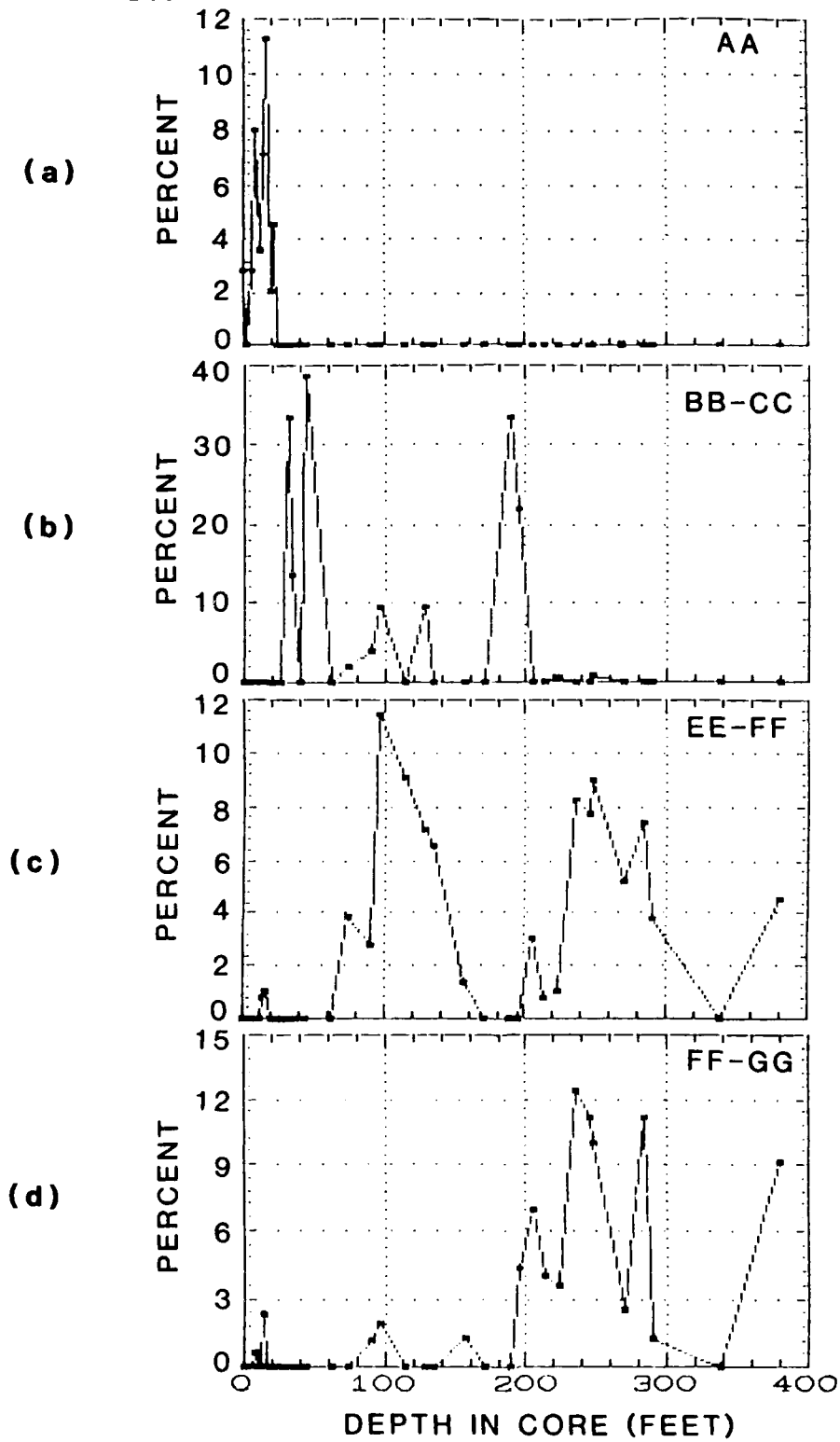


Figure 3-1. -- Borehole OAR-2/2A. Plot of percentages of diagnostic ostracode species. (1a) zone AA; (1b) zones BB-CC; (1c) zones EE-FF; (1d) zones FF-GG.

OOR-17

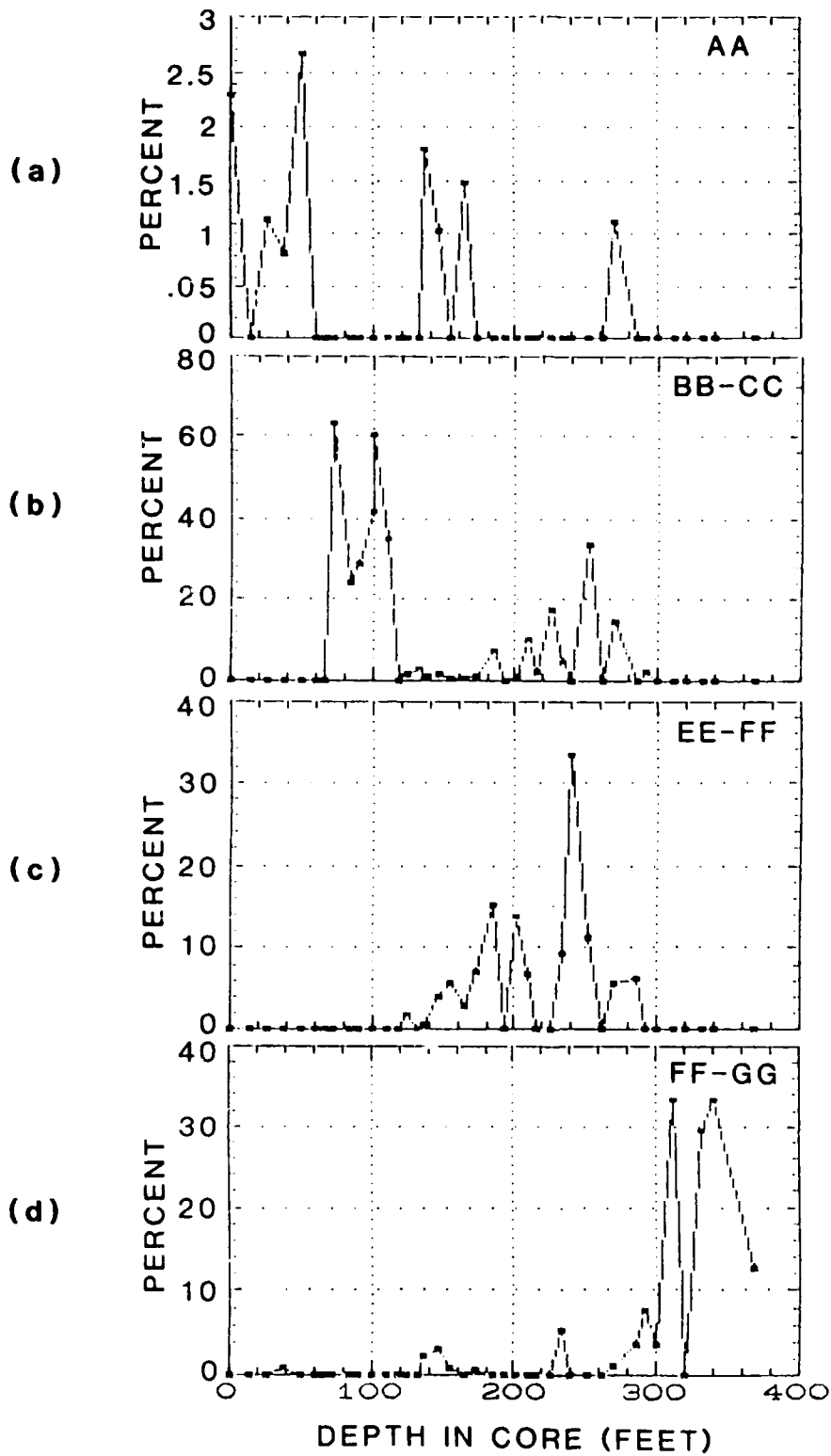


Figure 3-2. --- Borehole OOR-17: Plot of percentages of diagnostic ostracode species. (2a) zone AA; (2b) zones BB-CC; (2c) zones EE-FF; (2d) zones FF-GG.

Confirmation of a zone assignment from both fossil groups increases significantly the probability that the zone assignment is correct.

The use of percentages of specimens from zones II-MM probably underestimates the real percentages by no more than 5 to 10%, because far fewer species from the upper 300 ft of section range downward into these zones. This index of piped specimens is considered an accurate indicator of the proportion of piped material represented in a sample. The percentage piped from a depth interval may be considered representative of the entire sedimentary assemblage at that level if two assumptions are correct. First, we must assume all particles of all sizes behave the same as those between 63 and 850 μm (the size range from which ostracodes were extracted). Second, we must assume sediment particles of different shapes and densities behave the same as the ostracode valves and carapaces. With these assumptions in mind, and given the error margins associated with the limits to microfossils zonations discussed above, these data are useful in making volumetric estimates of the proportion of crater-fill sediments piped from depth.

The percentage of Neonesidea schulzi having setae is a distinct type of index that gives an approximate estimate of the actual percentage of surface material, at least to the extent that it can be determined from using this one common species of ostracodes.

A large proportion of the foraminifer assemblage in most samples is composed of Amphistigina madagascarensis. This species is abundant in the modern reef environments on Enewetak and continues downward into the Miocene strata in the Enewetak boreholes. Therefore, its occurrence alone cannot be used for biostratigraphic determination; however, its preservation state is indicative of its zone of origin or provenance. Translucent specimens of this species occur only in zone AA. Below this zone (i.e., in the Pleistocene section and in older strata), they are opaque. Thus, the occurrence of translucent specimens of A. madagascarensis indicates that their provenance is the Holocene section (zone AA). Many other foraminifer species also have long ranges and cannot be placed definitely. However, the evolutionary changes in the Calcarina lineage are most helpful for determination of the horizons, particularly because they are among the most numerous species in the assemblage.

In some other cases, the preservation of ostracodes and foraminifers also is important in identifying provenance. For example, conspicuous brown specimens of long-ranging species clearly could be identified as originating from deeper zones II-MM. Also, in the injection dikes between 189 and 208 ft bsf and at 233 ft bsf in OPZ-18, the preservation state is almost identical to that of specimens in the upper part of zone AA; therefore, the origin of even non-diagnostic species with the appropriate shell preservation can be shown confidently to be from zone AA.

RESULTS

The following results can be shown from our current studies of samples from OAK crater.

Central Crater (Ground Zero) Boreholes

Boreholes OBZ-4 and OPZ-18 were cored near ground zero in OAK crater; we examined 39 and 21 samples, respectively, from each. The following is an informal zonation of the crater-fill materials based on the characteristics of the mixing of microfossils. The zones of material in the crater-fill from top to bottom are: (1) the **Homogenized Zone**, (2) the **Upwardly Mixed Zone**, (3) the **Maximum Piping Zone**, and (4) the **Basal Mixed Zone**. The boundaries between these zones are gradational and their depths approximate. In addition, we examined material from several injection dikes. The results are based on the ostracode-occurrence data given in Appendices 3-3 and 3-4, many of which are presented graphically in Figures 3-3 and 3-4, and the benthic foraminifer data is summarized in Tables 3-2 through 3-6, located at the end of this Chapter immediately preceding the Appendices. To appreciate the nature of the mixing described in the next few pages and to see the actual percentage values, it is useful to compare directly the "normal" pattern of ostracodes (figs. 3-1 and 3-2) with that of the mixed sequence (figs. 3-3 and 3-4).

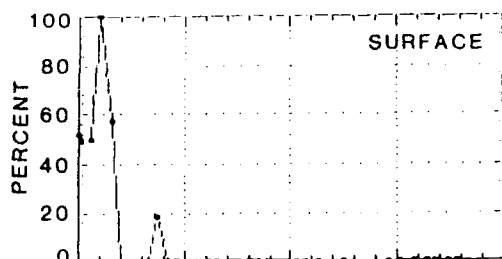
Homogenized Zone (0 to 40 ft). -- In this interval, high percentages (50 to 60%) of Neonesidea schulzi with preserved setae and specimens of Discorbis and Cymbaloporetta with chitinous inner linings originated from the Surface. High percentages of AA species, low to moderate numbers of specimens from CC, low to moderate occurrences of EE-GG species, low percentages of presumably piped specimens of II-MM species, and 3 to 6% BB-CC mixed material also characterize the Homogenized Zone. In general, this interval is easily identified by its anomalously high species diversity, resulting from the homogenization of material from virtually all zones with apparently equal contributions from most sub-AA zones. Specimens from the Homogenized Zone are characterized by widely varying preservation states.

Upwardly Mixed Zone (40 to 100 ft). -- This interval contains consistently low percentages of EE-GG ostracodes and greater percentages of piped material from zones II-MM than occur in the upper 40 ft of OAK crater-fill. The absence of surface material is conspicuous (with the exception of a single sample from 84 ft bsf from OBZ-4). Some samples from the Upwardly Mixed Zone contain less AA material than the overlying Homogenized Zone; in others, zone AA foraminifers still predominate. This interval characteristically contains moderate amounts of BB-CC material. The boundary between the Homogenized Zone and the underlying Maximum Piping Zone is not sharp, although this may be due to sample spacing. However, the relative contributions to the Upwardly Mixed Zone of foraminifers and ostracodes from various zones are quite distinct from the rest of the crater-fill. The piped specimens from this zone are from KK-LL and possibly from MM.

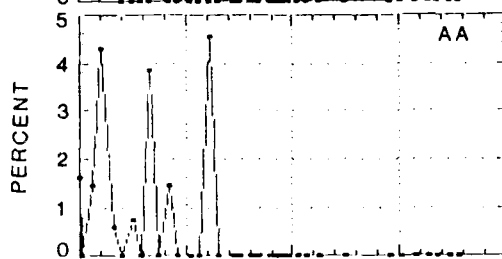
Maximum Piping Zone (100 to 160 ft). -- The highest percentages of piped specimens (9 to 12% in both OBZ-4 and OPZ-18) occur in this zone. LL-MM zone foraminifers and ostracodes are common at 121.8 ft bsf in OBZ-4, where at least eight separate ostracode species were emplaced from depth. Low percentages of AA foraminifers are characteristic of the upper part of the Maximum Piping Zone; however, no definite AA ostracodes or foraminifers are recorded from below about 125 ft in OBZ-4. This interval contains low to moderate numbers of specimens from zones CC and EE-GG. Here, piped foraminifers are not as obvious in OPZ-18 as in OBZ-4. Anomalously large numbers of single ostracode valves and still-articulated carapaces are broken

OBZ-4

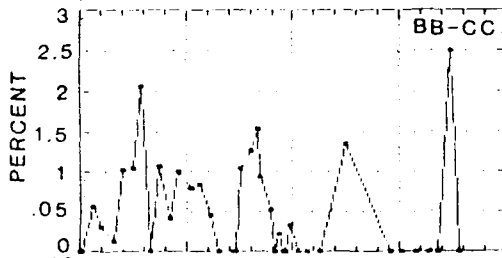
(a)



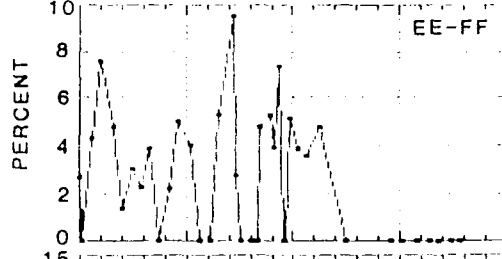
(b)



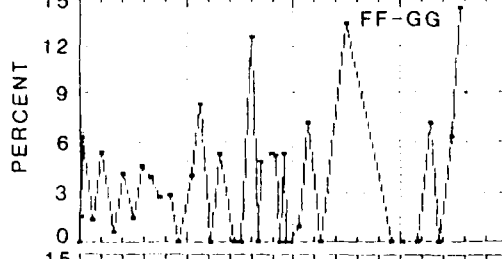
(c)



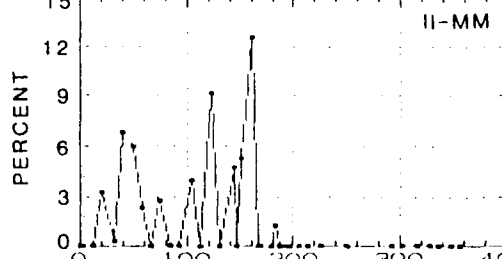
(d)



(e)



(f)



DEPTH IN CORE (FEET)

Figure 3-3. -- Borehole OBZ-4: Plot of percentages of diagnostic ostracode species. (3a) lagoon bottom species; (3b) zone AA; (3c) zones BB-CC; (3d) zones EE-FF; (3e) zones FF-GG; (3f) zones II-MM.

OPZ-18

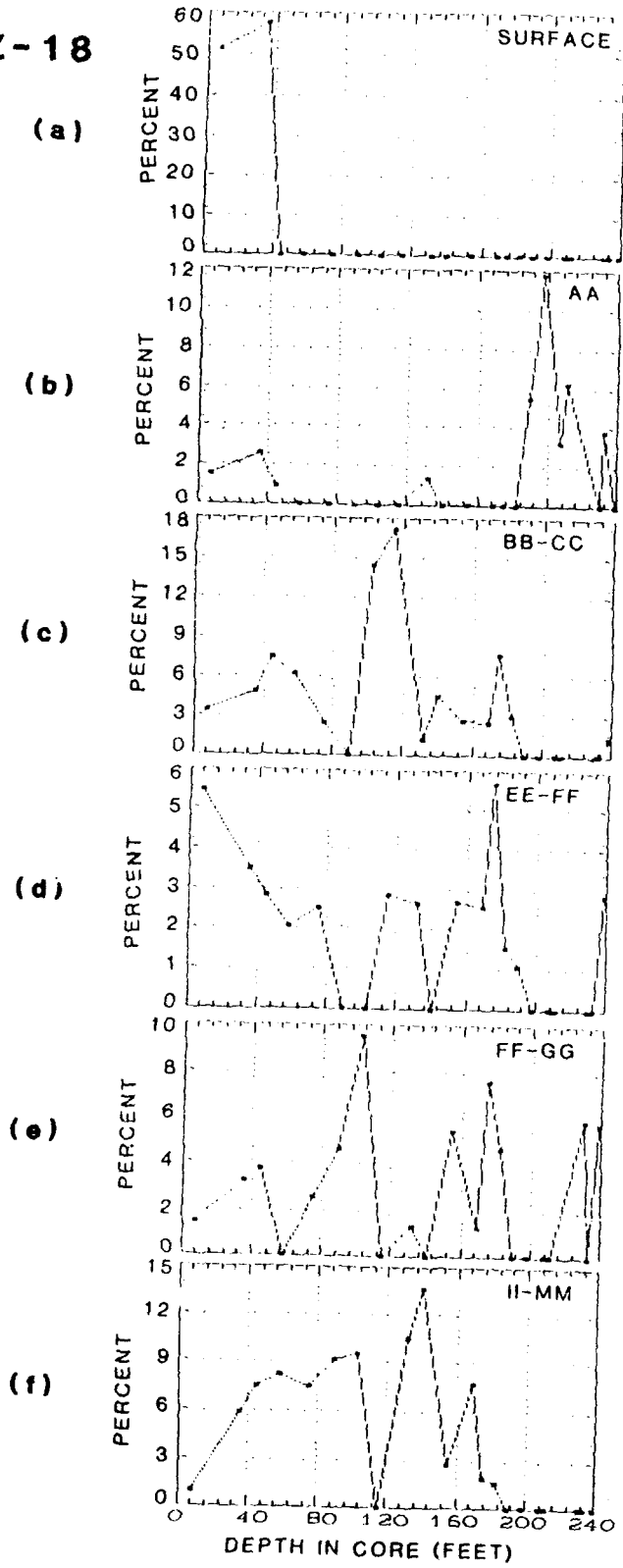


Figure 3-4. --- Borehole OPZ-18: Plot of percentages of diagnostic ostracode species. (4a) species from lagoon floor; (4b) zone AA; (4c) zones BB-CC; (4d) zones EE-FF; (4e) zones FF-GG; (4f) zones II-MM.

in samples from the Maximum Piping Zone, suggesting a kind of shock fracturing. The base of the Maximum Piping Zone is marked by an abrupt drop in the percentage of piped specimens in the samples.

Basal Mixed Zone (160 to 190 ft). -- The Basal Mixed Zone contains low percentages of piped material, low percentages of zone AA foraminifers, and high percentages of zone EE-FF material. Most of the sediment in the Basal Mixed Zone probably originated from zones EE and FF.

Statistical Analysis of Crater-Fill Materials. -- A simple linear-regression analysis of depth versus percentage of piped specimens was performed for samples from the upper 160 ft of OBZ-4 and the upper 145 ft of OPZ-18 (i.e., for all of the samples taken from above the Basal Mixed Zone in both boreholes). This statistical analysis was conducted to further analyze piping in the crater-fill from boreholes OBZ-4 and OPZ-18. Figures 3-5a and 3-5b show this relationship for 20 upper samples from OBZ-4 and 14 samples from OPZ-18. A positive correlation exists with correlation coefficients of $r = 0.46$ and $r = 0.52$, respectively. If samples from these depth intervals containing no piped specimens are excluded (9 samples in OBZ-4, 1 in OPZ-18; see Appendices 3-3 and 3-4), the correlation coefficients are much higher, $r = 0.64$ and $r = 0.93$, respectively (figs. 3-5c and 3-5d). The absence of piped specimens in some samples may be a result of the small number of specimens that could be extracted. Nonetheless, in both boreholes there is a positive correlation, suggesting a diminishing contribution of piped material toward the upper intervals of crater-fill.

Injection Dikes. -- Injection dikes were sampled only in borehole OPZ-18 from 189 to 208 ft and 233 ft bsf. Well-preserved AA foraminifers and ostracodes and many articulated, translucent ostracode carapaces occur in these samples. Bright-red Homotrema is also common. The samples from 189.25, 198.0, and 207.3 ft bsf are composed of almost identical assemblages of species, and the preservation is almost identical also. In these dikes, material from BB-CC is conspicuously missing. All evidence suggests an origin for almost all material between 189 and 208 ft from the upper part of zone AA; however, the lack of Neonesidea schulzi with setae argues against any material originating from the Surface. The sample at 210.4 ft contains recrystallized microfossils, and the samples at 229.95 and 232.1 ft bsf contain zone AA species. These are mixed with zone EE-GG species. No piped II-MM zone material occurs in this dike.

Transition Boreholes

Transition boreholes OCT-5, OFT-8, and OKT-13 were sampled for microfossils for the current mixing study.

OCT-5. -- Samples from borehole OCT-5 were analyzed semiquantitatively for ostracodes (Appendix 3-5) and foraminifers. Both microfossil groups, particularly ostracodes, are much less abundant than in samples from OBZ-4 and OPZ-18, and the following zonation is based more heavily on the foraminifers.

0-9 ft. -- Samples from this interval in OCT-5 have anomalously high diversity, with approximately equal contributions from all mid-upper zones (AA-GG), as was the case in the Homogenized Zone of OBZ-4 and OPZ-18. A few piped foraminifers are found at 8.8 ft bsf.

PIPED SPECIMENS VS DEPTH

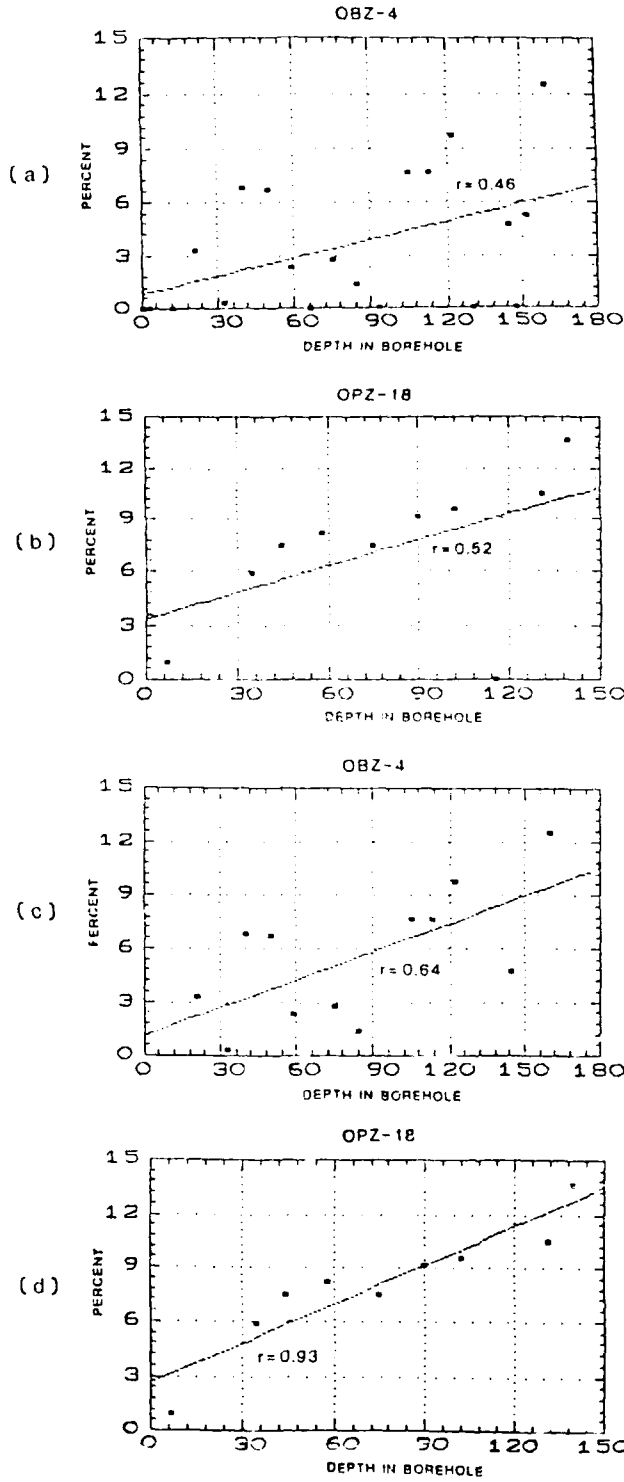


Figure 3-5. -- Plot of percentages of piped specimens versus depth. (5a) borehole OBZ-4, upper 160 ft; (5b) borehole OPZ-18, upper 145 ft; (5c) borehole OBZ-4, upper 160 ft, samples having no piped specimens omitted; (5d) borehole OPZ-18, upper 145 ft, samples having no piped specimens omitted.

39-77 ft. -- Abundant zone AA foraminifers, sparse BB-CC ostracodes, and low percentages of EE-GG material are found in samples from these depths.

86-105 ft. -- Samples from here differ from the overlying ones in lacking zone AA species; this interval has mostly CC-GG foraminifers; however both ostracodes and foraminifers are extremely sparse.

113-140 ft. -- Zone AA species predominate in these samples; preservation of the specimens is similar to specimens from zone AA and bright-red Homotrema (indicative of zone AA) also occurs; samples from here contain low percentages of CC-GG foraminifers.

149-187 ft. -- In this borehole, samples from this interval are almost barren and contain no diagnostic species of either ostracodes or foraminifers. Part of the explanation for the paucity of ostracodes may be that zone EE (normally at roughly comparable depths in the reference boreholes) typically contains few ostracodes in the normal stratigraphic section. However, samples from 149 to 187 ft in OCT-5 also lack even benthic foraminifers, which do occur in zone EE.

OFT-8. -- This borehole has diagnostic microfaunas in all samples examined, allowing a threefold subdivision of the upper 75 ft (Appendix 3-6).

0-19 ft.-- This is a mixed interval containing material from zones AA to probably no deeper than FF. Samples from this interval resemble the Homogenized Zone of the upper parts of other central crater and transitional boreholes. In the uppermost sample at 0.0 to 0.25 ft bsf, a single foraminifer and a single ostracode specimen occur, suggesting piping from zones JJ-MM.

27-50 ft. -- This interval consists almost entirely of material from zone AA, as indicated by the foraminifers. The ostracode species also occur typically in AA and are preserved like those from that zone. There is a noticeable absence of zone BB-CC material, also indicating a lack of mixing.

64-75 ft. -- At 64 ft bsf, a mixture of AA and sparse FF-GG foraminifers occurs with typical BB-CC ostracodes. The 74.0-ft sample appears to be from sediment that is essentially in place and consists exclusively of BB-CC material. A detailed sampling across the interval from 50 to 75 ft would be necessary to better document the transition into undisturbed sediments at this borehole site.

OKT-18. -- This borehole contained highly diagnostic ostracodes and foraminifers that allowed a fourfold subdivision of the upper 80 ft (Appendix 3-11). The results from the two fossil groups match each other more consistently, and, thus, these zones are more definitive than in any borehole yet analyzed.

0-19 ft. -- Samples from this interval are noted for their anomalously high species diversity and homogenization of zone AA-GG material. These samples resemble those from the uppermost parts of boreholes OBZ 4, OPZ 13, and OCT-5. No piped specimens are found.

25-37 ft. -- These samples contained almost exclusively material from zone AA; small percentages from EE-GG are noted from the sample at 25.4 ft

bsf. The microfaunas from this interval resemble those from the injection dike in OPZ-18 in both species composition and preservation.

55-66 ft. -- The samples studied contain only material from zones CC-DD. Especially noteworthy is the occurrence of Paracytheridea remanei (which has its acme in DD in all reference boreholes) in OKT-13 at 55.65 (abundant), 59.9, and 68.3 ft. Also, the abundance of Orionina sp. at 59.9 ft is noteworthy. This latter very distinctive species is abundant in OAR-2A at 62 to 75 ft, and a biostratigraphic correlation is probable for strata between 59.9 ft in OKT-13 and 62-75 ft in borehole OAR-2A.

68-81 ft. -- A typical EE-FF assemblage occurs in this interval; there is no obvious mixing from AA or BB.

SUMMARY AND CONCLUSIONS

Our primary conclusions from the mixing study for the OAK crater area follow:

1. Piped material: an inverse relationship exists between sample depth and the percentage of piped material (from zones II-MM) in OBZ-4 between the surface and 160 ft bsf and in OPZ-18 between the surface and 145 ft bsf. Sparse piped specimens occur in the upper 10 ft of OCT-5 and the upper 1 ft of OFT-8; no piped specimens were found in OKT-13.
2. Mixing of abundant Surface material occurs in OBZ-4 and OPZ-18 downward to a depth of 35 ft, although sparse specimens from the Surface occur as deep as 84 ft in OBZ-4.
3. Mixing of abundant material from zone AA is evident in OBZ-4 and OPZ-18 to about 50 to 60 ft bsf; AA material is less common to a depth of about 120 ft bsf in both boreholes.
4. Mixing of moderate amounts of material from zones EE-GG (occurring from 100 to 300 ft bsf in the normal stratigraphic sequence) is encountered in the upper 100 ft of the two central-crater boreholes (OBZ-4 and OPZ-18) and in the upper 20 ft of the transition boreholes. Mixing of BB-CC material is less significant than that of EE-GG material in all boreholes.
5. An apparent injection dike between 189 and 208 ft bsf in OPZ-18 contains almost exclusively AA microfossils. In addition, sediment from these dikes is greenish-gray, like that from the normal AA section. Distinctive microfaunas at 25 to 37 ft in OKT-13 and 27 to 50 ft in OFT-8 are extremely similar to those in this injected OPZ-18 material, although it is not clear if they are genetically related.
6. A Homogenized Mixed Zone containing approximately equal proportions of AA-GG material is a general characteristic of all central-crater (ground-zero) boreholes (down to 40 ft) and in transition boreholes (down to 20 ft).

7. The overall consistency between the ostracodes and foraminifers and our ability to quantitatively revise the standard and mixing zonations to a high degree of resolution gives us confidence that the only limits to our ability to further refine zonations of mixed material, to more accurately identify provenance, and to improve volumetric computations of mixed materials are manpower constraints and sample/core recovery.

REFERENCES

- Brouwers, E.M., Cronin, T.M., and Gibson, T.G., 1986, Chapter 11: Additional paleontologic studies, OAK and KOA Craters: 18 p., 5 figs., 5 tpls., 1 pl.; in Henry, T.W., and Wardlaw, B.R., editors, Pacific Enewetak Atoll Crater Exploration (PEACE) Program, Enewetak Atoll, Republic of the Marshall Islands; Part 3: Stratigraphic analysis and other geologic and geophysical studies in vicinity of OAK and KOA craters: U.S. Geological Survey Open-file Report 86-555.
- Cronin, T.M., Brouwers, E.M., Bybell, L.M., Edwards, L.E., Gibson, T.G., Margerum, R., and Poore, R.Z., 1986, Pacific Enewetak Atoll Crater Exploration (PEACE) Program, Enewetak Atoll, Republic of the Marshall Islands: Part 2; Paleontology and biostratigraphy, application to OAK and KOA craters. U.S. Geological Survey Open-file Report 86-159, 39 p., 20 figs., 12 tpls., 3 appendices.
- Gibson, T.G. and Hill, E.E., in preparation, Late Pliocene to Holocene benthonic Foraminifera from Enewetak Atoll.
- Henry, T.W., and Wardlaw, B.R., 1986, Chapter 1: Introduction: 13 p., 3 figs., 1 tbl.; in Henry, T.W., and Wardlaw, B.R., editors, Pacific Enewetak Crater Exploration (PEACE) Program, Enewetak Atoll, Republic of the Marshall Islands; Part 3: Stratigraphic analysis and other geologic and geophysical studies in vicinity of KOA and OAK craters: U.S. Geological Survey Open-File Report 86-555.
- Henry, T.W., Wardlaw, B.R., Skipp, B., Major, R.P., and Tracy, J.I., Jr., 1986, Pacific Enewetak Atoll Crater Exploration (PEACE) Program, Enewetak Atoll, Republic of the Marshall Islands: Part 1; Drilling operations and descriptions of the boreholes in the vicinity of KOA and OAK craters: U.S. Geological Survey Open-File Report 86-419, 497 p., 32 figs., 29 pls., 13 tpls., 3 appendices.
- Wardlaw, B.R., and Henry, T.W., 1986, Chapter 14: Geologic interpretation of OAK and KOA craters; 39 p., 21 figs., 2 tpls.; in Henry, T.W., and Wardlaw, B.R., editors, Pacific Enewetak Atoll Crater Exploration (PEACE) Program, Enewetak Atoll, Republic of the Marshall Islands; Part 3: Stratigraphic analysis and other geologic and geophysical studies in vicinity of KOA and OAK craters: U.S. Geological Survey Open-File Report 86-555.

Table 3-2.--Summary of foraminifer occurrences in OAK crater borehole OBZ-4.

DEPTH (ft bsf)	FORAMINIFER DATA
2.8-3.05	Mostly AA, some mixing from CC-GG (most likely CC), piping from KK-MM.
11.8-12.05	Mostly AA, moderate amount of CC-GG (most likely CC), piping from JJ-KK.
21.1-21.35	Moderate amount of AA, some CC and EE-GG, piping from II-KK.
33.0-33.25	Mostly AA, mixed with minor CC.
40.05-40.3	Moderate amounts of AA, CC, and EE-GG, moderate amount of piping from II-LL.
58.50-58.75	Mixed AA, CC, and EE-GG, moderate amount of piping from KK-LL.
66.35-66.60	Mixed AA, CC, and EE-GG, more of ?CC or EE-GG than in above sample, some brown specimens presumably from KK-LL.
75.15-75.4	Mixed AA, CC, and EE-GG, more of EE-GG, some brown specimens presumably from KK-LL.
84.15-84.4	Mixed AA, CC, and EE-GG, some piping from KK-LL, possibly MM.
93.1-93.35	Mostly CC and EE-GG, sparse AA, some brown specimens presumably from KK-LL.
104.55-104.8	Mostly CC and EE-GG, sparse AA, piping from KK-LL.
112.9-113.15	No definite AA; some from ?CC, definite EE-GG, piping from KK-LL and possibly from MM.
121.8-122.05	Definite AA and CC and ?EE-GG, some piping from KK-LL.
130.0-130.25	Mostly CC with some EE-GG, sparse brown specimens possibly from deeper zones.
144.5-144.75	?CC and EE-GG.
151.55-151.8	?CC and EE-GG, some brown specimens presumably from deeper zones.
166.85-167.1	?CC and EE-GG.
178.6-178.85	?CC and EE-GG, some brown specimens presumably from deeper zones.
186.8-187.05	?CC and EE-GG.
193.6-193.85	?CC and EE-GG.
196.5-196.75	EE-GG (probably FF) with ?CC.
205.1-205.35	EE-GG (probably FF) with ?CC.
213.9-214.15	EE-GG.
225.65-225.9	EE-GG.

Table 3-3.--Summary of foraminifer occurrences in OAK crater borehole OCT-5.

DEPTH (ft bsf)	FORAMINIFER DATA
0.2-0.45	Specimens from EE-GG, abundant AA, CC; some specimens from II-MM.
8.80-9.05	Mostly specimens from EE-GG, some from AA, some from KK-MM.
17.5-17.75	Some EE-GG, probably BB-CC, no AA.
39.50-39.75	AA and EE-GG with possibly CC and possibly deep zones.
57.55-57.8	Abundant AA and EE-GG.
66.8-67.05	Abundant AA, probable CC and definite EE-GG.
76.65-76.9	Mostly AA, some EE-GG.
86.15-86.4	All from CC-GG, no AA.
95.35-95.6	Same as above sample.
104.25-104.5	Very few specimens, but similar to above sample.
113.15-113.4	Few specimens, definite AA dominant, some from CC.
124.0-124.25	Abundant AA, sparse specimens probably from CC, possibly CC-GG.
132.8-133.05	Almost entirely AA, few specimens from CC or CC-GG.
140.9-141.15	Same as above sample.
149.65-149.9	Barren.
159.6-157.85	Only 1 specimen probably from CC, possibly from BB-GG.
166.4-166.65	Only 1 specimen, provenience uncertain.
176.25-176.5	Only 1 specimen, provenience uncertain, probably CC-GG.
186.0-186.25	Few specimens of CC-GG, probably CC.

Table 3-4.--Summary of foraminifer occurrences in OAK crater borehole OFT-9.

DEPTH (ft bsf)	FORAMINIFER DATA
0.0-0.25	Few specimens, definitely AA (but not uppermost AA), few specimens from EE-GG, scattered light-brown material with 1 immature specimen possibly from JJ-MM, not certain there is deep material.
8.75-9.00	More abundant AA (with more from uppermost AA), sparse specimens from CC, moderate amount from EE-GG, no brown material.
18.60-18.85	Abundant specimens from upper AA, few specimens probably from EE-GG.
27.90-28.15	All specimens from upper part of AA.
35.1-35.35	All specimens from upper part of AA.
43.1-43.35	All specimens from AA, probably slightly lower AA than two samples above.
48.85-49.1	All specimens from AA.
64.0-64.25	Mixture of older part of AA with few from EE-GG.
74.0-74.25	Appears to be unmixed BB-CC.

Table 3-5.--Summary of foraminifer occurrences in OAK crater borehole OKT-13.

DEPTH (ft bsf)	FORAMINIFER DATA
10.4-10.65	Mostly EE-GG, some from lower AA.
18.5-18.75	Mostly CC, some from EE-GG mixed with specimens from AA.
25.4-25.65	Specimens from ?CC mixed with few from EE-GG, more abundant AA than in above two samples
28.75-29.00	All from AA.
36.00-36.25	All from AA.
55.65-55.90	All apparently from CC-DD.
59.5-59.75	All probably from CC-DD.
68.2-68.45	All probably from EE-FF, possibly some CC-DD.
80.00-80.25	All from CC-GG.

Table 3-6.--Summary of foraminifer occurrences in OAK crater borehole OPZ-18.

DEPTH (ft bsf)	FORAMINIFER DATA
7.0-7.25	Mostly AA, with some CC and EE-GG mixed, has light-brown material but no diagnostic specimens.
35.0-35.25	Mostly AA, with some CC and EE-GG mixed, has more light-brown material than above sample but only one probable specimen from KK-MM.
44.6-44.85	AA, with some CC and more EE-GG than above, moderate amount of light-brown material but no diagnostic specimens.
57.85-58.1	More AA than above sample, with EE-GG common, moderate amount of light-brown material but no diagnostic specimens.
74.3-74.55	Mostly AA with some specimens from EE-GG, moderate amount of light-brown but no diagnostic specimens.
89.45-89.7	Mostly AA with some EE-GG, moderate amount of light-brown material with 1 specimen possibly from KK-LL.
102.0-102.25	Few specimens, some AA, some EE-GG, and moderate amount of light-brown material with one specimen questionably from LL-MM.
115.05-115.3	Few specimens, some AA, some EE-GG, moderate amount of light-brown material.
131.0-131.25	Few specimens, some AA, some EE-GG, 1 specimen possibly from KK-MM.
139.7-139.95	Some AA, some EE-GG, some light-brown material.
154.2-154.45	Some AA, some EE-GG, some light-brown material.
169.35-169.6	Some AA and some EE-GG, sparse light-brown material.
174.95-175.1	Some EE-GG, some probably AA, mostly uncertain.
182.3-182.55	Some AA, some EE-GG, very little light brown material.
189.25-189.5	All AA, apparently upper AA.
198.0-198.25	All AA, apparently upper AA.
207.3-207.55	All AA, apparently upper AA.
210.4-210.65	All recrystallized, but no markers??
229.95-230.2	No diagnostic species, most look like ?CC-GG, possibly few AA.
232.1-232.35	Mostly AA, probably upper A, except for 1 specimen from EE-GG.
239.15-239.4	Apparently all EE-GG, probably FF-GG.

APPENDIX 3-1

BOREHOLE OAR-2/ZA

DIAGNOSTIC SPECIES	0.25	2.3	6.0	9.3	11.85	14.5	17.1	20.8	22.75	23.75	26.05	31.9	34.75	40.2	43.55	62.5	74.8	90.4	95.8
1. <i>Australimoesella</i> sp.																		1	2
2. <i>Bythoceratina</i> sp.																			
3. <i>Callistocythere</i> sp. A								6	2	2				1		4	1		
4. <i>C. sp. B</i>		1	3			1	2	1										1	2
5. <i>Cardobairiia</i> sp.						3		1											
6. <i>Caudites</i> sp. A																			
7. <i>C. sp. B</i>																		2	2
8. <i>Cletocythereis</i> sp. A												1	1					1	2
9. <i>C. carolinulata</i>																		7	2
10. <i>C. rastromarginata</i>																			
11. <i>Cytherelloidea</i> sp.						4													
12. <i>Hemicythere</i> sp.																			4
13. <i>Hemicythere</i> sp.			1			1	1	1											
14. <i>Hemmites mooneyi</i>					10	4	9	11	2										
15. <i>H. parvifolia</i>			1		9	6		21							2			7	4
16. <i>H. transoceanica</i>			4		1	4	8	12	10	3	6		1				2	9	5
17. <i>Jugosocythereis</i> sp.					4	16	4	5	2	33	20						17	9	5
18. <i>Kejia dentata</i>																		2	3
19. <i>Loxocoche heronislankensis</i>												16	3	5					8
20. <i>L. huachinensis</i>	8	2	9	32	45	31	30	17	4	1	8	4		2		10	6	61	20
21. <i>L. insularienseis</i>														3	2			3	11
22. <i>L. labyrinthica</i>																		2	1
23. <i>L. n. sp. A</i>																			7
24. <i>Loxocoche</i> sp. A			2						2										
25. <i>L. sp. B</i>																			1
26. <i>L. sp. C</i>							1												3
27. <i>Mioeypridais</i> sp.																			
28. <i>Morbhovia inconspicua</i>										1									
29. <i>Neoesidea schulzi</i>	3		11	23	1	13	9	28	23	54		21					1	5	9
30. <i>Occultocythereis</i> sp.																			
31. <i>Orionina</i> sp.							1												
32. <i>Ornatoleberis</i> sp.																		14	5
33. <i>Paracytheriidea nemani</i>	2		4	6	5	5	9	3										1	
34. <i>Ponticythereis</i> sp.	1			1		3	3	1											10
35. <i>Procythereis</i> sp. A																			
36. <i>P. sp. B</i>																			
37. <i>Pterobatwita maddockae</i>																			
38. <i>Semicythereura</i> sp.						1													1
39. <i>Triebelina sertata</i>																			
40. Other	10	1	24	43	37	37	25	67	35	39	7	7	24	17	4	9	9	42	29
TOTAL	35	5	69	151	110	127	98	189	88	101	15	51	30	23	13	43	52	180	105

(continued on next page)

BOREHOLE OAR-2/ZA (continued)

DIAGNOSTIC SPECIES	115.1	127.8	134.0	157.45	171.2	188.25	195.3	204.9	212.45	223.9	234.6	244.55	246.8	268.45	282.55	289.7	337.05	379.5	TOTAL
1. <i>Australamoosella</i> sp.										1	1	2	9	2	3	1			25
2. <i>Rythoceratina</i> sp.																			1
3. <i>Calliothyra</i> sp. A																			16
4. <i>C.</i> sp. B	2			1				2	5	13		1		2					38
5. <i>Candohaimia</i> sp.													2						5
6. <i>Caudites</i> sp. A								1		2									8
7. <i>C.</i> sp. B												4	1						10
8. <i>Cleocythereis</i> sp. A							2			1									21
9. <i>C. canaliculata</i>											6	3							12
10. <i>C. rastromarginata</i>	1	1						5	1										9
11. <i>Cytherelloidea</i> sp.												1							4
12. <i>Hemicytherura</i> sp.										3									9
13. <i>Hemicythere</i> sp.			1					4											44
14. <i>Hemmarites mooneyi</i>														5					111
15. <i>H. parviflora</i>			9					16	2	23	1		5						142
16. <i>H. transoceanica</i>	5	8						4	1	14	3	10	13	7					218
17. <i>Jugocythereis</i> sp.	2	2	4	1				9	7	13	7	9	20	7					5
18. <i>Ketia demissa</i>																			36
19. <i>Loxocoche hemontalanaensis</i>		4																	27
20. <i>L. huahinensis</i>	1	18	30	37				82	34	51	8	31	12	15	10	24			679
21. <i>L. insulariensis</i>														3	2	4			4
22. <i>L. labrynthica</i>	2		5								6	5	6	6	3	2			46
23. <i>L. n. sp. A</i>														10	7	6			25
24. <i>Loxococheia</i> sp. A																			8
25. <i>L. sp. B</i>																			2
26. <i>L. sp. C</i>													1						12
27. <i>Miocypridae</i> sp.														2	4				1
28. <i>Morkhovenia inconspicua</i>																			21
29. <i>Neonestidea schulzi</i>	8		3	15	1			10	4	1	2	3							260
30. <i>Oculocythereis</i> sp.																			2
31. <i>Oriolina</i> sp.																			19
32. <i>Ornatobebis</i> sp.																			53
33. <i>Panocythereidea nemati</i>																			25
34. <i>Panocythereis</i> sp.																			1
35. <i>Procythereis</i> sp. A																			7
36. <i>P. sp. B</i>																			11
37. <i>Pterohaimia maddocensis</i>																			2
38. <i>Semicytherura</i> sp.																			19
39. <i>Trieheimia senkita</i>																			3
40. Other	12	14	9	18		1	6	23	230	125	196	73	117	111	116	54	80	1	88
TOTAL	33	42	76	76	1	6	23	230	125	196	73	117	111	116	54	80	1	88	2033

APPENDIX 3-2

BOREHOLE OOR-17

DIAGNOSTIC SPECIES	0.25	14.15	25.75	38.4	49.7	60.2	66.75	72.8	83.7	89.8	100.45	101.4	110.5	119.1	125.25	131.95	137.15	146.1	154.25	165.6	173.05
1. <i>Australimoesella</i> sp.	-	-	-	-	-	-	-	-	-	-	-	-	-	-	-	-	2	-	-	-	-
2. <i>Bythoceratina</i> sp.	-	-	-	-	-	-	-	-	-	-	-	-	-	-	-	-	-	-	-	-	-
3. <i>Callistocythere</i> sp. A	-	-	-	18	-	2	2	1	1	2	6	1	-	-	3	3	1	1	-	1	10
4. <i>C. sp. B</i>	-	-	-	-	-	-	-	-	-	-	-	-	-	-	-	-	-	-	-	-	-
5. <i>Cardobairdia</i> sp.	-	-	2	-	1	-	1	-	-	-	1	-	-	-	-	-	-	1	1	1	-
6. <i>Caudites</i> sp. A	-	-	-	-	-	-	-	-	-	-	-	-	-	-	-	-	-	-	-	-	-
7. <i>C. sp. B</i>	-	-	-	-	-	-	-	42	16	8	-	1	3	-	1	2	2	2	1	1	2
8. <i>Cleocythereis</i> sp. A	-	-	-	-	-	-	-	-	-	-	-	-	-	-	-	-	-	-	-	-	-
9. <i>C. canaliculata</i>	-	-	-	-	-	-	-	-	-	-	-	-	-	-	-	-	1	-	-	-	-
10. <i>C. rastromarginata</i>	-	-	-	-	-	-	-	-	-	-	-	-	-	-	-	-	-	-	-	-	-
11. <i>Cytherelloidea</i> sp.	-	-	1	-	-	-	-	-	-	-	-	-	-	-	-	-	-	-	-	-	1
12. <i>Hemicytherura</i> sp.	-	1	-	-	-	-	-	-	-	-	-	-	1	-	-	-	-	-	-	-	1
13. <i>Hemicythere</i> sp.	-	-	2	-	1	-	-	-	-	-	-	-	-	-	-	-	3	1	-	2	-
14. <i>Hermanites mooneyi</i>	-	2	2	3	2	17	19	-	-	-	-	-	-	-	2	1	6	1	2	-	-
15. <i>H. parviflora</i>	1	2	2	3	2	17	19	-	-	-	-	-	-	-	2	1	6	1	2	-	-
16. <i>H. transoceanica</i>	12	11	12	9	2	7	3	-	10	4	2	-	8	-	2	-	3	8	6	12	12
17. <i>Jugocythereis</i> sp.	8	2	1	-	2	7	18	-	-	-	-	-	1	-	3	-	8	-	6	10	11
18. <i>Ketia demissa</i>	-	-	-	-	-	-	-	-	-	-	-	-	-	-	-	-	-	1	1	1	1
19. <i>Loxocochia heroniana</i>	-	-	-	-	-	-	-	7	8	6	10	2	23	-	-	-	-	-	-	-	-
20. <i>L. huahimense</i>	30	10	34	9	24	6	9	-	2	1	-	-	2	-	8	-	24	12	6	1	-
21. <i>L. insulariense</i>	-	-	-	-	-	-	-	-	-	-	-	-	-	-	-	-	-	2	6	3	10
22. <i>L. labrynthica</i>	-	-	-	-	-	-	-	-	-	-	-	-	-	-	-	-	-	-	-	-	-
23. <i>L. n. sp. A</i>	4	-	-	1	1	-	-	-	-	-	-	-	-	-	-	-	-	-	-	-	-
24. <i>Loxocochella</i> sp. A	-	-	-	-	-	-	-	-	-	-	-	-	-	-	-	-	-	-	-	-	-
25. <i>L. sp. B</i>	-	-	-	-	-	-	-	-	-	-	-	-	-	-	-	-	-	-	-	-	-
26. <i>L. sp. C</i>	-	-	-	-	-	-	-	-	-	-	-	-	-	-	-	-	-	-	-	-	-
27. <i>Miocypridris</i> sp.	-	-	-	-	-	-	-	-	-	-	-	-	-	-	-	-	-	-	-	-	-
28. <i>Monchoventia inconspicua</i>	-	-	-	-	-	1	-	-	-	-	-	-	-	-	4	-	-	-	-	-	-
29. <i>Neonesidea schulzei</i>	45	32	41	32	12	32	39	3	2	-	-	-	2	-	-	1	7	2	12	29	17
30. <i>Oculocythereis</i> sp.	-	-	-	-	-	-	-	-	-	-	-	-	-	-	-	-	-	-	-	-	-
31. <i>Orionina</i> sp.	-	-	-	-	-	-	-	-	-	-	-	-	-	-	-	13	-	-	-	-	-
32. <i>Ornatoleberis</i> sp.	1	3	4	1	1	-	-	6	5	-	-	-	-	-	1	-	-	-	1	2	2
33. <i>Paracytheridea romani</i>	2	1	1	-	-	-	-	1	-	-	-	-	31	-	2	-	6	2	7	5	6
34. <i>Pontocythereis</i> sp.	-	-	-	-	-	-	-	-	-	-	-	-	-	-	-	1	-	-	-	-	-
35. <i>Procythereis</i> sp. A	-	-	-	-	-	-	-	-	-	-	-	-	-	-	-	-	-	-	-	-	-
36. <i>P. sp. B</i>	-	-	-	-	-	-	-	-	-	-	-	-	-	-	-	-	-	-	-	-	-
37. <i>Pterohamitia madlockana</i>	-	-	1	-	-	-	-	-	-	-	-	-	-	-	-	-	-	-	-	-	-
38. <i>Semicytherura</i> sp.	-	-	-	1	-	-	-	-	-	-	-	-	-	-	-	-	2	1	1	-	1
39. <i>Triebelina serrata</i>	-	1	-	-	1	-	-	-	-	-	-	-	-	-	-	-	-	-	-	-	-
40. Other	72	31	75	48	28	53	36	18	55	28	4	1	4	-	13	6	68	51	51	52	45
TOTAL	175	94	176	122	75	125	127	78	99	49	24	5	75	-	57	33	168	98	125	137	141

(continued on next page)

BOREHOLE OOR-17 (continued)

DIAGNOSTIC SPECIES	184.25	193.6	200.9	209.3	215.5	226.05	233.35	239.0	250.3	261.5	270.1	285.65	292.1	299.15	310.7	320.2	331.2	339.0	367.9	TOTAL
	SAMPLE DEPTH (ft bsf)																			
1. <i>Australimorcella</i> sp.	-	-	-	-	-	-	1	-	-	-	-	-	-	-	-	-	3	2	0	14
2. <i>Bythoseratina</i> sp.	-	-	-	-	-	-	-	-	-	-	1	-	-	-	-	-	-	-	-	1
3. <i>Callistocythere</i> sp. A	5	-	-	-	-	-	-	-	-	-	-	-	-	-	-	-	-	-	-	47
4. <i>C.</i> sp. B	-	-	-	-	-	1	2	-	1	-	-	-	-	1	-	-	-	-	-	25
5. <i>Cardobairmia</i> sp.	-	-	-	-	-	-	4	1	-	-	1	1	-	-	-	-	-	-	-	5
6. <i>Caudites</i> sp. A	-	-	-	-	-	-	-	-	-	-	4	-	-	-	-	-	-	-	-	11
7. <i>C.</i> sp. B	-	-	-	-	-	-	-	-	-	-	4	-	-	-	-	-	-	-	-	5
8. <i>Cletocythereis</i> sp. A	-	-	1	6	1	3	6	3	3	13	-	-	-	1	-	-	1	2	-	113
9. <i>C. canaliculata</i>	-	-	-	-	-	-	1	-	-	-	-	-	-	-	-	-	-	-	-	7
10. <i>C. rastromarginata</i>	2	-	1	1	-	-	3	-	-	-	-	-	-	-	-	-	-	-	-	7
11. <i>Cytherelloidea</i> sp.	-	-	-	-	-	-	-	-	-	-	1	-	-	-	-	-	-	-	-	2
12. <i>Hemicytherura</i> sp.	-	-	-	-	-	-	-	-	-	-	-	-	-	-	-	-	-	-	-	5
13. <i>Hemicythere</i> sp.	-	1	1	-	-	-	-	-	-	-	-	-	-	-	-	-	-	-	-	4
14. <i>Hemantides mooneyi</i>	-	-	-	-	-	-	-	-	-	-	-	-	-	-	-	-	-	-	-	9
15. <i>H. parviflora</i>	-	1	1	5	-	-	-	-	-	-	-	9	-	4	-	-	-	-	-	87
16. <i>H. transoceanica</i>	8	1	9	2	4	-	2	-	1	7	4	4	1	4	-	-	-	-	1	177
17. <i>Jugocythereis</i> sp.	11	-	6	4	2	-	-	-	-	-	1	1	2	2	1	1	7	2	-	117
18. <i>Katja demissa</i>	-	-	-	-	-	-	-	-	-	-	-	-	-	-	-	-	-	-	-	4
19. <i>Loxocoche heronielandensis</i>	3	-	-	-	-	-	-	-	-	-	-	-	1	-	-	-	-	-	-	60
20. <i>L. huahinensis</i>	-	3	35	25	14	7	62	-	1	16	31	12	26	1	-	3	3	1	475	
21. <i>L. theulariaensis</i>	-	-	-	-	-	3	3	5	-	5	3	2	2	-	-	2	-	-	-	79
22. <i>L. Labrynthica</i>	3	-	11	3	-	-	7	-	1	-	-	-	-	-	-	-	-	-	-	46
23. <i>L. n. sp. A</i>	-	-	-	-	-	-	-	-	-	-	-	-	-	-	-	-	-	-	2	4
24. <i>Loxococheilla</i> sp. A	-	-	-	-	-	-	-	-	-	-	1	-	-	-	-	-	-	-	-	7
25. <i>L. sp. B</i>	-	-	-	-	-	-	4	-	-	-	3	-	-	-	-	-	-	-	-	8
26. <i>L. sp. C</i>	-	-	-	-	-	-	-	-	-	-	-	5	-	-	-	-	-	-	-	6
27. <i>Miocypridea</i> sp.	-	-	-	-	-	-	-	-	-	-	-	-	-	-	-	-	-	-	-	-
28. <i>Morikovenia inconspicua</i>	-	1	-	-	2	2	2	-	-	-	-	-	3	-	-	-	-	-	-	13
29. <i>Reonaidia schulzei</i>	1	-	5	2	2	2	9	1	-	3	3	-	3	-	-	-	-	-	-	336
30. <i>Occultocythereis</i> sp.	-	-	-	-	-	-	-	-	-	-	-	-	-	-	-	-	-	-	-	-
31. <i>Orionina</i> sp.	-	-	-	-	-	-	-	-	-	-	-	-	-	-	-	-	-	-	-	13
32. <i>Omatoleberis</i> sp.	-	-	6	-	-	-	1	-	-	1	4	-	-	-	-	-	-	-	-	39
33. <i>Paracytheridea nemani</i>	-	-	-	-	-	1	2	-	-	8	2	-	-	-	-	-	-	-	2	79
34. <i>Pontocythereis</i> sp.	-	-	-	-	-	-	-	-	-	-	-	-	-	-	-	-	-	-	-	1
35. <i>Procythereis</i> sp. A	-	-	-	-	-	-	-	-	-	-	-	-	3	2	1	-	-	-	-	7
36. <i>P. sp. B</i>	-	-	-	-	-	-	-	-	-	-	-	-	-	-	-	-	-	-	-	1
37. <i>Pterohatmia madlockeae</i>	-	-	-	-	-	-	-	-	-	-	-	-	-	-	-	-	-	-	-	1
38. <i>Semicytherura</i> sp.	-	-	-	-	-	-	3	-	-	-	-	-	-	-	-	-	-	-	-	10
39. <i>Trieblina serrata</i>	-	-	-	-	-	-	-	-	-	-	-	-	-	-	-	-	-	-	-	5
40. Other	5	-	2	12	12	-	17	1	2	-	24	47	12	38	-	-	-	1	1	913
TOTAL	40	6	88	60	41	17	131	3	9	1	89	112	39	83	3	1	17	12	8	2743

APPENDIX 3-3

BOREHOLE OBZ-4

DIAGNOSTIC SPECIES	0.0	2.8	11.8	21.1	33.0	40.05	49.7	58.5	66.35	75.15	84.15	93.1	104.55	112.9	121.8	130.0	144.5	147.75	151.55	160.05
1. <i>Australimooeella</i> sp.	-	-	-	2	-	1	1	2	1	-	2	-	-	-	1	-	-	-	-	-
2. <i>Bythoeseratina</i> sp.	-	-	-	1	-	-	-	-	-	-	1	-	-	-	-	-	-	-	-	-
3. <i>Callistocythere</i> sp. A	7	-	-	1	-	-	-	-	-	-	1	-	-	-	-	-	-	-	-	-
4. <i>C. sp. B</i>	1	-	-	-	4	-	1	-	1	-	2	1	-	-	-	-	-	-	1	-
5. <i>Cardobairdia</i> sp.	-	-	-	-	-	-	-	-	-	-	-	-	-	-	-	-	-	-	-	-
6. <i>Caudites</i> sp. A	-	-	-	-	-	-	-	-	-	-	-	-	-	-	-	-	-	-	-	-
7. <i>C. sp. B</i>	-	-	-	-	-	-	-	-	-	-	-	-	-	-	2	-	-	-	-	-
8. <i>Cletoocythereis</i> sp. A	-	-	3	1	-	7	3	3	-	-	2	1	-	-	1	-	-	-	-	-
9. <i>C. canaliculata</i>	-	-	-	-	-	2	-	-	-	-	-	-	-	-	-	-	-	-	-	-
10. <i>C. rastrovarghathi</i>	-	-	-	-	-	-	-	-	-	-	-	-	-	-	-	-	-	-	-	-
11. <i>Cytherelloidea</i> sp.	1	-	-	-	-	1	1	-	-	-	-	-	-	-	-	-	-	-	-	-
12. <i>Hemicytherura</i> sp.	-	-	-	-	-	2	3	-	-	-	-	-	-	-	-	-	-	-	-	-
13. <i>Hemicythere</i> sp.	-	-	1	-	2	2	-	-	-	1	1	-	-	-	-	-	-	-	-	-
14. <i>Hermanites mooneyi</i>	3	-	1	3	2	-	1	-	1	2	-	-	-	-	2	-	-	-	-	-
15. <i>H. parviflora</i>	5	-	10	2	2	-	-	-	1	7	-	-	-	-	10	3	-	-	3	-
16. <i>H. transoceanica</i>	8	-	8	2	-	25	5	8	-	2	3	2	-	1	11	1	-	-	2	-
17. <i>Jugocythereis</i> sp.	7	3	1	7	6	11	12	4	-	3	10	1	2	1	9	-	-	-	4	2
18. <i>Ketia demissa</i>	-	-	-	-	1	-	-	-	-	-	1	-	-	-	1	-	-	-	-	-
19. <i>Loxocoche heronislansensis</i>	-	-	-	1	2	4	8	11	6	-	3	4	3	2	1	-	-	-	1	-
20. <i>L. huahinensis</i>	18	9	11	27	25	24	26	5	3	9	31	8	3	4	22	2	6	13	6	2
21. <i>L. inaulandensis</i>	5	-	5	2	7	7	5	1	1	1	4	1	-	-	6	-	-	-	1	1
22. <i>L. labrynthica</i>	-	-	-	6	1	2	3	1	1	-	3	2	-	-	2	-	-	-	1	-
23. <i>L. n. sp. A</i>	-	-	-	-	-	-	-	-	-	-	-	-	-	-	-	-	-	-	-	-
24. <i>Loxococheella</i> sp. A	-	-	-	1	-	-	-	-	-	-	-	-	-	-	-	-	-	-	-	-
25. <i>L. sp. B</i>	-	-	-	-	-	-	-	-	-	-	-	-	-	-	-	-	-	-	-	-
26. <i>L. sp. C</i>	5	-	2	1	14	-	-	-	-	-	-	-	-	-	-	-	-	-	-	-
27. <i>Miocypridea</i> sp.	-	-	-	-	-	3	4	-	-	-	-	-	-	-	-	-	-	-	-	-
28. <i>Mo-Khoueria inconspicua</i>	1	1	-	-	3	3	1	-	-	-	3	-	2	-	-	-	-	-	-	-
29. <i>Neonesidea schulzi</i>	33	2	8	2	61	-	13	7	4	5	11	1	-	-	-	-	-	-	3	1
30. <i>Oculocythereis</i> sp.	-	-	-	-	1	-	-	-	-	-	-	-	-	-	-	-	-	-	-	-
31. <i>Oriolina</i> sp.	-	-	-	-	-	3	1	-	-	-	1	1	-	-	2	-	-	-	1	-
32. <i>Ornatolabris</i> sp.	4	-	1	-	-	1	3	-	-	-	2	2	-	-	-	-	-	-	1	-
33. <i>Paracytheridea remani</i>	2	-	-	3	3	6	3	-	-	2	2	-	-	-	8	2	1	-	-	-
34. <i>Pontocythereis</i> sp.	-	-	-	-	-	-	-	-	-	-	-	-	-	-	-	-	-	-	-	-
35. <i>Procythereis</i> sp. A	-	-	-	1	-	2	1	-	-	-	-	-	-	1	-	-	-	-	-	-
36. <i>P. sp. B</i>	-	-	-	-	-	1	2	-	-	-	-	-	-	-	-	-	-	-	-	-
37. <i>Pterobairdia maddockae</i>	-	-	-	-	-	-	-	-	-	-	-	-	-	-	-	-	-	-	-	-
38. <i>Semicytherura</i> sp.	-	-	1	1	1	2	1	-	-	1	1	-	-	-	4	-	-	-	-	-
39. <i>Triebelina serrata</i>	-	-	-	-	-	-	-	-	-	-	-	-	-	-	-	-	-	-	-	-
40. Other	88	10	23	27	171	47	23	14	13	7	44	17	8	4	37	8	6	12	-	2
41. "Piped" specimens	-	-	-	3	1	9	7	1	-	-	2	-	1	1	13	-	-	-	-	1
TOTAL	188	32	70	93	336	147	134	44	26	37	140	40	26	13	133	19	21	37	19	8

(continued on next page)

BOREHOLE OBZ-4 (continued)

DIAGNOSTIC SPECIES	166.85	169.85	178.6	182.35	186.8	190.3	193.6	196.5	205.1	213.9	225.65	250.05	291.45	300.5	314.75	327.1	336.25	347.15	356.45	TOTAL
1. <i>Australimoesella</i> sp.	-	-	-	4	1	1	-	-	-	-	-	1	-	-	-	-	-	2	1	21
2. <i>Rythoceratina</i> sp.	-	-	-	-	-	-	-	-	1	1	-	-	-	-	-	-	-	-	-	4
3. <i>Callistocythere</i> sp. A	-	-	-	-	-	-	-	9	6	1	-	-	-	-	-	-	-	1	-	27
4. <i>C.</i> sp. B	-	-	1	-	-	-	-	-	-	-	-	-	-	-	-	-	-	1	-	17
5. <i>Cardobairdia</i> sp.	-	-	-	-	-	-	-	-	-	-	-	-	-	-	-	-	-	1	-	1
6. <i>Caudites</i> sp. A	-	-	-	-	-	-	-	2	-	1	-	-	-	-	-	-	-	-	-	8
7. <i>C.</i> sp. B	-	-	-	-	-	-	-	-	-	-	-	-	-	-	-	-	-	-	-	3
8. <i>Cleocythereis</i> sp. A	1	-	1	-	-	-	-	6	-	-	-	2	-	-	-	-	-	1	-	35
9. <i>C. canaliculata</i>	-	-	-	-	-	-	-	-	-	-	-	-	-	-	-	-	-	-	-	3
10. <i>C. wastromarginata</i>	-	-	-	-	2	-	-	-	-	-	-	-	-	-	-	-	-	-	-	2
11. <i>Cytherelloidea</i> sp.	-	-	-	-	-	-	-	1	-	-	-	-	-	-	-	-	-	-	-	6
12. <i>Hemicytherura</i> sp.	-	-	-	-	-	-	-	-	-	-	-	-	-	-	-	-	-	-	-	-
13. <i>Hemicythere</i> sp.	-	-	-	-	-	-	-	-	-	-	-	-	-	-	-	-	-	-	-	10
14. <i>Hemaritis mooneyi</i>	-	-	-	-	-	-	-	-	-	-	-	-	-	-	-	-	-	-	-	15
15. <i>H. parviflora</i>	1	-	1	7	5	-	1	6	3	-	1	-	-	-	-	-	-	2	1	78
16. <i>H. transoceanica</i>	-	-	-	2	-	3	-	4	1	-	-	-	-	1	-	-	-	-	-	82
17. <i>Juposoocythereis</i> sp.	-	1	3	6	4	-	2	17	22	2	8	2	3	-	1	2	-	-	-	158
18. <i>Ketia lemisa</i>	-	-	-	-	-	-	-	-	-	-	-	-	-	-	-	-	-	-	-	5
19. <i>Loxocochia heronislaniensis</i>	1	2	-	-	1	-	-	-	-	-	-	-	-	-	-	-	-	7	-	57
20. <i>L. huahinensis</i>	2	7	4	17	6	5	4	27	12	14	4	2	-	1	-	3	-	1	-	363
21. <i>L. inaulaensis</i>	-	-	1	4	1	1	2	11	13	1	1	1	1	-	-	-	-	1	-	88
22. <i>L. labrynthica</i>	-	1	1	2	1	-	-	7	4	-	1	-	-	-	-	-	-	-	-	40
23. <i>L. n. sp. A</i>	-	-	-	-	-	-	-	-	-	-	-	-	-	-	-	-	-	-	-	-
24. <i>Loxocochella</i> sp. A	-	-	-	-	-	-	-	-	-	-	-	-	-	-	-	-	-	-	-	1
25. <i>L. sp. B</i>	-	-	-	-	-	-	-	-	-	-	-	-	-	-	-	-	-	-	-	-
26. <i>L. sp. C</i>	-	-	-	1	-	-	-	-	-	-	-	-	-	-	-	-	-	-	-	23
27. <i>Miocyprideis</i> sp.	-	-	-	-	-	-	-	-	-	-	-	-	-	-	-	-	-	-	-	8
28. <i>Monkhoumella inconspicua</i>	-	-	-	2	-	-	-	-	-	-	-	1	-	-	-	-	-	-	-	17
29. <i>Neoneisida schulzei</i>	-	3	1	5	3	-	-	7	4	2	1	-	-	1	-	-	-	2	-	180
30. <i>Oculocythereis</i> sp.	-	-	-	-	-	-	-	-	-	-	-	-	-	-	-	-	-	-	-	-
31. <i>Orionina</i> sp.	-	-	-	-	-	-	-	22	14	-	-	-	-	-	-	-	-	-	-	46
32. <i>Ornatoleberis</i> sp.	-	-	-	-	-	-	-	4	-	-	-	-	-	-	-	-	-	3	-	23
33. <i>Paracytheridea remani</i>	-	1	-	1	2	-	1	-	-	-	-	-	-	1	-	-	-	-	1	39
34. <i>Pontocythereis</i> sp.	-	-	-	-	-	-	-	-	-	-	-	-	-	-	-	-	-	-	-	-
35. <i>Procythereis</i> sp. A	-	-	-	-	-	-	-	-	-	-	-	-	-	-	-	-	-	-	-	9
36. <i>P. sp. B</i>	-	-	-	-	-	-	-	-	-	-	-	-	-	-	-	-	-	-	-	6
37. <i>Pterobairdia madidochana</i>	-	-	-	-	-	-	-	1	-	-	-	-	-	-	-	-	-	-	-	1
38. <i>Semicythemum</i> sp.	-	-	-	-	-	-	-	-	-	1	-	-	-	-	-	-	-	-	-	15
39. <i>Trieblina serrata</i>	-	-	-	-	-	-	-	-	-	-	-	-	-	-	-	-	-	-	-	-
40. Other	8	5	5	25	13	9	7	51	23	5	5	5	2	-	2	5	2	11	3	747
41. "piped" specimens	-	-	-	1	-	-	-	-	-	-	-	-	-	-	-	-	-	-	-	41
TOTAL	13	21	19	77	41	19	18	175	103	28	21	15	6	3	3	14	2	32	7	2180

APPENDIX 3-4

BOREHOLE OPZ-18

DIAGNOSTIC SPECIES	7.0	35.0	44.6	57.85	74.3	89.45	102.0	115.05	131.0	139.7	154.2	169.35	174.95	182.3	189.25	198.0	207.3	210.4	229.95	232.1	239.15	TOTAL	
1. <i>Australimossella</i> sp.	1	4	1	1	1	1	1	1	1	1	1	1	1	1	1	1	1	1	1	1	1	1	12
2. <i>Bythoceratina</i> sp.	1	1	1	1	1	1	1	1	1	1	1	1	1	1	1	1	1	1	1	1	1	1	4
3. <i>Callistocythere</i> sp. A	1	1	1	1	1	1	1	1	1	1	1	1	1	1	1	1	1	1	1	1	1	1	5
4. <i>C. sp. B</i>	1	2	1	1	2	1	2	1	1	1	2	2	2	2	1	4	4	4	1	1	2	2	26
5. <i>Cardobairiia</i> sp.	1	1	1	1	1	1	1	1	1	1	1	1	1	1	1	1	1	1	1	1	1	1	11
6. <i>Caudites</i> sp. A	1	1	1	1	1	1	1	1	1	1	1	1	1	1	1	1	1	1	1	1	1	1	11
7. <i>C. sp. B</i>	1	1	1	1	1	1	1	1	1	1	1	1	1	1	1	1	1	1	1	1	1	1	11
8. <i>Cleocythereis</i> sp. A	3	14	2	2	1	1	2	1	1	1	1	1	1	1	1	1	1	1	1	1	1	1	23
9. <i>C. canaliculata</i>	1	2	1	1	1	1	1	1	1	1	1	1	1	1	1	1	1	1	1	1	1	1	5
10. <i>C. rastromarginata</i>	1	1	1	1	1	1	1	1	1	1	1	1	1	1	1	1	1	1	1	1	1	1	5
11. <i>Cytherelloidea</i> sp.	1	1	1	1	1	1	1	1	1	1	1	1	1	1	1	1	1	1	1	1	1	1	4
12. <i>Hemicytherura</i> sp.	2	2	1	1	1	1	1	1	1	1	1	1	1	1	1	1	1	1	1	1	1	1	9
13. <i>Hemicythere</i> sp.	1	6	1	1	1	1	1	1	1	1	1	1	1	1	1	1	1	1	1	1	1	1	43
14. <i>Hemartites mooneyi</i>	1	8	10	5	1	1	1	1	3	2	5	2	3	4	5	22	3	1	1	3	3	3	75
15. <i>H. parviflora</i>	8	18	10	5	1	1	1	1	3	2	5	2	3	4	5	22	3	1	1	3	3	3	75
16. <i>H. transoceanica</i>	16	11	8	1	1	1	2	1	2	1	3	3	3	3	14	28	8	2	2	5	6	6	110
17. <i>Jugosocythereis</i> sp.	8	17	11	5	4	1	1	3	11	1	7	7	7	11	6	2	11	1	1	9	5	5	111
18. <i>Keifia demissa</i>	1	1	1	1	1	1	1	1	1	1	1	1	1	1	1	1	1	1	1	1	1	1	6
19. <i>Loxocncha hemoniaLandensis</i>	4	3	8	1	1	1	1	6	1	1	2	2	4	2	1	1	1	1	1	1	1	1	35
20. <i>L. huahinensis</i>	29	82	17	13	7	4	7	11	5	19	23	13	17	33	72	40	3	5	34	13	13	447	447
21. <i>L. insulariense</i>	6	16	3	1	2	1	1	3	4	4	2	2	2	4	1	1	1	1	1	1	2	2	52
22. <i>L. labrynthica</i>	4	4	2	1	1	1	1	1	2	1	1	1	1	1	1	1	1	1	1	1	1	1	20
23. <i>L. n. sp. A</i>	2	3	1	1	1	1	1	1	1	1	1	1	1	1	1	1	1	1	1	1	1	1	8
24. <i>Loxocnchella</i> sp. A	1	1	1	1	1	1	1	1	1	1	1	1	1	1	1	1	1	1	1	1	1	1	8
25. <i>L. sp. B</i>	1	1	1	1	1	1	1	1	1	1	1	1	1	1	1	1	1	1	1	1	1	1	8
26. <i>L. sp. C</i>	7	1	1	1	1	1	1	1	1	1	1	1	1	1	1	1	1	1	1	1	1	1	9
27. <i>Miocyprideis</i> sp.	1	1	1	1	1	1	1	1	1	1	1	1	1	1	1	1	1	1	1	1	1	1	15
28. <i>Morkhouenia inconspicua</i>	1	2	1	1	1	1	1	1	1	1	2	2	1	1	2	1	1	1	1	1	1	1	15
29. <i>Neosetidea echulai</i>	41	19	1	1	6	1	3	3	1	1	1	1	1	1	1	6	4	1	1	5	1	1	85
30. <i>Oculocythereis</i> sp.	1	1	1	1	1	1	1	1	1	1	1	1	1	1	1	1	1	1	1	1	1	1	1
31. <i>Ontonina</i> sp.	1	1	1	1	1	1	1	1	1	1	1	1	1	1	1	1	1	1	1	1	1	1	3
32. <i>Omatoleberis</i> sp.	3	7	1	1	1	1	1	1	1	1	1	1	1	1	6	9	2	1	1	1	1	1	32
33. <i>Paracytheroidea remazi</i>	1	22	5	2	2	1	1	1	1	2	10	9	1	3	6	27	5	1	1	2	8	107	107
34. <i>Pontocythereis</i> sp.	1	1	1	1	1	1	1	1	1	1	1	1	1	1	1	1	1	1	1	1	1	1	1
35. <i>Proocythereis</i> sp. A	1	1	1	1	1	1	1	1	1	1	1	1	1	1	1	1	1	1	1	1	1	1	1
36. <i>P. sp. B</i>	1	1	1	1	1	1	1	1	1	1	1	1	1	1	1	1	1	1	1	1	1	1	2
37. <i>Pterobairiia madidockense</i>	1	1	1	1	1	1	1	1	1	1	1	1	1	1	1	1	1	1	1	1	1	1	1
38. <i>Semicytherura</i> sp.	1	4	2	1	1	1	1	1	1	1	4	1	1	2	1	1	1	1	1	1	1	1	19
39. <i>Trieblina serrata</i>	58	73	26	11	10	12	5	17	29	8	17	19	14	13	20	26	15	8	3	41	22	447	447
40. Other	2	19	8	4	3	2	2	1	8	3	2	6	1	1	1	1	1	1	1	1	1	1	60
41. "piped" specimens	202	343	107	49	40	22	21	35	76	22	74	78	53	65	92	205	95	16	17	106	70	1788	1788

APPENDIX 3-5

BOREHOLE OCT-5

DIAGNOSTIC SPECIES	0.2	8.8	17.5	39.5	48.05	57.55	66.8	76.65	86.15	95.35	104.25	113.15	124.0	132.8	140.9	149.65	157.6	166.4	176.25	186.0	TOTAL		
1. <i>Australimoesella</i> sp.																						1	
2. <i>Bythoceratina</i> sp.																							4
3. <i>Callistocythere</i> sp. A																							2
4. <i>C. sp. B</i>																							1
5. <i>Cardobairmia</i> sp.																							1
6. <i>Caudites</i> sp. A																							3
7. <i>C. sp. B</i>																							6
8. <i>Cletocythereis</i> sp. A																							1
9. <i>C. canaliculata</i>																							1
10. <i>C. mastromarginata</i>																							1
11. <i>Cythereilloidea</i> sp.																							5
12. <i>Hemicytherura</i> sp.																							2
13. <i>Hemicythere</i> sp.																							6
14. <i>Hermanites mooneyi</i>																							17
15. <i>H. parvuloba</i>																							28
16. <i>H. transoceanica</i>																							2
17. <i>Jugocythereis</i> sp.																							6
18. <i>Keijia damiaa</i>																							2
19. <i>Loxocncha hemerislandensis</i>																							6
20. <i>L. huahinesis</i>																							61
21. <i>L. insulariensis</i>																							11
22. <i>L. labrynthica</i>																							4
23. <i>L. n. sp. A</i>																							1
24. <i>Loxocnchella</i> sp. A																							1
25. <i>L. sp. B</i>																							1
26. <i>L. sp. C</i>																							1
27. <i>Miocypridae</i> sp.																							5
28. <i>Morbouvenia inconspicua</i>																							11
29. <i>Neomesstia schulzi</i>																							1
30. <i>Oeculocythereis</i> sp.																							1
31. <i>Omionia</i> sp.																							1
32. <i>Omatoleberis</i> sp.																							1
33. <i>Paracytheridea nemani</i>																							13
34. <i>Pontocythereis</i> sp.																							2
35. <i>Procythereis</i> sp. A																							2
36. <i>P. sp. B</i>																							3
37. <i>Pterobairmia madloctana</i>																							3
38. <i>Semicytherura</i> sp.																							3
39. <i>Tyebelina nemata</i>																							88
40. Other																							1
41. "Piped" specimens																							1
TOTAL	170	2	8	4	1	55	1	10	1	3	1	7	4	3	8	5	1	3	6	1	1	292	

APPENDIX 3-6
BOREHOLE OFT-8

DIAGNOSTIC SPECIES	SAMPLE DEPTH (ft bsf)									TOTAL
	0.0	8.75	18.6	27.9	35.1	43.1	48.85	64.0	74.0	
1. <i>Australimoosella</i> sp.	-	-	-	-	-	-	-	-	-	-
2. <i>Bythoceratina</i> sp.	-	-	-	-	-	-	-	-	-	-
3. <i>Callistocythere</i> sp. A	-	-	-	-	-	1	-	1	-	2
4. <i>C.</i> sp. B	-	-	-	-	-	-	-	-	-	-
5. <i>Cardohairdia</i> sp.	-	-	-	1	-	-	-	-	-	1
6. <i>Caudites</i> sp. A	-	1	-	-	-	-	-	-	-	1
7. <i>C.</i> sp. B	-	-	-	-	-	-	-	-	-	-
8. <i>Cletocythereis</i> sp. A	-	-	1	-	-	-	-	1	-	2
9. <i>C. canaliculata</i>	-	-	-	-	-	-	-	-	-	-
10. <i>C. rastrmarginata</i>	-	-	-	-	-	-	-	-	-	-
11. <i>Cytherelloidea</i> sp.	-	-	-	-	-	-	-	-	-	-
12. <i>Hemicytherura</i> sp.	-	-	-	-	-	-	-	-	-	-
13. <i>Hemicythere</i> sp.	-	1	-	-	-	-	-	-	-	1
14. <i>Hermanites mooneyi</i>	-	-	-	1	1	-	-	-	-	2
15. <i>H. parviloba</i>	1	-	-	-	-	-	-	-	-	1
16. <i>H. transoceanica</i>	-	-	-	3	4	-	-	-	-	7
17. <i>Jugosocythereis</i> sp.	-	1	-	-	-	8	-	4	-	13
18. <i>Keijia demissa</i>	-	-	-	-	-	-	-	-	-	-
19. <i>Loxoconcha heronislandensis</i>	-	2	-	-	-	-	-	2	-	4
20. <i>L. huahinensis</i>	1	4	1	5	3	3	1	9	1	28
21. <i>L. insularaensis</i>	-	1	-	-	-	-	-	1	-	2
22. <i>L. labyrinthica</i>	-	-	-	-	-	-	-	-	-	-
23. <i>L. n.</i> sp. A	-	-	-	-	-	-	-	-	-	-
24. <i>Loxoconchella</i> sp. A	-	-	-	-	-	-	-	-	-	-
25. <i>L.</i> sp. B	-	-	-	-	-	-	-	-	-	-
26. <i>L.</i> sp. C	-	-	-	-	-	-	-	-	-	-
27. <i>Miocyprideis</i> sp.	-	-	-	-	-	-	-	-	-	-
28. <i>Morkhovenia inconspicua</i>	-	-	-	-	-	-	-	-	-	-
29. <i>Neonesidea schulzi</i>	-	2	-	-	-	1	-	1	-	4
30. <i>Occultocythereis</i> sp.	-	-	-	-	-	-	-	-	-	-
31. <i>Orionina</i> sp.	-	-	-	-	-	-	-	-	-	-
32. <i>Ornatoleberis</i> sp.	-	1	-	3	-	-	-	-	-	4
33. <i>Paracytheridea nemani</i>	-	1	-	2	1	1	-	-	-	5
34. <i>Ponticythereis</i> sp.	-	-	-	-	-	-	-	-	-	-
35. <i>Procythereis</i> sp. A	-	-	-	-	-	-	-	-	-	-
36. <i>P.</i> sp. B	-	-	-	-	-	-	-	-	-	-
37. <i>Pterohairdia maddocksaе</i>	-	-	-	-	-	-	-	-	-	-
38. <i>Semicytherura</i> sp.	-	-	-	-	-	-	-	-	-	-
39. <i>Triebelina sertata</i>	-	-	-	-	-	-	-	-	-	-
40. Other	7	7	2	6	4	4	-	10	-	40
41. "Piped" specimens	1	-	-	-	-	-	-	-	-	1
TOTAL	10	21	4	21	13	18	1	29	1	118

APPENDIX 3-7
BOREHOLE OKT-13

DIAGNOSTIC SPECIES	SAMPLE DEPTH (ft bsf)									TOTAL
	10.4	18.5	25.4	28.75	36.0	55.65	59.9	68.2	80.0	
1. <i>Australimoosella</i> sp.	-	1	-	-	-	-	-	-	-	1
2. <i>Bythoceratina</i> sp.	-	1	-	-	-	-	-	-	-	1
3. <i>Callistocythere</i> sp. A	-	-	-	-	-	-	13	-	3	16
4. <i>C.</i> sp. B	3	2	-	-	-	-	-	-	-	5
5. <i>Carlobairdia</i> sp.	-	-	-	-	-	-	-	-	-	-
6. <i>Caudites</i> sp. A	1	-	-	-	-	-	-	-	-	1
7. <i>C.</i> sp. B	-	-	-	-	-	2	-	-	-	2
8. <i>Cletocythereis</i> sp. A	2	2	2	-	-	2	-	3	3	14
9. <i>C. canaliculata</i>	-	-	-	-	-	-	-	-	-	-
10. <i>C. rastromarginata</i>	-	-	-	-	-	-	-	-	-	-
11. <i>Cytherelloidea</i> sp.	-	1	-	-	-	-	-	-	-	1
12. <i>Hemicytherura</i> sp.	-	-	-	-	-	-	-	-	-	-
13. <i>Hemicythere</i> sp.	-	-	-	-	-	-	-	1	-	1
14. <i>Hermanites mooneyi</i>	-	-	4	5	2	-	-	-	-	11
15. <i>H. parviflora</i>	2	1	3	8	3	1	-	1	-	19
16. <i>H. transoceanica</i>	3	3	5	6	3	1	5	3	4	33
17. <i>Jugosocythereis</i> sp.	5	7	1	-	3	-	12	3	11	42
18. <i>Keijia demissa</i>	-	1	-	-	-	1	-	-	-	2
19. <i>Lorococoncha heronislaniensis</i>	2	2	-	-	-	-	-	-	-	4
20. <i>L. huahinensis</i>	11	19	17	19	11	12	3	8	12	112
21. <i>L. insulandaensis</i>	-	1	-	-	-	-	2	2	4	9
22. <i>L. labrynthica</i>	-	-	4	-	-	-	2	2	3	11
23. <i>L. n.</i> sp. A	-	-	-	-	-	-	-	-	-	-
24. <i>Loxococonchella</i> sp. A	-	-	1	3	-	-	-	-	-	4
25. <i>L.</i> sp. B	-	-	-	-	-	-	-	-	-	-
26. <i>L.</i> sp. C	1	-	-	-	-	-	-	-	-	1
27. <i>Miocyprideis</i> sp.	-	-	-	-	-	-	-	-	-	-
28. <i>Morkhovenia inconspicua</i>	-	-	-	-	-	-	-	1	-	1
29. <i>Neonesidea schulzei</i>	1	3	1	15	8	1	1	2	-	42
30. <i>Occultocythereis</i> sp.	-	-	-	-	-	-	-	-	-	-
31. <i>Onionina</i> sp.	-	-	1	-	-	-	12	-	1	14
32. <i>Ornatoleberis</i> sp.	-	1	1	1	5	-	-	-	-	8
33. <i>Paracytheridea nemani</i>	4	6	5	-	2	8	1	3	-	29
34. <i>Ponticythereis</i> sp.	-	-	-	-	-	-	-	-	-	-
35. <i>Procythereis</i> sp. A	-	-	-	-	-	-	-	-	-	-
36. <i>P.</i> sp. B	-	-	-	-	-	-	-	-	-	-
37. <i>Pterobairdia maddoxsae</i>	-	-	1	-	-	-	-	-	-	1
38. <i>Semicytherura</i> sp.	1	4	-	2	-	2	-	7	-	16
39. <i>Trieblina serrata</i>	-	-	-	-	-	-	-	-	-	-
40. Other	11	21	29	22	13	7	11	7	26	147
41. "Piped" specimens	-	-	-	-	-	-	-	-	-	-
TOTAL	47	76	84	81	50	37	62	43	67	547

CHAPTER 4:

ELECTRON PARAMAGNETIC RESONANCE STUDIES OF SELECTED BOREHOLE SAMPLES AND DEBRIS MATERIAL FROM OAK CRATER

by

Carol A. Polanskey¹ and Thomas J. Ahrens¹

INTRODUCTION

Electron paramagnetic resonance (EPR) spectrometry was used to measure the peak shock stress experienced by a variety of carbonate samples as a result of the detonation of the OAK nuclear device. The following results are based on EPR spectra from 136 samples taken from six boreholes and 17 debris samples recovered from the crater floor. Shock pressures were determined by comparing the sample spectra with spectra of Enewetak carbonate samples and Solenhofen Limestone that had been shocked to known pressures in the laboratory. Preliminary work on this procedure was developed by Vizgirda and Ahrens (1980) using Enewetak material from CACTUS crater obtained during Project EXPOE. Their work demonstrated a linear relationship between shock pressure and the hyperfine splitting of Mn^{2+} in the calcite component of CACTUS carbonate samples. The current report contains the analysis of the OAK samples and expands upon the previous calibration technique.

EPR ANALYSIS

The EPR spectrum of calcium carbonate, $CaCO_3$, is a result of Mn^{2+} substituting for Ca^{2+} in a single site in the crystal lattice. The theory of Mn^{2+} resonance absorption in single crystal of calcite is described by Hurd and others (1954). The calcite spectrum is dominated by six hyperfine peaks due to the central transitions $M = + 1/2$, where M is the electronic magnetic quantum number. The hyperfine splitting results from the coupling between electronic and nuclear magnetic moments (Hurd and others, 1954). The spectrum of a powdered sample of single crystal calcite, Iceland spar, is shown in Figure 4-1. The central transitions are labeled along with the forbidden transitions. Of particular interest to this study are the two outer most peak doublets at the lowest and highest field positions.

Sample Preparation and Spectrometer Settings

The carbonate samples were ground into a coarse powder and placed into Wilmad® 707SQ fused EPR tubes. The spectra were taken at room temperature with a Varian® E-Line Century Series spectrometer. The calcite spectrum is centered near 3,400 Gauss (G), and ranges from approximately 3,150 to 3,650 G.

¹California Institute of Technology, Division of Geological
and Planetary Sciences; Pasadena, California 91125.

CALCITE POWDER SPECTRUM

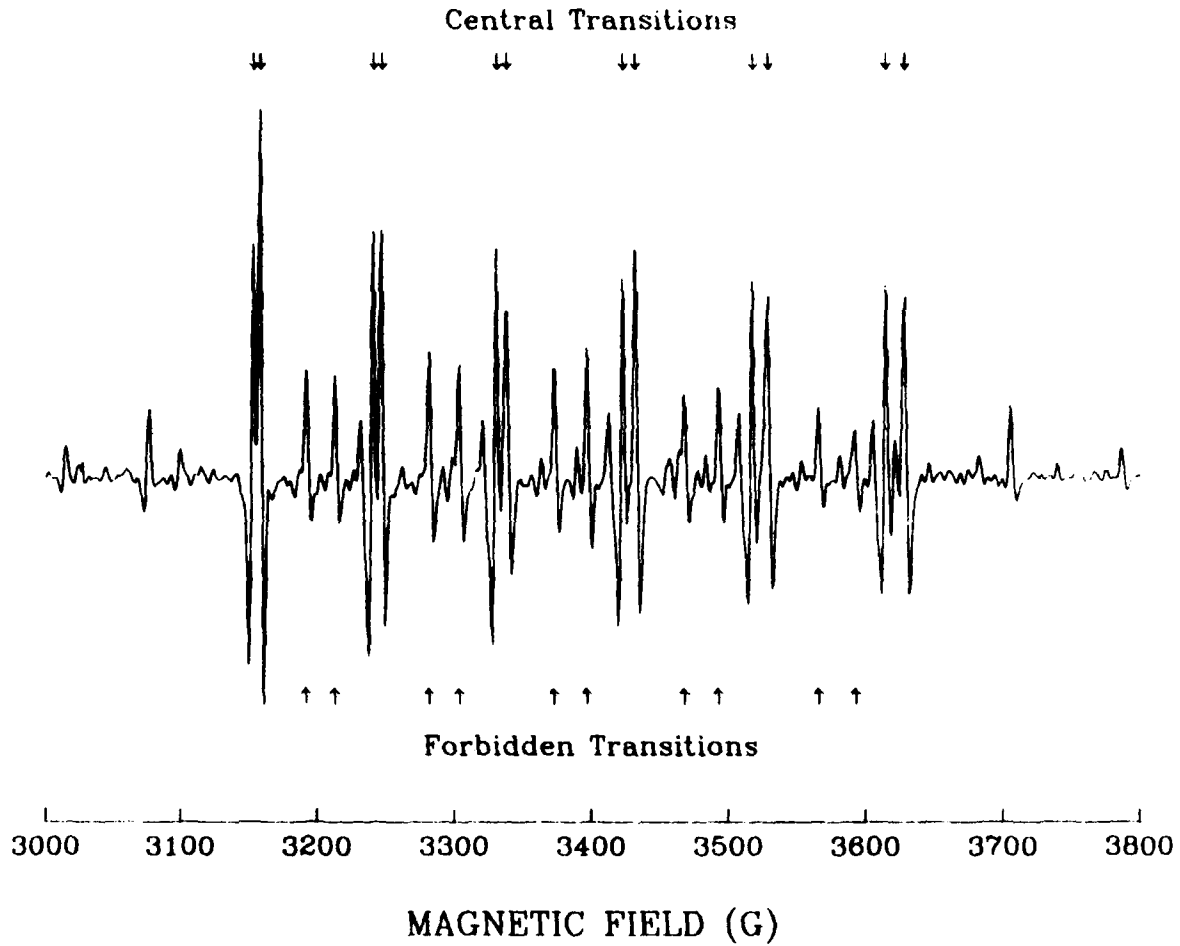


FIGURE 4-1. -- EPR spectrum of powdered single crystal calcite. The central transitions are due to $M = +1/2$, $\Delta m = 0$, where M and m are the electronic and nuclear magnetic quantum numbers, respectively. The forbidden transitions occur when $\Delta m = 1$. G = Gauss.

The spectrometer was set at a microwave frequency of 9.56 GigaHertz (GHz), modulation amplitude of 3.2 G, time constant of 0.25 seconds (sec), and microwave power of 20 milliwatts (mWatt). A scan time of 8 minutes (min) was used to obtain the full spectrum over a 1000-G scan range; however, high-resolution spectra were also recorded for both the extreme lower and higher field components of the spectrum. For these spectra, the magnetic field was swept over 100 G in 4 min. The high resolution spectra provided greater details of the modification of the hyperfine doublets from the shocked samples. As a result, the high-resolution spectra were used in all of the subsequent analyses.

In addition, all spectra were recorded digitally by the spectrometer. Therefore, it was possible to average several scans to improve the signal-to-noise ratio in samples with low signal strength. Signal averaging proved to be extremely useful for the highly shocked samples because there is a definite correlation between decreasing signal strength and increasing shock pressure. Finally, to remove the slope from the spectrum and reduce the line width of the signal, the spectrometer was operated in the second derivative mode. This was accomplished by setting the modulation frequency of the cavity 90 degrees out of phase with the receiver frequency.

SHOCK PRESSURE CALIBRATION OF EPR SPECTRA

Shock-Wave Calibration Experiments

The calibration experiments were a combination of two different data sets. The first set consisted of Enewetak carbonate samples shocked in the laboratory over 10 years ago. The samples were taken from two different depths, 10 ft and 146 ft, from the borehole XRU-3 located outside of CACTUS crater on the eastern side of Enewetak Atoll. These samples and experiments are described in detail by Vizgirda and Ahrens (1980). One reason for reprocessing these samples was to determine if the shock effects observed by Vizgirda and Ahrens (1980) had changed with time. New spectra were taken of each sample and the results confirmed that the effect of shock on the hyperfine splitting had not altered over the time scale of a decade. Secondly, high-resolution spectra were taken from these samples in order to test the pressure-calibration technique; however, these samples were not used for the pressure calibration which is described subsequently in this Chapter.

A series of Solenhofen Limestone samples also were shocked in the laboratory, and these samples became the basis for the pressure calibration. This material was chosen because its EPR spectrum, also due to Mn^{2+} substitution, is orders of magnitude more intense than the Enewetak samples. The Solenhofen is also more chemically homogeneous, although it is still a polycrystalline material. Limestone cores (diameter 0.25 in.) were cut into 0.4-in.-long cylinders and pressed into stainless-steel sample chambers. The sample chambers were sealed in the rear by a stainless-steel plug which was notched to vent any impact generated gases. The sample chamber was then inserted into a large stainless-steel momentum trap and mounted in a 40-mm propellant gun. Projectiles were made of polycarbonate-resin plastic (Lexan) that contained flyer plates of aluminium or Lexan. These impacted the target assembly at velocities between 0.8 and 1.6 km/sec to yield initial shock

pressures of 1.3 to 9.8 Giga Pascals (GPa). Initial shock pressure (rather than final reverberated shock pressure) is reported, because most of the entropy generated by the shock (and hence the shock damage) is associated with the initial shock wave.

Shock pressures were calculated using the projectile velocities and the impedance match technique (Stoffler, 1972). The average bulk density of the limestone samples was 2.61 g/cm^3 , and the Hugoniot for Solenhofen Limestone samples was taken from Tyburczy and Ahrens (1986). The remaining Hugoniots for Lexan[®] aluminium 2024, and stainless steel 304 are found in Marsh (1980).

Description of Shocked Spectra

Figure 4-2 shows a series of shocked-limestone spectra. The spectra have all been normalized such that the highest peaks (low-resolution spectra) or the highest subpeaks (high-resolution spectra) are of equal height. The shocked-limestone spectra not only reflect in much greater detail the decrease in the hyperfine splitting as a function of increasing pressure, observed previously in the carbonate, but also reveal that the relative signal strength and width of the two subpeaks also varies in a consistent manner with increasing pressure. It is clear from the last two columns in Figure 4-2 that the extreme low-field subpeak in the low-field doublet and the extreme high-field subpeak in the high-field doublet both decrease in relative amplitude and broaden with increasing shock pressure. Because the spectrum of each doublet is the sum of two individual subpeaks, a change in the magnitude or shape of one subpeak can be enough to create the observed decrease in peak separation of the doublet as a whole. In this case, a shift in the actual line position of either subpeak is not required.

The same general trend in peak variation also can be seen in the shocked-carbonate spectra shown in Figure 4-3. Because of the low signal in several samples, these spectra were not uniformly normalized. The specific behavior of the subpeaks in the high-field doublet is less obvious in this series, and the subpeaks are difficult to distinguish at higher shock pressures. The high-field doublet is ultimately lost in the noise (as seen in the sample shocked to 10 GPa). Another factor which complicates the carbonate analysis is that there is also variation between spectra of some of the "unshocked" carbonate samples. Material from two different depths in borehole XR11-3 was used in the calibration experiments of Vizgirda and Ahrens (1980). It appears that the material taken from a depth of 10 ft is not typical of the bulk of the unshocked samples analyzed from Enewetak Atoll. As a result, a systematic difference exists between the spectra taken from these calibration shots and that of the shocked material from 146 ft depth. Both sets of spectra show consistent variation in hyperfine splitting with increasing shock pressure; however, they do differ in the degree to which they are affected by shock deformation.

A second observation, mentioned earlier, is that the amplitude of the entire spectrum tends to decrease with increasing shock pressure. This effect is much more obvious in the Enewetak samples than in the Solenhofen Limestone samples. A loss of signal could be due to a reduction of the Mn^{2+} concentration in the Ca^{2+} lattice sites. The specific mechanism responsible for this reduction has not yet been identified.

SOLENHOFEN LIMESTONE

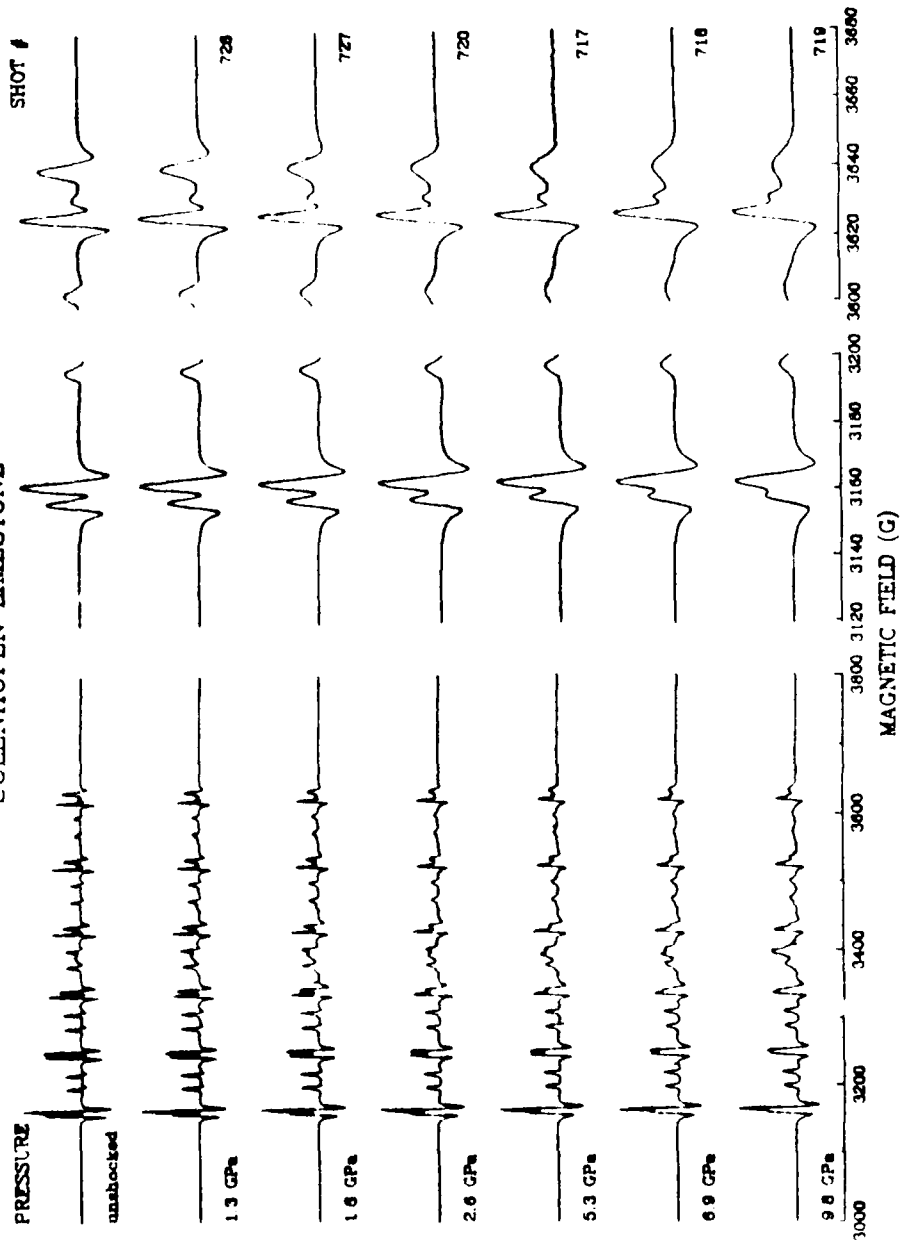


FIGURE 4-2. -- Comparison of limestone spectra shocked in the laboratory. The full spectrum is shown in the first column and centered at 3,400 Gauss (G). High-resolution spectra of the lowest and highest field components are shown in the latter two columns and centered at 3,160 G and 3,630 G, respectively.

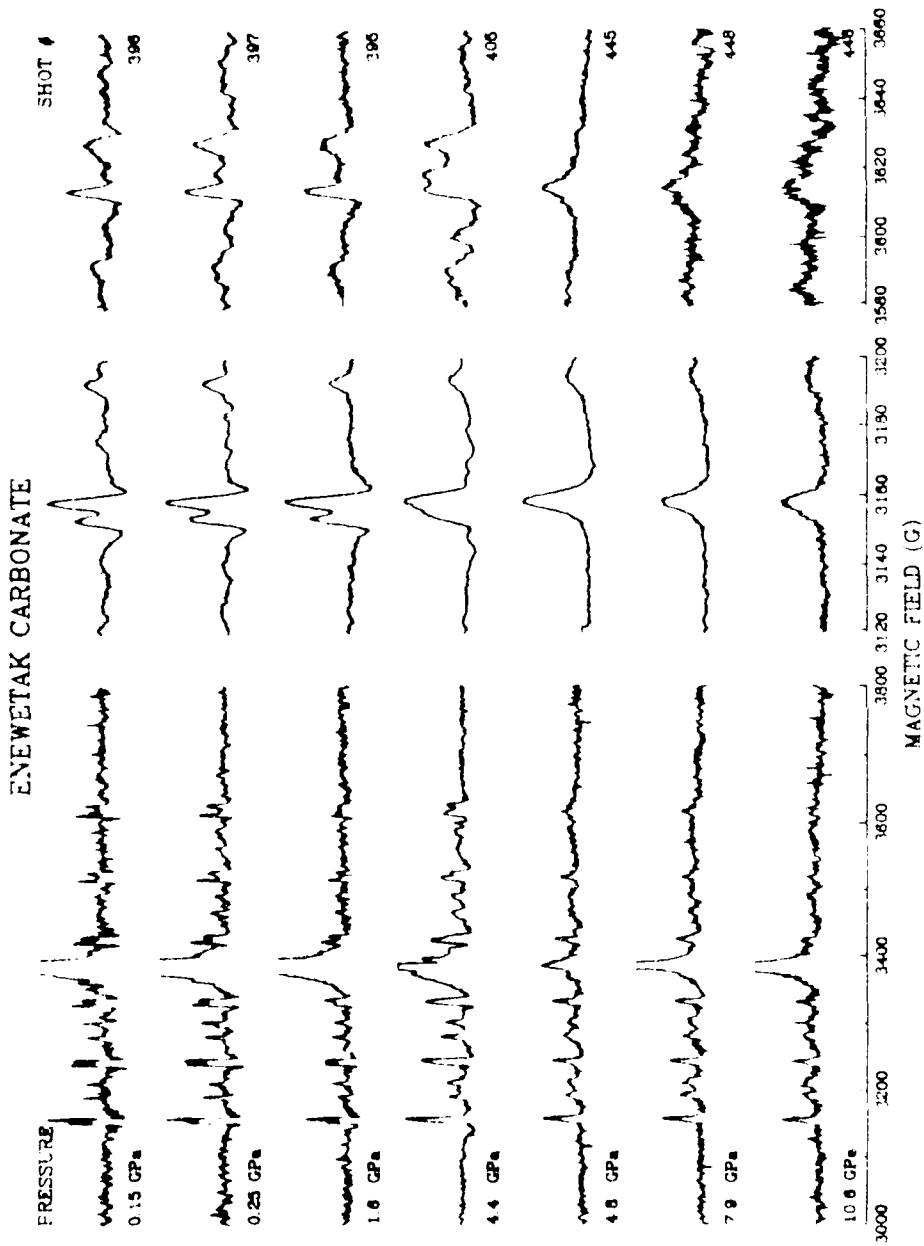


FIGURE 4-3. -- Comparison of coral spectra shocked in the laboratory. The full spectrum is shown in the first column and centered at 3,400 Gauss (G). High-resolution spectra of the lowest and highest field components are shown in the latter two columns and centered at 3,160 G and 3,030 G, respectively.

Pressure Calibration by Differencing Spectra

The previous calibration technique of Vizgirda and Ahrens (1980) relied on measuring the separation, in Gauss (G), of the two subpeaks of the highest field component of each spectrum. The hyperfine peak splitting, HPS, was related to shock pressure, P, by the relationship:

$$\text{HPS(G)} = - 0.60\text{P(GPa)} + 13.85 \quad (\text{high field})$$

Although the decrease in hyperfine splitting is most evident in the high field component, the signal strength of this peak is also the lowest. Therefore, as the signal intensity decreases, the error in measuring hyperfine peak splitting increases. The following technique was developed to incorporate the variations in hyperfine splitting as well as relative peak amplitudes and widths. In addition, the analysis will work equally well for the lowest field component of the spectrum which always has a higher amplitude.

Digital spectra were used to compare each carbonate sample to a pure, single-crystal calcite standard. Both high-resolution spectra from each end of the spectrum were used in the comparison. The digital spectra consisted of 1000 amplitude values evenly spaced over a 100-G field range. Both sample and standard spectra were first normalized by the amplitude of their respective highest subpeaks. The sample spectrum was then translated along the magnetic-field axis until the position of its highest subpeak coincided with that of the standard spectrum. Next the absolute value of the difference in amplitude between the two spectra was calculated for each point over the extent of the doublet. Finally, these individual differences were summed to determine a measure of the "likeness" or "unlikeness" of the sample spectrum to the standard. This number shall be referred to as the integrated difference, or ID, of the sample, which is given analytically by the equation:

$$\text{ID} = \int_{n=n_0}^{n=400} |Y[\text{standard}] - Y[\text{sample}]| / 40\text{G}$$

where n_0 is the index of the amplitude array corresponding to a magnetic field value 20 G below that of the highest peak of the standard spectrum; $Y[\text{standard}](i)$ and $Y[\text{sample}](i)$ are the normalized amplitudes of the standard and sample spectra, respectively, and N is the number of data points that are integrated. In this case, N is 400. The error in ID is determined by performing a similar calculation, where $Y[\text{sample}](i)$ are points in the flat baseline signal on either side of the Mn^{2+} peak.

Figure 4-4 illustrates this procedure with examples of two spectra from the limestone calibration experiments. The first frame shows an unshocked Solenhofen Limestone spectrum normalized, translated, and plotted over the standard calcite spectrum. The second frame is a plot of the absolute value of the difference between the amplitudes at each point over a 40-G range in magnetic field. The final two frames demonstrate the same technique using a sample which has been shocked to 9.8 GPa. The error is determined by using the same scheme to calculate the integrated difference along a flat portion of the spectrum. This value gives an estimate of the contribution of noise to the ID over the region containing the signal.

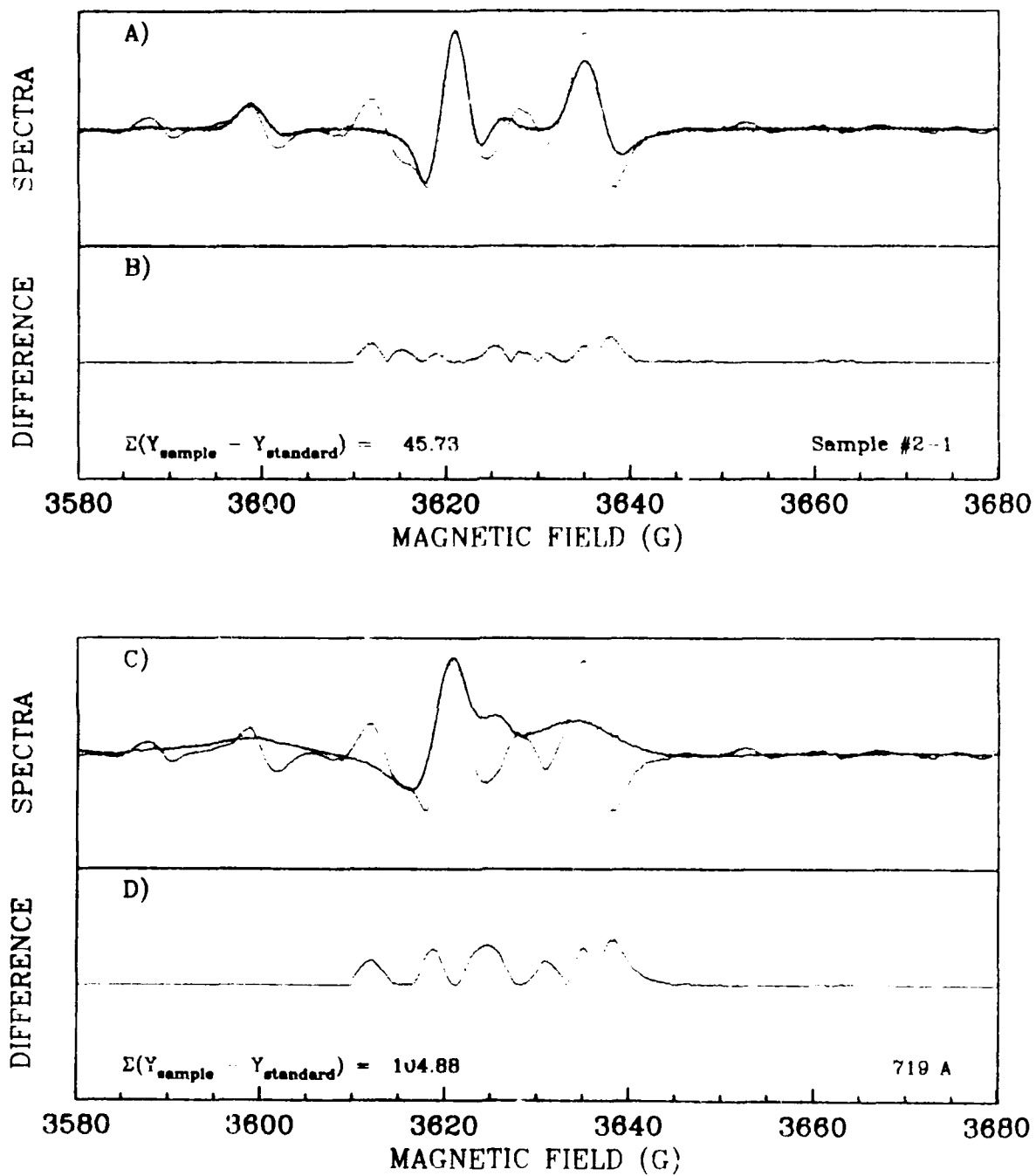


FIGURE 4-4. -- Illustration of the differencing technique showing (A) an overlay of the standard spectra and an unshocked Solenhofen Limestone sample; and (B) a plot of the individual absolute differences at each point along the field. Frames (C) and (D) correspond to (A) and (B) for a limestone sample shocked to 9.8 GigaPascals (GPa).

SOLENHOFEN LIMESTONE

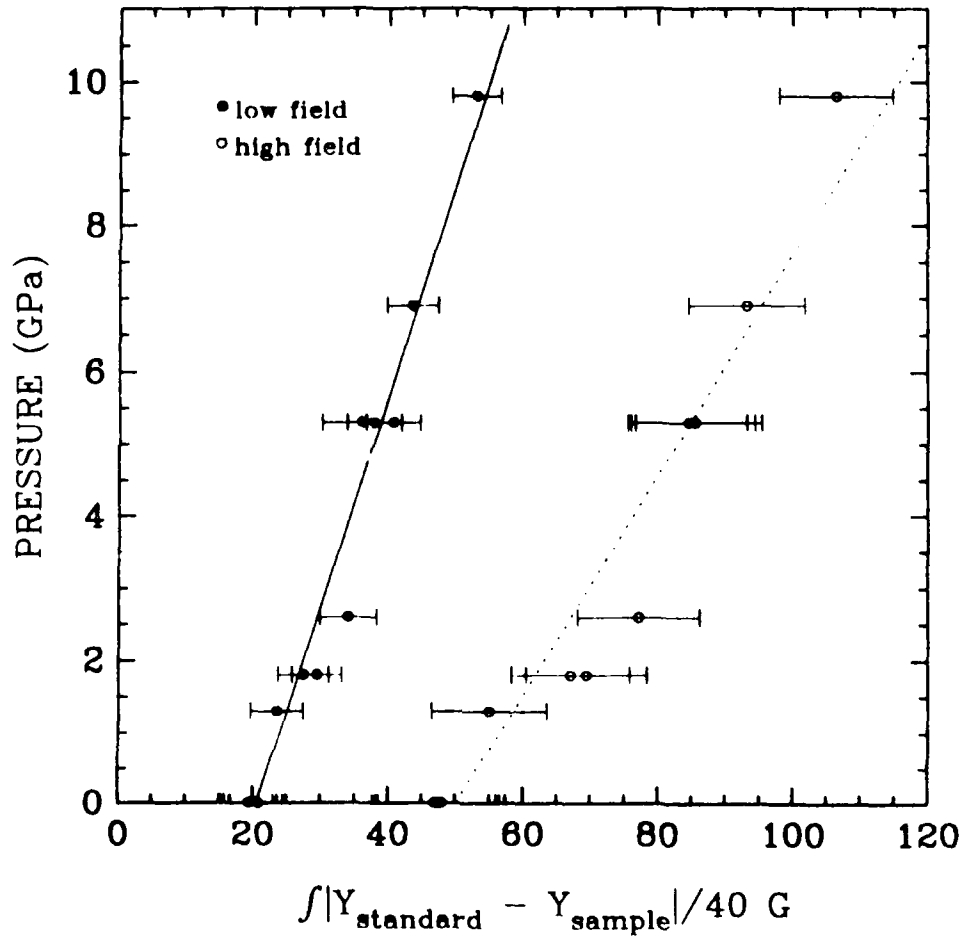


FIGURE 4-5. -- Plot of the summed differences for the low and high field components of the Solenhofen Limestone samples as a function of shock pressure. The ID value is normalized by 40 Gauss (G), the magnetic field range over which the differences were integrated.

TABLE 4-1. Pressure (Giga Pascal) and Integrated Difference (ID) Data for High Resolution Spectra from Samples Shocked in Laboratory Recovery Experiments.

SOLENHOFEN LIMESTONE			
SHOT NUMBER	P (GPa)	ID Low Field	ID High Field
—	0.0	20.79	47.61
717	5.3	38.12	85.13
718	6.9	43.53	93.17
719	9.8	52.99	106.43
720	2.6	34.03	77.16
726	1.3	23.44	55.14
727	1.8	28.42	68.23

ENEWETAK CARBONATES			
SHOT NUMBER	P (GPa)	ID Low Field	ID High Field
394	1.4	37.43	74.68
395	1.6	37.83	84.80
396	0.2	33.67	66.51
397	0.3	33.00	74.79
405	4.4	73.85	146.09
442	1.9	78.25	146.22
443	1.5	68.33	166.97
445	4.8	73.61	165.60
446	10.6	75.70	181.03
448	7.9	70.71	161.79

The results of these calculations for the limestone calibration experiments are plotted in Figure 4-5. The ID values are plotted against pressure for both the low- and high-field components of the spectrum. To determine the pressure to integrated difference calibration, a line was fit to each data set using linear least squares. The resulting equations are listed below:

$$\begin{aligned} P \text{ (GPa)} &= 0.290(\text{ID}) - 5.97 && \text{(low field)} \\ P \text{ (GPa)} &= 0.152(\text{ID}) - 7.59 && \text{(high field)} \end{aligned}$$

The correlation coefficients for the fit were 0.966 and 0.943, respectively. Table 4-1 contains a list of the ID results for both limestone and Enewetak sample experiments. The average ID values are given for shots where several samples were analyzed.

Using the calibration curves above, shock pressures were then assigned to the OAK carbonate samples. In general, the Enewetak carbonate samples have a much weaker EPR signal than those from the Solenhofen Limestone. Therefore, it was necessary to adjust the intercept of the calibration curves to compensate for the average ID value of the unshocked Enewetak samples. It follows that this method will then assign negative pressures to some samples, because the previous adjustment was made to accommodate the "average" background noise. To avoid this obviously unphysical result, and because this technique is not extremely sensitive for low-shock damage, all samples with shock pressures calculated to be below 2.0 GPa were classified as unshocked. Similarly, the high-pressure cut-off was chosen to be 15 GPa. This is necessary because: (1) no data exist for very high shock pressures, and (2) the intensity of the Enewetak sample spectrum is low even at 10 GPa. Samples with shock pressures calculated to be above 10 GPa were classified as highly shocked.

In most cases, shock pressures were calculated for each sample using both the low- and high-field components of the spectrum. These values were then averaged to determine the final calculated pressure.

OAK DATA

Borehole Sample Selection

The borehole samples consisted of uncemented sediments and carbonate rock clasts from boreholes OAR-2A, OBZ-4, OCT-5, OET-7, OFT-8, and OPZ-18, the locations of which are shown on Figure 4-6. Samples are referred by the appropriate borehole name succeeded by depth in feet below sea level (bsl).

The carbonate material from Enewetak is extremely inhomogeneous and consists of a mixture of both calcite and aragonite. Because aragonite does not have a detectable EPR spectrum (Low and Zeira, 1972), samples were selected, where possible, for their high-calcite content. For example, those samples containing carbonate grains replaced by solution-deposited calcite crystals were preferred because they would yield stronger EPR signals. Choosing good sample material is important because it provides a consistent base for analysis, and because it guards against mistaking a sample with an inherently poor EPR spectrum as being highly shocked. The difference between the two cases generally can be recognized by visual inspection, although it is

more difficult to assess with numerical techniques. As a result, the samples chosen were much less porous than the CACTUS samples used in the earlier shock-wave experiments; consequently, the OAK spectra tended to resemble the Solenhofen Limestone spectra more closely. For each borehole, the majority of samples were taken from depths above the gamma (γ) geologic crater zone, defined by Wardlaw and Henry (1986, p. 3) as that interval of rock and sediment that is fractured and displaced beneath the crater. A more specific description of each sample analyzed is given in Tables 4-2 through 4-7 (located at the end of this Chapter). Detailed descriptions of each borehole are given in Henry, Wardlaw, and others (1986).

Results of Borehole Sample Analysis

The two boreholes drilled almost directly below the position of the explosive device (ground-zero, GZ, and bathymetric-center boreholes OBZ-4 and OPZ-18, respectively) were the most heavily sampled for the EPR study. A very highly shocked layer of uncemented material was found in samples from borehole OPZ-18 between 399.9 ft and 415.9 ft bsl. This layer was distinguished visually by the characteristic greenish color of the muddy carbonate sand. The shocked zone was interrupted at 412.4 ft bsl by a thin zone of lighter-colored material. The location and nature of this shocked material coincides with a zone of Holocene sediments described by Wardlaw and Henry (1986) as a possible example of material that has been injected. The present results are consistent with such a hypothesis since this material most likely originated near the pre-shot sea-floor surface. Three other sand samples above this layer, 386.9 ft, 368.5 ft, and 357.2 ft bsl, were moderately shocked to at most 3.2 GPa. The highly shocked samples were located primarily in the geologic crater zone beta-2 (β_2) --the transition sands-- whereas the moderately shocked material came from zone beta-1b (β_{1b}) (Wardlaw and Henry, 1986; and Chapter 6 of current Report). The remaining 24 of the 31 samples from OPZ-18 appear to be unshocked.

Remarkably, not one of the 26 samples from OBZ-4 showed significant shock damage. Three samples from the β_{1b} zone registered only marginally detectable degrees of shock damage. Sufficient samples were analyzed from the transition sands and vicinity to characterize the core; therefore, it appears that OBZ-4 did not share the same history as OPZ-18.

Thick zones of highly shocked material were found in each of the three northeastern-radial transition boreholes OCT-5, OET-7, and OFT-8. The transition sands have not been identified in any of these boreholes; however, the spectra of the shocked material are similar to those from the shocked material in OPZ-18.

Spectra were taken of 25 samples from borehole OCT-5, drilled 658 ft from GZ. The results of six of these samples define a heavily shocked zone at least 25 ft thick, extending from 285.3 ft to 309.9 ft bsl. This region occurs within zone β_{1b} (early stage collapse rubble), and these samples are also primarily uncemented sands. Aside from the highly shocked material in this region, four widely dispersed samples appear to be moderately shocked. However, two of these samples (368.4 and 464.0 ft bsl in OCT-5) are examples of the aforementioned situation where poor signal quality biases a pressure determination. Simple visual analysis of these spectra suggest that both samples are actually unshocked. The elevated pressures calculated for

OAK CRATER BOREHOLES

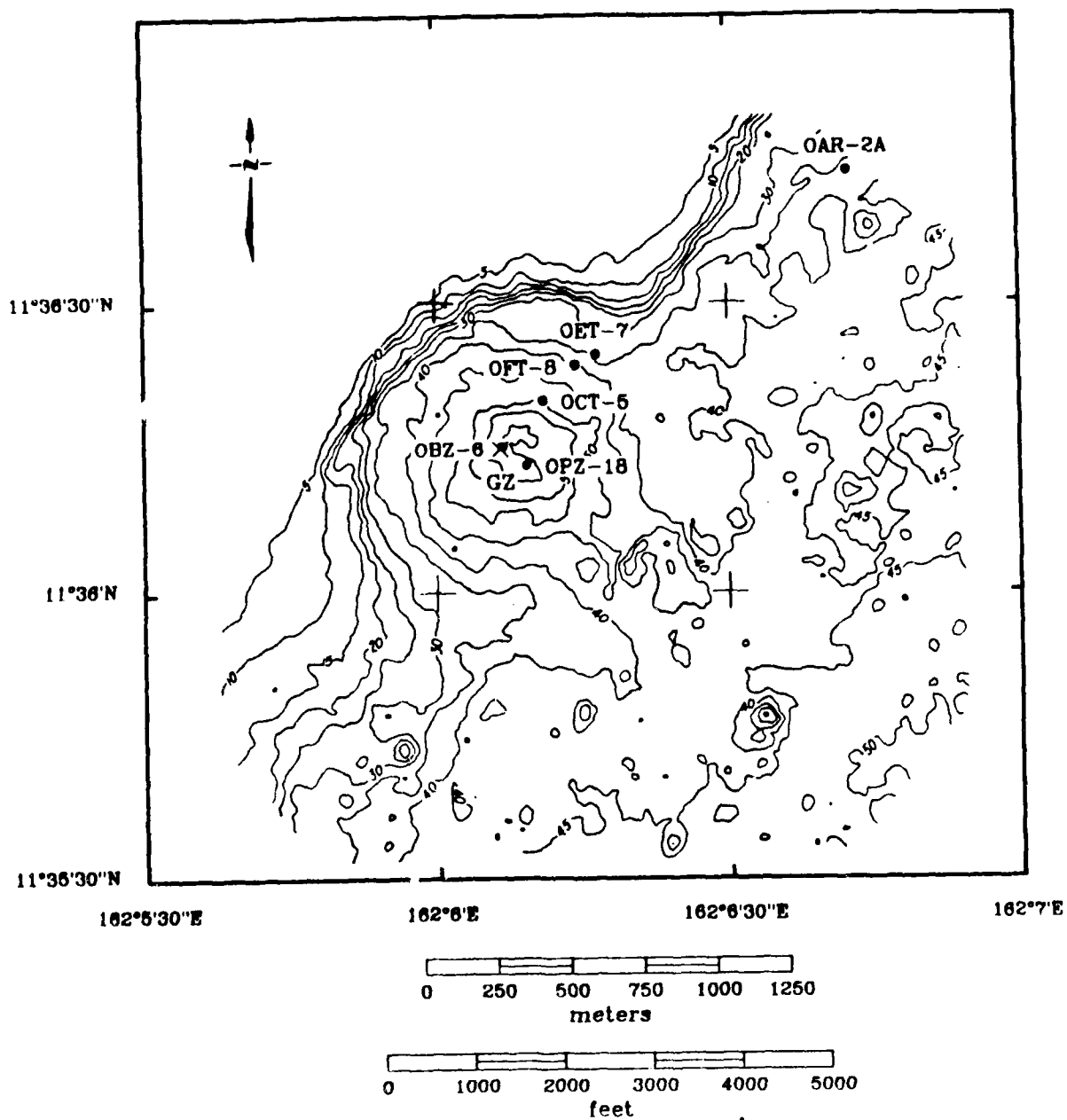


FIGURE 4-6. -- Map of OAK crater showing the location of the boreholes sampled for this study. Bathymetric contours given in 5-meter intervals.

these depths are an artifact of the noisiness of the spectra due to the small fraction of calcite in these samples.

Borehole OFT-8 is located 1,129 ft from GZ, just within the excavational crater (Henry, Wardlaw, and others, 1986). This borehole was sampled at 24 depths. In OFT-8, the region of heavily shocked material begins near the top of the β_{1b} zone and extends downward for approximately 27 ft. Included within this zone were seven heavily shocked samples located between 153.6 ft and 180.9 ft bsl. Bordering this region above and below are zones containing moderately shocked material. Two moderately shocked samples, 149.2 ft and 151.3 ft bsl, were taken at the base of the β_{1a} (late-stage collapse rubble) geologic zone, and three samples deeper in the β_{1b} extending to a depth of 195.3 ft bsl.

The next farthest borehole (OET-7) is 1,374 ft from GZ. Based on seismic-reflection, paleontologic, and lithostatigraphic data, this borehole is thought to be located outside of the excavational crater (Henry, Wardlaw, and others, 1986). The majority of the nine samples were from the GAMMA zone; however, all but the uppermost sample were heavily to moderately shocked. Of the highly shocked samples, six out of seven were uncemented sediment samples. The highly shocked zone extended from 118.9 to 147.5 ft bsl, and a moderately shocked, cemented sample was detected at 173.6 ft bsl.

Borehole OAR-2A, located 4,458 ft from OAK GZ, initially was sampled only as a reference core; however, six of 21 samples from this borehole have been heavily shocked. Two other samples were moderately shocked to pressures of 3.5 and 4.4 GPa. All of the shocked samples were located within the top 39 ft of the core and the most heavily shocked material within the first 24 ft. The proximity of this borehole to the reef may suggest that some highly shocked, fine-grain ejecta was transported from the slope and deposited at the site of OAR-2A.

The combined results from the OAK borehole sample analysis are presented in Figure 4-7. The solid horizontal line in each panel indicates the present sea-floor depth. The depth and thickness of each zone containing highly shocked material ($P > 10$ GPa) as a function of the distance of the borehole from GZ is shown in a simplified manner in Figure 4-8.

Results from Debris Samples

The debris analyzed consists of 14 samples collected throughout the crater by submersible and three samples collected by scuba divers from roughly a single site. The former samples are a subset of a series of debris samples analyzed by Halley, Ludwig, and others (1986). Figure 4-9 shows the locations where each debris sample was recovered. The range values that will be discussed in a subsequent section were measured from this map. Unfortunately, the debris samples included in this study were all taken from roughly the same distance from GZ. Only one sample (OAK 201) was recovered at a significantly different range.

The results of the debris analysis are plotted in Figure 4-10A and listed in Table 4-8 (located at end of Chapter). The majority of the debris samples were relatively unshocked; however, all of the highly shocked debris was found

OAK CRATER BOREHOLE RESULTS

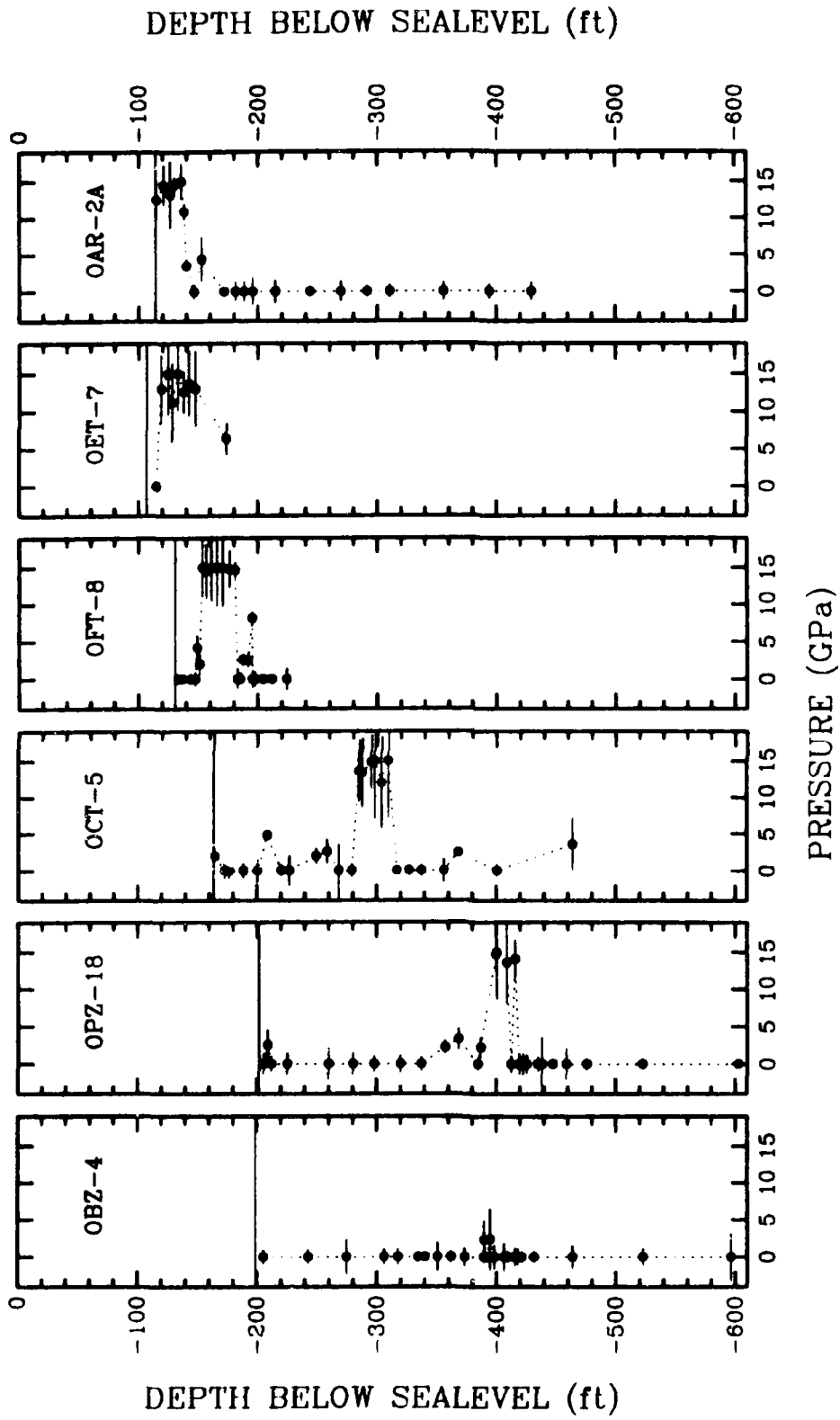


FIGURE 4-7. -- Combined results of the borehole-sample analysis showing the calculated shock pressure in relation to the sample depth in ft below sea level. The boreholes are presented in order of increasing distance from ground zero.

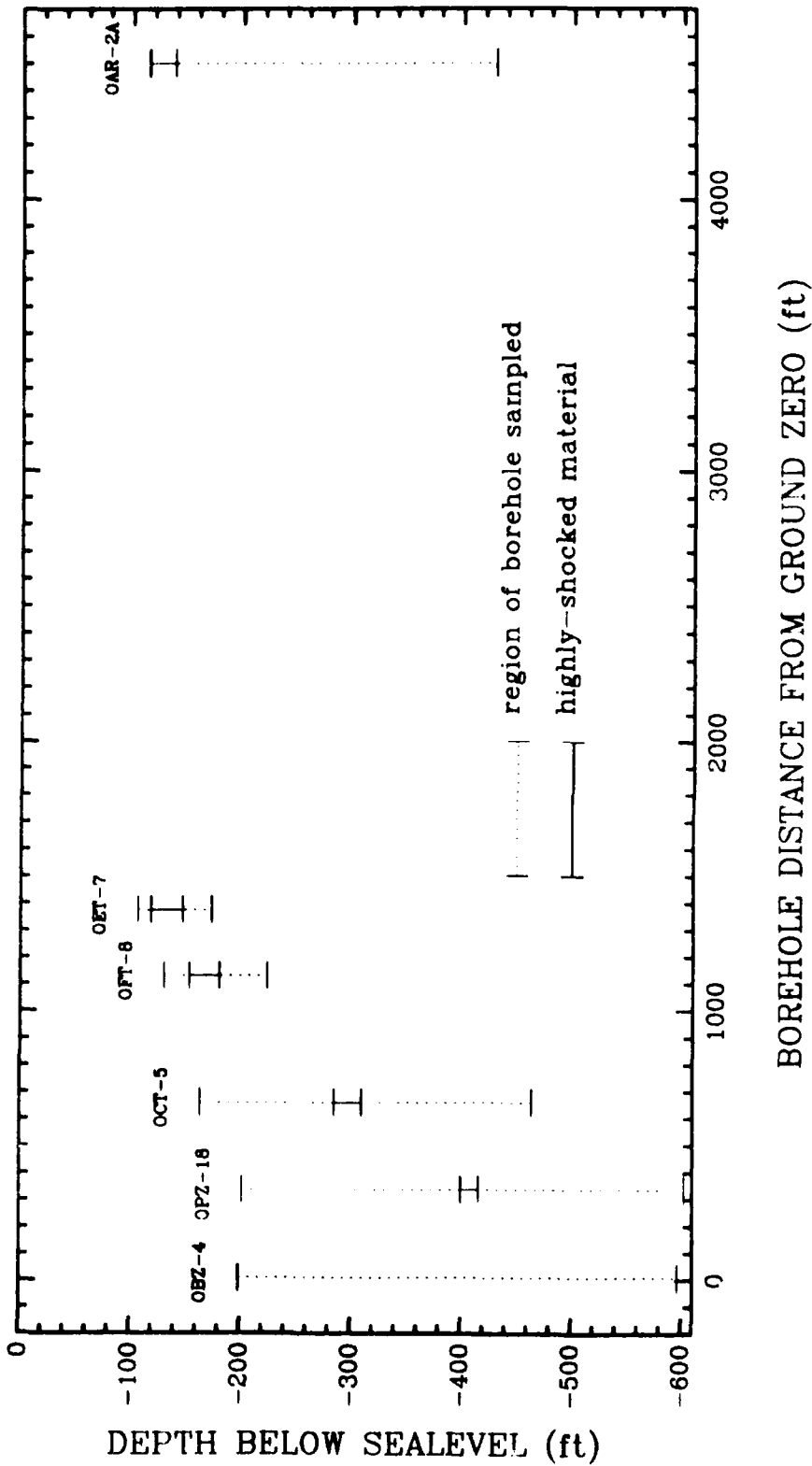


FIGURE 4-8. -- Illustration of the depth and thickness of regions of highly shocked carbonates recovered from each borehole. The dotted line indicates the extent of the borehole sampled, and the solid line defines the highly shocked zone.

OAK CRATER DEBRIS SAMPLES

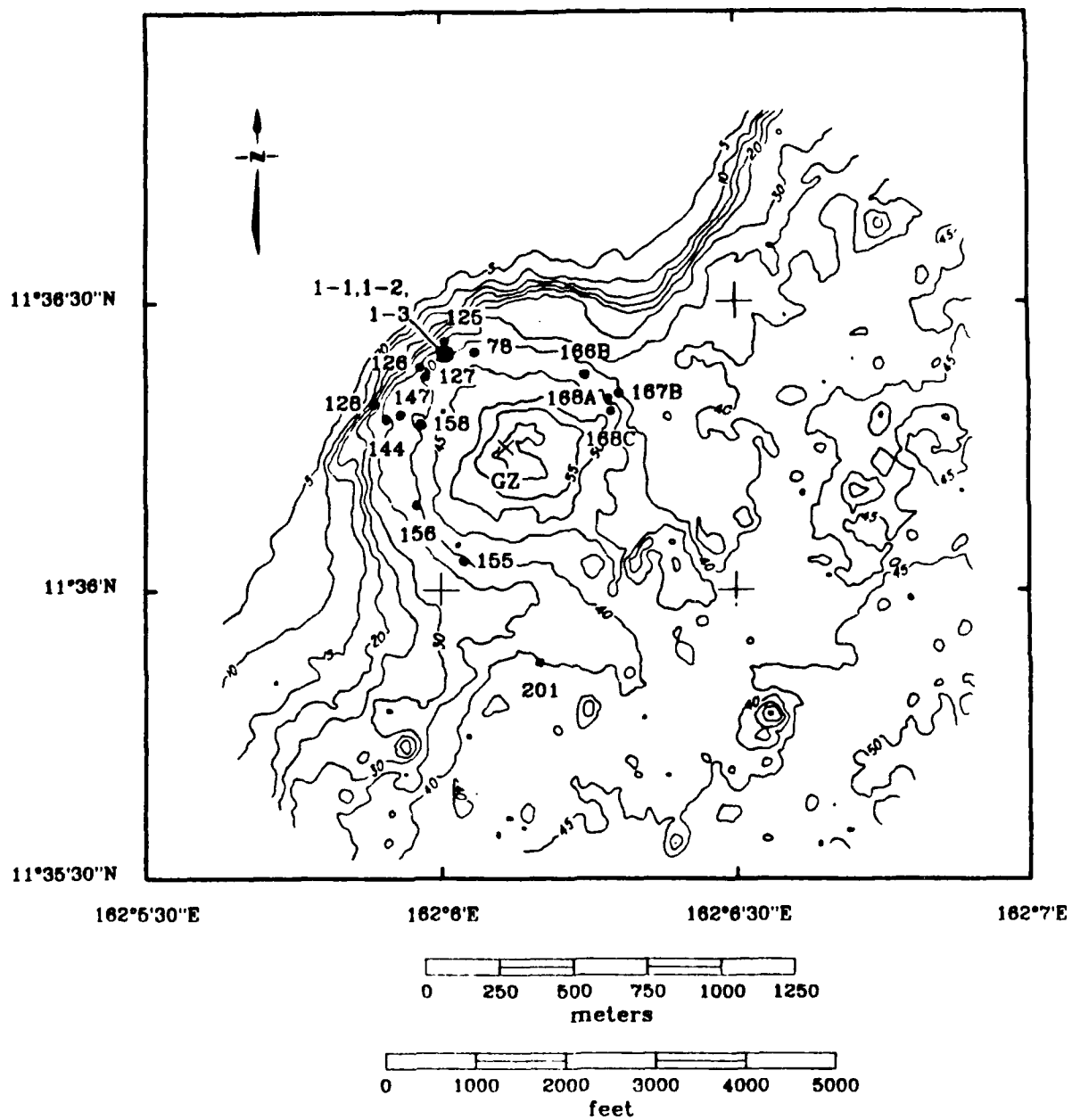


FIGURE 4-9. -- Map of OAK crater showing the debris-sample recovery sites. Bathymetric contours given in 5-meter intervals.

OAK DEBRIS

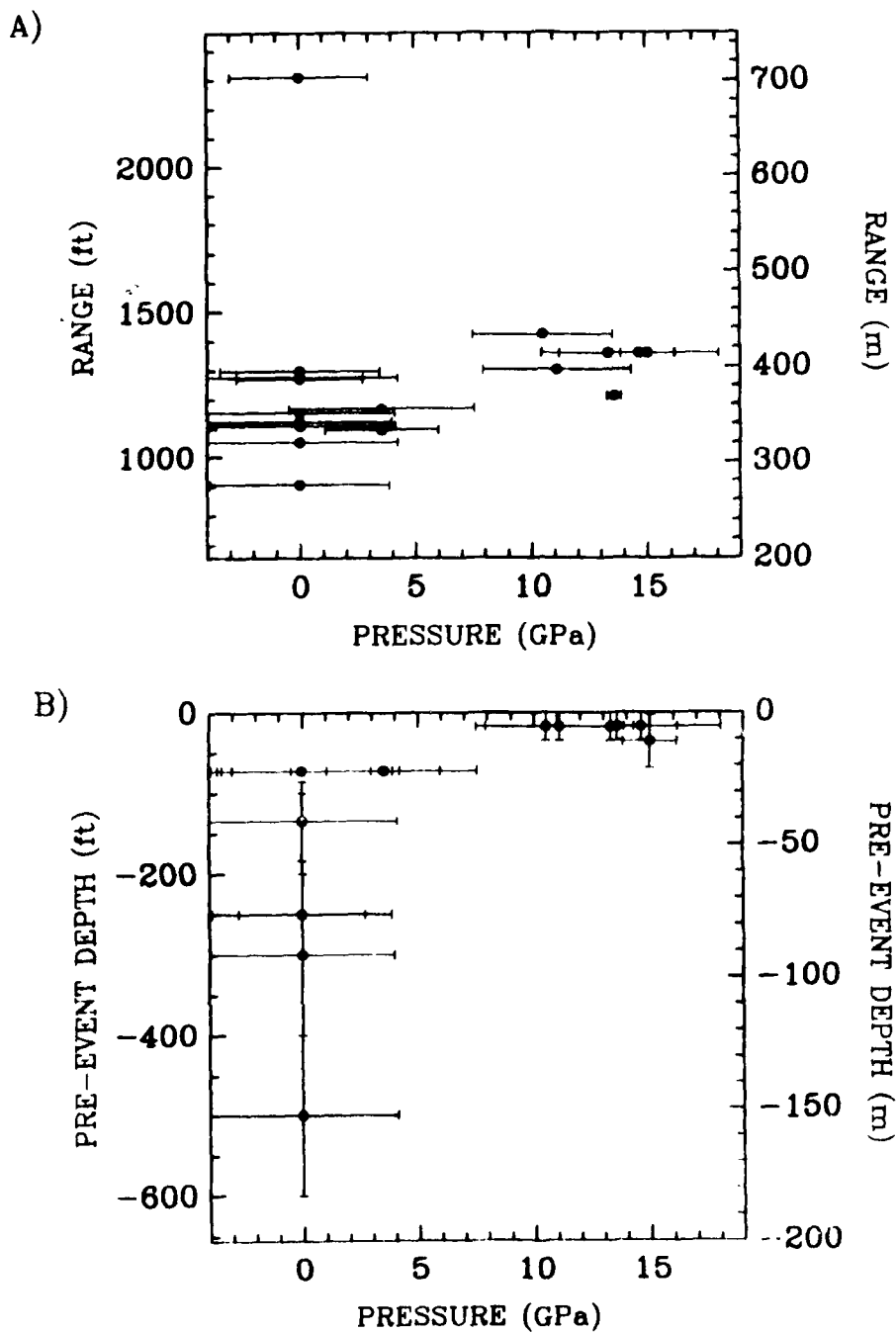


FIGURE 4-10. -- Results of the debris-sample analysis showing (A) shock pressure as a function of range from ground zero, and (B) shock pressure versus estimated pre-event depth below sea level.

at the base of the reef slope. The reef may have blocked some of the highly shocked material from leaving the crater as ejecta, or this material (ejected from the crater) could have been transported craterward back down the reef slope some time after the crater was formed.

In addition to the range measurements, the estimated pre-event initial depth of a limited number of the debris samples was available from strontium-isotope analysis (Halley, Major, and others, 1986; and Ludwig, Halley, and others, 1986) and gross paleontologic and petrographic analysis by B.L. Ristvet in 1981 (see Ristvet, 1986) and corroborated by subsequent analysis by USGS personnel. The pre-event depth below sea level is plotted against shock pressure for these samples in Figure 4-10. Although the pre-event depth estimates are crude in some cases, a strong correlation is evident between shock pressure and depth for this limited data set. This correlation is consistent with the assertion that the pre-event surface material near GZ was the most severely shocked.

DISCUSSION

With a few exceptions, the bulk of the samples analyzed can be split into two categories, unshocked and very highly shocked. There were relatively few samples which can be assigned to intermediate pressure categories. This suggests that the majority of the shocked material shares a common origin. Presumably, the material right at or near the surface near GZ received the highest shock pressure from the blast. During the cratering event, some of this material was incorporated in the lining of the transient crater cavity and was then buried almost immediately by the collapse of the crater walls. Subsequent backwash of ejecta and slumping and deformation of the crater would tend to mix this highly shocked material with other rubble and breccia and consequently obscure any stratigraphically discernable zone of highly shocked material.

This hypothesis can be applied to explain the presence of the shocked regions in OPZ-18 and in the transition boreholes. Because slumping and collapse become increasingly more important toward the rim of the crater, it is not unreasonable that OPZ-18 is the only borehole to have the shocked material preserved in a stratigraphically discernable unit such as the transition sands. The thickness of the region of highly shocked material does remain fairly constant throughout the three transition boreholes (Figure 4-8), although the region is located at consistently shallower depths as the distance between the borehole and GZ increases. This is a further indication that these regions were at one time related.

Late-stage debris slumping and the influence of sedimentation also have contributed to borehole stratigraphy. Post-event slumps from the reef have deposited at least 8 ft of unshocked debris at OET-7, and possibly as much as 17 ft at OFT-8. The location of the shocked debris samples collected from the floor of the crater suggest that highly shocked ejecta may also be deposited from the reef slope, and the shocked upper layer of OAR-2A could be the result of accumulated deposition over many years.

ACKNOWLEDGEMENTS

The authors would like to thank the following people: Lt. Col. Robert F. Couch, Jr., for his support of this project; Thomas W. Henry for assistance with sample acquisitions from the boreholes; Robert B. Halley for providing debris samples; Papo Celle, Mike Long, and Leon Young for preparing the recovery samples for the shock-wave experiments; and Sunney Chan for use of the EPR facilities.

Contribution # 4473, Division of Geological and Planetary Sciences, California Institute of Technology, Pasadena, CA 91125.

REFERENCES CITED

- Blanchard, S.C., and Chasteen, N.D., 1976, Electron paramagnetic resonance spectrum of a sea shell, Mytilus edulis: *Journal of Physical Chemistry*, v. 80, p. 1362-1367.
- Halley, R.B., Major, R.P., Ludwig, K.R., Peterman, Z.L., and Matthews, R.K., 1986, Preliminary analyses of OAK debris samples; 11 p., 7 figs., 4 tbls.; in Folger, D.W., ed., *Sea-floor observations and subbottom seismic characteristics of OAK and KOA craters, Enewetak Atoll, Marshall Islands*: U.S. Geological Survey Bulletin 1678.
- Henry, T. W., Wardlaw, B. R., Skipp, B., Major, R.P., and Tracey, J. I., Jr., 1986, Pacific Enewetak Atoll Crater Exploration (PEACE) Program Enewetak Atoll, Republic of the Marshall Islands; Part 1: Drilling operations and descriptions of boreholes in vicinity of KOA and OAK craters: U.S. Geological Survey Open-File Report 86-419, 502 p., 29 figs., 13 tbls., 3 appendices.
- Hurd, F. K., Sachs, M., and Hershberger, W. D., 1954, Paramagnetic resonance absorption of Mn^{++} in single crystals of $CaCO_3$: *Physics Review*, vol. 93, p. 373-380.
- Low, W. and Zeira, S., 1972, ESR spectra of Mn^{++} in heat-treated aragonite: *American Mineralogist*, v. 57, p. 1115-1124.
- Ludwig, K.R., Halley, R.B., Simmons, K.R., and Peterman, Z.E., 1986, Sr-isotope stratigraphy of disturbed and undisturbed carbonates: 23 p., 8 figs., 6 tbls.; in Henry, T.W., and Wardlaw, B.R., eds., *Pacific Enewetak Atoll Crater Exploration (PEACE) Program Enewetak Atoll, Republic of the Marshall Islands; Part 3: Stratigraphic analysis and other geologic and geophysical studies in vicinity of OAK and KOA craters*: U.S. Geological Survey Open-File Report 86-555.
- Marsh, S.P. (Ed.), 1980, LASL Shock Hugoniot Data: University of California Press, Berkeley.
- Ristvet, B.L., 1986, Personal oral communication.

Stoffler, D., 1972, Deformation and transformation of rock-forming minerals by natural and experimental shock processes: *Fortschrift Mineralogie*, v. 49, p. 50-113.

Tyburczy, J.A., and Ahrens, T.J., 1986, Dynamic compression and volatile release of carbonates: *Journal of Geophysical Research*, v. 91, p. 4730-4744.

Vizgirda, J. and Ahrens, T. J., 1980, Shock-induced effects in calcite from Cactus Crater: *Geochimica Cosmochimica Acta*, v. 44, p. 1059-1069.

Wardlaw, B. R., and Henry, T. W., 1986, Geologic interpretation of OAK and KOA craters; 39 p., 21 figs., 3 tpls., 1 appendix; in *Pacific Enewetak Atoll Crater Exploration (PEACE) Program Enewetak Atoll, Republic of the Marshall Islands; Part 3: Stratigraphic analysis and other geologic and geophysical studies in vicinity of OAK and KOA craters*: U.S. Geological Survey Open-File Report 86-555.

TABLE 4-2. Results for Borehole OAR-2A Samples. The pressures and accompanying errors are given in Giga Pascal (GPa). Depths are provided in both feet below seafloor (ft bsf) and feet below sealevel (ft bsl). For explanation of carbonate petrographic names used under DESCRIPTION column in this and succeeding tables, see Henry, Wardlaw, and others (1986, p. 83-97).

DEPTH		P	ERROR	DESCRIPTION
(ft bsf)	(ft bsl)	(GPa)	(GPa)	
0.6	111.1	12.5	2.6	uncemented sand
6.6	117.1	14.5	2.7	uncemented wackestone
12.2	122.7	13.2	4.5	uncemented wackestone
15.8	126.3	14.5	1.0	uncemented wackestone
21.4	131.9	15.0	2.4	uncemented packstone
23.8	134.3	10.9	1.0	uncemented wackestone/packstone
25.8	136.3	3.5	0.6	uncemented packstone below AA/BB bndry
32.2	142.7	0.0	1.0	cemented packstone
38.4	148.9	4.4	3.0	poorly-cemented packstone
57.3	167.8	0.0	0.7	cemented packstone
67.1	177.6	0.0	1.2	poorly-cemented wackestone
74.2	184.7	0.0	1.3	uncemented wackestone
81.6	192.1	0.0	1.9	uncemented wackestone
100.3	210.8	0.0	1.6	coral fragment, <i>Astreopora</i>
129.3	239.8	0.0	0.6	cemented wackestone
155.3	265.8	0.0	1.4	spar-replaced coral
177.4	287.9	0.0	0.7	well-cemented mudstone
196.3	306.8	0.0	0.8	cemented wackestone
241.6	352.1	0.0	1.2	uncemented grainstone
280.0	390.5	0.0	0.9	cemented wackestone burrow
315.6	426.1	0.0	1.1	cemented wackestone

TABLE 4-3. Results for Borehole OBZ-4 samples. The pressures and accompanying errors are given in Giga Pascal (GPa). Depths are provided in both feet below seafloor (ft bsf) and feet below sealevel (ft bs!).

CRATER ZONE	DEPTH (ft bsf)	DEPTH (ft bs!)	P (GPa)	ERROR (GPa)	DESCRIPTION
α_1	6.7	205.4	0.0	0.9	mud
α_2	44.0	242.7	0.0	1.0	wackestone
	75.9	274.6	0.0	2.3	coarse-grain packstone
β_{1a}	107.5	306.2	0.0	1.0	cemented
	119.1	317.8	2.3	1.0	cemented packstone
	136.0	334.7	0.0	0.6	cemented packstone
	141.8	340.5	0.0	0.5	cemented
	152.1	350.8	0.0	2.0	cemented
	163.3	362.0	0.0	0.8	cemented
β_{1b}	174.8	373.5	0.0	1.2	spar
	190.8	389.5	0.0	0.7	cemented wackestone burrow
	191.0	389.7	2.3	2.6	lithoclast and spar
	193.2	391.9	0.0	0.6	cemented packstone
	196.1	394.8	2.4	4.2	spar-replaced <i>Favia</i>
	199.6	398.3	0.0	1.6	fine grain muddy sand
β_2	199.9	398.6	0.0	0.7	uncemented wackestone
	207.7	406.4	0.0	1.8	cemented wackestone burrow
	210.9	409.6	0.0	0.7	cemented packstone burrow
	216.6	415.3	0.0	0.7	recrystallized <i>Tridacna</i>
	217.1	415.8	0.0	1.2	well-cemented tea-brown micrite
β_3	219.4	418.1	0.0	1.1	spar-replaced coral
	222.7	421.4	0.0	0.7	cemented packstone
	233.0	431.7	0.0	0.7	uncemented
	265.1	463.8	0.0	1.5	poorly-cemented
	324.0	522.7	0.0	1.1	cemented burrow
γ	397.7	596.4	0.0	3.2	spar-replaced coral

TABLE 4-4. Results for Borehole OCT-5 Samples. The pressures and accompanying errors are given in Giga Pascal (GPa). Depths are provided in both feet below seafloor (ft bsf) and feet below sealevel (ft bsl).

CRATER ZONE	DEPTH (ft bsf)	DEPTH (ft bsl)	P (GPa)	ERROR (GPa)	DESCRIPTION
α_1	0.9	164.6	0.0	1.0	uncemented grainstone
α_2	9.4	173.1	0.0	1.1	coarse-grain packstone
	13.0	176.7	0.0	1.0	uncemented packstone
	25.0	188.7	0.0	0.9	fall-in (?)
β_{1a}	36.7	200.4	0.0	1.5	cemented wackestone burrow
	45.0	208.7	4.8	0.6	echinoid spine
	56.7	220.4	0.0	0.8	cemented packstone lithoclast
	63.4	227.1	0.0	2.0	rounded cemented burrow
	85.8	249.5	0.0	1.0	cemented packstone
	95.1	258.8	2.6	1.6	<i>Cardium</i> with internal filling
β_{1b}	104.7	268.4	0.0	3.5	spar-replaced <i>Cardium</i>
	115.7	279.4	0.0	0.8	cemented wackestone
	121.6	285.3	13.6	4.2	uncemented med-grained grainstone
	124.3	288.0	13.3	4.7	uncemented coarse-grained grainstone
	131.9	295.6	14.8	3.6	uncemented grainstone
	135.1	298.8	15.0	8.0	cemented grainstone
	140.6	304.3	12.0	6.3	uncemented <i>Halimeda</i> packstone
	146.2	309.9	15.0	7.8	uncemented <i>Halimeda</i> packstone
	153.4	317.1	0.0	0.6	cemented burrow
	163.6	327.3	0.0	0.6	cemented packstone
	174.1	337.8	0.0	0.8	cemented packstone
γ	192.6	356.3	0.0	1.6	cemented packstone
	204.7	368.4	2.5	0.4	tea-brown cemented rhizolith
	237.0	400.7	0.0	0.8	tea-brown cemented packstone
	300.3	464.0	3.6	3.5	spar-replaced coral

TABLE 4-5. Results for Borehole OET-7 Samples. The pressures and accompanying errors are given in Giga Pascal (GPa). Depths are provided in both feet below seafloor (ft bsf) and feet below sealevel (ft bsl).

CRATER ZONE	DEPTH (ft bsf)	DEPTH (ft bsl)	P (GPa)	ERROR (GPa)	DESCRIPTION
α_2	8.3	115.2	0.0	0.7	pebble-sized lithoclast
	12.0	118.9	13.0	4.5	uncemented grainstone
	17.8	124.7	15.0	5.5	coral pebble
γ	21.2	128.1	11.2	5.2	uncemented <i>Halimeda</i> grainstone
	25.9	132.8	15.0	4.8	uncemented packstone-grainstone
	30.7	137.6	12.6	2.7	uncemented packstone-grainstone
	35.3	142.2	13.7	4.3	uncemented packstone-grainstone
	40.6	147.5	13.0	5.0	uncemented fine-grain packstone
	66.7	173.6	6.4	2.1	cemented pebble-sized

TABLE 4-6. Results for Borehole OFT-8 Samples. The pressures and accompanying errors are given in Giga Pascal (GPa). Depths are provided in both feet below seafloor (ft bsf) and feet below sealevel (ft bsl).

CRATER ZONE	DEPTH (ft bsf)	DEPTH (ft bsl)	P (GPa)	ERROR (GPa)	DESCRIPTION
α_2	2.7	133.5	0.0	0.6	tea-brown cemented rhizolith
	6.4	137.2	0.0	0.6	tea-brown cemented lithoclast
β_{1a}	13.1	143.9	0.0	0.6	tea-brown cemented packstone
	17.0	147.8	0.0	0.9	cemented packstone
	18.4	149.2	4.2	1.6	cemented matrix within pelecypod
	20.5	151.3	2.0	1.4	partly spar-replaced coral
	22.8	153.6	15.0	4.0	uncemented packstone
	26.0	156.8	14.5	3.7	uncemented grainstone
β_{1b}	30.4	161.2	15.0	4.5	uncemented <i>Halimeda</i>
	35.0	165.8	15.0	5.2	uncemented packstone
	39.8	170.6	15.0	5.3	uncemented packstone
	45.5	176.3	14.8	2.5	partly spar-replaced coral
	50.1	180.9	14.7	1.0	uncemented packstone
	52.3	183.1	0.0	1.2	<i>Cardium</i> with cemented matrix
	52.6	183.4	0.0	0.9	partly spar-replaced coral
	54.4	185.2	0.0	0.6	moderately cemented packstone
	57.0	187.8	2.6	0.7	moderately cemented <i>Halimeda</i>
	61.1	191.9	2.5	0.9	poorly-cemented packstone
	64.5	195.3	8.1	0.8	cemented shell rubble
	64.9	195.7	0.0	1.1	spar-replaced <i>Astreopora</i>
γ	67.0	197.8	0.0	1.0	mudstone filled cemented burrow
	73.8	204.6	0.0	0.4	moderately cemented packstone
	81.2	212.0	0.0	0.5	cemented packstone
	93.5	224.3	0.0	1.4	spar-replaced <i>Porites</i>

TABLE 4-7. Results for Borehole OPZ-18 Samples. The pressures and accompanying errors are given in Giga Pascal (GPa). Depths are provided in both feet below seafloor (ft bsf) and feet below sealevel (ft bsl).

CRATER ZONE	DEPTH (ft bsf)	DEPTH (ft bsl)	P (GPa)	ERROR (GPa)	DESCRIPTION
α_1	3.6	205.5	0.0	1.4	uncemented mudstone
	7.0	208.9	2.5	2.1	uncemented mudstone
	10.0	210.9	0.0	1.0	uncemented mudstone
	23.3	225.2	0.0	1.4	uncemented mudstone
β_{1a}	57.8	259.7	0.0	2.1	uncemented wackestone
	78.2	280.1	0.0	1.4	uncemented grainstone
	95.9	297.8	0.0	1.0	uncemented grainstone
	117.8	319.7	0.0	1.1	uncemented grainstone
β_{1b}	135.3	337.2	0.0	0.9	uncemented grainstone
	155.3	357.2	2.2	0.9	uncemented packstone
	166.6	368.5	3.3	1.4	uncemented packstone
β_2	182.6	384.5	0.0	0.8	spar-cemented grainstone
	185.0	386.9	2.2	1.3	uncemented
	198.0	399.9	14.7	2.5	uncemented
	198.6	400.5	15.0	6.3	green Holocene wackestone mud
	207.0	408.9	13.6	5.4	uncemented
β_3	210.5	412.4	0.0	1.1	cemented packstone burrow
	214.0	415.9	14.1	2.5	uncemented
	217.0	418.9	0.0	0.9	tea-brown cemented packstone
	217.1	419.0	0.0	0.7	cemented wackestone
	217.5	419.4	0.0	1.4	cemented wackestone burrow
	220.4	422.3	0.0	1.3	coarse-grain spar
	220.5	422.4	0.0	0.8	cemented packstone
	223.5	425.4	0.0	1.2	cemented packstone burrow
	232.9	434.8	0.0	0.9	poorly-cemented packstone
	236.3	438.2	0.0	3.5	partially spar-replaced coral
	245.4	447.3	0.0	0.6	cemented wackestone
	256.9	458.8	0.0	2.0	spar-replaced coral
273.8	475.7	0.0	0.7	spar-cemented packstone burrow	
320.5	522.4	0.0	0.7	spar-filled grstropod	
γ	400.5	602.4	0.0	0.6	cemented wackestone

TABLE 4-8. Results for OAK Debris Samples. The pressures and accompanying errors are given in Giga Pascal (GPa). Source-depths are converted to feet below sea level from Ludwig and others (1987) and Ristvet (1981).

SAMPLE	RADIUS (ft)	ERROR (ft)	P (GPa)	ERROR (GPa)	SOURCE- DEPTH (ft bsl)
78	1053	13	0.0	0.9	-
125a	1273	13	0.0	1.8	200-500
126	1211	13	13.6	4.2	105-140
127	1095	13	3.0	2.0	-
128	1421	13	10.5	8.0	105-140
144	1302	13	12.5	2.3	105-140
147	1170	30	2.7	0.9	-
155	1299	13	0.0	1.4	-
156	1109	13	0.0	1.1	-
156b	1109	13	0.0	0.9	-
158	906	13	0.0	1.0	200-500
166B	1109	13	0.0	1.0	500-700
167B	1276	13	0.0	0.6	-
168A	1155	13	0.0	0.8	-
168C	1122	13	0.0	1.4	300-500
201	2310	16	0.0	1.4	420
1-1	1358	157	13.1	1.6	105-140
1-2	1358	157	15.0	3.4	>140
1-3	1358	157	14.6	1.6	105-140

CHAPTER 5:

BATHYMETRIC STUDIES OF OAK CRATER

By

John L. Peterson¹ and Robert W. Henny²

INTRODUCTION

This chapter summarizes recent work done by the Air Force Weapons Laboratory (AFWL) and the New Mexico Engineering Research Institute (NMERI) in a first-order assessment of OAK crater bathymetry (Peterson and Henny, 1987). The starting points for this study were the 1958 pre- and postshot bathymetric maps and a new 1984 bathymetric map of the OAK crater (ALICE reef) area of Enewetak Atoll (fig. 5-1).

Objectives and General Procedures

The primary objectives were to characterize and to quantify changes in bathymetry resulting both from the detonation of the OAK device and from subsequent geologic processes. A secondary objective was to provide a set of working maps at a common scale of 1:2400 for use both by the PEACE Program and future investigations.

The approach was to prepare contour maps by digitizing and reprocessing each of the three bathymetric basemaps and to construct three isopach maps from the contour-map pairs with the aid of a computer. Areas and volumes were computed by contour interval for each of the isopach maps, and planar and cross-sectional features were examined critically on all six maps.

Terminology

The following terms are used in this Chapter. No attempt is made here to correlate the cratering terms with those used in other portions of this Open-File Report; this can only be accomplished after synthesis of the various data sets (see statement 8 of the Conclusions).

Circular crater -- crater region consisting of an inner circular component, as defined by the minus 145-ft closed contour in the postshot contour maps, which is enclosed by an outer-circular component as defined by approximately the minus 50-ft partially closed contour on the same maps.

¹ New Mexico Engineering Research Institute, Albuquerque, NM.

² Air Force Weapons Laboratory, Kirtland Air Force Base, NM.

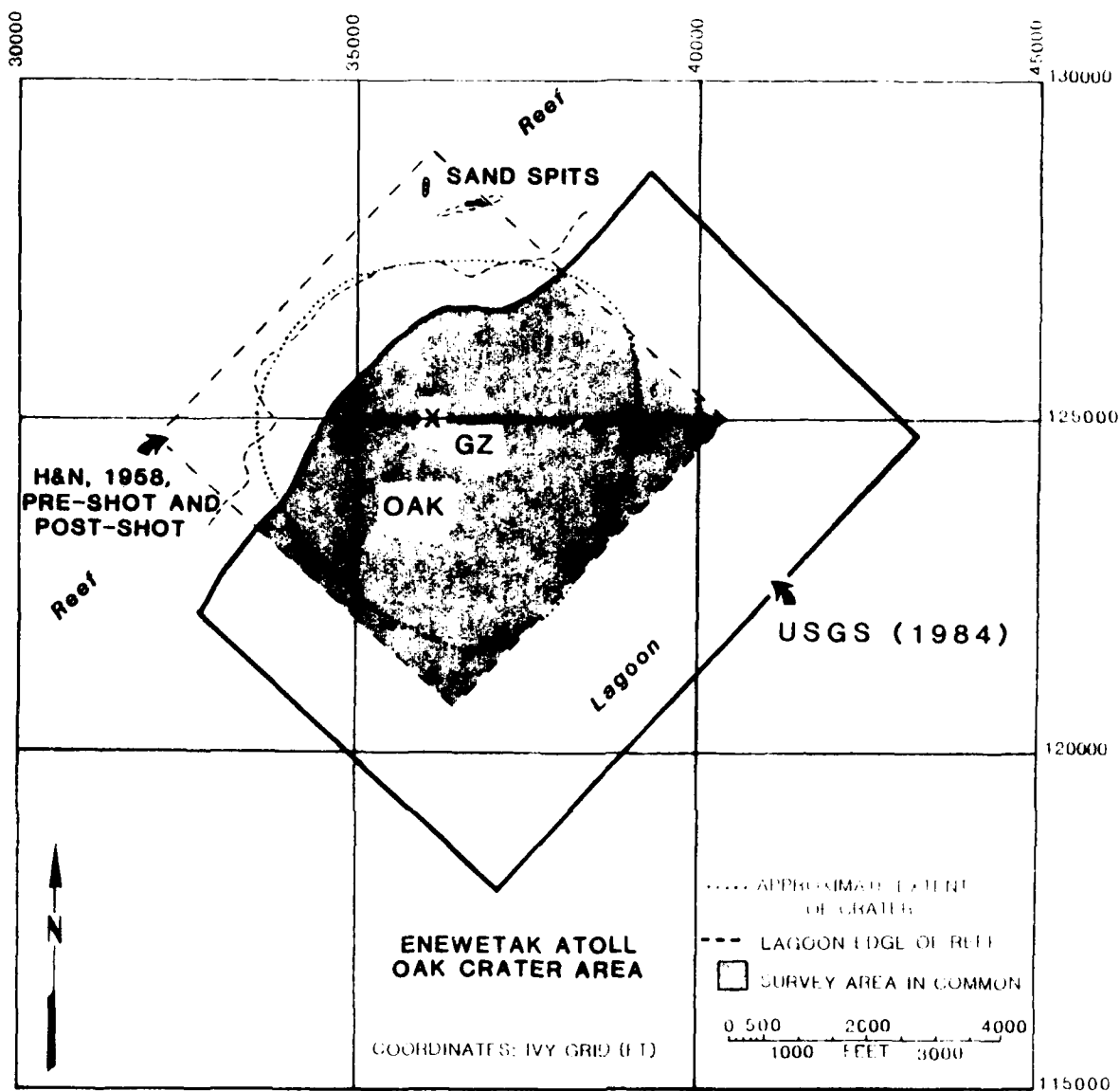


FIGURE 5-1. -- Map showing OAK crater region and areas included in Holmes and Narver pre- and postshot surveys (H&N, 1958a and 1958b) and the U.S. Geological Survey map (USGS, 1984). Area in common to all three basemaps shown in stippled pattern. OAK surface ground zero (SGZ) depicted by "X", and apparent crater shown by dotted line.

Crater wings -- areas primarily within the reef slope and just beyond the boundary of the circular crater.

Elliptical crater -- crater region consisting of the circular crater and portions of the crater wings as defined by the closed minus 20-ft contour of the isopach maps.

Apparent crater -- the final observed crater, composed of the elliptical crater and the encompassing areas of subsidence. Note that the apparent crater boundary extends beyond the mapped areas of this study.

Differential relief (subsequently abbreviated Δ -relief) -- term used in describing the net positive and negative changes in relief of an area with time. This is depicted by isopach maps showing the areas of change of relief derived from comparison of the digitized bathymetric base maps.

Subsidence -- term used to denote an increase in negative Δ -relief without subscribing to any particular mechanism.

Units used in this Chapter are those of the original works; metric for the 1984 bathymetry, engineering for the remainder.

DATA BASE

H&N Preshot Bathymetric Map

Prior to the OAK nuclear event (29 June 1958), a bathymetric survey of the site (ALICE-reef area) was conducted between 3 and 26 June by Holmes and Narver Engineering Company (H&N) for the U.S. Atomic Energy Commission (AEC) using standard rod, fathometer, and lead-line surveying techniques (fig. 5-1). Datum was 0.5 ft below Approximate Mean Low Water Spring (AMLWS). The survey, tied into the Eniwetok Ivy Grid Coordinate System (H&N, 1952; U.S. Army, 1970), originally was planned to cover a 6,000- x 6,000-ft square centered on the OAK surface ground zero (SGZ) and aligned with the oceanward edge of ALICE reef. A baseline approximately 6,000-ft long was established along the highest topographic area of the reef flat (specifically, along a line of sand bars midway on the reef flat) with benchmarks (BMs) placed on 300-ft centers.

A standard rod survey was conducted perpendicular to the baseline at each BM oceanward to near the reef edge and lagoonward to approximately the minus 5-ft elevation. Each survey line was continued lagoonward to 3,000 ft beyond SGZ using an LCM vessel equipped with a Raytheon Recording Fathometer. Vessel course was controlled by theodolite from each BM and at 300-ft intervals by triangulation from the two terminal baseline BMs. Vertical control was provided at these 300-ft intervals by a lead-line sounding. No cross-tie survey lines were run, and a data gap of a few hundred feet at the lagoonward reef edge resulted because of the inability of the LCM-vessel to obtain fathometer readings in water shallower than 10 to 15 ft (H&N, 1958a).

The resultant bathymetric map was hand-contoured with 5-ft intervals (1-ft intervals above the minus 5-ft contour) (pl. 5-1)¹. The map did not include the surveyed ocean side of the reef for reasons discussed below.

H&N Postshot Bathymetric Map

A postshot survey of the OAK crater area, using the same techniques described above, was run between 16 August and 4 September 1958 (D + 47 to 67 days). Numerous major problems were encountered in relocating the baseline along the reef flat opposite the crater because it was significantly disturbed (lowered and covered with debris) by the event. Eventually, the terminal BMs were located and the baseline reconstructed. As in the preshot survey, there was a data gap between rod and fathometer surveys that probably was increased by the difficult postshot conditions. These conditions also resulted in little of the reef oceanward of the baseline being resurveyed. Finally, toward the end of the survey, operationally imposed time constraints may have resulted in only every other line being surveyed in the far eastern quadrant of the grid. The resultant map (H&N, 1958b), contoured at a 5-ft interval, covered the same area as the preshot survey except oceanward of the reef baseline (fig. 5-1), thus giving a common pre-/postshot map area of approximately 6,000 x 5,000 ft or 30 million sqft (pl. 5-2).

Detailed documentation of the H&N surveys does not exist. Most of the information presented here is from B.L. Ristvet (oral communication, 1986) who has reviewed the original field survey books and maps referenced and has conducted extended discussions with several of the original workers.

USGS 1984 Bathymetric Map

The third basemap used in this study was the bathymetric map of the OAK crater and surrounding area prepared from a detailed echo-sounder survey conducted in 1984 (D + 26 years) by the U.S. Geologic Survey (USGS) during the Marine Phase of the PEACE Program (USGS, 1984; see Folger, Hampson, and others, 1986, for details of the survey). This survey also was tied into the Eniwetok Ivy Grid; however, datum was Mean Lower Low Water (MLLW), which is 0.18 m (0.6 ft) below the MLWS established for the earlier H&N surveys. Most of the echo-sounder data were collected along 25-m- (82-ft-) spaced lines oriented parallel to the reef. Perpendicular tie lines were run on the average at 180-m (590-ft) intervals (fig. 5-2). Thus, the USGS survey had a sampling density greater than four times that of the H&N surveys. Although smaller boats provided some data at shallower water depths, nearly all data contoured were obtained from the 41-m R/V Egabrag II, which, because of her draft, effectively excluded data above minus 4 m (minus 13 ft). Therefore, although the greatly increased sample density allowed a 1-m contour interval and the survey extended a 1,000 ft both farther out into the lagoon and along the reef slope (figs. 5-1 and 5-2), no bathymetric data were obtained from

¹ Plates 5-1, 5-2, and 5-3 are digitized, reprocessed versions of the referenced original bathymetric maps; these are located at the end of the Open-File Report in the map pocket.

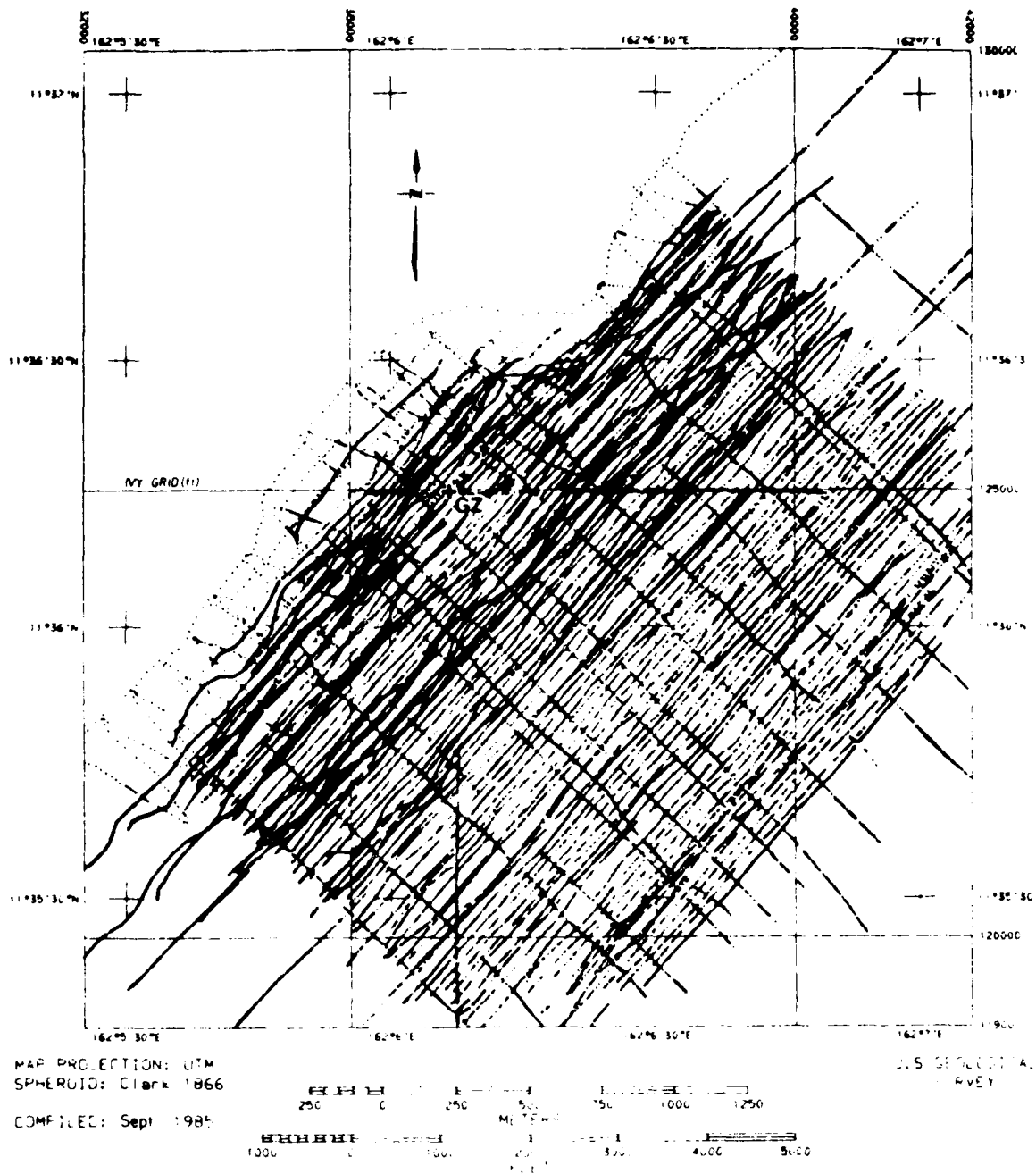


FIGURE 5-2. -- Fathometer lines used in the 1984 USGS study (from Folger, Hampson, and others, 1986, fig 2, p. A-3).

near the reef or on the reef flat itself. This reduced the contoured area common to all three maps to approximately 25.5 million sqft or 85 percent of the digitized H&N maps (see fig. 5-1).

DATA PROCESSING

Digitized Base Contour Maps

All data input and processing were performed using an Arc/Info Geographic Information System software package (ESRI, 1986). Processing was done on a VAX 11/750 computer at the Technology Application Center (TAC), University of New Mexico.

The data-input process for the two H&N maps (pls. 5-1 and 5-2, located in the map pocket at the end of the Report) was complicated because the maps were not on base-stable media. Both were digitized manually from 1:2400-scale bluelines using a 36- x 48-in. Summagraphics Digitizer Tablet operating in the continuous-string sampling mode. All data entered into the system were initialized and recorded in the Eniwetok Ivy Grid Coordinate System.

Digitization of the 1984 USGS basemap (pl. 5-3) required that a photographic enlargement be made from the original mylar map (1:6000). The enlargement was redrafted to separate contour lines along steep slopes within the study area. This redrafted map was photographically enlarged again to increase digitizing accuracy of the contours.

Three minor corrections were required to standardize and update the USGS map. The first was a simple conversion of metric contours to feet. However, since no interpolation was applied to the converted metric units, non-integer engineering-unit contours were generated. The second was a depth correction. This resulted from the comparison of the water-depth values interpolated from the USGS bathymetric map to those measured at each borehole site during the Drilling Phase of the PEACE Program. Linear fits to these data pairs showed that fathometer depths exceeded borehole-site depths by 1 percent down to minus 120 ft, and that borehole-site depths exceeded fathometer depths by 2 percent below minus 120 ft (E.L. Tremba, oral communication, 1986). Third, only those portions of the USGS map that overlaid the H&N map boundaries were digitized.

All digitized basemaps were quality-control checked by interactive zoom editing with a 13-in. Techtronix 4107A Color Graphics Terminal. The maps were scale-corrected by the computer to be compatible for overlaying data sets.

Derived Isopach Maps

Three pairs of isopach maps were computer-generated by digitally subtracting combinations of the three contour maps. The contour-map combinations and descriptions of the resulting three pairs of isopach maps are listed below. The first isopach map of each pair presents negative Δ -relief; the second map shows the positive Δ -relief. All (as plates) are located in the pocket in the back of this Report.

H&N Postshot - H&N Preshot Map Pair: Plates 5-4 and 5-5 display distribution of short-term elevation changes (event to D + 67 days) primarily due to cratering effects.

USGS 1984 - H&N Preshot Map Pair: Plates 5-6 and 5-7 display distribution of long-term elevation changes (event to D + 26 years) primarily due to cratering effects and redistribution of crater-produced and natural debris.

USGS 1984 - H&N Postshot Map Pair: Plates 5-8 and 5-9 display distribution of post-crater long-term elevation changes (from D + 67 days to D + 26 years) primarily due to continued subsidence and redistribution of crater-produced and natural debris.

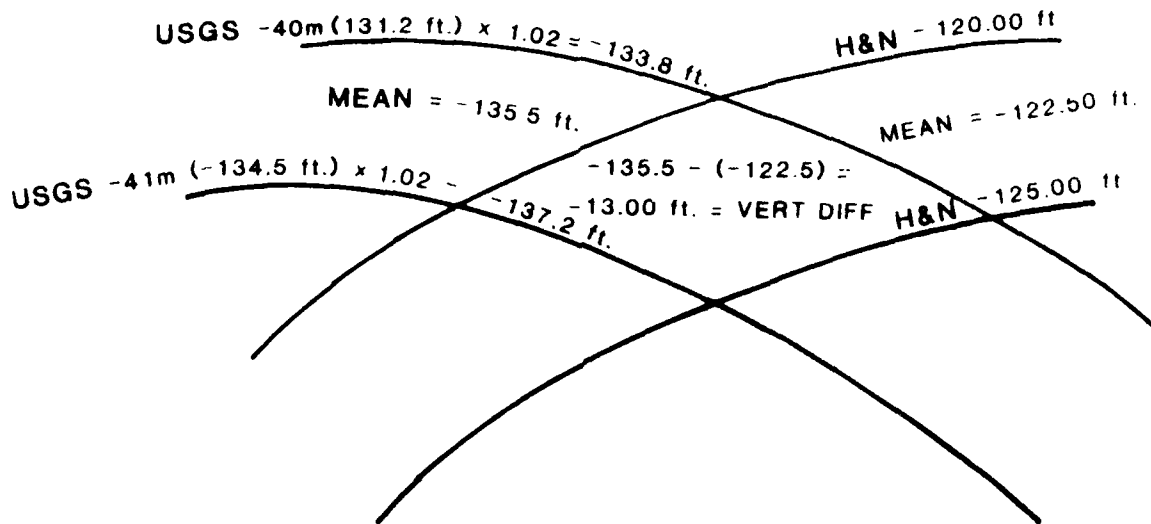
Figure 5-3 illustrates how vertical differences in elevation were calculated within the Arc/Info computer framework. As indicated, a polygon is formed where the two sets of elevation contours, one from each map, intersect. To account for as much of the elevation variance inside the polygon as possible, the mean between the two contours was always used. The vertical difference for each polygon, therefore, is the difference between the means of the two contour sets. In the production of the isopach maps, vertical differences were computed for all polygons formed by the intersection of one map overlaid on another. Typically, five thousand polygons were formed per isopach map. Areas for each polygon were computed in square feet and stored as associated attributes. The vertical-difference files and individual polygons were then sorted into 5-ft increments by a decision rule that grouped polygons with similar vertical differences (i.e.; 0 to 5 ft, 5 to 10 ft, etc.) into the same file.

To reduce required computer memory for the graphic displays, a dissolve module was run on the computer map files that combined adjacent polygons having the same 5-ft increment. Tabular data used to compute areas and volumes for each polygon were saved separately. The final groupings of polygons, representing an increment of 5 ft of positive or negative elevation difference (Δ -relief) between two maps, was then assigned a color and/or symbol for the slides or a shade and/or symbol for the hardcopy maps presented in this Report (pls. 5-4 through 5-9). The jagged appearance of many boundaries on the isopach maps results from the oblique angles formed by intersecting contour sets.

Map Products

Table 5-1 summarizes all maps produced during this study. Each map was produced as a color 35-mm slide, and selected maps were output as hardcopy at a scale of 1:2400 using a 36-in. Versatec Electrostatic Plotter. Because of the large number of contour increments required to fully delineate the crater and disturbed region, the color slides provided the best means to make first-order assessments of the maps. Hardcopy maps were necessary for more detailed analysis and publication. The three digitized contour maps are presented as Plates 5-1 through 5-3, and a positive and a negative display for each of the three derived isopach-map pairs are presented as Plates 5-4 thru 5-9, located in the map pocket of this Report.

EXAMPLE OF VERTICAL DIFFERENCE CALCULATION



VOLUME OF POLYGON = AREA OF POLYGON X VERT DIFF

FIGURE 5-3. -- Diagram showing isopach computational grid.

TABLE 5-1. -- Summary of digitized bathymetric map products for OAK crater for PEACE Program. Note that the 10-ft contour increment is depicted on the negative Δ -relief isopach maps (i.e., pls. 5-4, 5-6, and 5-8) for depth increments greater than minus 20 ft.

MAP PRODUCTS

MAP TYPE	PLATE	MAP TITLE	CONTOUR INTERVAL (ft)				SLIDE SETS	PAPER MAPS	AREA & VOLUME SUMMARS	
			3.3	5	10	25				
Contour	5-1	H&N Preshot	-	+	-	-	+	+	-	
	5-2	H&N Postshot	-	+	-	-	+	+	-	
	5-3	USGS Postshot	+	-	-	-	+	+	-	
Overlaid Contour	-	H&N Post- on H&N Pre- Overlay (contours only)	-	+	-	-	+	-	-	
	-	USGS on H&N Pre- Overlay (contours only)	-	+	-	-	+	-	-	
	-	USGS on H&N Post- Overlay (contours only)	+	+	-	-	+	-	-	
Isopach	5-4	H&N Isopach (Pre- & Post-)	Negative Δ -relief	-	+	-	-	+	+	+
	5-5	H&N Isopach (Pre- & Post-)	Positive Δ -relief	-	+	-	-	+	+	+
	-	H&N Isopach (Pre- & Post-)	Combined Pos. & Neg. Δ -relief	-	-	-	+	+	+	+
	5-6	USGS/Pre- H&N Isopach	Negative Δ -relief	-	+	+	-	+	+	+
	5-7	USGS/Pre- H&N Isopach	Positive Δ -relief	-	+	-	-	+	+	+
	5-8	USGS/Post- H&N Isopach	Negative Δ -relief	-	+	+	-	+	+	+
	5-9	USGS/Post- H&N Isopach	Positive Δ -relief	-	+	-	-	+	+	+

Plus (+) symbol indicates presence of product, minus (-) absence.

ANALYSIS

On comparing the three bathymetric basemaps discussed above (see fig. 5-1) and knowledge of the extent of the apparent crater of OAK, it is obvious that neither the 1958 H&N maps nor the 1984 USGS map continue outward far enough in any direction to fully cover the total area affected by the OAK event. This forms a significant limitation to any bathymetric analysis.

Map Derived Quantities

Several problems are associated with obtaining numerical values from the contour and isopach maps. These are complexly related to the previously discussed survey-sampling differences and deficiencies. They include the following: (1) the differences in areas mapped between surveys; (2) problems with positioning of the survey and drilling ships; and (3) the continuing redistribution of debris with time. The interpretation of the results are further hampered by the fact that both the pileup of debris from the crater (positive Δ -relief) and subsidence after the event (negative Δ -relief) occur over nearly the entire map area yet are inseparable solely from bathymetric data alone. However, even cursory examination of the maps shows clearly recognizable Δ -relief patterns that are easily followed from map to map (with time). Therefore, in general, the larger the area over which measurements are averaged, the higher the confidence of those values. Below are presented selected point (depths), line (cross sections), and area (area and volumes) estimates.

Water Depths. -- Table 5-2 compares water depths at each borehole drilled during the PEACE Program that are located within the map areas. Borehole water depths are those measured in the field at time of drilling and reported in the USGS (Henry, Wardlaw, and others, 1986a), whereas bathymetric water depths are the arithmetic mean of the bounding contours (3.3-ft contour interval). However, although the precision of the former are probably to within 0.1 ft, the latter could be in error by up to 1.7 ft. Additional errors probably occur due to borehole location uncertainties (± 10 ft), which could easily translate into several vertical feet in areas of rough postshot terrain.

Because the USGS bathymetry and drilling programs were completed within a year of each other, the differences in water depths provide a measure of the inaccuracies inherent on the USGS contour map. Fourteen of the boreholes exhibit differences ranging from plus 2.9 to minus 1.7 ft, with a mean of only 0.4 ft and an absolute average of 1.6 ft. The other four boreholes (OCT-2, ODT-6, OLT-14, and OUT-24) exhibit differences exceeding 4 ft (range from plus 4.8 to minus 5.8 ft), have a mean difference of 1.9 ft and an absolute average of 4.9 ft. For OLT-14, there was a problem in locating the position of the borehole (see Henry, Wardlaw, and others, 1986b, p. 390-391). For the other three, no trends are obvious nor is the reason for the larger differences known. These differences do illustrate the problem in relying solely on the bathymetric data to obtain point estimates.

Another important observation is that postshot water depths for boreholes located at roughly equal distances, but on opposite sides of SGZ, are similar

TABLE 5-2. -- Summary of water depths and vertical differences at PEACE Program borehole locations. Water depths are compared between measured values at borehole sites in 1985 (Henry, Wardlaw, and others, 1986, p. 60, tbl. 10) and interpolated values from Holmes and Narver preshot and postshot maps (H&N, 1958a, 1958b) and U.S. Geological Survey postshot map (USGS, 1984), compiled from echo-sounding data from Marine Phase of PEACE Program. All depths given in ft below sea level (bsl); vertical differences are given in ft. Note that the location of borehole OLT-14 is questionable (see Henry, Wardlaw, and others, 1986, p. 390-391).

WATER DEPTHS AND VERTICAL DIFFERENCES

BOREHOLE NUMBER	H&N PRESHOT DEPTH*	USGS DRILL LOG DEPTH** (1985)	USGS MAP DEPTH* (1984)	USGS 1984-85 DIFF.	H&N POSTSHOT DEPTH*	H&N POSTSHOT VS USGS 1984 DIFF.	
PARALLEL TO REEF							
1	ORT-20	67.5	101.4	102	-0.9	87.5	-14.8
2	OQT-19	47.5	117.5	115	2.2	107.5	- 7.8
3	OTG-23	47.5	164.0	166	-1.6	152.5	-13.1
4	OPZ-18	47.5	201.9	199	2.8	197.5	- 1.6
5	OBZ-4	12.5	198.7	199	-0.4	197.5	- 1.6
6	OCT-5	17.5	163.7	159	4.8	142.5	-16.4
7	OGT-9	17.5	134.8	136	-0.7	122.5	-13.0
8	OFT-8	17.5	130.8	129	2.0	117.5	-11.3
9	OET-7	17.5	106.9	106	1.4	92.5	-13.0
10	ODT-6	17.5	90.1	86	4.0	72.5	-13.6
PERPENDICULAR TO REEF							
1	OUT-24	1.5	147.0	142	4.8	127.5	-14.7
2	OBZ-4	12.5	198.7	199	-0.4	197.5	- 1.6
3	OPZ-18	47.5	201.9	199	2.8	197.5	- 1.6
4	OKT-13	102.5	164.7	166	-0.9	152.5	-13.1
5	OIT-11	122.5	155.0	152	-2.8	147.5	- 4.7
6	OHT-10	122.5	137.3	139	-1.5	122.5	-16.3
7	OJT-12	112.5	143.8	146	-1.7	132.5	-13.0
8	ONT-16	132.5	135.1	132	2.9	122.5	- 9.7
9	OMT-15	142.5	110.9	112	-1.1	127.5	15.5
10	OLT-14	127.5	139.7	146	-5.8	132.5	-13.0

* From Arc/Info File.

** From Henry, Wardlaw, and others (1986, p. 60, tbl. 10).

regardless of differences in the preshot water depths. For example, at roughly 900 ft from SGZ, preshot differences in water depths between OUT-24 on the reefward side and OKT-13 on the lagoonward side are 101 ft; postshot differences are only 18 ft. At 1,800 ft from SGZ, ODT-6 and ORT-20 differ by 50 ft preshot compared to only 11 ft postshot. Another pair (OQT-19 and OET-19 at 1,400 ft) exhibit preshot and postshot differences of 30 and 10 ft, respectively. These data suggest that the net cratering effects in both the "coral" media and water were about the same.

Except for OMT-15, which lies along the lagoon radial (southwest transect) of a large debris tongue, all 1984 USGS water depths at borehole locations exceed the 1958 H&N postshot depths by 2 to 16 ft (see tbl. 5-2). Although no other trends are obvious, these values represent the minimum net downward displacement (i.e., downward movement of the surface plus any addition of debris that may have occurred between surveys). At OMT-15, there is a 15-ft decrease in water depth which, if valid, can only be explained by a late-time addition of debris possibly from a neighboring high.

Cross Sections. -- Figure 5-4 presents two composite cross sections through the OAK SGZ parallel to (southwest to northeast) and perpendicular to (northwest to southeast) the trend of the reef. Each profile of the composite was prepared by manually digitizing the respective contour maps. Note that a vertical exaggeration of 10:1 results in slopes accordingly out of proportion. The H&N preshot profiles illustrate that the OAK device was placed above a sharp break in slope of the lagoonward edge of the reef. Comparisons of the H&N pre- and postshot profiles show that a large part of the lagoon side of the crater was originally water, and, therefore, most of the ejecta from that side of the crater was water. Within the circular crater, the flat floor is offset lagoonward from SGZ by 300 ft, and sets of terraces on the reefward side of the crater are evident.

The H&N postshot profile, perpendicular to the reef, crosses the most complex portion of the map near the apex of a large debris mass rising over 100 ft above the preshot level near the 1,900-ft mark. A slightly smaller debris mass, 500 ft further out, is some 30 ft above the preshot level and appears to have built up against and engulfed a preshot coral knoll. The cross section parallel to the reef shows the break at the boundary of the circular crater and the crater wings. Several distinct terraces within the crater are visible.

Comparisons of the 1984 USGS and 1958 H&N profiles show that the entire region subsided. Maximum downward displacement is concentrated in the mid- to lower depths of the circular crater and out into the lagoon. Significantly less downward displacement has occurred on the wings of the crater, whereas, on the reefward side, material has moved up and in toward SGZ. In assessing these profiles it is important to consider that redistribution of sediments probably resulted in material moving out of and into the plane of the cross sections.

Areas and Volumes. -- Tabulated areas and volumes for each of the three computed bathymetric maps are given in Tables 5-3 thru 5-5, located at the end of

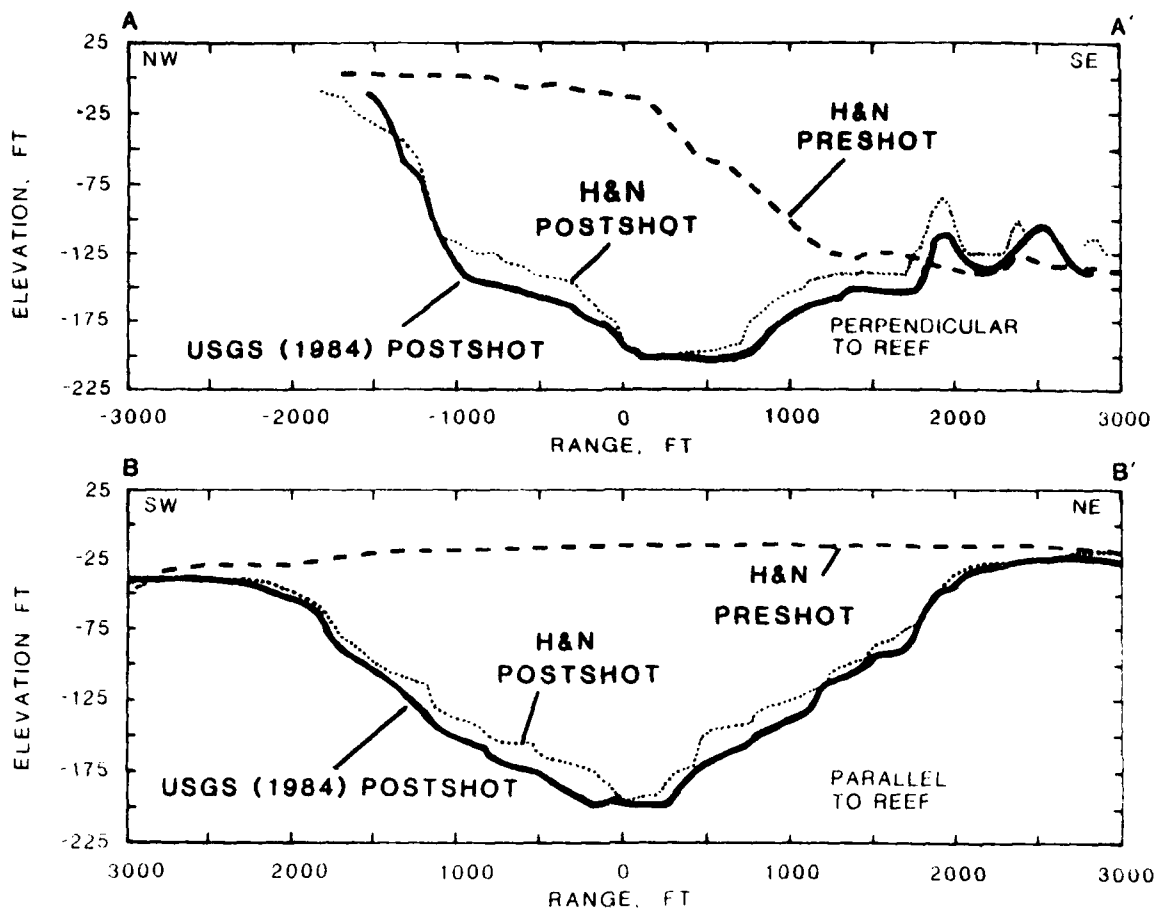


FIGURE 5-4. -- Cross sections through surface ground zero (SGZ) of OAK crater.

the Chapter¹, and summarized in Table 5-6. Volumes were computed in 5-ft increments by multiplying the vertical differences for each polygon by their respective areas and then totaling all of the volumes. Dimensions given are for each map area which, as discussed previously, differ somewhat between maps. The data demonstrate clearly that the entire area subsided an average of 23 ft by D + 67 days and another 12 ft during the next 26 years. As the surface of the crater and surrounding areas dropped, so did the coverage of positive relief, from 27 percent of the area at D + 67 days to only 14 percent of the area after 26 years.

MAP CHARACTERISTICS

The following is a first-order assessment of each contour and isopach map in terms of topographic patterns and characteristics. Because it is difficult to accurately quantify many of the features discussed, dimensions stated are only approximate.

H&N Preshot Contour Map

The northwest one-third (reefward side) of the 1958 H&N preshot map (pl. 5-1) shows the lagoonward side of the reef flat with sand bars along the upper margin. At the wave-break line, there is a well-defined, nearly linear scarp that is distinctly sharper north of SGZ. Approximately 400 ft reefward from SGZ, the scarp is cut by a 400 x 400-ft embayment. Beyond the scarp, a gently sloping shelf, dipping 1.5 degrees into the lagoon, ranges in width from 1,000 ft south of SGZ to less than 500 ft north of SGZ.

The southeast two-thirds of the H&N map (lagoonward side) comprises the reef slope and the lagoon floor, which contains numerous patch reefs. The reef slope, steepest (up to 15 degrees) north and shallowest (up to 5 degrees) south of SGZ, extends 1,000 ft beyond SGZ. Lagoonward from the foot of the reef slope, the lagoon floor slopes very gently (1 degree) toward the lagoon interior. Just south of SGZ is a 75-ft deep, 200-ft wide ravine with a steep, 25-degree headwall. This ravine flattens and widens lagoonward over a distance of about 1,500 ft but retains its identity to at least 2,500 ft as a clear path extending through the patch reefs. On the lagoon floor, numerous patch reefs, roughly aligned in two lineaments parallel to the reef at 1,700 and 2,600 ft lagoonward of SGZ, rise as high as 40 ft above the bottom and range up to several hundred feet in diameter. Their elliptical to triangular shapes on the map are due to the 300-ft H&N-survey spacing. Actually, they are in fact smaller and nearly circular as shown in the 1984 USGS map with its nearly fourfold increase in sampling density.

¹ Tables 5-3 through 5-5, summarizing the data calculated from the computer analysis of the pairs of derivative maps, and Table 5-6, presenting the grand summary of Tables 5-3 through 5-5, are all located at the end of the current Chapter.

Inspection of the H&N Preshot Contour Map (pl. 5-1) shows that the device was placed at a position along the Alice Reef marked by a large embayment. In addition, SGZ was located near the beginning of the lagoonward edge of the reef slope and close to the head of the large ravine that cuts into that slope. Although water depth, interpolated from the preshot map for the OAK SGZ, was almost 13 ft at shot time, according to B.L. Ristvet (oral communication, 1986), it was closer to 14 ft due to a 1.4-ft tide.

H&N Postshot Contour Map

The most striking feature of the OAK crater is its symmetry with respect to the geometric center (GC), which is offset nearly 300 ft lagoonward of SGZ. This is shown clearly in the 1958 H&N postshot map (pl. 5-2). All contours from the bottom of the crater up to the minus 145-ft contour, averaging 850 ft from the GC, are closed. The minus 125-ft contour, averaging 1,200 ft from the GC, closes except for a 45-degree sector on the lagoonward side. Furthermore, on the same side at roughly 1,500 ft from GC, the minus 100-ft contour closes to within 120 degrees. Slopes within the crater are much steeper on the reef side with distinct terraces and slump features evident throughout. Contours in the preshot embayment area are noticeably more distorted than at other locations along the reef.

A second major feature shown by the H&N postshot map is the extension of the debris blanket into the lagoon. This blanket is dominated by a 3,000-ft-long tongue of material, 1,500 ft wide at the crater edge and 55 ft thick at the highest point. Actually, the maximum thickness must be at least 75 ft due to an estimated subsidence in that region of at least 20 ft. The debris tongue is cut radially near the middle by a 400-ft wide channel closely aligned with the preshot ravine. This channel, breaching the crater rim at 1,200 ft from SGZ, passes between two topographic highs at 1,500 ft and bifurcates against another topographic high at 2,700 ft from SGZ.

A third major characteristic is the difference in the preshot to postshot topography in the area of the crater wings along the reef slope. North of SGZ the postshot contours virtually overlay the preshot contours, whereas south of SGZ, the contours have changed considerably and most of the reef slope clearly has been modified by the event.

Many of the patch reefs surveyed preshot do not appear on the H&N postshot map. Some were obviously destroyed, others buried by debris; however, many were probably not mapped in the H&N surveys. Resolution of this issue will require a better understanding of the exact survey lines used by H&N. The 1984 USGS Map (pl. 5-3), with its greater sampling density, adds important information regarding these features and probably could be used as a base to rectify the H&N maps.

USGS 1984 Contour Map

The 1984 USGS map (pl. 5-3) depicts many of the same features shown in the 1958 H&N postshot map (pl. 5-2), except that, with its fourfold increase in sampling density, features such as the coral patch reefs, crater terraces, and slump regions are much more sharply defined. After 26 years, the crater

is larger but retains its basic circular appearance; the crater wings have broadened, especially to the southwest. The inner component of the circular crater, still defined by the minus 145-ft contour, has expanded in radius about the GC from 850 to 1,050 ft. Contours are noticeably smoother, and slopes within the crater are steeper, particularly along the reef where at least two distinct scarps are now present. The debris tongue continues to dominate the lagoonward side, and the preshot ravine is still clearly visible as a remnant feature. Folger, Hampson, and others (1986) discuss the features of the 1984 USGS bathymetric map in terms of "physiographic provinces" and compare them to observations from the submersible, scuba-diving, and sidescan-sonar operations.

H&N Postshot - H&N Preshot Isopach Map

This pair of isopach maps (pls. 5-4 and 5-5) documents the areal distribution of Δ -relief (the net changes in negative and positive elevations), referenced to the preshot datum, resulting from OAK and extending to 67 days after the event.

The most striking feature of the map pair is the nature and distribution of the Δ -relief. Areas of positive Δ -relief, ranging up to 55 ft, cover only 27 percent of the total map of which Δ -relief greater than 5 ft (16 percent of the total map) is restricted to areas lagoonward of the crater. Negative Δ -relief dominates all other areas and covers 63 percent of the map, approximately one-half of that is outside the elliptical crater. The remaining 10 percent of the area shows no change in Δ -relief.

Although it is likely that at least some debris from the crater extends over nearly all of the area covered by the H&N postshot map, most of the reef and large regions on the crater wings and beyond are at a lower elevation than preshot. Therefore, this isopach map grossly understates the amount of debris present because of the unknown amount of event-related subsidence which is very difficult to isolate and measure. In fact, the total amount of debris is further understated because a substantial amount of the debris mass, particularly on the lagoon side, was water. Also, a small amount of ejecta impacted beyond the map area. And finally, an unknown amount of the debris mass may have been transported beyond the confines of the map.

A first-cut estimate of the downward displacement can be obtained by viewing the upper corners of the map (north and west of SGZ) that contain the reef flat. Most distant from SGZ, at 3,000 ft from SGZ, there are areas with a maximum of 5 ft of positive Δ -relief. In contrast at 2,000 ft along the same radials, but still beyond the elliptical crater, there are regions of 5 to 10 ft of negative Δ -relief. Because the positive Δ -relief is probably due to debris, and because debris thickness should increase toward the crater, it is concluded that at least 10 to 15 ft of negative Δ -relief is present at the 2,000 ft range. High-explosive craters in wet media typically display such downwardly displaced profiles, although large azimuthal variations often exist.

A second striking feature of this isopach pair is the elliptically shaped crater, defined by the minus 20-ft contour, which is in sharp contrast to the circular crater of the postshot contour maps (see pls. 5-2 and 5-3). This

elliptical crater, composed of the inner and outer components of the circular crater and the crater wings, has a long axis (4,000 ft) parallel to the reef and a short axis (2,800 ft) perpendicular to the reef.

Difference contours from the deepest point on the crater floor up to the minus 140-ft contour (400-ft radius) are roughly circular and symmetric about the GC of the crater. Above and up to the minus 110-ft contour (1,000-ft radius), the contour lines are roughly circular, but about the SGZ. Above, the largest rates of increasing difference (narrowest contour bands) occur between the minus 60- and minus 20-ft contours and probably represent a series of scarps surrounding the elliptical crater.

The elliptical shape of the crater is primarily due to the crater wings and to the sloping lagoon floor. This suggests that the crater wings, although controlled by the reef structure, are related to the circular crater. The elliptical crater is notably broken along the southeast by a remnant feature of the ravine and its headwall, previously described for the 1958 H&N preshot map. Finally, beyond the crater wings and predominately to the southwest, the en echelon pattern of difference contours suggests successive slumping parallel to the reef and well out into the lagoon.

USGS 1984 - H&N Preshot Isopach Map

This isopach map set (pls. 5-6 and 5-7) documents the distribution of net positive and negative Δ -relief from the preshot datum to 26 years after the detonation of the OAK device. Generally, the same basic difference patterns and features are displayed as at 67 days (previously discussed isopach map), but with some notable changes.

First, the entire area has subsided further so that now 86 percent of the map area exhibits a negative Δ -relief and only 14 percent exhibits a positive Δ -relief. The reef flat in the upper right corner of the map (north of SGZ) indicates an additional 5 to 10 ft of subsidence since the detonation of OAK. At the bottom of the map, 3,300 ft southeast of SGZ, an additional drop of 5 to 10 ft has occurred since the event. The previous maximum high of 55 ft on the ejecta tongue is now only 40 ft, indicating subsidence and possibly some redistribution of debris. Note that the new small circular highs in the bottom right of the map (east of SGZ) are probably artifacts of the higher density sampling by the USGS and were not detected by the earlier H&N surveys.

Second, the elliptical crater, as defined by the minus 20-ft contour, has expanded parallel to the reef in the crater wings and into the lagoon, but has contracted reefward. The net result is an increase of 500 ft in the long axis to 4,500 ft, but only an increase in the short axis of 100 ft to 2,900 ft.

Third, the difference contours near the crater floor have changed from circular to elliptical. However, the contours above that level (i.e., the minus 160- to minus 100-ft contours) have remained circular, expanded considerably, and shifted toward the reef.

USGS 1984 - H&N Postshot Isopach Map

This pair of isopach maps (pls. 5-8 and 5-9) shows the negative and positive changes in Δ -relief relative to the H&N postshot datum (47 to 67 days after the event) caused by redistribution of debris and long-term subsidence. In general, the entire map area is displaced downward increasing from 5 ft at the map boundaries (3,500 ft from SGZ) to 20 ft over much of the lagoon to 30 ft within the crater. Areas of negative Δ -relief now constitute 89 percent of the map area.

Areas of maximum negative Δ -relief are associated with deeper portions of the crater, the debris tongue, and isolated topographic highs in the lagoon. The concentric patterns of increasing negative Δ -relief vary from 5 to 10 ft at the edge of the circular crater (1,700 ft from SGZ) up to 25 to 30 ft just above the crater floor. This indicates that the circular crater has continued to subside with time. The multiple, repeating circumferential patterns in the elliptical-crater walls and along portions of the reef probably represent en echelon slumping of debris.

Beyond the elliptical crater, the debris tongue exhibits 5 to 15 ft greater negative Δ -relief compared with surrounding areas, even at its maximum extent of 3,300 ft, where a negative change of 20 to 25 ft is measured. Localized areas of 30 to 45 ft of negative Δ -relief occur in the lagoon associated with topographic highs. These areas are complex with converging zones of negative and positive Δ -relief probably representing slumping and redistribution of debris.

Areas of positive Δ -relief are associated with the flanks of several topographic highs, suggesting (as mentioned above) movement of debris downslope. The small positive Δ -relief on the floor of the crater is due to infillin and probably masks a 20-ft plus Δ -relief. The positive lineaments along the reef scarp probably reflect movement of reef blocks and washback of debris into the crater. The narrow positive lineaments bordering the extended crater probably represent movement of debris downslope along the crater rim scarps. The positive circular highs on the middle and lower right side of the map are probably artifacts of the previously mentioned bathymetry sampling density. The positive highs in the lower left portion of the map (south of SGZ) are unexplained.

CONCLUSIONS

Based primarily on analysis of the OAK bathymetric data presented herein, the following conclusions are reached:

1. The OAK event produced a circular explosion-type crater with debris distributed outward in all directions, probably continuously, to at least 3,000 ft from SGZ.
2. The circular crater, consisting of an inner circular component on the order of 850 ft in radius, probably formed initially by ejection and outward flow of material. This expanded outward by crater-wall collapse, slumping, and inflow of material to form an outer circular component. By $D + 67$ days, and probably much sooner, the circular crater had grown to a radius of 1,700 ft and a depth of 200 ft.

3. A very large tongue of debris, 1,500 ft wide at the crater edge and tapering to 500 ft at 3,000 ft from SGZ, was deposited outward onto the lagoon floor. This is cut by a 400-ft-wide channel that closely tracks the preshot ravine.
4. Also by D + 67 days, the entire area out to at least 3,000 ft from SGZ had subsided 5 to 10 ft with crater wings forming and expanding along the reef slope on either side of the circular crater. This resulted in an elliptical crater 4,000 ft parallel to and 2,800 ft perpendicular to the reef.
5. Over the next 26 years, the entire area continued to subside. This subsidence ranged from a minimum of 5 to 10 ft at 3,000 ft from SGZ up to 10 to 20 ft just outside the elliptical crater. Even greater subsidence occurred within the circular crater, particularly the lower portions, and out on the debris tongue. The length of the elliptical crater increased 500 ft (from 4,000 to 4,500 ft), but the width increased only 100 ft (from 2,800 to 2,900 ft).
6. Also, over this 26-year period, debris within the crater, on the debris tongue, and along the crater walls continued to slump. Elsewhere debris was selectively redistributed.
7. In retrospect, preshot topographic features (reef, embayment, ravine, and reef/lagoon slope) had a significant influence on the final size and shape of the crater and on the initial distribution and subsequent reworking of debris.
8. Finally, it is believed that a synthesis of the bathymetric data with the drilling, seismic, side-scan sonar, and gravity data will lead to a significant improvement in the quantification of the postshot topography which, in turn, should provide substantial improvement in the understanding of the cratering mechanics of the OAK event.

ACKNOWLEDGEMENTS

We are indebted to Gar Clark and his staff at the Technology Application Center (TAC), University of New Mexico, for their excellent and painstaking work in digitizing the basemaps and producing the contour and isopach maps. We also greatly appreciate the extended discussions with B.L. Ristvet of S-Cubed on the many details of the 1958 H&N surveying and for providing us the last "originals" of those maps.

This effort was jointly funded by the Defense Nuclear Agency (DNA). Project Officer for DNA was Lt. Col. Robert Couch; the Air Force Systems Command Project Officer was Maj. William Clark.

REFERENCES CITED

- Environmental Systems Research Institute (ESRI), 1986. ARC/INFO Users Manual v. 3.2, April 1986.
- Folger, D.W., Hampson, J.C., Robb, J.M., Woellner, R.A., Foster, D.S., and Tavares, L.A., 1986, Bathymetry of OAK and KOA craters; 32 p., 1 fig., 2 appendices; in Folger, D.W., editor, Sea-floor observations and subbottom seismic characteristics of OAK and KOA craters, Enewetak Atoll, Marshall Islands: U.S. Geological Survey Bulletin 1678.
- Henry, T.W., and Wardlaw, B.R., editors, 1986, Pacific Enewetak Atoll Crater Exploration (PEACE) Program, Enewetak Atoll, Republic of the Marshall Islands; Part 3: Stratigraphic analysis and other geologic and geophysical studies in vicinity of KOA and OAK craters: U.S. Geological Survey Open-File Report 86-555, 486 p., 92 figs., 90 tbls., 34 pls.
- Henry, T.W., Wardlaw, B.R., Skipp, B.A., Major, R.P., and Tracey, J.L., 1986, Pacific Enewetak Atoll Crater Exploration (PEACE) Program, Enewetak Atoll, Republic of the Marshall Islands; Part 1: Drilling operations and descriptions of boreholes in vicinity of KOA and OAK craters: U.S. Geological Survey Open-File Report 86-419, 497 p., 32 figs., 29 pls., 10 tbls., 3 appendices.
- Holmes and Narver Engineering Co. (H&N), 1952, Completion Report, Enewetak Proving Ground Facilities, Operation IVY; v. 1, book 1, p. 2-11 thru 2-25, Los Angeles, CA, 31 December 1952 [Unclassified]. Survey conducted for U.S. Atomic Energy Commission (AEC).
- Holmes and Narver Engineering Co. (H&N), 1958a, OAK preshot topography and hydrography map; Alice Reef Station #25: Field Book # 257, p. 2-15 thru 2-26 [June 9 through 26, 1958], Map Sheets J/S 03-001-C11 [compiled September 13, 1958]. Survey conducted for U.S. Atomic Energy Commission (AEC).
- Holmes and Narver Engineering Co. (H&N), 1958b, OAK postshot topography and hydrography map; Alice Reef Station #25: Field Book # 252, p. 2-1 thru 2-14 [August 14 thru September 4, 1958], Map Sheets J/S 03-001-C11 [compiled October 1, 1958]. Survey conducted for U.S. Atomic Energy Commission (AEC).
- Peterson, J.L., and Henny, R.W., 1987, Bathymetric studies of the 1952-53 nuclear cratering event, Pacific Proving Grounds: New Mexico Desert Research Institute Task Report WA6-16, September 1987, Albuquerque, NM.
- U.S. Army, 1970, Eniwetok Trig List: U.S. Army Topographic Command, Ft. Belvoir, VA.
- U.S. Geological Survey (USGS), 1984 [1985], Bathymetric Map of the OAK Crater Area, Enewetak Atoll [surveyed June 17 thru September 20, 1984, compiled September 1985]. [This is a working-scale map at 1:6000 of the map published as fig. 7, p. A8, of Folger, Hampson, and others, 1986]. Survey conducted for Defense Nuclear Agency (DNA).

TABLE 5-3. -- Summary of areas and volumes calculated from derivative map pair formed by combination of Holmes and Narver (H&N) preshot bathymetric/topographic map (pl. 5-1) and H&N postshot isopach map (pl. 5-2). Corresponding maps are Plates 5-4 for the negative Δ -relief and Plate 5-5 for the positive Δ -relief, respectively.

H&N PRESHOT VS H&N POSTSHOT -- VOLUMES AND AREAS

Δ -RELIEF CATEGORY	CONTOUR INTERVAL (ft)	AREA (sq ft)	TOTAL MAP AREA (2)	VOLUME (cu ft)
	50-55	1,348	0.004	74,160
	45-50	4,176	0.01	208,796
	40-45	6,201	0.02	279,045
Positive	35-40	21,735	0.07	869,344
	30-35	122,071	0.4	4,272,490
Δ -relief	25-30	299,352	1.0	8,480,567
	20-25	317,622	1.1	7,940,551
	15-20	727,271	2.4	14,545,419
	10-15	1,265,755	4.2	18,986,328
	5-10	2,118,996	7.0	21,187,252
	>0-5	<u>3,134,338</u>	<u>10.4</u>	<u>13,788,992</u>
Total Positive Δ -relief		8,018,865	26.6	91,132,994
Total Zero (0) Δ -relief		3,223,946	10.6	0
	>0-5	4,597,830	15.2	19,366,933
	5-10	3,090,431	10.2	29,015,023
	10-15	1,856,139	6.1	27,033,099
	15-20	1,133,271	3.8	22,237,414
	20-25	700,073	2.3	17,178,469
	25-30	454,545	1.5	13,423,574
	30-35	375,716	1.2	12,903,993
	35-40	330,047	1.1	13,017,456
	40-45	276,989	0.9	12,300,535
	45-50	307,840	1.0	15,220,082
	50-55	256,148	0.8	13,975,590
	55-60	294,104	1.0	17,531,655
	60-65	254,941	0.8	16,485,412
	65-70	258,841	0.9	18,033,970
	70-75	264,372	0.9	19,743,284
	75-80	244,716	0.8	19,493,811
	80-85	274,512	0.9	23,247,576
	85-90	269,727	0.9	24,166,199
	90-95	294,963	1.0	27,771,543
	95-100	338,887	1.1	33,472,777
Negative	100-105	291,674	1.0	30,298,728
	105-110	346,830	1.1	37,791,053
Δ -relief	110-115	355,535	1.2	40,539,123
	115-120	320,563	1.1	38,067,852
	120-125	391,098	1.3	48,674,321
	125-130	401,628	1.3	51,943,142
	130-135	324,904	1.1	43,586,633
	135-140	230,240	0.8	31,933,508
	140-145	76,917	0.3	11,138,929
	145-150	61,249	0.2	9,487,333
	150-155	63,632	0.2	9,862,944
	155-160	55,269	0.2	8,843,002
	160-165	41,603	0.1	6,864,133
	165-170	32,152	0.1	5,465,870
	170-175	8,008	0.1	4,901,403
	175-180	22,978	0.1	4,135,995
	180-185	23,807	0.1	4,404,134
	185-190	<u>7,449</u>	<u>0.03</u>	<u>1,415,289</u>
Total Negative Δ -relief		18,951,568	62.8	784,972,178

TABLE 5-4. -- Summary of areas and volumes calculated from derivative map pair formed by combination of U.S. Geological Survey (USGS, 1984) postshot isopach map (pl. 5-3) and Holmes and Narver (H&N) preshot map (pl. 5-1). Corresponding figures are Plates 5-6 for the negative Δ -relief and Plate 5-7 for the positive Δ -relief, respectively

H&N PRESNOT VS USGS POSTSHOT -- AREAS AND VOLUMES					
Δ -RELIEF CATEGORY	CONTOUR INTERVAL (ft)	AREA (sq ft)	TOTAL MAP AREA (%)	VOLUME (cu ft)	
Positive Δ -relief	35-40	3,874	0.01	142,848	
	30-35	45,563	0.20	1,431,653	
	25-30	83,634	0.30	2,269,071	
	20-25	222,615	0.9	5,202,429	
	15-20	203,841	0.8	3,683,457	
	10-15	399,046	1.6	4,865,145	
	5-10	897,017	3.5	6,635,921	
	0-5	1,678,303	6.5	3,792,121	
	Total Positive Δ-relief		3,533,893	13.7	28,022,645
Negative Δ -relief	0-5	2,933,886	11.4	9,388,814	
	5-10	3,826,724	15.0	30,180,137	
	10-15	3,220,256	12.5	40,631,938	
	15-20	2,359,641	9.2	40,622,228	
	20-25	1,191,911	4.6	26,888,750	
	25-30	676,404	2.6	18,451,376	
	30-35	450,900	1.8	14,086,145	
	35-40	371,889	1.5	14,086,246	
	40-45	324,188	1.3	13,924,608	
	45-50	312,580	1.2	14,978,353	
	50-55	302,003	1.2	15,895,082	
	55-60	289,656	1.1	16,078,999	
	60-65	275,562	1.1	17,264,649	
	65-70	253,538	1.0	17,161,790	
	70-75	245,220	1.0	17,773,609	
	75-80	223,971	0.9	17,360,741	
	80-85	252,353	1.0	20,796,354	
	85-90	288,305	1.1	25,364,923	
	90-95	286,225	1.1	26,602,615	
	Negative Δ -relief	95-100	270,795	1.1	26,505,055
		100-105	317,440	1.2	32,581,806
		105-110	338,915	1.3	36,342,656
		110-115	292,983	1.1	33,043,380
		115-120	256,188	1.0	30,203,119
		120-125	339,398	1.3	41,856,235
		125-130	306,752	1.2	39,182,244
		130-135	329,502	1.3	43,234,343
		135-140	274,305	1.0	37,830,334
		140-145	285,822	1.1	4,886,445
		145-150	387,055	1.5	57,054,655
		150-155	244,093	1.0	37,287,965
		155-160	127,398	0.5	20,112,575
		160-165	70,272	0.3	11,453,367
	165-170	67,390	0.3	11,340,488	
	170-175	54,923	0.2	9,519,263	
	175-180	48,496	0.2	8,659,313	
	180-185	58,401	0.2	10,717,498	
	185-190	41,979	0.2	7,869,618	
Total Negative Δ-relief		22,197,319	86.3	935,058,002	

TABLE 5-5. -- Summary of areas and volumes calculated from derivative map pair formed by combination of U.S. Geological Survey postshot map (USGS, 1984) and Holmes and Narver (H&N) postshot isopach map. Corresponding figures are Plates 5-8 for the negative Δ -relief and Plate 5-9 for the positive Δ -relief, respectively.

H&N PRESHOT VS USGS POSTSHOT -- AREAS AND VOLUMES

Δ -RELIEF CATEGORY	CONTOUR INTERVAL (ft)	AREA (sq ft)	TOTAL MAP AREA (%)	VOLUME (cu ft)
Positive Δ -relief	35-40	478	0.002	16,843
	30-35	844	0.003	26,802
	25-30	3,856	0.02	102,241
	20-25	17,189	0.1	378,356
	15-20	112,704	0.4	1,976,824
	0-15	272,512	1.1	3,386,556
	5-10	721,865	2.8	5,217,536
	0- 5	<u>1,820,125</u>	<u>7.1</u>	<u>3,739,364</u>
Total Positive Δ -relief		2,949,573	11.5	14,844,523
Negative Δ -relief	0- 5	4,053,640	15.8	11,485,025
	5-10	6,555,275	25.5	51,868,217
	10-15	7,707,037	30.0	97,957,905
	15-20	3,372,562	13.1	59,101,780
	20-25	857,090	3.3	19,181,484
	25-30	178,053	0.7	4,838,022
	30-35	28,472	0.1	921,606
	35-40	6,822	0.03	257,019
	40-45	3,177	0.01	136,916
	45-50	2,052	0.01	99,545
50-55	<u>579</u>	<u>0.002</u>	<u>30,640</u>	
Total Negative Δ -relief		22,764,759	88.5	245,878,159

TABLE 5-6. -- Grand summary of areas and volumes of negative, zero, and positive Δ -relief for OAK crater area. Summary derived from Tables 5-2 through 5-5. Area given in sq ft, volume in cu ft, net Δ -relief in ft.

TYPE Δ -RELIEF	H&N PRESHOT VS. H&N POSTSHOT		USGS POSTSHOT VS. H&N PRESHOT		USGS POSTSHOT VS. H&N POSTSHOT	
	Value	Percent	Value	Percent	Value	Percent
AREA: (sq ft)						
Positive Δ -relief	8,018,865	26.56	3,533,893	13.73	2,949,573	11.47
Negative Δ -relief	18,951,568	62.77	22,197,319	86.27	22,764,759	88.53
Zero (0) Δ -relief	<u>3,223,337</u>	10.68	<u>-----</u>	---	<u>-----</u>	---
TOTAL	30,193,770 sq ft		25,731,212 sq ft		25,714,302 sq ft	
VOLUME: (cu ft)						
Positive Δ -relief	91,132,994	10.39	28,022,645	2.91	14,844,523	5.69
Negative Δ -relief	<u>789,972,178</u>	89.61	<u>935,058,002</u>	97.09	<u>245,878,159</u>	94.31
NET	(693,809,189) cu ft		(907,035,357) cu ft		(231,033,636) cu ft	
AVERAGE NET Δ -RELIEF:						
	minus 22.99 ft		minus 35.25 ft		minus 8.98 ft	

CHAPTER 6:

CONSTRAINTS ON DENSIFICATION AND PIPING FOR THE OAK EVENT

By

John G. Trulio¹

BACKGROUND AND SUMMARY

PPG (Pacific Proving Grounds) sites differ widely from typical CONUS (Continental U.S.) sites in structure and composition. Hence, plausibly, high-yield near-surface nuclear explosions might dig much different craters in one setting than the other. But do they? The question cannot be answered by direct comparison of craters from such bursts. It therefore raises the kindred one of mechanism: The crater from a given burst could vary greatly from a CONUS site to the PPG, because dominant cratering mechanisms might -- but do they?

A "subsidence hypothesis" proposed in the early 1980's got to the physical nub of this issue:²

Explosive loading causes widespread fracturing of PPG coral, whose parts then settle slowly under gravity to form the outer one-half to three-fourths (in radius) of the apparent crater -- its "wing." By contrast, the inner one-half to one-fourth grows in several ways, including ejection of solid; indeed, virtually all ejecta come from that inner region -- or (hence) "excavation crater."

In sum, the subsidence hypothesis posits cave-in of a "coral" skeleton³ to fill the space left by water flowing out of it. Here, we call that process "simple subsidence." Its hallmark is an increase in coral density, since coral solids are denser than the water they replace [but for that, gravity (its cause) could not drive it]. Hence, alternatively, we speak of simple subsidence as "densification."

¹ Applied Theory, Inc., Los Angeles, CA 90036.

² The basic idea appears to have been suggested independently by S. Blouin, H.L. Brode, and B.L. Ristvet, years before the PEACE Program began. In the form stated here, the simple subsidence hypothesis is credited mainly to K.D. Pyatt and K. Kreyenhagen.

³ The OAK medium is referred to herein simply as coral. Said medium is a mixture of carbonate sediment, carbonate rock, and sea water with small amounts of other substances (see Chapter 7 of this Report for details of composition of the OAK medium). Used as an adjective herein, the meaning of coral is controlled by the noun it modifies; for example, "coral solid" denotes the solid components of the medium just described.

PEACE Program data do tell of excavation craters about one-fourth to one-third as large in radius as present apparent craters, widened by later slumping of their walls to about 0.4 of the latter radii (B.R. Wardlaw, oral communication, November 9, 1987). Thus, if the wings of apparent PPG craters did form by simple subsidence, then, for a given burst, most CONUS craters would have half the radii (or less) seen at the PPG. By the same token, coral under the wings would be denser now than pre-shot. PEACE Program measurements [borehole gravimetry and gamma-gamma (γ - γ) logging], however, disclose only minor changes in density there: Layers of coral (roughly horizontal) from the sea floor to clearly identified interfaces below have thinned much more than the measured densities alone imply. Hence, on the available data, most of the sea-floor lowering had other causes than simple subsidence. Succeeding sections summarize the evidence for and against this last statement; though not airtight, the case for it is strong.

When the mean density of solids in a column grows by a smaller factor than the column's vertical compression, lateral transport must take place. Such transport can occur during plastic flow, as in a tube of toothpaste. Another kind, termed "piping", calls for the flow of slurry (here, water plus coral particles) to the sea floor, where currents may sweep it out of the crater. Signs of piping abound in the OAK crater (Wardlaw and Henry, 1986b, p. 10; Halley and others, 1986, p. 4), but not in its wing, reducing the importance of PEACE measurements as constraints on piping (nonetheless discussed below). Plastic flow, perhaps with some "internal piping" (transport), seems the most likely means whereby the wings of OAK's crater formed. If so, similar wings could form at most CONUS sites -- and early, relative to such gravity-driven processes as slumping and densification. For structures, the wing would still be more benign than the excavation crater, but operating there would be no cinch.

BASIC FACTS AND PARAMETERS

Both the OAK and KOA craters were explored during the PEACE Program, but emphasis fell on OAK because many nearby shots preceded KOA; cratering-mechanism puzzles are made knottier by the effects of prior shots (example: How did MIKE affect KOA coral?). Indeed, even with the focus on OAK, and OAK's relative simplicity, the data base for assessing density changes remains slim. Priority rightly went to OAK.

In the OAK crater area, vital maps of the sea floor were drawn before the event, shortly after, and during the PEACE Program (see Chapter 5 of this Report). The bathymetric maps tell us how far the sea floor has sunk as a result of the shot. That does more than quantify what it is that we have to explain (essential enough). For, PEACE exploration has shown that, in the wing and beyond, the coral is split into layers by clearly identifiable Lagrangian surfaces (termed "horizons" by the geologists) that are critical here; several appear in Figure 6-1.

The horizons' great value lies in knowledge of their undisturbed (hence pre-shot) depths. By geologic means, those depths are reproducible down boreholes to within a few tens of feet, and most often to ± 10 ft, in this part of the atoll. More important still, they can be located generally to within a foot in any one borehole. Thus, the depth of each has been determined in boreholes inside the crater and out. So, therefore, has the shortening of

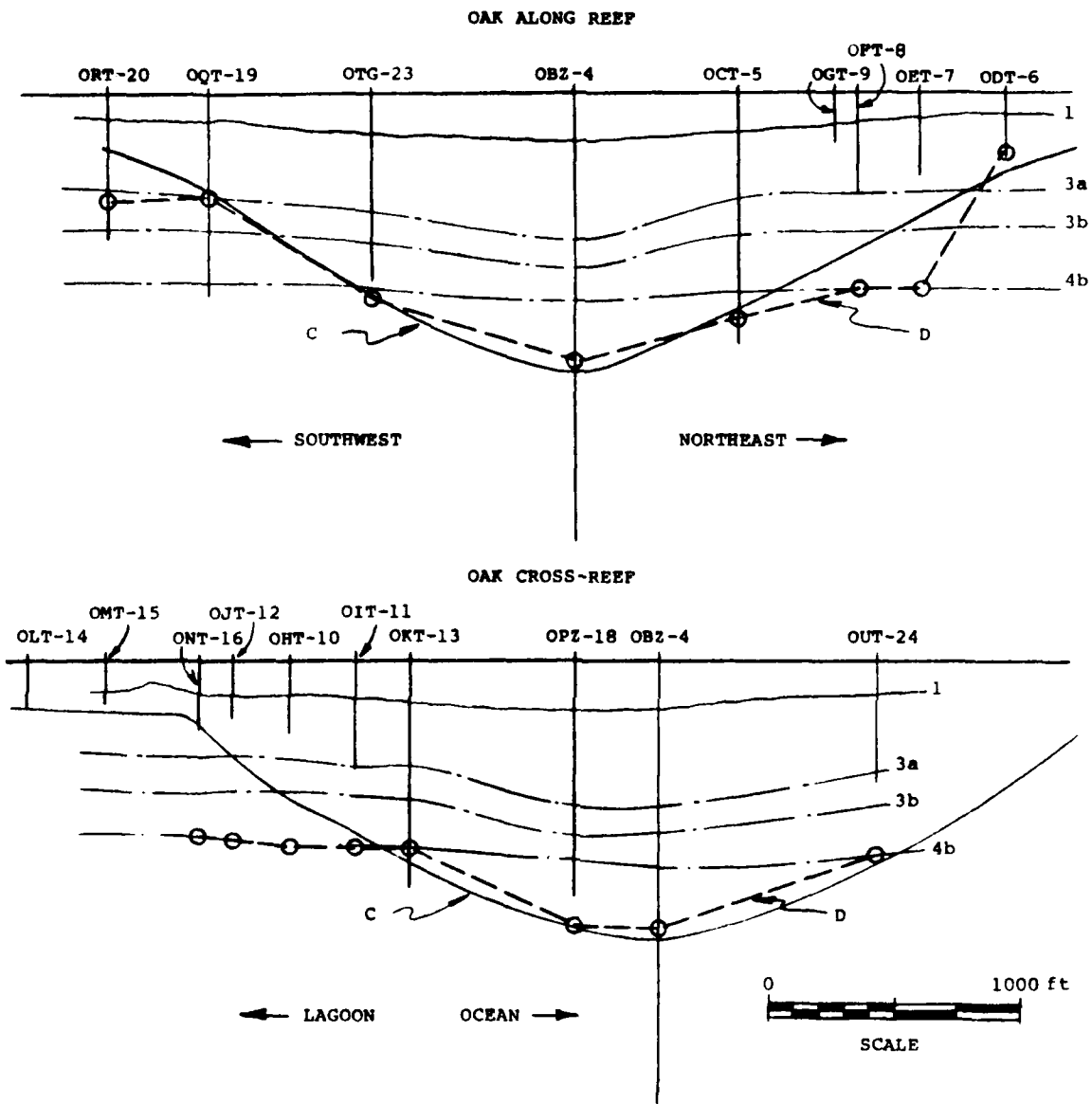


FIGURE 6-1. -- Vertical sections at the OAK site. Contours C and D, respectively, mark the bases of regions of (a) measurable decrease in sonic wavespeed and (b) measurable downward displacement. The SCALE (in ft) applies to all distances.

vertical columns between the sea floor and these horizons.¹ Mapped out too is the base of the region of sensible downward displacement of coral below the crater (contour D; fig. 6-1); its border lies close to the contour (C; fig. 6-1) that marks the limit of the region in which seismic wave-speed has decreased measurably (see Chapter 7 of this Report, particularly tbls. 7-2 and 7-4). Evidently, the shortening of any vertical coral column, flagged by lowering of the sea floor, takes place above the contour D -- and the column's mean vertical shrinkage is given by the ratio of sea-floor lowering at the top of the column, to the column's pre-shot height (current height plus sea-floor drop).

The OAK boreholes lay along two lines through the center of the crater (see Chapter 1, fig. 1-3), one parallel to the reef ("reef-wise") and the other at right angles to it ("cross-reef"). By design, most density logs (and results on densification) came from the reef-wise line (see Chapter 2, fig. 2-2). The reason: We need pre-shot density profiles to compute density changes and their effects. Now -- long after OAK -- those profiles have to come from logging in near-pristine coral outside the crater. For geologic reasons, however, systematic changes in material properties occur along cross-reef lines; on well-chosen reef-wise lines, the medium is subject mainly to smaller, random, local variations. Most actual borehole locations were chosen for OAK by PEACE geologists on that basis. The line those holes form runs close to the crater's center, so that density profiles along it can stand as rough cylindrical crater-averages at their respective reef-wise stations. What "rough" means rests with actual PPG measurements; so does the gut issue of reef-wise fluctuations in natural density profiles (below).

Table 6-1 presents basic PEACE data from the OAK crater, including the mean compressions of coral columns at borehole locations. All OAK boreholes are listed in the table; for reference, so is the estimated peak airblast pressure that acted above each. Of special weight are the table's mean vertical shrinkages $\Delta D/L$. Their average of 13 percent (16-1/2 percent for the reef-wise holes), if achieved via simple subsidence, would entail a mean density increase of $\sim .13$ g/cc (.18 g/cc reef-wise). That is larger by almost a factor of ten than the limit of BHG (and γ - γ) resolution achieved in the PEACE Program (.01 to .02 g/cc). Hence, direct on-site evaluation of the subsidence hypothesis was indeed feasible (not known when the program began). Concern therefore lies instead with systematic error and the natural reef-wise scatter of density/depth profiles. Further, as readily confirmed,

¹ The pre-shot depth of the sea floor is known at borehole locations, as are the depths of some horizons (depth uncertainties and confidence questions are taken up later). For a given borehole and horizon, the difference between horizon depth and sea-floor depth is the pre-shot height of the vertical column between horizon and sea floor. Likewise, for that same borehole and horizon, the post-shot height of the column from horizon to sea floor is also known. Between those two levels (horizon and sea floor), the particles of solid in the column may or may not be the same pre-shot as post-shot. The simple subsidence hypothesis says they are the same. The hypothesis is tested herein by adopting it, and comparing the column shortening it implies (when coupled with measured densities) to the observed shortening.

Hole	Range (ft) from GZ	L I N E	Preshot Depth L, (ft): Sea Floor to C to D		Water Depth (ft) Preshot D1 PEACE D2		ΔD, ft D2 - D1	Shrinkage ΔD/L, %; Column to D	Peak Overpressure MPa
			to C	to D	D1	D2			
JOR-17	6057.8		NA	NA	-	55.2	0	NA	1.0
OSM-22	5538.6		NA	NA	-	76.0	0	NA	1.3
OSR-21	5495.3	A	NA	NA	-	84.0	0	NA	1.3
OPT-20	1845.8	L	144.5	375	70.0	101.4	31.4	8	34
OQT-19	1444.3	O	360.0	380	46.0	117.5	71.5	19	72
OTG-23	804.6	N	796.4	787	45.6	164.0	118.4	15	620
OBZ-4	7.1	G	1125.6	1068	13.1	198.7	185.6	17	>690
OCT-5	658.3		841.5	891	16.2	163.7	147.5	17	>690
OGT-9	1043.5	R	-	-	16.0	134.8	118.8	-	228
OFT-8	1129.1	E	598.8	779	15.4	130.8	115.4	15	172
OET-7	1374.8	E	47.7	775	18.4	106.9	88.5	11	85
ODT-6	1714.9	F	291.6	211	20.0	87.4	67.4	32	41
OAM-3	4510.2		NA	NA	-	108.0	0	NA	2.3
OAR-2A	4500.2		NA	NA	-	110.5	0	NA	2.3
OAM-11	4458.4		NA	NA	-	114.2	0	NA	2.4
OAR-21									
OLT-14	2511.2	C	-	-	132.5	139.7	7.2	-	13
OMT-15	2203.6	R	-	-	141.8	110.9	30.9	-	19
ONT-16	1827.3	O	93.0	207	130.9	135.1	4.2	2	34
OJT-12	1695.5	S	257.3	617	115.0	143.8	28.8	5	43
OHT-10	1462.2	S	446.5	626	124.6	137.3	12.7	2	70
OIT-11	1205.5		568.5	636	121.6	155.0	33.4	5	136
OAT-13	988.7	R	730.0	664	101.7	164.7	63.0	9	269
OPZ-18	334.8	E	1032.6	1043	46.3	201.9	155.6	15	>690
OBZ-4	7.1	E	1125.6	1068	13.1	198.7	185.6	17	>690
OUT-24	858.0	F	828.4	782	1.6	147.0	145.4	19	510

TABLE 6-1. -- Column-height changes down boreholes at the OAK site. Contour C is the base of region of decrease in sonic wavespeed; contour D is the base of the region of downward displacement; GZ is ground zero.

Head- ing	Hole	RANGE,ft to OBZ-4	PEACE Depth, in ft bsl												
			Hole Base	Horizon											
				Surface D	2b	2c	2d	3a	3b	4b	5a	5b	5c		
SW R E E P W I S E NE	OOR-17	6060.6	1146.3	NA	363.1	405.7	552.4	765.2	961.2						
	OSR-21	5498.2	438.3	NA	290.1	344.2	391.7								
	ORT-20	1847.8	593.2	445	216.2	262.7	346.7	411.7	552.0	(1013.5)					
	OQT-19	1446.1	819.0	426	233.9	274.7	365.3	413.3	548.3	(1020.1)					
	OTG-23	805.5	751.3	(834)	/	434.0	484.0	610.0	(1000.4)						
	OBZ-4	0	1803.9	1081	/	593.0	701.2	847.7	1013.8	1065.1	1114.6				
	OCT-5	654.3	1015.2	9074	368.4	417.9	432.7	572.2	799.7	944.6					
	OGT-9	1039.6	209.8		/	/	/	/	/	/	/	/	/	/	/
	OFT-8	1125.0	414.3	(794)	223.3	272.0	344.6	(419.8)	(565.0)	(794.0)	(925.0)				
	OET-7	1370.5	338.6	(793)	220.6	294.7	320.4	(410.0)	(555.0)	(793.0)	(925.0)				
SE A C R O S S R E E P NW	ODT-6	1710.5	251.6	231	219.0	231.3	(315.0)	(397.0)	(546.0)	(792.0)	(925.0)				
	OAR-2A	4495.5	521.0	NA	310.0	355.6	410.6	(556.8)	(812.2)						
	OLT-14	2517.3	188.9	(700)	227.0	(341.1)	(383.8)	(534.6)	(700.0)	(1010.2)					
	OMT-15	2209.7	187.5	(702)	225.0	(334.6)	(373.9)	(529.7)	(701.9)	(1013.5)					
	ONT-16	1833.4	287.4	(715)	238.6	(337.8)	(395.2)	(537.9)	(715.0)	(991.8)					
	OJT-12	1701.6	241.1	(732)	238.0	(350.0)	(390.3)	(531.0)	(732.0)	(991.0)					
	OHT-10	1456.3	299.8	(751)	213.3	(360.8)	(403.4)	(531.4)	(751.0)	(987.3)					
	OIT-11	1199.4	441.5	(758)	274.4	375.0	434.8	(562.0)	(758.0)	(980.0)					
	ORT-13	982.7	920.0	766	232.9	326.1	411.6	431.3	564.0	765.8	(1036.5)				
	OPZ-18	329.1	950.5	(1089)	568.9	593.0	723.5	809.9	(1000.0)	(1063.0)	(1114.0)				
OBZ-4	0	1803.9	1081	373.0	407.0	457.1	592.0	784.0	847.7	1013.8	1065.1	1114.6			
OUT-24.	864.2	498.1	(784)												

TABLE 6-2. -- Uniformity of horizons in OAK area. Parentheses () signifies seismic data because borehole ends above depth shown; cross-hatching covers downward-displacement region; blank spaces signify missing values. Below sea level (given in ft) is abbreviated bsl.

the few tens of feet or less by which horizon depths vary (tbl. 6-2) have scant effect on the values of $\Delta D/\Delta z$ in Table 6-1.

SHORTENING OF CORAL COLUMNS BY DENSIFICATION: BOOKKEEPING

Let subscripts L and S refer, respectively, to the liquid and solid components of saturated coral. In a volume V of the mixture, let V_L and V_S be the volumes of the two components and ρ_L and ρ_S their densities. The mass, m, of the mixture is then equal to the mass of its liquid component ($=\rho_L V_L$) plus the mass of its solid component ($=\rho_S V_S$). Hence, if ρ denotes the density of the mixture, we can write:

$$\rho_L V_L + \rho_S V_S = m = \rho V$$

or

$$\rho_L \alpha_L + \rho_S \alpha_S = \rho \quad \text{Eq. (1)}$$

where α_L and α_S denote the volume-fractions of liquid and solid in the mixture:

$$\alpha_L = V_L/V \quad ; \quad \alpha_S = V_S/V \quad ; \quad \alpha_L + \alpha_S = 1 \quad \text{Eq. (2)}$$

Using the last of Eqs. (2) to eliminate α_L from Eq. (1), and rearranging, we get:

$$\text{Volume Fraction of Solid in Mixture} = \alpha_S = (\rho - \rho_L) / (\rho_S - \rho_L) \quad \text{Eq. (3)}$$

Hence, in volume V of the mixture, we find that:

$$\text{Mass of Solid} = \rho_S V_S = \rho_S \alpha_S V = V \rho_S (\rho - \rho_L) / (\rho_S - \rho_L) \quad \text{Eq. (4)}$$

Now consider a vertical column of coral of unit cross-section. Let the column be divided into short vertical sections. A section of the column of height dh then subtends a volume V, and Eq. (4) -- with dh replacing V -- gives the mass of solid in that section. Summing over all sections of the column from a height z_0 to a greater height z, the total solid mass m_S between those heights is given by:

$$M_S = \rho_S \int_{z_0}^z \frac{\rho - \rho_L}{\rho_S - \rho_L} dh \quad \text{Eq. (5)}$$

In Eq. (5), ρ_L , ρ_S , and ρ can all vary with height h in the column. Here however ρ_L (the density of sea water) is constant, while ρ_S can run only from about calcite's density to aragonite's (ρ_S can be set uniformly to the mean of the calcite/aragonite densities, with negligible error in m_S ; below). Thus,

the measured density of the mixture, ρ , holds the key to simple subsidence in the OAK event.

With the key, goes a key assumption: The pre-shot density profile down any crater hole is the same as that found now in holes outside the crater ("control holes"), where the medium is almost unmarred. Then, taking z_0 [Eq. (5)] at a level in the column where coral has not been vertically displaced, the vertical thickness subtended by solid mass m_s [from Eq. (5)] in a control hole, is equal to the pre-shot thickness of mass m_s of solid in the crater hole. On that basis, the hypothesis of simple subsidence can be tested via its mandate to conserve the column's solid mass. For, the present thickness of that mass [also from Eq. (5)], subtracted from its pre-shot thickness, will give the actual change in height of its topmost particle -- if that change is due to simple subsidence.

In particular, if z [Eq. (5)] refers to the crater floor, the change in question should equal the observed sea-floor lowering. Moreover, knowledge of the pre- and post-shot depths of horizons below the crater allows us a stronger result: By letting z_0 and z refer to any two horizons, Eq. (5) should give the same solid mass m_s pre-shot as now -- if the distance between horizons changed by means of simple subsidence. We therefore integrate upward from one and the same horizon R , both pre-shot ($z_0 = z_R^P$) and now ($z_0 = z_R^N$). When that is done (with a control-hole profile taken as "pre-shot"), a given solid mass m_s , reached at $z = z^P$ pre-shot, will be reached at $z = z^N$ now. For that solid (between z_R^P and z^P pre-shot), the difference $(z^N - z_R^N) - (z^P - z_R^P) \equiv \delta z$ specifies the change in thickness implied by the observed density-profile changes, if the solid moved only up or down. Thus, the meaning of measured density profiles for simple subsidence is shown by plotting δz (but with z increasing downward, not upward; i.e., with depth in place of altitude). Such plots tell how coral solid at any depth below the present OAK crater had its depth changed by the shot -- if simple subsidence caused the change.

DENSITY PROFILES, THEIR TREATMENT, AND DOWNWARD DISPLACEMENTS

Logs of back-scattered neutron and γ -ray intensity (see Melzer, 1986), and of gravity-field variations (Beyer, Ristvet, and Oberste-Lehn, 1986) furnished density profiles down boreholes in the OAK crater region ("neutron", " γ - γ ", and "BHG" profiles, respectively). On the reef-wise line (see second section), control-holes OOR-17 and OSR-21 were logged in all three ways, whereas neutron and γ - γ logs were taken in control-hole OAR-2A. There were no cross-reef control holes. On the crater's wing, however, the only reef-wise holes logged close to contour C or D were OQT-19 and ORT-20;¹ that was done by all three methods, save for neutron logging of ORT-20.

¹ That can be seen by comparing (1) the depths listed for contours C and D in Table 6-2 and (2) the density profiles presented in full in Appendix 6-1.

It was known before PEACE operations began at the PPG that we would have to look mainly to BHG for density profiles. Why? Because γ - γ logs tell about the medium only within a few centimeters of our 4-inch-diameter boreholes, where the drilling disturbance is greatest; neutron logs "see" about 4 inches farther out (L.S. Melzer, conversations, summer 1987). By contrast, BHG logs give average densities out to about 10 times the vertical interval between readings (generally an interval of 25 ft for the boreholes in question); BHG densities are thus virtually free of man-made or natural local variations in the medium. It was not known, however, whether BHG logging could be done with useful precision under PPG conditions; doing so was a first, and a major PEACE Program success (see Beyer, Ristvet, and Oberste-Lehn, 1986, and Chapter 2 of this Report).

BHG aside, steel borehole casing that ran downward from the sea floor for 100 to 150 ft, interfered with γ - γ logs; the tool was not calibrated for measurement in coral through such a pipe (L.S. Melzer, conversations, summer 1987). In view of that problem, and of changes to the medium from drilling, γ - γ density profiles are probably reliable only at depths greater than a few hundred feet (where they match BHG profiles fairly well). Further, if neutron logs are to add density profiles to the BHG/ γ - γ set, a way will be needed to calibrate the neutron tool for PPG coral (L.S. Melzer, conversations, early summer 1987). Thus, at present, density changes from the OAK event must be evaluated from BHG density profiles, augmented somewhat by γ - γ profiles.

Copies of all BHG density profiles from OAK's reef-wise line are shown in Figure 6-2, and the γ - γ profiles in Figure 6-3; all profiles appear at full scale in Appendix 6-1. For use in Eq. (5), each profile was fit by a piecewise linear function, an especially simple matter for the BHG step-profiles; the linear coefficients are listed in Appendix 6-1, where the fits are also plotted. At full scale, the fits overlap the measured profiles everywhere, reproducing them about as closely as their finite line width allows. Those fits embody almost all the depth-dependence of the integrand of Eq. (5); the rest stems from the solid component's density ρ_S , whose extremes lie within 4 percent of their mean (see preceding section). As measured, the variation of ρ_S over that small range is also no more than piecewise-linear with depth. Thus, at its worst, Eq. (5) calls only for integrating a ratio of two linear functions [since $\rho_S/(\rho_S - \rho_L) = 1 + \rho_L/(\rho_S - \rho_L)$] -- whence, down a given borehole, the solid mass m_S is easily found in closed form vs. depth. When m_S for a crater hole is equated to m_S for a borehole, however, the resulting equation for z^P in terms of z^n is transcendental. By taking ρ_S as constant over each of the many linear intervals of measured density ρ , we avoid that complication; m_S becomes (at worst) piecewise-quadratic in depth, and $z^n - z^P$ becomes an explicit function of z^n . The results, plotted in Figures 6-4 through 6-7, are identical (when plotted) with those obtained by solving the transcendental equation; indeed, simply replacing ρ_S by its mean (2.821 g/cc), and ignoring its depth-dependence, makes no significant change in the figures. Full equations and details of calculation, including the fits to ρ_S , are presented in Appendix 6-2.

The dotted and dashed curves in our thickness-change figures (figs. 6-4 through 6-7) and in Appendix 6-1 speak to a subtler point in the treatment of density profiles: They make direct use of all horizon-depths measured for a given control-hole/crater-hole pair. Specifically, Eq. (5) was integrated from any one horizon to the next higher one in the given control hole. Starting from the same lower horizon in the crater hole, the z^D -value dictated by equal solid mass m_S in the two holes, was computed from Eq. (5) (in the usual way; above) for each z^D -value. On reaching the next horizon in the control hole, z^D fell above or below -- but not on -- that horizon in the crater hole; the reasons: natural density-profile variations along the rock-wise line, and sources of thickness-change other than simple subsidence. Integration proceeded nonetheless from that horizon in both holes, until the horizon above it was reached in the control hole -- and so on until density data gave out in one hole or the other. A full thickness-change curve was thus developed in sections, with the assurance that integration started for each section from the bottom of the same geologic (bio- or lithostratigraphic) layer -- and hence in as nearly equivalent material as possible in both holes. Dots track that curve in our plots of thickness change. The process was then repeated with the roles of crater hole and control hole reversed (i.e., going from one horizon to the next higher one in the crater hole; dashes limb that curve in our plots of thickness-change. The mean of the dotted and dashed curves -- a solid curve -- also appears in the plots. All three curves are clearly distinguishable on the right half of Figure 6-4 (for example); note the horizontal step on the dotted curve, where integrating to the upper surface of a layer in control-hole OQR-17 took us past the corresponding surface in the crater hole (OPZ-18).

As the density profiles show (figs. 6-2, 6-3, and Appendix 6-1), logging began in each hole at a significant depth below the sea floor -- not at it. Calculated thickness changes (figs. 6-4 through 6-7 and Appendix 6-1) must therefore be extrapolated up to the sea floor from the smallest depths the logs cover. With OQR-21 as the control hole, the gaps spanned by extrapolation at boreholes OQT-19 and ORT-20, respectively, come to about 5 and 6 percent of the present distance between the sea floor and surface B (downward displacement limit; see preceding section). Using control-hole OQR-17, these figures grow to 23 and 21 percent -- large enough to have three people separately set reasonable upper and lower limits of extrapolation; arrows on Figures 6-6 and 6-7 mark the lines that gave the extremes of the six estimates and their mean.

The downward trend of every BHG-derived curve near its shallow end probably influenced all extrapolations (γ - γ curves go both ways; Appendix 6-2). If so, the bias can hardly be called a defect, given the trend's persistence. Indeed, it suggests forcibly that, down to 100 to 200 ft below the sea floor, the medium is somewhat less dense now than pre-shot.

CONTRIBUTION OF SIMPLE SUBSIDENCE TO THE OAK CRATER

The solid curves of Figures 6-4 through 6-7 (and Appendix 6-1) present final estimates of thickness change due to densification below Oak Crater. Extrapolating those curves to the sea floor produced the mean values listed as \bar{z} in Table 6-3.

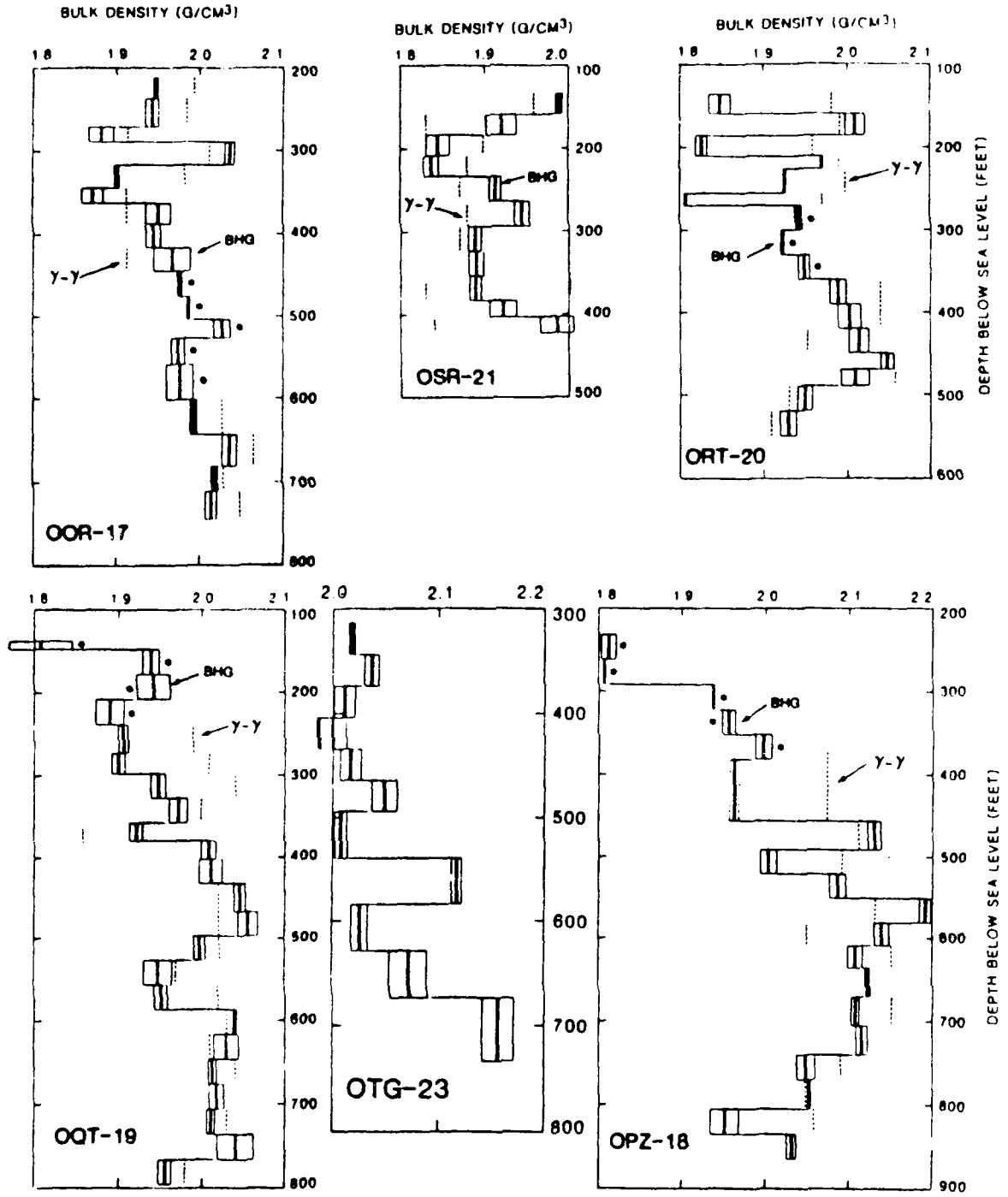


FIGURE 6-2. --Density profiles determined by borehole gravimetry (BHG) in the OAK crater area (Courtesy of L. Beyer, see Chapter 2). Depth below sea level (bsl) given in ft; bulk density in g/cm³. Inferred densities derived from gamma-gamma (Y-Y) logs shown as dotted lines. Asterisks (*) denote intervals where Y-Y logs are not available due to drillpipe.

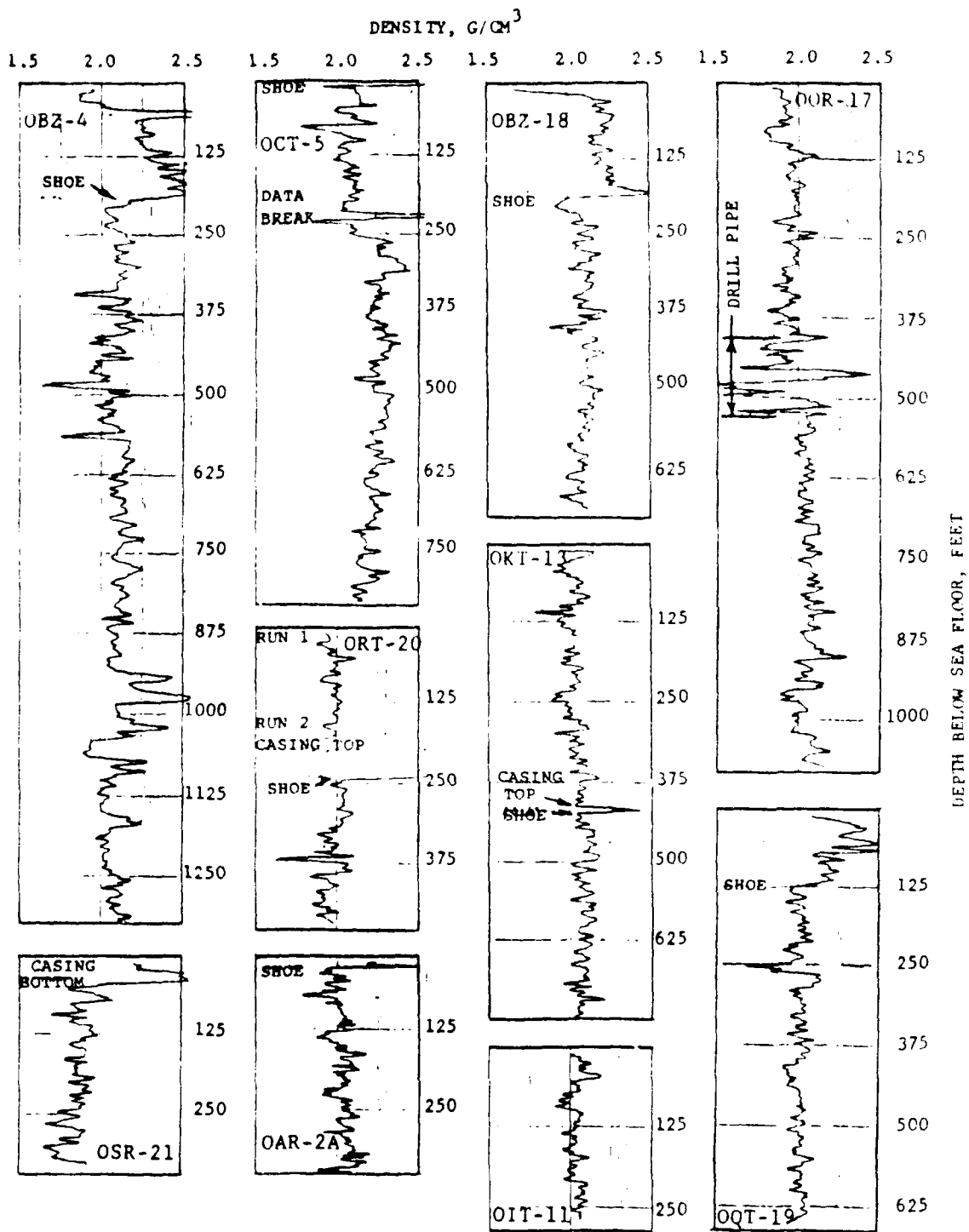


FIGURE 6-3. -- Density profiles from gamma-gamma (γ - γ) logging in OAK crater area (data from Meizer, 1986). Depth below sea floor given in ft.

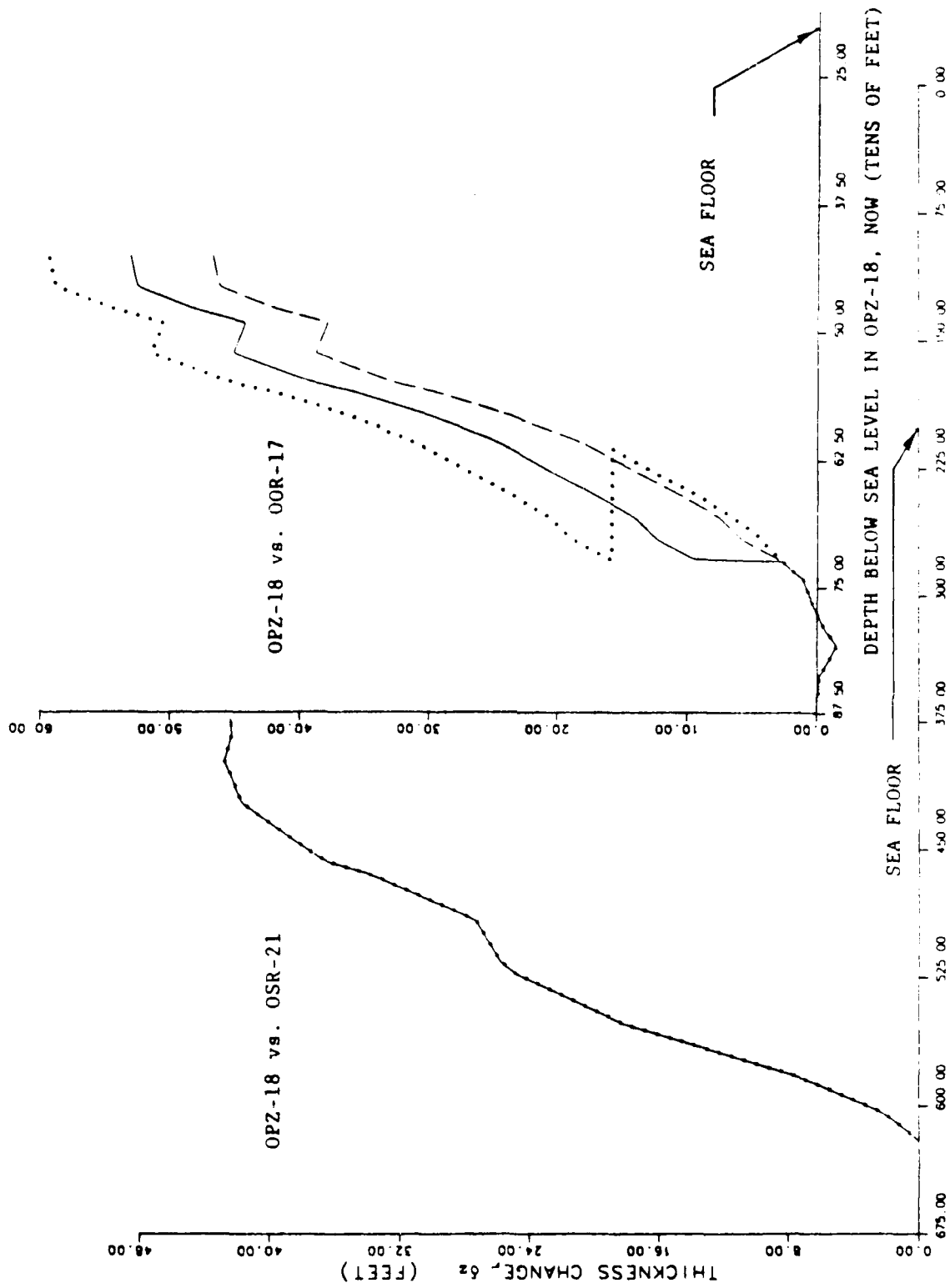


FIGURE 6-4. -- Change in rock thickness from borehole-gravity (BHG) densities, assuming simple subsidence. Boreholes OPZ-18 vs OSR-21 and OPZ-8 vs OOR-17. Strictly speaking, "NOW" refers to December 1984 throughout this Chapter.

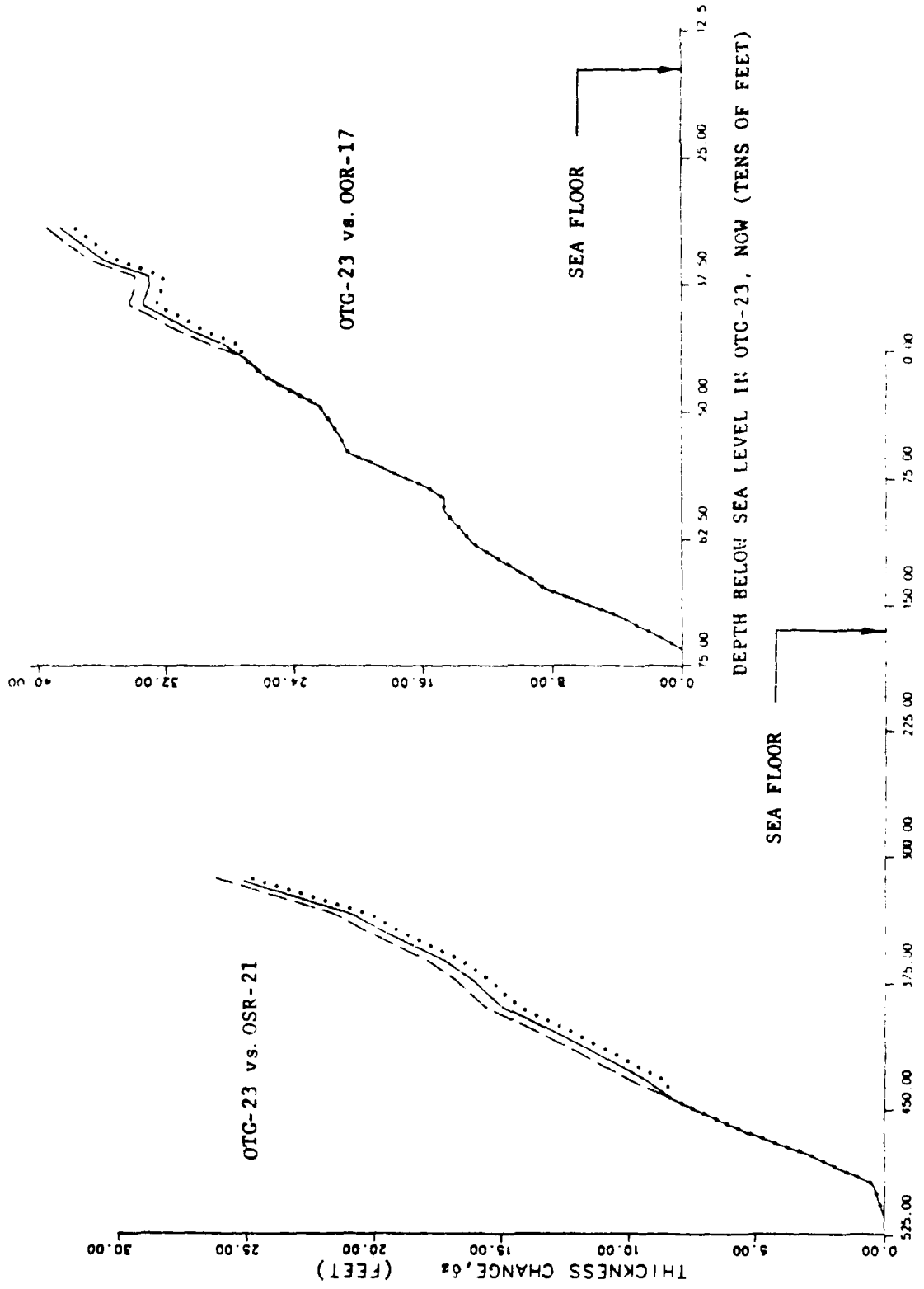


FIGURE 6-5. -- Change in rock thickness from borehole-gravity (BHG) densities, assuming sample subsidence. Boreholes OTG-23 vs. OSR-21 and OTG-23 vs. OOR-17.

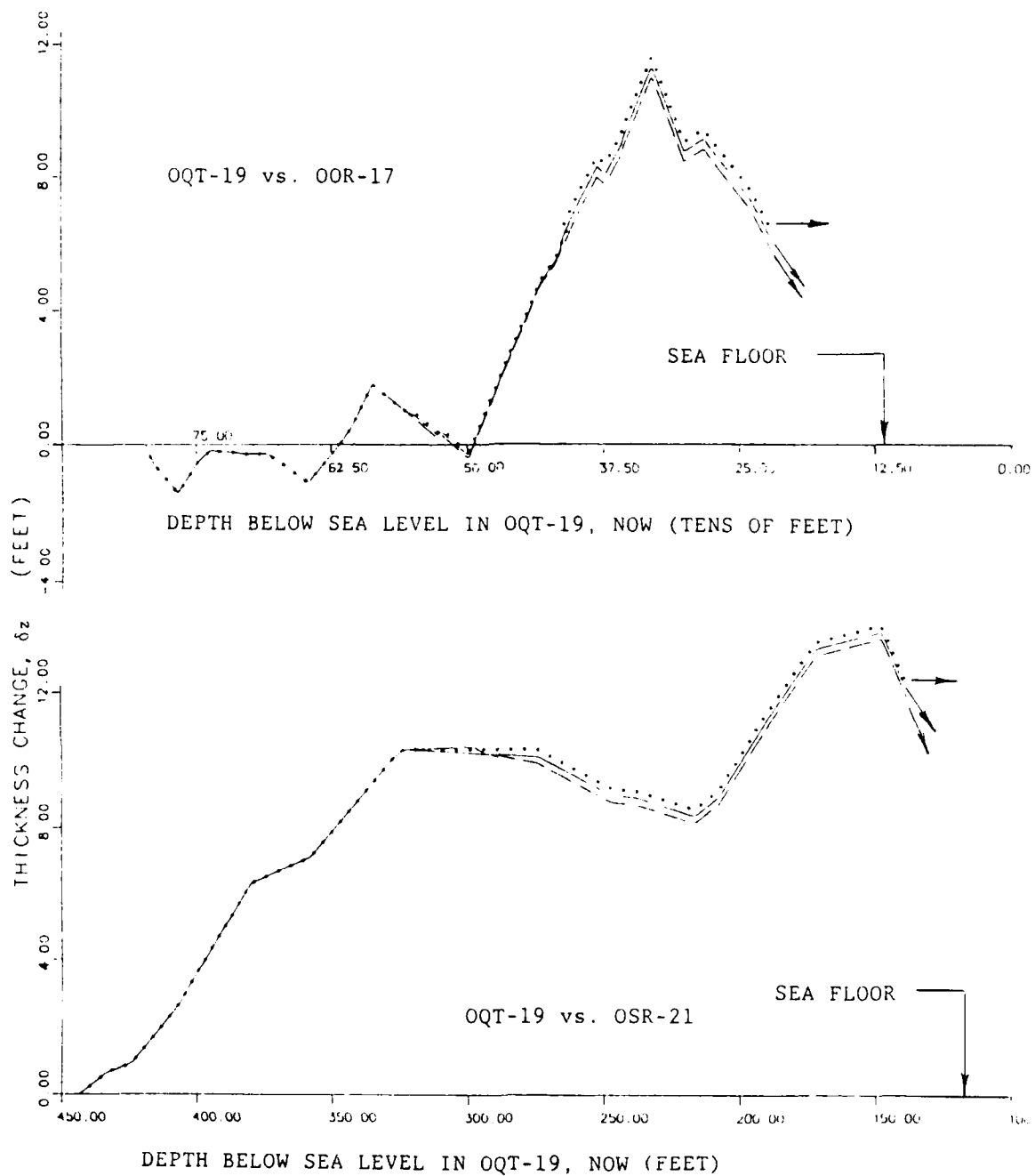


FIGURE 6-6. -- Change in rock thickness from borehole-gravity (BHG) densities, assuming simple subsidence. Boreholes OQT-19 vs OSR-21 and OQT-19 vs OOR-17.

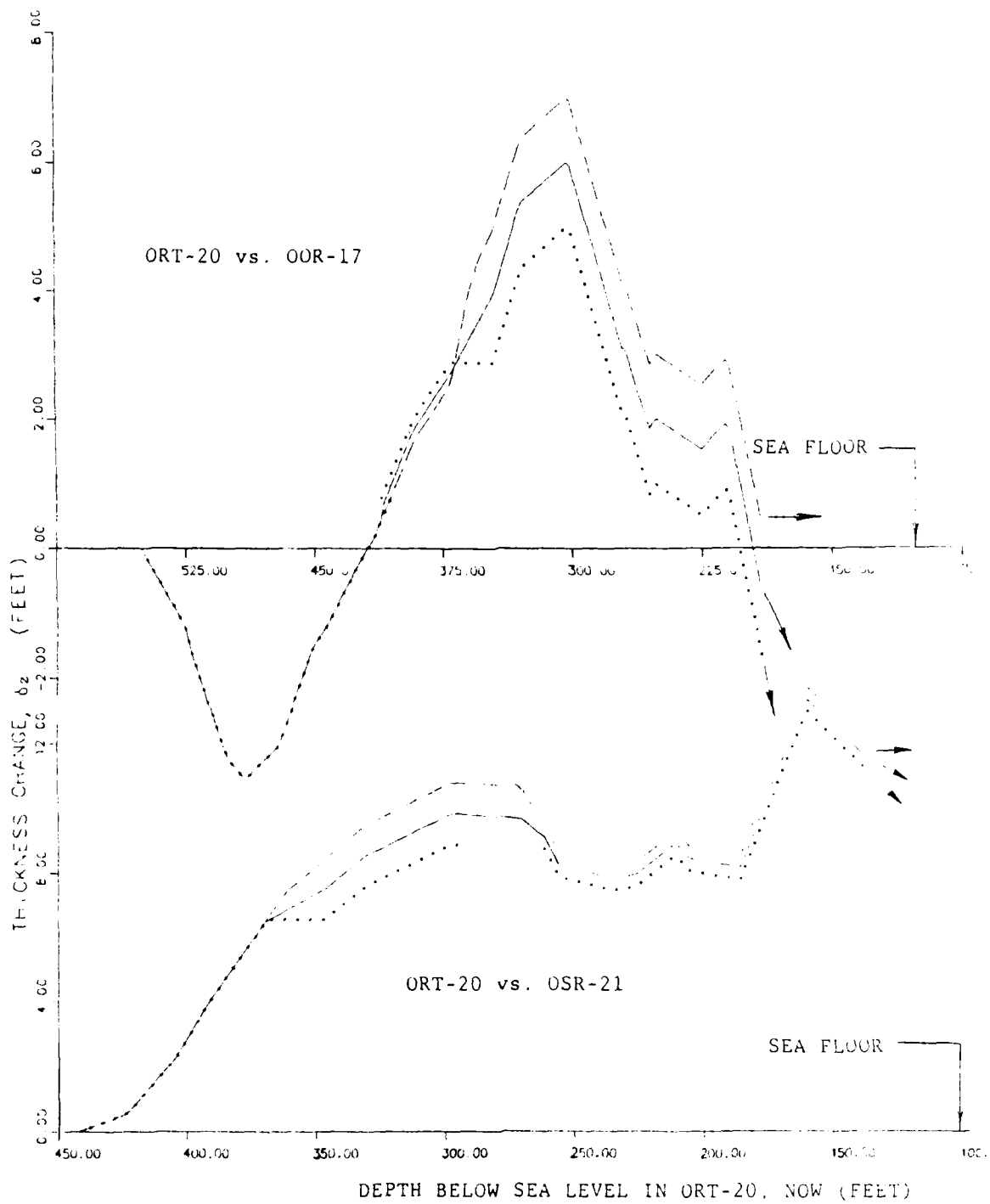


FIGURE 6-7. -- Change in rock thickness from borehole-gravity (BHG) densities, assuming simple subsidence. Boreholes ORT-20 vs. OSR-21 and ORT-20 vs OOR-17.

(Length Unit = 1 ft; $f \equiv \delta z / \Delta z$)

Pairs	Δz	AS MEASURED: D: 423 ft bsl for OQT-19 442 ft bsl for ORT-20				BIASED TO INCREASE f: D: 498 ft bsl for OQT-19 $\delta z = 3$ ft at D for ORT-20			
		δz	f	σ_3	δz	f	σ_3		
19/17	71.5	1.6	.02	.17	7.0	.10	.17	High Estimate <f> = { .153, no bias .238, bias up	
19/21	71.5	11.4	.16	.20	16.8	.23	.20		
20/17	31.4	1.6	.05	.18	4.6	.15	.19		
20/21	31.4	11.9	.38	.07	14.9	.47	.07		
19/17	71.5	-3.6	-.05	.24	1.8	.03	.24	Best Estimate <f> = { .060, no bias .146, bias up	
19/21	71.5	8.6	.12	.25	14.0	.20	.25		
20/17	31.4	-4.7	-.15	.19	-1.7	-.05	.20		
20/21	31.4	10.1	.32	.14	13.1	.42	.13		
19/17	71.5	-4.2	-.06	.30	1.2	.02	.30	Low Estimate <f> = { -.079, no bias .077, bias up	
19/21	71.5	6.5	.09	.29	11.9	.17	.30		
20/17	31.4	-10.3	-.32	.16	-7.3	-.23	.17		
20/21	31.4	8.2	.26	.21	11.2	.36	.20		

TABLE 6-3. -- Column-height changes (in ft) due to densification. Borehole pairs shown in left-hand column; f denotes the fraction $\delta z / \Delta z$.

If a column of material between D and the sea floor changed thickness via simple subsidence, then the thickness change δz computed from density profiles measured pre-shot (under our key assumption, see p. 6-8 above) and post-shot should equal the observed sea-floor lowering at the top of the column. The latter lowering is the column's actual thickness-change Δz (tbl. 6-3), whereas δz is the virtual change which densification provides, as computed from measured density profiles. For each control-hole/crater-hole pair, the ratio $\delta z/\Delta z$ appears in Table 6-3 as the fraction "f" of the sea-floor drop due to simple subsidence. On the wing of the OAK crater, the BHG profiles at hand (crater-holes OQT-19, ORT-20; control-holes OOR-17, OSR-21) tell a clear story: Only a small part of the sea-floor drop can be laid to simple subsidence. The highlights, subsumed in the f-values of Table 6-3, follow:

- (1). For the sea-floor drop, best estimates of the fraction (f) due to densification run from -.15 to .32, with a mean of .06.
- (2). With each variable (some not yet discussed) pushed to a reasonable extreme so as to increase f, the minimum, maximum, and mean of f are .02, .38, and .15.
- (3). With each variable pushed to a reasonable extreme to decrease f, the least, greatest, and mean f-values are -.32, .26, and .01.
- (4). With further possible but unlikely increases in all δz -values (right side of tbl. 6-3), the best-estimate values of f [(1), above] increase by .10, .10, and .09, respectively; the f-values in (2) and (3), above, also increase by about those amounts.

Items (1) through (4) above cover systematic errors in determining the fractions by which densification changed column-heights. A major question remains, however, especially with so small a data-set: What confidence can be placed in these results?

CONFIDENCE ASSESSMENT

To fix levels of confidence, we look first at "thickness-changes" caused not by the OAK shot but by natural density-profile variations from one reef-wise borehole to another. To that end, the profile from OSR-21 has been used as a crater profile with the one from control-hole OOR-17 (fig. 6-8) -- and vice versa (fig. 6-9). With OSR-21 as crater hole, extrapolation to the sea floor gives "thickness-change" extremes of -16.3 and -22.5 ft; with OOR-17 as the crater hole, the extremes become 19.8 and 30.4 ft. These are thickness-changes that the two profiles would imply if simple subsidence, in a single coral column down to about 400 ft below sea level (bsl), turned one profile into the other. Thus, not only is density steadily higher in OOR-17 than OSR-21 to about 442 ft bsl, but, as forseen,¹ the "changes" in question are a good deal larger than those due to the burst (the measured δz 's in tbl. 6-3

¹ Letters of July 12, 1984, and April 21, 1985, from author to Dean Oberste-Lehn, Research and Development Associates (RDA), and to Maj. Robert F. Couch, Defense Nuclear Agency (DNA), respectively.

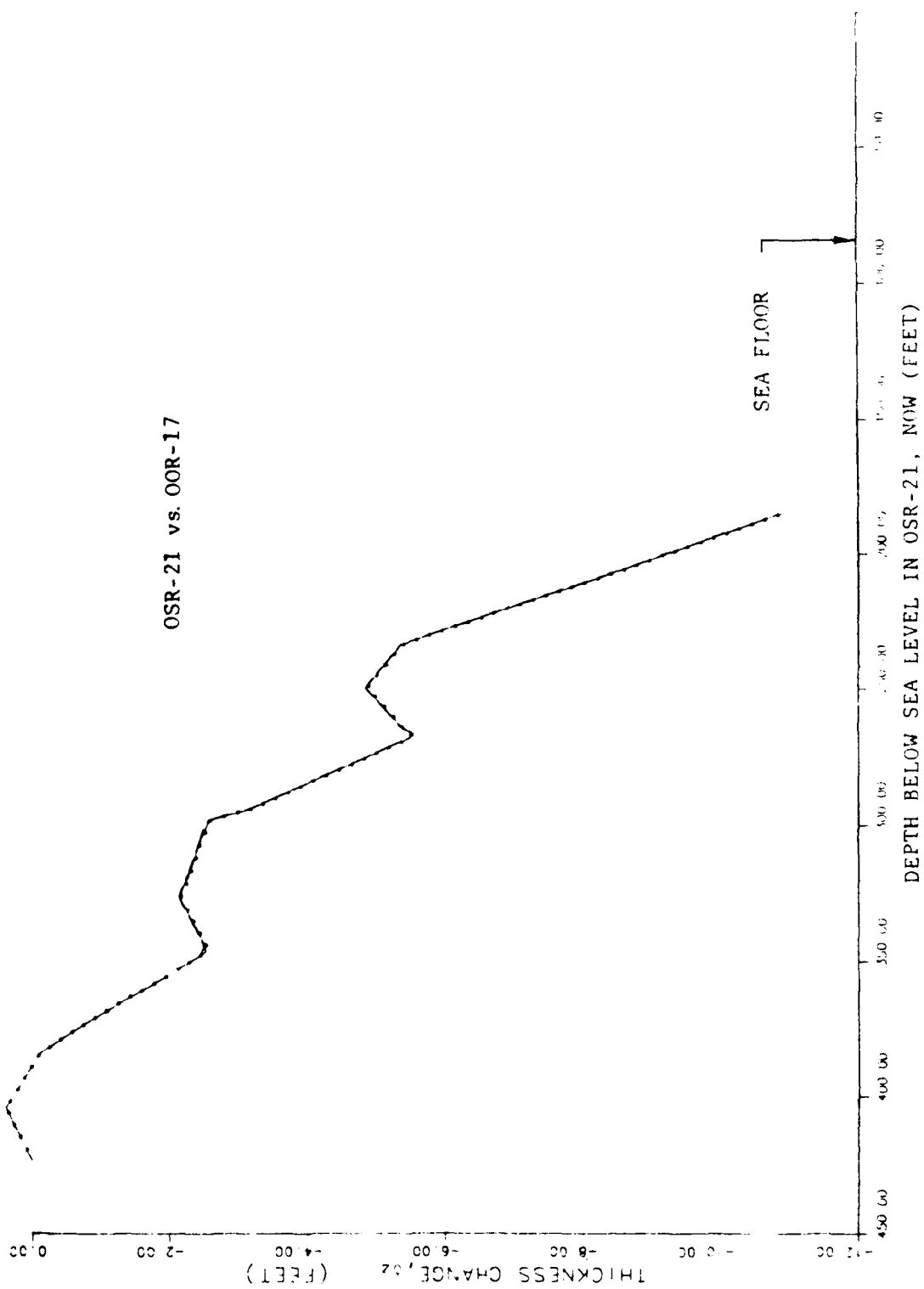


FIGURE 6-8. -- Change in rock thickness from borehole-gravity (BHG) densities, assuming simple subsidence. Boreholes OSR-21 vs OOR-17.

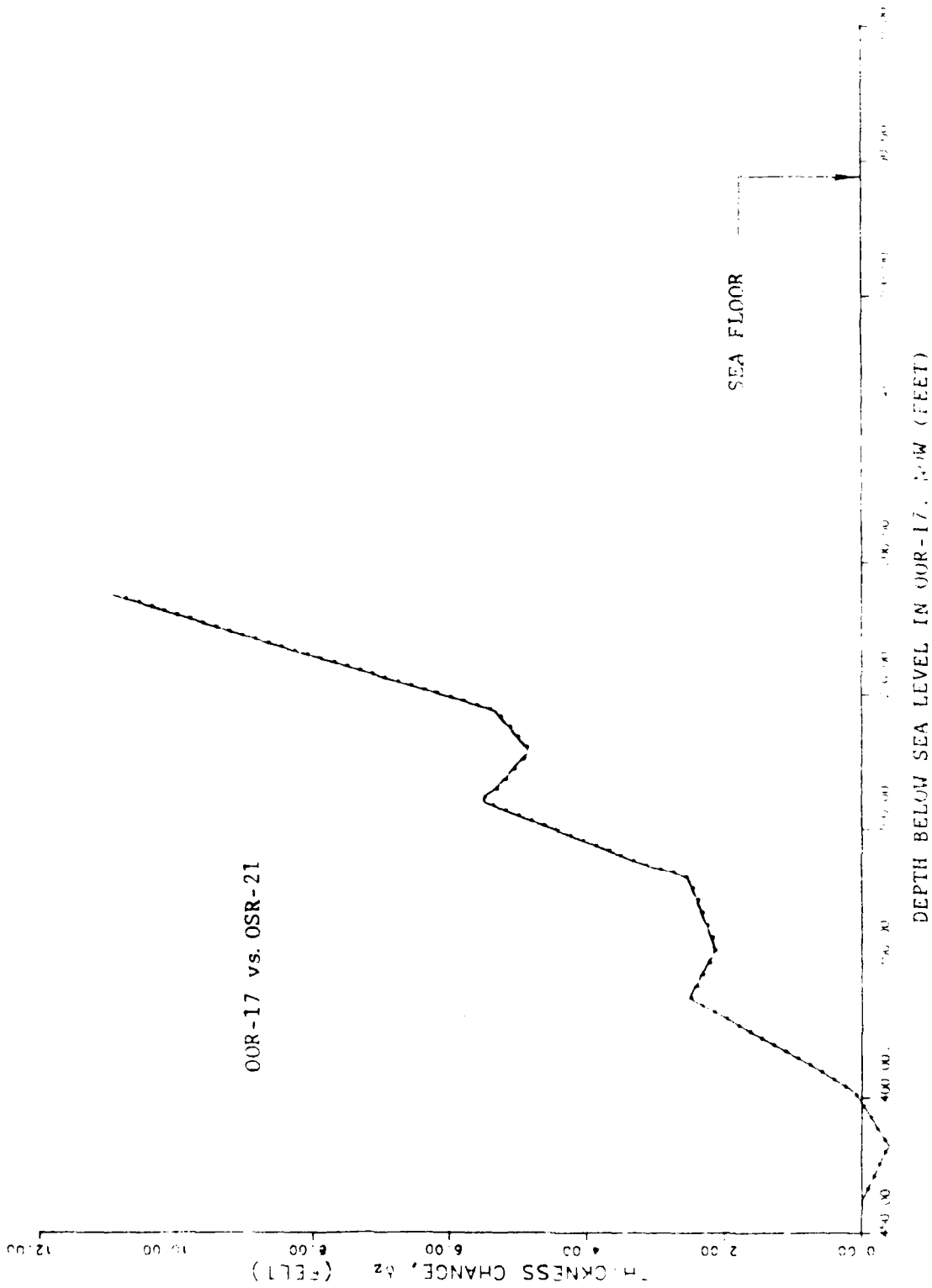


FIGURE 6-9. -- Change in rock thickness from borehole-gravity (BHG) densities, assuming simple subsidence. Boreholes 00R-17 vs OSR-21.

are ≤ 12.4 ft and average 3.0, 6.1, and .1 ft, respectively, for our best, high, and low extrapolations). With nature causing so much variation (presumably at random) in our calculated thickness-change δz , natural density variations dominate the δz -values. Indeed, for equal depths (442 ft) and the same control hole, absolute differences in δz between OQT-19 and ORT-20 come to < 4 ft and average only 1.8 ft. Hence, treating all four of the resulting f-values as randomly distributed about a mean appears, at the least, a fair approximation (actually, three sets of four must be dealt with, owing to uncertainty in extrapolating δz to the sea floor). On that basis, the question of confidence turns to one of confidence in the estimated mean of a distributed random variable, and can be answered for a data-set of any size by standard statistical methods.

By reason of central tendency, and lacking data that would establish a precise distribution, we assume (as usual) that f-values are normally distributed. In each case (best, highest, and lowest extrapolation), the data of Table 6-3 then supply both a sample mean of f and a sample standard deviation. In computing the latter, however, it must be recognized that only three of the four f-values are independent. For example, given z in both OQT-19 and ORT-20, vs. z in OOR-17, we know z in OQT-19 vs. z in ORT-20; z in OQT-19 vs. z in OSR-21, then yields z in ORT-20 vs z in OSR-21. Since any three of the four f-values can be taken as independent, four estimates emerge of the standard deviation σ_3 ; two degrees of freedom enter the calculation of each (par for the standard deviation of three independent measurements). For each mode of extrapolation (high, best, low), every one of the four σ_3 -estimates is listed in Table 6-3 alongside the f-value omitted in its calculation; also listed are the drop Δz of the sea floor, and the part (δz) of the sea-floor drop due to densification.

For each estimate in Table 6-3 (high, best, and low) the mean $\langle f \rangle$ and a standard deviation imply a distribution of the true mean of the densification-fraction f. In its cumulative form, that "t-distribution" states the probability $\text{Prob}(f > v)$ that the true mean of f (denoted f) lies above any stated value v. Since $\text{Prob}(f > v)$ increases monotonically with σ_3 for a given sample mean $\langle f \rangle$, the largest of the four pertinent σ_3 -values was chosen to get a high estimate of $\text{Prob}(f > v)$, and the smallest σ_3 -value for a low estimate; for the best estimate, the four σ_3 -values were averaged. With those respective values of the standard deviation σ_3 , we computed $\text{Prob}(f > .5)$ and $\text{Prob}(f > 1)$ for each estimate of $\langle f \rangle$ [high, low, and best; a value of about 1/2 would be expected for $\text{Prob}(f > 1)$ if densification accounted for all of the sea-floor drop]. The net result -- fundamental to the whole study -- is that every case $\text{Prob}(f > .5) \leq .05$, with much smaller values for $\text{Prob}(f > 1)$. That is, the odds against densification having caused as much as half the observed sea-floor drop are at least 20-to-1. The left side of Table 6-4 presents a detailed, though brief, summary of all key quantities. As for the right sides of Tables 6-3 and 6-4, the following applies.

The thickness-change curve for OQT-19 vs OOR-17 rises at its greatest rate at a depth of about 426 ft, from a minimum at 498 ft (fig. 6-6). The rise between 498 and 426 ft, and the curve's wiggles below 498 ft, may well stem from the medium's random reef-wise variations, rather than any error in estimating the depth of D at OQT-19. In addition, at ORT-20 (and elsewhere), non-zero downward displacement of a few feet might have been missed at D. Both hypothetical errors would act to decrease f; errors of opposite sign -- about as likely -- would make our f-values too large. Nonetheless, to bias f

Estimate	AS MEASURED: D: 423 ft bsl for OQT-19 442 ft bsl for ORT-20						BIASED TO INCREASE \bar{f} D: 498 ft bsl for OQT-19 $\Delta z = 3$ ft at D for ORT-20					
	$\bar{f} > .5$		$\bar{f} > 1$		$\bar{f} > .5$		$\bar{f} > 1$		$\bar{f} > .5$		$\bar{f} > 1$	
	<f>	σ_3	t	Prob	t	Prob	<f>	σ_3	t	Prob	t	Prob
High	.153	.07	8.31	.007	20.29	.001	.238	.07	6.52	.011	18.98	.001
	.153	.15	3.89	.030	9.50	.005	.238	.16	2.85	.052	8.31	.007
	.153	.20	3.03	.047	7.40	.009	.238	.20	2.21	.079	6.44	.012
Best.	.060	.14	5.58	.015	11.92	.003	.146	.13	4.80	.020	11.58	.004
	.060	.20	3.77	.032	8.06	.008	.146	.20	3.02	.047	7.28	.009
	.060	.25	3.06	.046	6.55	.011	.146	.25	2.43	.068	5.86	.014
Low	-.009	.16	5.50	.016	10.92	.004	.077	.17	4.30	.025	9.39	.006
	-.009	.24	3.63	.034	7.20	.009	.077	.24	3.03	.047	6.61	.011
	-.009	.30	2.91	.050	5.76	.014	.077	.30	2.44	.068	5.32	.017

TABLE 6-4. -- Likelihood that true mean \bar{f} exceeds .5 or 1, given a sample mean $\langle f \rangle$. Symbol f denotes the fraction of column-height change due to densification. For each estimate (high, best, low), the three standard deviations shown are the greatest, mean, and least of the four values of Table 6-3.

as far toward higher values as common sense allows, we have assumed on the right of Tables 6-3 and 6-4 that: (a) the depth of D at OQT-19 is 498 ft, causing δz to increase by 5.4 ft (vs. OOR-17); (b) δz is also greater by 5.4 ft at D for OQT-19 vs OSR-21; (c) for ORT-20, the downward displacement is 3 ft (not zero) at 442 ft bsl, where the geologist's horizons place D; and (d) the 3-ft drop at D for ORT-20 is due entirely to densification at greater depths (contrary to all evidence above D). These assumptions lead to the values of f on the right of Figures 6-2 and 6-3, under the heading "BIASED TO INCREASE f". The main result (besides raising $\langle f \rangle$ -values by $\sim .10$): $\text{Prob}(f > .5) \leq .08$. Strengthened, therefore, is our central conclusion: Densification accounts for just a small part of the wing of OAK's crater.

LONG-TERM SETTLING

Within 67 days of the OAK shot (viz., B+67 days), the sea floor had been re-surveyed to $\sim 3,000$ ft from ground zero (GZ). Coupling that survey with PEACE bathymetry has brought to light notable changes in sea-floor depth between August 1958 and December 1984 (see Chapter 5 of this Report). Specifically, in that period, the sea floor sank by ~ 12 ft at ORT-20, 11 ft at OQT-19, and 4-1/2 ft outside the crater (3,000 ft southwest of GZ on the reef-wise line). That cuts the respective sea-floor drops at ORT-20 and OQT-19 to ~ 20 and 60 ft seven to ten weeks after the event; i.e., "early". What those results mean for densification -- still our working hypothesis -- is perhaps plainest in terms of ORT-20.

Suppose first that the 1958 to 1984 sea-floor drop was caused by vertical settling of coral from the floor down to surface D; such densification is both simple and credible (any net settling below D, for example, would entail an error in present estimates of D's depth). The early sea-floor drop of ~ 20 ft at ORT-20 would take less densification to produce than the drop from pre-shot time to now (31.4 ft) -- but the column between D and the sea floor would have been 12 ft taller in 1958 than now, lowering its mean density. More precisely, the sea-floor drop δz due to densification would be less by 12 ft than in 1984 (see tbl. 6-3); the high, best, and low estimates of its value would all fall by that amount, making negative every f on Table 6-3 but one (for ORT-20). The opposite, less likely scenario has contour D move downward by the same amount as the sea floor above it. Above D, density profiles (and hence δz) are then unaffected; mean densification there stays in the small positive range shown in Tables 6-3 and 6-4 [$f = \delta z / (\Delta z - \Delta z_D)$; δz unaffected; equal changes in Δz and in the drop Δz_D at D] -- even if the drop Δz_D has other causes than densification.

Both extremes (D-depth unchanged vs. equal change at D and at sea floor) lead to the same fraction f of the sea-floor drop due to densification. For, if h_D is the increase in D-depth due to slow densification below D, then δz_D (the part of Δz_D due to densification) evolved to zero in 1984 from $-h_D$ at B+67 days (48 to 67 days after the OAK burst); similarly, if h denotes the increase in sea-floor depth due to slow densification above D, then (for coral above D) δz in 1984 becomes $\delta z - h$ at B+67 days. On the densification hypothesis, we have $h + h_D = 11.8$ ft (the total sea-floor drop at ORT-20 from B+67 to 1984) for any value of h_D ; at OQT-19, $h + h_D = 11.2$ ft. Hence δz (densification's part of the total sea-floor drop by 1984) becomes $\delta z - h - h_D$ at day B+67 -- i.e., $\delta z - 11.8$ ft for ORT-20 and $\delta z - 11.2$ ft for OQT-19. Likewise,

the sea-floor drop Δz (in 1984) becomes $\Delta z - 11.8$ ft for ORT-20 at day B+67, and $\Delta z - 11.2$ ft for OQT-19. The f 's, reckoned as $\delta z / \Delta z$ for 1984, change to $(\delta z - h - h_D) / (\Delta z - h - h_D)$ for day B+67. Thus, with the 1958 to 1984 sea-floor drop $h + h_D$ fixed (no matter how it is split into parts h and h_D due to densification above and below D), the change in f during that period is also fixed. Accordingly, at B+67, the f - and σ_3 -values of Table 6-3, and the probabilities of Table 6-4, becomes those of Table 6-5 below.

Table 6-5, like Tables 6-3 and 6-4, tells a clear and simple tale: As in 1984, the odds against densification having caused half or more of the sea-floor drop measured at B+67, are ≥ 18 -to-1 in all cases; biased to favor densification, the odds remain ≥ 16 -to-1. At B+67, however, all values of $\langle f \rangle$ are negative, with a best estimate of $-.30$ (vs. $.06$ in 1984). Hence, had f -values been as precise for B+67 as for 1984, $\text{Prob}(f > .5)$ would have been a good deal smaller than $.05$; higher σ_3 's at B+67 blocked that (the largest were almost twice as big at B+67). Still, simple subsidence points to negative densification at B+67 (f -values < 0), and it may actually have been negative then (dilatancy). More likely, though, the simple subsidence hypothesis is at fault; it is hard to believe that a medium with 40 to 60 percent porosity, even though fully saturated, would show sizable volume increases on loading and unloading either in uniaxial strain [peak overpressures: ~ 30 to 78 MegaPascals (MPa) (Table 6-1)] or thereafter.

Larger σ_3 's, and the increased scatter of f -values they reflect, take some explaining. They stem primarily from the reduced value, for ORT-20, of the column-height change that forms the denominator of f (a factor of 1.6 smaller at B+67 than 1984). Physically, small column-height changes can flag a breakdown of the f -criterion for measuring the part densification played in forming the crater. That measure makes sense only if the column-height change ($\Delta z - h - h_D$ in this case) is large compared to random ups and downs (standard deviation) in the part densification contributes to the change. Otherwise values of f for columns with small changes in height (changes adding little to the sea-floor drop and crater volume) will dominate the mean value $\langle f \rangle$ used to characterize the whole set of f 's (including f 's for holes with much larger changes in height). The problem can perhaps be finessed (below, last section), but the true cure lies in computing f as a fraction of crater volume due to densification -- given axial symmetry, a sum (over all crater holes) of products $R\delta z$, divided by a sum of products $R\Delta z$ (R = horizontal range at a given crater hole). That fraction, after all, is the ultimate object sought. On present knowledge, its uncertainty would come mostly from its dependence on the choice of control hole for computing each δz . Here, however, we have density profiles from just two crater holes and two control holes. They yield too small a sample (2 ratios) to make such a criterion practical; the one adopted here, despite the drawback under discussion, permits more efficient use of those data (3 independent f 's). Given profiles from a half-dozen or more holes of each kind, the volume criterion appears the better choice.

As for slow settling beyond the presently defined crater, pre-shot and 1984 contour maps show ~ 4 to 6 ft of it. So do the maps for B+67. The drop appears widespread as to direction, occurring (for example) at both 2-to-4 o'clock relative to GZ (north = 12 o'clock), and 6-to-8 o'clock. Here, however, it matters only if it means that the shot appreciably disturbed control-hole material. That is not at all likely for the following reasons:

Pairs	Δz	AS MEASURED			BIASED TO INCREASE \bar{f}		
		$\delta z - (h+h_p)$	f	σ_3	$\delta z - (h+h_p)$	f	σ_3
19/17	60.3	1.6-11.2	-0.16	.30	7.0-11.2	-0.07	.29
19/21	60.3	11.4-11.2	.00	.27	16.8-11.2	.09	.26
20/17	19.6	1.6-11.8	-0.52	.09	4.6-11.8	-0.37	.12
20/21	19.6	11.9-11.8	.01	.27	14.9-11.8	.16	.23
19/17	60.3	-3.6-11.2	-0.25	.45	1.8-11.2	-0.16	.43
19/21	60.3	8.6-11.2	-0.04	.40	14.0-11.2	.05	.39
20/17	19.6	-4.7-11.8	-0.84	.11	-1.7-11.8	-0.69	.12
20/21	19.6	10.1-11.8	-0.09	.42	13.1-11.8	.07	.38
19/17	60.3	-4.2-11.2	-0.26	.58	1.2-11.2	-0.17	.56
19/21	60.3	6.5-11.2	-0.08	.53	11.9-11.2	.01	.51
20/17	19.6	-10.3-11.8	-1.13	.09	-7.3-11.8	-0.97	.09
20/21	19.6	8.2-11.8	-0.18	.56	11.2-11.8	-0.03	.53

LIKELIHOOD THAT THE TRUE MEAN \bar{f} EXCEEDS .5 OR 1, GIVEN A SAMPLE MEAN $\langle f \rangle$

Estimate	$\langle f \rangle$	AS MEASURED:			BIASED TO INCREASE \bar{f}		
		σ_3	t	Prob	$\langle f \rangle$	σ_3	Prob
High	-0.17	.09	12.26	.003	21.44	.001	.008
	-0.17	.23	4.95	.019	8.66	.007	.026
	-0.17	.30	3.81	.031	6.68	.011	.040
Best	-0.30	.11	13.08	.003	21.22	.001	.005
	-0.30	.34	4.07	.028	6.60	.011	.035
	-0.30	.45	3.10	.045	5.03	.019	.055
Low	-0.41	.09	17.68	.002	27.38	.001	.002
	-0.41	.44	3.60	.035	5.57	.015	.042
	-0.41	.58	2.73	.056	4.23	.026	.067

TABLE 6-5. -- Column-height changes due to densification in OAK crater 48 to 67 days after burst. Borehole pairs given in left-hand column.

- (1). Whereas 4-to-6 ft of subsidence appears to have occurred around most of the crater, the pre-shot map runs only about 1.2 crater radii; there, peak overpressure was greater by a factor of 5-to-10 than at control-holes OSR-21 and OOR-17.
- (2). As horizontal range increases, a steady decrease occurs in the sea-floor drop observed between 1958 (pre-shot) and 1984. On the reef-wise line of BHG logging, those drops run from ~120 ft one-fourth of the way to the crater's edge, to ~64 ft halfway there, to ~5 ft at the edge itself. They and their rapid decrease with range were doubtless both caused by the explosive loads the medium bore -- loads which also decreased rapidly with range. Like those loads, the sea-floor drop should be a good deal smaller at two crater radii than one -- and the drop of 5 ft at the crater's edge is already small, whether it came about by densification or not.
- (3). Uncemented layers were breached in the crater's central region, opening new routes for leakage of water to the surface from great ranges; at a speed of only 1 cm/hr, water would have flowed ~7,500 ft by 1984. Driving such flow, however, would be gravity, just as it has tended over geologic ages to force water upward through the local fissures and passages present in coral. Balancing gravity over that time has been the ability of the solid skeleton to support vertical loads without transferring them to interstitial water; owing to those very loads, the strength of uncemented sand is >0 . Gravity and strength act no differently now than in the past -- and the absence of detectable change in the separation of horizons in control holes argues that the balance between them remains where it was struck ages ago.

PIPING

During simple subsidence, skeletal coral replaces water that flows from it; since coral solids are denser than water, the medium then densifies, in accord with Eqs. (1)-(5). Yet, as discussed above, applying Eqs. (1)-(5) to the observed density profiles accounts for only some of the observed sea-floor drop; in material below the crater floor, density has increased by only a small fraction of the requisite amount. However, the finding that material hundreds of feet below the excavation crater had risen to the crater floor (see Wardlaw and Henry, 1986b; and Chapters 3 and 7 of this Report), suggests a way out -- namely, transport of solid particles by upwelling water. Any observed changes in density and column-height can be brought about by such "piping", given the right ratio of solid to liquid in piped slurry; for example, no density changes will be seen if the density of the slurry equals that of the pre-shot medium. In addition, of course, the right amount of material must be piped. On that point, the idea founders; evidence of

substantial piping is limited to the central crater region.¹ There is also an implicit demand that piped solid be transported not just to the sea floor, but out of the apparent crater; that puts direct measurement of the amount of piped material beyond reach now. Nevertheless, piping was noted at OAK; some of its properties follow.

Eqs. (1)-(5) remain valid, but it is no longer useful to ask what pre- and post-shot heights are subtended in a column by a given solid mass m_s . Rather, with solid leaving the column, the mass of solid between two coral particles that remain in it will be different before the shot than after; moreover, the distance between them changes as both solids and liquid are lost. To compute the effects of both losses, let V denote a pre-shot control volume of the medium in which the following definitions apply:

α = pre-shot volume-fraction of liquid in V

β = pre-shot volume fraction of solid in $V = 1 - \alpha$

ρ_L = density of liquid component

ρ_S = density of solid component

ρ = mean pre-shot density of mixture in V .

As on page 6-7 of this Chapter, it then follows that:

$$\alpha\rho_L + \beta\rho_S = \rho \qquad \text{Eq. (6)}$$

To describe the post-shot state of the same material, let

γ = piped-out fraction (volume or mass) of the liquid within V

$k\gamma$ = piped-out fraction (volume or mass) of the solid within V

$\bar{\rho}$ = present mean density of mixture not piped from V .

¹ For a cratering mechanism, a useful measure of significance lies in the fraction of the apparent crater's volume that can be laid to it. The piping observed at OAK crater occurred only within ~ 4 apparent radii from GZ -- the central crater -- whereas the main PEACE problem is to account for the wing beyond the central crater. Piping will merit great attention if it can be shown, by tight quantitative arguments, to have produced something like half the wing's volume. By that standard, the fact that piping occurred can only suggest it as a possibly significant mechanism. The same holds for other observations as well, applying (for example) to any sand boils outside the apparent KOA crater; what their quantitative relation might be to the volume of KOA crater (let alone OAK's) is not at all obvious [mud boils also appeared above the Tatum salt dome after the SALMON event (Werth and Randolph, 1966, p. 3409) -- clear proof of piping, but piping played no role in forming SALMON's cavity].

Since αV and βV are the respective pre-shot volumes of liquid and solid, the volumes of liquid and solid piped out of V equal $\gamma\alpha V$ and $k\gamma\beta V$. Hence, of the volume V , the piped-out fraction ϕ is given by:

$$\phi = \frac{\text{Volume of Mixture Piped}}{\text{Pre-shot Volume, } V} = (\gamma\alpha V + k\gamma\beta V)/V = \gamma(\alpha+k\beta) \quad \text{Eq. (7)}$$

Likewise, the mean density of the remaining mixture becomes:

$$\begin{aligned} \bar{\rho} &= [(1-\gamma)\alpha V\rho_L + (1-k\gamma)\beta V\rho_S]/[(1-\phi)V] \\ &= [(\alpha\rho_L + \beta\rho_S) - \gamma(\alpha\rho_L + k\beta\rho_S)]/(1-\phi) - [\rho - \gamma(\alpha\rho_L + k\beta\rho_S)]/(1-\phi) \quad \text{Eq. (8)} \end{aligned}$$

Using Eq. (7) to eliminate γ from Eq. (8), the direct result is:

$$\bar{\rho} = [\rho - (\alpha\rho_L + k\beta\rho_S)\phi/(\alpha+k\beta)]/(1-\phi)$$

Slight rearrangement of this last equation makes it linear in $k\beta/\alpha$, whence

$$\begin{aligned} k\beta/\alpha &= [(\bar{\rho} - \rho_L)\phi - (\bar{\rho} - \rho)\phi + (\bar{\rho} - \rho)] \\ &= \frac{k\gamma\beta V}{\gamma\alpha V} = \frac{\text{Volume of Solid Piped}}{\text{Volume of Liquid Piped}} \equiv \frac{V_{SP}}{V_{LP}} \quad \text{Eq. (9)} \end{aligned}$$

The sludge density, $\bar{\rho}_{SL}$, follows from the ratio V_{SP}/V_{LP} :

$$\bar{\rho}_{SL} = (\rho_L V_{LP} + \rho_S V_{SP})/(V_{LP} + V_{SP}) = [\rho_L + \rho_S (V_{SP}/V_{LP})]/[1 + (V_{SP}/V_{LP})] \quad \text{Eq. (10)}$$

Values for the mean densities ρ and $\bar{\rho}$ come from density profiles measured, respectively, in control holes and crater holes. Also, for a vertical column of OAK coral, the fraction ϕ is just the change in column-height, divided by the column's pre-shot height. Hence, from PEACE observations, Eq. (9) allows us to compute the ratio of solid and liquid volumes in piped material, and Eq. (10) its density, if piping caused the changes observed. Perforce, then, those quantities constrain the piping process, whereas γ and $k\gamma$ simply fix the unmeasurable total amount piped. For example, if no density changes occur ($\bar{\rho}=\rho$), then the volume and mass ratios implied by Eq. (9) will be those of pre-shot material, and piped sludge will have the same density as the rest of the medium -- in which case, gravity cannot cause it to be piped. However, if a shot raises the medium's density a bit (as the PEACE logs indicate for OAK), the resulting small pressure head can push sludge upward. To help quantify that push, estimates of the density of piped material have been made from PEACE measurements using Eqs. (7), (9), and (10).

In Table 6-6 below are recorded: (a) the mean densities (ρ and $\bar{\rho}$) measured for OOR-17, OSR-21, OQT-19, and ORT-20 from their shallowest common horizon, down to each of three others (the deepest at base D of the downward-displacement region); (b) the depths z and z_0 , respectively, of the top and bottom of the column to which each mean density refers; (c) the measured

column shrinkage, ϕ , between z and z_0 for OQT-19 and ORT-20¹ (together with the changes in depth Δz and Δz_0 at z and z_0)²; (d) volume ratios implied by those data and Eq. (9), for the four control-hole/crater-hole pairs; (e) a mean density of piped material (also listed) follows from each volume ratio by Eq. (10), and with it (f) a "density decrement" $\rho_{SL} - \bar{\rho}$ (the difference between the densities of piped and remaining material). Evidently, subsidence by piping would require extruded material to have a bit lower density than that not piped. Note, however, that the residue's density $\bar{\rho}$ runs from slightly greater than that of the supposed sludge, to $\sim .45$ g/cc less. That wide spread reflects sensitivity of the volume ratio [Eq. (9)] to random differences among borehole density profiles, when column shrinkages (ϕ) are $\ll 1$. Thus, the most consistent sludge densities and density decrements are obtained for the longest columns (third quartet of tbl. 6-6, running down to D at ~ 443 ft bsl for OQT-19 and ORT-20).

From the decrements in Table 6-6, it appears that slurry would be driven upward by pressures of about a tenth of the lithostatic head (mean decrement $\sim .2$ g/cc), though the standard deviation of decrements is also that large (.21 and .26 g/cc; second and third quartets). At an upward acceleration of .1 g (decrement $\sim .2$ g/cc), sludge would take ~ 11 sec to rise 200 ft in a wide, unobstructed pipe -- but there's more to piping than that.

OTHER CONSTRAINTS; HORIZONTAL PIPING

The densities in Table 6-6 apply to vertical columns 200 to 300 ft in height. Within such a column, single layers could have been driven by a density decrement as large as 1/3 g/cc. However, the path of sludge piped from the crater's wing leads first to the central crater, where lie nearly all the vents known to have guided solids from depth to the sea floor. That first path-leg has its pitfalls. For one, all horizons grow in depth along it; the horizons crossed by contour D at boreholes OQT-19 and ORT-20 (roughly 3a in fig. 6-1) run ~ 70 ft deeper at OTG-23, 800 ft from GZ (tbl. 6-2), and the sea floor lies ~ 55 ft deeper. Adding 55 ft of sea water and 15 ft (70 minus 55 ft) of coral makes the overburden ~ 11 percent greater than at the intersection of D with OQT-19 (or ORT-20). Along the horizon in question (H, say), the resulting overburden gradient opposes inward flow to the vents -- and while 11

¹ The "Volume of Mixture Piped", needed to calculate ϕ by Eq. (7), is equal to the change in depth Δz_0 of the column's bottom end, minus the change in depth Δz of its top end. The column's "Pre-shot Volume, V" is equal to the pre-shot depth $z_0 - \Delta z_0$ of its bottom end minus the pre-shot depth $z - \Delta z$ of its top end, where z_0 and z are the current (1984) depths of its bottom and top ends, respectively.

² Values of z , z_0 , Δz and Δz_0 were obtained for Table 6-6 from Table 7-4 of the present Report. For several horizons, the latter table lists both 1984 depths measured in crater holes, and estimates of pre-shot depth based on the full set of 1984 measurements (including horizon depths in control holes). Given a 1984 depth, the pre-shot depth of the same horizon was obtained for Table 6-6 by linear interpolation in Table 7-4 -- with the change in its depth equal to the difference between the 1984 and pre-shot values.

Pair	z_0	z	Δz_0	Δz	ϕ	$\bar{\rho}$	ρ	V_{SP}/V_{LP}	$\bar{\rho}_{SL}$	$\bar{\rho}_{SL} - \bar{\rho}$
19/17	309	220	35.0	38.9	.042	1.91	1.96	<0	> ρ	>0
19/21	309	220	35.0	38.9	.042	1.91	1.89	.36	1.50	-.40
20/17	300	192	19.7	29.7	.085	1.91	1.96	4.66	> ρ	>0
20/21	300	192	19.7	29.7	.085	1.91	1.89	.62	1.71	-.19
19/17	410	220	9.2	38.9	.135	1.94	1.94	1.04	1.94	.00
19/21	410	220	9.2	38.9	.135	1.94	1.89	.44	1.57	-.37
20/17	408	192	6.0	29.7	.099	1.94	1.94	1.14	1.98	.04
20/21	408	192	6.0	29.7	.099	1.94	1.89	.34	1.48	-.46
19/17	444	220	0	38.9	.148	1.95	1.94	.92	1.89	-.06
19/21	444	220	0	38.9	.148	1.95	1.90	.47	1.60	-.35
20/17	442	192	0	29.7	.106	1.95	1.94	.97	1.91	-.04
20/21	442	192	0	29.7	.106	1.95	1.90	.37	1.51	-.44

TABLE 6-6. -- Piping hypothesis. Symbol $\bar{\rho}_{SL}$ denotes density of piped material; densities in g/cm³; lengths in ft.

percent of overburden may be a small pressure, it is two-thirds or more of the total head available to pipe sludge from H. That head acts at the vents; slurry near them can, of course, be piped upward. At bigger ranges, however, their influence weakens relative to that of overburden. Hence, if we are dealing with a liquefied layer (all sludge), the denser layers above probably settle soonest near the vents, replacing piped material but pinching off the flow. Note also that slurry converges cylindrically as it moves inward, slowing its passage to the vents. The "aperture" available to it (proportional to horizontal radius) decreases by a factor of 2-1/2, for example, as slurry goes from 2,000 ft of radius to 800.

An unliquefied layer presents added bars to piping. For, in a layer with strength, unpiped material bears at least part of the overburden; the pressure that drives piping is smaller than the head that the density decrement would otherwise supply. Indeed, the slurry pressure may simply equal its own head, as in any drained unit; then no piping occurs. More generally, creep of the layer's strong component, like weakening induced by the blast, provides some impetus for piping -- but reduced from that which the full density decrement could furnish, and on a wholly different time-scale. Indeed, creep can be so slow that almost no solid particles are entrained by piped water (simple subsidence), which may well have been the mechanism for settling between B+67 and 1984 (see preceding section). In addition, members with strength physically block piping; sludge has to flow between and around those solid parts. Such flow -- through a porous solid -- is described in simplest quantitative terms as diffusion, in accord with D'Arcy's Law, with flow rates set mainly by the medium's permeability. The lower the rates, however, the more solid settles out (under gravity) on its way to the crater's floor; further, at any given rate, entrained particles will not accelerate upward unless the drag on them exceeds their submerged weight.

These remarks suggest detailed calculations of upward/inward diffusion that have not been made, partly because the medium's post-shot permeability is poorly known, but more because PEACE disclosed no piping of note on the crater's wing.

Once at the surface, slurry particles would have to ride out of the crater on reef-wise currents of perhaps 1 knot (~1.5 ft/sec) (Halley and others, 1986, p. 5). During that half-hour trip, gravity would cause particles to settle; those with diameters $>1/8$ mm would drop an estimated 100 ft or more along the way (Stokes flow), and hence would leave the crater, if at all, only by other, slower means. The same forces of drag, weight and buoyancy also act on the particles during their rise to the crater's floor; treating them again as isolated spheres, the buoyancy and drag of water rising 200 ft in one hour (1/18 ft/sec) can move them only if their diameters are $<1/8$ mm, while for 10 and 100 hours of rise, respectively, the critical diameters are $3/80$ and $1/80$ mm. These estimates are rough, since the particles are not spheres (nor do spheres bound drag \div mass), they and their wakes overlap [increasing drag \div mass if they do not clump (Soo, 1967, Ch. 5)], and they rise in ragged, twisty channels (not straight, free streams) that may be <10 diameters wide in places.

Fissures, and cones of debris containing coral fragments raised hundreds of feet, were seen in the central region, where coral was most damaged (Halley and others, 1986; Slater, and others, 1986). Piping accounts neatly for that, and much of it could have occurred in a few seconds or less. For, with

overpressure at the .1-MPa level, burst-induced sub-crater pressures up to ~100 MPa would furnish the required vertical stress gradients. Relief of those pressures would be rapid, requiring a volume increase of <1/2 percent for decay to .1 MPa (from 100 MPa). Though slight in relation to crater volume, enough material would be extruded in such an expansion to make impressive deposits on the sea floor, and cloud the reef currents that cross the crater.

DENSIFICATION: SUMMARY AND CRITIQUE

Borehole cores have let geologists fix the depths of many layer interfaces ("horizons") below and outside the OAK crater. Further, in two holes on the crater's wing, gravimetry has furnished density profiles down to horizons not moved by the OAK burst; to the same horizons, but well outside the crater, borehole gravimetry (BHG) also has given two density profiles. All four holes lie on a curve roughly parallel to the reef. There, in pristine coral, geology argues for random density-profile variations about some mean. The present coral medium formed in about the same way at different points on any one of a set of curves roughly parallel to the reef. Moreover, PEACE cores and density profiles support the idea of such variations about a mean. Treating the far-field pair as pristine profiles then yields density changes due to the burst, from depth to 20-100 ft below the crater floor. From those changes come the downward displacements that densification implies for sub-crater coral, vs. depth, and for the crater floor itself. Comparing the latter displacements to actual sea-floor drops yields the result that densification played but a small role in forming the crater's wing.

Except for converting density profiles to downward displacements, significant uncertainty attends each step noted:

1. The general increase of coral density from lagoon to ocean is a source of systematic error in the measured profiles. Specifically, prior to OAK, departures from the mean density profile would have been random along the curve on which boreholes were supposed to lie. That curve is not known precisely. Actual boreholes therefore depart from it, but are about as likely to fall on one side of it as the other. Hence, given the oceanward density gradient, the general effect of such misplacement is to increase the differences among measured profiles. The unlikely opposite result, however, is more apt to have occurred in our four-profile set than in a large set. The scatter of profiles would then have been underestimated.
2. A horizon's drop (or rise) by a few feet could have escaped notice. That holds for the "unmoved" horizons above which we reckoned density-change effects in the two crater-wing holes.
3. From the shallowest point of BHG logging in a given borehole to the sea floor, horizon-depth changes due to densification were estimated by extrapolation from below.
4. Limits of precision render BHG-measured densities uncertain, but by $< \pm .02$ g/cc. Further, BHG densities are averages over such large regions that the effects of them of local site inhomogeneities (vugs, etc.) are believed negligible (for PEACE, a great advantage of BHG over other methods).

5. The sea-floor drop δz implied by density changes down a borehole, divided by the actual sea-floor drop at the hole (Δz), measures the contribution of densification to the crater. That ratio (f), however, gives too much weight to holes where the actual drop is small. Further, though f is a random variable, its distribution may not be near-normal (as assumed).
6. The largest values of δz (vs. depth) come from pairing the two wells outside the crater, just 560 ft apart ("control-holes," ~5,500 and 6,000 ft from GZ). Moreover, paired with the same control hole, the two holes 400 ft apart in the crater's wing (~4,000 ft from the control holes) have much the same curve of δz -vs.-depth. Nature, not the OAK burst, thus appears the chief source of variation among the four density profiles; our signals (density changes due to OAK) were buried in noise (random natural differences in density). As a result, the likelihood that the crater wing formed by simple subsidence could be assessed using three independent values of δz (the maximum from four profiles) -- despite our having just two profiles from the wing. Strictly, that can be correct only as f , divided by its standard deviation, approaches zero. The crater-wing profiles show some densification ($f > 0$), however, and may differ systematically therein owing to their different ranges.

Caveats 1 through 6 forced us to assess confidence in the overall finding of low densification ($\delta z < .1 \Delta z$). To that end, our data base and calculations were altered (within reason) to maximize f :

i) Since oceanward density gradients could have acted to reduce differences among our f -values [caveat 1 above], the standard deviation of f was assigned the largest value found from the data (of the four deviations at hand when three of four f 's are independent).

ii) For each borehole, δz was set at the sea floor to the highest δz -value found by extrapolating δz -vs.-depth to the floor [point 2 above].

iii) Unseen displacement of the shallowest "unmoved horizon" D in a given borehole would probably have been downward. Each δz -value from item (ii) above was increased by 3 ft or more to offset such an error [caveat 3 above].

iv) Adding offsets (iii) directly to δz -values credits the unseen drop of D entirely to densification below D -- even though densification accounted for just a small part of the horizon-drops observed above D (in the crater's wing).

v) On the PEACE data, the tendency of f to place undue weight on holes with small sea-floor drops [point 5 above] led to high -- but accepted -- values of both f and its standard deviation (ORT-20 has smaller Δz -values than OQT-19 and higher f -values).

The overstatement of f flagged by item (v) looks correctible (next section). That correction would probably be cancelled, and then some, if no appeal were made to the limit where f , divided by its standard deviation, tends to zero (item 6 above). How to avoid that limit without giving f another strong ad hoc lift is not clear. As it is, each upward bias lent to f appears within reason. Having them all act at once to make high f -values likely does not. But even so, only minor densification results.

CONCLUSIONS

If the wing of the OAK crater resulted from densification, then the sea-floor drop at a wing-station, W, can be computed exactly from density profiles before and after the shot in a vertical column below W. No such profiles were measured pre-shot. That heightens the problem of reading density increases due to OAK through the noise of random natural variations in density. Below the crater's wing, those variations were found to dominate shot-driven changes in density. More important, however, the noise level proved low enough to admit a clear answer to the main question posed -- **on the wing of OAK's crater, most of the sea-floor drop had causes other than densification.**

As a best estimate, 6 percent of the sea-floor drop on the crater's wing can be laid to density increases caused by the burst. That figure follows from profiles down two crater holes and down two control holes outside the crater -- profiles that yield four estimates (3 independent) of the fraction, f , contributed by densification to the sea-floor drop. Each of the four has a high, best, and low value, depending on how a gap in data just below the sea floor is bridged (fig. 6-10). To be sure, the sample is small, but its size has been taken into account in assessing confidence in the mean of f . The results: The probability that densification caused half or more of the sea-floor drop is $<.1$. That result holds even if the main parameters of the calculation are all varied at once (each within reasonable limits) so as to increase f . The PEACE density profiles could be of course atypical, but, at most, that observation only supports measuring more profiles; with the data at hand, the results are as stated.

Extant maps show that, in the crater wing, the sea floor sank appreciably between August 1958 (a few months after OAK) and December 1984 (PEACE). The crater was therefore significantly shallower in 1958 than now. By the same token, given simple subsidence, the medium was notably less dense (on average), from the base of the region of downward displacement to the crater floor. Combining that slow sea-floor drop with the PEACE density profiles leads to a best estimate of $\sim -.2$ for f at August 1958 -- and again (by chance) the probability that densification caused half or more of the sea-floor drop at that date is $<.1$.

The same data base of sea-floor maps and PEACE density profiles also yields mean values for the density of materials piped up to the sea floor, if the piping hypothesis is correct. From those values, the densities of piped and residual material differ by an average of $\sim .2$ g/cc, but with a standard deviation at least that large. A density difference of $.2$ g/cc can drive piping, but weakly -- and the chain of events leading to transport of piped material out of the crater has many weak links (e.g., it appears that particles $>.1$ mm in diameter will settle before they can exit).

The statistical grounds for assessing densification probably can be strengthened, using only extant data. Given the cost of the data, that should be done. Specifically, both the sea-floor drop (Δz) and the part of it due to density changes (δz) can be expressed as fractions of the pre-shot depth to D. The probability that the latter fraction exceeds half (say) of the former can then be computed, using standard deviations supplied by PEACE data. A BHG profile from the central region could also be added to the present set, but not without giving a further strong upward bias to the estimated extent of

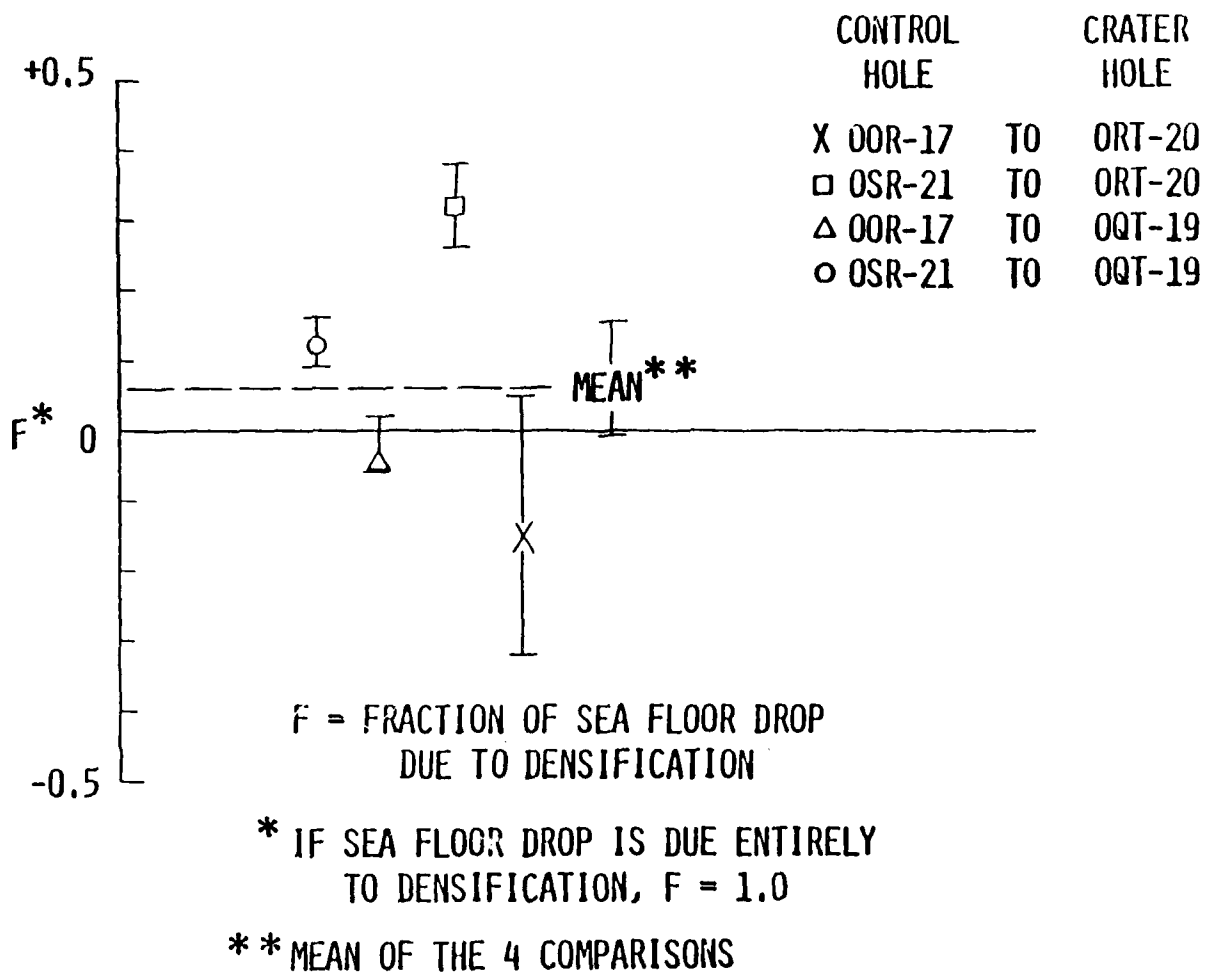


FIGURE 6-10. -- High, low, and best estimates of the fraction contributed to sea-floor drop by densification at boreholes OQT-19 and ORT-20.

densification. In addition, the plausibility of the piping hypothesis should be examined further. With densification as an unlikely mechanism for forming OAK's crater-wing, however, plastic flow appears to offer the simplest and most plausible explanation for it. Whether that explanation will withstand close scrutiny is unclear; flow is well understood in principle, but not much is known about the displacement field around a flow crater.

ACKNOWLEDGEMENTS

For the PEACE Program data herein, and much kind assistance besides, my sincere thanks go to Larry Beyer, Scott Blouin, Bob Henny, Woody Henry, Steve Melzer, Dean Oberste-Lehn, John Peterson, Byron Ristvet, Ed Tremba, and Bruce Wardlaw. Larry, John, Woody, and Byron, and (above all) Steve and Bruce are due special thanks for extended discussions of both the data and its implications; so are my co-workers Neil Perl, Jim Workman, and Ken Burrell, for reducing PEACE data to forms from which conclusions more readily follow.

REFERENCES CITED

- Beyer, L.A., Ristvet, B.L., and Oberste-Lehn, D., Chapter 8, Preliminary density and porosity data and field techniques of borehole gravity surveys, OAK crater; 28 p., 4 figs. 10 tpls; in Henry, T.W., and Wardlaw, B.R., eds., Pacific Enewetak Atoll Crater Exploration (PEACE) Program, Enewetak Atoll, Republic of the Marshall Islands; Part 3: Stratigraphic analysis and other geologic and geophysical studies in vicinity of KOA and OAK craters: U.S. Geological Survey Open-File Report 86-555.
- Halley, R.B., Slater, R.A., Shinn, E.A., Folger, D.W., Hudson, J.H., Kindinger, J.L., and Roddy, D.J., 1986, Observations of OAK and KOA craters from the submersible; 32 p., 13 figs., 1 appendix; in Folger, D.W., ed., Sea-floor observations and subbottom seismic characteristics of OAK and KOA craters, Enewetak Atoll, Marshall Islands: U.S. Geological Survey Bulletin 1678.
- Melzer, L.S., 1986, Chapter 7, Downhole geophysical logs; 32 p., 16 figs., 7 tpls., in Henry, T.W., and Wardlaw, B.R., eds., Pacific Enewetak Atoll Crater Exploration (PEACE) Program, Enewetak Atoll, Republic of the Marshall Islands; Part 3: Stratigraphic analysis and other geologic and geophysical studies in vicinity of KOA and OAK craters: U.S. Geological Survey Open-File Report 86-555.
- Pierce, B.O., 1929, A Short Table of Integrals; Third Revised Edition, Ginn and Company, Boston, New York (etc.).
- Slater, R.A., Roddy, D.J., Folger, D.W., Halley, R.B., and Shinn, E.A., 1986, Chapter 13; Additional submersible studies; detailed observations of the sea floor of OAK, KOA, and MIKE craters; 153 p., 2 tpls., 4 pls.; in Henry, T.W., and Wardlaw, B.R., eds., Pacific Enewetak Atoll Crater Exploration (PEACE) Program, Enewetak Atoll, Republic of the Marshall Islands; Part 3: Stratigraphic analysis and other geologic and geophysical studies in vicinity of KOA and OAK craters: U.S. Geological Survey Open-File Report 86-555.
- Soo, S.L., 1967, Chapter 5; in Fluid Dynamics of Multiphase Systems; Blaisdell Publishing Company, Division of Ginn and Company, Waltham, Massachusetts, Toronto, London.
- Tremba, E.L., and Ristvet, B.L., 1986, Chapter 4; X-ray diffraction mineralogy; 49 p., 11 figs., 35 tpls., in Henry, T.W., and Wardlaw, B.R., eds., Pacific Enewetak Atoll Crater Exploration (PEACE) Program, Enewetak Atoll, Republic of the Marshall Islands; Part 3: Stratigraphic analysis and other geologic and geophysical studies in vicinity of KOA and OAK craters: U.S. Geological Survey Open-File Report 86-555.

Wardlaw, B.R., and Henry, T.W., 1986b, Chapter 14; Geologic interpretation of OAK and KOA craters; 39 p., 21 figs., 2 tbls.; in Henry, T.W., and Wardlaw, B.R., eds., Pacific Enewetak Atoll Crater Exploration (PEACE) Program, Enewetak Atoll, Republic of the Marshall Islands; Part 3: Stratigraphic analysis and other geologic and geophysical studies in vicinity of KOA and OAK craters: U.S. Geological Survey Open-File Report 86-555.

Werth, G., and Randolph, P., 1966, The Salmon seismic experiment: Journal of Geophysical Research, v. 71, no. 14, p. 3405-3413.

APPENDIX 6-1

This appendix contains (1) all PEACE density profiles measured in the OAK area, with (2) plots of the fits made to those profiles as part of the work reported here. Also presented are (3) tables of coefficients for the piecewise linear function used to fit all profiles. That function is defined as follows:

$$\rho = [(z-z_j) \rho_{j+1}^- + (z_{j+1}-z) \rho_j^+] / (z_{j+1} - z_j); \quad j = 1, 2, \dots, J \quad \text{Eq. (11)}$$

where ρ and z denote density and depth, respectively. For the BHG profiles [received as step-functions from L.A. Beyer, written communication, May 15, 1987]; see Chapter 2, this Report], ρ_j^+ and ρ_{j+1}^- have the same value $\rho_{j+1/2}$. Otherwise, $\rho_j^- = \rho_j^+ = \rho_j$, and (z_j, ρ_j) gives the coordinates of an endpoint of either two or one straight-line segments of the complete function. Specifically, for $j \neq 1$ or J , a segment runs from (ρ_{j-1}, z_{j-1}) to (ρ_j, z_j) , and another from (ρ_j, z_j) to (ρ_{j+1}, z_{j+1}) ; the single segment for $j=1$ runs from (ρ_1, z_1) to (ρ_2, z_2) , and the single segment for $j=J$ connects (ρ_J, z_J) to (ρ_{J+1}, z_{J+1}) .

The measured BHG profiles, in graphic form, comprise the first exhibit below (figs. 6-11 to 6-16). In each case, for ready comparison, a graph of the density-function fit to a given profile [Eq. (11)] is shown next to it, with the pair on identical scales. Then, in exactly the same format, a set of figures (6-17 to 6-26) follows in which appear all the profiles derived from γ - γ logging, together with the density function fit to each. Next, on a single page (tbl. 6-7), come all the (ρ_j, z_j) -points that specify the functions fit to BHG profiles (points supplied by the tables of Chapter 2 of this report). A corresponding table for fits to all the γ - γ profiles comes last (tbl. 6-8). The latter table was compiled by measuring coordinates from the profiles themselves, having overlain them with thin graph paper; thus, at the outset, our measures of density and depth, denoted "DIV" in the tables, were a pair of coordinates read off graph paper. Conversion was made from DIV to g/cc, and from DIV to ft, by means of the following formulas:

$$\text{density (g/cc)} = Q + (\text{DIV} - Y_0)/S; \quad \text{depth (ft)} = A + B(\text{DIV} - X_0)/C \quad \text{Eq. (12)}$$

Values of Q , Y_0 , S , A , B , X_0 , and C are given for each profile in Table 6-8.

BOREHOLE GRAVITY SURVEY: HOLE OOR-17

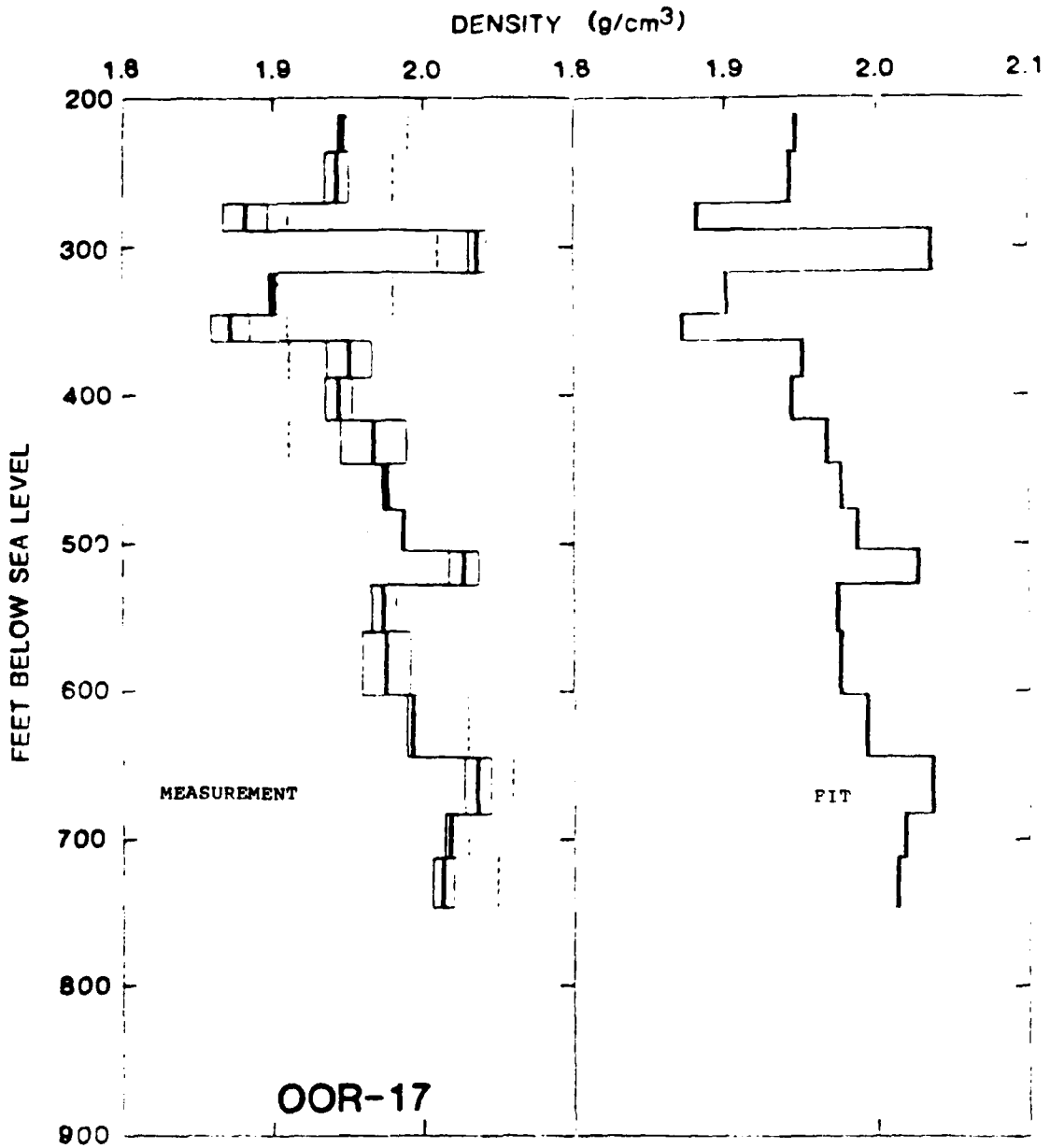


FIGURE 6-11. -- Left: profile of density vs. depth from BHG logging in control hole OOR-17, as received. Right: plot of broken-straight-line fit [Eq. (11)] to profile at left. The left- and right-hand plot scales are identical.

BOREHOLE GRAVITY SURVEY: HOLE OSR-21

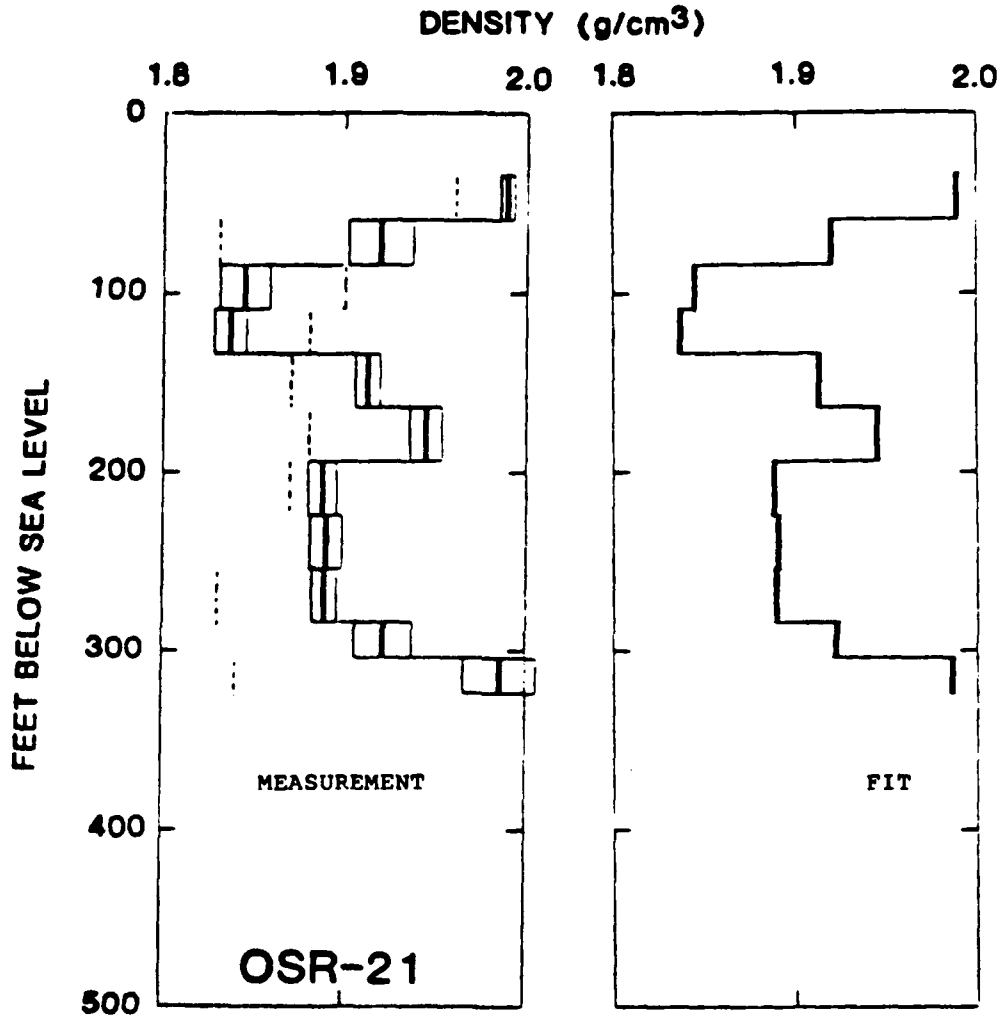


FIGURE 6-12. -- Left: profile of density vs. depth from BHG logging in control hole OSR-21, as received. Right: plot of broken-straight-line fit [Eq. (11)] to profile at left. The left- and right-hand plot scales are identical.

BOREHOLE GRAVITY SURVEY: HOLE ORT-20

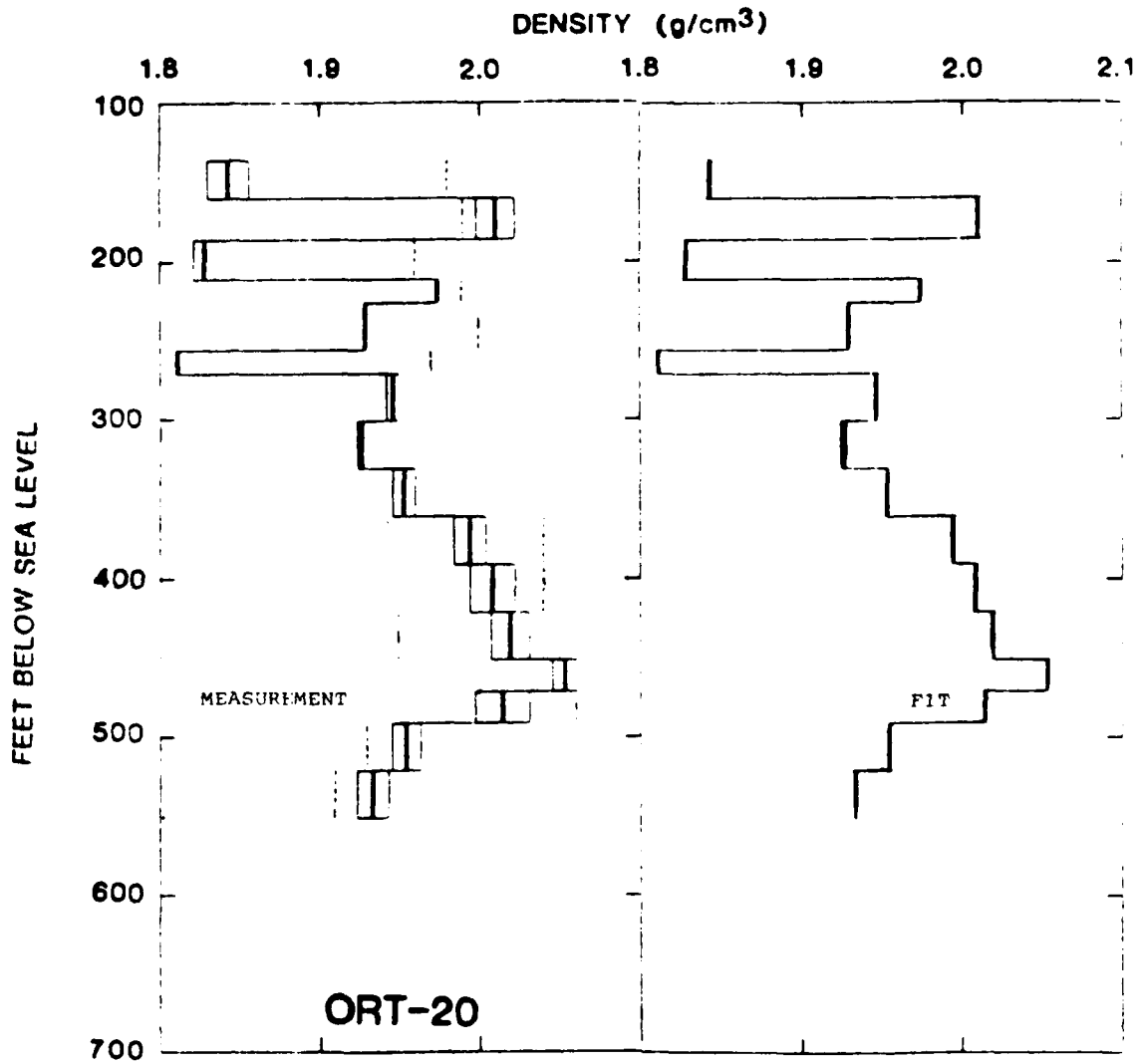


FIGURE 6-13. -- Left: profile of density vs. depth from BHG logging in crater hole ORT-20, as received. Right: plot of broken-straight-line fit [Eq. (11)] to profile at left. The left- and right-hand plot scales are identical.

BOREHOLE GRAVITY SURVEY: HOLE OQT-19

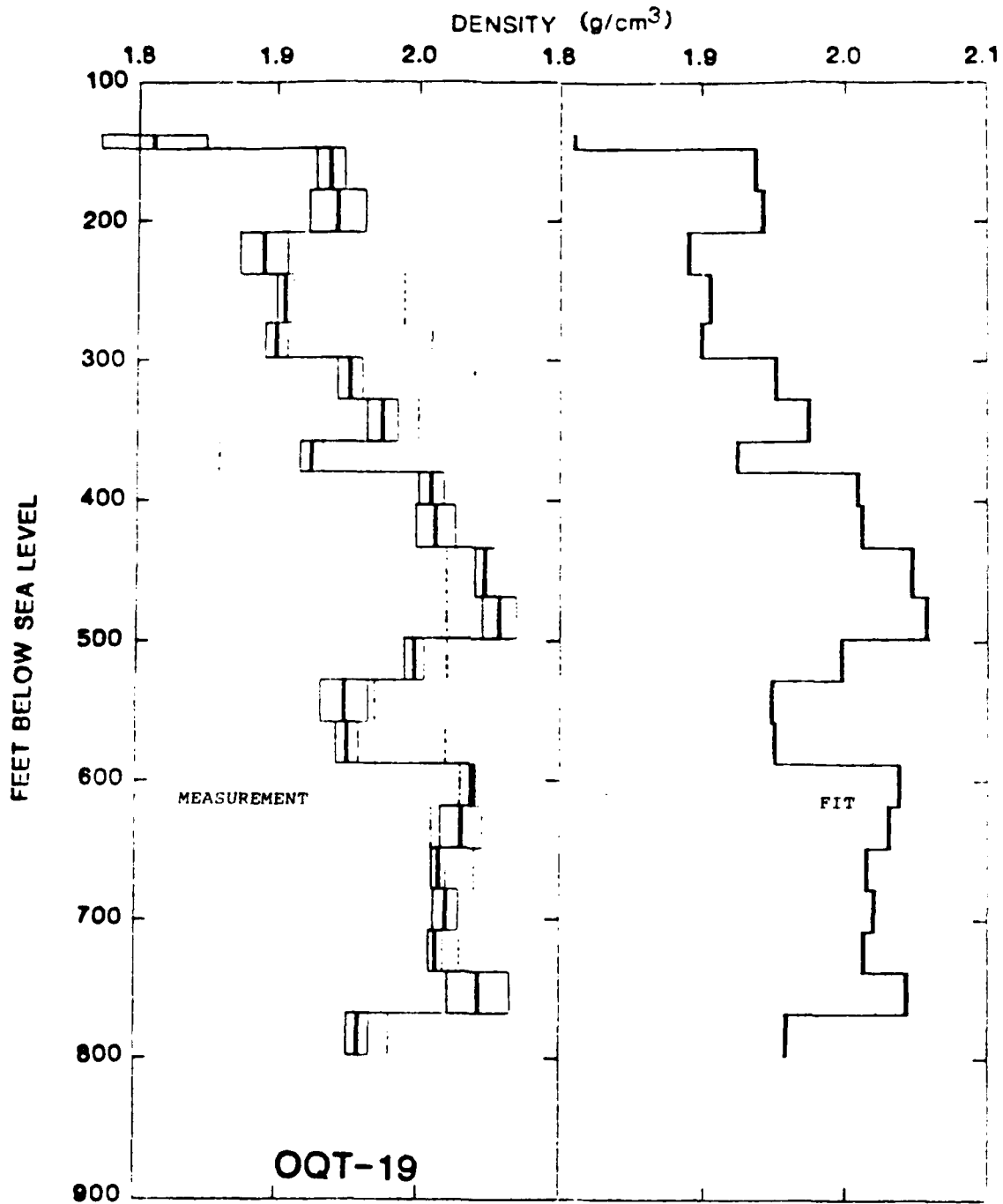


FIGURE 6-14. -- Left: profile of density vs. depth from BHG logging in crater hole OQT-19, as received. Right: plot of broken-straight-line fit [Eq. (11)] to profile at left. The left- and right-hand plot scales are identical.

BOREHOLE GRAVITY SURVEY: HOLE OTG-23

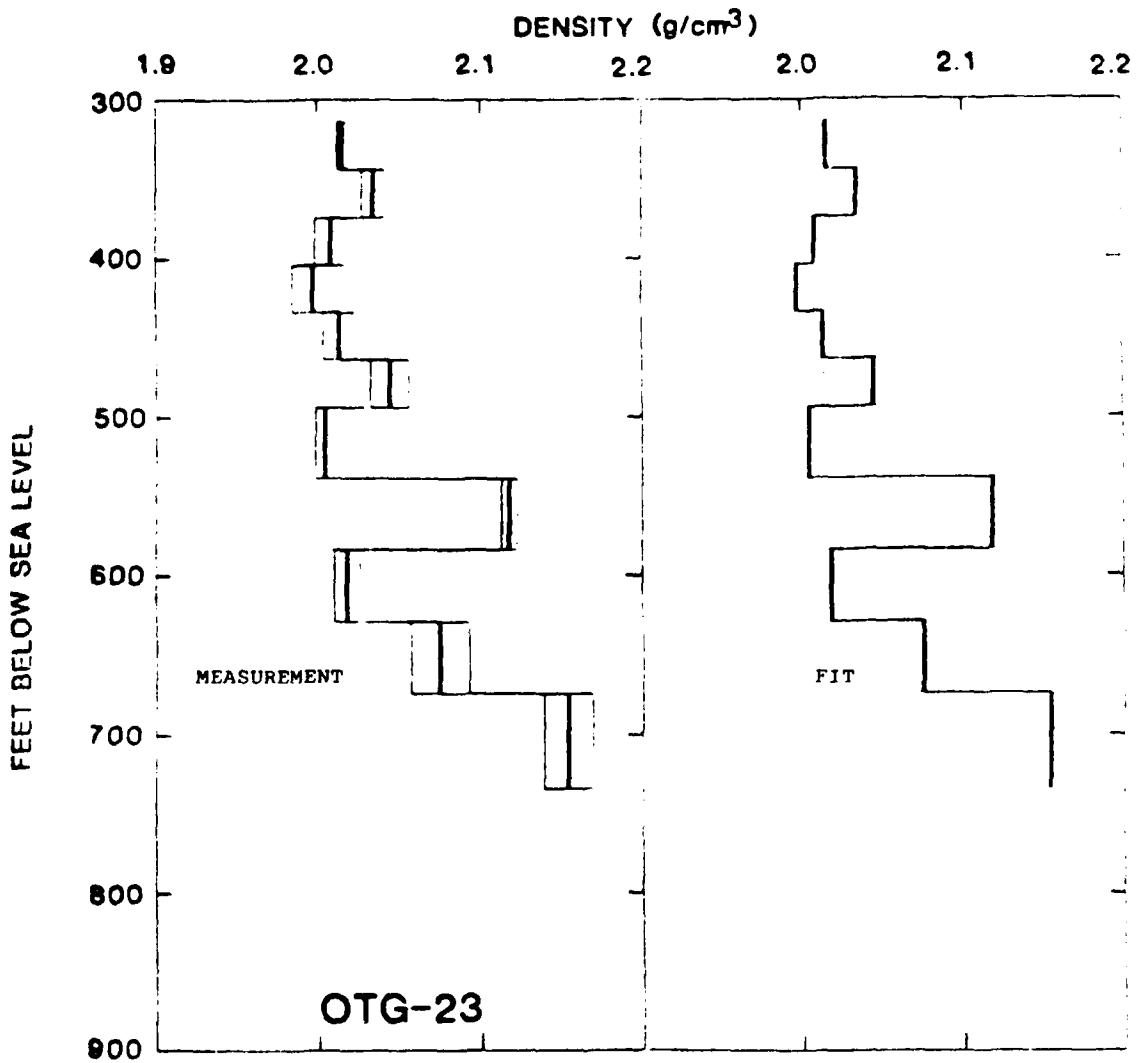


FIGURE 6-15. -- Left: profile of density vs. depth from BHG logging in crater hole OTG-23, as received. Right: plot of broken-straight-line fit [Eq. (11)] to profile at left. The left- and right-hand plot scales are identical.

BOREHOLE GRAVITY SURVEY: HOLE OPZ-18

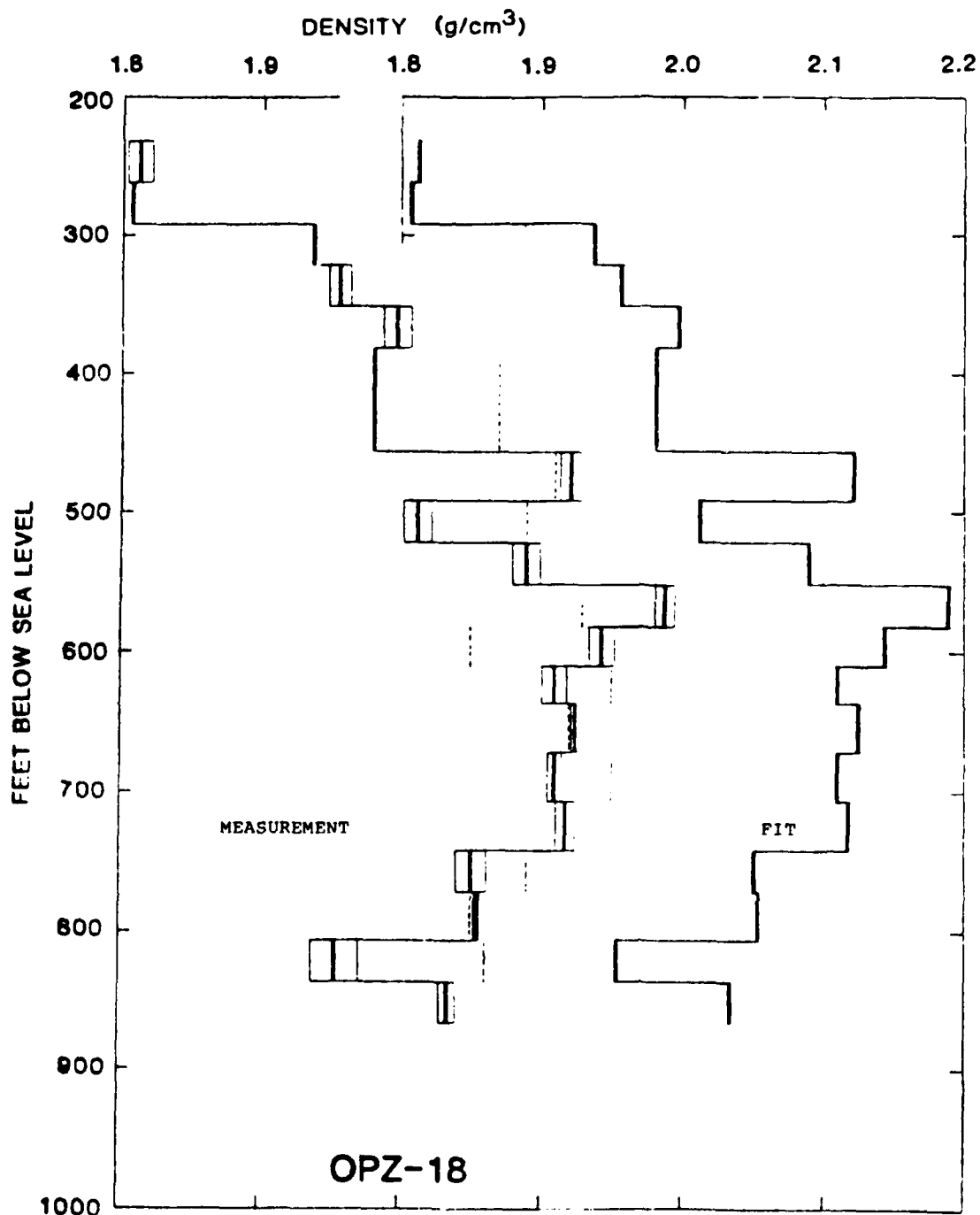


FIGURE 6-16. -- Left: profile of density vs. depth from BHG logging in crater hole OPZ-18, as received. Right: plot of broken-straight-line fit [Eq. (11)] to profile at left. The left- and right-hand plot scales are identical.

BOREHOLE OOR-17: GAMMA-GAMMA LOGGING

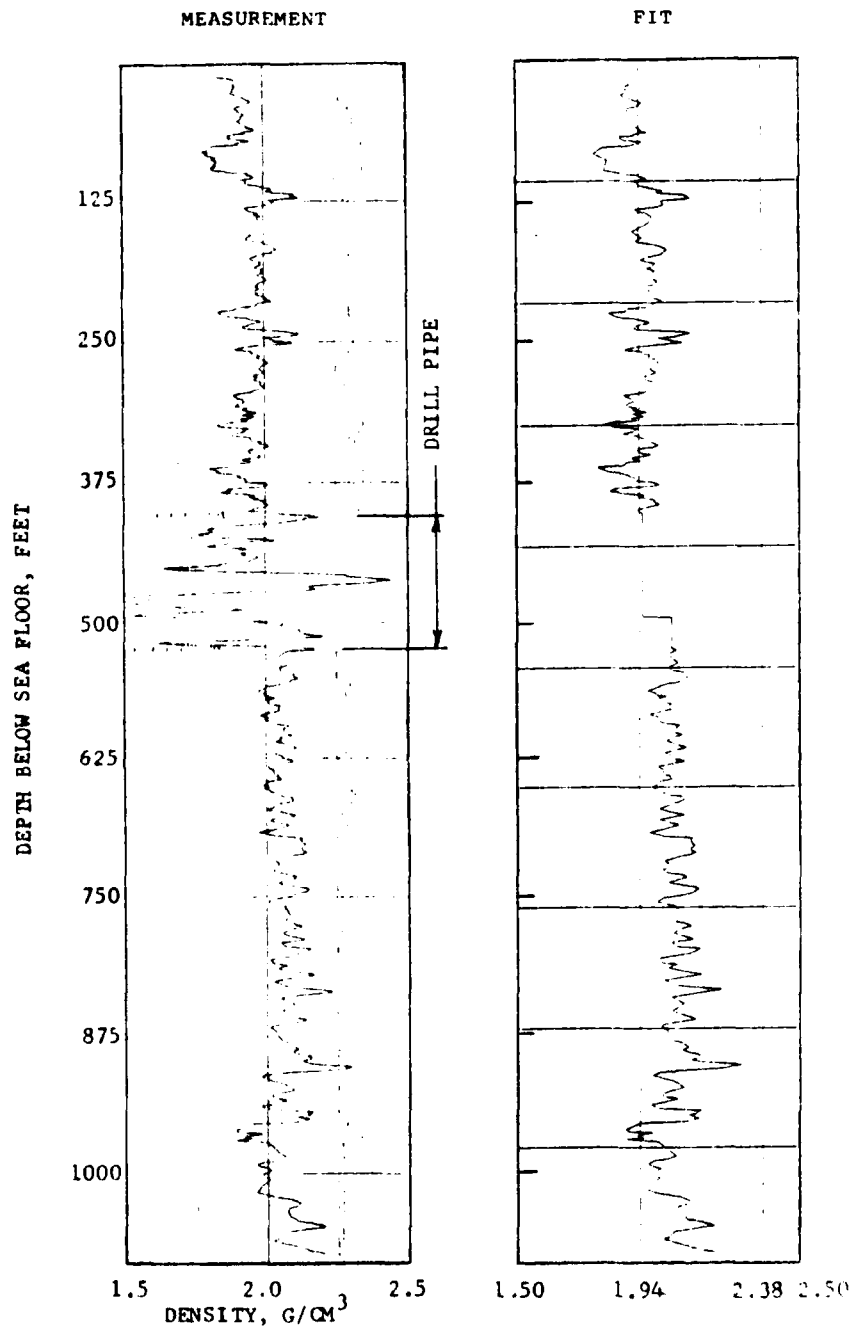


FIGURE 6-17. -- Left: profile of density vs. depth from γ - γ logging in control hole OOR-17, at .70 times the scale of the plot as received. Right: plot of broken-straight-line fit [Eq. (11)] to profile at left. The left- and right-hand plot scales are identical.

BOREHOLE OSR-21: GAMMA-GAMMA LOGGING

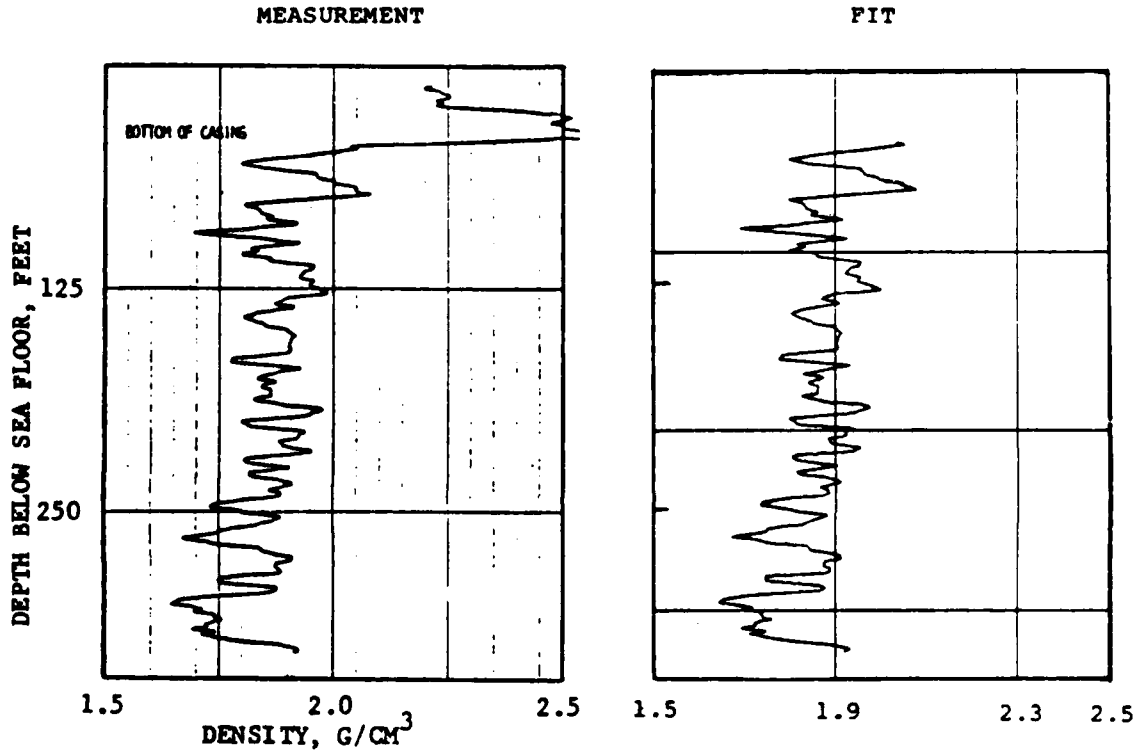


FIGURE 6-18. -- Left: profile of density vs. depth from Y-Y logging in control hole OSR-21, at 1.0 times the scale of the plot as received. Right: plot of broken-straight-line fit [Eq. (11)] to profile at left. The left- and right-hand plot scales are identical.

BOREHOLE ORT-20: GAMMA-GAMMA LOGGING

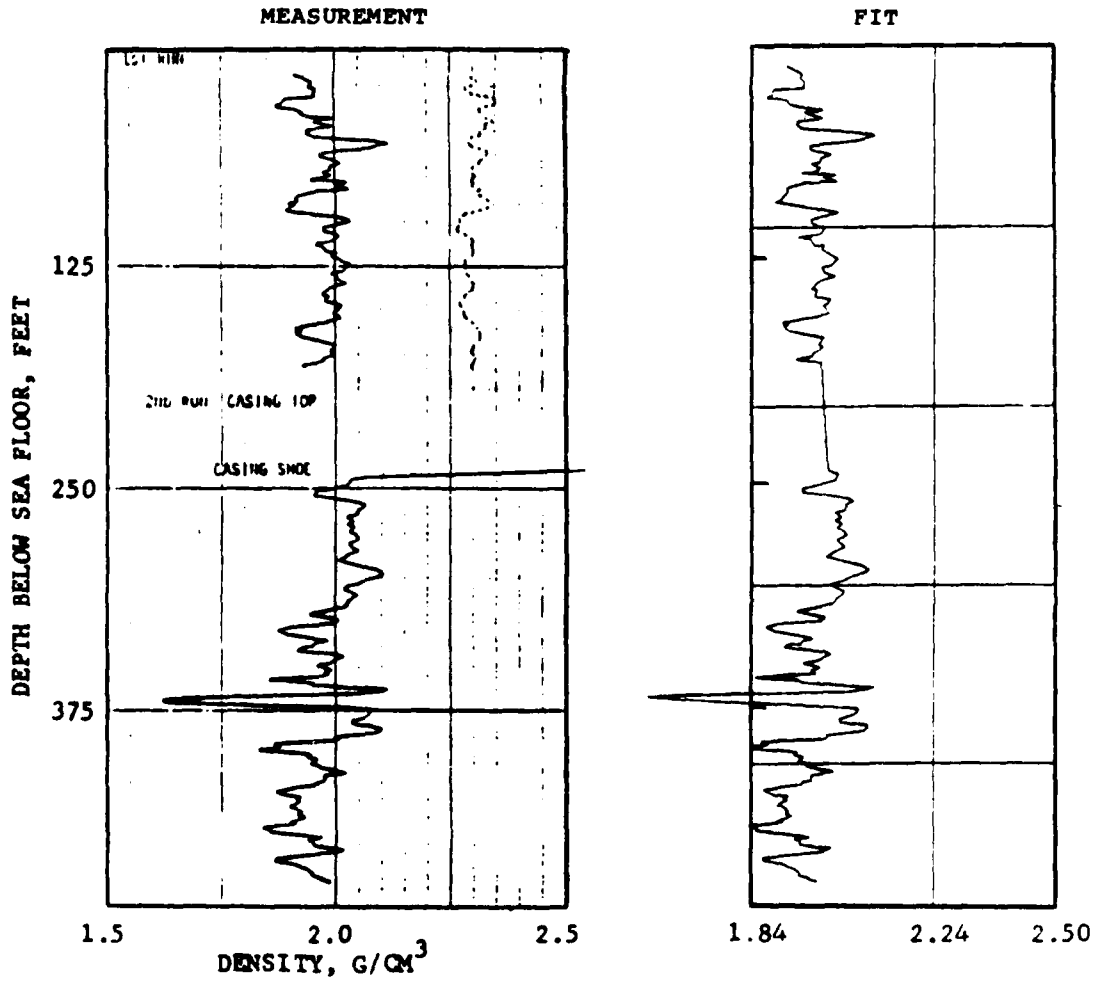


FIGURE 6-19. -- Left: profile of density vs. depth from γ - γ logging in crater hole ORT-20 at 1.0 times the scale of the plot as received. Right: plot of broken-straight-line fit [Eq. (11)] to profile at left. The left- and right-hand plot scales are identical.

BOREHOLE OQT-19: GAMMA-GAMMA LOGGING

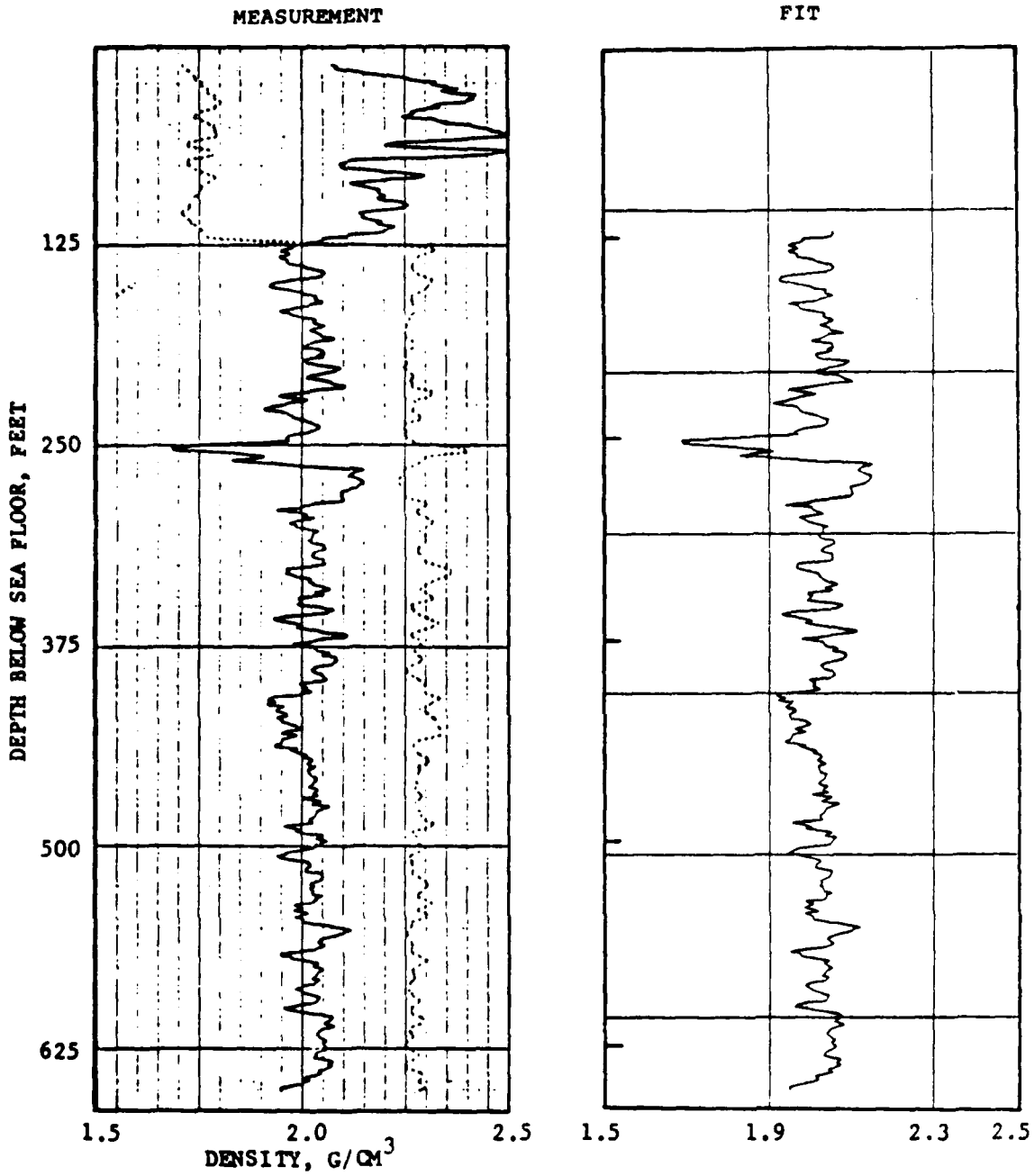


FIGURE 6-20. -- Left: profile of density vs. depth from γ - γ logging in crater hole OQT-19, at 1.0 times the scale of the plot as received. Right: plot of broken-straight-line fit [Eq. (11)] to profile at left. The left- and right-hand plot scales are identical.

BOREROLE OBZ-4: GAMMA-GAMMA LOGGING

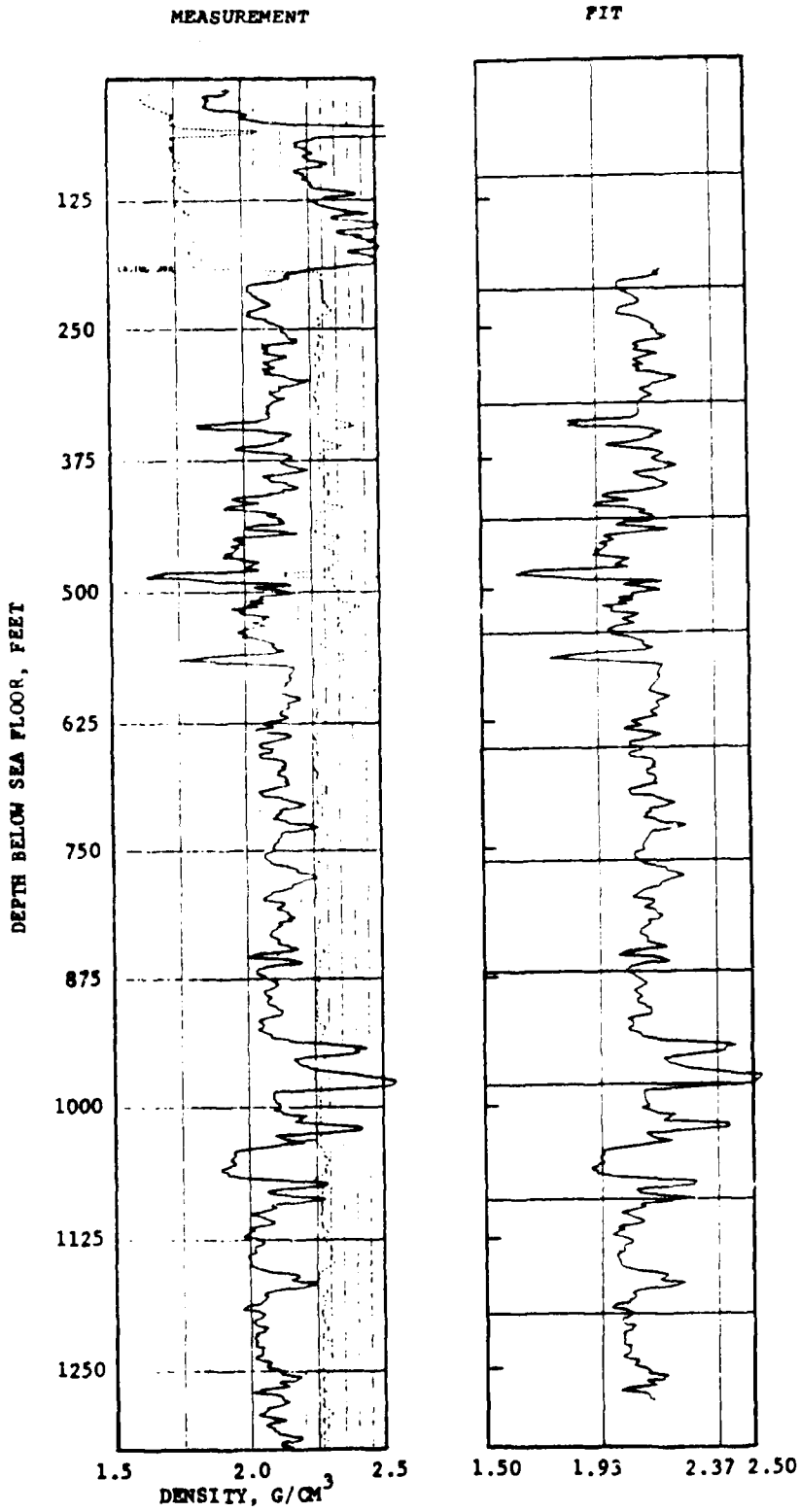


FIGURE 6-21. -- Left: profile of density vs. depth from γ - γ logging in crater hole OBZ-4, at .70 times the scale of the plot as received.
Right: plot of broken-straight-line fit [Eq. (11)] to profile at left. The left- and right-hand plot scales are identical.

BOREHOLE OCT-5: GAMMA-GAMMA LOGGING

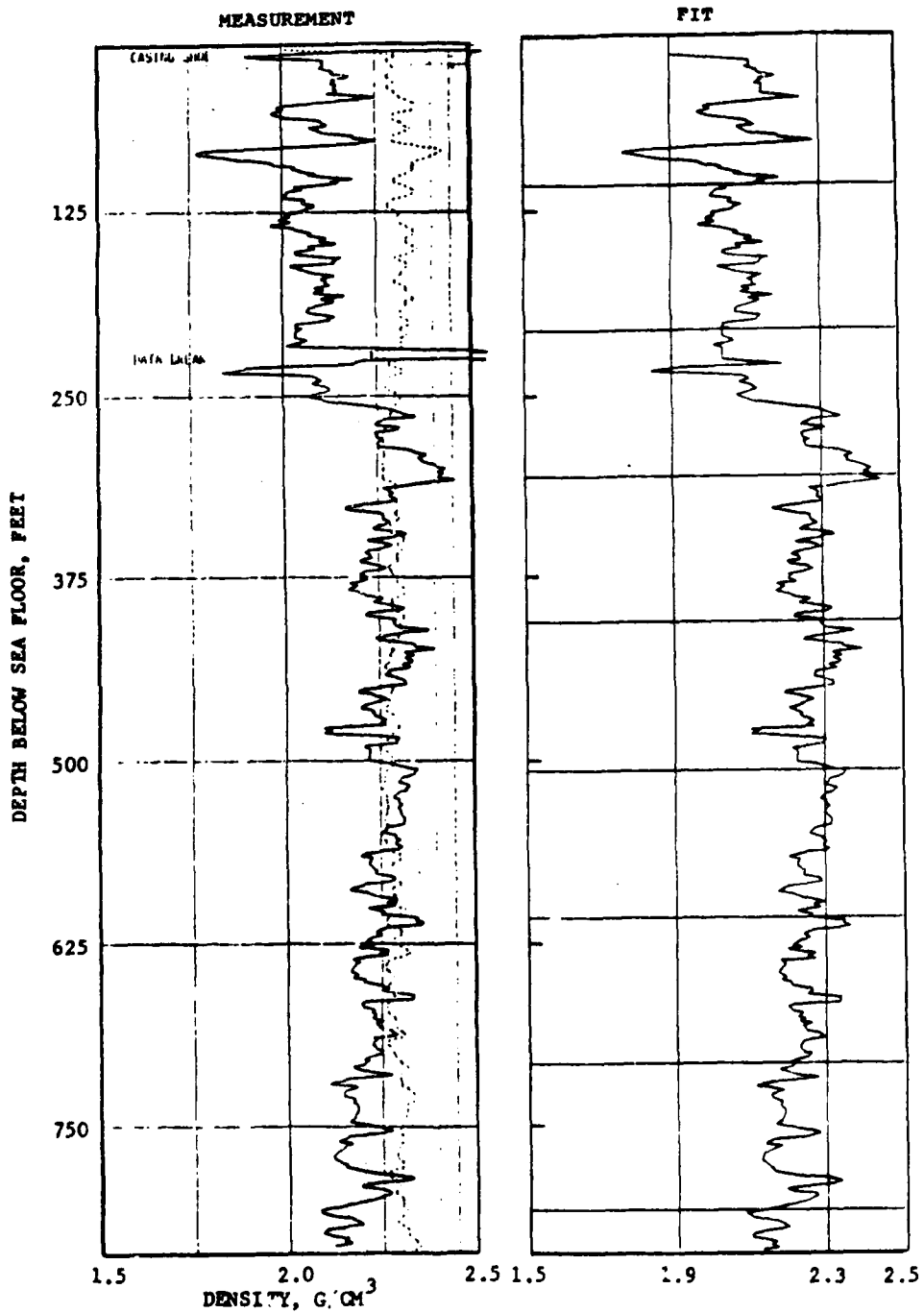


FIGURE 6-22. -- Left: profile of density vs. depth from γ - γ logging in crater hole OCT-5, at 1.0 times the scale of the plot as received. Right: plot of broken-straight-line fit [Eq. (11)] to profile at left. The left- and right-hand plot scales are identical.

BOREHOLE OAR-2A: GAMMA-GAMMA LOGGING

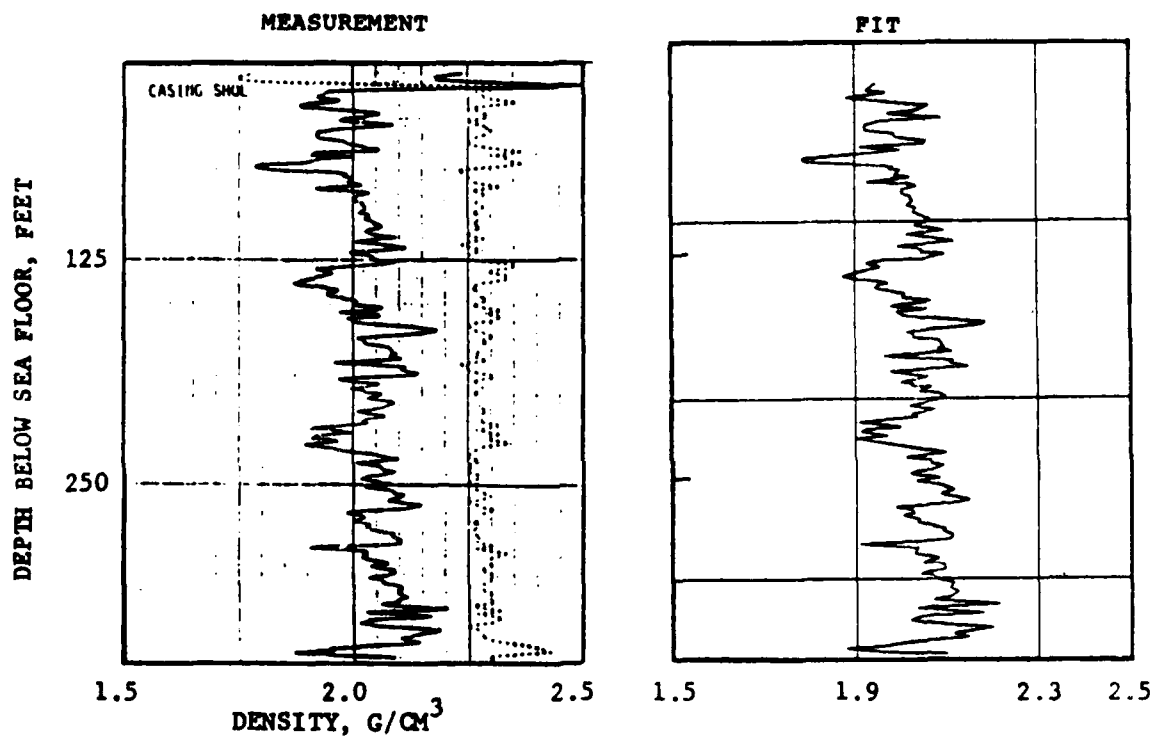


FIGURE 6-23. -- Left: profile of density vs. depth from γ - γ logging in control hole OAR-2A, at 1.0 times the scale of the plot as received. Right: plot of broken-straight-line fit [Eq. (11)] to profile at left. The left- and right-hand plot scales are identical.

BOREHOLE OIT-11: GAMMA-GAMMA LOGGING

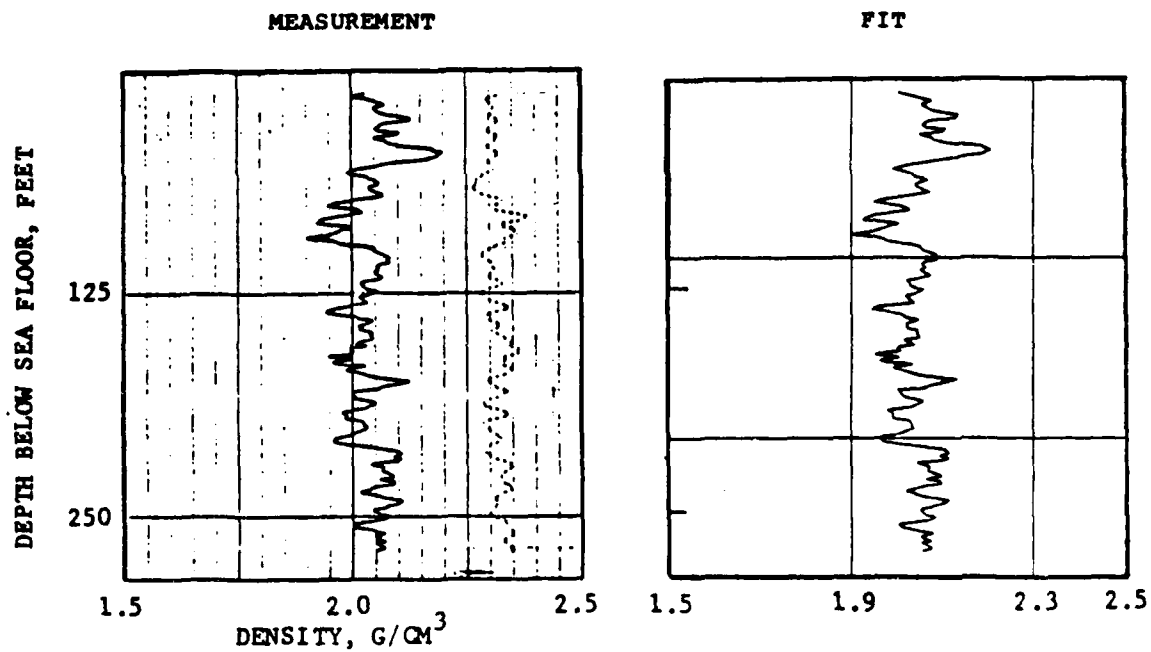


FIGURE 6-24. -- Left: profile of density vs. depth from γ - γ logging in crater hole OIT-11, at 1.0 times the scale of the plot as received. Right: plot of broken-straight-line fit [Eq. (11)] to profile at left. The left- and right-hand plot scales are identical.

BOREHOLE OKT-13: GAMMA-GAMMA LOGGING

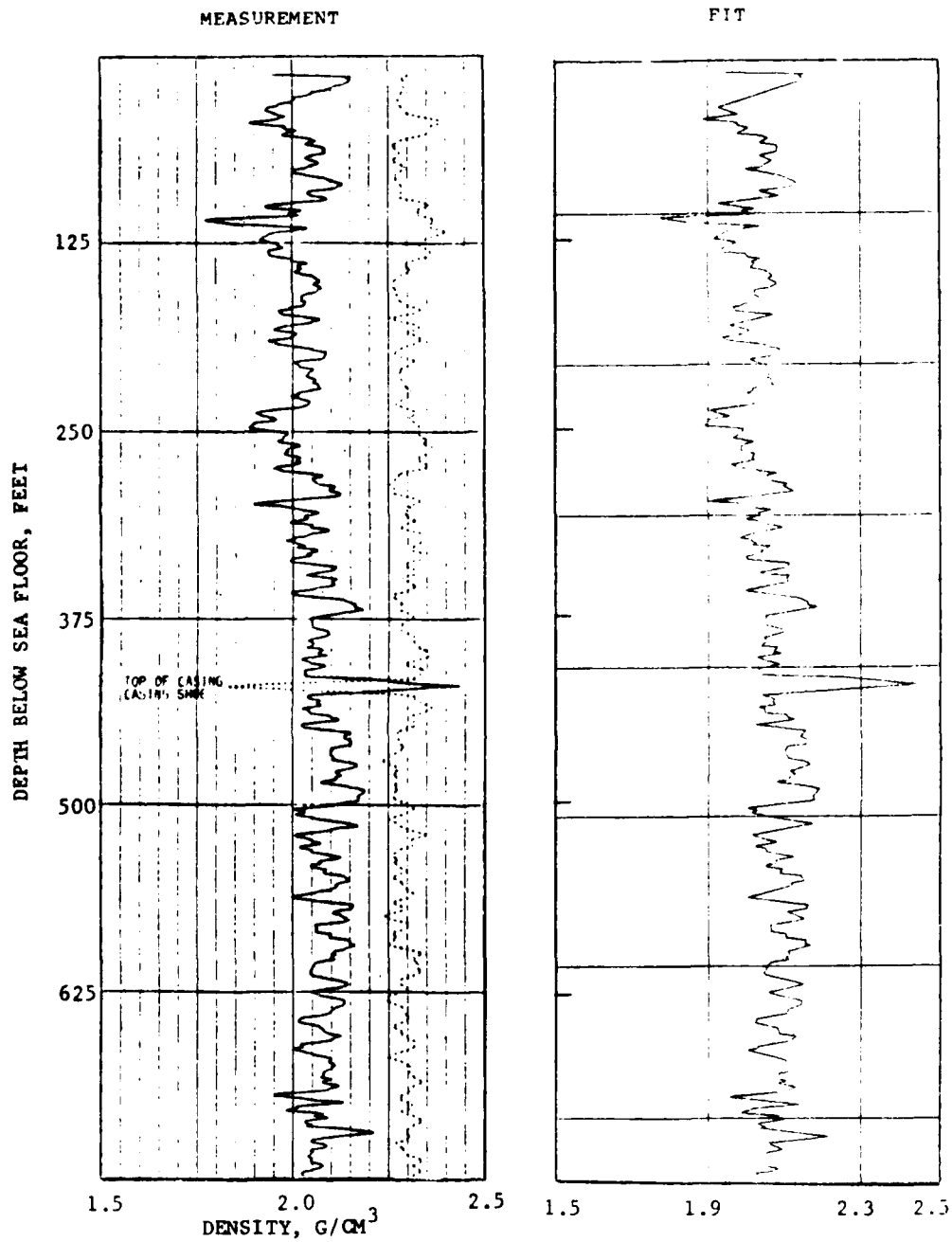


FIGURE 6-25. -- Left: profile of density vs. depth from γ - γ logging in crater hole OKT-13, at 1.0 times the scale of the plot as received. Right: plot of broken-straight-line fit [Eq. (11)] to profile at left. The left- and right-hand plot scales are identical.

BOREHOLE OPZ-18: GAMMA-GAMMA LOGGING

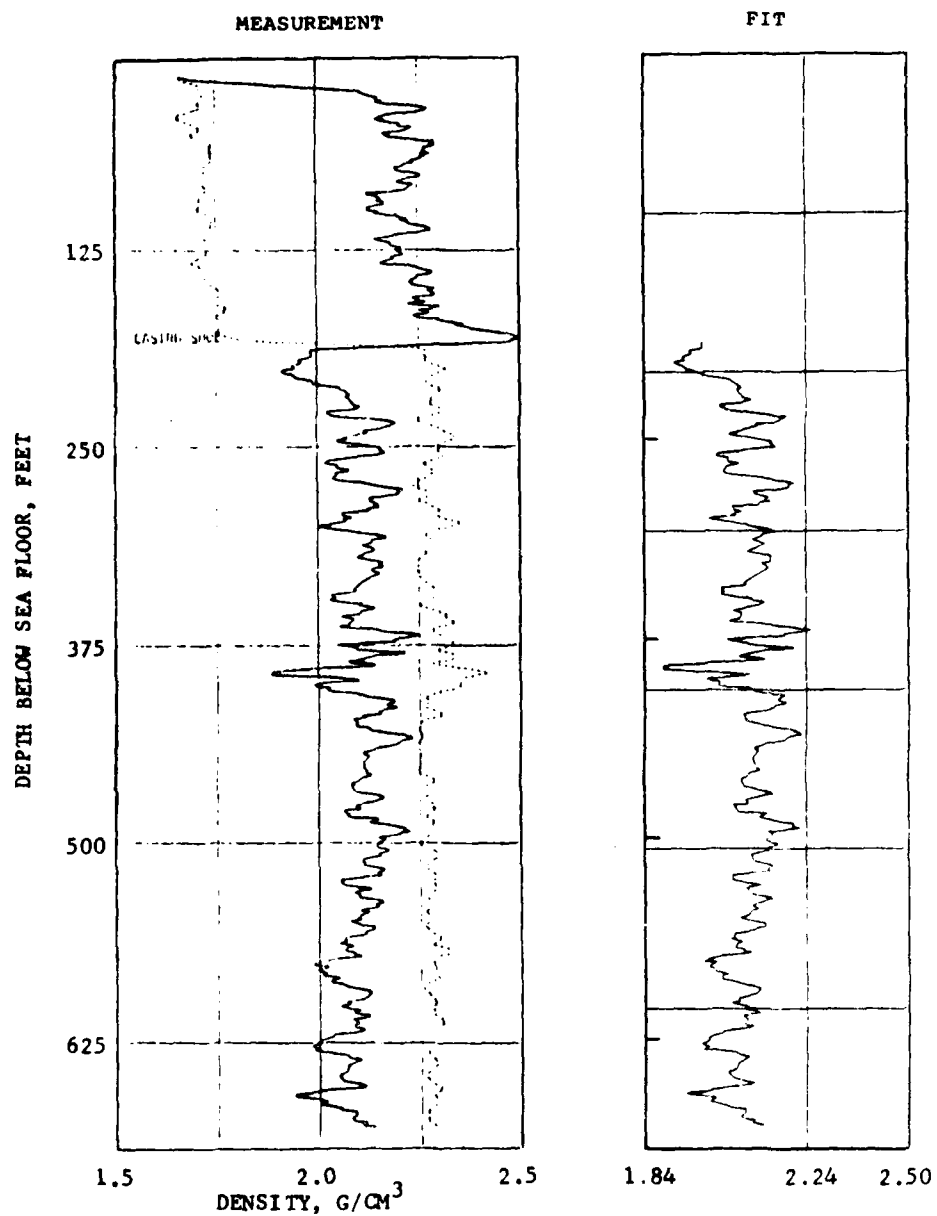


FIGURE 6-26. -- Left: profile of density vs. depth from γ - γ logging in crater hole OPZ-18, at 1.0 times the scale of the plot as received. Right: plot of broken-straight-line fit [Eq. (11)] to profile at left. The left- and right-hand plot scales are identical.

PLACE BOREHOLE UOR-17			PLACE BOREHOLE OPR-18			PLACE BOREHOLE DJF-19			PLACE BOREHOLE UNT-20			PLACE BOREHOLE OSN-21			PLACE BOREHOLE WTS-23		
J	DEPTH (FT)	DENSITY (GM/CC)	J	DEPTH (FT)	DENSITY (GM/CC)	J	DEPTH (FT)	DENSITY (GM/CC)	J	DEPTH (FT)	DENSITY (GM/CC)	J	DEPTH (FT)	DENSITY (GM/CC)	J	DEPTH (FT)	DENSITY (GM/CC)
1	412	1.987	1	252	1.912	1	138	1.907	1	156	1.949	1	134	1.949	1	514	2.014
2	437	1.987	2	262	1.912	2	143	1.907	2	160	1.948	2	139	1.949	2	524	2.014
3	457	1.983	3	262	1.907	3	173	1.913	3	160	4.010	3	139	1.920	3	534	2.017
4	471	1.983	4	292	1.907	4	179	1.913	4	186	4.010	4	146	1.920	4	574	2.025
5	489	1.982	5	292	1.917	5	208	1.912	5	206	1.926	5	186	1.920	5	574	2.025
6	489	1.982	6	342	1.917	6	208	1.912	6	211	1.926	6	209	1.926	6	604	2.025
7	517	1.901	7	352	1.916	7	233	1.910	7	226	1.971	7	234	1.917	7	634	2.025
8	549	1.901	8	382	1.917	8	233	1.910	8	226	1.971	8	234	1.917	8	634	2.025
9	563	1.912	9	382	1.917	9	273	1.905	9	226	1.971	9	234	1.917	9	634	2.025
10	563	1.912	10	437	1.916	10	273	1.905	10	226	1.971	10	234	1.917	10	634	2.025
11	588	1.951	11	472	2.130	11	298	1.900	11	273	1.901	11	234	1.917	11	634	2.025
12	588	1.944	12	472	2.130	12	298	1.900	12	273	1.901	12	234	1.917	12	634	2.025
13	517	1.944	13	542	2.003	13	320	1.944	13	301	1.944	13	234	1.917	13	634	2.025
14	517	1.944	14	542	2.003	14	320	1.944	14	301	1.944	14	234	1.917	14	634	2.025
15	546	1.947	15	542	2.086	15	350	1.972	15	351	1.922	15	234	1.917	15	634	2.025
16	546	1.947	16	552	2.086	16	350	1.972	16	351	1.922	16	234	1.917	16	634	2.025
17	577	1.976	17	582	2.191	17	350	1.972	17	351	1.922	17	234	1.917	17	634	2.025
18	577	1.976	18	582	2.191	18	350	1.972	18	351	1.922	18	234	1.917	18	634	2.025
19	603	1.993	19	610	2.139	19	403	2.009	19	351	1.922	19	234	1.917	19	634	2.025
20	603	1.993	20	610	2.139	20	403	2.009	20	351	1.922	20	234	1.917	20	634	2.025
21	645	1.994	21	637	2.107	21	433	2.011	21	351	1.922	21	234	1.917	21	634	2.025
22	645	1.994	22	637	2.107	22	433	2.011	22	351	1.922	22	234	1.917	22	634	2.025
23	683	2.036	23	772	2.048	23	468	2.045	23	351	1.922	23	234	1.917	23	634	2.025
24	683	2.036	24	772	2.048	24	468	2.045	24	351	1.922	24	234	1.917	24	634	2.025
25	713	2.016	25	807	2.052	25	468	2.045	25	351	1.922	25	234	1.917	25	634	2.025
26	713	2.016	26	807	2.052	26	468	2.045	26	351	1.922	26	234	1.917	26	634	2.025
27	767	2.013	27	897	2.051	27	578	2.013	27	351	1.922	27	234	1.917	27	634	2.025
28	767	2.013	28	897	2.051	28	578	2.013	28	351	1.922	28	234	1.917	28	634	2.025
29			29	867	2.031	29	678	2.019	29	351	1.922	29	234	1.917	29	634	2.025
30			30	867	2.031	30	678	2.019	30	351	1.922	30	234	1.917	30	634	2.025

TABLE 6-7. -- Endpoints of segments of piecewise linear fits [Eq. (11)] to density profiles from borehole gravity surveys.

PEACE BOREHOLE OOR-17				PEACE BOREHOLE OOR-17			
J	DIGITIZED DEPTH (DIV)	DENSITY (G/CC)	COMPUTED DENSITY (G/CC)	J	DIGITIZED DEPTH (DIV)	DENSITY (G/CC)	COMPUTED DENSITY (G/CC)
1	5.00	23.30	72.72	101	76.00	42.00	352.17
2	5.46	23.56	74.44	102	76.00	42.10	356.04
3	5.70	24.20	75.74	103	71.00	42.30	350.19
4	6.30	25.00	76.31	104	71.50	43.20	358.42
5	6.70	22.40	80.83	105	74.20	42.80	361.63
6	7.50	22.50	82.61	106	72.60	42.90	363.35
7	7.60	23.60	82.90	107	76.00	42.00	365.07
8	9.20	46.00	90.76	108	75.50	47.00	367.22
9	10.00	44.00	94.22	109	73.00	44.00	368.51
10	10.20	23.20	95.06	110	74.00	26.50	371.00
11	10.80	22.00	97.65	111	74.70	43.00	372.50
12	12.00	44.90	102.01	112	75.20	25.00	374.55
13	12.00	44.20	106.75	113	75.50	40.30	375.91
14	14.40	43.40	100.43	114	76.00	16.70	377.84
15	14.00	44.20	111.41	115	76.50	40.00	380.11
16	14.70	25.00	114.42	116	76.70	45.10	380.97
17	15.00	45.20	115.71	117	77.00	24.20	384.41
18	15.40	27.10	117.45	118	78.00	21.80	386.54
19	15.50	27.70	118.74	119	78.50	25.30	388.71
20	18.00	44.00	120.01	120	80.00	49.50	394.40
21	16.20	41.50	120.87	121	80.00	26.30	394.66
22	16.90	41.70	123.08	122	81.00	26.00	399.46
23	17.50	26.00	125.60	123	81.00	45.00	401.19
24	18.20	23.30	129.87	124	82.10	25.80	404.19
25	18.50	17.00	138.76	125	82.00	24.00	405.98
26	19.00	16.00	135.92	126	84.00	23.70	404.46
27	21.20	18.00	142.37	127	85.70	25.60	411.07
28	23.20	18.20	150.97	128	84.00	43.00	412.36
29	24.00	42.20	154.90	129	84.70	42.00	415.37
30	24.10	25.00	154.03	130	85.00	16.00	416.66
31	25.00	27.10	158.70	131	86.00	19.00	420.96
32	25.00	24.00	146.42	132	84.20	22.00	421.80
33	25.60	25.20	161.20	133	87.50	44.50	424.55
34	26.30	25.30	164.29	134	87.90	24.70	429.15
35	27.50	30.30	169.45	135	88.10	48.30	429.99
36	27.90	29.00	171.17	136	88.60	49.50	432.13
37	28.50	34.00	172.80	137	89.00	27.00	433.85
38	29.10	36.10	174.55	138	89.50	41.20	435.14
39	29.60	38.00	178.46	139	90.00	19.50	438.15
40	30.40	38.70	181.92	140	90.00	26.50	441.59
41	30.80	39.50	183.64	141	91.20	25.20	443.31
42	31.30	44.70	185.79	142	92.00	46.70	446.75
43	31.80	25.30	187.90	143	92.30	48.40	448.04
44	34.10	47.20	189.25	144	94.00	49.60	450.19
45	35.00	48.20	193.10	145	94.00	46.00	453.63
46	36.20	27.50	198.26	146	94.00	25.80	455.85
47	36.00	24.00	206.00	147	94.70	46.00	458.36
48	37.20	26.10	211.15	148	116.00	26.00	451.65
49	38.00	24.00	214.54	149	116.50	32.00	452.04
50	38.00	49.00	218.44	150	125.00	32.00	460.05
51	39.00	51.20	222.34	151	125.50	35.00	462.18
52	40.80	20.00	226.63	152	124.00	51.80	464.33
53	41.20	47.20	228.74	153	124.70	51.70	467.34
54	41.90	25.80	231.56	154	126.00	53.40	469.93
55	42.70	46.00	234.80	155	126.70	51.60	469.94
56	43.50	48.00	238.24	156	127.50	52.00	469.87
57	44.60	46.00	236.67	157	128.00	44.80	469.82
58	44.80	48.00	241.25	158	129.00	55.80	469.82
59	46.70	48.00	243.40	159	130.00	63.40	470.12
60	48.00	47.00	245.95	160	130.80	51.00	471.41
61	48.80	49.00	250.88	161	131.00	57.00	471.64
62	47.00	28.50	253.89	162	134.50	78.00	472.16
63	47.10	27.60	253.72	163	134.80	48.00	472.16
64	47.50	46.90	255.44	164	133.00	51.00	473.02
65	48.20	27.70	258.45	165	133.40	49.30	474.74
66	48.70	47.00	264.60	166	134.10	49.30	474.74
67	49.70	47.20	264.89	167	134.00	42.00	474.90
68	50.00	49.20	266.18	168	135.00	51.60	475.12
69	50.60	34.40	265.76	169	135.50	51.60	475.77
70	51.00	28.00	270.44	170	135.70	42.00	476.63
71	51.80	47.00	275.79	171	136.50	49.00	477.64
72	52.00	45.50	274.10	172	137.00	49.00	477.64
73	54.70	42.30	277.79	173	137.50	29.30	478.37
74	53.00	47.20	279.08	174	138.00	49.00	478.37
75	53.90	40.80	282.95	175	138.70	30.00	478.52
76	54.10	24.20	283.81	176	139.50	33.70	480.11
77	55.80	48.00	287.60	177	140.00	42.00	480.22
78	55.50	25.50	289.83	178	140.00	52.00	484.55
79	56.20	24.20	292.04	179	141.20	34.30	484.27
80	56.50	26.00	294.13	180	141.00	42.00	484.85
81	56.90	34.00	295.85	181	142.60	51.00	484.29
82	57.30	36.00	297.57	182	144.00	35.00	484.31
83	58.00	22.40	300.80	183	145.00	30.50	484.67
84	58.20	29.50	301.44	184	145.00	52.20	484.95
85	59.20	34.50	305.74	185	146.30	51.00	488.20
86	60.00	29.00	309.14	186	147.00	44.70	488.21
87	60.60	22.40	311.76	187	148.20	49.00	488.37
88	61.00	46.00	313.48	188	148.90	30.30	489.38
89	61.50	26.40	315.63	189	149.00	51.50	489.25
90	61.60	27.70	316.06	190	150.00	42.00	489.55
91	64.50	27.30	319.07	191	150.00	42.00	489.55
92	62.50	28.80	319.92	192	151.50	49.30	491.70
93	63.40	29.50	323.79	193	152.70	48.20	491.72
94	64.60	27.50	326.95	194	154.20	51.00	491.16
95	63.30	49.00	331.96	195	155.00	34.00	491.54
96	64.00	24.50	334.97	196	155.00	34.50	491.03
97	64.90	24.00	338.04	197	157.00	29.50	491.20
98	67.00	46.10	339.27	198	158.30	50.60	491.79
99	68.30	28.60	344.86	199	159.20	49.30	491.66
100	69.50	26.00	350.92	200	160.40	53.50	490.82

TABLE 6-8. -- Endpoints of segments of piecewise linear fits [Eq. (11)] to density profiles from gamma-gamma logging. Table continues on succeeding pages. Data given for boreholes OOR-17, OSR-21, ORT-20, OQT-19, ORZ-4, OCT-5, OAR-2A, OIT-11, OKT-13, and OPZ-18 in OAK crater and KAR-1 in KOA crater.

TABLE 6-8 (Continued)

J	REAL BOREHOLE		COMPUTER		J	REAL BOREHOLE		COMPUTER	
	DENSITY DEPTH (IDIV)	DENSITY (IDIV)	DEPTH (FT)	COMPUTED DENSITY (GM/CC)		DENSITY DEPTH (IDIV)	DENSITY (IDIV)	DEPTH (FT)	COMPUTED DENSITY (GM/CC)
201	164.00	27.50	747.70	1.972	301	241.00	35.70	1083.04	2.110
202	162.00	28.40	751.14	2.024	302	241.74	34.90	1084.05	2.104
203	163.20	28.20	752.06	2.124	303	241.31	35.30	1087.77	2.074
204	164.00	35.00	756.30	2.117	304	242.00	38.00	1091.50	2.071
205	164.00	36.70	759.74	2.135	305	242.20	35.50	1092.57	2.074
206	165.00	36.00	761.04	2.123	306	242.10	34.90	1096.37	2.080
207	164.00	36.00	764.89	2.190	307	243.51	34.90	1098.08	2.104
208	164.30	37.00	766.16	2.110	308	243.00	35.00	1099.57	2.106
209	166.70	35.70	767.50	2.110	309	243.90	36.10	1099.00	2.125
210	167.00	38.00	769.19	2.005	310	244.20	38.10	1101.00	2.134
211	168.00	30.40	773.40	2.026	311	244.60	38.90	1102.81	2.173
212	168.50	31.10	775.64	2.042	312	244.80	40.20	1103.57	2.196
213	169.00	31.50	779.53	2.042	313	245.10	40.60	1104.64	2.192
214	169.00	30.00	781.23	2.019	314	245.50	37.70	1106.64	2.124
215	170.00	31.00	784.67	2.034	315	247.70	36.30	1107.50	2.065
216	171.00	34.00	786.14	2.000	316	248.20	32.70	1109.69	2.061
217	171.50	35.00	788.50	2.036	317	248.50	34.00	1111.37	2.054
218	172.00	31.10	793.27	2.030	318	248.60	31.90	1112.77	2.047
219	173.00	36.70	797.57	2.017	319	248.90	31.80	1114.56	2.045
220	174.00	37.40	799.24	2.117	320	249.10	31.60	1116.28	2.024
221	174.50	36.10	802.30	2.040	321	249.51	31.50	1117.15	2.081
222	175.00	34.00	804.84	2.022	322	249.80	30.30	1117.43	2.022
223	175.00	30.20	807.05	2.002	323	249.00	30.70	1119.15	2.034
224	176.00	29.00	810.97	2.002	324	249.00	32.00	1121.73	2.081
225	177.00	22.70	814.50	2.005	325	249.00	33.90	1122.16	2.092
226	179.00	23.00	822.50	2.067	326	249.10	35.20	1124.45	2.112
227	180.00	22.00	828.52	2.093	327	249.41	35.60	1124.74	2.142
228	181.00	24.50	829.30	2.123	328	249.70	37.10	1126.48	2.145
229	181.00	24.00	832.02	2.085	329	250.20	37.50	1129.04	2.204
230	182.50	23.80	836.97	2.010	330	250.70	40.70	1129.04	2.204
231	183.10	22.20	838.43	2.040					
232	184.50	26.40	844.43	2.034					
233	185.00	21.70	846.54	2.134					
234	186.00	23.00	852.60	2.114					
235	186.00	27.00	857.33	2.019					
236	187.50	23.50	861.63	2.019					
237	188.00	29.50	865.93	2.071					
238	189.50	30.00	867.22	2.036					
239	189.00	33.00	870.23	2.117					
240	190.00	28.00	874.84	2.026					
241	191.00	28.00	880.97	2.007					
242	193.00	22.00	884.19	2.227					
243	194.00	22.00	890.00	2.042					
244	195.10	21.70	896.05	2.099					
245	196.00	24.60	902.47	2.036					
246	197.50	22.30	907.63	2.039					
247	199.20	22.30	909.74	2.140					
248	199.70	27.00	916.46	2.024					
249	201.50	30.30	920.96	2.016					
250	202.50	29.00	923.11	2.035					
251	204.00	10.00	924.12	2.040					
252	205.50	10.00	925.56	2.039					
253	205.00	11.70	934.00	2.092					
254	206.00	32.30	936.15	2.092					
255	206.10	35.00	942.45	2.090					
256	207.00	34.10	944.60	2.116					
257	208.00	35.70	947.16	2.147					
258	208.00	37.00	950.00	2.186					
259	209.50	37.00	950.42	2.148					
260	209.70	36.00	952.77	2.137					
261	210.50	36.00	955.35	2.137					
262	211.00	34.00	958.43	2.239					
263	211.00	34.00	961.37	2.235					
264	212.50	29.00	964.01	2.010					
265	213.00	27.00	967.82	1.901					
266	213.00	24.00	973.43	2.061					
267	215.00	34.40	974.00	2.095					
268	217.00	30.00	984.36	2.019					
269	217.00	30.10	987.36	2.021					
270	219.00	33.00	989.31	2.071					
271	219.00	30.00	992.75	2.019					
272	219.50	27.50	994.90	1.974					
273	220.10	28.00	997.91	1.990					
274	220.70	30.00	1000.06	2.157					
275	221.00	27.00	1003.07	2.190					
276	221.00	35.00	1004.79	2.104					
277	222.20	37.50	1006.31	2.199					
278	223.00	34.50	1009.95	2.087					
279	223.00	23.50	1011.67	1.961					
280	224.00	22.30	1014.83	1.986					
281	225.10	23.00	1019.84	1.986					
282	225.10	28.00	1020.27	1.986					
283	226.00	24.70	1022.89	1.927					
284	226.00	26.00	1025.43	1.950					
285	226.00	22.00	1026.29	1.888					
286	227.50	29.00	1028.44	2.002					
287	228.00	22.90	1031.76	2.069					
288	228.00	30.00	1034.34	2.033					
289	231.00	28.00	1035.63	1.985					
290	232.00	27.00	1040.64	1.967					
291	232.50	28.00	1050.74	1.984					
292	233.00	29.70	1052.94	2.014					
293	233.00	28.00	1055.95	1.988					
294	234.00	28.10	1058.53	1.984					
295	235.70	29.50	1061.54	2.010					
296	236.20	27.00	1066.70	1.981					
297	237.00	27.00	1073.58	1.967					
298	238.20	34.00	1074.60	2.088					

TO = 0.5; .00 1.50 57.60
 TO = 0.5; C: 30.00 100.20 500.00 116.30

TABLE 6-8 (Continued)

PEACE FORMHOLE OSR-21				PEACE BOWHOLE OSR-21					
J	DIGITIZED DEPTH, A (DIV)	DIGITIZED DENSITY, Y (DIV)	COMPUTED DENSITY (GM/CC)	J	DIGITIZED DEPTH, A (DIV)	DIGITIZED DENSITY, Y (DIV)	COMPUTED DENSITY (GM/CC)		
1	10.00	30.70	130.64	4.033	101	61.00	19.00	333.92	1.799
2	10.30	33.00	131.44	2.009	102	62.10	19.50	334.71	1.806
3	11.00	40.00	134.50	1.959	103	62.60	20.00	336.47	1.876
4	11.60	43.70	136.74	1.871	104	64.00	20.30	337.45	1.881
5	12.30	49.00	139.69	1.790	105	64.50	22.00	340.10	1.805
6	14.00	51.60	142.03	1.839	106	64.00	21.00	342.15	1.829
7	14.60	49.00	144.74	1.955	107	64.30	18.00	343.32	1.782
8	14.30	49.60	146.50	1.964	108	64.60	16.00	344.50	1.751
9	14.00	31.00	144.47	1.992	109	65.00	15.00	346.06	1.748
10	13.20	31.00	151.04	1.990	110	65.00	11.00	349.20	1.672
11	13.00	24.00	152.61	2.047	111	66.00	14.50	350.76	1.727
12	13.00	24.60	153.50	2.042	112	66.70	16.00	352.72	1.751
13	14.70	26.00	154.92	2.077	113	67.10	21.70	354.24	1.840
14	17.20	30.00	156.07	1.970	114	67.70	21.90	356.44	1.843
15	18.00	19.00	167.01	1.794	115	68.00	23.00	357.81	1.875
16	18.30	41.00	163.74	1.829	116	68.00	26.20	359.36	1.911
17	18.30	21.40	167.10	1.857	117	67.00	26.20	361.73	1.911
18	19.00	43.00	169.06	1.841	118	69.20	24.00	362.51	1.876
19	20.20	42.00	170.62	1.845	119	70.00	23.70	364.44	1.871
20	21.00	44.50	172.97	1.841	120	70.20	24.60	366.45	1.886
21	21.30	41.20	174.93	1.832	121	70.70	24.60	368.30	1.891
22	21.10	40.00	174.10	1.813	122	71.00	23.00	369.56	1.875
23	22.10	17.20	176.04	1.691	123	71.00	18.00	370.34	1.782
24	23.00	22.00	181.59	1.845	124	71.00	25.00	371.13	1.794
25	23.40	27.00	183.55	1.925	125	72.00	15.70	373.40	1.746
26	24.20	40.20	186.24	1.817	126	72.70	25.00	376.22	1.861
27	24.00	41.20	187.46	1.832	127	73.00	24.00	377.34	1.876
28	24.20	19.00	190.20	1.748	128	73.00	23.70	378.96	1.865
29	25.50	42.70	191.38	1.854	129	74.10	13.70	381.70	1.735
30	26.10	42.40	193.73	1.854	130	74.50	10.20	383.27	1.680
31	26.00	49.00	196.44	1.955	131	75.00	9.10	385.23	1.643
32	27.30	48.30	199.45	1.951	132	75.00	12.00	386.74	1.680
33	27.60	47.70	197.60	1.934	133	75.00	13.00	388.36	1.716
34	28.00	46.00	202.73	1.920	134	76.10	12.60	389.53	1.697
35	29.00	49.00	205.06	1.955	135	76.50	15.20	391.10	1.736
36	29.10	48.70	207.43	1.947	136	77.10	15.40	392.25	1.741
37	30.00	50.70	209.00	1.970	137	77.40	16.50	394.62	1.759
38	31.70	31.00	211.74	1.994	138	78.00	14.20	396.97	1.723
39	31.00	40.00	212.92	1.970	139	78.00	14.40	398.50	1.726
40	31.30	45.50	214.09	1.980	140	78.70	12.30	399.72	1.693
41	32.70	45.30	216.83	1.864	141	79.10	15.00	401.80	1.746
42	32.70	46.00	219.57	1.908	142	79.00	13.60	403.05	1.713
43	33.30	28.00	222.71	1.826	143	79.00	15.40	404.41	1.741
44	34.30	19.30	226.06	1.803	144	80.50	19.00	406.76	1.798
45	34.90	40.80	228.44	1.824	145	81.00	24.50	408.72	1.884
46	35.00	28.00	223.70	1.845	146	81.60	27.40	411.07	1.929
47	35.00	42.40	230.15	1.891	147	82.10	26.70	413.88	1.918
48	36.00	25.30	232.11	1.897					
49	36.00	46.30	236.02	1.932					
50	37.30	24.00	234.00	1.908					
51	38.20	49.70	241.11	1.903					
52	39.20	25.00	245.03	1.904					
53	39.00	20.00	247.35	1.826					
54	40.00	18.00	248.16	1.782					
55	40.60	40.00	250.51	1.779					
56	41.00	22.00	252.00	1.845					
57	41.50	27.30	254.00	1.920					
58	42.00	24.70	255.99	1.887					
59	42.00	21.00	259.13	1.829					
60	43.10	40.00	266.30	1.861					
61	43.30	23.00	261.80	1.873					
62	44.00	41.70	263.61	1.840					
63	44.20	21.00	264.61	1.842					
64	44.50	43.00	265.78	1.861					
65	45.60	23.00	270.89	1.861					
66	46.00	40.70	271.66	1.824					
67	46.70	44.00	274.40	1.876					
68	46.90	24.00	275.18	1.869					
69	47.00	29.00	274.57	1.955					
70	47.50	30.20	277.53	1.975					
71	48.00	29.00	278.44	1.954					
72	48.40	28.00	281.06	1.930					
73	49.00	40.00	285.43	1.820					
74	49.20	19.00	284.10	1.798					
75	50.00	20.30	287.32	1.810					
76	50.40	27.00	288.09	1.923					
77	50.60	28.00	289.67	1.937					
78	50.90	26.00	290.85	1.922					
79	51.60	46.90	293.59	1.922					
80	51.90	24.50	294.74	1.864					
81	52.40	24.00	297.50	1.889					
82	53.20	48.00	299.85	1.951					
83	53.70	48.00	301.81	1.937					
84	54.20	23.20	303.77	1.817					
85	54.60	19.40	305.34	1.804					
86	55.00	20.00	304.90	1.813					
87	55.70	25.70	309.44	1.903					
88	56.60	20.00	313.17	1.813					
89	57.20	40.40	314.74	1.820					
90	57.30	23.30	315.91	1.866					
91	57.80	25.30	317.87	1.900					
92	58.10	26.00	319.04	1.908					
93	58.00	23.20	321.70	1.864					
94	59.10	24.30	322.96	1.881					
95	59.60	24.50	324.92	1.884					
96	60.00	23.30	326.48	1.864					
97	60.20	19.00	327.87	1.804					
98	60.70	16.00	329.88	1.751					
99	60.90	15.00	330.01	1.735					
100	61.20	15.00	331.18	1.735					

TOTALS: .00 1.50 63.40
 # OF A. B. C.: 30.00 209.00 1.00 .25530467

TABLE 6-8 (Continued)

PEACE BORHOLE OCT-63				PEACE BORHOLE CHAL. 7					
	DIGITIZED DEPTH (Ft)	DIGITIZED DENSITY (Lb/CC)	COMPUTED DEPTH (Ft)	COMPUTED DENSITY (Lb/CC)		DIGITIZED DEPTH (Ft)	DIGITIZED DENSITY (Lb/CC)	COMPUTED DEPTH (Ft)	COMPUTED DENSITY (Lb/CC)
201	172.80	47.60	848.94	2.247	1	7.50	28.30	141.87	1.949
202	172.60	49.40	850.12	2.276	2	6.80	27.00	142.56	1.927
203	173.40	50.50	853.27	2.293	3	7.10	24.70	144.53	1.970
204	174.60	46.80	855.63	2.255	4	7.40	24.30	145.84	1.964
205	175.20	48.30	859.57	2.277	5	9.00	25.70	153.91	2.065
206	176.00	47.00	863.50	2.258	6	9.40	25.20	156.24	2.050
207	176.20	48.10	864.29	2.255	7	10.00	20.00	157.80	1.974
208	176.70	47.90	866.24	2.252	8	10.80	27.31	160.87	2.029
209	177.20	46.00	868.24	2.227	9	11.20	29.01	162.84	1.954
210	177.70	44.70	870.20	2.204	10	11.80	46.00	164.70	1.924
211	178.00	44.40	871.58	2.211	11	12.60	48.00	167.40	1.924
212	178.20	45.00	873.34	2.204	12	13.00	30.00	167.80	1.960
213	178.00	42.80	875.31	2.172	13	13.40	31.00	171.01	1.891
214	178.80	45.80	878.44	2.219	14	14.70	35.20	172.17	2.021
215	180.30	49.50	880.83	2.277	15	14.00	35.10	173.34	2.029
216	181.00	41.80	883.19	2.156	16	14.30	25.00	174.50	2.004
217	181.80	46.90	885.34	2.211	17	24.90	46.20	174.20	1.917
218	184.50	43.50	889.04	2.183	18	15.20	31.80	176.00	2.001
219	183.20	41.60	891.85	2.150	19	15.70	47.00	176.94	1.921
220	183.90	41.90	894.41	2.151	20	16.00	44.00	181.11	1.881
221	184.50	43.50	896.97	2.180	21	16.50	18.00	183.50	1.780
222	185.20	42.00	899.72	2.173	22	17.00	18.50	184.84	1.792
223	186.00	43.80	902.87	2.188	23	17.40	46.80	186.00	1.924
224	187.00	43.70	906.81	2.188	24	17.80	30.70	187.30	1.902
225	187.60	43.20	909.94	2.170	25	18.00	30.20	188.84	1.874
226	188.50	42.20	912.72	2.162	26	18.20	31.80	189.87	2.021
227	189.50	48.70	916.65	2.254	27	18.40	31.00	192.10	1.771
228	190.00	49.60	918.62	2.274	28	18.40	31.00	193.10	2.022
229	190.50	47.90	920.59	2.252	29	19.90	47.00	194.74	2.030
230	191.00	42.00	922.46	2.159	30	20.10	42.00	197.04	2.019
231	191.90	40.30	926.10	2.133	31	20.40	24.00	198.20	2.032
232	192.70	45.00	927.28	2.175	32	21.00	32.00	200.40	2.006
233	192.60	41.70	928.84	2.135	33	21.50	35.00	202.64	2.006
234	193.60	40.00	932.74	2.118	34	21.00	35.20	203.64	2.029
235	194.50	49.60	936.34	2.182	35	22.60	206.75	206.75	2.030
236	196.20	41.70	943.03	2.133	36	23.20	52.80	209.04	2.019
237	196.60	41.80	944.61	2.134	37	23.50	34.10	210.27	2.020
238	197.00	46.00	947.74	2.222	38	24.10	35.50	212.54	2.050
239	197.80	51.20	949.31	2.304	39	25.10	35.80	216.44	2.064
240	198.30	53.20	951.30	2.335	40	26.00	33.80	218.94	2.024
241	198.80	41.40	953.27	2.308	41	26.80	37.70	225.17	2.071
242	199.30	46.00	955.24	2.222	42	27.30	42.70	225.74	2.071
243	199.64	44.00	956.42	2.191	43	28.30	39.30	228.51	2.021
244	200.10	45.00	957.99	2.206	44	29.00	31.40	231.60	1.997
245	200.40	46.40	959.17	2.240	45	29.20	34.10	232.34	2.040
246	200.70	47.20	960.75	2.272	46	29.60	34.80	233.85	2.051
247	201.60	47.50	964.29	2.246	47	29.90	34.60	235.11	2.047
248	202.90	42.00	969.41	2.159	48	30.10	37.90	235.89	2.100
249	203.70	37.00	972.34	2.081	49	30.60	35.00	238.61	2.054
250	204.50	38.20	975.73	2.100	50	31.00	29.00	239.39	1.945
251	205.28	48.70	978.94	2.170	51	31.50	47.00	241.44	1.927
252	206.34	46.80	982.78	2.145	52	31.80	48.00	242.27	1.959
253	207.14	40.50	985.44	2.104	53	33.40	43.80	248.71	1.877
254	207.84	37.80	988.70	2.093	54	33.80	45.00	250.24	1.894
255	208.74	42.00	992.24	2.153	55	34.00	38.80	251.04	1.948
256	209.24	41.20	995.21	2.137	56	34.50	30.00	252.59	1.975
257	209.74	42.30	996.14	2.144	57	35.20	29.00	254.84	1.954
258	210.00	39.70	997.34	2.123	58	35.00	46.20	254.93	1.994
					59	35.30	49.00	254.94	1.959
					60	36.00	32.40	254.81	2.014
					61	36.00	32.00	260.57	2.006
					62	37.00	49.00	262.70	2.070
					63	37.70	30.50	263.42	1.983
					64	38.10	35.50	266.97	2.062
					65	38.50	41.30	266.52	1.995
					66	39.00	42.00	270.67	2.006
					67	40.00	48.60	274.34	2.190
					68	40.00	48.00	275.91	2.100
					69	41.80	42.70	279.74	2.071
					70	41.50	38.50	280.14	2.050
					71	42.20	33.50	282.90	2.030
					72	42.50	37.00	284.07	2.060
					73	43.80	37.70	287.45	2.097
					74	43.80	17.60	289.12	2.085
					75	44.20	38.80	290.47	2.114
					76	44.80	49.50	293.00	1.967
					77	45.50	29.00	295.72	2.117
					78	45.80	48.60	296.87	2.111
					79	46.30	41.00	298.03	2.068
					80	47.00	30.80	301.54	1.979
					81	47.60	35.40	304.64	2.040
					82	48.30	33.00	306.60	2.022
					83	48.50	31.80	307.34	2.081
					84	48.70	33.40	308.15	2.028
					85	49.00	34.30	309.32	2.097
					86	49.24	36.00	310.10	2.070
					87	49.34	34.30	312.43	2.043
					88	50.10	37.00	313.54	2.085
					89	50.40	37.40	314.74	2.094
					90	51.00	46.50	317.08	2.078
					91	51.64	33.00	320.20	2.024
					92	52.30	36.40	322.14	2.074
					93	53.00	33.30	324.44	2.027
					94	53.30	24.00	326.03	2.018
					95	54.10	46.30	328.13	1.911
					96	54.84	31.60	331.85	2.003
					97	55.00	27.00	332.43	1.927
					98	55.40	46.70	334.18	1.916
					99	56.00	29.80	336.52	1.972
					100	56.40	25.50	338.07	1.903
TOTAL S:		48.00	1.90	65.70					
TOTAL B: C:		33.00	284.70	1.00	.254				

TABLE 6-8 (Continued)

PEACE BUREAU				GTT-11			
J	DISTANCE (LEPM, # DUV)	DENSIFIED DENSITY, % (DUV)	COMPUTED DEPTH (FT)	J	DISTANCE (LEPM, # DUV)	DENSIFIED DENSITY, % (DUV)	COMPUTED DEPTH (FT)
101	58.00	38.00	375.04	1	1.00	22.00	169.37
102	59.00	38.50	379.17	2	2.00	22.00	173.70
103	59.00	39.00	380.11	3	3.00	22.00	176.04
104	60.00	39.00	382.06	4	4.00	22.00	179.21
105	62.00	37.50	382.83	5	5.00	22.00	180.79
106	63.00	38.00	385.16	6	6.00	22.00	181.57
107	63.00	39.00	385.94	7	7.00	22.00	183.94
108	63.00	39.00	387.11	8	8.00	22.00	183.15
109	63.00	37.00	389.03	9	9.00	22.00	185.94
110	64.00	38.00	391.38	10	10.00	22.00	189.72
111	63.00	37.00	393.71	11	11.00	22.00	191.00
112	63.00	37.00	396.04	12	12.00	22.00	190.65
113	64.00	37.00	398.76	13	13.00	22.00	190.63
114	65.00	41.00	371.48	14	14.00	22.00	192.60
115	65.00	39.00	373.04	15	15.00	22.00	194.57
116	66.00	38.00	375.57	16	16.00	22.00	195.35
117	67.00	38.50	376.55	17	17.00	22.00	197.32
118	68.00	38.50	378.44	18	18.00	22.00	198.90
119	67.00	38.00	380.13	19	19.00	22.00	201.26
120	67.00	39.00	381.97	20	20.00	22.00	203.62
121	68.00	39.00	383.55	21	21.00	22.00	206.38
122	68.00	39.00	387.02	22	22.00	22.00	209.97
123	69.00	39.00	390.29	23	23.00	22.00	211.94
124	69.00	39.00	390.22	24	24.00	22.00	214.25
125	70.00	39.00	392.07	25	25.00	22.00	215.93
126	70.00	39.00	393.29	26	26.00	22.00	218.22
127	71.00	39.00	395.57	27	27.00	22.00	217.80
128	71.00	39.00	397.51	28	28.00	22.00	220.16
129	72.00	39.00	399.42	29	29.00	22.00	222.13
130	72.00	37.00	401.79	30	30.00	22.00	224.08
131	73.00	39.00	403.06	31	31.00	22.00	226.02
132	74.00	37.00	407.23	32	32.00	22.00	230.34
133	74.00	37.00	409.76	33	33.00	22.00	232.76
134	75.00	39.00	411.89	34	34.00	22.00	235.12
135	75.00	39.00	412.67	35	35.00	22.00	237.87
136	76.00	37.00	415.38	36	36.00	22.00	240.63
137	76.00	39.00	416.94	37	37.00	22.00	241.81
138	77.00	39.00	420.05	38	38.00	22.00	242.60
139	78.00	39.00	421.99	39	39.00	22.00	244.57
140	78.00	39.00	424.71	40	40.00	22.00	246.54
141	79.00	39.00	426.26	41	41.00	22.00	248.90
142	79.00	39.00	428.98	42	42.00	22.00	250.47
143	80.00	39.00	430.93	43	43.00	22.00	252.44
144	81.00	39.00	433.65	44	44.00	22.00	255.20
145	81.00	39.00	435.20	45	45.00	22.00	257.17
146	82.00	39.00	437.53	46	46.00	22.00	260.31
147	82.00	39.00	439.70	47	47.00	22.00	263.46
148	83.00	39.00	441.82	48	48.00	22.00	266.25
149	84.00	39.00	443.30	49	49.00	22.00	269.03
150	85.00	41.00	447.24	50	50.00	22.00	272.40
151	85.00	39.00	449.57	51	51.00	22.00	274.67
152	86.00	41.00	451.91	52	52.00	22.00	277.24
153	86.00	41.00	453.17	53	53.00	22.00	279.67
154	86.00	41.00	455.51	54	54.00	22.00	282.08
155	86.00	39.00	458.14	55	55.00	22.00	284.57
156	87.00	41.00	460.11	56	56.00	22.00	287.04
157	87.00	41.00	462.11	57	57.00	22.00	289.50
158	88.00	41.00	464.11	58	58.00	22.00	291.99
159	88.00	41.00	466.11	59	59.00	22.00	294.42
160	89.00	41.00	468.11	60	60.00	22.00	296.80
161	89.00	41.00	470.11	61	61.00	22.00	299.29
162	90.00	41.00	472.11	62	62.00	22.00	301.67
163	90.00	41.00	474.11	63	63.00	22.00	304.05
164	91.00	41.00	476.11	64	64.00	22.00	306.42
165	91.00	41.00	478.11	65	65.00	22.00	308.79
166	92.00	41.00	480.11	66	66.00	22.00	311.16
167	92.00	41.00	482.11	67	67.00	22.00	313.53
168	93.00	41.00	484.11	68	68.00	22.00	315.90
169	93.00	41.00	486.11	69	69.00	22.00	318.27
170	94.00	41.00	488.11	70	70.00	22.00	320.64
171	94.00	41.00	490.11	71	71.00	22.00	323.01
172	95.00	41.00	492.11	72	72.00	22.00	325.38
173	95.00	41.00	494.11	73	73.00	22.00	327.75
174	96.00	41.00	496.11	74	74.00	22.00	330.12
175	96.00	41.00	498.11	75	75.00	22.00	332.49
176	97.00	41.00	500.11	76	76.00	22.00	334.86
177	97.00	41.00	502.11	77	77.00	22.00	337.23
178	98.00	41.00	504.11	78	78.00	22.00	339.60
179	98.00	41.00	506.11	79	79.00	22.00	341.97
180	99.00	41.00	508.11	80	80.00	22.00	344.34
181	99.00	41.00	510.11	81	81.00	22.00	346.71
182	100.00	41.00	512.11	82	82.00	22.00	349.08
183	100.00	41.00	514.11	83	83.00	22.00	351.45
184	100.00	41.00	516.11	84	84.00	22.00	353.82
185	100.00	41.00	518.11	85	85.00	22.00	356.19
186	100.00	41.00	520.11	86	86.00	22.00	358.56
187	100.00	41.00	522.11	87	87.00	22.00	360.93
188	100.00	41.00	524.11	88	88.00	22.00	363.30
189	100.00	41.00	526.11	89	89.00	22.00	365.67
190	100.00	41.00	528.11	90	90.00	22.00	368.04
191	100.00	41.00	530.11	91	91.00	22.00	370.41
192	100.00	41.00	532.11	92	92.00	22.00	372.78
193	100.00	41.00	534.11	93	93.00	22.00	375.15
194	100.00	41.00	536.11	94	94.00	22.00	377.52
195	100.00	41.00	538.11	95	95.00	22.00	379.89
196	100.00	41.00	540.11	96	96.00	22.00	382.26
197	100.00	41.00	542.11	97	97.00	22.00	384.63
198	100.00	41.00	544.11	98	98.00	22.00	387.00
199	100.00	41.00	546.11	99	99.00	22.00	389.37
200	100.00	41.00	548.11	100	100.00	22.00	391.74

TOTAL: 1.00 1.50 63.23
 SUM OF R.C. 30.60 235.90 1.00 .25734647

TABLE 6-8 (Continued)

PEACE BOREHOLE U1-11					PEACE BOREHOLE U1-11				
J	DIGITIZED DEPTH (DIV)	DIMITIALIZED DEPTH (DIV)	COMPUTED DEPTH (FT)	COMPUTED DENSITY (G/CC)	J	DIGITIZED DEPTH (DIV)	DIMITIALIZED DEPTH (DIV)	COMPUTED DEPTH (FT)	COMPUTED DENSITY (G/CC)
101	53.00	53.00	370.55	2.111	1	1.00	20.50	180.53	1.907
102	53.00	57.00	372.13	2.092	2	2.00	41.50	181.52	2.150
103	53.00	59.00	373.31	2.111	3	2.20	40.60	182.11	2.136
104	53.00	50.50	374.40	2.103	4	3.00	41.10	185.26	2.144
105	54.00	50.00	375.20	2.063	5	7.40	27.20	203.47	1.926
106	54.00	44.70	376.06	2.044	6	8.70	40.50	207.71	1.978
107	54.00	46.30	376.03	2.064	7	9.50	44.70	210.86	1.887
108	55.00	36.10	380.34	2.266	8	10.40	30.40	213.61	1.974
109	55.00	47.70	381.97	2.083	9	10.60	30.40	215.19	1.976
110	56.00	50.00	383.34	2.096	10	11.00	32.30	216.76	2.006
111	56.00	53.90	384.72	2.063	11	11.90	30.20	220.31	1.973
112	56.00	47.90	385.91	2.094	12	12.30	34.30	221.88	2.030
113	57.00	40.00	387.40	2.096	13	14.00	35.60	223.85	2.058
114	57.00	43.30	388.66	2.053	14	13.40	34.10	224.22	2.034
115	58.00	33.20	391.42	2.020	15	14.00	37.00	228.56	2.080
116	58.00	35.00	393.78	1.955	16	15.00	37.00	232.47	2.080
117	59.00	39.80	396.54	2.121	17	15.60	34.00	234.80	2.033
118	60.00	30.70	398.11	2.107	18	16.50	36.20	236.91	2.061
119	60.00	37.00	399.69	2.080	19	17.50	34.00	242.36	2.033
120	60.00	33.00	401.65	2.044	20	17.00	41.70	243.54	1.997
121	61.00	36.00	404.00	2.054	21	19.00	37.60	248.27	2.009
122	62.00	37.20	405.98	2.081	22	20.20	40.20	253.00	2.130
123	62.00	36.50	407.17	2.072	23	20.00	34.00	255.75	2.111
124	63.00	32.00	409.52	2.082	24	21.60	34.00	258.41	2.033
125	63.00	32.80	411.50	2.006	25	22.50	37.40	262.04	2.084
126	64.00	33.20	413.86	2.054	26	23.80	47.20	267.17	1.926
127	64.00	36.80	415.94	2.077	27	24.60	33.20	270.32	2.020
128	64.00	35.00	417.81	2.049	28	25.00	31.00	271.90	1.986
129	65.00	46.60	419.37	2.074	29	25.50	48.00	275.87	2.017
130	65.00	43.20	420.55	2.052	30	26.00	47.50	275.84	1.774
131	66.00	36.60	422.91	2.074	31	26.80	41.80	278.94	1.842
132	66.00	36.40	424.04	2.071	32	27.50	34.20	281.74	2.036
133	66.00	33.30	424.94	2.053	33	28.30	29.00	284.90	1.955
					34	29.60	26.40	290.07	1.914
					35	30.00	49.00	291.59	1.935
					36	30.40	60.20	293.17	1.973
					37	31.20	27.80	296.32	1.936
					38	32.00	48.00	297.47	1.939
					39	32.10	51.80	299.86	1.998
					40	32.80	32.00	302.62	2.002
					41	33.00	34.30	303.91	2.038
					42	33.50	32.80	305.37	2.014
					43	33.90	33.20	306.95	2.020
					44	34.30	32.70	309.31	2.004
					45	35.00	35.00	311.89	2.049
					46	36.00	36.20	313.82	2.067
					47	36.50	35.40	317.19	2.055
					48	37.20	36.90	319.95	2.078
					49	37.90	35.80	322.77	2.061
					50	38.40	43.20	324.67	2.078
					51	39.00	48.20	328.22	2.082
					52	39.80	45.90	329.00	2.081
					53	40.10	43.80	331.37	2.030
					54	40.70	41.30	333.75	1.991
					55	40.90	43.00	334.52	1.986
					56	41.10	49.60	335.30	1.964
					57	41.80	40.00	338.04	1.970
					58	42.40	38.30	340.42	2.069
					59	42.20	49.00	347.51	1.955
					60	43.00	32.20	350.66	2.005
					61	43.60	31.60	353.05	1.995
					62	44.20	47.00	355.39	1.936
					63	44.70	49.00	357.36	1.955
					64	47.50	35.00	360.51	2.049
					65	48.00	36.00	362.88	2.064
					66	48.10	37.80	362.87	2.086
					67	49.10	47.00	366.41	2.080
					68	49.90	32.20	364.99	1.905
					69	50.50	33.00	371.74	2.017
					70	50.90	35.20	373.97	2.054
					71	51.10	35.20	374.64	2.054
					72	52.10	34.20	378.63	2.036
					73	52.50	35.60	380.27	2.058
					74	53.00	35.60	382.17	2.058
					75	53.10	35.10	382.56	2.050
					76	53.20	36.00	382.96	2.064
					77	54.00	36.00	384.11	2.064
					78	54.90	36.50	386.90	2.072
					79	54.90	32.90	388.87	2.016
					80	55.20	42.00	390.83	2.016
					81	55.30	31.70	392.02	1.997
					82	55.80	43.00	393.20	2.017
					83	56.10	34.30	394.38	2.038
					84	56.30	34.00	395.94	2.043
					85	57.00	42.00	397.32	2.038
					86	57.50	42.80	394.89	2.082
					87	58.00	45.70	401.44	1.983
					88	59.00	49.10	407.37	1.956
					89	60.00	45.30	409.74	1.900
					90	60.90	44.90	413.28	1.880
					91	61.50	41.20	415.67	1.989
					92	62.00	41.20	417.61	1.989
					93	63.10	29.70	421.94	1.966
					94	63.80	48.20	424.70	2.020
					95	64.10	41.70	425.88	1.997
					96	64.50	41.00	427.46	1.986
					97	65.00	41.00	429.85	1.986
					98	65.20	40.80	430.22	1.983
					99	65.80	43.80	432.58	2.022
					100	66.50	42.80	435.34	2.014

YOU G. S.: .04 1.50 63.47
 YOU G. R. C.: 30.04 280.00 1.00 .254

TABLE 6-8 (Continued)

PEACE BOREHOLE				OPZ-18					
J	DIGITIZED (CMM) (DIY)	DIGITIZED (CMM) (DIY)	COMPUTER (CMM) (DIY)	CUMULATIVE (CMM) (DIY)	J	DIGITIZED (CMM) (DIY)	DIGITIZED (CMM) (DIY)	COMPUTER (CMM) (DIY)	CUMULATIVE (CMM) (DIY)
1	46.00	9.00	387.79	1.900	101	104.00	17.50	610.56	2.110
2	47.00	9.00	393.83	1.900	102	102.00	16.00	611.94	2.109
3	47.00	7.10	395.00	1.954	103	102.10	16.00	611.70	2.110
4	47.00	7.10	397.37	1.954	104	102.60	16.20	616.64	2.102
5	48.00	6.10	399.34	1.959	105	100.00	16.00	618.94	2.104
6	48.00	6.10	401.51	1.962	106	100.00	15.00	621.37	2.151
7	49.00	6.60	402.00	1.915	107	105.10	17.00	622.57	2.116
8	49.00	6.20	405.24	1.940	108	105.00	15.50	625.74	2.086
9	50.00	6.50	406.82	1.965	109	104.70	16.00	626.87	2.094
10	51.00	9.30	409.50	1.989	110	107.00	16.00	630.05	2.126
11	51.00	9.30	411.55	1.989	111	111.00	16.20	630.04	2.129
12	52.00	13.30	413.51	4.052	112	104.00	23.30	635.99	2.209
13	53.30	15.70	418.63	4.082	113	108.70	24.70	636.74	2.231
14	53.00	15.90	419.01	2.071	114	109.00	15.30	637.92	2.204
15	55.10	15.70	425.72	2.000	115	109.60	16.00	640.29	2.189
16	55.00	16.70	426.51	2.105	116	110.10	19.30	642.25	2.194
17	55.00	15.00	428.47	2.079	117	111.00	17.00	645.00	2.110
18	56.00	12.00	429.74	2.031	118	111.00	17.00	647.37	2.124
19	56.30	11.70	430.44	2.027	119	111.00	17.00	649.10	2.110
20	56.00	13.00	432.41	2.047	120	114.20	17.70	655.40	2.121
21	56.00	12.30	437.14	2.195	121	114.60	16.20	657.97	2.129
22	59.00	17.60	441.07	2.157	122	115.00	16.50	661.55	2.102
23	59.20	17.60	441.06	2.119	123	115.00	16.20	663.91	2.097
24	59.50	17.90	443.67	2.124	124	115.00	15.20	665.09	2.082
25	60.00	13.50	446.14	2.052	125	117.10	15.60	668.81	2.086
26	61.50	17.20	450.92	4.113	126	116.20	16.10	671.14	2.154
27	62.00	16.00	452.00	2.157	127	117.30	15.90	674.07	2.094
28	62.00	18.00	456.07	2.134	128	118.00	16.30	680.84	2.064
29	62.70	18.00	459.77	2.147	129	120.00	16.00	681.25	2.064
30	63.90	11.60	460.34	2.025	130	121.10	16.70	685.56	2.074
31	64.30	11.30	461.94	2.027	131	121.10	19.20	686.74	2.180
32	64.50	13.20	462.73	4.050	132	124.10	16.00	689.50	2.124
33	65.20	13.20	465.00	2.050	133	123.10	16.30	693.04	2.209
34	65.00	15.00	466.27	2.074	134	123.60	23.30	693.00	2.223
35	65.00	18.00	468.70	2.047	135	124.70	19.20	698.16	2.194
36	66.00	12.60	471.78	2.041	136	124.70	19.30	698.95	2.140
37	67.10	13.00	472.96	2.050	137	125.00	16.90	701.67	2.140
38	67.50	17.00	474.54	2.114	138	125.70	20.00	705.64	2.171
39	68.00	20.00	476.51	2.157	139	126.20	19.50	707.61	2.169
40	68.60	23.00	478.07	2.234	140	126.70	19.50	709.58	2.109
41	68.70	22.90	479.34	2.203	141	127.20	19.30	712.33	2.107
42	69.50	22.70	481.62	2.200	142	127.20	16.00	716.64	2.112
43	70.00	17.20	484.38	2.113	143	127.40	17.00	719.05	2.157
44	70.00	17.00	485.96	2.116	144	129.60	16.00	720.94	2.145
45	70.00	19.40	487.92	2.160	145	130.10	19.20	722.94	2.151
46	71.00	18.90	489.10	2.103	146	131.20	18.70	725.35	2.058
47	71.50	19.70	490.29	1.153	147	131.00	14.70	728.47	2.058
48	72.60	18.20	490.68	2.129	148	132.00	16.10	732.02	2.127
49	72.10	17.90	492.65	2.174	149	132.00	15.00	733.20	2.091
50	72.20	13.90	495.04	4.061	150	133.20	15.00	735.99	2.087
51	72.50	14.20	495.43	2.066	151	135.10	16.20	736.74	2.087
52	73.00	14.00	496.14	2.083	152	136.10	16.20	739.04	2.157
53	73.20	14.00	496.94	4.069	153	136.10	16.00	741.07	2.183
54	73.60	14.20	499.55	2.066	154	136.20	16.70	745.03	2.109
55	74.00	10.00	501.31	4.000	155	136.60	17.00	746.59	2.123
56	75.00	15.50	504.07	4.084	156	136.00	16.70	747.77	2.105
57	75.50	16.50	506.05	2.166	157	136.60	17.00	750.52	2.181
58	76.00	20.70	508.74	2.166	158	137.00	16.00	752.10	2.079
59	76.70	16.40	510.74	2.135	159	137.00	16.70	754.07	2.105
60	77.10	16.40	512.33	2.133	160	139.00	16.00	756.05	2.190
61	77.60	17.00	514.30	2.110	161	139.00	16.90	757.63	2.190
62	78.20	18.90	516.64	2.180	162	139.00	17.30	758.79	2.118
63	79.50	16.30	521.76	2.079	163	140.00	17.50	759.97	2.118
64	80.10	19.00	524.14	2.154	164	140.00	16.10	762.33	2.064
65	82.10	19.00	528.08	2.154	165	140.00	16.10	765.09	2.064
66	81.50	18.00	529.07	2.132	166	141.30	16.00	765.06	2.055
67	82.20	19.60	532.02	2.151	167	141.30	15.20	767.05	2.082
68	84.00	18.00	535.36	2.126	168	141.60	14.00	767.04	2.072
69	85.30	15.70	541.47	2.050	169	141.90	15.20	770.60	2.064
70	86.00	19.00	543.04	2.095	170	142.00	14.60	770.60	2.064
71	86.00	18.10	545.81	2.053	171	142.70	15.50	771.76	2.086
72	86.00	18.00	546.59	2.030	172	143.00	15.70	773.34	2.090
73	86.30	11.00	548.55	2.030	173	143.50	16.60	775.75	2.104
74	87.00	16.60	551.31	2.109	174	144.00	12.30	775.72	2.034
75	87.90	16.70	553.67	2.138	175	144.00	9.20	776.87	2.087
76	87.60	18.00	556.05	2.121	176	145.10	11.20	780.05	2.019
77	88.20	17.70	556.05	2.079	177	145.70	9.90	782.41	2.098
78	88.40	13.00	559.79	2.060	178	146.20	10.90	784.30	2.014
79	89.10	15.00	559.50	2.079	179	146.40	10.80	785.17	2.013
80	89.00	14.00	560.70	2.083	180	146.90	15.00	787.14	2.097
81	89.00	14.00	563.91	2.075	181	147.10	12.20	787.92	2.035
82	90.50	13.50	565.99	4.082	182	147.70	11.90	790.24	2.030
83	92.00	19.70	567.06	2.153	183	147.70	11.90	791.84	2.063
84	92.00	16.00	570.99	2.058	184	148.10	16.00	791.19	2.124
85	92.60	28.00	573.36	2.189	185	148.20	17.50	794.34	2.118
86	92.90	22.00	574.34	2.189	186	150.00	17.50	802.48	2.074
87	93.50	13.00	576.90	2.047	187	150.00	14.70	804.07	2.074
88	94.10	16.10	579.36	2.099	188	151.20	14.70	804.85	2.055
89	94.10	16.20	580.05	2.097	189	151.40	16.20	807.21	2.097
90	95.90	43.50	582.41	2.212	190	151.40	15.50	808.70	2.064
91	95.20	19.00	583.59	2.142	191	152.00	19.50	811.15	2.124
92	96.70	14.90	587.53	2.077	192	152.00	18.00	813.12	2.082
93	96.00	18.90	589.09	2.140	193	153.50	15.20	815.40	2.094
94	96.00	3.10	592.03	1.002	194	154.00	15.50	816.24	2.086
95	97.20	24.00	595.34	3.010	195	154.00	16.00	819.01	2.108
96	97.90	9.50	598.10	1.994	196	154.00	12.00	822.06	2.085
97	99.20	11.70	603.00	2.027	197	154.00	12.00	823.75	2.085
98	100.00	11.00	606.93	2.020	198	154.90	10.00	826.51	2.000
99	100.00	11.00	607.21	2.020	199	157.50	20.00	828.06	2.080

TABLE 6-8 (Continued)

J	PEACE BOREHOLE OPZ-1A				I	WAR-01			
	DIGITIZED DEPTH (DIV)	DENSITY (G/CC)	COMPUTED DEPTH (FF)	COMPUTED DENSITY (G/ACC)		DIGITIZED DEPTH (DIV)	DENSITY (G/CC)	COMPUTED DEPTH (FF)	COMPUTED DENSITY (G/ACC)
001	157.00	8.96	838.44	1.983	1	20.00	46.00	189.94	1.921
002	158.00	10.00	832.41	1.988	2	20.70	46.30	192.74	1.960
003	159.00	9.10	831.70	1.986	3	21.20	46.00	194.75	1.955
004	159.20	14.30	835.54	2.000	4	21.40	48.00	195.95	1.978
005	159.60	10.70	837.14	2.074	5	21.80	27.00	197.14	1.931
006	160.00	16.30	838.71	2.099	6	22.20	10.00	198.74	1.659
007	161.00	14.60	842.65	2.072	7	22.40	1.00	199.57	1.514
008	162.00	19.20	846.30	2.066	8	23.40	7.00	201.90	1.612
009	162.60	18.00	848.95	2.047	9	23.30	4.10	203.10	1.644
010	163.30	18.00	852.49	2.064	10	23.70	7.70	204.79	1.623
011	164.00	16.00	854.46	2.094	11	24.10	10.00	206.40	1.639
012	164.30	17.00	855.64	2.119	12	24.30	17.00	208.00	1.704
013	165.00	6.30	861.95	1.942	13	24.80	14.00	209.21	1.755
014	166.00	10.00	863.91	2.000	14	24.90	3.00	209.61	1.742
015	166.80	11.00	865.48	2.016	15	25.10	15.10	210.41	1.761
016	167.20	10.00	867.04	2.000	16	25.20	14.00	210.82	1.723
017	168.00	13.20	870.21	2.050	17	25.40	16.00	211.62	1.760
018	168.20	13.20	870.99	2.050	18	26.00	10.00	214.03	1.659
019	169.00	13.00	871.78	2.091	19	26.40	2.30	215.64	1.532
020	169.30	15.70	874.94	2.090	20	26.80	3.00	217.65	1.568
021	169.60	15.00	876.51	2.074	21	27.20	13.00	218.85	1.707
022	169.80	15.10	877.29	2.083	22	27.50	45.60	220.04	1.900
023	170.20	17.20	878.87	2.113	23	28.00	4.30	225.28	1.569
024	170.60	16.91	880.44	2.100	24	29.30	10.40	227.24	1.666
025	171.00	18.50	882.02	2.154	25	29.80	10.60	229.30	1.669
					26	30.10	17.70	230.50	1.782
					27	31.00	1.20	234.10	1.519
					28	31.50	4.00	236.11	1.564
					29	31.60	5.90	236.53	1.561
					30	31.90	5.10	237.73	1.581
					31	32.40	3.00	239.74	1.548
					32	32.50	4.70	240.10	1.511
					33	33.20	12.70	242.94	1.703
					34	33.40	13.20	243.74	1.711
					35	33.70	16.80	244.94	1.800
					36	34.20	11.90	246.97	1.690
					37	34.60	11.00	248.58	1.675
					38	34.90	8.90	249.74	1.628
					39	35.60	16.00	252.60	1.755
					40	36.00	18.00	254.26	1.730
					41	36.80	16.70	256.62	1.764
					42	37.00	17.00	258.22	1.771
					43	37.30	40.50	259.43	1.827
					44	37.70	41.30	261.03	1.840
					45	37.90	20.00	261.84	1.819
					46	38.20	19.00	263.04	1.803
					47	38.30	18.80	263.44	1.787
					48	38.70	17.90	265.05	1.785
					49	39.40	13.20	267.86	1.711
					50	39.70	13.00	269.20	1.739
					51	40.10	45.20	270.68	1.902
					52	40.60	42.60	272.64	1.860
					53	41.00	42.50	274.24	1.859
					54	41.20	42.00	275.10	1.851
					55	41.60	43.20	276.70	1.870
					56	42.10	43.20	278.73	1.870
					57	42.50	44.00	279.51	1.883
					58	42.70	46.20	281.12	1.910
					59	43.50	43.20	284.34	1.870
					60	43.80	25.00	285.54	1.899
					61	44.30	43.80	287.55	1.880
					62	44.70	44.70	289.14	1.894
					63	44.90	43.60	289.94	1.874
					64	45.40	17.40	291.17	1.778
					65	45.80	24.20	293.58	1.886
					66	46.70	10.00	297.19	1.659
					67	47.30	43.70	299.60	1.910
					68	47.50	42.90	300.41	1.867
					69	47.60	42.90	300.91	1.885
					70	47.70	41.20	301.21	1.837
					71	48.20	30.80	303.22	1.931
					72	48.30	48.20	303.62	1.930
					73	48.80	30.80	304.02	1.931
					74	48.80	40.00	305.43	1.819
					75	49.20	45.40	307.23	1.915
					76	49.80	42.10	309.65	1.852
					77	50.10	44.10	310.85	1.884
					78	50.50	40.30	312.46	1.824
					79	51.10	49.60	314.87	1.972
					80	51.50	29.70	316.48	1.974
					81	52.00	48.00	318.48	1.910
					82	52.20	31.00	319.29	1.894
					83	52.80	21.90	321.70	1.849
					84	53.60	40.80	324.91	2.151
					85	54.10	40.00	326.92	1.978
					86	54.30	44.80	328.33	1.919
					87	54.90	29.40	330.13	1.877
					88	55.30	15.00	332.54	1.734
					89	55.80	12.90	333.75	1.704
					90	56.40	18.00	336.16	1.787
					91	56.70	19.50	337.87	1.811
					92	57.00	18.20	338.97	1.771
					93	57.80	19.90	341.79	1.817
					94	58.80	20.60	345.80	1.829
					95	49.00	42.80	346.61	1.864
					96	59.00	43.60	348.21	1.876
					97	59.80	40.30	349.82	1.983
					98	60.50	16.40	352.63	1.762
					99	61.00	25.00	355.44	1.899
					100	61.60	26.60	357.25	1.924

YU = S: 10.00 2.00 63.40
 XJ = B, C: 30.00 32.90 1.00 .254

TABLE 6-8 (Continued)

PEICE BOREHOLE #44-01				PEICE BOREHOLE #44-01			
DEPT. (FT)	DENSITY (DIV)	DEPTH (FT)	COMPUTED DENSITY (GM/CC)	DEPT. (FT)	DENSITY (DIV)	DEPTH (FT)	COMPUTED DENSITY (GM/CC)
201	175.30	39.00	2.122	401	230.00	38.00	2.077
202	175.27	40.00	2.106	402	231.00	38.50	2.077
203	176.10	39.00	2.099	403	231.00	39.50	2.074
204	176.70	38.00	2.087	404	232.50	40.00	2.074
205	175.40	38.00	2.078	405	233.00	40.00	2.074
206	176.00	39.20	2.085	406	233.20	40.50	2.074
207	176.20	42.20	2.094	407	233.50	41.00	2.074
208	176.50	42.00	2.094	408	234.50	41.00	2.074
209	176.90	40.00	2.093	409	234.70	42.50	2.074
210	177.00	38.10	2.090	410	235.00	43.00	2.074
211	176.00	38.10	2.088	411	236.00	42.00	2.074
212	176.70	40.00	2.082	412	236.00	42.00	2.074
213	179.20	40.30	2.103	413	237.00	42.00	2.074
214	180.10	41.30	2.109	414	238.20	41.00	2.074
215	180.00	37.00	2.090	415	238.00	42.50	2.074
216	181.00	37.00	2.095	416	239.20	42.00	2.074
217	181.10	36.00	2.074	417	240.00	40.00	2.074
218	181.00	31.00	2.077	418	240.20	43.50	2.074
219	184.30	36.50	2.082	419	241.00	44.00	2.074
220	184.90	36.70	2.117	420	241.00	44.00	2.074
221	184.70	31.30	2.099	421	241.00	44.00	2.074
222	185.30	35.00	2.095	422	241.00	44.00	2.074
223	185.30	36.00	2.074	423	242.20	44.00	2.074
224	185.70	36.00	2.074	424	242.20	44.00	2.074
225	186.00	36.20	2.085	425	242.20	44.00	2.074
226	186.40	42.00	2.022	426	242.20	44.00	2.074
227	187.30	39.00	2.128	427	242.20	44.00	2.074
228	187.00	37.70	2.101	428	242.20	44.00	2.074
229	188.20	40.00	2.112	429	242.20	44.00	2.074
230	188.30	47.60	2.100	430	242.20	44.00	2.074
231	188.90	39.20	2.085	431	242.20	44.00	2.074
232	189.50	35.50	2.066	432	242.20	44.00	2.074
233	190.00	42.30	2.015	433	242.20	44.00	2.074
234	190.30	42.30	2.015	434	242.20	44.00	2.074
235	190.60	41.20	2.098	435	242.20	44.00	2.074
236	191.20	30.00	2.105	436	242.20	44.00	2.074
237	192.00	36.00	2.106	437	242.20	44.00	2.074
238	192.60	35.40	2.065	438	242.20	44.00	2.074
239	193.20	33.70	2.037	439	242.20	44.00	2.074
240	193.80	30.30	2.089	440	242.20	44.00	2.074
241	194.50	47.50	2.090	441	242.20	44.00	2.074
242	195.10	36.00	2.082	442	242.20	44.00	2.074
243	195.70	38.10	2.100	443	242.20	44.00	2.074
244	196.10	38.00	2.106	444	242.20	44.00	2.074
245	197.00	40.00	2.102	445	242.20	44.00	2.074
246	197.30	41.30	2.151	446	242.20	44.00	2.074
247	197.00	40.80	2.151	447	242.20	44.00	2.074
248	198.00	39.30	2.127	448	242.20	44.00	2.074
249	198.60	40.50	2.130	449	242.20	44.00	2.074
250	199.20	40.00	2.109	450	242.20	44.00	2.074
251	199.50	40.50	2.086	451	242.20	44.00	2.074
252	199.90	40.50	2.083	452	242.20	44.00	2.074
253	200.40	40.00	2.104	453	242.20	44.00	2.074
254	200.60	42.00	2.170	454	242.20	44.00	2.074
255	201.00	48.00	2.174	455	242.20	44.00	2.074
256	201.30	41.00	2.154	456	242.20	44.00	2.074
257	201.00	38.00	2.089	457	242.20	44.00	2.074
258	202.40	38.00	2.120	458	242.20	44.00	2.074
259	202.90	49.10	2.124	459	242.20	44.00	2.074
260	203.00	43.10	2.107	460	242.20	44.00	2.074
261	203.00	41.00	2.194	461	242.20	44.00	2.074
262	204.00	47.00	2.090	462	242.20	44.00	2.074
263	204.60	40.70	2.109	463	242.20	44.00	2.074
264	205.70	47.70	2.101	464	242.20	44.00	2.074
265	206.10	40.50	2.146	465	242.20	44.00	2.074
266	206.60	39.00	2.127	466	242.20	44.00	2.074
267	207.00	40.90	2.152	467	242.20	44.00	2.074
268	207.50	41.20	2.157	468	242.20	44.00	2.074
269	208.10	40.60	2.211	469	242.20	44.00	2.074
270	208.80	40.50	2.182	470	242.20	44.00	2.074
271	209.00	36.50	2.092	471	242.20	44.00	2.074
272	209.50	38.10	2.094	472	242.20	44.00	2.074
273	210.00	40.00	2.151	473	242.20	44.00	2.074
274	211.00	40.00	2.086	474	242.20	44.00	2.074
275	212.20	36.00	2.089	475	242.20	44.00	2.074
276	213.50	36.40	2.081	476	242.20	44.00	2.074
277	214.00	37.30	2.095	477	242.20	44.00	2.074
278	214.70	39.30	2.072	478	242.20	44.00	2.074
279	215.50	36.00	2.074				
280	216.00	39.50	2.117				
281	216.50	38.70	2.090				
282	218.20	47.50	2.090				
283	219.00	39.30	2.127				
284	219.50	40.00	2.130				
285	220.00	40.00	2.106				
286	220.50	38.00	2.084				
287	224.10	46.60	2.097				
288	224.70	43.00	2.024				
289	224.90	42.50	2.018				
290	224.50	40.00	2.130				
291	228.00	40.00	2.100				
292	225.40	40.50	2.100				
293	226.00	40.70	2.111				
294	226.70	35.50	2.034				
295	227.10	37.90	2.074				
296	228.00	36.10	2.055				
297	228.70	37.00	2.090				
298	229.20	40.50	2.105				
299	231.00	52.40	2.018				
300	231.50	52.40	2.017				
				YU M S:	.00	1.50	62.90
				RU A B C:	30.00	250.10	875.00 217.80

APPENDIX 6-2

DENSITIES OF "CORAL" AND ITS SOLID COMPONENT
AS CONTINUOUS FUNCTIONS OF DEPTH

Data on the composition of coral solids¹ place its density ρ_S in a narrow range of values (2.71 to 2.93 g/cc; see Tremba and Ristvet, 1986). Within that range, however, ρ_S varies erratically over the discrete set of borehole depths for which solid composition has been measured. Hence, in a given borehole, straight-line connections between measured (ρ_S, z) -points embody virtually all the extant information on the continuous change of ρ_S with depth (or altitude) z . At that level of description, we have:

$$\rho_S = [(z-z_m)\rho_S^{m+1} + (z_{m+1}-z)\rho_S^m]/(z_{m+1}-z_m) \quad ; m=1,2,\dots,M \quad \text{Eq. (13)}$$

with (ρ_S^m, z_m) denoting point m of the set measured for a given borehole, and with the points so ordered that depth decreases as m increases.

For the same borehole, let the z_j -points of Eq. (11) also be ordered so that depth decreases as j increases. Now, merge the two sets of z -values, and number different z 's of the combined set in the order of decreasing depth (again), obtaining thereby the values z_k ($k=1,2,\dots,K+1$). The z -interval between z_k and z_{k+1} ($k=1,2,\dots,K$) must then lie entirely within one of the z -intervals on which ρ (the density of coral) has the linear depth-dependence specified by Eq. (11); it must also lie entirely within one of the z -intervals of linear variation of ρ_S (the density of the coral solid) specified by Eq. (13). However, a given z_k -value need not appear among the z_j 's of Eq. (11); if not, then, at $z=z_k$, the value of ρ ($=\rho_k$) is obtained from Eq. (11) for the z_j -interval in which $z=z_k$ falls. Likewise, for a z_k -value not among the z_m 's of Eq. (13), we find the z_m -interval in which z_k falls, and use Eq. (13) to compute ρ_S at z_k ($\rho_S=\rho_S^k$). Eqs. (11) and (13) can then be replaced by the following equivalent relations:

$$\begin{aligned} \rho &= [(z-z_k)\rho_{k+1}^- + (z_{k+1}-z)\rho_k^+]/(z_{k+1}-z_k) \\ \rho_S &= [(z-z_k)\rho_S^{k+1} + (z_{k+1}-z)\rho_S^k]/(z_{k+1}-z_k) \end{aligned} \quad ; k=1,2,\dots,K \quad \text{Eq. (14)}$$

In accord with Appendix 6-1, $\rho_k^- = \rho_k^+ = \rho_k$ for the γ - γ profiles; for the BHG profiles, $\rho_k^+ = \rho_{k+1}^- = \rho_{k+1/2}$ where $\rho_{k+1/2} = \rho_{j+1/2}$ -- the value of j being set by the requirement that the interval from z_k to z_{k+1} lie on the interval of Table 6-7 from z_j to z_{j+1} .

For each borehole included in the BHG survey, Table 6-9 (located in this Appendix) presents the depths z_k ($k=1,2,\dots,K+1$) that mark the endpoints of

¹ See footnote 3 on page 6-1 for explanation of use of "coral" in this text.

the depth-intervals on which both ρ and ρ_S are simple linear functions of z [Eq. (14)]. For each depth z_k , the density of either coral or its solid component is also shown (third and fourth columns of table). Where blank spaces appear between two listed values of coral density ρ (called "BHG DENSITY" in tbl. 6-9), those two ρ 's are identical; that same value applies everywhere between them. Also, where values of ρ appear, the density ρ_S of coral's solid component does not; the value of ρ_S at that blank spot is given by Eq. (13) with z equal to the depth listed (or to its negative, if z denotes height).

MASS OF SOLID AS A CONTINUOUS FUNCTION
OF DEPTH IN A BOREHOLE

Table 6-9 (in this Appendix 6-2) and Eqs. (13) allow ρ and ρ_S to be computed for any depth and borehole covered by the BHG survey. Hence, the mass m_S of coral solid can also be computed from Eq. (5). In fact, given piecewise linear dependence of ρ and ρ_S on z [Eq. (14)], m_S can be expressed in terms of z using only elementary functions. In particular, if z lies between z_k and z_{k+1} , then:

$$m_S^k = m_S^k + \int_{z_k}^z \rho_S \left(\frac{\rho - \rho_L}{\rho_S - \rho_L} \right) dh \quad ; \quad k = 1, 2, \dots, K \quad \text{Eq. (15)}$$

where $m_S^1 = 0$ and

$$m_S^k = m_S^{k-1} + \int_{z_{k-1}}^{z_k} \rho_S \left(\frac{\rho - \rho_L}{\rho_S - \rho_L} \right) dh \quad ; \quad k = 2, 3, \dots, K+1 \quad \text{Eq. (16)}$$

Next, observing that $\rho_S / (\rho_S - \rho_L) = (\rho_S - \rho_L + \rho_L) / (\rho_S - \rho_L)$, we can write Eq. (15) as follows:

$$m_S = m_S^k + \int_{z_k}^z [(\rho - \rho_L) + \rho_L \left(\frac{\rho - \rho_L}{\rho_S - \rho_L} \right)] dh \quad \text{Eq. (17)}$$

Replacing ρ and ρ_S in Eq. (17) by their linear equivalents in terms of z [Eq. (14)], we obtain

$$m_S = m_S^k + \int_{z_k}^z \left\{ a_k + b_k(h - z_k) + \rho_L \left[\frac{a_k + b_k(h - z_k)}{a_k' + b_k'(h - z_k)} \right] \right\} dh \quad \text{Eq. (18)}$$

where

$$a_k = \rho_k - \rho_L, \quad b_k = (\rho_{k+1} - \rho_k) / (z_{k+1} - z_k); \quad a_k' = \rho_S - \rho_L, \quad b_k' = (\rho_S^{k+1} - \rho_S^k) / (z_{k+1} - z_k) \quad \text{Eq. (19)}$$

The integral of Eq. (17) is readily found as an explicit function of z (Pierce, 1929)

$$m_S = m_S^k + a_k x + b_k x^2 + \rho_L \left[\frac{b_k x}{b_k'} + \frac{(a_k b_k' - a_k' b_k)}{(b_k')^2} \cdot \ln \left(\frac{a_k' + b_k' x}{a_k'} \right) \right] \quad \text{Eq. (20)}$$

where $x = z - z_k$.

From Eq. (16), it follows that $m_S = m_S^{k+1}$, when z is set equal to z_{k+1} in Eq. (20); with m_S^{k+1} known, a similar computation then gives m_S^{k+2} , etc. Thus, using the depths and densities of Table 6-9, the m_S^k -values ($k=2, \dots, K+1$) can be computed in sequence from Eq. (20). For each borehole of the BHG survey, the resulting values of m_S^2, m_S^3, m_S^{K+1} appear in the seventh column of Table 6-9, starting at the greatest depth logged in that hole. Listed in the sixth column is an approximation to m^k -- \underline{m}_S , say -- obtained by setting ρ_S equal to its mid-value $\underline{\rho}_S^k \equiv 1/2(\rho_S^{k+1} + \rho_S^k)$, the mean of ρ_S on the z -interval from z_k to z_{k+1} . Using that value for ρ_S in the integral of Eq. (15), but with ρ still related to z by Eq. (14), we can write

$$m_S \approx \underline{m}_S = \underline{m}_S^k + \frac{\rho_S^k}{\rho_S^k - \rho_L} \int_{z_k}^z (\rho - \rho_L) dh = \underline{m}_S^k + (a_k x + b_k x^2) \rho_S^k / (\rho_S^k - \rho_L) \quad \text{Eq. (21)}$$

where $\underline{m}_S^1 = 0$, and \underline{m}_S^{k+1} is the value obtained for \underline{m}_S by setting z equal to z_{k+1} in Eq. (21) (or $x = z_{k+1} - z_k$). Replacing the ρ_S^k ($k=1, 2, \dots, K$) of Eq. (21), for all k , by the single value 2.821 g/cc (half the sum of aragonite and calcite densities) yields yet a coarser estimate of m_S , and the approximate values of m_S^k listed in the fifth column of Table 6-9.

Table 6-10 (also located in Appendix 6-2), identical in format and derivation to Table 6-9, differs from Table 6-9 only in that the density profiles on which it rests came from γ - γ logging (not from BHG surveys).

DENSIFICATION: THICKNESS CHANGES AS CONTINUOUS FUNCTIONS OF DEPTH IN CRATER HOLES

Eq. (20) allows us to compute the solid mass per unit cross-section, m_S^a , from the greatest depth logged to the depth at $z = z_a$ in a given borehole. The horizon at z_a in the given borehole -- horizon "a" -- will generally have somewhat different depth in a second borehole¹. Let $z = z_a^*$ at that horizon in the latter hole, with m_S^{a*} denoting solid mass (per unit cross-section) in the second hole, from the greatest depth logged therein to horizon "a". For any

¹ As needed, the depths to a given horizon in different boreholes have been found herein by linear interpolation among the horizon-depths fixed by PEACE Program geologists (see Chapter 7 of the current Report, particularly tbls. 7-2 and 7-4).

depth above "a" in the first borehole, the solid mass between "a" and that depth is equal to $m_S - m_S^a$ ($\equiv \Delta m_S$), where m_S is computed to the depth in question from Eq. (20), using the a_k - and b_k -values for that first borehole. Likewise, in the second borehole, the solid mass from "a" to a given depth above "a" is equal to $m_S - m_S^{a^*}$ ($\equiv \Delta m_S^*$), with m_S computed from Eq. (20) using a_k - and b_k -values appropriate to that borehole. For each choice of z in the second hole -- $z=z^*$, say -- Δm_S^* can be computed simply by evaluating the right-hand member of Eq. (20) and subtracting $m_S^{a^*}$ from the result. However, in the first hole, finding the value of z at which the solid mass Δm_S above "a" is equal to Δm_S^* , plainly requires equating Δm_S to Δm_S^* . The relation determining z is therefore the following:

$$\Delta m_S^* + m_S^a = m_S^k + a_k x + b_k x^2 + \rho_L \left[\frac{b_k x}{b_k'} + \frac{(a_k b_k' - a_k' b_k)}{(b_k')^2} \ln \left(\frac{a_k' + b_k' x}{a_k'} \right) \right] \quad \text{Eq. (22)}$$

where $x = z - z_k$.

Eq. (22), which is transcendental, can be solved for x (hence z) by numerical means. Exactly one value of x satisfies it because m_S [Eq. (20)] increases monotonically as depth decreases, and the mass Δm_S^* above horizon "a" in the second borehole is ≥ 0 . Solution of Eq. (22) for x is greatly expedited by foreknowledge of m_k ($k=1,2,\dots,K$): As k is increased from $k=1$, it reaches a level at which positive values of $\Delta m_S^* + m_S^a - m_S^k$ turn negative; the root of Eq. (21) must lie on the z_k -interval over which that change of sign occurs. With the root of Eq. (22) so bounded, it can be found easily by search or iteration. Repeating the process for a series of ever-shallower z 's gives a set of (z^*, z) pairs for which the solid mass between horizon "a" ($z=z_a^*$) and level z^* in the second hole is equal to that between "a" ($z=z_a$) and level z in the first. The height of the column between z_a and z is $z - z_a$ (or its negative if z denotes depth); $z^* - z_a^*$ gives the corresponding height in the second hole (for equal mass above "a"). If the two holes are actually the same, but with pre- and post-shot density profiles representing the "second" and "first" holes, respectively, then $z - z_a$ and $z^* - z_a^*$ (or their negatives) give the post- and pre-shot thicknesses of a column above "a" that contains the same mass of solid at both times. The change in that column's thickness due to shot-induced changes in density is just $(z^* - z_a^*) - (z - z_a)$ (or its negative).

Under the key assumption given previously on pages 6-7 and 6-8, the pre-shot profiles are found today in control holes -- whence, we do in fact compute (z^*, z) pairs from profiles in different holes. A detail of the calculation (noted previously on pages 6-8 through 6-10) lies in redefining horizon "a" at each successive geologic horizon met along the stepwise march in z^* (from depth toward the sea floor). With z^* referring to the control hole, z is then allowed to shift suddenly to its value, in the crater hole, at a newly encountered geologic horizon. Geologic horizons are thereby strictly retained as Lagrangian surfaces, regardless of departures from the ideal of simple subsidence, or of actual differences between pre-shot density profiles

and control-hole profiles. In addition (see p.6-8 through 6-10), differences in column height are thereby computed from densities in materials that are (as nearly as possible) the same.¹

Curves of thickness-change vs. depth are plotted as a series of dots when z^* refers to a control hole (jumps in z can then occur, marking shifts to geologic crater-hole horizons). When z^* refers to a crater hole, curves of thickness-change vs. depth are drawn with dashes (jumps in z then mark shifts to geologic horizons in control holes). The mean of a dotted and dashed curve is also drawn, as a continuous line.

As functions of present crater-hole depth, the thickness changes computed from profiles of the BHG survey were presented in preceding sections (p. 6-7 and 6-8 and 6-8 through 6-10) (see figs. 6-4 through 6-9). Corresponding curves, deduced from γ - γ density profiles, appear on succeeding pages as Figures 6-27 through 6-53.

REFERENCES CITED

See pages 6-35 and 6-36 for references cited in this Appendix.

¹ Thickness-change curves were first computed with horizon "a" fixed near Contour D. Except for larger gaps between end-of-data and the sea floor, there are no appreciable differences between those curves and the ones presented in this report -- and no change at all in conclusions drawn from them (conclusions first reached, in fact, with horizon "a" fixed).

PEACE (LEFT) DEPTH	BHG DENSITY (%W/C)	BOREHOLE DGR-17		PEACE DEPTH DIFF	BHG DENSITY (%W/C)	BOREHOLE DGR-17		PEACE DEPTH DIFF	BHG DENSITY (%W/C)	BOREHOLE DGR-17		PEACE DEPTH DIFF	BHG DENSITY (%W/C)	BOREHOLE DGR-17	
		DENSITY OF SOLID CORRECTED (%W/C)	CUMULATIVE AMOUNT			NO. TO CORRECT	DENSITY OF SOLID CORRECTED (%W/C)			CUMULATIVE AMOUNT	NO. TO CORRECT			DENSITY OF SOLID CORRECTED (%W/C)	CUMULATIVE AMOUNT
1	1190.00	2.8210	0.	101	209.00	2.036	0.	101	209.00	2.036	27813.	27734.	27734.		
2	1190.00	2.8210	0.	102	209.00	1.992	0.	102	209.00	1.992	27813.	27734.	27734.		
3	1190.00	2.7262	0.	103	209.00	2.746	0.	103	209.00	2.746	27813.	27734.	27734.		
4	1190.00	2.7149	0.	104	209.00	2.8361	0.	104	209.00	2.8361	27813.	27734.	27734.		
5	1190.00	2.7366	0.	105	209.00	1.982	0.	105	209.00	1.982	27813.	27734.	27734.		
6	1190.00	2.7303	0.	106	209.00	1.993	0.	106	209.00	1.993	27813.	27734.	27734.		
7	1190.00	2.7394	0.	107	209.00	2.8361	0.	107	209.00	2.8361	27813.	27734.	27734.		
8	1190.00	2.7291	0.	108	209.00	2.8454	0.	108	209.00	2.8454	27813.	27734.	27734.		
9	1190.00	2.7242	0.	109	209.00	1.993	0.	109	209.00	1.993	27813.	27734.	27734.		
10	1190.00	2.7242	0.	110	209.00	1.997	0.	110	209.00	1.997	27813.	27734.	27734.		
11	1190.00	2.7242	0.	111	209.00	2.8655	0.	111	209.00	2.8655	27813.	27734.	27734.		
12	1190.00	2.7242	0.	112	209.00	2.8452	0.	112	209.00	2.8452	27813.	27734.	27734.		
13	1190.00	2.7242	0.	113	209.00	1.997	0.	113	209.00	1.997	27813.	27734.	27734.		
14	1190.00	2.7242	0.	114	209.00	2.8655	0.	114	209.00	2.8655	27813.	27734.	27734.		
15	1190.00	2.7242	0.	115	209.00	2.8452	0.	115	209.00	2.8452	27813.	27734.	27734.		
16	1190.00	2.7242	0.	116	209.00	1.997	0.	116	209.00	1.997	27813.	27734.	27734.		
17	1190.00	2.7242	0.	117	209.00	2.8655	0.	117	209.00	2.8655	27813.	27734.	27734.		
18	1190.00	2.7242	0.	118	209.00	2.8452	0.	118	209.00	2.8452	27813.	27734.	27734.		
19	1190.00	2.7242	0.	119	209.00	1.997	0.	119	209.00	1.997	27813.	27734.	27734.		
20	1190.00	2.7242	0.	120	209.00	2.8655	0.	120	209.00	2.8655	27813.	27734.	27734.		
21	1190.00	2.7242	0.	121	209.00	2.8452	0.	121	209.00	2.8452	27813.	27734.	27734.		
22	1190.00	2.7242	0.	122	209.00	1.997	0.	122	209.00	1.997	27813.	27734.	27734.		
23	1190.00	2.7242	0.	123	209.00	2.8655	0.	123	209.00	2.8655	27813.	27734.	27734.		
24	1190.00	2.7242	0.	124	209.00	2.8452	0.	124	209.00	2.8452	27813.	27734.	27734.		
25	1190.00	2.7242	0.	125	209.00	1.997	0.	125	209.00	1.997	27813.	27734.	27734.		
26	1190.00	2.7242	0.	126	209.00	2.8655	0.	126	209.00	2.8655	27813.	27734.	27734.		
27	1190.00	2.7242	0.	127	209.00	2.8452	0.	127	209.00	2.8452	27813.	27734.	27734.		
28	1190.00	2.7242	0.	128	209.00	1.997	0.	128	209.00	1.997	27813.	27734.	27734.		
29	1190.00	2.7242	0.	129	209.00	2.8655	0.	129	209.00	2.8655	27813.	27734.	27734.		
30	1190.00	2.7242	0.	130	209.00	2.8452	0.	130	209.00	2.8452	27813.	27734.	27734.		
31	1190.00	2.7242	0.	131	209.00	1.997	0.	131	209.00	1.997	27813.	27734.	27734.		
32	1190.00	2.7242	0.	132	209.00	2.8655	0.	132	209.00	2.8655	27813.	27734.	27734.		
33	1190.00	2.7242	0.	133	209.00	2.8452	0.	133	209.00	2.8452	27813.	27734.	27734.		
34	1190.00	2.7242	0.	134	209.00	1.997	0.	134	209.00	1.997	27813.	27734.	27734.		
35	1190.00	2.7242	0.	135	209.00	2.8655	0.	135	209.00	2.8655	27813.	27734.	27734.		
36	1190.00	2.7242	0.	136	209.00	2.8452	0.	136	209.00	2.8452	27813.	27734.	27734.		
37	1190.00	2.7242	0.	137	209.00	1.997	0.	137	209.00	1.997	27813.	27734.	27734.		
38	1190.00	2.7242	0.	138	209.00	2.8655	0.	138	209.00	2.8655	27813.	27734.	27734.		
39	1190.00	2.7242	0.	139	209.00	2.8452	0.	139	209.00	2.8452	27813.	27734.	27734.		
40	1190.00	2.7242	0.	140	209.00	1.997	0.	140	209.00	1.997	27813.	27734.	27734.		
41	1190.00	2.7242	0.	141	209.00	2.8655	0.	141	209.00	2.8655	27813.	27734.	27734.		
42	1190.00	2.7242	0.	142	209.00	2.8452	0.	142	209.00	2.8452	27813.	27734.	27734.		
43	1190.00	2.7242	0.	143	209.00	1.997	0.	143	209.00	1.997	27813.	27734.	27734.		
44	1190.00	2.7242	0.	144	209.00	2.8655	0.	144	209.00	2.8655	27813.	27734.	27734.		
45	1190.00	2.7242	0.	145	209.00	2.8452	0.	145	209.00	2.8452	27813.	27734.	27734.		
46	1190.00	2.7242	0.	146	209.00	1.997	0.	146	209.00	1.997	27813.	27734.	27734.		
47	1190.00	2.7242	0.	147	209.00	2.8655	0.	147	209.00	2.8655	27813.	27734.	27734.		
48	1190.00	2.7242	0.	148	209.00	2.8452	0.	148	209.00	2.8452	27813.	27734.	27734.		
49	1190.00	2.7242	0.	149	209.00	1.997	0.	149	209.00	1.997	27813.	27734.	27734.		
50	1190.00	2.7242	0.	150	209.00	2.8655	0.	150	209.00	2.8655	27813.	27734.	27734.		

TABLE 6-9. -- Mass of solid in vertical columns of unit cross-section, from BHG-survey data (continued on next 3 pages).

A	PEACE DEPTH (FEET)	BHC DENSITY (G/CC)	SOREHOLE DHT-20			A	PEACE DEPTH (FEET)	BHC DENSITY (G/CC)	SOREHOLE DHT-19						
			DENSITY OF SOLID COMPONENT (G/CC)	CUMULATIVE RHO*0.021	SOLID MASS RHO*CMO				DENSITY OF SOLID COMPONENT (G/CC)	CUMULATIVE RHO*0.021	SOLID MASS RHO*CMO				
0	1000.00		2.0210			0	1000.00		2.0210						
1	591.41		2.0210			1	010.51		2.0210						
2	591.00		2.0670			2	020.50		2.0096						
3	581.00	1.929		0.	0.	3	030.50		2.0191						
4	572.00		2.7571	072.	075.	4	040.50		2.0082						
5	551.00		1.7292	1460.	1270.	5	050.00	1.956							
6	551.00	1.929		1099.	1319.	6	060.50		2.0190						
7	537.00		2.7242	1800.	1919.	7	070.00		2.0257						
8	527.00		2.7241	2021.	2061.	8	080.00	1.956							
9	521.00	1.909		2590.	2000.	9	090.00		2.0091						
10	521.00	1.949		2590.	2000.	10	100.00		2.0091						
11	511.00		2.7100	3014.	2069.	11	110.00		2.0091						
12	491.00	1.909		3726.	2000.	12	120.00	2.001							
13	491.00	2.009		3726.	2000.	13	130.00	2.711							
14	481.00		2.7242	4360.	2000.	14	140.00		2.0110						
15	471.00	2.009		4960.	2000.	15	150.00		2.0110						
16	471.00	2.000		4960.	2000.	16	160.00		2.0110						
17	460.00		2.7091	5172.	2273.	17	170.00		2.0070						
18	451.00	2.000		5800.	2000.	18	180.00	2.010							
19	451.00	2.014		5800.	2000.	19	190.00	2.013							
20	442.00		2.7101	6437.	2061.	20	200.00		2.0000						
21	432.00		2.7140	6745.	2079.	21	210.00		2.0000						
22	421.00	2.010		7269.	2016.	22	220.00	2.013							
23	421.00	2.005		7269.	2016.	23	230.00	2.030							
24	416.00		2.7304	8161.	2017.	24	240.00		2.7242						
25	401.00		2.7146	8161.	2017.	25	250.00	2.040							
26	391.00	2.001		8674.	2029.	26	260.00	2.000							
27	391.00	1.919		8674.	2029.	27	270.00		2.0001						
28	387.00		2.9974	8827.	2000.	28	280.00	2.000							
29	367.00		2.0301	9760.	2000.	29	290.00	1.901							
30	361.00	1.909		10000.	10203.	30	300.00		2.0000						
31	361.00	1.900		10000.	10203.	31	310.00	1.951							
32	351.00		2.0090	10000.	10203.	32	320.00	1.900							
33	342.00		2.0002	11324.	11009.	33	330.00		2.7241						
34	331.00	1.900		11000.	11510.	34	340.00		2.7140						
35	331.00	1.922		11000.	11510.	35	350.00	1.900							
36	318.00		2.7044	12196.	12000.	36	360.00	1.999							
37	303.00		2.0201	12700.	12700.	37	370.00		2.7140						
38	301.00	1.022		12675.	12799.	38	380.00	1.990							
39	301.00	1.902		12675.	12799.	39	390.00	2.050							
40	280.00		2.0277	13550.	13550.	40	400.00		2.7101						
41	272.00		2.0505	13901.	14052.	41	410.00	2.050							
42	271.00	1.900		13900.	14113.	42	420.00	2.000							
43	271.00	1.007		13900.	14113.	43	430.00	2.000							
44	256.00		2.0090	14550.	14573.	44	440.00	2.000							
45	256.00	1.920		14550.	14573.	45	450.00	2.011							
46	250.00		2.0301	15025.	14709.	46	460.00		2.7090						
47	250.00	2.0505		15025.	14709.	47	470.00	2.011							
48	230.00	1.920		15000.	15000.	48	480.00	2.000							
49	226.00	1.971		15000.	15000.	49	490.00	2.000							
50	222.00		2.0051	16021.	16129.	50	500.00		2.0000						
51	211.00		2.0059	16012.	16012.	51	510.00	2.000							
52	211.00	1.971		16029.	16030.	52	520.00	1.922							
53	211.00	1.000		16029.	16030.	53	530.00	1.922							
54	200.00		2.0036	16916.	17012.	54	540.00		2.0000						
55	190.00		2.7044	17119.	17014.	55	550.00	1.972							
56	186.00	1.020		17000.	17000.	56	560.00		2.0020						
57	186.00	2.010		17000.	17000.	57	570.00	1.972	2.0305						
58	170.00		2.0090	17061.	17053.	58	580.00	1.900							
59	165.00		2.0299	18056.	18053.	59	590.00	1.900							
60	161.00		2.9190	18063.	18077.	60	600.00		2.7073						
61	160.00	2.010		18015.	18000.	61	610.00	1.900							
62	160.00	1.000		18015.	18000.	62	620.00		2.0233						
63	146.00		2.0297	19203.	19316.	63	630.00	1.900							
64	146.00	1.000		19061.	19226.	64	640.00	1.900							
65	131.00		2.0090			65	650.00		2.0700						
66	131.00		2.0210			66	660.00	1.900							
67	131.00		2.0210			67	670.00	1.900							

TABLE 6-9 (page 2 of 3 pages). -- Mass of solid in vertical columns of unit cross-section, from BHC-survey data.

A	BUREHOLE 076-23						BUREHOLE 072-16					
	DEPTH (FEET)	BHG DENSITY (GM/CC)	DENSITY OF SOLID COMPONENT (GM/CC)	CUMULATIVE VOLUME (CM ³)	CO TO MASS RATIO (CM ³ /G)	CO TO MASS RATIO (CM ³ /G)	DEPTH (FEET)	BHG DENSITY (GM/CC)	DENSITY OF SOLID COMPONENT (GM/CC)	CUMULATIVE VOLUME (CM ³)	CO TO MASS RATIO (CM ³ /G)	CO TO MASS RATIO (CM ³ /G)
0	1000.00		2.8210				0	1000.00	2.8310	7.0010		
1	734.00	2.156		0.	0.	0.	1	1062.00	2.831		0.	0.
2	728.00		2.8210	740.	740.	740.	2	1052.00	2.831	1445.	1445.	1445.
3	728.00		2.8253	750.	740.	750.	3	1052.00	1.951	1445.	1445.	1447.
4	689.00		2.8779	2921.	5305.	5305.	4	1002.00	1.951	2776.	2776.	2776.
5	674.00	2.136		3250.	5214.	5214.	5	1002.00	2.052	4776.	2776.	2776.
6	674.00	2.072		3250.	5214.	5214.	6	967.00	2.052	4488.	4488.	4488.
7	659.00		2.8059	3972.	5049.	5049.	7	947.00	2.048	4488.	4488.	4488.
8	659.00	2.072		5006.	4449.	5049.	8	937.00	2.048	5967.	4967.	5967.
9	629.00	2.026		5506.	4449.	5049.	9	937.00	2.115	5967.	4967.	5967.
10	600.00	2.026		7064.	7615.	7615.	10	892.00	2.115	7704.	7704.	7704.
11	584.00	2.117		7664.	7615.	7615.	11	892.00	2.107	7704.	7704.	7704.
12	566.00		2.7889	8079.	8785.	8785.	12	871.00		8874.	8874.	8874.
13	569.00	2.117		10017.	10006.	10006.	13	871.00		9274.	8874.	9374.
14	559.00	2.088		10017.	10006.	10006.	14	867.00	2.107	9608.	8874.	9608.
15	555.00		2.7967	10380.	10170.	10170.	15	867.00	2.031	9608.	8874.	9608.
16	555.00		2.7973	11880.	11695.	11695.	16	866.00		9608.	8874.	9608.
17	494.00	2.008		12140.	12140.	12140.	17	852.00		2.9189	10421.	10421.
18	494.00	2.008		12140.	12140.	12140.	18	851.00	2.081	2.9196	11051.	11051.
19	478.00		2.7134	13145.	13142.	13142.	19	837.00	1.951	11051.	11051.	11051.
20	464.00	2.069		13807.	13597.	13597.	20	832.00		2.9252	11205.	11205.
21	464.00	2.017		14751.	14706.	14706.	21	815.00	2.048	2.9206	11866.	11866.
22	440.29		2.8005	14751.	14706.	14706.	22	809.00		2.9206	12424.	12424.
23	434.00	2.617		15012.	14706.	15005.	23	807.00	1.951	2.9206	12424.	12424.
24	434.00	2.000		15012.	14706.	15005.	24	807.00	2.152	2.9185	12424.	12424.
25	404.00	2.000		16433.	16406.	16406.	25	799.00		2.9185	13023.	13023.
26	376.00	2.011		16433.	16406.	16406.	26	772.00	2.052	13106.	14718.	14718.
27	376.00	2.011		17050.	17023.	17023.	27	772.00	2.048	13106.	14718.	14718.
28	374.00	2.037		17850.	17823.	17823.	28	766.00		2.9206	14284.	14284.
29	344.00	2.037		18004.	18277.	18277.	29	742.00	2.048	15075.	14641.	14641.
30	344.00	2.018		18504.	18277.	18277.	30	742.00	2.115	15075.	14641.	14641.
31	314.00		2.9210	20711.	20703.	20703.	31	737.00		2.8059	15000.	15000.
32	314.00		2.9210	20711.	20703.	20703.	32	739.00		2.7241	16729.	16617.
							33	709.00		2.7303	17888.	17888.
							34	707.00	2.115	17402.	17304.	17304.
							35	672.00	2.107	17402.	17304.	17304.
							36	672.00	2.122	19216.	19216.	19216.
							37	660.00		2.9146	19800.	19800.
							38	661.00	2.7803	20283.	20283.	20283.
							39	667.00	2.122	21095.	21019.	21019.
							40	667.00	2.107	21095.	21019.	21019.
							41	631.00		2.7241	21535.	21535.
							42	618.00	2.187	2.7241	23122.	23122.
							43	618.00	2.139	22444.	22444.	22444.
							44	602.00		2.7140	22444.	22444.
							45	598.00	2.139	2.7140	22444.	22444.
							46	582.00	2.131	23548.	23548.	23548.
							47	578.00		2.9146	24121.	24121.
							48	558.00	2.873	2.873	24711.	24711.
							49	552.00	2.191	25623.	25623.	25623.
							50	552.00	2.066	2.8882	26451.	26451.
							51	522.00	2.008	27147.	27147.	27147.
							52	522.00	2.004	27147.	27147.	27147.
							53	517.00		2.8683	27349.	27349.
							54	492.00	2.003	2.8683	28552.	28552.
							55	492.00	2.130	28552.	28552.	28552.
							56	491.00		2.8059	28552.	28552.
							57	479.00	2.070	2.8059	29404.	29404.
							58	457.00	2.180	30405.	30405.	30405.
							59	457.00	1.962	30405.	30405.	30405.
							60	452.00		2.8541	30509.	30509.
							61	435.00		2.8541	31449.	31449.
							62	418.00		4.8101	32019.	32019.
							63	393.00		2.9665	32236.	32236.
							64	382.00	1.962	33770.	33770.	33770.
							65	382.00	1.997	33770.	33684.	33684.
							66	376.00		2.8098	34031.	34031.
							67	361.00		2.8585	34704.	34615.
							68	352.00	1.997	35167.	35167.	35167.
							69	352.00	1.956	35167.	35167.	35167.
							70	347.00		2.8768	35272.	35272.
							71	331.00	2.8765	36099.	36099.	36099.
							72	322.00	1.956	36505.	36505.	36505.
							73	322.00	1.937	36505.	36505.	36505.
							74	313.00		4.5765	36505.	36505.
							75	294.00	2.8882	37669.	37669.	37669.
							76	292.00	1.887	37615.	37615.	37615.
							77	277.00		2.8005	38244.	38244.
							78	266.00	2.8059	38778.	38641.	38641.
							79	262.00	1.807	38778.	38641.	38641.
							80	249.00	1.812	38778.	38641.	38641.
							81	249.00		2.8814	39395.	39395.
							82	238.00	2.8683	40033.	40033.	40033.
							83	232.00	2.8210	40533.	40442.	40442.
							84	224.00	1.812	40533.	40442.	40442.
							85	224.00		2.8210	40570.	40442.

TABLE 6-9 (page 3 of 3 pages). -- Mass of solid in vertical columns of unit cross-section, from BHG-survey data.

TABLE 6-10 (Continued)

DEPTH (FEET)	BUREAU OF MINES			DENSITY OF SOLID COMPONENT (G/CC)			DENSITY OF SOLID COMPONENT (G/CC)			DENSITY OF SOLID COMPONENT (G/CC)		
	DEPTH (FEET)	W - S (G/CC)	DENSITY (G/CC)	CUMULATIVE SOLID MASS (G/CM ²)	W - S (G/CC)	DENSITY (G/CC)	CUMULATIVE SOLID MASS (G/CM ²)	W - S (G/CC)	DENSITY (G/CC)	CUMULATIVE SOLID MASS (G/CM ²)	W - S (G/CC)	DENSITY (G/CC)
201	647.20	2.019	24465.	24452.	24552.	801	344.20	1.996	2.9206	34320.	34305.	34205.
202	648.37	2.007	24405.	24442.	24492.	802	345.27	1.984	34227.	34227.	34127.	18229.
203	649.54	2.007	24706.	24592.	24592.	803	346.54	1.964	34143.	34143.	34043.	34043.
204	650.71	1.974	24806.	24691.	24691.	804	347.81	1.958	34059.	34059.	34059.	34059.
205	651.88	2.082	24929.	24809.	24809.	805	349.08	2.002	34020.	34020.	34020.	34020.
206	653.05	2.058	25046.	24952.	24952.	806	350.35	1.974	34000.	34000.	34000.	34000.
207	654.22	2.047	25111.	24994.	24994.	807	351.62	2.010	2.8565	34015.	34015.	34015.
208	655.39	2.047	25177.	24998.	25048.	808	352.89	2.010	34015.	34015.	34015.	34015.
209	656.56	2.054	25301.	24987.	25182.	809	354.16	1.998	34015.	34015.	34015.	34015.
210	657.73	2.070	25376.	24984.	25299.	810	355.43	1.972	34015.	34015.	34015.	34015.
211	658.90	2.007	25476.	25025.	25289.	811	356.70	1.979	34015.	34015.	34015.	34015.
212	660.07	2.007	25546.	25025.	25289.	812	357.97	1.997	34015.	34015.	34015.	34015.
213	661.24	2.036	25628.	25007.	25507.	813	359.24	1.950	34015.	34015.	34015.	34015.
214	662.41	2.000	25669.	25007.	25507.	814	360.51	1.994	34015.	34015.	34015.	34015.
215	663.58	1.994	25749.	24987.	25647.	815	361.78	1.951	34015.	34015.	34015.	34015.
216	664.75	2.040	25844.	24911.	25711.	816	363.05	2.003	34015.	34015.	34015.	34015.
217	665.92	1.987	25948.	24874.	25784.	817	364.32	2.007	40166.	40166.	40166.	40166.
218	667.09	2.056	26177.	24843.	26003.	818	365.59	2.061	40166.	40166.	40166.	40166.
219	668.26	2.070	26233.	24810.	26106.	819	366.86	2.023	40261.	40261.	40261.	40261.
220	669.43	2.070	26353.	24824.	26224.	820	368.13	1.983	40361.	40361.	40361.	40361.
221	670.60	2.089	26405.	24875.	26275.	821	369.40	2.088	40461.	40461.	40461.	40461.
222	671.77	2.082	26476.	24869.	26384.	822	370.67	1.970	40561.	40561.	40561.	40561.
223	672.94	2.082	26548.	24869.	26484.	823	371.94	1.974	40661.	40661.	40661.	40661.
224	674.11	2.082	26653.	24817.	26584.	824	373.21	1.954	40761.	40761.	40761.	40761.
225	675.28	2.090	27381.	24800.	27200.	825	374.48	1.984	40861.	40861.	40861.	40861.
226	676.45	2.089	27437.	24825.	27205.	826	375.75	1.970	40961.	40961.	40961.	40961.
227	677.62	2.050	27520.	24807.	27307.	827	377.02	1.980	41022.	41022.	41022.	41022.
228	678.79	2.071	27619.	24798.	27406.	828	378.29	1.982	41170.	41170.	41170.	41170.
229	679.96	2.054	27742.	24762.	27402.	829	379.56	1.986	41266.	41266.	41266.	41266.
230	681.13	2.054	27817.	24778.	27478.	830	380.83	1.986	41354.	41354.	41354.	41354.
231	682.30	2.054	27943.	24775.	27575.	831	382.10	1.987	41452.	41452.	41452.	41452.
232	683.47	2.056	28119.	24806.	27606.	832	383.37	1.967	41549.	41549.	41549.	41549.
233	684.64	2.056	28119.	24806.	27606.	833	384.64	1.984	41646.	41646.	41646.	41646.
234	685.81	2.056	28258.	24822.	27622.	834	385.91	1.984	41743.	41743.	41743.	41743.
235	686.98	2.056	30479.	24990.	27606.	835	387.18	2.005	41840.	41840.	41840.	41840.
236	688.15	2.056	31463.	24988.	27606.	836	388.45	1.971	41937.	41937.	41937.	41937.
237	689.32	2.056	31463.	24988.	27606.	837	389.72	1.967	42034.	42034.	42034.	42034.
238	690.49	2.056	31463.	24988.	27606.	838	390.99	1.974	42131.	42131.	42131.	42131.
239	691.66	2.056	31463.	24988.	27606.	839	392.26	1.985	42228.	42228.	42228.	42228.
240	692.83	2.056	31463.	24988.	27606.	840	393.53	1.970	42325.	42325.	42325.	42325.
241	694.00	2.056	31463.	24988.	27606.	841	394.80	1.984	42422.	42422.	42422.	42422.
242	695.17	2.056	31463.	24988.	27606.	842	396.07	1.964	42519.	42519.	42519.	42519.
243	696.34	2.056	31463.	24988.	27606.	843	397.34	1.984	42616.	42616.	42616.	42616.
244	697.51	2.056	31463.	24988.	27606.	844	398.61	1.984	42713.	42713.	42713.	42713.
245	698.68	2.056	31463.	24988.	27606.	845	399.88	1.984	42810.	42810.	42810.	42810.
246	699.85	2.056	31463.	24988.	27606.	846	401.15	1.984	42907.	42907.	42907.	42907.
247	701.02	2.056	31463.	24988.	27606.	847	402.42	1.984	43004.	43004.	43004.	43004.
248	702.19	2.056	31463.	24988.	27606.	848	403.69	1.984	43101.	43101.	43101.	43101.
249	703.36	2.056	31463.	24988.	27606.	849	404.96	1.984	43198.	43198.	43198.	43198.
250	704.53	2.056	31463.	24988.	27606.	850	406.23	1.984	43295.	43295.	43295.	43295.

TABLE 6-10 (Continued)

PEACE DEPTH D(FT)	S - S DENSITY (GM/CC)	BOREHOLE DENSITY OF SOLID COMPONENT (GM/CC)	BOREHOLE COR-17			PEACE DEPTH D(FT)	S - S DENSITY (GM/CC)	BOREHOLE DENSITY OF SOLID COMPONENT (GM/CC)	BOREHOLE COR-21		
			CUMULATIVE RHO(SG.821)	SOLID MASS RHO(CORHO)	TP/CORHO21 LINEAR SP. LINE FOR RHO				CUMULATIVE RHO(SG.821)	SOLID MASS RHO(CORHO)	TP/CORHO21 LINEAR SP. LINE FOR RHO
401	119.71	1.986	4085.	40567.	40367.	0	1800.00	2.0210			
402	119.97	1.986	40861.	40623.	40423.	1	452.71	2.0210			
403	118.00		2.9275	40869.	40631.	2	452.70	2.0432			
404	111.41	1.919		40992.	40591.	3	421.50	2.7202			
405	108.09	1.905		40782.	40659.	4	412.05	1.938			
406	107.40		2.9290	40771.	40726.	5	411.00	2.0144			
407	106.25	1.919		40811.	40765.	6	411.07	1.929			
408	102.01	1.931		40959.	40911.	7	408.74	1.984			
409	97.65	1.894		40179.	40129.	8	406.76	1.798			
410	95.00	1.901		40207.	40201.	9	406.41	1.761			
411	94.44	1.929		40229.	40267.	10	402.85	1.715			
412	90.78	1.950		40074.	40015.	11	401.60	2.7760			
413	88.20		2.9272	40671.	40608.	12	401.28	1.788			
414	85.90	1.874		40764.	40701.	13	399.74	1.693			
415	82.81	1.884		40917.	40953.	14	398.24	1.726			
416	80.49	1.888		40926.	40957.	15	396.97	1.723			
417	78.51	1.898		40907.	40928.	16	396.64	1.759			
418	75.75	1.884		40105.	40035.	17	396.43	1.741			
419	74.44	1.907		40159.	40084.	18	395.16	1.738			
420	72.74	1.905		40231.	40157.	19	394.53	1.697			
421	66.40		2.9270			20	388.26	1.716			
422	56.52		2.9252			21	386.79	1.688			
423	56.49		2.8211			22	385.25	1.643			
424	.00		2.8210			23	383.70	1.660			
						24	381.70	1.715			
						25	378.96	1.665			
						26	377.24	1.876			
						27	376.44	1.861			
						28	373.48	1.786			
						29	371.15	1.748			
						30	370.24	1.762			
						31	369.39	1.873			
						32	368.27	1.886			
						33	364.90	1.886			
						34	365.04	1.871			
						35	363.00	2.8387			
						36	362.21	1.876			
						37	361.73	1.911			
						38	359.38	1.921			
						39	357.81	1.873			
						40	356.68	1.883			
						41	356.49	1.880			
						42	354.74	1.751			
						43	350.76	1.727			
						44	349.20	1.672			
						45	346.00	2.8543			
						46	348.06	1.788			
						47	348.50	1.751			
						48	343.84	1.782			
						49	342.11	1.829			
						50	340.19	1.885			
						51	337.45	1.891			
						52	336.67	1.874			
						53	336.00	2.8588			
						54	334.71	1.886			
						55	333.94	1.798			
						56	331.18	1.755			
						57	330.01	1.755			
						58	329.44	1.751			
						59	327.47	1.806			
						60	326.48	1.886			
						61	324.92	1.884			
						62	322.76	1.881			
						63	321.78	1.884			
						64	320.90	2.8365			
						65	319.04	1.888			
						66	317.87	1.900			
						67	315.91	1.868			
						68	314.74	1.820			
						69	313.17	1.815			
						70	309.64	1.903			
						71	308.90	1.815			
						72	305.24	1.884			
						73	304.20	2.8476			
						74	303.77	1.817			
						75	301.01	1.844			
						76	299.85	1.951			
						77	297.20	1.888			
						78	296.76	1.884			
						79	293.59	1.922			
						80	291.00	2.7718			
						81	290.85	1.922			
						82	289.87	1.936			
						83	288.89	1.923			
						84	287.32	1.818			
						85	284.19	1.798			
						86	283.41	1.820			
						87	281.86	1.939			
						88	279.44	1.955			
						89	277.44	1.879			
						90	275.57	1.955			
						91	275.18	1.889			
						92	274.40	1.876			
						93	271.86	1.874			
						94	270.70	2.8146			
						95	270.00	1.861			
						96	265.70	1.881			
						97	264.41	1.882			
						98	263.83	1.890			
						99	261.48	1.875			
						100	260.00	2.8635			

TABLE 6-10 (Continued)

NO	WELL DEPTH (FEET)	S.G. DENSITY (60/60 F)	BIRMINGHAM COMPONENT DENSITY (60/60 F)	05N-21		CORRECTED LINEAR SCALE FOR WMC	FLUID DENSITY (60/60 F)	BIRMINGHAM COMPONENT DENSITY (60/60 F)		CORRECTED LINEAR SCALE FOR WMC
				CUMULATIVE SOLID MASS FRACTION (%)	S.G. DENSITY (60/60 F)			CUMULATIVE SOLID MASS FRACTION (%)	S.G. DENSITY (60/60 F)	
101	260.30	1.861		5878	4877	5877	0	1806.00		
102	259.35	1.829		5928	4922	5922	1	1811.91		
103	258.40	1.807		6049	6046	6046	4	1817.82		
104	257.45	1.828		6132	6129	6129	7	1823.73		
105	256.50	1.845		6213	6209	6209	10	1829.64		
106	255.55	1.879		6272	6267	6267	13	1835.55		
107	254.60	1.908	2.8586	6289	6289	6289	16	1841.46	0	0
108	253.65	1.922		6397	6392	6392	19	1847.37	48	48
109	252.70	1.926		6505	6501	6501	22	1853.28	107	107
110	251.75	1.909		6588	6583	6583	25	1859.19	173	173
111	250.80	1.903		6645	6640	6640	28	1865.10	229	229
112	249.85	1.908		6645	6638	6638	31	1871.01	285	285
113	248.90	1.912		6827	6819	6819	34	1876.92	341	341
114	247.95	1.931		6860	6852	6852	37	1882.83	397	397
115	247.00	1.897		7025	7015	7015	40	1888.74	453	453
116	246.05	1.931		7105	7095	7095	43	1894.65	509	509
117	245.10	1.826		7166	7156	7156	46	1900.56	565	565
118	244.15	1.803		7182	7171	7171	49	1906.47	621	621
119	243.20	1.826		7200	7189	7189	52	1912.38	677	677
120	242.25	1.826		7389	7377	7377	55	1918.29	733	733
121	241.30	1.908		7515	7502	7502	58	1924.20	789	789
122	240.35	1.888	2.8541	7588	7581	7581	61	1930.11	845	845
123	239.40	1.900		7625	7615	7615	64	1936.02	901	901
124	238.45	1.970		7783	7777	7777	67	1941.93	957	957
125	237.50	1.999		7847	7841	7841	70	1947.84	1013	1013
126	236.55	1.970		7972	7966	7966	73	1953.75	1069	1069
127	235.60	1.967		7986	7979	7979	76	1959.66	1125	1125
128	234.65	1.955	2.8631	8043	8026	8026	79	1965.57	1181	1181
129	233.70	1.920		8147	8129	8129	82	1971.48	1237	1237
130	232.75	1.934		8248	8231	8231	85	1977.39	1293	1293
131	231.80	1.951		8345	8336	8336	88	1983.30	1349	1349
132	230.85	1.935		8436	8417	8417	91	1989.21	1405	1405
133	229.90	1.959		8523	8504	8504	94	1995.12	1461	1461
134	228.95	1.934		8639	8619	8619	97	2001.03	1517	1517
135	228.00	1.936		8738	8713	8713	100	2006.94	1573	1573
136	227.05	1.826		8780	8758	8758	103	2012.85	1629	1629
137	226.10	1.832	2.8541	8866	8853	8853	106	2018.76	1685	1685
138	225.15	1.817		8927	8906	8906	109	2024.67	1741	1741
139	224.20	1.837		9038	9017	9017	112	2030.58	1797	1797
140	223.25	1.845		9118	9098	9098	115	2036.49	1853	1853
141	222.30	1.891		9244	9225	9225	118	2042.40	1909	1909
142	221.35	1.813		9312	9291	9291	121	2048.31	1965	1965
143	220.40	1.882	2.8368	9314	9295	9295	124	2054.22	2021	2021
144	219.45	1.915		9377	9356	9356	127	2060.13	2077	2077
145	218.50	1.887		9435	9416	9416	130	2066.04	2133	2133
146	217.55	1.867		9495	9474	9474	133	2071.95	2189	2189
147	216.60	1.947		9572	9551	9551	136	2077.86	2245	2245
148	215.65	1.879		9746	9723	9723	139	2083.77	2301	2301
149	214.70	1.929		9889	9866	9866	142	2089.68	2357	2357
150	213.75	2.077		10090	10067	10067	145	2095.59	2413	2413
151	212.80	2.082		10265	10243	10243	148	2101.50	2469	2469
152	211.85	2.007		10303	10283	10283	151	2107.41	2525	2525
153	210.90	1.998		10378	10356	10356	154	2113.32	2581	2581
154	209.95	1.992		10511	10490	10490	157	2119.23	2637	2637
155	209.00	1.964		10588	10582	10582	160	2125.14	2693	2693
156	208.05	1.955	2.8589	10662	10639	10639	163	2131.05	2749	2749
157	207.10	1.989		10775	10752	10752	166	2136.96	2805	2805
158	206.15	1.871		10826	10811	10811	169	2142.87	2861	2861
159	205.20	1.955		10972	10966	10966	172	2148.78	2917	2917
160	204.25	2.009		11077	11045	11045	175	2154.69	2973	2973
161	203.30	2.009		11200	11171	11171	178	2160.60	3029	3029
162	202.35	2.085	2.9886	11242	11212	11212	181	2166.51	3085	3085
163	201.40	2.088		11287	11287	11287	184	2172.42	3141	3141
164	200.45	2.029					187	2178.33	3197	3197
165	199.50	2.029					190	2184.24	3253	3253
166	198.55	2.029					193	2190.15	3309	3309
167	197.60	2.007					196	2196.06	3365	3365
168	196.65	2.007					199	2201.97	3421	3421
169	195.70	2.007					202	2207.88	3477	3477
170	194.75	2.007					205	2213.79	3533	3533
171	193.80	2.007					208	2219.70	3589	3589
172	192.85	2.007					211	2225.61	3645	3645
173	191.90	2.007					214	2231.52	3701	3701
174	190.95	2.007					217	2237.43	3757	3757
175	190.00	2.007					220	2243.34	3813	3813
176	189.05	2.007					223	2249.25	3869	3869
177	188.10	2.007					226	2255.16	3925	3925
178	187.15	2.007					229	2261.07	3981	3981
179	186.20	2.007					232	2266.98	4037	4037
180	185.25	2.007					235	2272.89	4093	4093
181	184.30	2.007					238	2278.80	4149	4149
182	183.35	2.007					241	2284.71	4205	4205
183	182.40	2.007					244	2290.62	4261	4261
184	181.45	2.007					247	2296.53	4317	4317
185	180.50	2.007					250	2302.44	4373	4373
186	179.55	2.007					253	2308.35	4429	4429
187	178.60	2.007					256	2314.26	4485	4485
188	177.65	2.007					259	2320.17	4541	4541
189	176.70	2.007					262	2326.08	4597	4597
190	175.75	2.007					265	2331.99	4653	4653
191	174.80	2.007					268	2337.90	4709	4709
192	173.85	2.007					271	2343.81	4765	4765
193	172.90	2.007					274	2349.72	4821	4821
194	171.95	2.007					277	2355.63	4877	4877
195	171.00	2.007					280	2361.54	4933	4933
196	170.05	2.007					283	2367.45	4989	4989
197	169.10	2.007					286	2373.36	5045	5045
198	168.15	2.007					289	2379.27	5101	5101
199	167.20	2.007					292	2385.18	5157	5157
200	166.25	2.007					295	2391.09	5213	5213

TABLE 6-10 (Continued)

J	PEACK DEPTH (FT)	G - G DENSITY (GM/CC)	BOREHOLE DGT-19			J	PEACK DEPTH (FT)	G - G DENSITY (GM/CC)	BOREHOLE DGT-14		
			DENSITY OF SOLID COMPONENT (GM/CC)	CUMULATIVE RHO(=2.82)	SOLID MASS RHO(=RHO)				DENSITY OF SOLID COMPONENT (GM/CC)	CUMULATIVE RHO(=2.82)	SOLID MASS RHO(=RHO)
203	434.46	1.972		1694.	1699.	1699.	301	226.90		2.0700	
204	411.51	2.030		1693.	1702.	1702.	302	216.30		2.0541	
205	409.54	2.009		1704.	1712.	1712.	303	196.90		2.0039	
206	409.40		2.1995	1709.	1719.	1719.	304	189.00		2.0074	
207	407.50	2.003		1716.	1725.	1725.	305	171.00		2.0367	
208	406.79	1.982		1720.	1731.	1731.	306	160.00		2.0159	
209	404.88	2.003		1720.	1730.	1730.	307	163.90		2.0153	
210	403.60	2.003		1734.	1739.	1739.	308	148.70		2.0213	
211	402.47	2.005		1740.	1750.	1750.	309	128.00		2.0201	
212	400.48	2.007		1743.	1750.	1750.	310	122.90		2.0135	
213	399.74	2.104		1744.	1750.	1750.	311	118.00		2.0117	
214	399.50		2.0005	1755.	1759.	1759.	312	117.99			
215	397.09	2.091		1767.	1768.	1768.				2.0210	
216	393.04	2.134		1760.	1792.	1792.					
217	389.89	2.140		1808.	1809.	1809.					
218	388.71	2.149		1817.	1817.	1817.					
219	386.75	2.129		1822.	1840.	1840.					
220	385.19	2.138		1829.	1852.	1852.					
221	382.84	2.129		1853.	1864.	1864.					
222	381.64	2.151		1896.	1896.	1896.					
223	380.50		2.1020	1956.	1956.	1956.					
224	380.07	2.126		1957.	1960.	1960.					
225	379.67	2.037		1959.	1976.	1976.					
226	377.71	1.959		1968.	1977.	1977.					
227	375.74	1.830		1977.	1976.	1976.					
228	372.93	1.909		1982.	1996.	1996.					
229	370.44	1.814		1992.	1994.	1994.					
230	368.27	1.692		1960.	1982.	1982.					
231	366.81	1.889		1912.	1994.	1994.					
232	362.77	1.970		1929.	1978.	1978.					
233	361.53	1.962		1912.	1935.	1935.					
234	359.43	1.980		1919.	1935.	1935.					
235	356.40	2.035		1939.	1963.	1963.					
236	355.30		2.1020	1936.	1960.	1960.					
237	353.73	2.046		1942.	1969.	1969.					
238	350.59	2.011		1983.	1983.	1983.					
239	348.84	1.976		1925.	1993.	1993.					
240	345.87	1.967		2050.	2057.	2057.					
241	343.51	1.909		2035.	2059.	2059.					
242	340.76	1.961		2023.	2077.	2077.					
243	339.38	1.978		2034.	2082.	2082.					
244	338.70		2.0845	2036.	2072.	2072.					
245	337.64	2.013		2011.	2022.	2022.					
246	336.46	1.984		2025.	2050.	2050.					
247	333.69	1.999		2036.	2061.	2061.					
248	331.78	2.000		2039.	2059.	2059.					
249	330.19	2.004		2068.	2075.	2075.					
250	328.18	2.008		2068.	2073.	2073.					
251	326.44	2.044		2097.	2072.	2072.					
252	325.04	2.019		2102.	2102.	2102.					
253	323.07	2.016		2110.	2123.	2123.					
254	319.98	2.008		2127.	2127.	2127.					
255	317.90	2.096		2132.	2158.	2158.					
256	316.49	2.036		2151.	2156.	2156.					
257	315.21	2.017		2157.	2153.	2153.					
258	313.45	2.011		2160.	2167.	2167.					
259	311.48	2.053		2165.	2170.	2170.					
260	311.10		2.1973	2174.	2171.	2171.					
261	310.50	2.041		2173.	2171.	2171.					
262	309.48	2.057		2171.	2179.	2179.					
263	308.96	2.030		2197.	2193.	2193.					
264	308.49	2.003		2183.	2199.	2199.					
265	306.11	2.019		2209.	2207.	2207.					
266	301.66	2.046		2217.	2210.	2210.					
267	300.67	2.002		2210.	2219.	2219.					
268	299.18	2.000		2220.	2227.	2227.					
269	296.78	2.002		2240.	2213.	2213.					
270	296.30		2.0733	2216.	2228.	2228.					
271	295.17	2.024		2240.	2268.	2268.					
272	292.81	2.055		2245.	2263.	2263.					
273	290.06	2.020		2272.	2277.	2277.					
274	288.49	2.035		2284.	2282.	2282.					
275	285.74	1.976		2293.	2294.	2294.					
276	283.88	1.972		2301.	2308.	2308.					
277	282.98	1.988		2308.	2305.	2305.					
278	280.66	2.017		2317.	2313.	2313.					
279	279.45	2.028		2325.	2329.	2329.					
280	277.41	2.055		2329.	2335.	2335.					
281	275.91	2.036		2335.	2341.	2341.					
282	273.94	2.039		2341.	2346.	2346.					
283	273.18	2.011		2328.	2353.	2353.					
284	271.59	2.000		2360.	2367.	2367.					
285	268.84	1.925		2373.	2377.	2377.					
286	266.48	1.929		2385.	2388.	2388.					
287	264.14	1.981		2393.	2395.	2395.					
288	262.15	2.017		2404.	2407.	2407.					
289	260.17	2.038		2412.	2412.	2412.					
290	258.61	2.053		2421.	2421.	2421.					
291	257.09	2.022		2427.	2426.	2426.					
292	255.00	2.003		2437.	2436.	2436.					
293	253.99	1.970		2444.	2422.	2422.					
294	251.63	1.969		2453.	2451.	2451.					
295	251.00		2.1478	2453.	2451.	2451.					
296	250.88	1.948		2454.	2459.	2459.					
297	248.00	1.972		2472.	2466.	2466.					
298	246.45	1.988		2474.	2453.	2453.					
299	244.97	1.981		2448.	2441.	2441.					
300	243.70	2.003		2454.	2450.	2450.					
301	241.54	2.050		2494.	2485.	2485.					
302	239.77	2.057		2510.	2510.	2510.					

TABLE 6-10 (Continued)

DEPTH (FT)	W. G. DENSITY (GM/CC)	BOREHOLE 002-04			W. G. DENSITY (GM/CC)	BOREHOLE 002-04		
		DENSITY OF SOLID COMPONENT (GM/CC)	CUMULATIVE SOLID MASS (KG/CC)	ISIP/CORRECTED LINEAR ST. WT. FOR BWC		DENSITY OF SOLID COMPONENT (GM/CC)	CUMULATIVE SOLID MASS (KG/CC)	ISIP/CORRECTED LINEAR ST. WT. FOR BWC
0	2.8210	2.8210	0.	0.	2.8210	0.	0.	
1	2.8210	2.8210	101	1375.00	2.8210	101	1375.00	
2	2.7822	2.7822	104	1376.49	2.8210	104	1376.49	
3	2.7140	2.7140	108	1378.11	2.8210	108	1378.11	
4	2.7201	2.7201	109	1380.00	2.8210	109	1380.00	
5	2.7967	2.7967	108	1379.91	2.8210	108	1379.91	
6	2.7841	2.7841	106	1381.00	2.8210	106	1381.00	
7	2.7381	2.7381	107	1380.47	2.8210	107	1380.47	
8	2.7341	2.7341	108	1383.10	2.8210	108	1383.10	
9	2.7340	2.7340	110	1382.20	2.8210	110	1382.20	
10	2.7340	2.7340	113	1380.81	2.8210	113	1380.81	
11	2.7341	2.7341	114	1380.10	2.8210	114	1380.10	
12	2.7340	2.7340	114	1380.00	2.8210	114	1380.00	
13	2.7340	2.7340	115	1381.10	2.8210	115	1381.10	
14	2.7340	2.7340	116	1381.00	2.8210	116	1381.00	
15	2.7340	2.7340	117	1383.01	2.8210	117	1383.01	
16	2.7340	2.7340	119	1381.00	2.8210	119	1381.00	
17	2.196	2.196	119	1381.17	2.207	119	1381.17	
18	2.197	2.197	120	1380.00	2.207	120	1380.00	
19	2.197	2.197	121	1382.00	2.207	121	1382.00	
20	2.197	2.197	122	1384.10	2.207	122	1384.10	
21	2.197	2.197	124	1384.10	2.207	124	1384.10	
22	2.197	2.197	124	1384.10	2.207	124	1384.10	
23	2.197	2.197	124	1384.10	2.207	124	1384.10	
24	2.197	2.197	124	1384.10	2.207	124	1384.10	
25	2.197	2.197	124	1384.10	2.207	124	1384.10	
26	2.197	2.197	124	1384.10	2.207	124	1384.10	
27	2.197	2.197	124	1384.10	2.207	124	1384.10	
28	2.197	2.197	124	1384.10	2.207	124	1384.10	
29	2.197	2.197	124	1384.10	2.207	124	1384.10	
30	2.197	2.197	124	1384.10	2.207	124	1384.10	
31	2.197	2.197	124	1384.10	2.207	124	1384.10	
32	2.197	2.197	124	1384.10	2.207	124	1384.10	
33	2.8210	2.8210	124	1384.10	2.8210	124	1384.10	
34	2.8210	2.8210	124	1384.10	2.8210	124	1384.10	
35	2.8210	2.8210	124	1384.10	2.8210	124	1384.10	
36	2.8210	2.8210	124	1384.10	2.8210	124	1384.10	
37	2.8210	2.8210	124	1384.10	2.8210	124	1384.10	
38	2.8210	2.8210	124	1384.10	2.8210	124	1384.10	
39	2.8210	2.8210	124	1384.10	2.8210	124	1384.10	
40	2.8210	2.8210	124	1384.10	2.8210	124	1384.10	
41	2.8210	2.8210	124	1384.10	2.8210	124	1384.10	
42	2.8210	2.8210	124	1384.10	2.8210	124	1384.10	
43	2.8210	2.8210	124	1384.10	2.8210	124	1384.10	
44	2.8210	2.8210	124	1384.10	2.8210	124	1384.10	
45	2.8210	2.8210	124	1384.10	2.8210	124	1384.10	
46	2.8210	2.8210	124	1384.10	2.8210	124	1384.10	
47	2.8210	2.8210	124	1384.10	2.8210	124	1384.10	
48	2.8210	2.8210	124	1384.10	2.8210	124	1384.10	
49	2.8210	2.8210	124	1384.10	2.8210	124	1384.10	
50	2.8210	2.8210	124	1384.10	2.8210	124	1384.10	
51	2.8210	2.8210	124	1384.10	2.8210	124	1384.10	
52	2.8210	2.8210	124	1384.10	2.8210	124	1384.10	
53	2.8210	2.8210	124	1384.10	2.8210	124	1384.10	
54	2.8210	2.8210	124	1384.10	2.8210	124	1384.10	
55	2.8210	2.8210	124	1384.10	2.8210	124	1384.10	
56	2.8210	2.8210	124	1384.10	2.8210	124	1384.10	
57	2.8210	2.8210	124	1384.10	2.8210	124	1384.10	
58	2.8210	2.8210	124	1384.10	2.8210	124	1384.10	
59	2.8210	2.8210	124	1384.10	2.8210	124	1384.10	
60	2.8210	2.8210	124	1384.10	2.8210	124	1384.10	
61	2.8210	2.8210	124	1384.10	2.8210	124	1384.10	
62	2.8210	2.8210	124	1384.10	2.8210	124	1384.10	
63	2.8210	2.8210	124	1384.10	2.8210	124	1384.10	
64	2.8210	2.8210	124	1384.10	2.8210	124	1384.10	
65	2.8210	2.8210	124	1384.10	2.8210	124	1384.10	
66	2.8210	2.8210	124	1384.10	2.8210	124	1384.10	
67	2.8210	2.8210	124	1384.10	2.8210	124	1384.10	
68	2.8210	2.8210	124	1384.10	2.8210	124	1384.10	
69	2.8210	2.8210	124	1384.10	2.8210	124	1384.10	
70	2.8210	2.8210	124	1384.10	2.8210	124	1384.10	
71	2.8210	2.8210	124	1384.10	2.8210	124	1384.10	
72	2.8210	2.8210	124	1384.10	2.8210	124	1384.10	
73	2.8210	2.8210	124	1384.10	2.8210	124	1384.10	
74	2.8210	2.8210	124	1384.10	2.8210	124	1384.10	
75	2.8210	2.8210	124	1384.10	2.8210	124	1384.10	
76	2.8210	2.8210	124	1384.10	2.8210	124	1384.10	
77	2.8210	2.8210	124	1384.10	2.8210	124	1384.10	
78	2.8210	2.8210	124	1384.10	2.8210	124	1384.10	
79	2.8210	2.8210	124	1384.10	2.8210	124	1384.10	
80	2.8210	2.8210	124	1384.10	2.8210	124	1384.10	
81	2.8210	2.8210	124	1384.10	2.8210	124	1384.10	
82	2.8210	2.8210	124	1384.10	2.8210	124	1384.10	
83	2.8210	2.8210	124	1384.10	2.8210	124	1384.10	
84	2.8210	2.8210	124	1384.10	2.8210	124	1384.10	
85	2.8210	2.8210	124	1384.10	2.8210	124	1384.10	
86	2.8210	2.8210	124	1384.10	2.8210	124	1384.10	
87	2.8210	2.8210	124	1384.10	2.8210	124	1384.10	
88	2.8210	2.8210	124	1384.10	2.8210	124	1384.10	
89	2.8210	2.8210	124	1384.10	2.8210	124	1384.10	
90	2.8210	2.8210	124	1384.10	2.8210	124	1384.10	
91	2.8210	2.8210	124	1384.10	2.8210	124	1384.10	
92	2.8210	2.8210	124	1384.10	2.8210	124	1384.10	
93	2.8210	2.8210	124	1384.10	2.8210	124	1384.10	
94	2.8210	2.8210	124	1384.10	2.8210	124	1384.10	
95	2.8210	2.8210	124	1384.10	2.8210	124	1384.10	
96	2.8210	2.8210	124	1384.10	2.8210	124	1384.10	
97	2.8210	2.8210	124	1384.10	2.8210	124	1384.10	
98	2.8210	2.8210	124	1384.10	2.8210	124	1384.10	
99	2.8210	2.8210	124	1384.10	2.8210	124	1384.10	
100	2.8210	2.8210	124	1384.10	2.8210	124	1384.10	

TABLE 6-10 (Continued)

BOREHOLE 082-09					BOREHOLE 081-09				
DEPTH FEET	DENSITY G/CC	GRAVITY CORRECTED	CUMULATIVE VOLUME CM ³	CUMULATIVE MASS GRAMS	DEPTH FEET	DENSITY G/CC	GRAVITY CORRECTED	CUMULATIVE VOLUME CM ³	CUMULATIVE MASS GRAMS
401	2.098		59211.	54661.	4	2.125		2.8210	0.
402	2.104		59872.	54822.	5	2.164			63.
403	2.103		59992.	54942.	6	2.197			170.
404	2.187		59611.	54861.	7	2.159			276.
405	2.187		59799.	54908.	8	2.093			463.
406	2.184		59915.	54865.	9	2.104			605.
407	2.158		59871.	54827.	10	2.175			774.
408	2.090		59929.	54878.	11	2.170			915.
409	2.015		59897.	54817.	12	2.100			1015.
410	2.028		59841.	54791.	13	2.081			1161.
411	2.102		59921.	54791.	14	2.081			1322.
412	2.102		59957.	54607.	15	2.159			1467.
413	2.102		59954.	54784.	16	2.244			1774.
414	2.034		59959.	54709.	17	2.272			1905.
415	2.035		59701.	54751.	18	2.204			2079.
416	2.037		59805.	54755.	19	2.197			2283.
417	2.070		59887.	54757.	20	2.224			2502.
418	2.038		59815.	54665.	21	2.308			2719.
419	2.038		59795.	54745.	22	2.308			2911.
420	2.132		59554.	54804.	23	2.222			3087.
421	2.177		59624.	54874.	24	2.154			3232.
422	2.155		59554.	54886.	25	2.155			3348.
423	2.104	2.8710			26	2.122			3424.
424	2.104				27	2.128			3471.
425	2.104				28	2.159			3497.
426	2.104				29	2.159			3521.
427	2.104				30	2.252			3511.
428	2.104				31	2.274			3423.
429	2.104				32	2.254			3340.
430	2.104				33	2.184			3257.
431	2.104				34	2.151			3187.
432	2.104				35	2.150			3128.
433	2.104				36	2.103			3079.
434	2.104				37	2.131			3030.
435	2.104				38	2.156			2981.
436	2.104				39	2.277			2932.
437	2.104				40	2.254			2883.
438	2.104				41	2.219			2834.
439	2.104				42	2.174			2785.
440	2.104				43	2.204			2736.
441	2.104				44	2.213			2687.
442	2.104				45	2.202			2638.
443	2.104				46	2.222			2589.
444	2.104				47	2.252			2540.
445	2.104				48	2.254			2491.
446	2.104				49	2.254			2442.
447	2.104				50	2.254			2393.
448	2.104				51	2.254			2344.
449	2.104				52	2.254			2295.
450	2.104				53	2.254			2246.
451	2.104				54	2.254			2197.
452	2.104				55	2.254			2148.
453	2.104				56	2.254			2099.
454	2.104				57	2.254			2050.
455	2.104				58	2.254			2001.
456	2.104				59	2.254			1952.
457	2.104				60	2.254			1903.
458	2.104				61	2.254			1854.
459	2.104				62	2.254			1805.
460	2.104				63	2.254			1756.
461	2.104				64	2.254			1707.
462	2.104				65	2.254			1658.
463	2.104				66	2.254			1609.
464	2.104				67	2.254			1560.
465	2.104				68	2.254			1511.
466	2.104				69	2.254			1462.
467	2.104				70	2.254			1413.
468	2.104				71	2.254			1364.
469	2.104				72	2.254			1315.
470	2.104				73	2.254			1266.
471	2.104				74	2.254			1217.
472	2.104				75	2.254			1168.
473	2.104				76	2.254			1119.
474	2.104				77	2.254			1070.
475	2.104				78	2.254			1021.
476	2.104				79	2.254			972.
477	2.104				80	2.254			923.
478	2.104				81	2.254			874.
479	2.104				82	2.254			825.
480	2.104				83	2.254			776.
481	2.104				84	2.254			727.
482	2.104				85	2.254			678.
483	2.104				86	2.254			629.
484	2.104				87	2.254			580.
485	2.104				88	2.254			531.
486	2.104				89	2.254			482.
487	2.104				90	2.254			433.
488	2.104				91	2.254			384.
489	2.104				92	2.254			335.
490	2.104				93	2.254			286.
491	2.104				94	2.254			237.
492	2.104				95	2.254			188.
493	2.104				96	2.254			139.
494	2.104				97	2.254			90.
495	2.104				98	2.254			41.
496	2.104				99	2.254			0.
497	2.104				100	2.254			0.

TABLE 6-10 (Continued)

PLACED DEPTH FEET	G - S DENSITY G/CC	BOREHOLE DENSITY OF SOLID COMPONENT G/CC	OCT-95			PLACED DEPTH FEET	G - S DENSITY G/CC	BOREHOLE DENSITY OF SOLID COMPONENT G/CC	DAR-24			
			CUMULATIVE RHOx2.0Z	RHOxCRHOZ	(G/CM ³) LITERS FOR ONE				CUMULATIVE RHOx2.0Z	RHOxCRHOZ	(G/CM ³) LITERS FOR ONE	
301	1.90	2.007	39800.	39800.	39800.	1	1.900	2.010				
302	1.90	2.007	39932.	39932.	39932.	2	1.900	2.010				
303	1.90	2.007	40064.	40064.	40064.	3	1.900	2.010				
304	1.90	2.007	40196.	40196.	40196.	4	1.900	2.010				
305	1.90	2.007	40328.	40328.	40328.	5	1.900	2.010				
306	1.90	2.007	40460.	40460.	40460.	6	1.900	2.010				
307	1.90	2.007	40592.	40592.	40592.	7	1.900	2.010				
308	1.90	2.007	40724.	40724.	40724.	8	1.900	2.010				
309	1.90	2.007	40856.	40856.	40856.	9	1.900	2.010				
310	1.90	2.007	40988.	40988.	40988.	10	1.900	2.010				
311	1.90	2.007	41120.	41120.	41120.	11	1.900	2.010				
312	1.90	2.007	41252.	41252.	41252.	12	1.900	2.010				
313	1.90	2.007	41384.	41384.	41384.	13	1.900	2.010				
314	1.90	2.007	41516.	41516.	41516.	14	1.900	2.010				
315	1.90	2.007	41648.	41648.	41648.	15	1.900	2.010				
316	1.90	2.007	41780.	41780.	41780.	16	1.900	2.010				
317	1.90	2.007	41912.	41912.	41912.	17	1.900	2.010				
318	1.90	2.007	42044.	42044.	42044.	18	1.900	2.010				
319	1.90	2.007	42176.	42176.	42176.	19	1.900	2.010				
320	1.90	2.007	42308.	42308.	42308.	20	1.900	2.010				
321	1.90	2.007	42440.	42440.	42440.	21	1.900	2.010				
322	1.90	2.007	42572.	42572.	42572.	22	1.900	2.010				
323	1.90	2.007	42704.	42704.	42704.	23	1.900	2.010				
324	1.90	2.007	42836.	42836.	42836.	24	1.900	2.010				
325	1.90	2.007	42968.	42968.	42968.	25	1.900	2.010				
326	1.90	2.007	43100.	43100.	43100.	26	1.900	2.010				
327	1.90	2.007	43232.	43232.	43232.	27	1.900	2.010				
328	1.90	2.007	43364.	43364.	43364.	28	1.900	2.010				
329	1.90	2.007	43496.	43496.	43496.	29	1.900	2.010				
330	1.90	2.007	43628.	43628.	43628.	30	1.900	2.010				
331	1.90	2.007	43760.	43760.	43760.	31	1.900	2.010				
332	1.90	2.007	43892.	43892.	43892.	32	1.900	2.010				
333	1.90	2.007	44024.	44024.	44024.	33	1.900	2.010				
334	1.90	2.007	44156.	44156.	44156.	34	1.900	2.010				
335	1.90	2.007	44288.	44288.	44288.	35	1.900	2.010				
336	1.90	2.007	44420.	44420.	44420.	36	1.900	2.010				
337	1.90	2.007	44552.	44552.	44552.	37	1.900	2.010				
338	1.90	2.007	44684.	44684.	44684.	38	1.900	2.010				
339	1.90	2.007	44816.	44816.	44816.	39	1.900	2.010				
340	1.90	2.007	44948.	44948.	44948.	40	1.900	2.010				
341	1.90	2.007	45080.	45080.	45080.	41	1.900	2.010				
342	1.90	2.007	45212.	45212.	45212.	42	1.900	2.010				
343	1.90	2.007	45344.	45344.	45344.	43	1.900	2.010				
344	1.90	2.007	45476.	45476.	45476.	44	1.900	2.010				
345	1.90	2.007	45608.	45608.	45608.	45	1.900	2.010				
346	1.90	2.007	45740.	45740.	45740.	46	1.900	2.010				
347	1.90	2.007	45872.	45872.	45872.	47	1.900	2.010				
348	1.90	2.007	46004.	46004.	46004.	48	1.900	2.010				
349	1.90	2.007	46136.	46136.	46136.	49	1.900	2.010				
350	1.90	2.007	46268.	46268.	46268.	50	1.900	2.010				
351	1.90	2.007	46400.	46400.	46400.	51	1.900	2.010				
352	1.90	2.007	46532.	46532.	46532.	52	1.900	2.010				
353	1.90	2.007	46664.	46664.	46664.	53	1.900	2.010				
354	1.90	2.007	46796.	46796.	46796.	54	1.900	2.010				
355	1.90	2.007	46928.	46928.	46928.	55	1.900	2.010				
356	1.90	2.007	47060.	47060.	47060.	56	1.900	2.010				
357	1.90	2.007	47192.	47192.	47192.	57	1.900	2.010				
358	1.90	2.007	47324.	47324.	47324.	58	1.900	2.010				
359	1.90	2.007	47456.	47456.	47456.	59	1.900	2.010				
360	1.90	2.007	47588.	47588.	47588.	60	1.900	2.010				
361	1.90	2.007	47720.	47720.	47720.	61	1.900	2.010				
362	1.90	2.007	47852.	47852.	47852.	62	1.900	2.010				
363	1.90	2.007	47984.	47984.	47984.	63	1.900	2.010				
364	1.90	2.007	48116.	48116.	48116.	64	1.900	2.010				
365	1.90	2.007	48248.	48248.	48248.	65	1.900	2.010				
366	1.90	2.007	48380.	48380.	48380.	66	1.900	2.010				
367	1.90	2.007	48512.	48512.	48512.	67	1.900	2.010				
368	1.90	2.007	48644.	48644.	48644.	68	1.900	2.010				
369	1.90	2.007	48776.	48776.	48776.	69	1.900	2.010				
370	1.90	2.007	48908.	48908.	48908.	70	1.900	2.010				
371	1.90	2.007	49040.	49040.	49040.	71	1.900	2.010				
372	1.90	2.007	49172.	49172.	49172.	72	1.900	2.010				
373	1.90	2.007	49304.	49304.	49304.	73	1.900	2.010				
374	1.90	2.007	49436.	49436.	49436.	74	1.900	2.010				
375	1.90	2.007	49568.	49568.	49568.	75	1.900	2.010				
376	1.90	2.007	49700.	49700.	49700.	76	1.900	2.010				
377	1.90	2.007	49832.	49832.	49832.	77	1.900	2.010				
378	1.90	2.007	49964.	49964.	49964.	78	1.900	2.010				
379	1.90	2.007	50096.	50096.	50096.	79	1.900	2.010				
380	1.90	2.007	50228.	50228.	50228.	80	1.900	2.010				
381	1.90	2.007	50360.	50360.	50360.	81	1.900	2.010				
382	1.90	2.007	50492.	50492.	50492.	82	1.900	2.010				
383	1.90	2.007	50624.	50624.	50624.	83	1.900	2.010				
384	1.90	2.007	50756.	50756.	50756.	84	1.900	2.010				
385	1.90	2.007	50888.	50888.	50888.	85	1.900	2.010				
386	1.90	2.007	51020.	51020.	51020.	86	1.900	2.010				
387	1.90	2.007	51152.	51152.	51152.	87	1.900	2.010				
388	1.90	2.007	51284.	51284.	51284.	88	1.900	2.010				
389	1.90	2.007	51416.	51416.	51416.	89	1.900	2.010				
390	1.90	2.007	51548.	51548.	51548.	90	1.900	2.010				
391	1.90	2.007	51680.	51680.	51680.	91	1.900	2.010				
392	1.90	2.007	51812.	51812.	51812.	92	1.900	2.010				
393	1.90	2.007	51944.	51944.	51944.	93	1.900	2.010				
394	1.90	2.007	52076.	52076.	52076.	94	1.900	2.010				
395	1.90	2.007	52208.	52208.	52208.	95	1.900	2.010				
396	1.90	2.007	52340.	52340.	52340.	96	1.900	2.010				
397	1.90	2.007	52472.	52472.	52472.	97	1.900	2.010				
398	1.90	2.007	52604.	52604.	52604.	98	1.900	2.010				
399	1.90	2.007	52736.	52736.	52736.	99	1.900	2.010				
400	1.90	2.007	52868.	52868.	52868.	100	1.900	2.010				

TABLE 6-10 (Continued)

		BOREHOLE OIT-11						BOREHOLE OIT-11			
PEACE	4 - 5	DENSITY	CUMULATIVE	SOLID MASS	IGP(CRHOZ)	PEACE	4 - 5	DENSITY	CUMULATIVE	SOLID MASS	IGP(CRHOZ)
DEPTH	DENSITY	OF SOLID	DEPTH, 0.021	IN GRAMS	PER (CRHOZ)	DEPTH	DENSITY	OF SOLID	DEPTH, 0.021	IN GRAMS	PER (CRHOZ)
(M)	(G/CC)	COMPONENT	(M)	(G/CC)	FOR RMC	(M)	(G/CC)	COMPONENT	(M)	(G/CC)	FOR RMC
1000.00	2.8210		0.	0.	0.	101	252.76	2.811	9265.	9265.	9265.
1020.00	2.8210		39.	39.	39.	102	256.37	2.850	9375.	9375.	9375.
1040.00	2.8210		90.	90.	90.	104	258.84	2.870	9481.	9481.	9481.
1060.00	2.8210		140.	140.	140.	106	259.88	2.869	9581.	9581.	9581.
1080.00	2.8210		190.	190.	190.	108	262.18	2.892	9681.	9681.	9681.
1100.00	2.8210		240.	240.	240.	110	260.18	2.888	9781.	9781.	9781.
1120.00	2.8210		289.	289.	289.	112	217.80	2.868	9881.	9881.	9881.
1140.00	2.8210		339.	339.	339.	114	218.20	2.888	9979.	9979.	9979.
1160.00	2.8210		389.	389.	389.	116	218.40	2.888	10056.	10056.	10056.
1180.00	2.8210		439.	439.	439.	118	219.20	2.888	10152.	10152.	10152.
1200.00	2.8210		489.	489.	489.	120	219.20	2.888	10249.	10249.	10249.
1220.00	2.8210		539.	539.	539.	122	219.20	2.888	10346.	10346.	10346.
1240.00	2.8210		589.	589.	589.	124	219.20	2.888	10443.	10443.	10443.
1260.00	2.8210		639.	639.	639.	126	219.20	2.888	10540.	10540.	10540.
1280.00	2.8210		689.	689.	689.	128	219.20	2.888	10637.	10637.	10637.
1300.00	2.8210		739.	739.	739.	130	219.20	2.888	10734.	10734.	10734.
1320.00	2.8210		789.	789.	789.	132	219.20	2.888	10831.	10831.	10831.
1340.00	2.8210		839.	839.	839.	134	219.20	2.888	10928.	10928.	10928.
1360.00	2.8210		889.	889.	889.	136	219.20	2.888	11025.	11025.	11025.
1380.00	2.8210		939.	939.	939.	138	219.20	2.888	11122.	11122.	11122.
1400.00	2.8210		989.	989.	989.	140	219.20	2.888	11219.	11219.	11219.
1420.00	2.8210		1039.	1039.	1039.	142	219.20	2.888	11316.	11316.	11316.
1440.00	2.8210		1089.	1089.	1089.	144	219.20	2.888	11413.	11413.	11413.
1460.00	2.8210		1139.	1139.	1139.	146	219.20	2.888	11510.	11510.	11510.
1480.00	2.8210		1189.	1189.	1189.	148	219.20	2.888	11607.	11607.	11607.
1500.00	2.8210		1239.	1239.	1239.	150	219.20	2.888	11704.	11704.	11704.
1520.00	2.8210		1289.	1289.	1289.	152	219.20	2.888	11801.	11801.	11801.
1540.00	2.8210		1339.	1339.	1339.	154	219.20	2.888	11898.	11898.	11898.
1560.00	2.8210		1389.	1389.	1389.	156	219.20	2.888	11995.	11995.	11995.
1580.00	2.8210		1439.	1439.	1439.	158	219.20	2.888	12092.	12092.	12092.
1600.00	2.8210		1489.	1489.	1489.	160	219.20	2.888	12189.	12189.	12189.
1620.00	2.8210		1539.	1539.	1539.	162	219.20	2.888	12286.	12286.	12286.
1640.00	2.8210		1589.	1589.	1589.	164	219.20	2.888	12383.	12383.	12383.
1660.00	2.8210		1639.	1639.	1639.	166	219.20	2.888	12480.	12480.	12480.
1680.00	2.8210		1689.	1689.	1689.	168	219.20	2.888	12577.	12577.	12577.
1700.00	2.8210		1739.	1739.	1739.	170	219.20	2.888	12674.	12674.	12674.
1720.00	2.8210		1789.	1789.	1789.	172	219.20	2.888	12771.	12771.	12771.
1740.00	2.8210		1839.	1839.	1839.	174	219.20	2.888	12868.	12868.	12868.
1760.00	2.8210		1889.	1889.	1889.	176	219.20	2.888	12965.	12965.	12965.
1780.00	2.8210		1939.	1939.	1939.	178	219.20	2.888	13062.	13062.	13062.
1800.00	2.8210		1989.	1989.	1989.	180	219.20	2.888	13159.	13159.	13159.
1820.00	2.8210		2039.	2039.	2039.	182	219.20	2.888	13256.	13256.	13256.
1840.00	2.8210		2089.	2089.	2089.	184	219.20	2.888	13353.	13353.	13353.
1860.00	2.8210		2139.	2139.	2139.	186	219.20	2.888	13450.	13450.	13450.
1880.00	2.8210		2189.	2189.	2189.	188	219.20	2.888	13547.	13547.	13547.
1900.00	2.8210		2239.	2239.	2239.	190	219.20	2.888	13644.	13644.	13644.
1920.00	2.8210		2289.	2289.	2289.	192	219.20	2.888	13741.	13741.	13741.
1940.00	2.8210		2339.	2339.	2339.	194	219.20	2.888	13838.	13838.	13838.
1960.00	2.8210		2389.	2389.	2389.	196	219.20	2.888	13935.	13935.	13935.
1980.00	2.8210		2439.	2439.	2439.	198	219.20	2.888	14032.	14032.	14032.
2000.00	2.8210		2489.	2489.	2489.	200	219.20	2.888	14129.	14129.	14129.

TABLE 6-10 (Continued)

BOREHOLE DWT-13				BOREHOLE DWT-16							
PLACE DEPTH	G + S DENSITY (GM/CC)	DENSITY OF SOLID COMPONENT (GM/CC)	CUMULATIVE SOLID MASS RHO*2.R21	RHO*CRMO ₂	(RHO/CRMO)*2 LINEAR SP. INC FOR RHO	PLACE DEPTH	G + S DENSITY (GM/CC)	DENSITY OF SOLID COMPONENT (GM/CC)	CUMULATIVE SOLID MASS RHO*2.R21	RHO*CRMO ₂	(RHO/CRMO)*2 LINEAR SP. INC FOR RHO
201	395.95	2.047	25940.	25940.	25940.	0	1000.00		2.9210		
202	395.20	2.038	26027.	26027.	26027.	1	1005.81	1.134			
203	392.02	1.997	26085.	26083.	26083.	2	1008.00	1.108		83.	83.
204	390.67	2.016	26104.	26139.	26139.	4	1011.86	1.115		165.	165.
205	388.07	2.014	26200.	26200.	26200.	6	1010.29	2.093		246.	246.
207	386.70	2.072	26304.	26304.	26304.	8	1009.89	2.099		285.	285.
208	384.11	2.044	26380.	26380.	26380.	10	1008.99	2.091		328.	328.
209	382.76	2.046	26400.	26400.	26400.	12	1008.77	2.050		365.	365.
210	382.30	2.050	26419.	26419.	26419.	14	1008.99	2.050		404.	404.
211	382.17	2.050	26716.	26716.	26716.	16	1008.99	2.050		444.	444.
212	380.20	2.036	26790.	26790.	26790.	18	1008.99	2.050		482.	482.
213	378.63	2.036	26790.	26790.	26790.	20	1008.99	2.050		520.	520.
214	376.99	2.052	26790.	26790.	26790.	22	1008.99	2.050		558.	558.
215	373.90	2.052	26790.	26790.	26790.	24	1008.99	2.050		597.	597.
216	371.24	2.037	26790.	26790.	26790.	26	1008.99	2.050		635.	635.
217	369.70	2.005	26790.	26790.	26790.	28	1008.99	2.050		674.	674.
218	366.81	2.000	26790.	26790.	26790.	30	1008.99	2.050		712.	712.
219	362.87	2.004	26790.	26790.	26790.	32	1008.99	2.050		751.	751.
220	360.70	2.004	26790.	26790.	26790.	34	1008.99	2.050		790.	790.
221	360.51	2.049	26790.	26790.	26790.	36	1008.99	2.050		828.	828.
222	357.70	1.954	26790.	26790.	26790.	38	1008.99	2.050		867.	867.
223	355.59	1.936	26790.	26790.	26790.	40	1008.99	2.050		906.	906.
224	353.05	1.899	26790.	26790.	26790.	42	1008.99	2.050		945.	945.
225	351.90	2.004	26790.	26790.	26790.	44	1008.99	2.050		984.	984.
226	349.54	2.009	26790.	26790.	26790.	46	1008.99	2.050		1023.	1023.
227	347.90	1.970	26790.	26790.	26790.	48	1008.99	2.050		1062.	1062.
229	345.40	1.904	26790.	26790.	26790.	50	1008.99	2.050		1101.	1101.
230	344.50	1.986	26790.	26790.	26790.	52	1008.99	2.050		1140.	1140.
231	344.70	1.991	26790.	26790.	26790.	54	1008.99	2.050		1179.	1179.
232	341.70	2.050	26790.	26790.	26790.	56	1008.99	2.050		1218.	1218.
233	339.00	2.031	26790.	26790.	26790.	58	1008.99	2.050		1257.	1257.
234	337.00	2.020	26790.	26790.	26790.	60	1008.99	2.050		1296.	1296.
235	335.97	2.031	26790.	26790.	26790.	62	1008.99	2.050		1335.	1335.
236	332.70	2.061	26790.	26790.	26790.	64	1008.99	2.050		1374.	1374.
237	331.70	2.078	26790.	26790.	26790.	66	1008.99	2.050		1413.	1413.
238	331.19	2.025	26790.	26790.	26790.	68	1008.99	2.050		1452.	1452.
239	329.22	2.047	26790.	26790.	26790.	70	1008.99	2.050		1491.	1491.
240	328.40	2.049	26790.	26790.	26790.	72	1008.99	2.050		1530.	1530.
241	328.21	2.009	26790.	26790.	26790.	74	1008.99	2.050		1569.	1569.
242	326.95	2.020	26790.	26790.	26790.	76	1008.99	2.050		1608.	1608.
243	325.97	2.038	26790.	26790.	26790.	78	1008.99	2.050		1647.	1647.
244	324.82	2.022	26790.	26790.	26790.	80	1008.99	2.050		1686.	1686.
245	323.90	1.990	26790.	26790.	26790.	82	1008.99	2.050		1725.	1725.
247	323.47	1.959	26790.	26790.	26790.	84	1008.99	2.050		1764.	1764.
248	323.32	1.936	26790.	26790.	26790.	86	1008.99	2.050		1803.	1803.
249	322.11	1.973	26790.	26790.	26790.	88	1008.99	2.050		1842.	1842.
250	321.50	1.955	26790.	26790.	26790.	90	1008.99	2.050		1881.	1881.
251	320.02	1.934	26790.	26790.	26790.	92	1008.99	2.050		1920.	1920.
252	320.90	1.955	26790.	26790.	26790.	94	1008.99	2.050		1959.	1959.
253	320.70	2.036	26790.	26790.	26790.	96	1008.99	2.050		1998.	1998.
254	319.99	1.982	26790.	26790.	26790.	98	1008.99	2.050		2037.	2037.
255	319.00	1.974	26790.	26790.	26790.	100	1008.99	2.050		2076.	2076.
256	318.07	2.017	26790.	26790.	26790.						
257	317.90	1.990	26790.	26790.	26790.						
258	317.54	2.020	26790.	26790.	26790.						
259	317.17	1.926	26790.	26790.	26790.						
260	316.05	2.006	26790.	26790.	26790.						
261	315.91	2.063	26790.	26790.	26790.						
262	315.70	2.111	26790.	26790.	26790.						
263	315.00	2.000	26790.	26790.	26790.						
264	314.27	1.989	26790.	26790.	26790.						
265	313.94	1.973	26790.	26790.	26790.						
266	313.30	2.033	26790.	26790.	26790.						
267	313.00	2.067	26790.	26790.	26790.						
268	313.00	2.033	26790.	26790.	26790.						
269	312.90	2.000	26790.	26790.	26790.						
270	312.00	2.000	26790.	26790.	26790.						
271	312.00	2.000	26790.	26790.	26790.						
272	312.00	2.000	26790.	26790.	26790.						
273	312.00	2.000	26790.	26790.	26790.						
274	312.00	2.000	26790.	26790.	26790.						
275	312.00	2.000	26790.	26790.	26790.						
276	312.00	2.000	26790.	26790.	26790.						
277	312.00	2.000	26790.	26790.	26790.						
278	312.00	2.000	26790.	26790.	26790.						
279	312.00	2.000	26790.	26790.	26790.						
280	312.00	2.000	26790.	26790.	26790.						
281	312.00	2.000	26790.	26790.	26790.						
282	312.00	2.000	26790.	26790.	26790.						
283	312.00	2.000	26790.	26790.	26790.						
284	312.00	2.000	26790.	26790.	26790.						
285	312.00	2.000	26790.	26790.	26790.						
286	312.00	2.000	26790.	26790.	26790.						
287	312.00	2.000	26790.	26790.	26790.						
288	312.00	2.000	26790.	26790.	26790.						
289	312.00	2.000	26790.	26790.	26790.						
290	312.00	2.000	26790.	26790.	26790.						
291	312.00	2.000	26790.	26790.	26790.						
292	312.00	2.000	26790.	26790.	26790.						
293	312.00	2.000	26790.	26790.	26790.						
294	312.00	2.000	26790.	26790.	26790.						
295	312.00	2.000	26790.	26790.	26790.						
296	312.00	2.000	26790.	26790.	26790.						
297	312.00	2.000	26790.	26790.	26790.						
298	312.00	2.000	26790.	26790.	26790.						
299	312.00	2.000	26790.	26790.	26790.						
300	312.00	2.000	26790.	26790.	26790.						

TABLE 6-10 (Continued)

BOREHOLE 092-18					BOREHOLE KAR-01				
WELL	S - G	DENSITY	CUMULATIVE	SP. MASS	WELL	S - G	DENSITY	CUMULATIVE	SP. MASS
DEPTH	GRAVITY	OF SOLID	RMHDZ-RZ1	RHOGRMHD	DEPTH	GRAVITY	OF SOLID	RMHDZ-RZ1	RHOGRMHD
(FT)	(GM/CC)	COMPONENT	(GM/CC)	(G/CM ³)	(FT)	(GM/CC)	COMPONENT	(GM/CC)	(G/CM ³)
		(GM/CC)		FOR RMHD			(GM/CC)		FOR RMHD
381	462.78	2.020	29722.	29670.	29670.	0	1886.00	2.010	0.
382	461.90	2.020	29760.	29707.	29707.	1	1105.00	2.005	0.
383	460.36	2.025	29835.	29782.	29782.	2	1103.00	2.001	61.
384	459.09	2.167	30077.	30022.	30022.	3	1102.40	2.057	140.
385	458.07	2.194	30163.	30107.	30107.	4	1101.45	2.030	210.
386	458.00		30226.	30170.	30170.	5	1119.84	2.000	297.
387	452.00	2.197	30227.	30171.	30171.	6	1117.01	2.050	375.
388	450.74	2.113	30232.	30277.	30277.	7	1115.01	2.040	455.
389	450.10	2.052	30471.	30415.	30415.	8	1114.40	2.042	536.
390	449.30	2.124	30732.	30671.	30671.	9	1112.19	2.044	632.
391	448.86	2.119	30794.	30752.	30752.	10	1109.70	1.994	746.
392	448.01	2.151	30836.	30774.	30774.	11	1106.17	2.002	818.
393	437.10	2.193	31053.	30987.	30987.	12	1104.10	2.025	1017.
394	433.50		31446.	31177.	31177.	13	1101.54	2.124	1157.
395	432.92	2.047	31300.	31231.	31231.	14	1100.14	2.005	1249.
396	430.50	2.027	31396.	31325.	31325.	15	1100.14	2.017	1317.
397	429.20	2.031	31453.	31381.	31381.	16	1100.32	2.005	1452.
398	428.97	2.070	31491.	31419.	31419.	17	1100.94	1.990	1557.
399	424.31	2.105	31542.	31519.	31519.	18	1100.90	2.038	1663.
400	423.74	2.090	31632.	31559.	31559.	19	1100.47	2.090	1744.
401	419.01	2.071	31731.	31656.	31656.	20	1100.09	2.052	1804.
402	418.50		31977.	31902.	31902.	21	1100.00	1.915	1897.
403	418.22	2.002	31990.	31916.	31916.	22	1100.67	2.076	2009.
404	415.24	2.072	32206.	32171.	32171.	23	1102.40	2.002	2094.
405	411.50	1.969	32440.	32265.	32265.	24	1102.06	2.070	2090.
406	409.30	1.907	32511.	32355.	32355.	25	1100.00	2.010	2149.
407	408.00	1.900	32555.	32479.	32479.	26	1100.04	2.010	2282.
408	405.25	1.900	32624.	32500.	32500.	27	1106.44	1.970	2402.
409	402.00	1.915	32728.	32649.	32649.	28	1100.00	2.001	2460.
410	401.51	1.902	32794.	32716.	32716.	29	1102.44	1.994	2545.
411	399.20	1.939	32801.	32802.	32802.	30	1100.01	2.034	2607.
412	397.27	1.974	32868.	32880.	32880.	31	1106.79	1.975	2608.
413	395.00	1.954	32936.	32974.	32974.	32	1123.90	2.050	2641.
414	393.90		33124.	33011.	33011.	33	1121.97	2.055	3011.
415	393.03	1.904	33127.	33004.	33004.	34	1120.37	2.022	3119.
416	389.09	1.904	33308.	33227.	33227.	35	1118.70	2.115	3185.
417	376.00					36	1116.75	1.990	3289.
418	361.00	2.056				37	1115.94	2.039	3423.
419	347.00	2.0760				38	1112.33	1.900	3499.
420	331.10	2.0705				39	1110.32	1.900	3591.
421	313.90	2.0705				40	1109.14	1.965	3685.
422	296.90	2.0002				41	1107.91	2.053	3701.
423	277.90	2.0595				42	1106.71	2.007	3760.
424	266.30	2.0059				43	1104.70	2.070	3861.
425	249.90	2.0014				44	1101.09	1.967	3996.
426	231.04	2.0043				45	1099.67	1.964	4223.
427	222.90	2.0210				46	1098.27	1.966	4159.
428						47	1097.47	1.970	4196.
429						48	1096.26	1.900	4241.
430						49	1095.06	1.974	4306.
431						50	1094.25	2.042	4345.
432						51	1093.05	2.005	4404.
433						52	1090.44	2.009	4525.
434						53	1087.42	2.074	4704.
435						54	1085.04	2.070	4765.
436						55	1083.01	2.001	4868.
437						56	1082.60	2.005	4929.
438						57	1081.50	2.120	4941.
439						58	1079.24	2.162	5094.
440						59	1077.70	2.202	5180.
441						60	1076.50	2.229	5257.
442						61	1074.57	2.174	5371.
443						62	1073.76	2.106	5414.
444						63	1070.35	2.017	5574.
445						64	1068.99	2.016	5650.
446						65	1066.33	1.904	5763.
447						66	1063.42	2.060	5910.
448						67	1060.10	2.010	6073.
449						68	1057.09	2.010	6187.
450						69	1055.00	1.970	6373.
451						70	1052.47	2.010	6429.
452						71	1050.06	2.004	6507.
453						72	1048.05	2.023	6643.
454						73	1046.45	2.034	6720.
455						74	1045.00	2.058	6754.
456						75	1043.45	2.070	6859.
457						76	1041.44	1.986	6975.
458						77	1037.01	1.986	7142.
459						78	1037.41	1.970	7160.
460						79	1035.60	2.017	7235.
461						80	1033.34	2.010	7351.
462						81	1030.30	2.143	7493.
463						82	1028.37	2.090	7598.
464						83	1025.55	2.004	7710.
465						84	1021.94	2.104	7920.
466						85	1018.00	2.034	8001.
467						86	1017.52	1.990	8133.
468						87	1015.41	2.111	8252.
469						88	1013.50	2.140	8337.
470						89	1011.49	2.130	8444.
471						90	1009.40	2.010	8546.
472						91	1008.40	2.006	8603.
473						92	1005.07	2.004	8722.
474						93	1002.00	1.947	8875.
475						94	999.04	2.106	8941.
476						95	990.00	2.180	9073.
477						96	989.00	2.127	9337.
478						97	986.10	2.250	9716.
479						98	979.25	2.117	10096.
480						99	974.00	2.130	10223.
481						100	970.00	2.074	10306.

ORT-20 vs. OOR-17

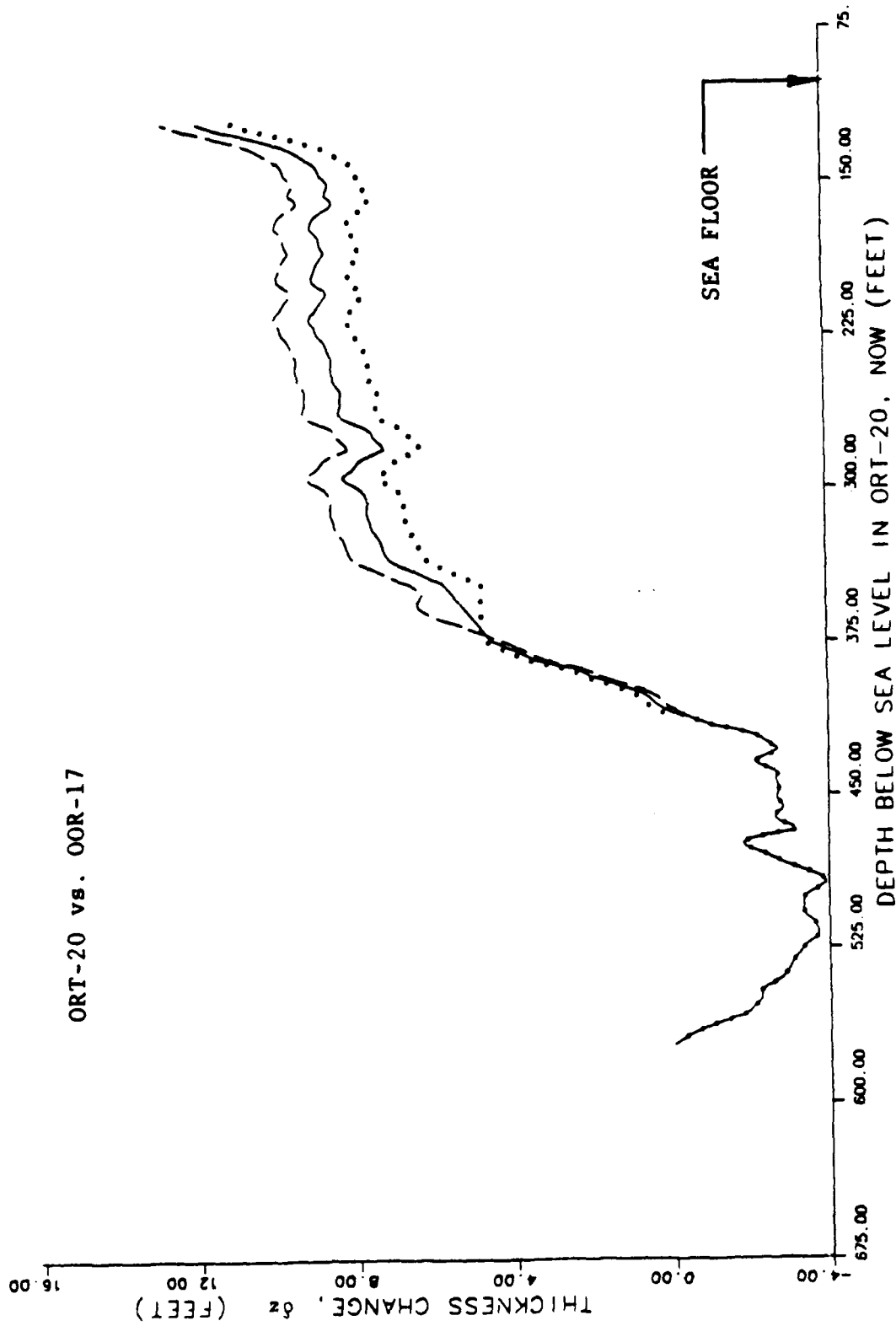


FIGURE 6-27. -- Change in rock thickness from γ - γ densities, assuming simple subsidence. Borehole ORT-20 vs. OOR-17.

ORT-20 vs. OSR-21

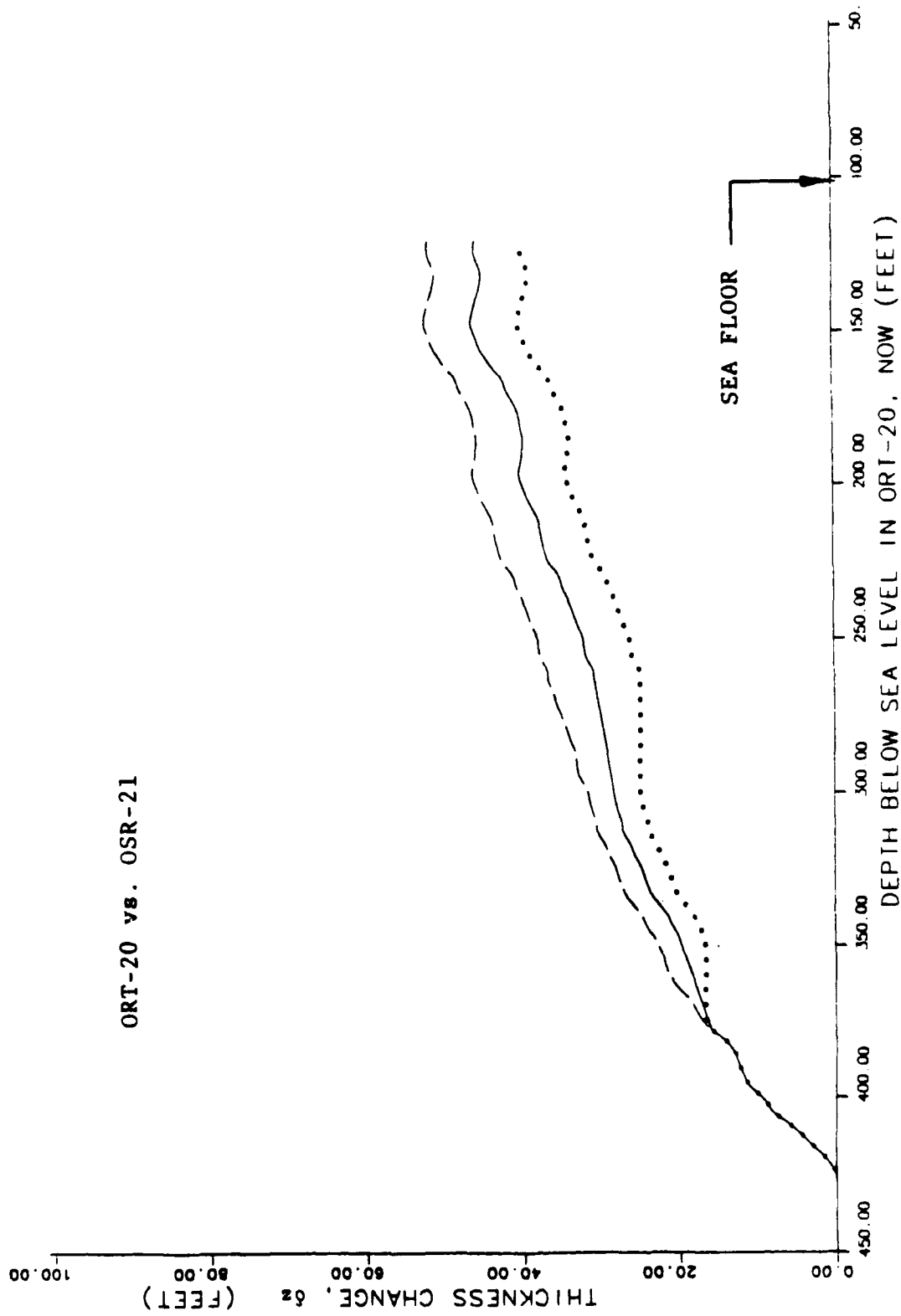


FIGURE 6-28. --- Change in rock thickness from Y-Y densities, assuming simple subsidence. Borehole ORT-20 vs. OSR-21.

ORT-20 vs. OAR-2A

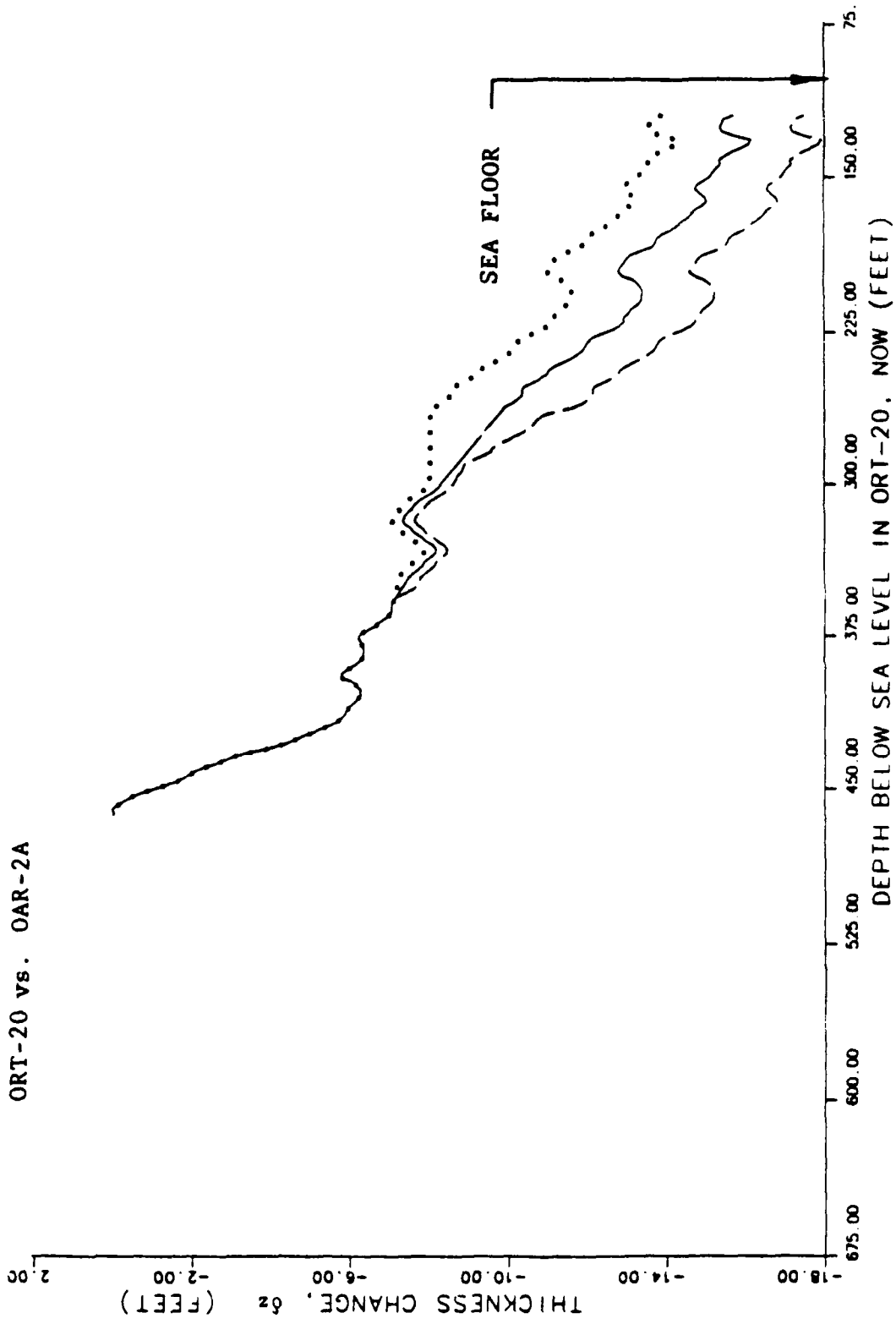
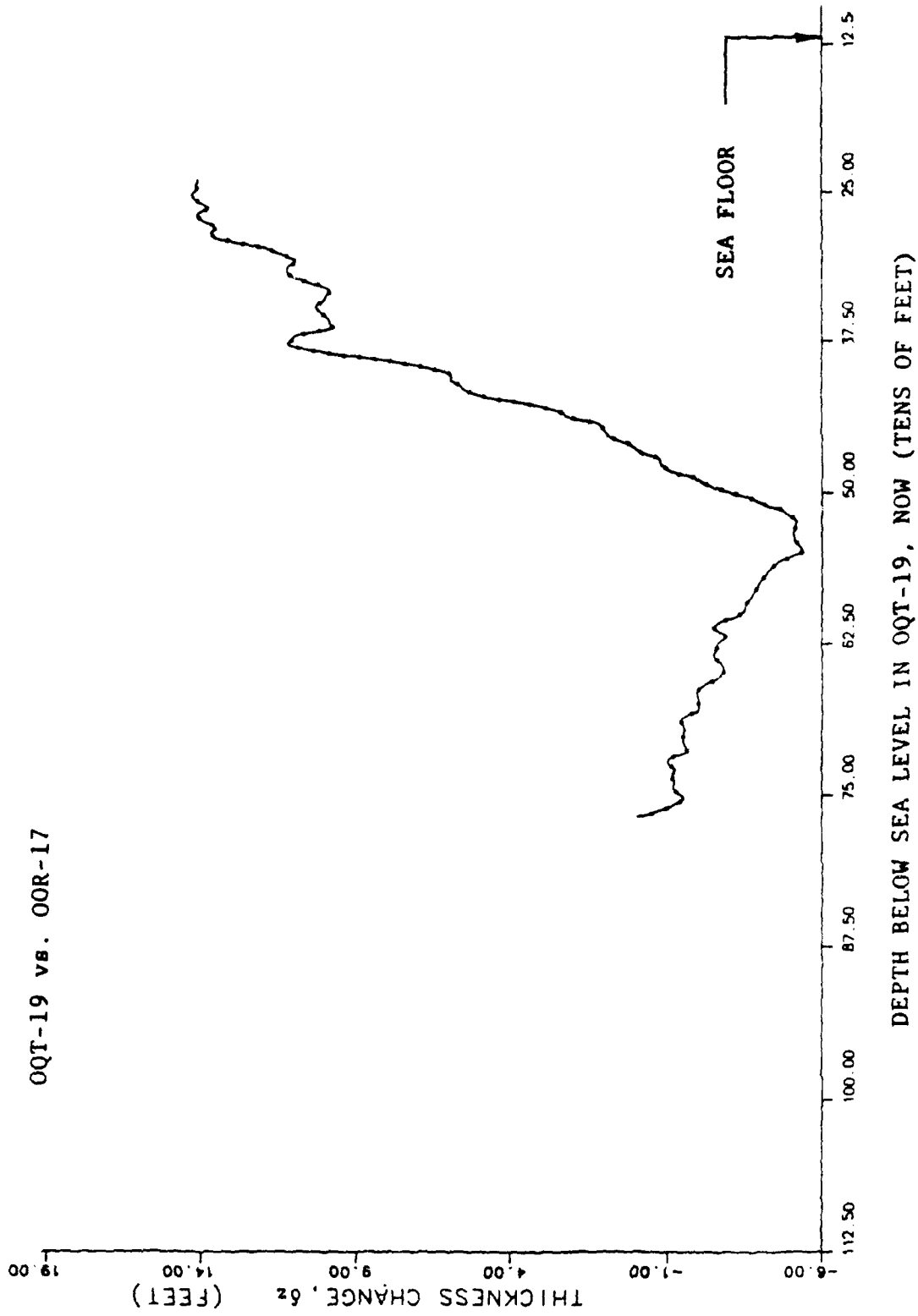


FIGURE 6-29. -- Change in rock thickness from γ - γ densities, assuming simple subsidence. Borehole ORT-20 vs. OAR-2A.

OQT-19 vs. OOR-17



DEPTH BELOW SEA LEVEL IN OQT-19, NOW (TENS OF FEET)

FIGURE 6-30. -- Change in rock thickness from γ - γ densities, assuming simple subsidence. Borehole OQT-19 vs. OOR-17.

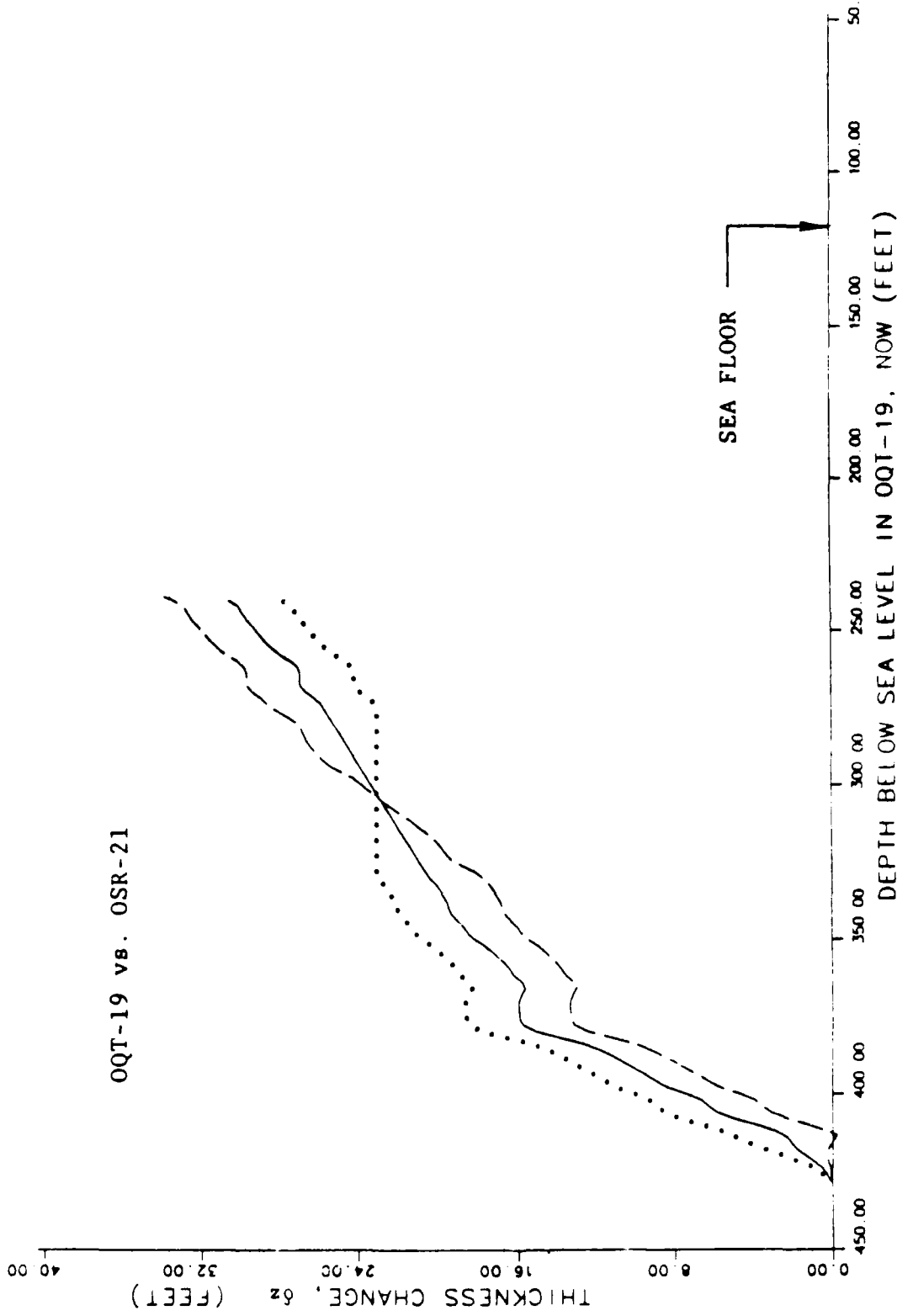


FIGURE 6-31. -- Change in rock thickness from γ - γ densities, assuming simple subsidence. Borehole OQT-19 vs. OSR-21.

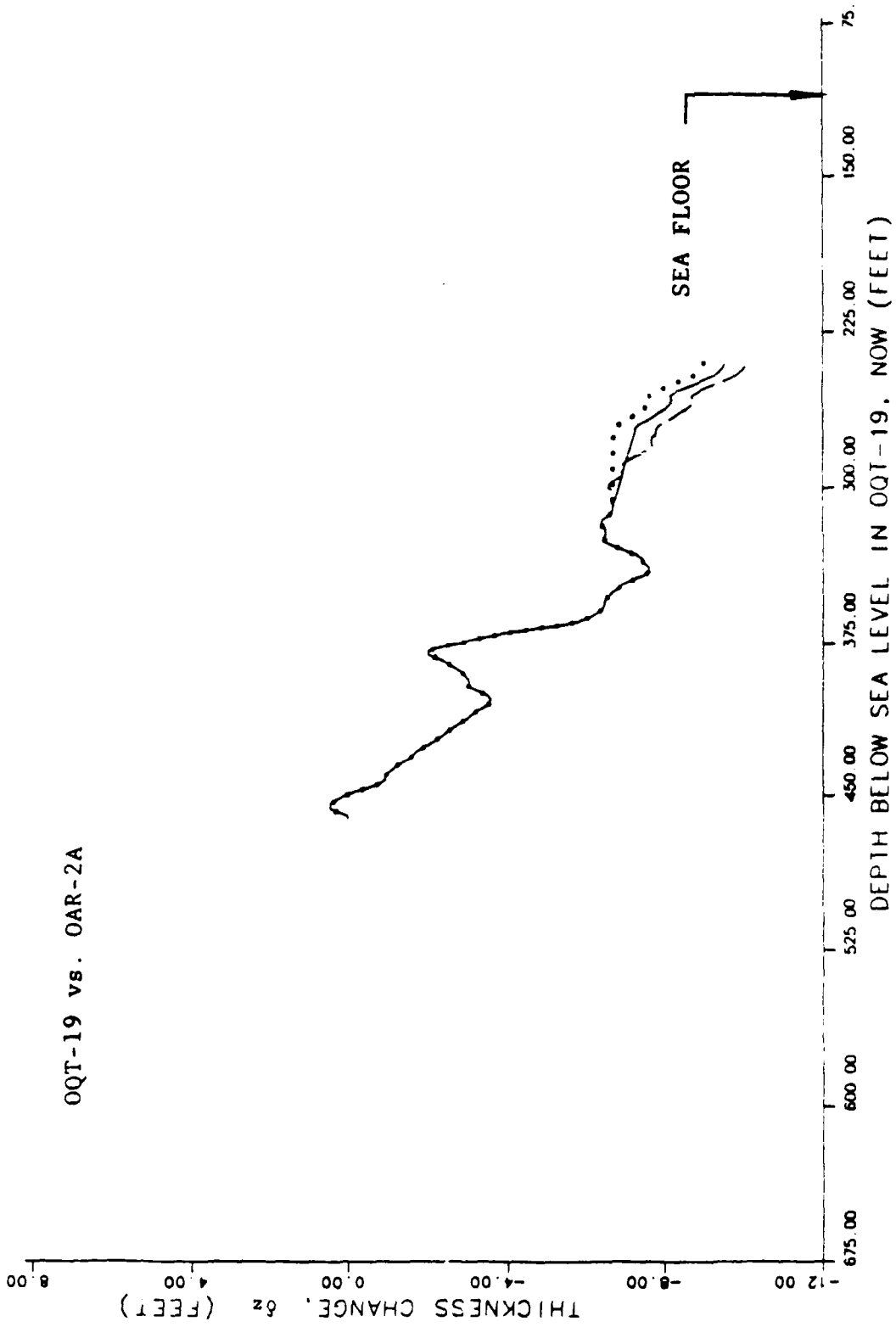


FIGURE 6-32. -- Change in rock thickness from γ - γ densities, assuming simple subsidence. Borehole OQT-19 vs. OAR-2A.

OBZ-04 vs. OOR-17

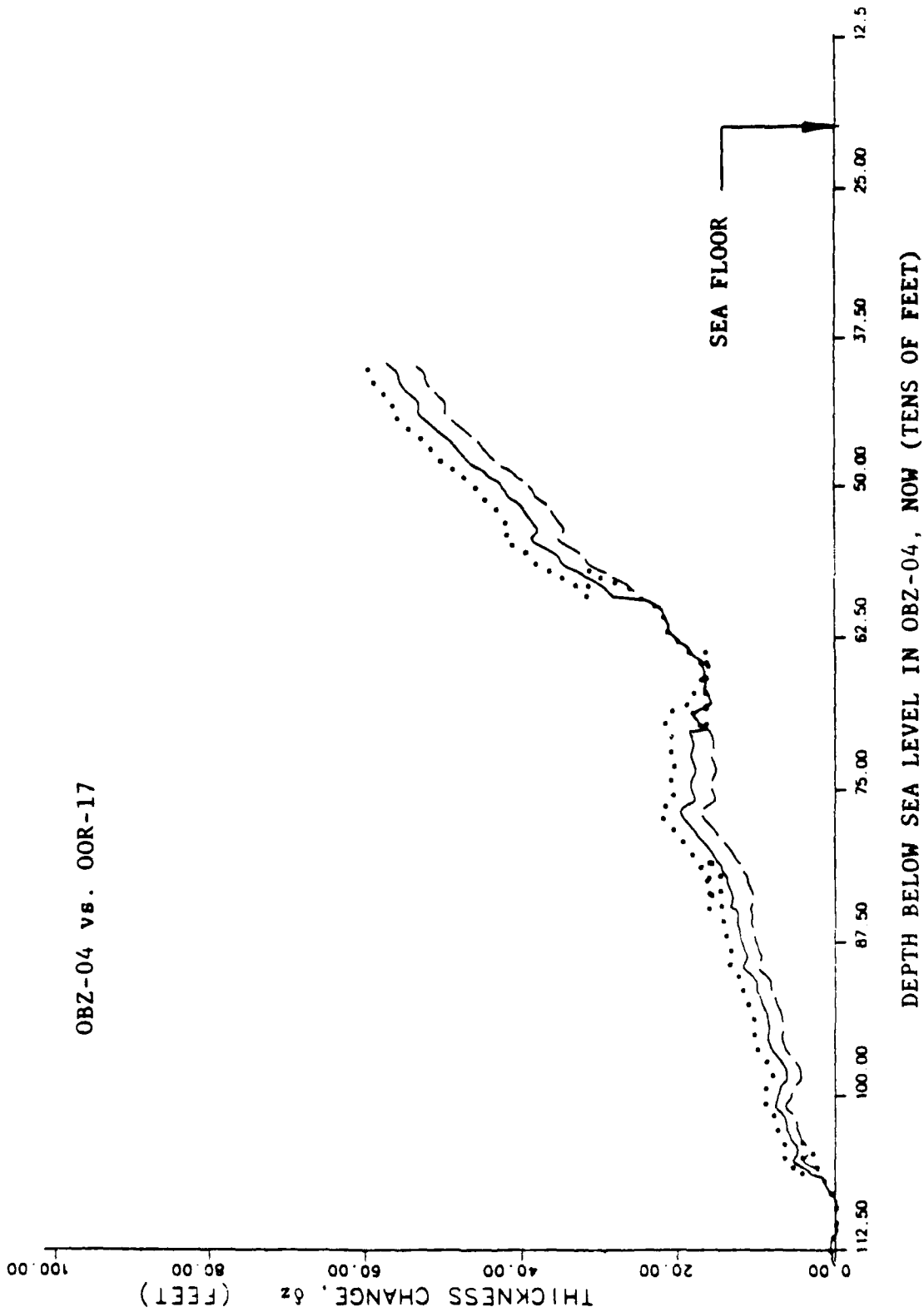


FIGURE 6-33. -- Change in rock thickness from γ - γ densities, assuming simple subsidence. Borehole OBZ-04 vs. OOR-17.

OBZ-04 vs. OSR-21

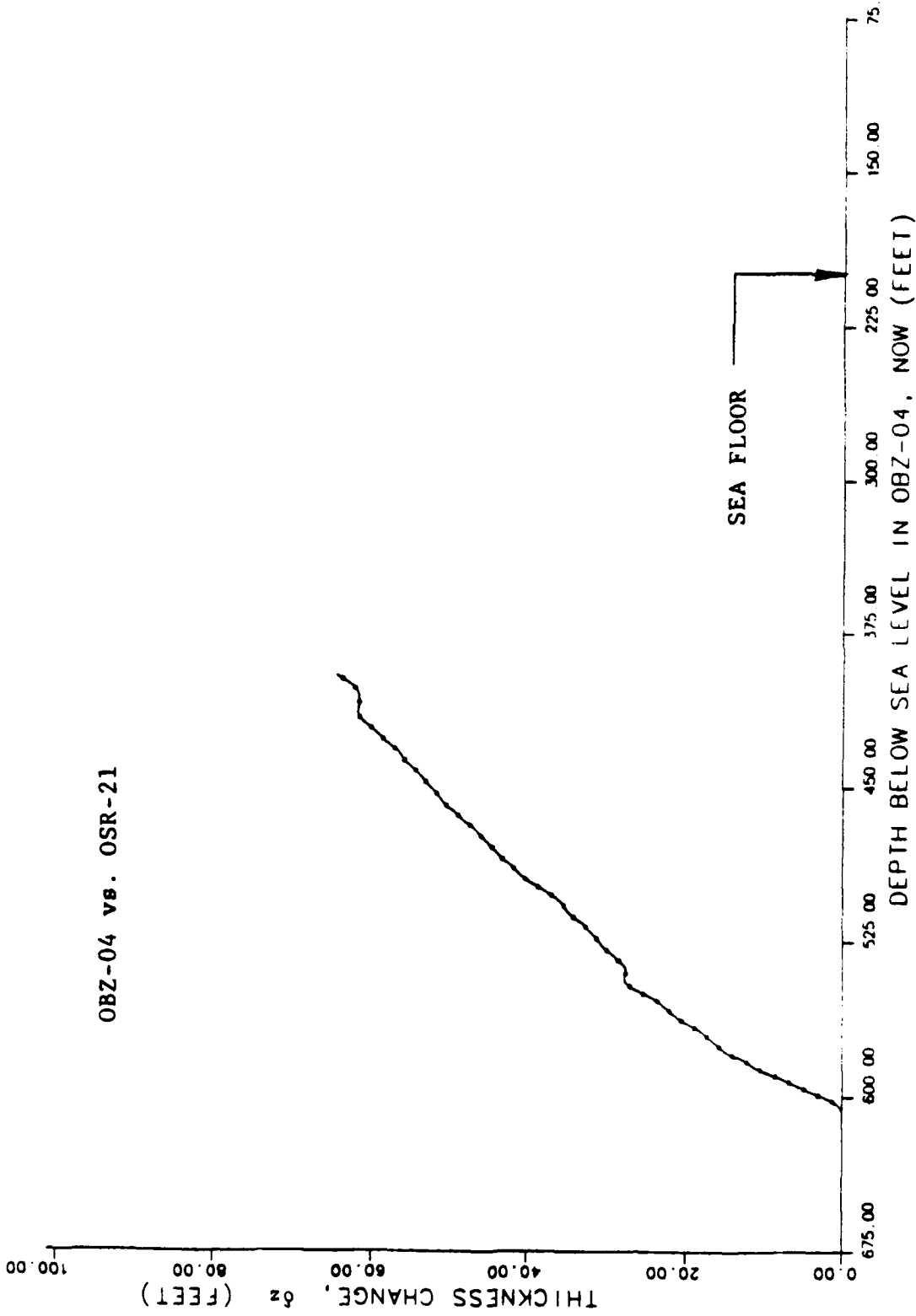


FIGURE 6-3+. -- Change in rock thickness from γ - γ densities, assuming simple subsidence. Borehole OBZ-04 vs. OSR-21.

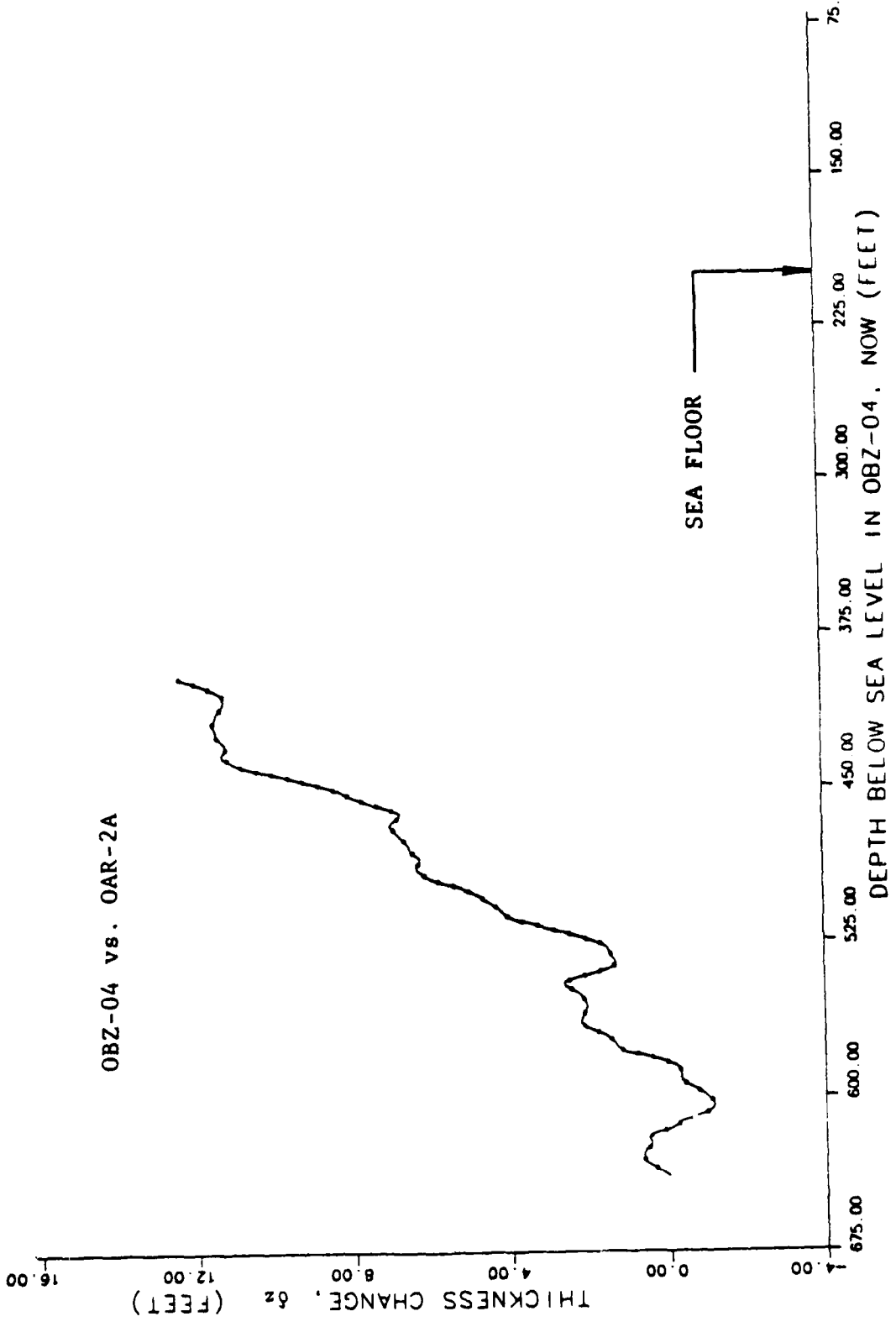


FIGURE 6-35. -- Change in rock thickness from γ - γ densities, assuming simple subsidence. Porehole OBZ-04 vs. OAR-2A.

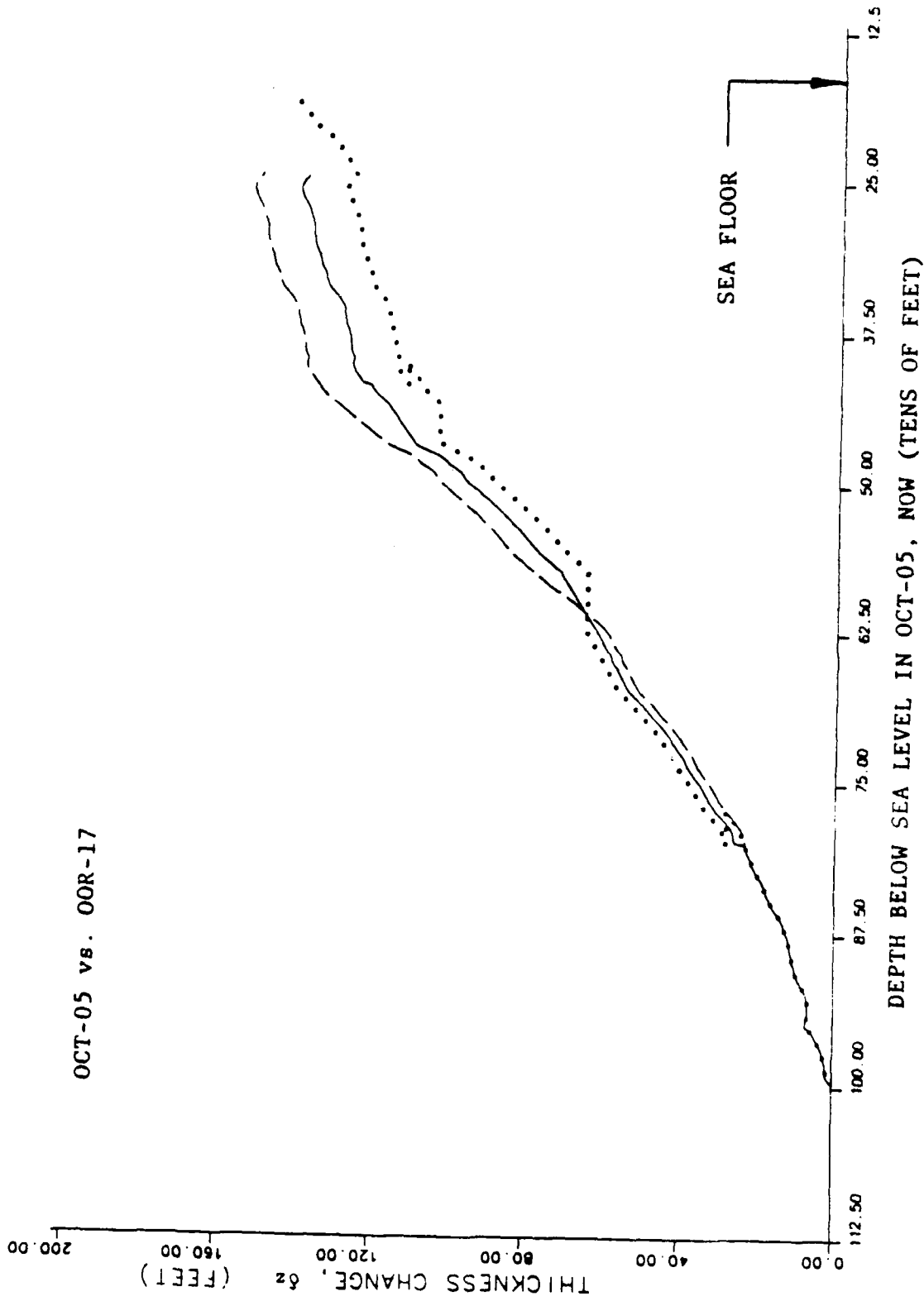


FIGURE 6-36. -- Change in rock thickness from γ - γ densities, assuming simple subsidence. Borehole OCT-05 vs. OOR-17.

OCT-05 vs. OSR-21

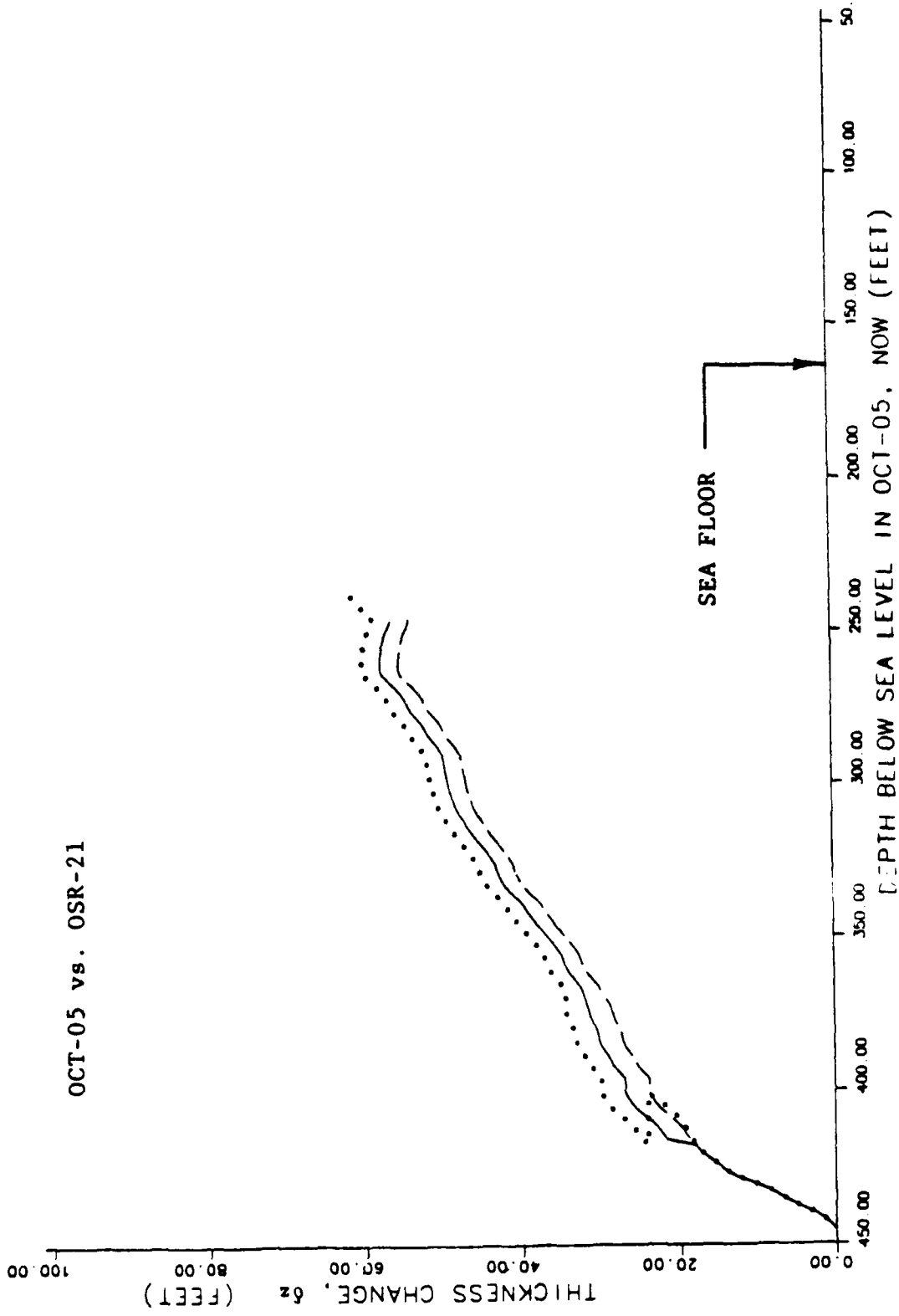


FIGURE 6-37. -- Change in rock thickness from γ - γ densities, assuming simple subsidence. Borehole OCT-05 vs. OSR-21.

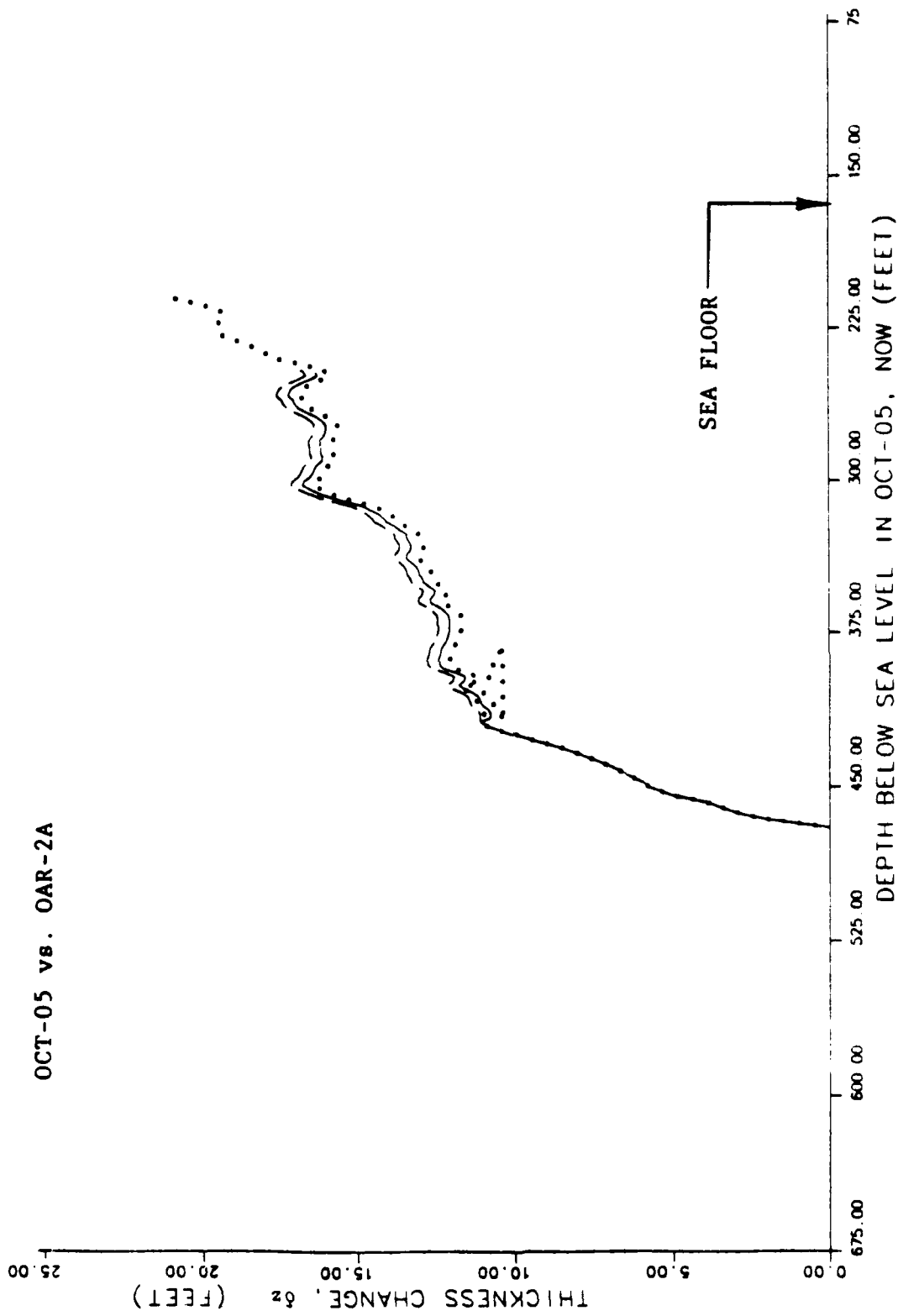


FIGURE 6-38. -- Change in rock thickness from γ - γ densities, assuming simple subsidence. Borehole OCT-05 vs. OAR-2A.

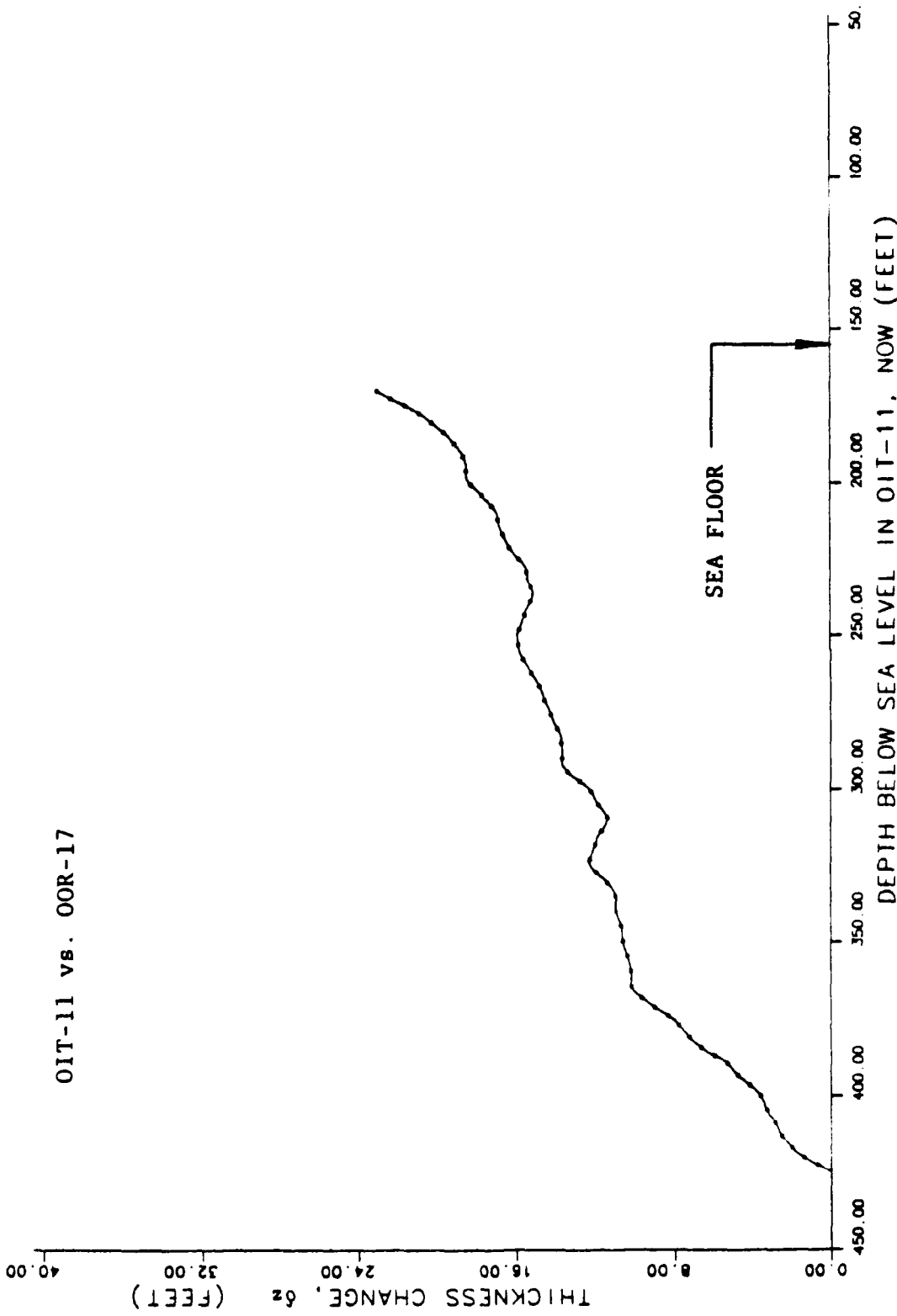


FIGURE 6-39. -- Change in rock thickness from γ - γ densities, assuming simple subsidence. Borehole OIT-11 vs. OOR-17.

OIT-11 vs. OSR-21

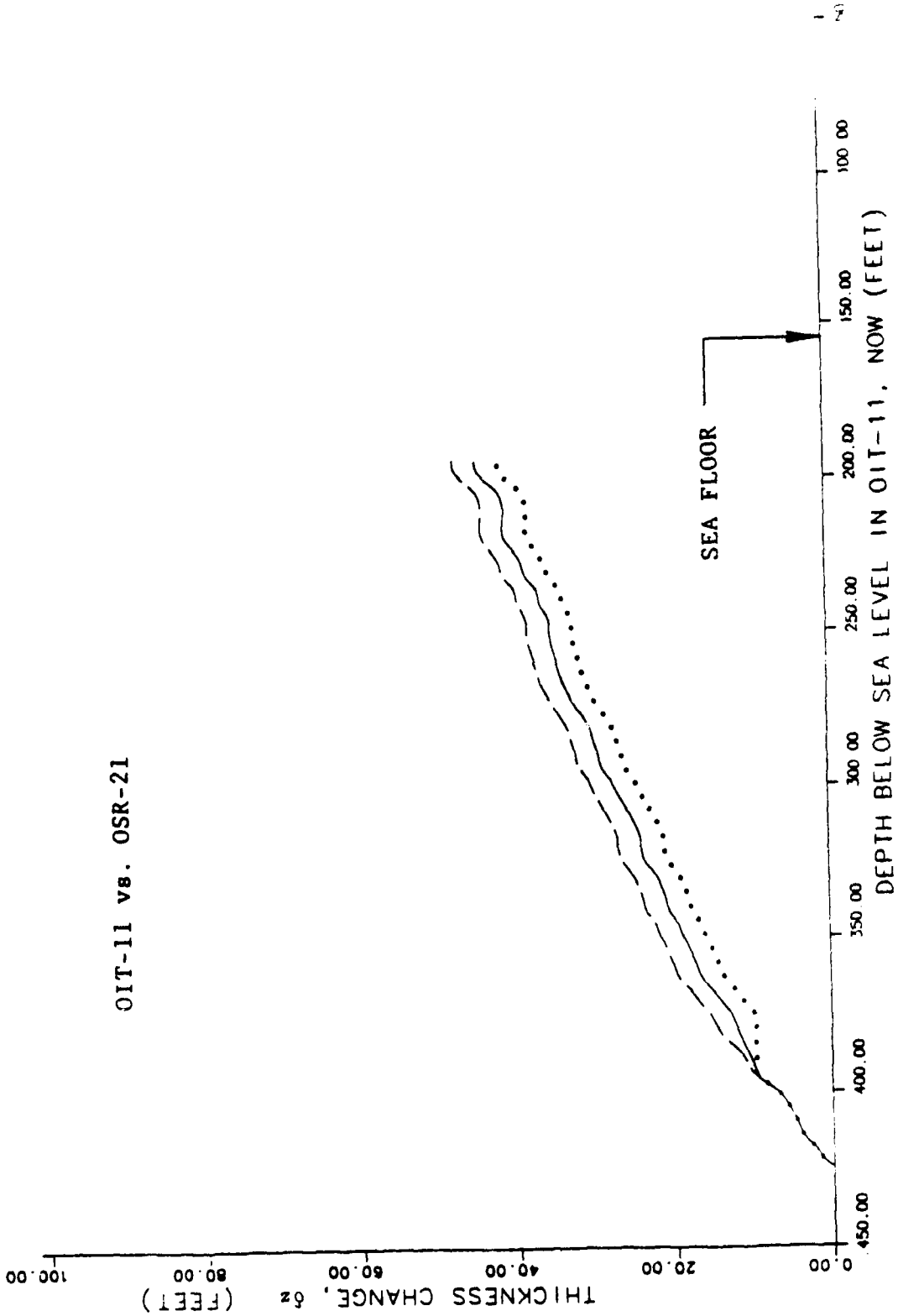


FIGURE 6-40. -- Change in rock thickness from γ - γ densities, assuming simple subsidence. Borehole OIT-11 vs. OSR-21.

OIT-11 vs. OAR-2A

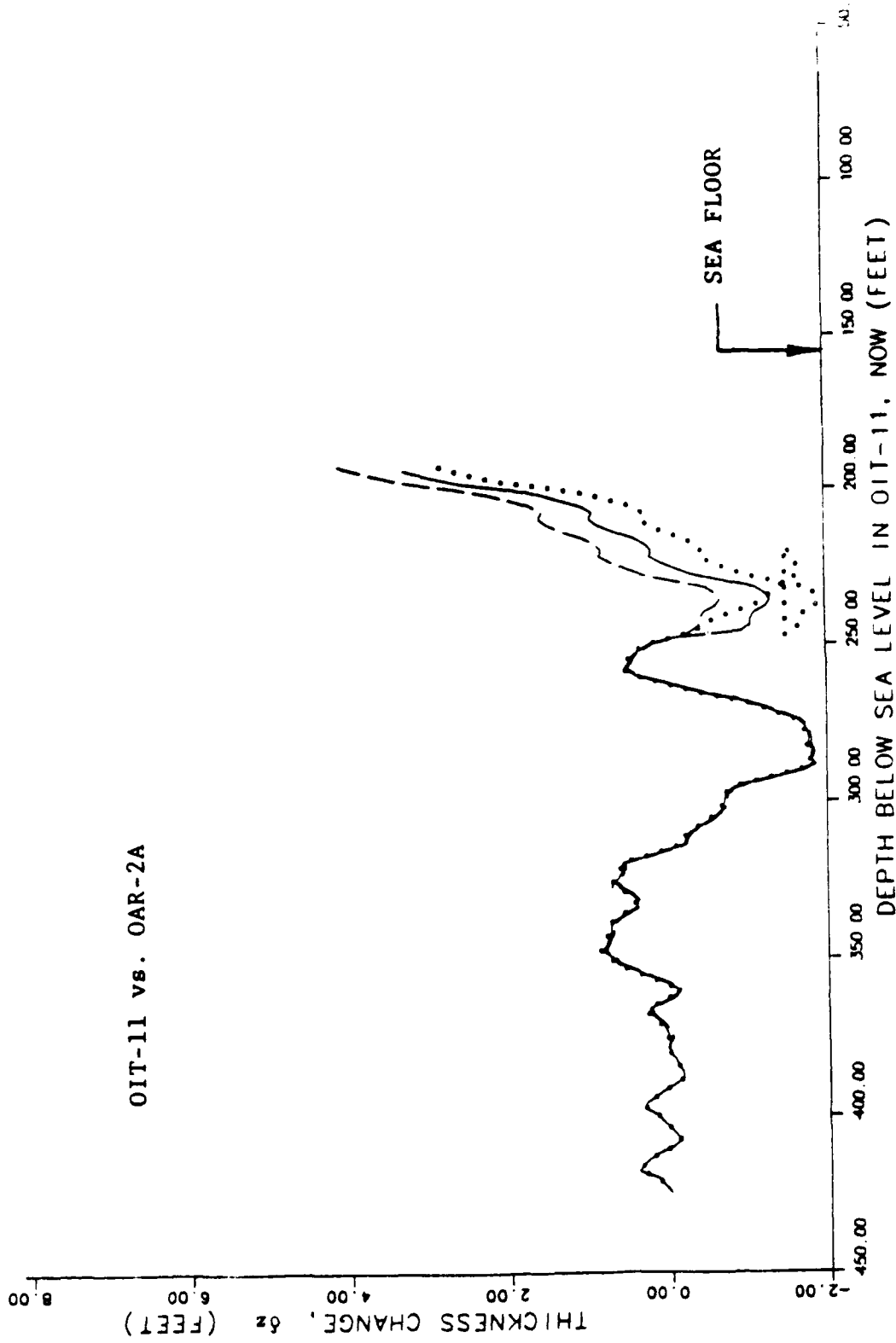
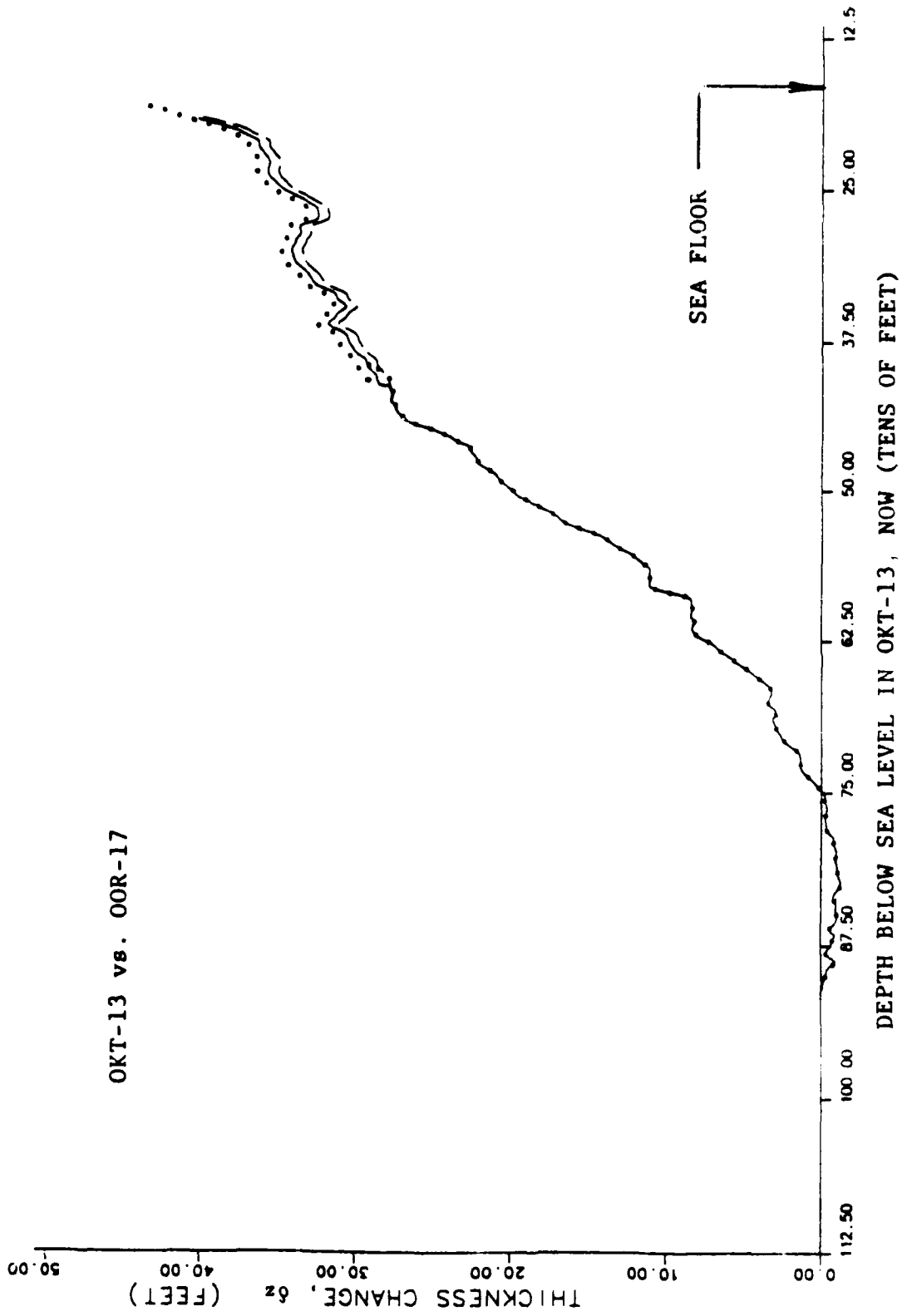


FIGURE 6-4J. -- Change in rock thickness from γ - γ densities, assuming simple subsidence. Borehole OIT-11 vs. OAR-2A.

OKT-13 vs. OOR-17



DEPTH BELOW SEA LEVEL IN OKT-13, NOW (TENS OF FEET)

FIGURE 6-42. --- Change in rock thickness from γ - γ densities, assuming simple subsidence. Borehole OKT-13 vs. OOR-17.

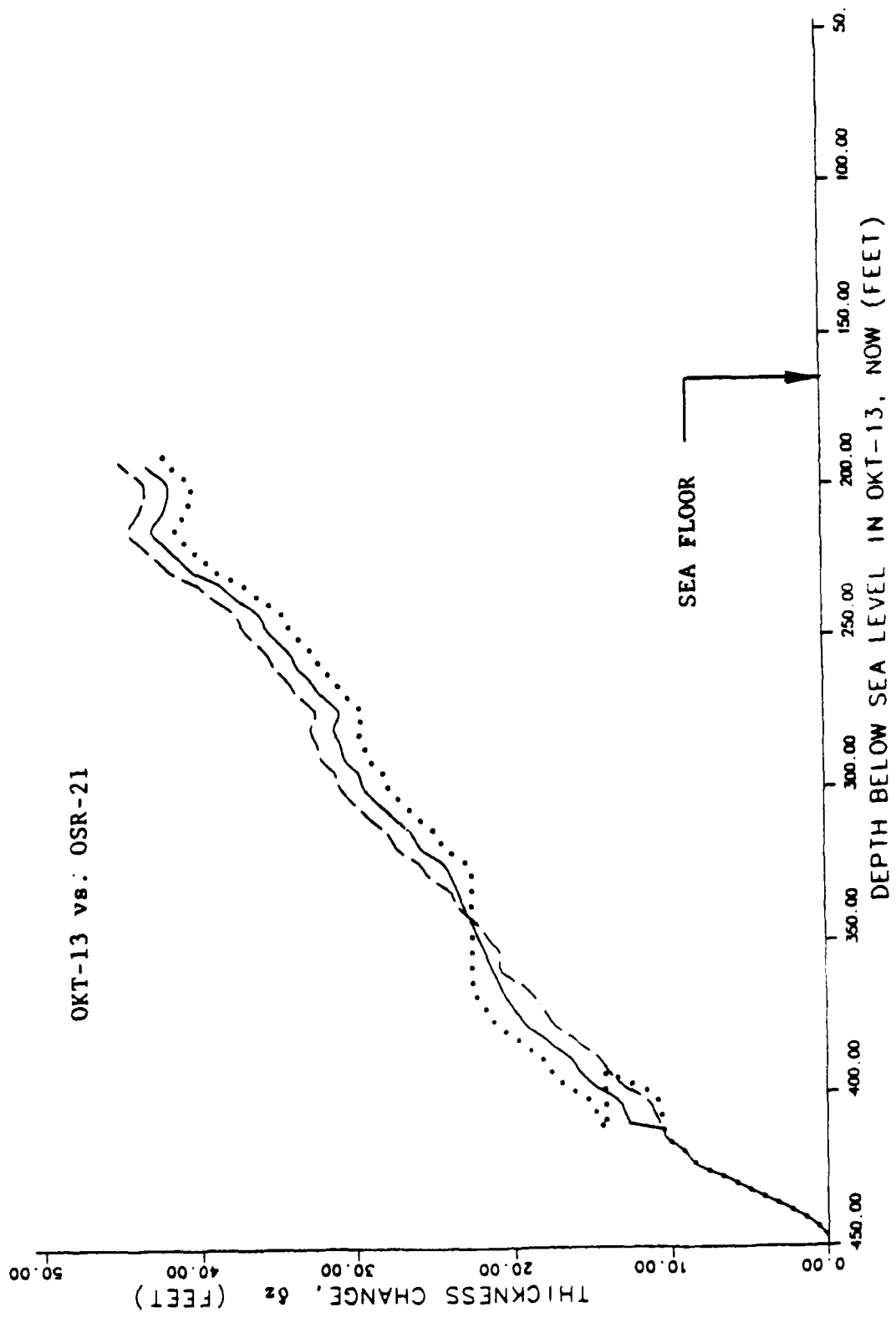


FIGURE 6-43. -- Change in rock thickness from γ - γ densities, assuming simple subsidence. Borehole OKT-13 vs. OSR-21.

OKT-13 vs. OAR-2A

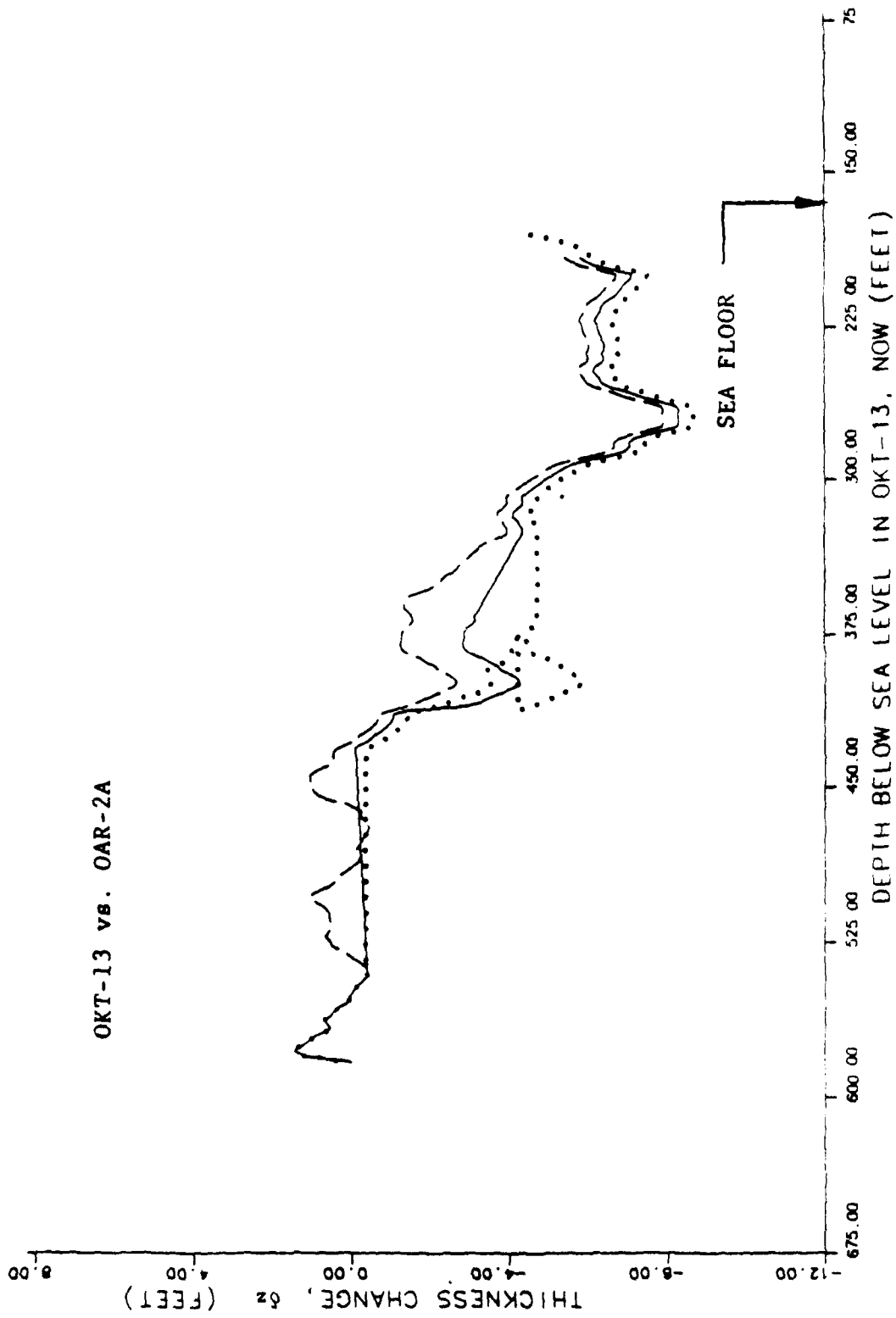


FIGURE 6-44. -- Change in rock thickness from γ - γ densities, assuming simple subsidence. Borehole OKT-13 vs. OAR-2A.

OPZ-18 vs. OOR-17

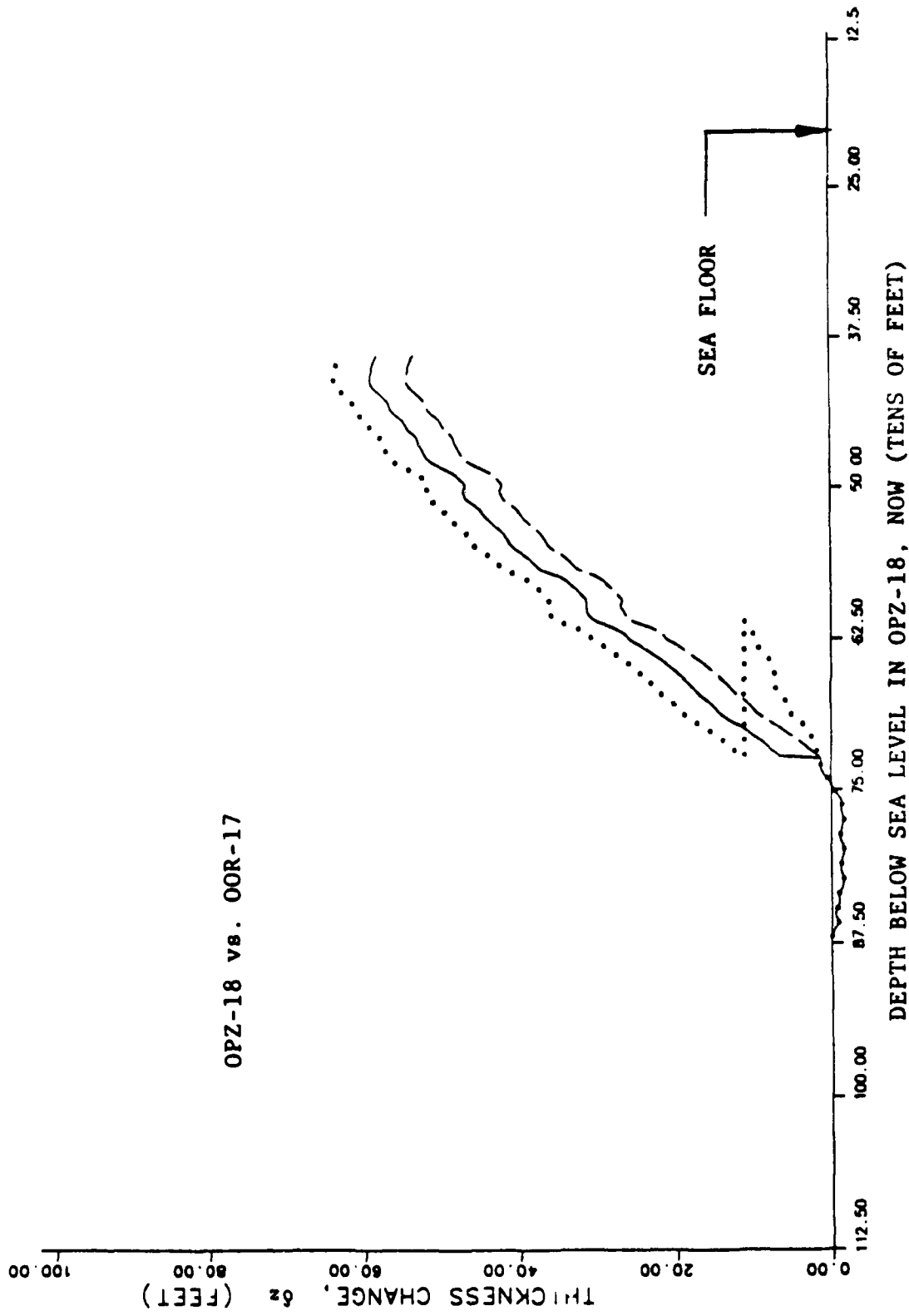


FIGURE 6-45. -- Change in rock thickness from γ - γ densities, assuming simple subsidence. Borehole OPZ-18 vs. OOR-17.

OPZ-18 vs. OSR-21

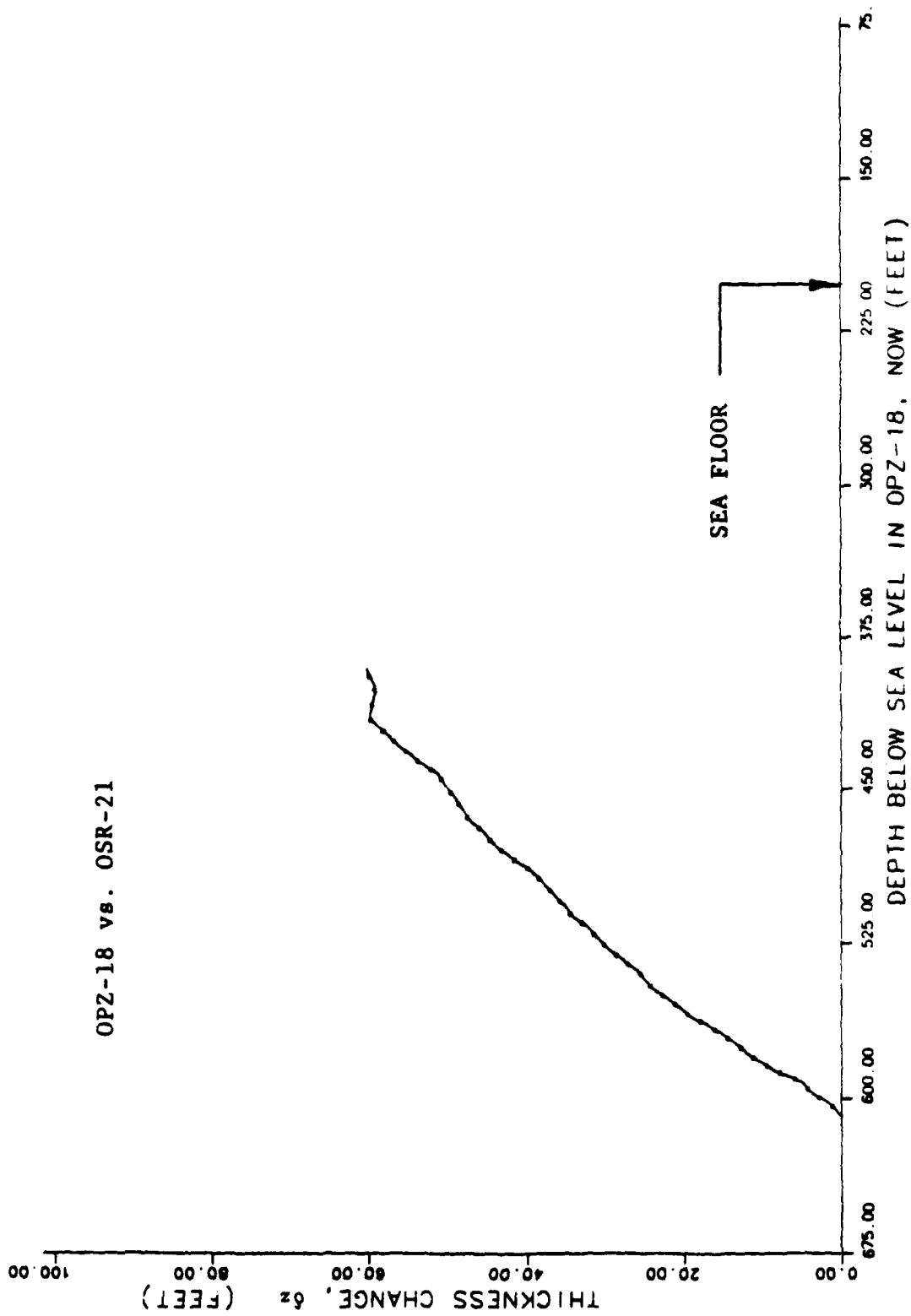


FIGURE 6-46. --- Change in rock thickness from Y-Y densities, assuming simple subsidence. Borehole OPZ-18 vs. OSR-21.

OPZ-18 vs. OAR-2A

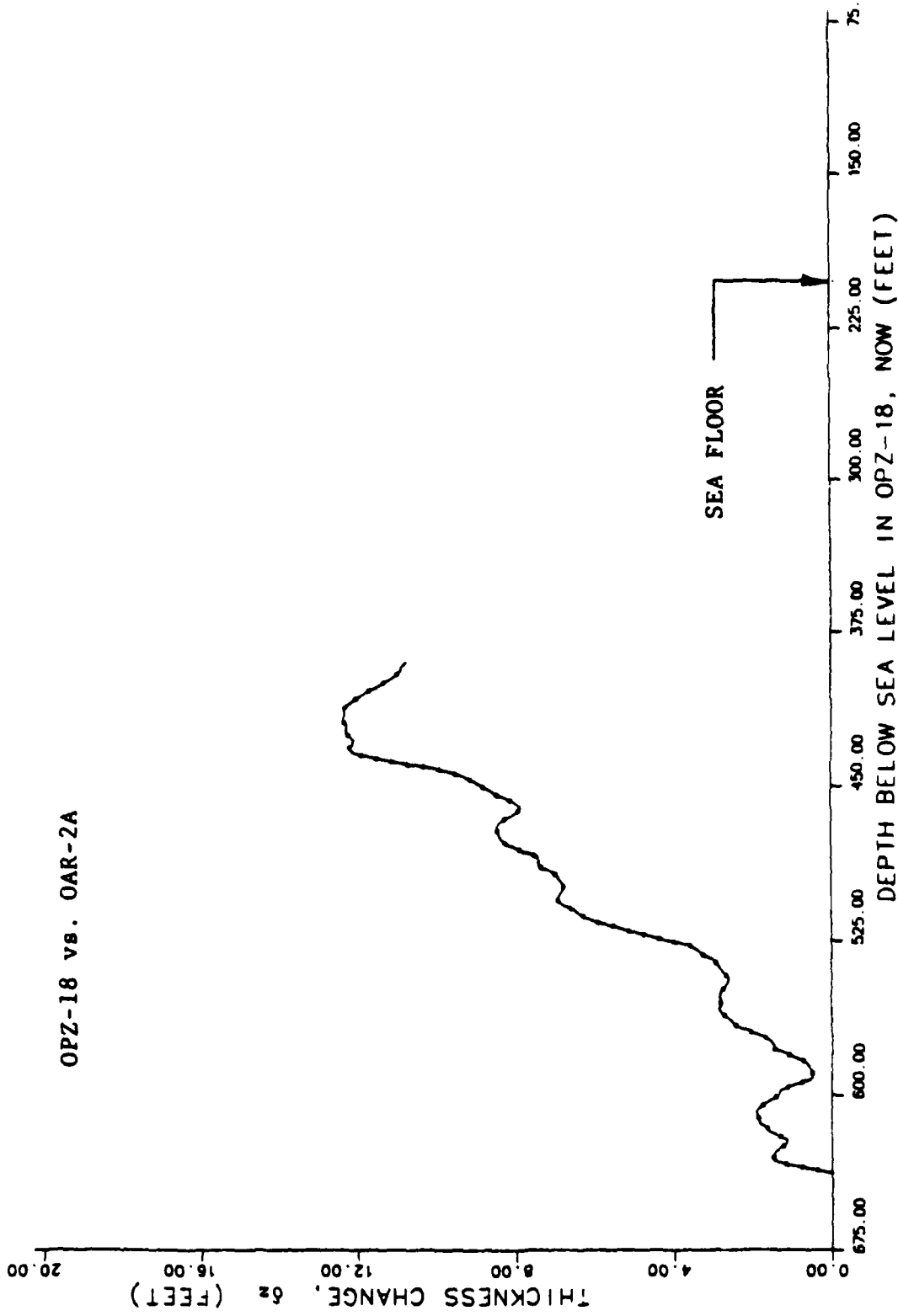


FIGURE 6-47. -- Change in rock thickness from γ - γ densities, assuming simple subsidence. Borehole OPZ-18 vs. OAR-2A.

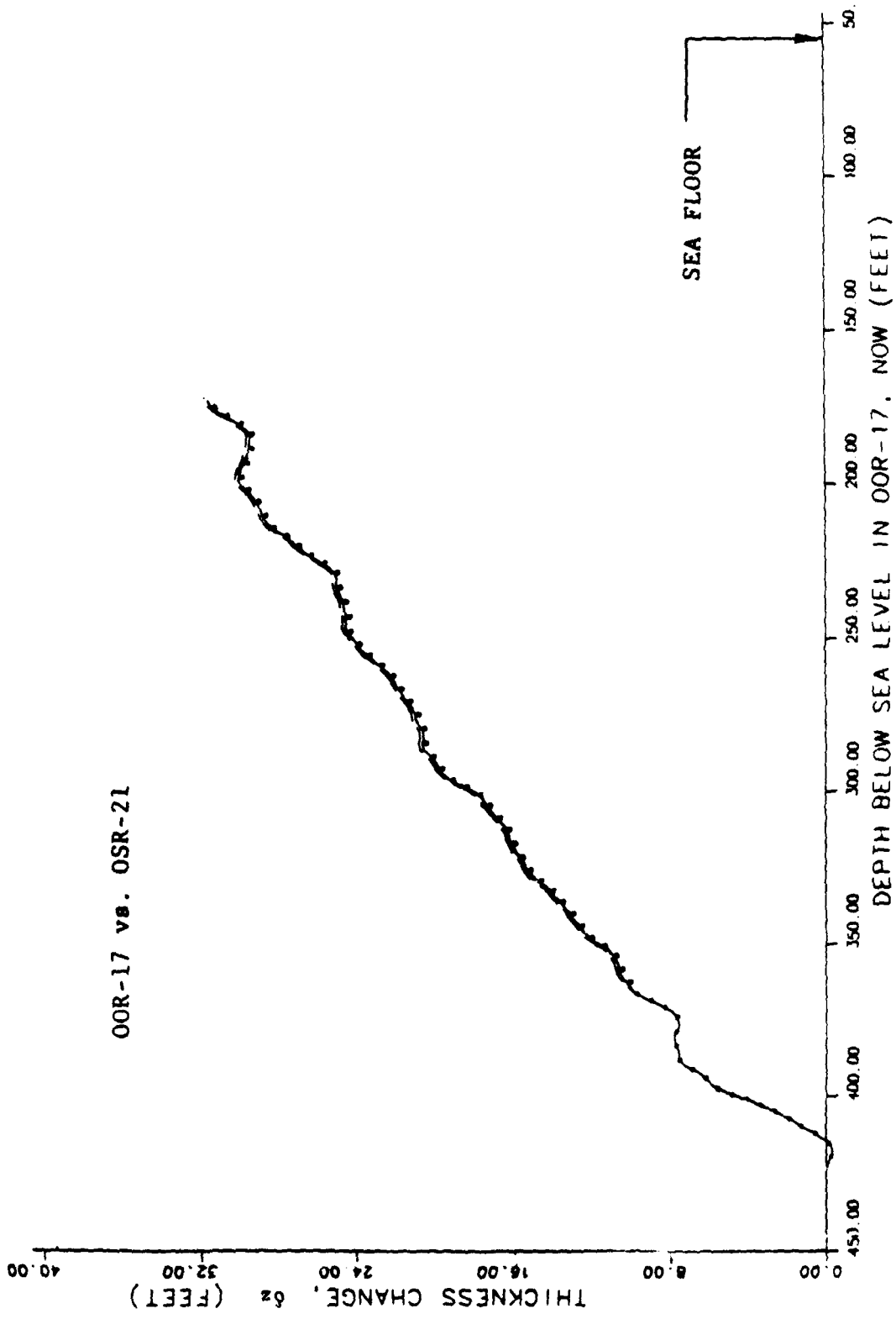


FIGURE 6-48. -- Change in rock thickness from γ - γ densities, assuming simple subsidence. Borehole OOR-17 vs. OSR-21.

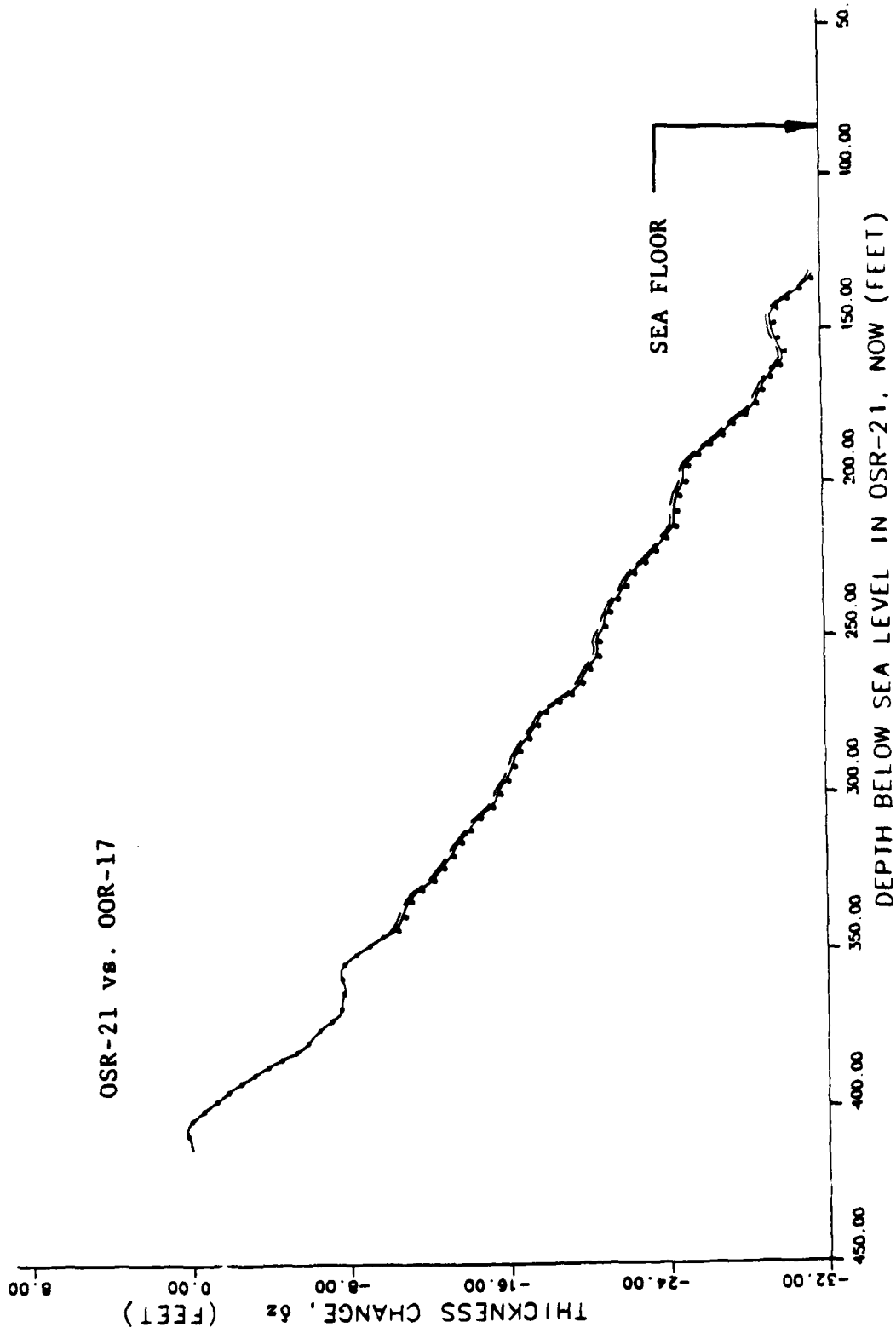


FIGURE 6-49. -- Change in rock thickness from γ - γ densities, assuming simple subsidence. Borehole OSR-21 vs. OOR-17.

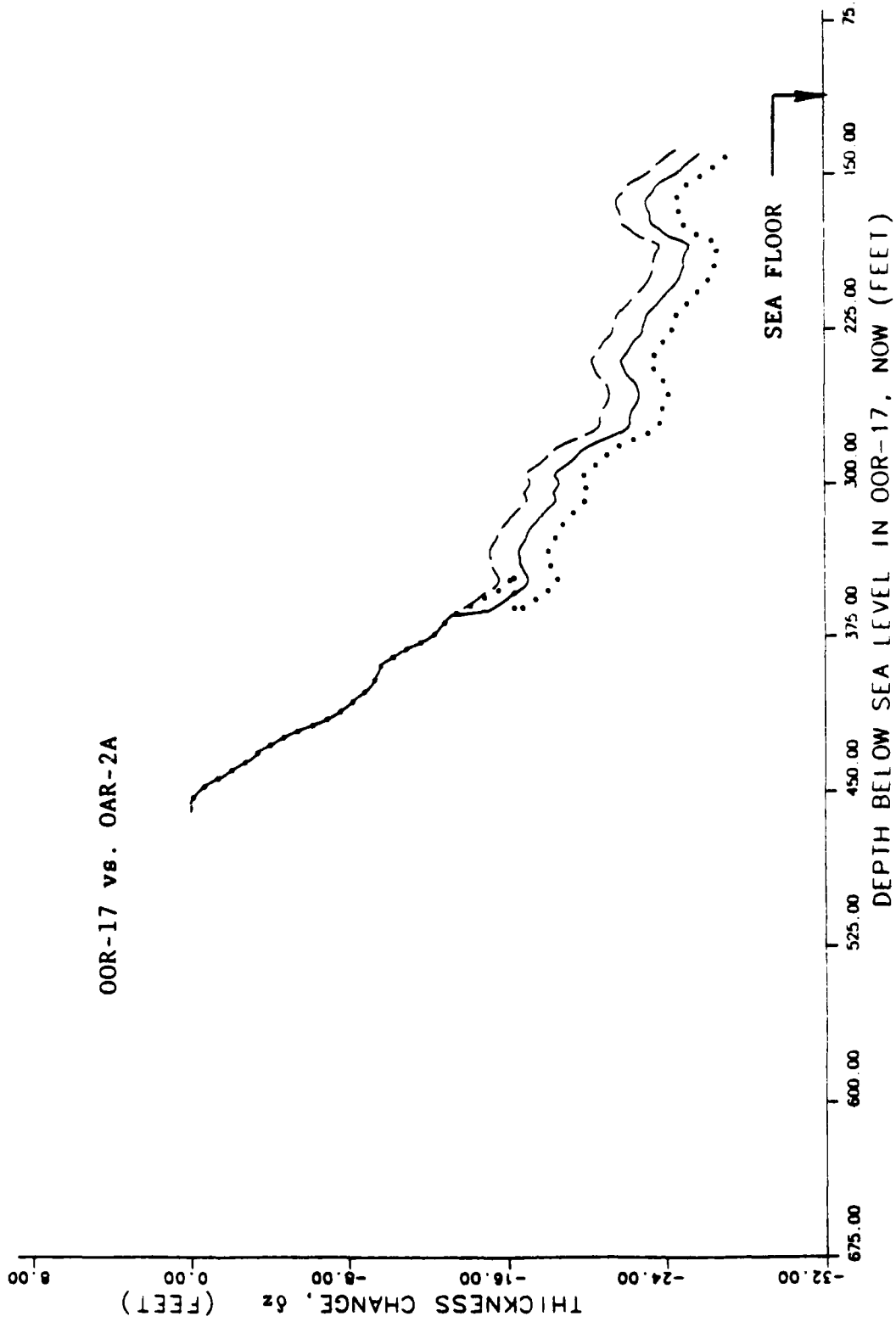


FIGURE 6-50. -- Change in rock thickness from γ - γ densities, assuming simple subsidence. Borehole OOR-17 vs. OAR-2A.

OAR-2A vs. OOR-17

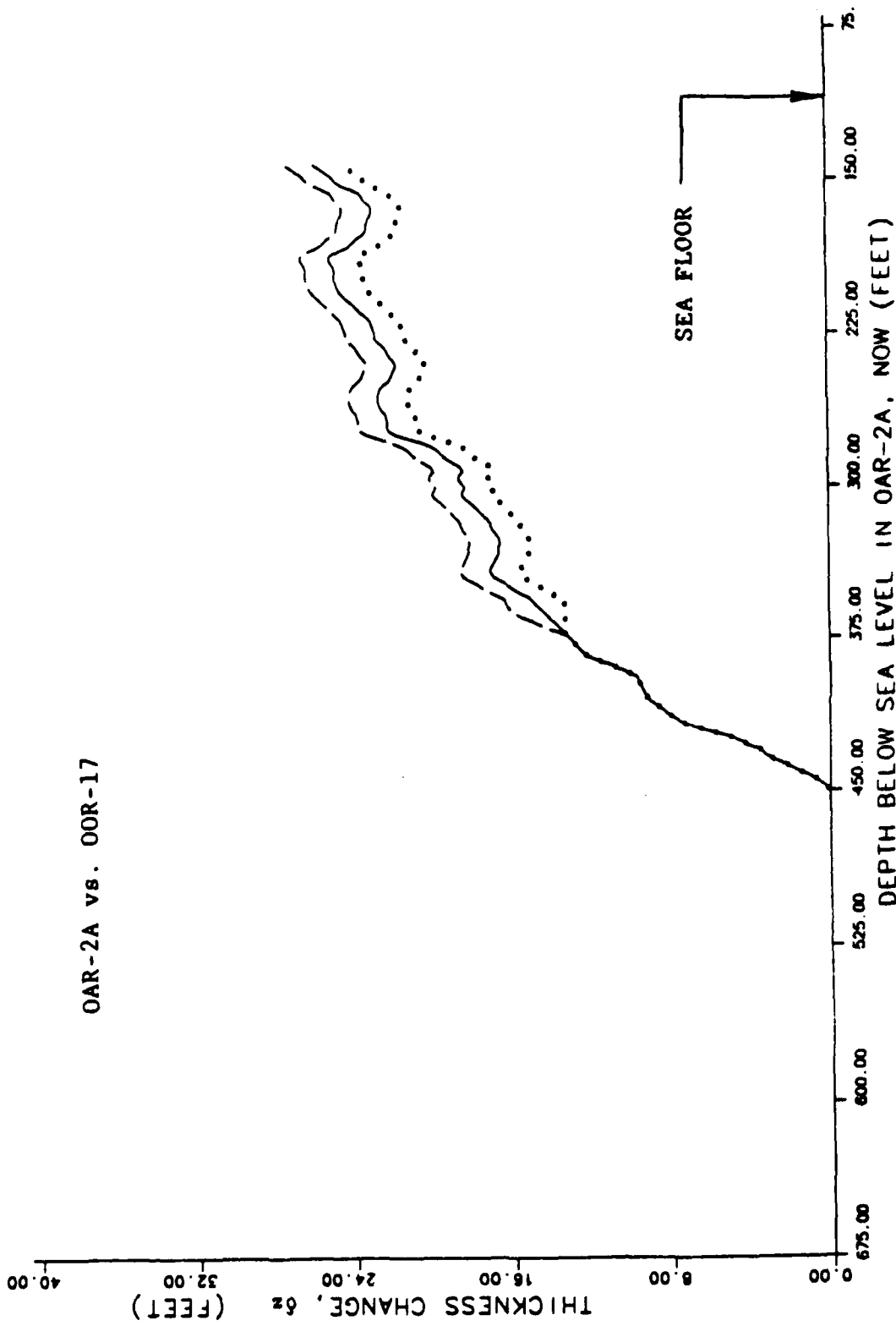


FIGURE 6-51. -- Change in rock thickness from γ - γ densities, assuming simple subsidence. Borehole OAR-2A vs. OOR-17.

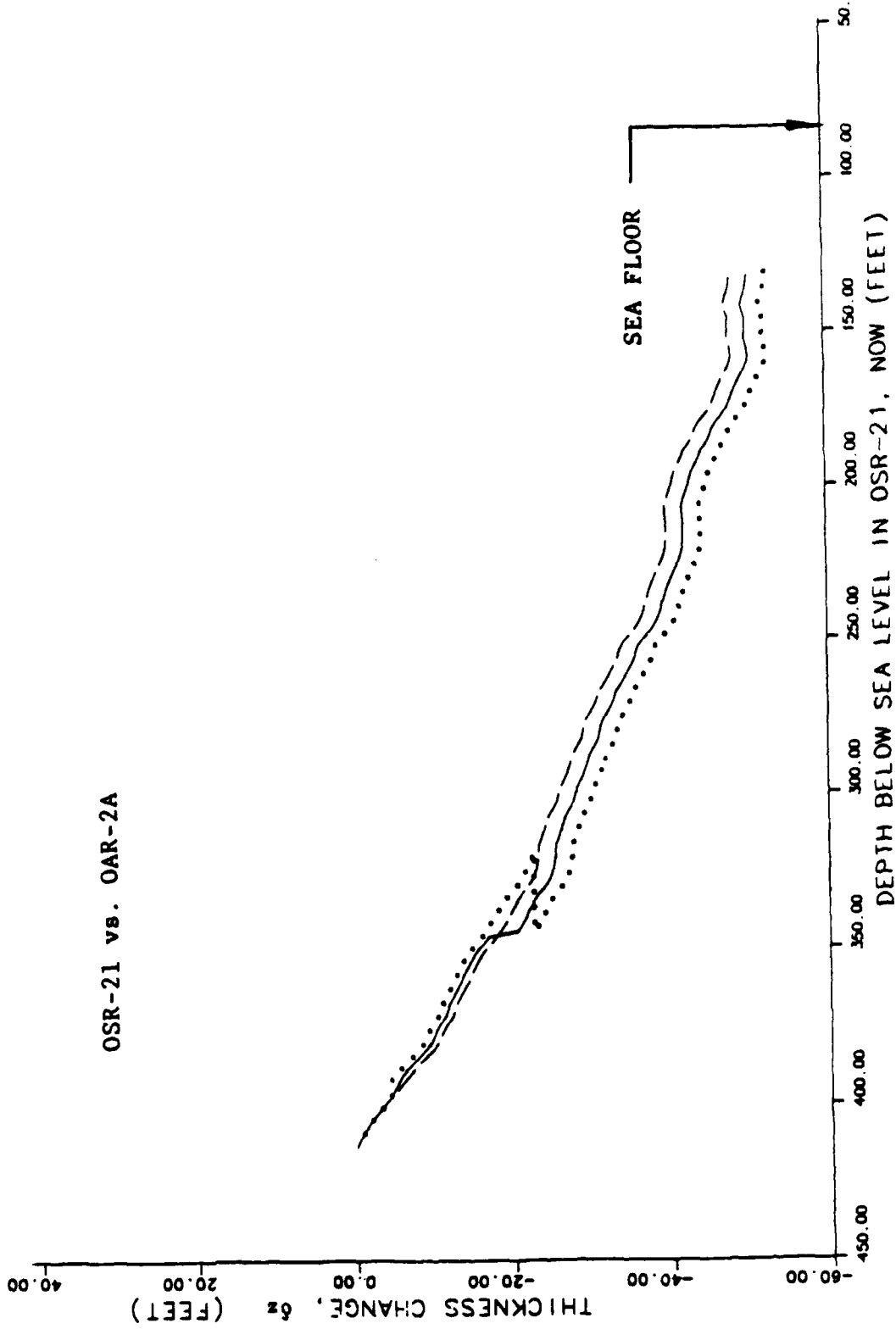


FIGURE 6-52. -- Change in rock thickness from γ - γ densities, assuming simple subsidence. Borehole OSR-21 vs. OAR-2A.

OAR-2A vs. OSR-21

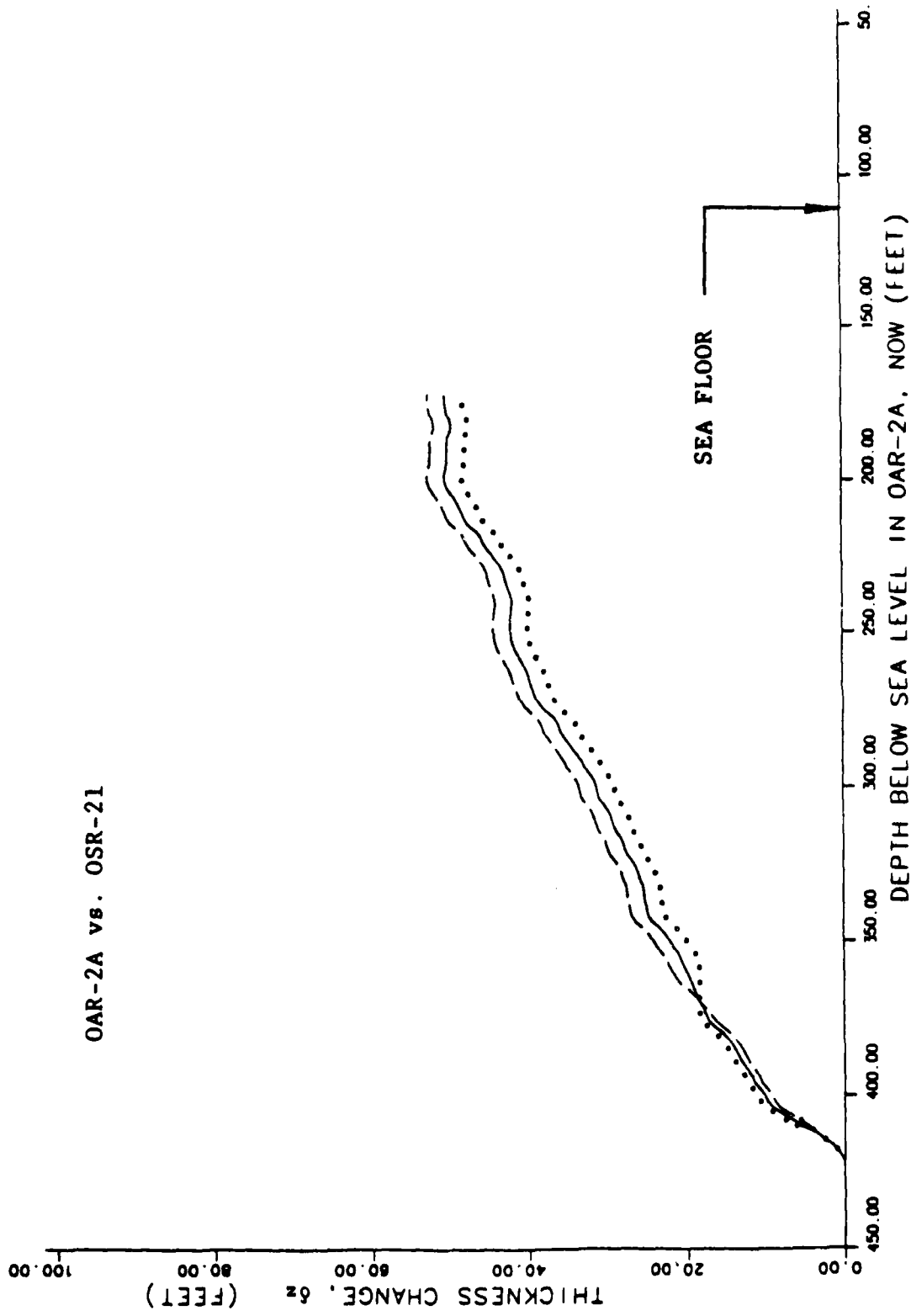


FIGURE 6-53. -- Change in rock thickness from γ - γ densities, assuming simple subsidence. Borehole OAR-2A vs. OSR-21.

CHAPTER 7:
INTEGRATION OF MATERIAL-PROPERTY UNITS, GRAVIMETRY,
AND ADDITIONAL STUDIES OF OAK AND KOA CRATERS

By

Bruce R. Wardlaw

INTRODUCTION

Preliminary interpretations of the geology of the OAK and KOA crater areas and of the craters themselves are presented in Wardlaw and Henry (1986a, 1986b). Since those reports, additional information was developed from analyses of borehole gravimetry, paleontologic mixing, thinning, and distribution of shocked calcite, most of which are presented in previous Chapters of the current Open-File Report. These new data require modification of the geologic interpretation of OAK and KOA craters. This Chapter incorporates these new salient data and presents a more comprehensive interpretation than that given by Wardlaw and Henry (1986b). Depths to a few horizons or zones have been reinterpreted, and all pertinent data are presented herein in corrected form as tables. These data supercede all previous information.

The most convenient way to relate the geology to crater phenomenology is to develop geologic material-property units that match the general material-property models for OAK and KOA craters. The geologic framework is reviewed briefly before presentation of the new geologic material-property units (MPs). These units will be used throughout this text in deference to previously used geologic schemes such as the sedimentary packages (SPs) of Wardlaw and Henry (1986a).

PRE-EVENT GEOLOGY OF OAK AND KOA CRATERS

The general stratigraphic sequence of Enewetak Atoll is punctuated by a series of discontinuities within the carbonate sedimentary rock column, of which nine are identified as major disconformities in the upper 1,200 ft (Wardlaw and Henry, 1986a). These major disconformities represent significant exposure and cementation surfaces over most of the atoll. Generally, pervasive cementation is confined to the reef margin (fig. 7-1a), but extends for a considerable distance beneath the lagoon beneath disconformities 5, 8, and 9 (fig. 7-2). Data from the EXPOE Project (Couch and others, 1975), which presents data from shallow boreholes drilled on islands on the reef tract, indicate that the geology is generally similar throughout the reef tract (fig. 7-1c), although the width of the cemented reef margin narrows on the leeward side of the atoll. Cementation also appears to generally decrease in areal distribution in the sequence from disconformity 5 (Pliocene) to disconformity 1

1 Branch of Paleontology and Stratigraphy,
U.S. Geological Survey, Reston, VA 22092.

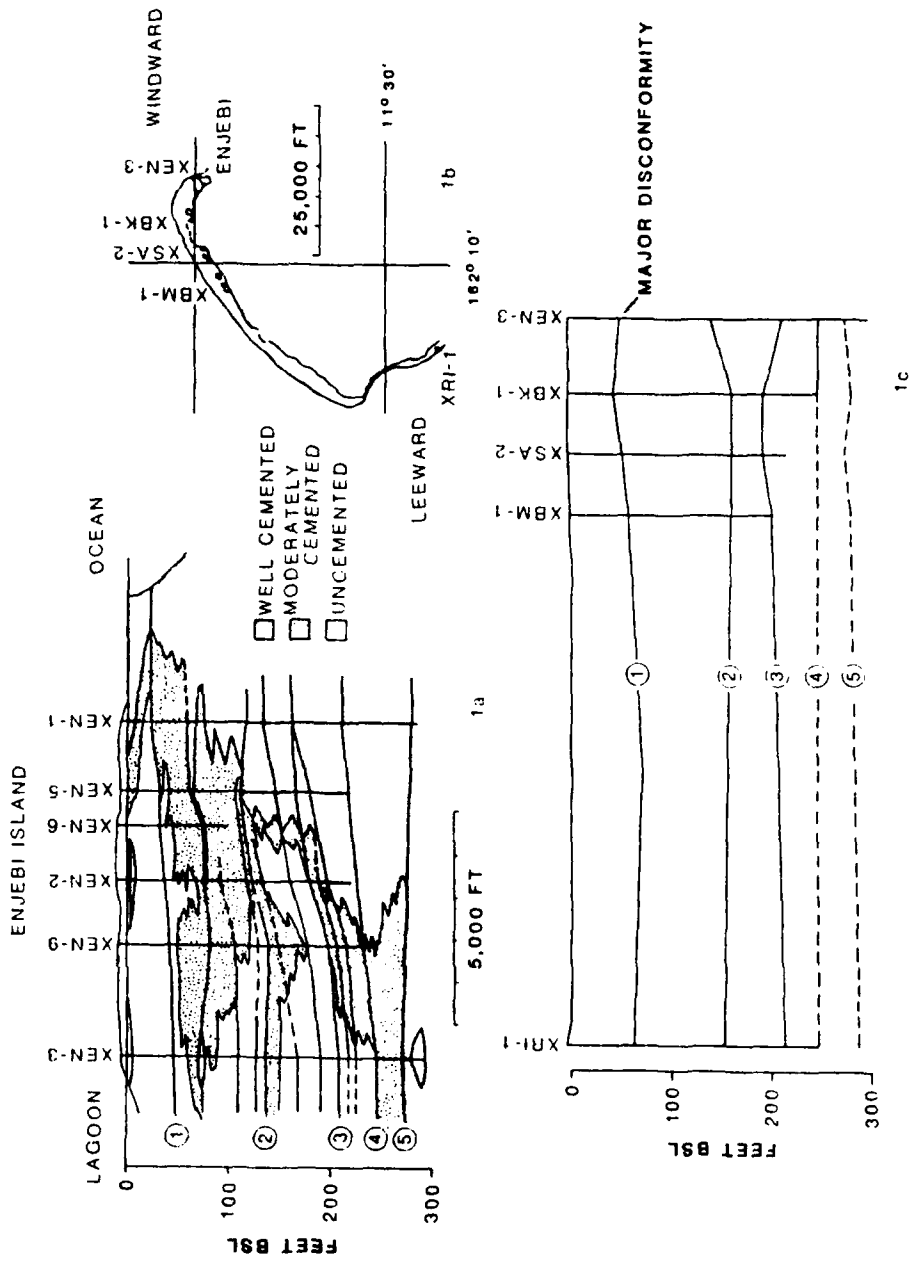


FIGURE 7-1. -- (1a) Distribution of cemented zones in shallow subsurface in transect on Enjebi Island from reef to lagoon from EXPOE cores (modified from Ristvet and others, 1978). (1b) Location of boreholes for 1c. (1c) Relationship of major discontinuities (1-5) in shallow subsurface on northern and western portion of Enewetak Atoll.

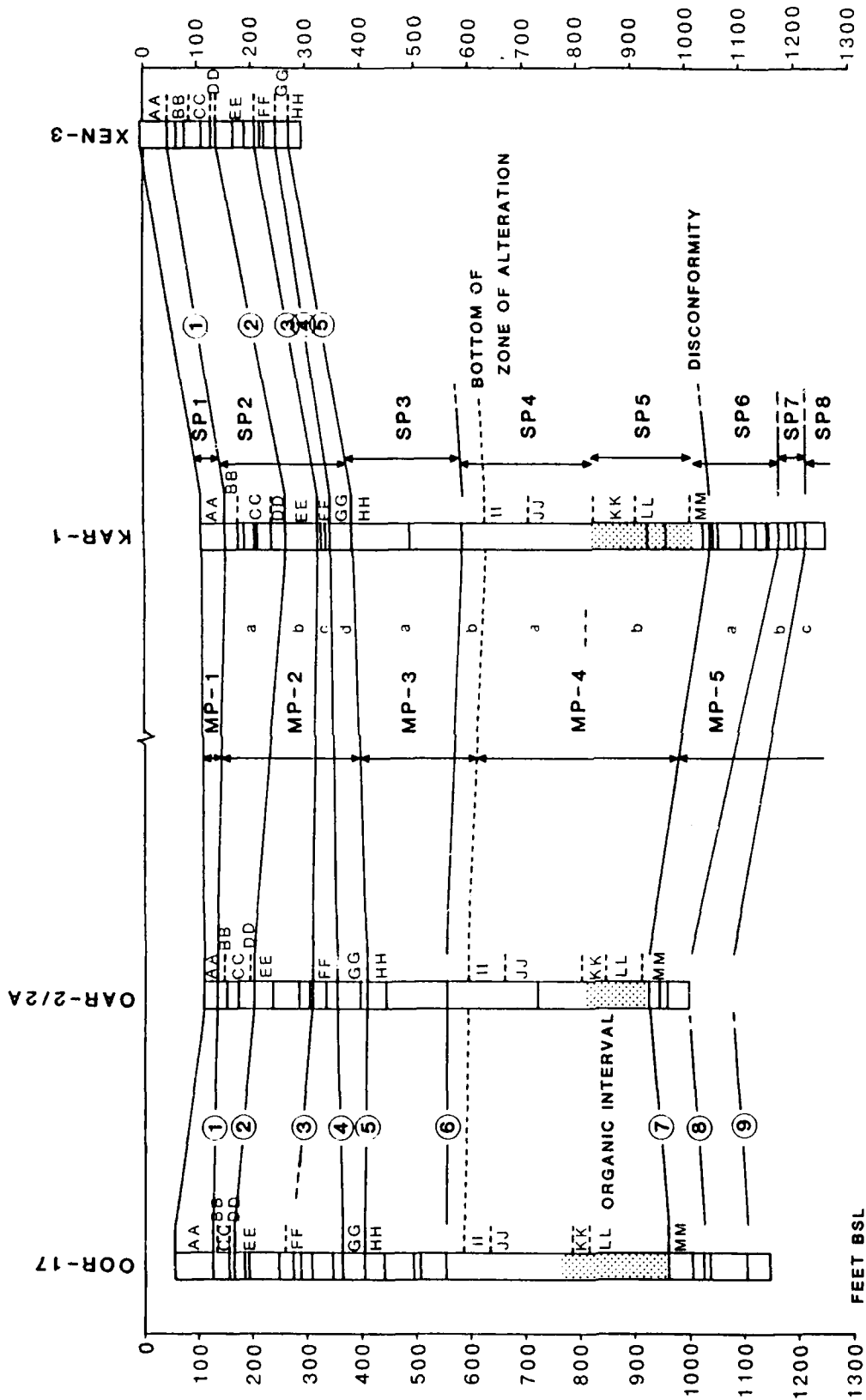


FIGURE 7-2. -- Relationship of discontinuities (shown in columns), major discontinuities (1-9), biostratigraphic zones (AA-MM), material property units (MP-1 to MP-5), and sedimentary packages (SP1 to SP8) in reference boreholes. Highly organic zone (SP5) is stippled in columns.

(Pleistocene) as represented in the cross section of Figure 7-1a. From disconformity 1 to the present surface, the area of cementation has increased (fig. 7-1a).

The major disconformities (Wardlaw and Henry, 1986a) and the biostratigraphic zones, based on the distribution of microfossils presented by Cronin, Brouwers, and others (1986), generally correlate readily from borehole to borehole and extend throughout the area of investigation (fig. 7-2). The sedimentary packages (SP) delimited by these disconformities (Wardlaw and Henry, 1986a) and the geologically defined material-property units (MP) proposed herein also are shown on Figure 7-2. The consistency and trends of the disconformities, the SP and MP units, and biostratigraphic zones allow reasonable prediction of pre-shot ground-zero geology for both OAK and KOA. The relationship of discontinuities, cementation zones, and general sediment type for the PEACE Program reference boreholes and the models of ground-zero geology for both OAK and KOA are shown in Figure 7-3. Excellent seismic-reflection profiles (Grow and others, 1986) allow mapping of key surfaces in the undisturbed areas away from the craters, and, combined with the pre-shot geologic models, allow mapping of the probable distribution of these surfaces in a pre-shot configuration below the crater (Wardlaw and Henry, 1986b). Figure 7-4 shows the probable pre-shot surfaces at the top of the Pleistocene (disconformity 1) and at the top of the Pliocene (disconformity 5) in the KOA and OAK areas.

The most convenient way to summarize the geology for crater considerations is in material-property (MP) units. These are units delimited by major geologic horizons that best fit the material model (viz, the geologically defined units that best conform to the mechanical properties important to cratering). Differences between the sedimentary packages (SP) and material-property units are minor (see below) but include, for example, the pervasively cemented zone that includes SP3 and the upper part of SP4 is represented as a single unit (MP-3), although it is divided by a major disconformity (6) that represents a significant exposure surface and geologic gap.

The upper 1,200 feet of sedimentary section at Enewetak is divided into five material-property units (fig. 7-3), as follows:

- MP-1** (Holocene, Sedimentary Package 1). -- Aragonitic sediments, from the surface to disconformity 1.
- MP-2** (Pleistocene, SP 2). -- Aragonitic sediments with thin calcitic limestones, from disconformity 1 to 5. This unit is subdivided by disconformities 2, 3, and 4.
- MP-3** (Upper Pliocene, SP 3 and part of SP 4). -- Cemented interval of vuggy, calcitic limestone and aragonitic or calcitic sands, from disconformity 5 to the base of the alteration zone (see Wardlaw and Henry, 1986b, p. 25 for discussion of alteration zone). This unit is subdivided by disconformity 6.
- MP-4** (Upper Miocene-Pliocene, part of SP 4, all of SP 5). -- Aragonitic sands, from base of the alteration zone to disconformity 7. High organic content and high activity on the natural gamma logs identifies a lower subunit.
- MP-5** (Miocene, SP 6, SP 7, and SP 8). -- Calcitic sands and limestones, limestone variably developed, from disconformity 7 to bottom of boreholes. This unit is subdivided by disconformities 8 and 9.

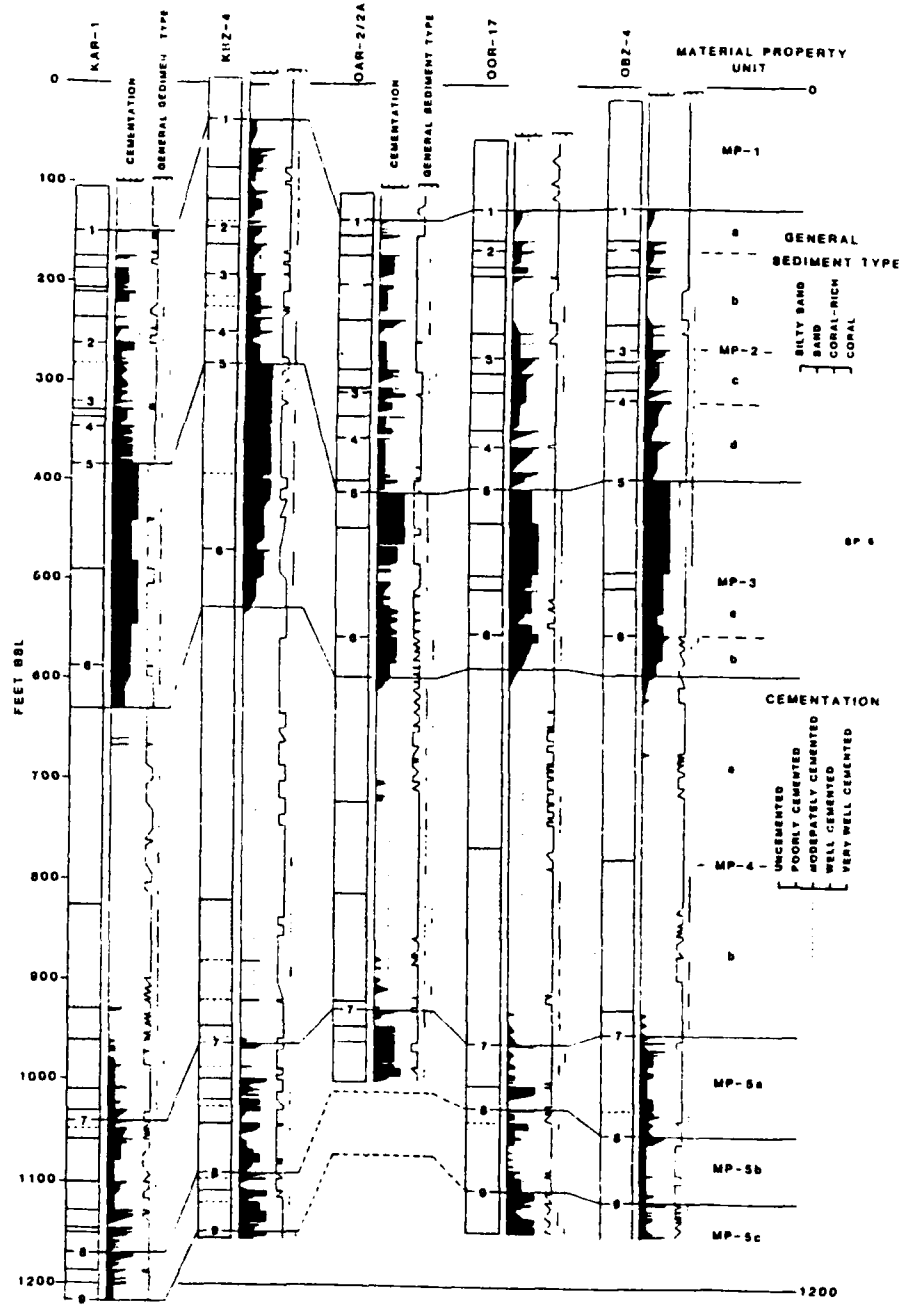


FIGURE 7-3. -- Characterization of cementation and general sediment type and relationship to material property units for reference boreholes and models for ground-zero geology. Discontinuities as lines in columns, major disconformities numbered in columns.

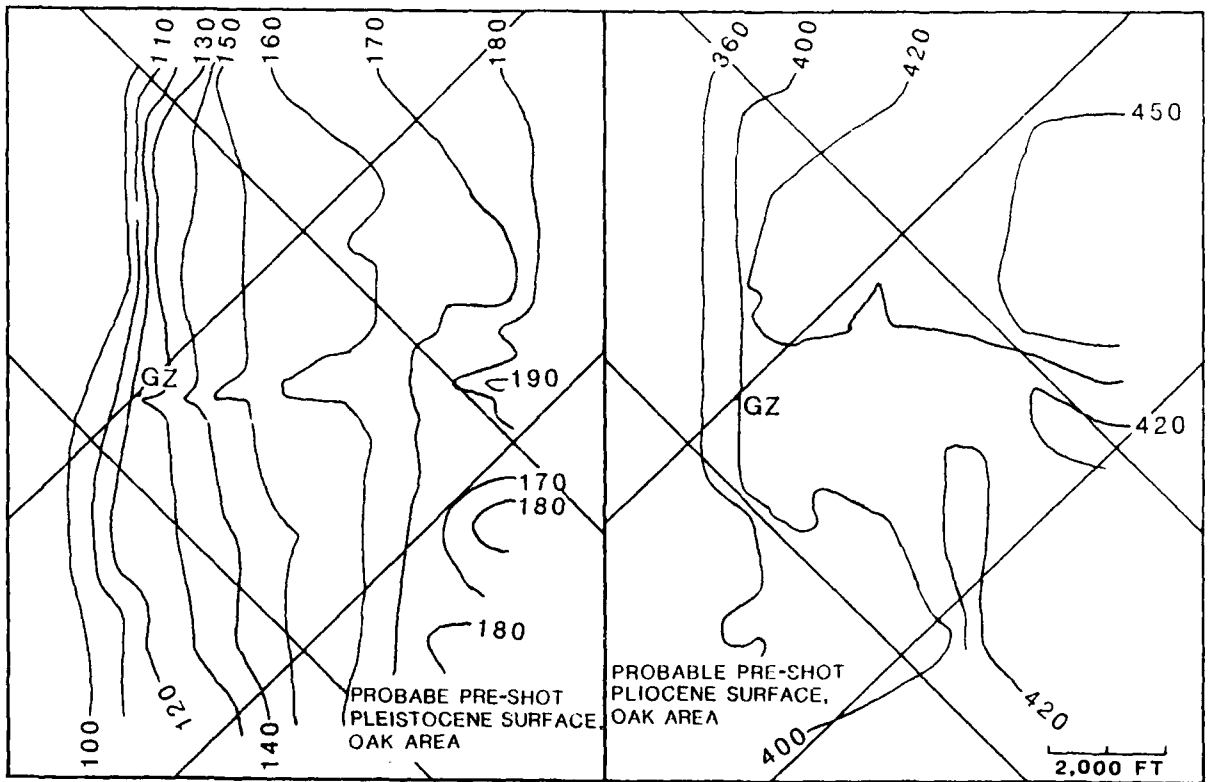
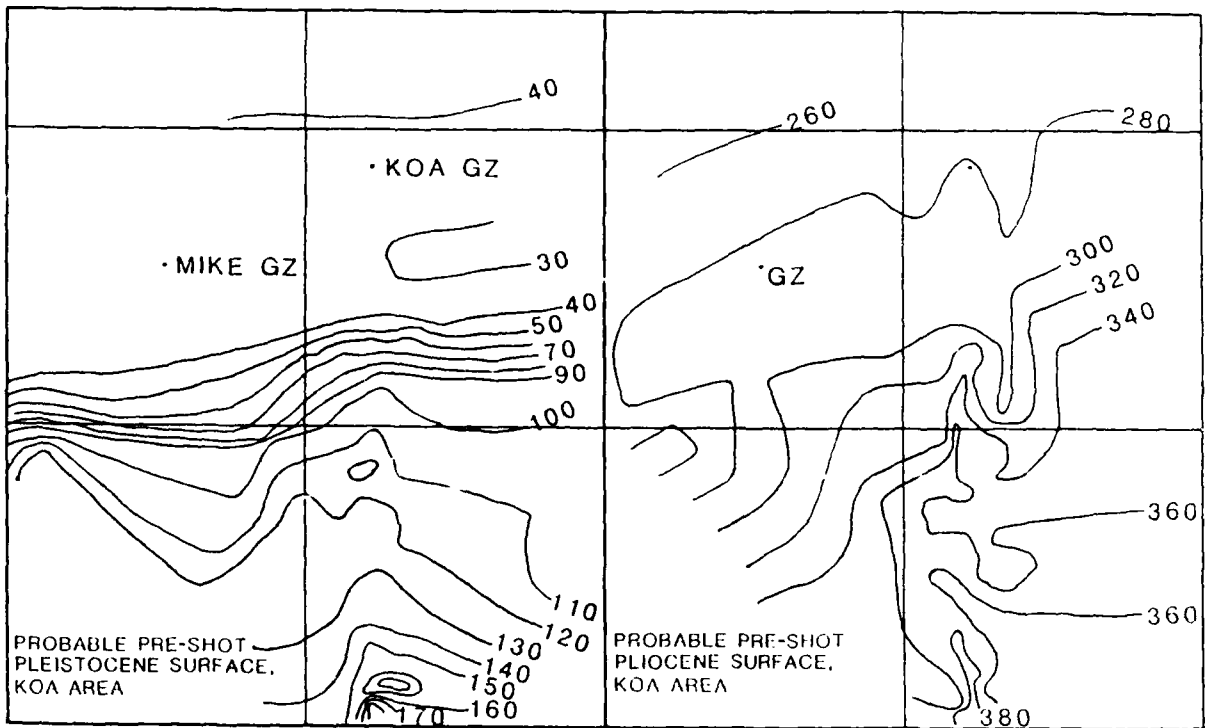


FIGURE 7-4. -- Probable pre-shot surfaces for the Pleistocene (Disconformity 1) and Pliocene (Disconformity 5) in the KOA and OAK areas. Contours in feet.

The pre-event subsurface geology in the KOA and OAK areas differs in three significant ways (fig. 7-5):

- (1). MP-2d is more consistently well-cemented in the KOA area.
- (2). MP-3 (the upper, well-cemented unit) is thicker (246 ft vs 197 ft) and shallower (top at 282 ft vs 395 ft bsl¹) in the KOA area.
- (3). MP-3 is homogeneous throughout the crater area at KOA. At OAK, this unit changes from a cemented limestone with calcitic sands beneath the reef tract to cemented limestone with aragonitic sands beneath the lagoon, and the cemented intervals appear to decrease in thickness lagoonward (contrast OAR-2/2A to OOR-17; see fig. 7-3).

In addition, the pre-event ground surfaces in OAK and KOA areas differ significantly. KOA is represented by a nearly flat shallow surface on a broad reef tract, whereas OAK is represented by a narrow, shallow reef tract, relatively steep slope, and a flat, deep lagoon bottom.

POST-EVENT GEOLOGY OF OAK AND KOA CRATERS

The excavational craters were modified profoundly by a set of processes that included shock-induced liquefaction and consolidation, subsequent flow and piping of liquefied materials from depth (both laterally and toward and/or to the surface), consequent subsidence of the region adjacent to and beneath the excavational craters, and major and repeated failures of the sidewalls of the initial and subsequent craters.

Crater Zones

OAK and KOA craters can be characterized in the subsurface by geologic, paleontologic, and seismic-reflection crater zones that, in turn, can be related to crater-event history.

Traditional crater terminology does not always adequately apply to the Enewetak craters studied; many subsurface features within the carbonate rock and sediment virtually were undescribed. Thus, limited new terminology was introduced by Wardlaw and Henry (1986b), and a few additional terms are introduced in the current Chapter (designated by an asterisk, *).

Geologic Crater Zones

1. Zone of sonic degradation (ZSD): the stratigraphic interval in which sonic velocities are depressed below expected velocities. Normal or (more correctly) pre-event sonic velocities are determined from the sonic signature of reference boreholes. On the multichannel-seismic profiles, the ZSD appears as a "fuzzy" area in which seismic reflectors are not coherent and are surrounded by an area where

¹ Below sea level is abbreviated bsl throughout this Volume.

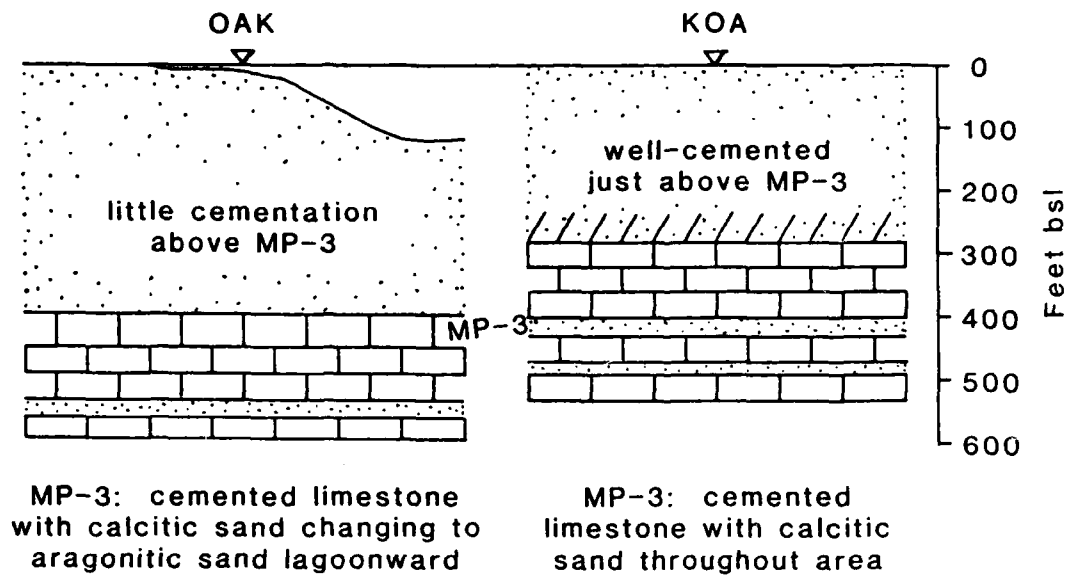


FIGURE 7-5. -- Comparison of pre-shot ground surface and subsurface geology for the OAK and KOA areas.

coherent reflectors are present but downturned. The ZSD represents units of rock and sediment that are fractured or shattered, mixed, and/or otherwise disturbed significantly enough to retard the sonic velocities relative to what they were before the nuclear events occurred. All geologic crater zones lie within the ZSD (fig. 7-6).

2. Geologic crater: the subsurface expression of the crater defined by the ZSD. The geologic crater zones encountered in the central crater are as follows:
3. Alpha 1 (α_1): Mud. Late-stage, fine-grained sediments with abundant brown, piped material in OAK.
4. Alpha 2 (α_2): Graded sand (distal) and slumps (proximal). Late-stage slope-failure and sand-turbidite flow deposits containing abundant brown, piped material. (Proximal means near material source; distal means far from the material source).
5. Beta 1a (β_{1a}): Graded Rubble. (*) This zone contains proximal rubble and distal sand (as in OPZ-18) with granules of rubblized material. The zone is transitional from the rubble below and slumps above and contains abundant brown, piped material near the top in the central crater area. Both Alpha 2 and Beta 1a show high gamma-ray activity (see fig. 7-17).
6. Beta 1s* (β_{1s}): Hiatus sand. (*) Highly shocked, uppermost unit (MP-1, Holocene) sediments.
7. Beta 1b (β_{1b}): Collapse rubble. (*) Thick rubble bed with sparse brown piped material within the zone in the central crater area. Both zones Beta 1a and Beta 1b are less distinct in the central-most part of the crater, and Beta 1s is missing in the same area because of mixing primarily due to late-stage pipping.
8. Beta 2 (β_2): Transition sand. Pulverized sand within the transition paleontologic zone (see below). It has a limited lateral extent. The sand grains show fractured surfaces but no internal microfracturing.
9. Beta 3 (β_3): Rubble floatstone. Rubble in which no paleontologic mixing can be shown.
10. Gamma (γ): Fractured and displaced rock and sediment.
11. Delta (δ): Fractured but undisplaced rock and sediment.

The base of the zone of sonic degradation:

12. Epsilon (ϵ): In-place, relatively unfractured stratigraphic section; outside and beneath the geologic crater.

The geologic crater zones in the debris blanket are as follows:

13. Beta 1a* (β_{1a}^*): Graded sand and rubble *. This zone is found only in boreholes OHT-10 and OJT-12 and may be related to a large collapse and debris flow that breached the debris blanket and flowed into the

lagoon (as seen on the OAK enhanced sea-floor image, Folger and others, 1986).

14. Beta 1b* (β_{1b}^*), or Beta (β) undifferentiated: Rubble. Debris with no brown piped material.
15. Disturbed zone: This zone represents slightly altered stratigraphy with no apparent discontinuities.
16. Delta (δ) and Epsilon (ϵ): Relatively unaffected stratigraphy.

The depths to various crater zones for the transition and ground-zero boreholes for both OAK and KOA craters are given in Table 7-2, and graphically displayed in fence diagrams in Figures 7-7 to 7-10. Interpretations of geologic crater zones on seismic reflection profiles through ground-zero for both OAK and KOA crater (from Wardlaw and Henry, 1986b) are shown in Figures 7-11 and 7-12.

Paleontologic Crater Zones

The paleontologic crater zones for the **central crater** follow. The depths to various paleontologic crater zones for both OAK and KOA craters are given in Table 7-3.

1. Mixed: Fossils from various biostratigraphic zones are mixed together. This zone can be crudely divided into three subzones:
 - a. Very mixed with material from mostly upper biostratigraphic zones and piped material from deeper zones.
 - b. Mixed material from most of MP-1 and MP-2 plus piped material that decreases in degree of mixing downward.
 - c. Mixed material from mostly lower biostratigraphic zones of crater and sparse piped material.

These zones were developed for KOA crater (Wardlaw and Henry, 1986b) and are applicable to OAK with minor modification. In OAK, an additional zone, represented by the "hiatus sand" (Beta 1s), occurs between paleontologic subzones b and c in the lateral part of the crater. This unit consists predominantly of Holocene (near-surface) material and shows little mixing.

2. Transition: Transitional paleontology from mixed to unmixed.
3. Unmixed: Paleontology in normal succession showing no mixing of materials from different biostratigraphic zones.

The paleontologic crater zones for **debris blanket** are:

4. Mixed, undifferentiated: generally like unit 1b within the crater, but without piped material.
5. Transition: as above.
6. Disturbed Zone: unmixed, but sparse faunas.
7. Unmixed: as above.

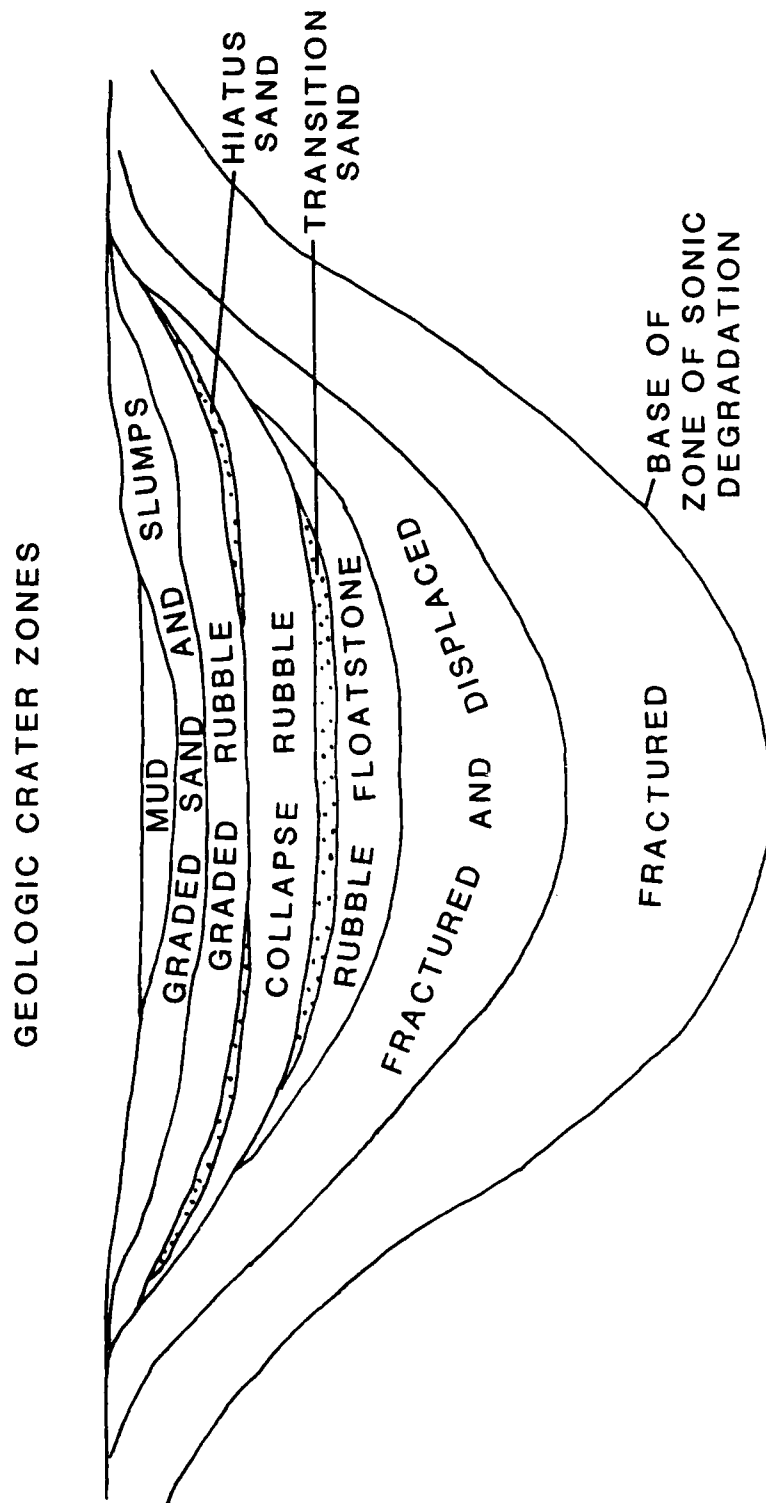


FIGURE 7-6. -- Geologic crater model.

TABLE 7-1. -- Relationship of geologic and paleontologic zones in the crater and debris blanket modified from Wardlaw and Henry (1986b). The hiatus sand { } is present only in the outer crater of OAK.

[PALEONTOLOGIC ZONES]	[GEOLOGIC ZONES]
CENTRAL CRATER	
MIXED	ALPHA 1 (α_1) Mud
a--Very mixed with mostly upper biostratigraphic zones and piped material	ALPHA 2 Graded sand (distal) (α_2) and slumps (proximal)
b--Mixed material from most units 1 and 2 and piped material, generally decreasing in mixing downward	BETA 1a Graded (β_{1a}) rubble
{Unmixed upper biostratigraphic zone}	{BETA 1s Hiatus Sand} (β_{1s})
c--Mixed material from mostly lower biostratigraphic zones and sparse piped material	BETA 1b Collapse (β_{1b}) rubble
TRANSITION	BETA 2 (β_2) Transition sand
UNMIXED	BETA 3 (β_3) Rubble floatstone
	GAMMA (γ) Fractured, displaced
	DELTA (δ) Fractured, relatively undisplaced
	EPSILON (ϵ) Relatively unfractured, in place
DEBRIS BLANKET	
MIXED (undifferentiated)	DEBRIS BETA 1a (β_{1a}) Graded (BETA) sand and rubble
TRANSITION	BETA 1b (β_{1b}) Rubble
DISTURBED	DISTURBED
UNMIXED	DELTA (δ) Fractured, relatively undisplaced
	EPSILON (ϵ) Relatively unfractured, in place

TABLE 7-2. -- Depth (ft bsl) to tops of the crater zones in OAK and KOA boreholes. ZSD = Zone of Sonic Degradation. Boreholes listed in order of increasing distance from ground-zero.

OAK AND KOA GEOLOGIC CRATER ZONES

ZONE	ç	OBZ-4	OPZ-18	OCT-5	OTG-23	OUT-24	OKT-13	OFT-8	OIT-11
Alpha 1		198.7	201.9	163.7	-	-	164.7	130.8	155.0
Alpha 2		229.2	-	164.6	164.0	147.0	165.3	131.1	
Beta 1a		271.7	246.5	174.1	174.0	249.2	177.0	139.4	155.1
Beta 1s		-	-	244.1	219.0	278.6	190.8	152.9	-
Beta 1b		309.1	337.2	310.7	235 ?	288.0	207.0	175.4	
Beta 2		394.9	377.0	-	-	-	-	-	-
Beta 3		415.1	412.3						
Gamma		564.2	522.4	346.3	314.0	332.0	227.3	204.1	171.7
ZSD		1138.7	1082.4	863.7	842.0	830.0	831.7	639.6	697.0

ZONE	ç	OET-7	OQT-19	OHT-10	OJT-12	ODT-6	ONT-16	ORT-20	OMT-15
Alpha 1		-	-	-	-	-	-	-	-
Alpha 2		106.9	-	-	-	-	-	-	-
Beta 1a		132.3	-	137.3	143.8	87.4	-	-	-
Beta 1s		-	-	-	-	-	-	-	-
Beta 1b		-	-	145.2	155.0	-	135.1	-	110.9
Beta 2		-	-	-	-	-	-	-	-
Beta 3				[191.1]	[164.7]	-	[148.0]	-	[119.8]
Gamma		156.3	117.5	286.8	238.0	91.9	176.7	101.4	139.4
ZSD		505.1	413.3	587.1	387.0	311.6	242.7	239.0	223.0

[] denotes disturbed zone

ZONE	ç	OLT-14	ç	KBZ-4	KCT-5	KFT-8	KDT-6	KET-7
Alpha 1		-	ç	109.1	-	-	-	-
Alpha 2		-	ç	137.3	98.9	77.8	56.2	-
Beta 1a		139.7	ç	167.7	120.0	96.5	79.9	-
Beta 1s		-	ç	-	154.5	-	-	-
Beta 1b		-	ç	238.5	156.1	106.0	-	-
Beta 2		-	ç	247.2	242.5	-	-	-
Beta 3		-	ç	266.2	259.9	-	-	-
Gamma		147.2	ç	316.2	274.3	153.8	110.1	51.1
ZSD		154.2	ç	1101.1	869.2	590.4	410.0	318.2

TABLE 7-3. -- Paleontologic crater zones and relation to the transition sand in OAK and KOA boreholes. Depths in ft below sea floor (ft bsf) are compatible with the footages presented in the paleontologic studies (Cronin, Brouwers, and others, 1986; Brouwers, Cronin, and Gibson, 1986; and Cronin and Gibson, 1987), which are consistently in feet below sea floor (bsf).

=====					
KOA CRATER					
	KBZ-4	KCT-5	KFT-8	KDT-6	

Mixed Zone	0-137.5	0-140.1	0-28.5	0-43.6	
Transition Zone	137.5-142	140.1-155.2	28.5-99.3	43.6-58.5	
Transition Sands	138.1-157.1	143.6-161.0	---	---	
=====					
OAK CRATER					
	OBZ-4	OPZ-18	OCT-5	OKT-13	

Mixed Zone	0-180	0-174	0-149	0-55	
Transition Zone	180-220	174-211	149-187	55-68	
Transition Sands	196.2-216.4	175.1-210.4	---	---	

	OFT-8	ODT-6			

Mixed Zone	0-64	1.8-4.4			
Transition Zone	64-74	---			
Transition Sands	---	---			

OAK CRATER DEBRIS BLANKET					
	OHT-10	OJT-12	ONT-16	OMT-15	OLT-14

Mixed Zone	0-54	0-20.9	0-12.9	0-8.9	0-7.5
Transition Zone	54-76	20.9-67	12.9-14.7	8.9-15.5	---
Disturbed Zone	76-149.5	67-94.2	14.7-41.6	15.5-28.5	---
=====					

Seismic Crater Zones

Grow, Lee, and others (1986) interpreted four subcrater seismic zones from the multichannel seismic-reflection records. They are, from top to bottom: (1) transparent zone, (2) zone of intense fracturing/depression, (3) zone of moderate fracturing/depression; and, 4, zone of minor fracturing/depression. The zone of minor fracturing/depression has not been defined in terms of depth. The seismic zones are compared to geologic craters zones in Table 7-4.

The transparent zone corresponds to the crater fill and the transition sand (where present). In OAK, reefward of SGZ, the base of the transparent zone is difficult to interpret because some large-scale slumps (crater fill) from the reef tract are not completely transparent seismically. The bottom of the zone of intense fracturing/depression falls within gamma, the zone of fracturing and displacement in KOA, and very near the bottom of the rubble zone in OAK. The bottom of the zone of moderate fracturing/depression appears to fall close to the gamma/delta transition or that change from fractured/displaced to fractured/in place material. The delta zone appears to be equivalent to the zone of minor fracturing/depression.

TABLE 7-4. -- Comparison of subcrater seismic zones to selected geologic crater zone boundaries for OAK and KOA craters.

SEISMIC ZONE	GEOLOGIC CRATER ZONE
KOA	
Bottom of Transparent Zone 262 ft bsl	Bottom of Transition Sand 266.2 ft bsl
Bottom of Zone of Intense Fracturing/Depression 460 ft bsl	Bottom of Rubble 316.2 ft bsl
Bottom of Zone of Moderate Fracturing/Depression 755 ft bsl	Bottom of ZSD 1101.1 ft bsl
OAK	
Bottom of Transparent Zone 361 ft bsl	Bottom of Transition Sand 377.0 ft bsl
Bottom of Zone of Intense Fracturing/Depression 590 ft bsl	Bottom of Rubble 564.2 ft bsl
Bottom of Zone of Moderate Fracturing/Depression 918 ft bsl	Bottom of ZSD 1138.7 ft bsl

CRATER FEATURES

Crater Material in the Lagoon

Muddy sediments in the northwestern portion of the lagoon (see fig. 7-13) are derived partly from crater material. Observations leading to this conclusion (Wardlaw and Henry, 1986b) include:

- (1). An anomalously high amount of low-Mg calcite in the sediments probably indicates mixing from diagenetically altered subsurface units.
- (2). The sediments have an anomalously high content of clay-size material, probably indicating crater-derived material. Normal lagoon sediments do not contain appreciable quantities of naturally produced clay-sized carbonate.
- (3). The sediments have measurable radioactivity, probably from the device-derived Cesium-137 (Ristvet and Tremba, 1986).

Thus, a substantial part of the mud in the northwestern portion of the lagoon (fig. 7-13) was derived from pulverization of sediment and rock particles by the nuclear detonations during the excavation of the craters. A considerable volume of fine-grained material was moved from the crater areas to the lagoon, although the volume of this lost material or proportion derived from each of the forty-one nuclear events other than OAK or KOA cannot be estimated.

Breach Deposit in the Lagoon

The enhanced sea-floor image of OAK crater displays a large flow deposit out into the lagoon (fig. 7-14). This feature extends out beyond the limits of the apparent crater, thus it, too, represents loss of material to the lagoon. This feature was not observed until after the field operations, so it was not sampled. The thickness or volume of the deposit is unknown. The deposit appears to represent a breach in the debris blanket through the "channel" (Peterson and Henny, Ch. 5 of this report, p. 5-15) and flow of material out onto the lagoon floor.

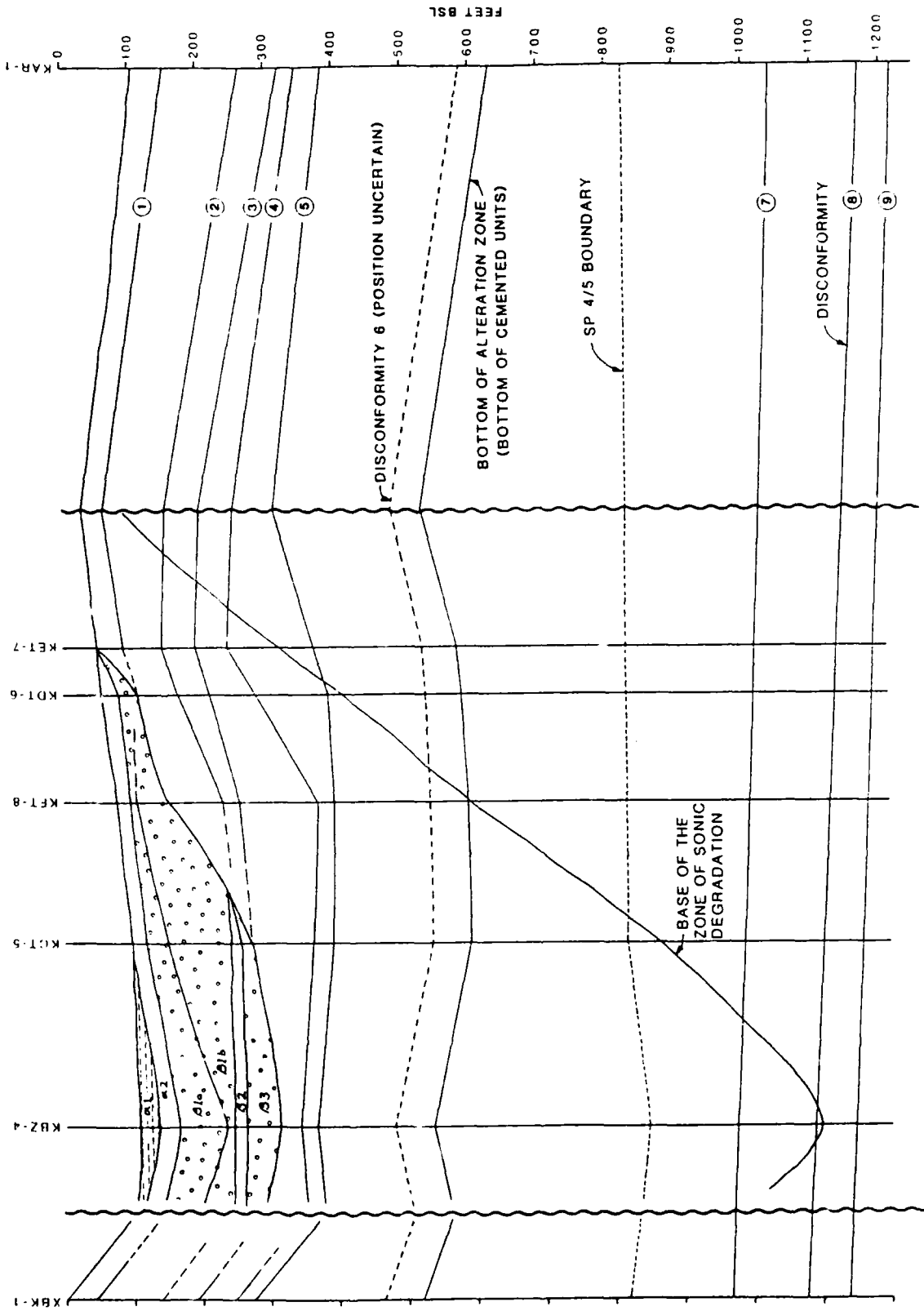


FIGURE 7-7. --- Fence diagram of KOA boreholes showing relationship of crater and geologic horizons. Scale is vertically exaggerated 2:1. Squiggly lines represent breaks to shorten the diagram.

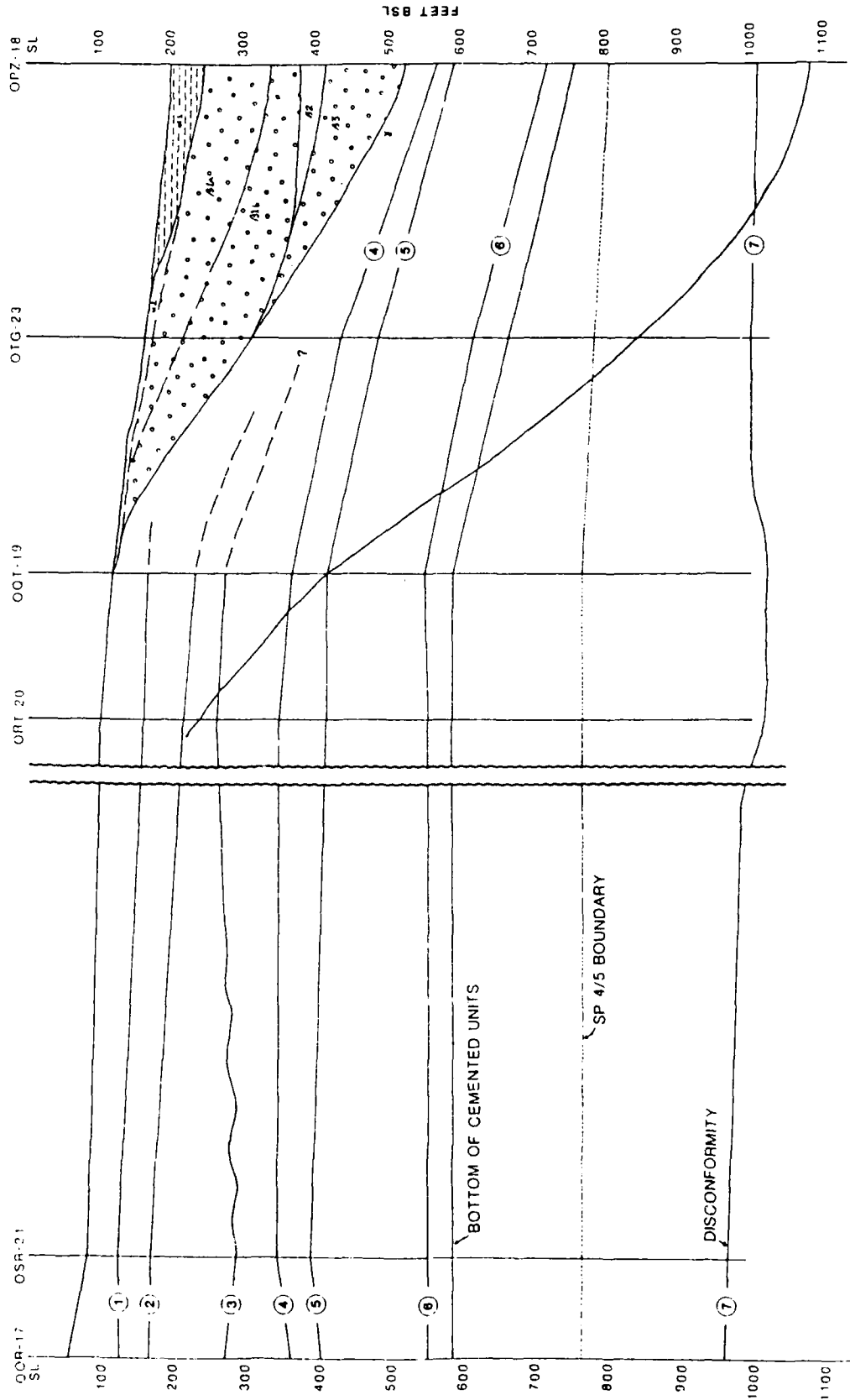


FIGURE 7-8. -- Fence diagram of OAK boreholes OOR-17 to OPZ-18 showing relationship of crater and geologic horizons. Double squiggly lines represent breaks and change in vertical exaggeration from 2:1 on right side to 4:1 on left side.

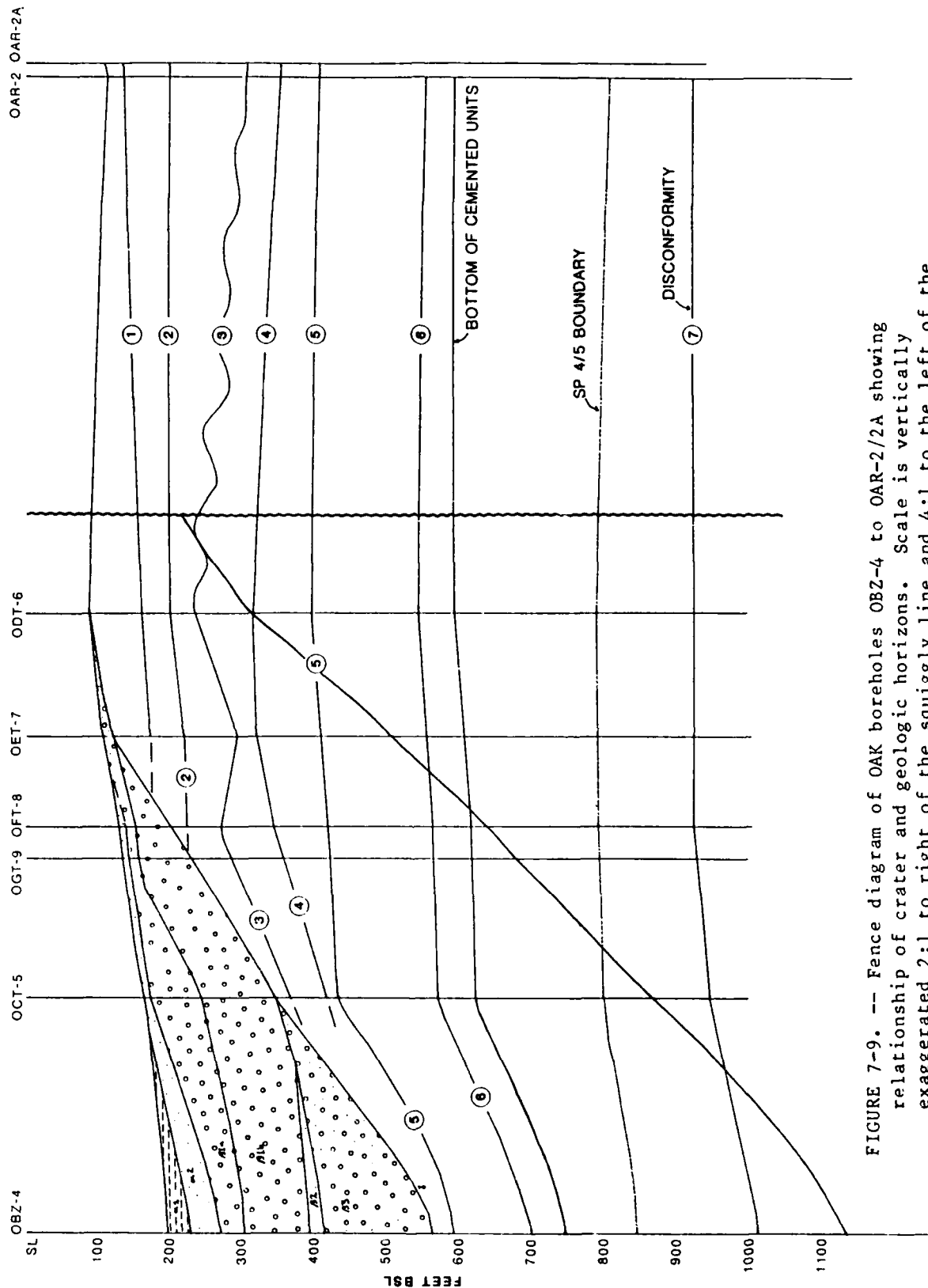


FIGURE 7-9. -- Fence diagram of OAK boreholes OBZ-4 to OAR-2/2A showing relationship of crater and geologic horizons. Scale is vertically exaggerated 2:1 to right of the squiggly line and 4:1 to the left of the line.

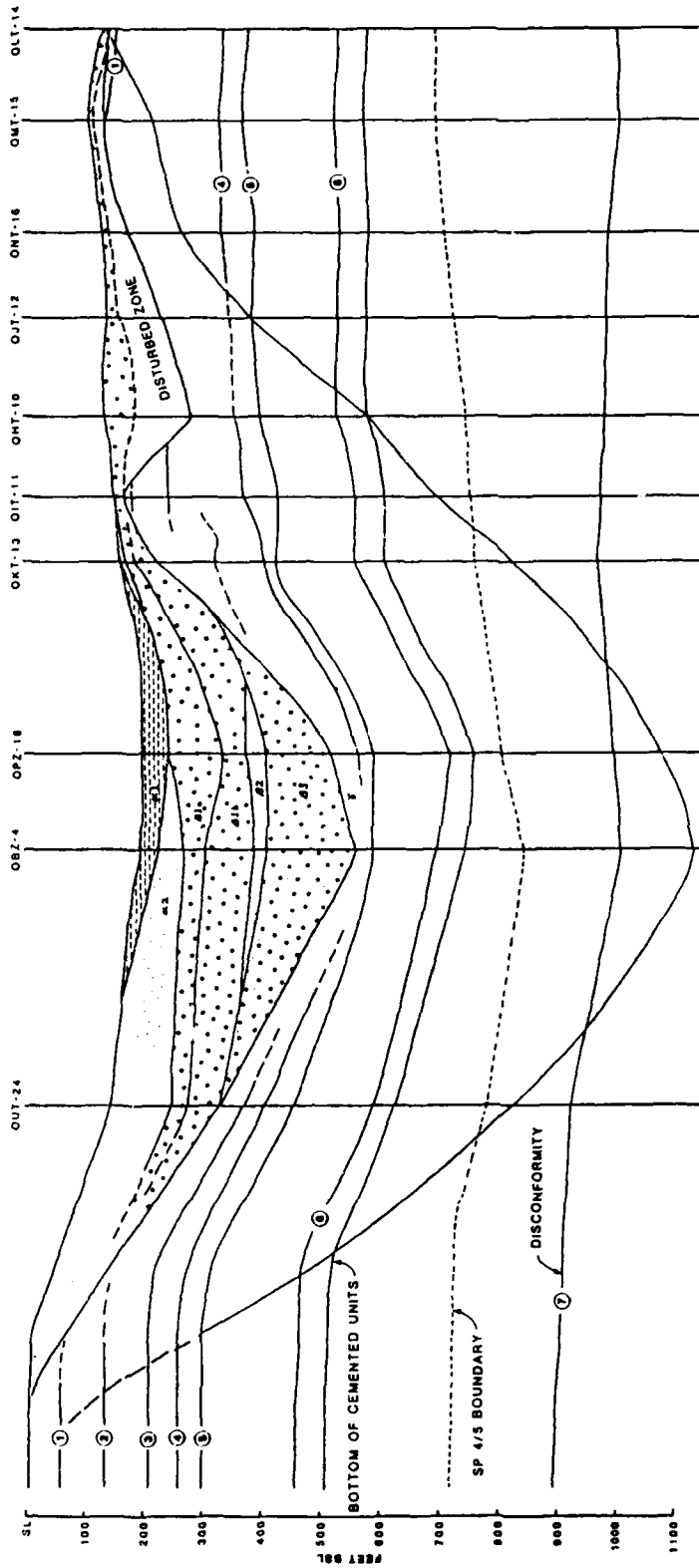


FIGURE 7-10. -- Fence diagram of OAK boreholes from reef tract to OLT-14 showing relationship of crater and geologic horizons. Scale is vertically exaggerated 2:1.

OAK CRATER

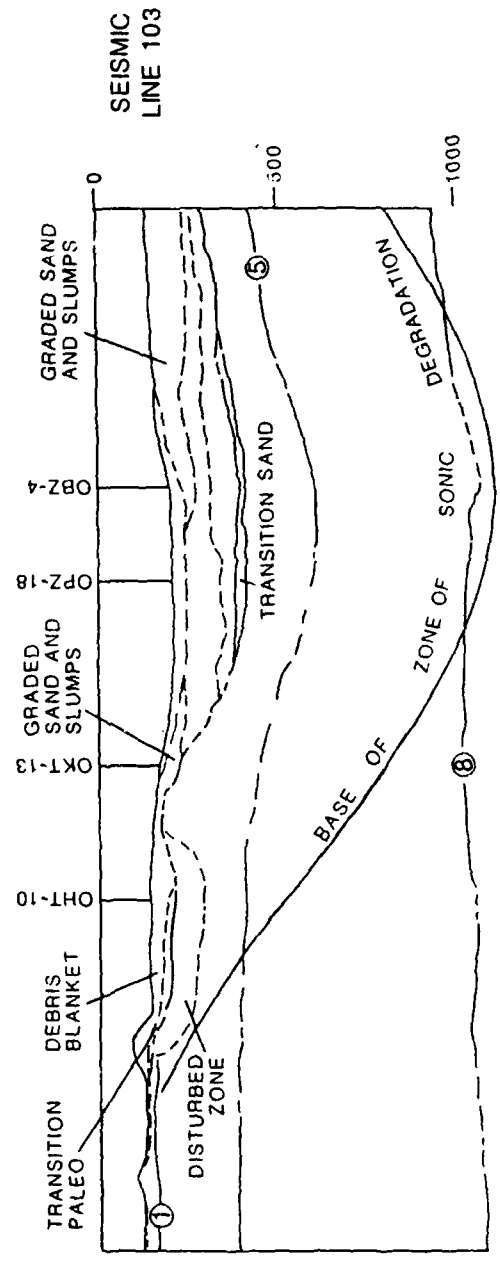
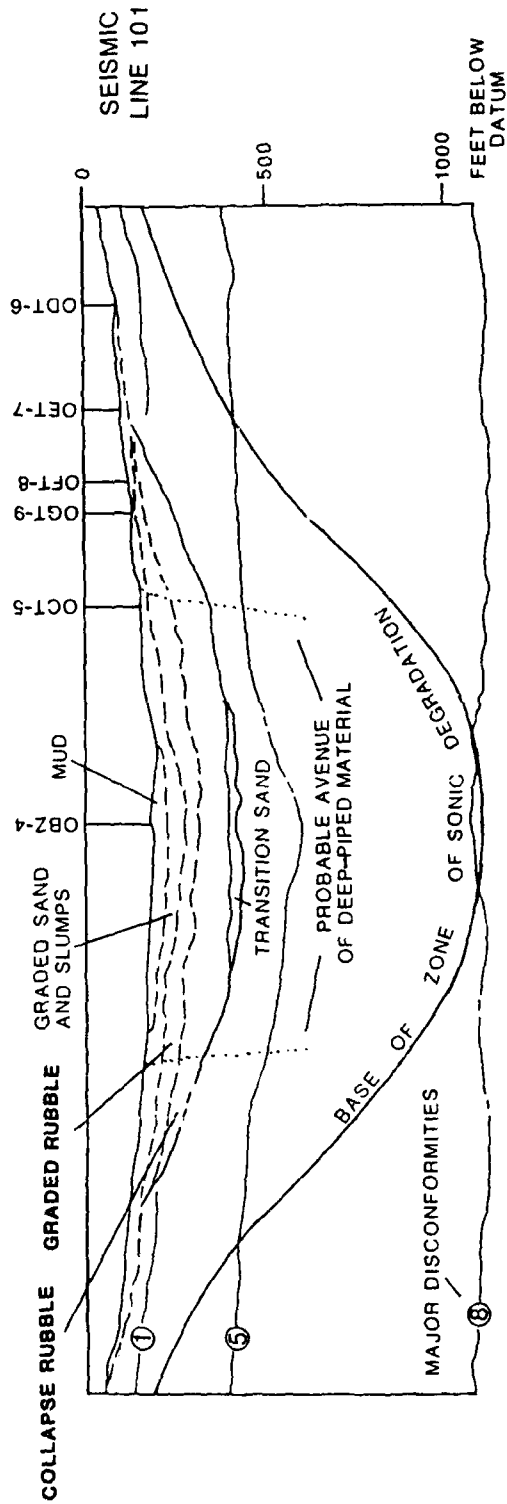


FIGURE 7-11. -- Geologic interpretation of multichannel seismic lines 101 and 103 in proximity of OAK crater (from Wardlaw and Henry, 1986b). Location of lines shown in Grow, Lee, and others (1986).

KOA CRATER

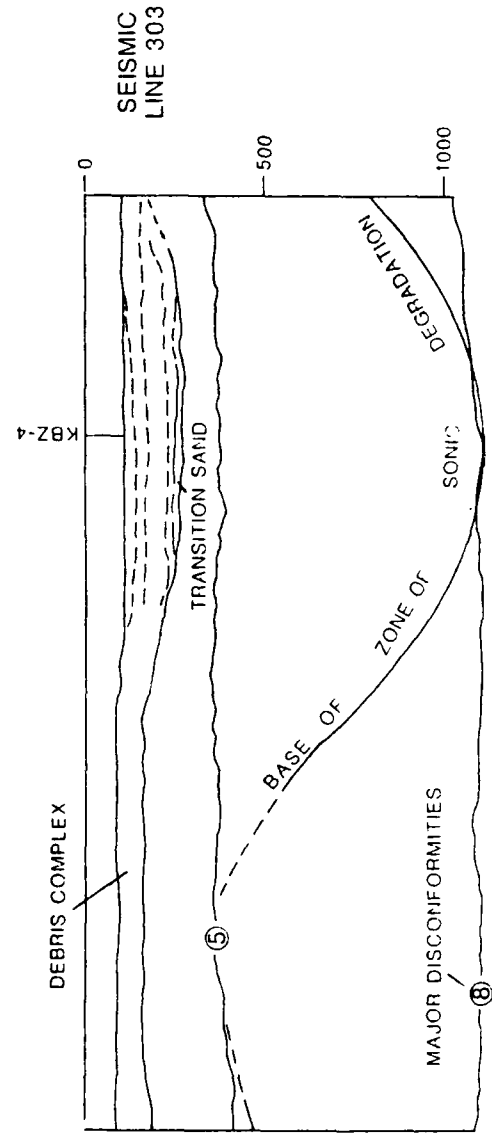
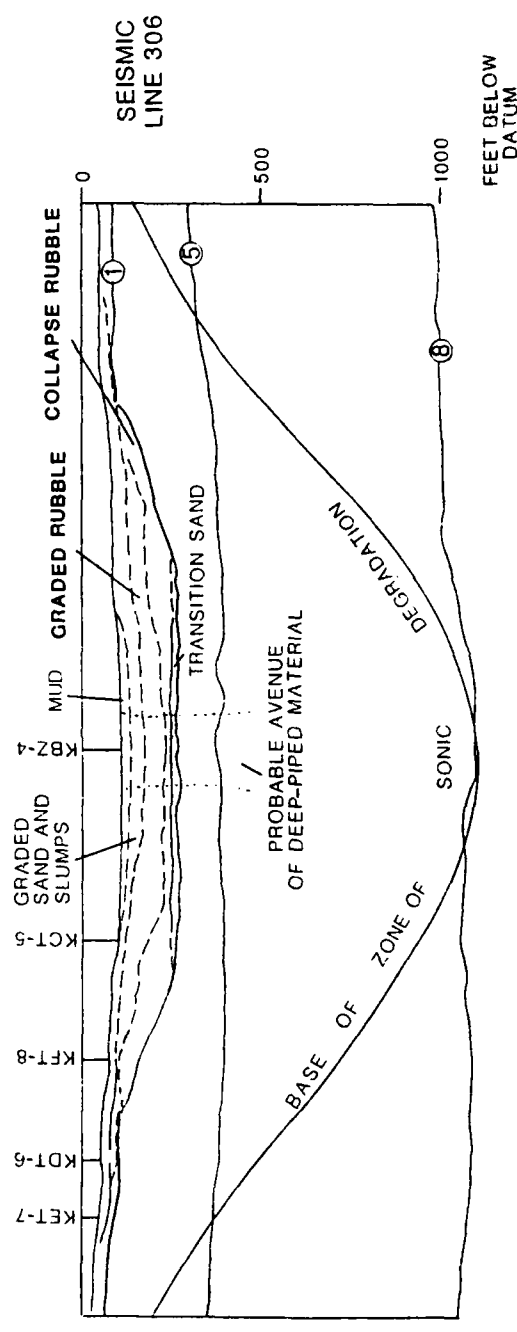


FIGURE 7-12. -- Geologic interpretation of multichannel seismic lines 303 and 306 in proximity of KOA crater (from Wardlaw and Henry, 1986b). Location of lines shown in Grow, Lee, and others (1986).

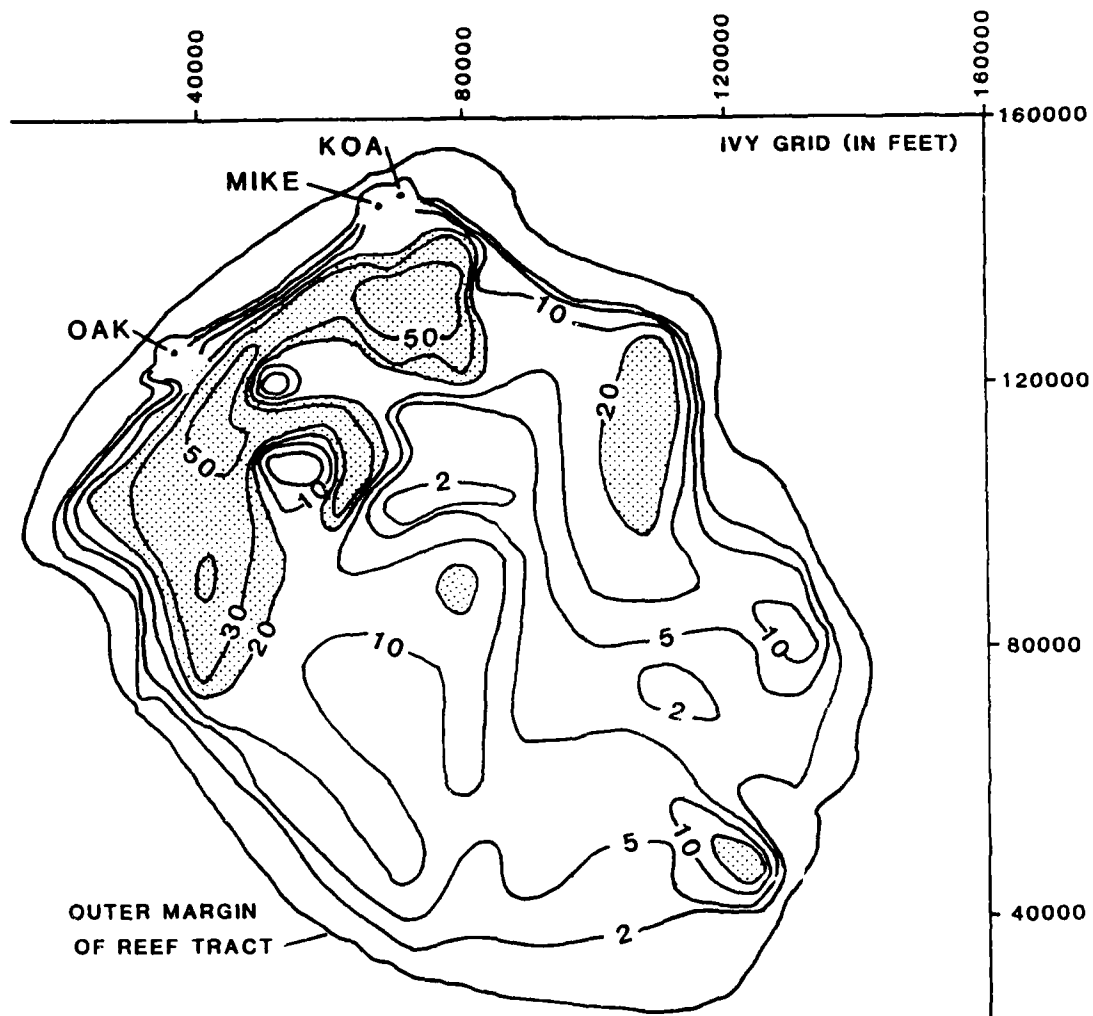


FIGURE 7-13. -- Weight percent mud in bottom sediments of lagoon. Sediments in excess of 10 percent mud are probably indicative of blast-derived mud contribution.

Piping

Brown-stained, organic-rich sediments from MP-4 were piped to the surface in substantial quantities. Several sand mounds (Halley and others, 1986) or "sand volcanoes", covered with moderate-brown, coarse-grained detritus are common on the terraces of OAK crater. This material commonly contains granule- and small-pebble-sized particles (2-64 mm) and may sparsely contain small cobble-sized materials (64-256 mm). The sand volcanoes observed are generally less than 10 ft high, are round to elongate, and are 16-33 ft across and up to 100 ft long. The eight volcanoes documented by Halley and others (1986a) are plotted on the enhanced sea-floor image (fig. 7-14). Similar features that are probably sand volcanoes are also shown. The volcanoes appear to exist in several clusters or swarms on the terraces of OAK crater. No sand volcanoes were observed in the KOA area; however, most surficial features have been obscured by extensive slumping and recent sedimentation (Folger and others, 1986).

Several thin sand dikes filled with brown-stained sediments, confirmed by paleontologic analysis to be from MP-4, were penetrated by the boreholes. These were inclined at a high angle to the borehole under the central crater region and terraces of OAK. Dikes were observed in boreholes OPZ-18 at 667.8 - 668.5 ft, OKT-13 at 615.0 to 615.2 ft, OTG-23 at 472.3 to 473.2 ft, and OFT-8 at 291.1 to 291.9 ft (all depths bsl; see Henry, Wardlaw, and others, 1986). No dikes were observed in the KOA boreholes.

Paleontologic Mixing

The distribution of mixed materials from different biostratigraphic zones within the geologic crater is complicated, but each fossil is a clue to unraveling the history of formation of crater-fill deposits. In addition to the general three to four mixed zones presented in the previous section, both KOA and OAK have an overprint of hydraulic sorting in the central region due to post-deposition upward flow of piped material from strata below the excavational crater. In KBZ-4, the piped material shows hydraulic sorting of various fossil groups (see Brouwers, Cronin, and Gibson, 1986). In OBZ-4 and OPZ-18, the faunas are depleted and represented by sparse piped material in the lower part of the crater fill (fig. 7-15; and Cronin and Gibson, 1987), thought to indicate preferential removal of contained faunas by hydraulic flow and scant deposition of MP-4 faunas.

The mixing within the crater is displayed in Figure 7-16 for OAK and Figure 7-17 for KOA. The biostratigraphic zones represented are defined in the reference boreholes in sequence of superposition and with increasing depth are: surficial (S), AA, BB, CC, DD, EE, FF, and GG. Piped material from depth designated as "piped" in the figures is represented by biostratigraphic zones II, JJ, KK, LL, and MM. Because the KOA event excavated down to the DD/EE zone boundary, most EE and all FF material in the crater-fill indicates shallow piping. Because the OAK event excavated down to a point within EE, possibly some EE and all FF and GG material in the crater-fill represents shallow piping. Each crater will be briefly discussed from bottom up (or as they filled).

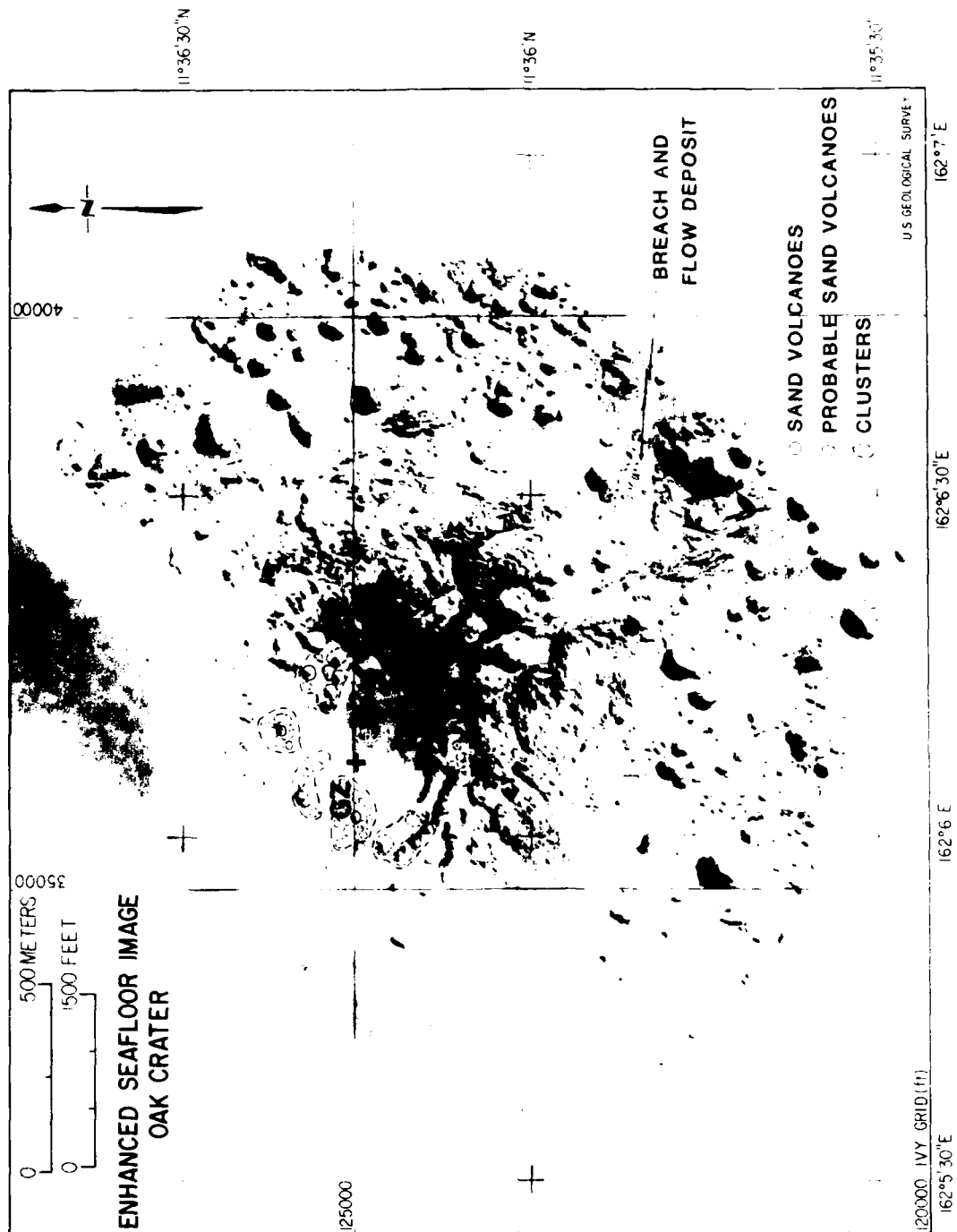


FIGURE 7-14. -- Distribution of observed (solid circles) and probable (dashed circles) sand volcanoes shown in clusters on enhanced sea-floor image of OAK crater and location of breach and flow deposit in lagoon.

DEEP-PIPED MATERIAL

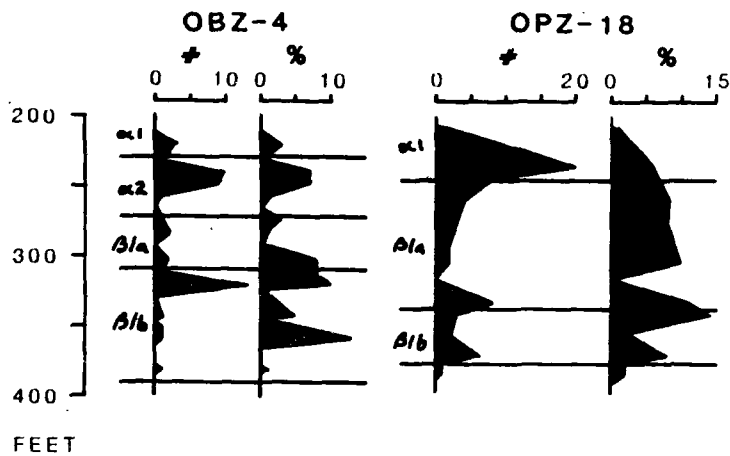


FIGURE 7-15. -- Number of specimens (#) from MP-4 and MP-5 (minor) and percent (%) of total ostracodes picked in crater zones in boreholes OBZ-4 and OPZ-18.

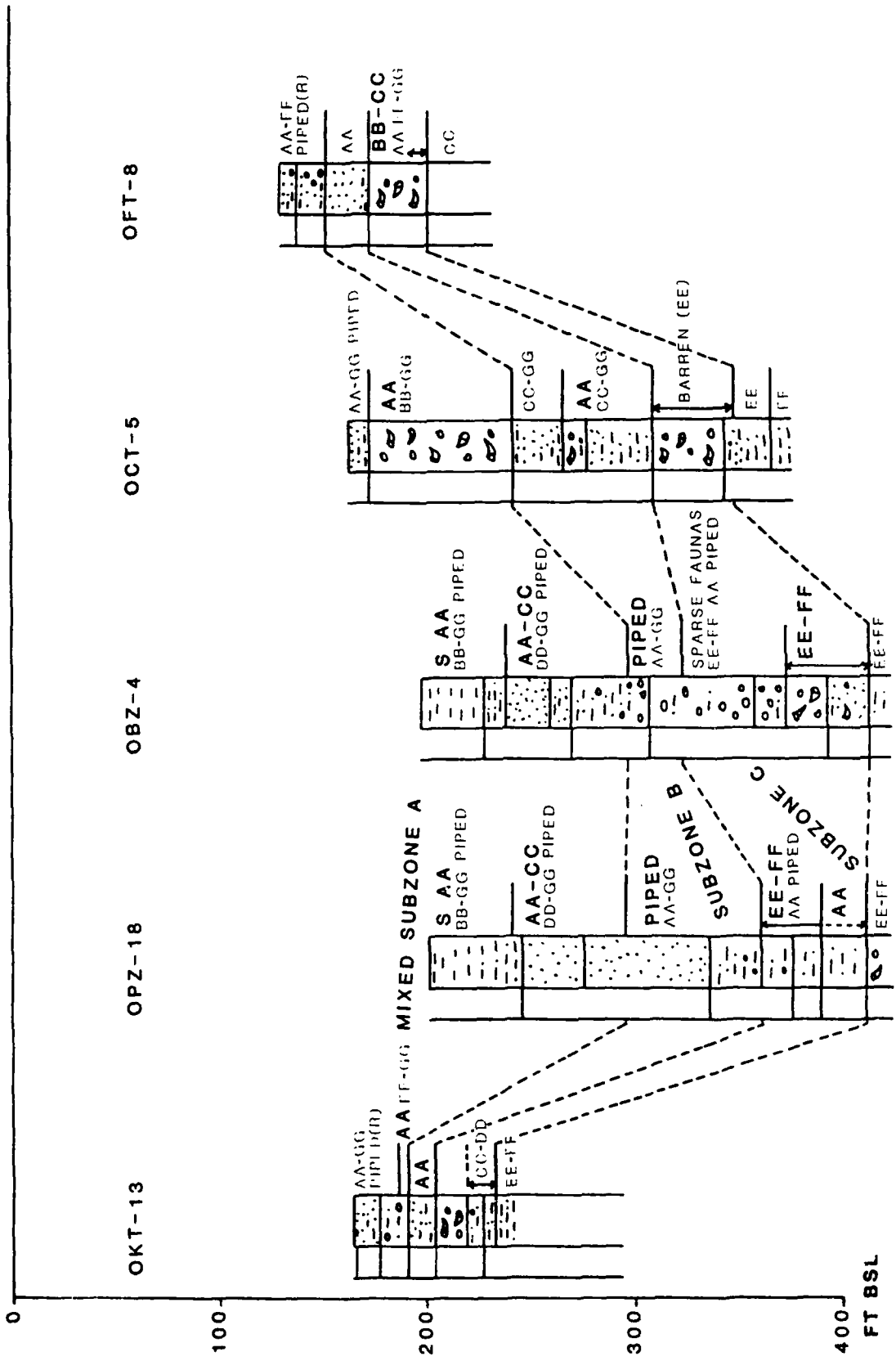


FIGURE 7-16. -- Paleontologic mixing in the mixed zone of OAK crater. Only boreholes with detailed analyses shown. Lithic symbols the same as Figure 7-19. Bold letters indicate abundant material from that particular biostratigraphic zone.

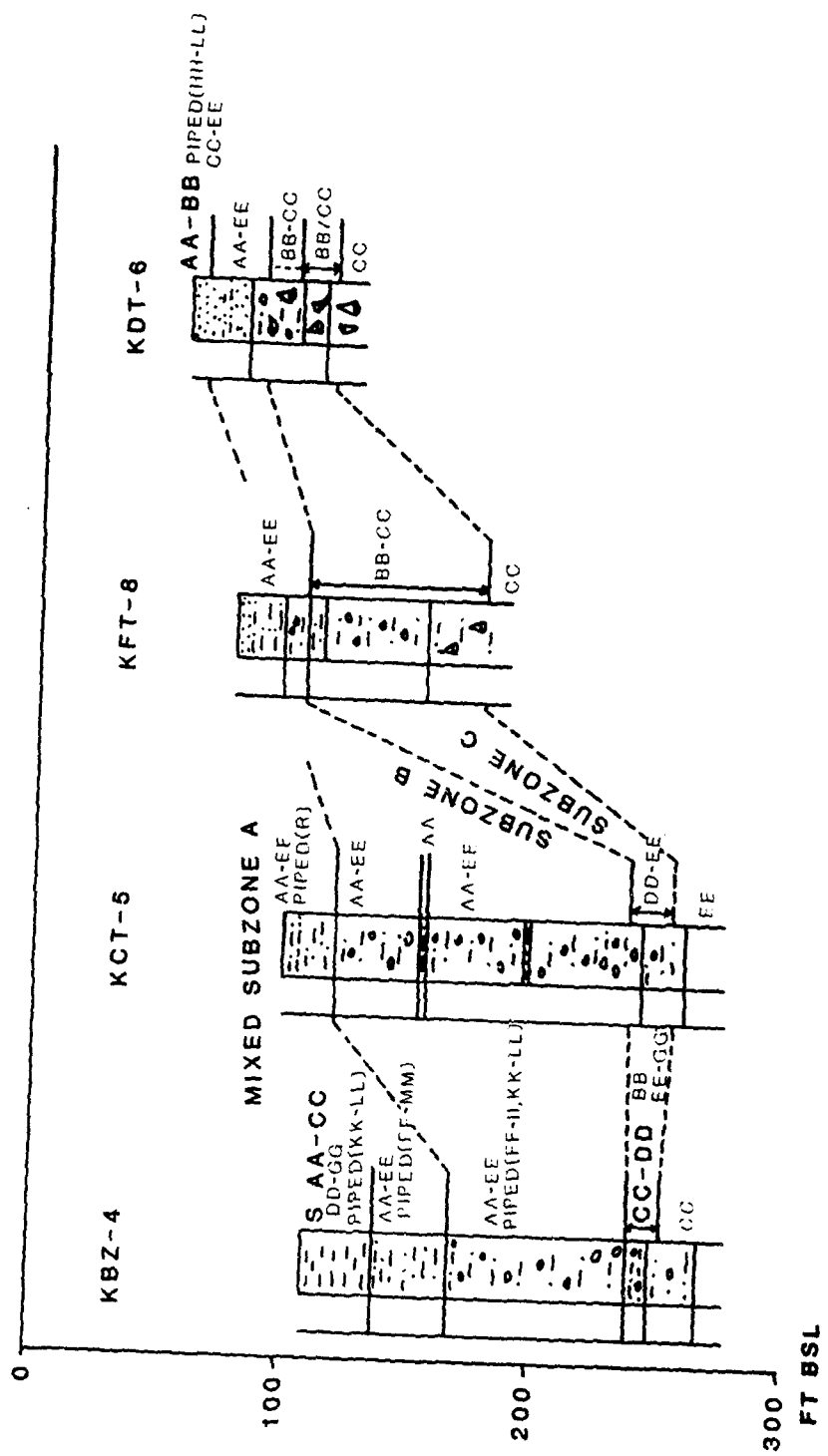


FIGURE 7-17. -- Paleontologic mixing in the mixed zone of KOA crater. Lithic symbols the same as Figure 7-19. Bold letters indicate abundant material from that particular biostratigraphic zone.

OAK Crater.

The lower mixed subzone (C, figs. 7-15 and 7-16) and the transition zone coincide for much of OAK crater (this is because of the limits of resolution, similarity of taxa in the zones, and gradational nature of these zones). This zone contains undifferentiated EE-FF material with sparse AA and deep-piped material in the central crater and of slightly mixed material from progressively stratigraphically higher zones outward to OFT-8 where it contains mostly BB-CC material.

The middle mixed subzone (B) represents a maximum of mixing of material in the central-crater area with components from zones AA-GG mixed with abundant deep-piped material in the upper part of Beta 1b and the lower part of Beta 1a. Laterally, this interval is represented by the "hiatus" sand (Beta 1s) which consists largely of AA material on top of Beta 1b. This situation is complicated at OCT-5 by an apparent local slump that covers and possibly involves the "hiatus" sand (fig. 7-16).

The upper mixed subzone (A) can be divided into two parts in the central-crater area and the inner terraces (OCT-5). In the central-crater area, the lower part consists of common AA-CC material and deep-piped and sparse DD-GG material, and the upper part consists of abundant surficial and AA components with common BB-GG and deep-piped material. Under the inner terraces (OCT-5), the upper mixed subzone consists of a lower part with abundant AA and common BB-GG material (no deep-piped material) and an upper part that is highly mixed with AA-GG and deep-piped material. Laterally, the upper mixed subzone commonly consists of very mixed AA-GG material decreasing outward to AA-FF material with sparse deep-piped material at its top. At OKT-13, the base of the upper mixed subzone (which coincides with the base of Beta 1a) is mixed with material from the underlying unit, the "hiatus" sand (Beta 1s).

Deep-piped material from MP-4 is mixed throughout the crater-fill in both OBZ-4 and OPZ-18, suggesting that the central crater bowl served as the common avenue for venting of MP-4 material. Although sand volcanoes are common on the terraces, mixing of deep-piped material from MP-4 is restricted to surface or near-surface deposits, suggesting that the volcanoes are a late-stage feature and did not represent the more common avenue of venting. Venting under the terraces probably did not take place until significant concentric fracture zones opened sufficiently in the subsiding crater to serve as conduits.

Shallow-piped material is that material in the crater-fill from shallow biostratigraphic zones that remained completely below the excavational crater. In OAK, this material is represented by components of biostratigraphic zones FF-GG. Shallow-piped material is common in the upper mixed subzone throughout the crater-fill, common in the middle mixed subzone, and sparse in the lower mixed subzone in the central crater.

KOA Crater.

The lower mixed subzone (C, fig. 7-17) and the transition zone coincide in most of KOA crater (for the same reasons as in OAK) and consist of CC-DD material with sparse BB and EE-GG material at KBZ-4, of DD-EE material at KCT-5, and of BB-CC material at KFT-8 and KDT-6.

The middle mixed subzone (B) consists of AA-EE material throughout the crater-fill. In addition, at KBZ-4, this zone contains deep-piped material that indicates hydraulic sorting in Beta 1a with FF-II ostracodes and KK-LL foraminifers, and a normal distribution of deep-piped FF-MM ostracodes and foraminifers in Alpha 2. A very thin, muddy "hiatus" sand may be preserved in KCT-5 within the middle of this unit.

The upper mixed subzone (A) is confined to Alpha zones. At KBZ-4, it is dominated by surficial (S) and AA-CC material with sparse DD-GG and deep-piped (KK-LL) material. At KCT-5, it consists of microfossils from AA-EE with very sparse deep-piped material. At KFT-8, the upper mixed subzone cannot be differentiated from the middle mixed subzone, and the whole interval consists of AA-EE material. At KDT-6, it is dominated by AA-BB with CC-EE and deep-piped (HH-LL) material.

Deep-piped material from MP-4 is mixed with other material throughout most of the crater-fill in KBZ-4. It is only found in surficial deposits in the transition boreholes. This suggests that the central bowl in KOA, which is now obscured by pervasive slumping, served as the common avenue for venting deep material from MP-4 just like in OAK.

In KOA, shallow-piped material is represented by components of biostratigraphic zones EE-GG, predominantly EE. The KOA crater-fill material shows much more pervasive shallow piping than in OAK. This shallow piping obscures some of the mixing subzones and yields fairly common mixed faunas of AA-EE. The pervasiveness of the mixing also implies that shallow piping occurred over a broad area. In addition, the paucity of samples and boreholes and a less rigorous study of the KOA material gives less definition of the mixing in KOA.

Estimates of Volume of Piped Material.

The volume of deep-piped material can be estimated with the techniques developed for the detailed paleontologic analysis of the OAK crater by Cronin and Gibson (Ch. 3 of this Report). Deep-piped material occurs only near the surface outside the central bowl and is essentially negligible in quantity. If all grain sizes behaved as those between 63 through 850 μ (the size range from which ostracodes are extracted) and if sedimentary particles of different shapes and densities (minor, all CaCO₃) behave the same as ostracode valves and carapaces, then the detailed percentages of piped ostracodes reflect the entire sedimentary assemblage (Cronin and Gibson, Ch. 3 of this report). A conservative volume estimate based on these data is 4.83 million cubic feet (5.1 % of the total volume of central bowl to a depth of 149 ft with a radius of 450 ft from GZ).

A semiquantitative approach also can be attempted for estimating the shallow-piped material in OAK. Shallow-piped material is identified as those ostracodes that characterize the FF/GG zones, those zones that remained completely below the excavational crater. Shallow-piped material is similar in distribution to deep-piped material within the central bowl, it occurs throughout the crater fill. Because of the general low abundance of FF/GG zone indicators, any patterns in the distribution within the crater-fill is difficult to discern. The crater bowl probably was an avenue for shallow

piping, and the piping probably obscures any patterns of distribution in a manner similar to that for deep-piped material. Ostracodes that characterize the FF/GG zones are typically sparse, averaging 0.4 percent in the faunas above the FF/GG zones in the reference boreholes. They average a sparing 7.5 percent in the faunas of the zones that they characterize in the reference boreholes. These ostracodes average 3.3 percent in the central crater-fill faunas. This implies a whopping 41 percent of the central crater-fill material may have been derived from the FF/GG zones. A volume estimate based on these data is 45.62 million cubic feet of shallow-piped material within the central bowl. However, unlike deep-piped material, shallow-piped material is distributed in significant quantities in Beta 1a and Alpha zones outside the central bowl, suggesting a much larger volume than that estimated for the central bowl was piped.

Paleontologic Model of Crater-Fill.

The paleontologic zonation of the crater-fill can be summarized into a simple model that is applicable to both craters studied. It is extremely relevant for constraints on timing of processes of crater-filling. It is presented in Figure 7-18. The zone of shallow-piped material coincides with that of the deep-piped material through mixed subzones B and C in the central crater but encompasses all of mixed subzone A throughout the crater. The zones of piped material indicate the relative timing of arrival of material to the surface. Shallow-piped material first arrived to the surface after the deposition of the hiatus sand (Beta 1s), which probably resulted from wash-back. Deep-piped material first arrived to the surface after the deposition of the graded rubble (Beta 1a), during deposition of Alpha.

The zone of piped material from depth has a strong overprint of mixing and hydraulic sorting in the central bowl, especially in mixed subzone B, where abundant deep-piped material was deposited. The central bowl served as the probable avenue for venting of the deep-piped material. Shallow-piped material also appears to have vented, in part, through the central region. However, shallow piping appears to have occurred throughout the crater wings which implies venting throughout the crater region.

Injection

Holocene sediment (from MP-1) appears at an anomalous depth in borehole OPZ-18 within the transition sand (390.6 to 410.0 ft bsl) and in thin dikes below the transition sand (434.5 to 435.2 ft bsl, and questionably at 415 ft). This appears to be injection of near-surface material at the base of the excavational crater.

Gamma Activity

In Enewetak boreholes, elevated gamma activity appears to reflect the following: (1) the presence of device-produced radionuclides; (2) the presence of brown-stained, organic-rich sediments from MP-4; and (3) various other factors. For example, a gamma peak of the third type occurs within muddy sediments overlying a discontinuity in OIT-11 (fig. 7-19). It appears that other peaks of the third type also can be related to thick zones of "tea-brown" (organically stained) micrite cement.

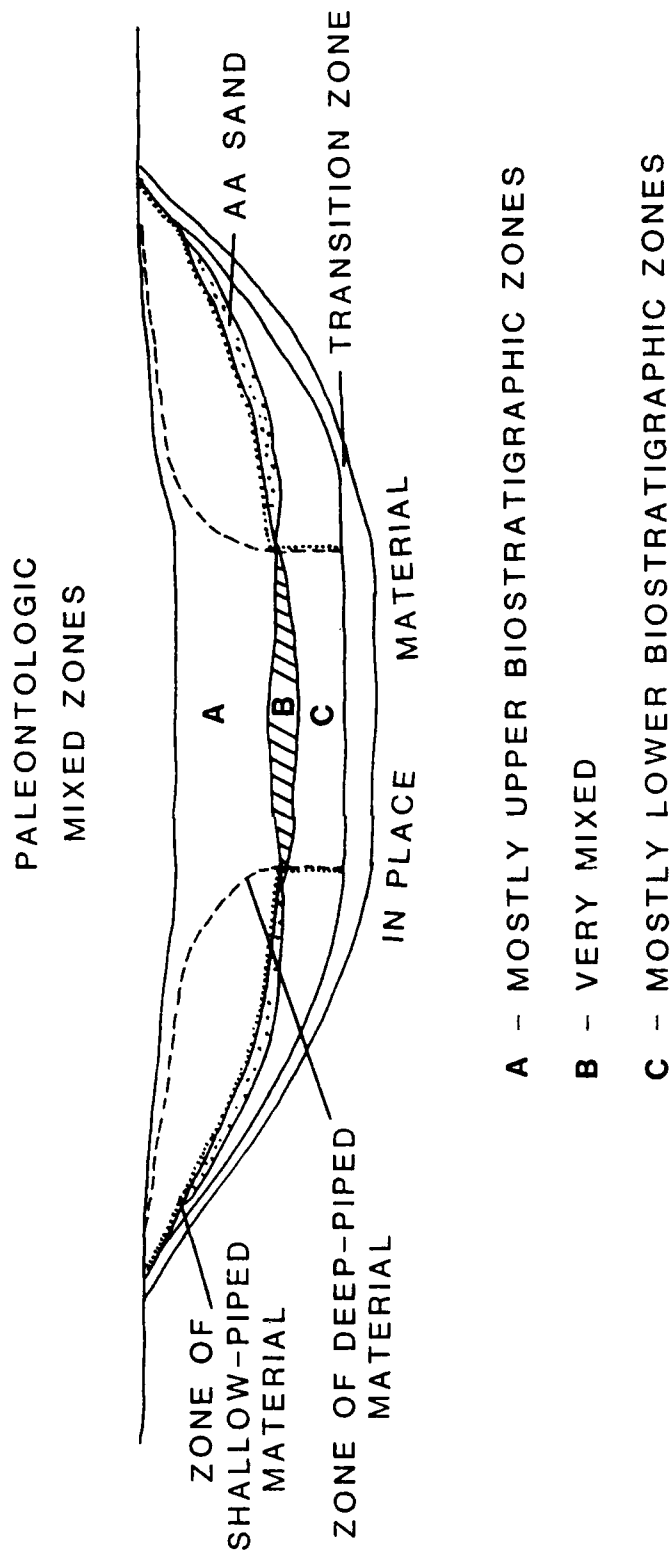


FIGURE 7-18. -- Paleontologic model of the crater-fill and the paleontologic mixed zones.

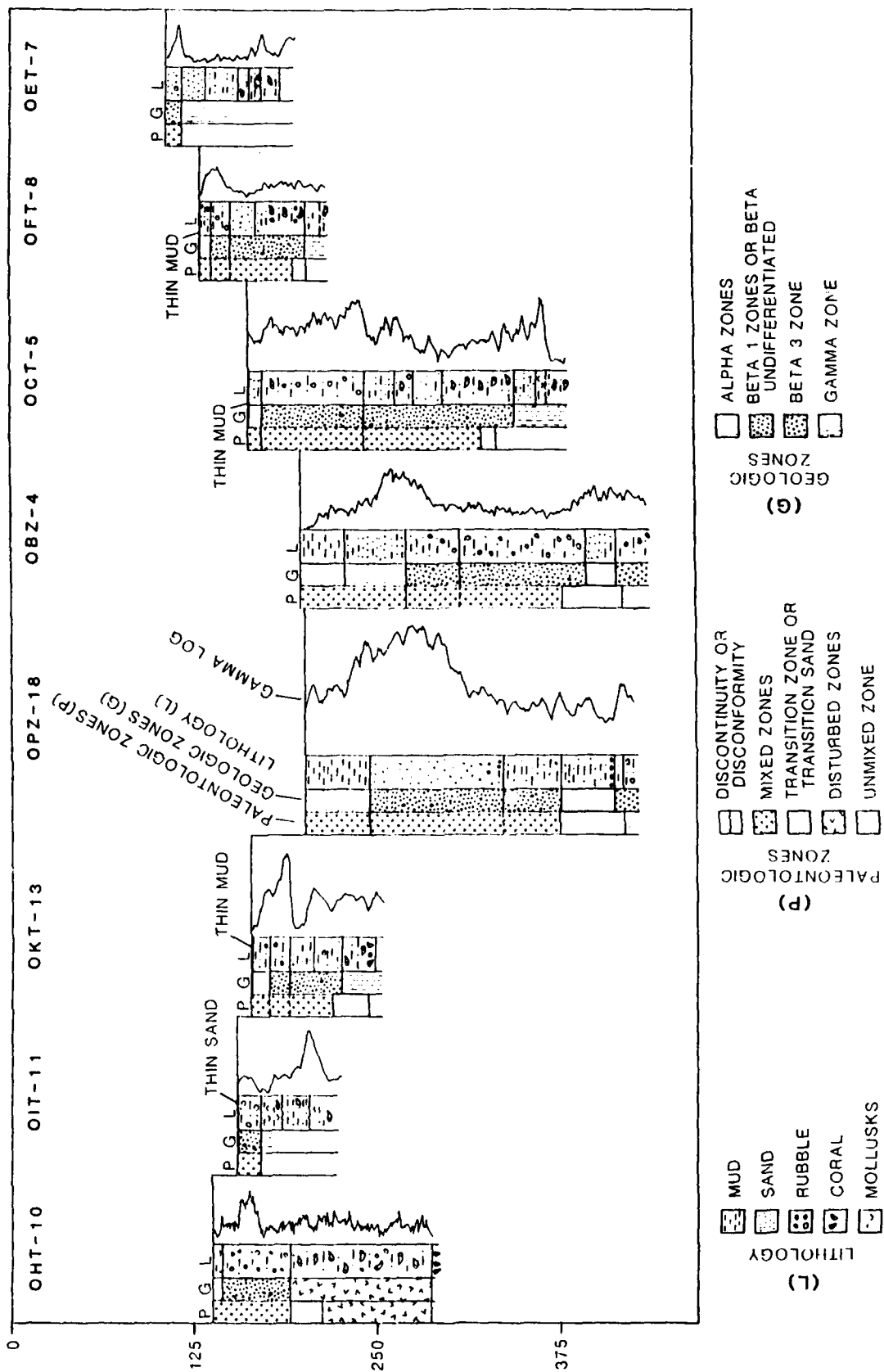


FIGURE 7-19.--Borehole lithology (L), geologic (G) and paleontologic (P) crater zones, and gamma-ray logs for selected boreholes, OAK crater. Location of boreholes shown on Figure 7-20.

Cesium-137 levels coincide directly to the gamma activity in the Alpha, Beta-1, and Beta-2 crater zones (Ristvet and Tremba, 1986). Furthermore, the gamma activity of the brown-stained, organic-rich sediments is caused largely by naturally occurring isotopes of thorium and uranium. These radionuclides were not observed within the Alpha, Beta-1, and Beta-2 crater zones.

Naturally occurring thorium and uranium isotopes were detected in borehole OIT-11 and probably account for the "other" peak (third type) in gamma activity noted above. Similarly, in borehole OHT-10, a small peak in the gamma activity probably reflects naturally occurring thorium and uranium (fig. 7-19).

Figures 7-19 and 7-20 compare the gamma log, paleontologic and geologic crater zones, and general lithologies for KOA and OAK crater areas. Only boreholes on transects with full geologic sampling and open-hole gamma logs were utilized for this comparison. Essentially, the gamma logs confirm the general trends in radionuclide abundance (Ristvet and Tremba, 1986; and fig. 7-21). The Beta-2 / Beta-3 boundary (where present) and the Beta-1 / Gamma boundary (where present) appear to represent the demarcation between occurrence and absence of device-produced radionuclides. Naturally occurring radionuclides appear to reflect the presence of deep-piped material in the Beta-3 crater zone. Device-produced radionuclides are most abundant within the bottom of Alpha-2 (graded sands) and top of Beta-1a (graded rubble) in OBZ-4 and OPZ-18, respectively. In KBZ-4, they are most abundant at the base of Alpha-1 and at the top of Alpha-2. In KCT-5, there is only a trace of radionuclides (device-produced and natural). In borehole OCT-5, device-produced radionuclides are most abundant within the lower part of the Beta-1a crater zone. In OKT-13, device-produced radionuclides show two peaks, one within Beta-1a and the other (larger) near the base of Beta 1b.

Distribution of Radionuclides

The distribution of radionuclides within OAK crater is shown in Figure 7-21 (Ristvet and Tremba, 1986). In OBZ-4, the device-produced radionuclide (Cesium-137) is common in Alpha 1, Alpha 2, and Beta 1a, with peak abundance in Alpha 2. Most of the crater-fill in OPZ-18 consists of muddier sediments than OBZ-4 and consequently contains higher concentrations of Cesium-137. In OPZ-18, radionuclides are common to Alpha 1, Beta 1a, Beta 1b, and Beta 2; the Beta 2 occurrences represent the injected material. Peak abundance is in the upper part of Beta 1a. A moderate amount of cesium is found in OKT-13 below and above the "hiatus" sand (Beta 1s), in Beta 1b, and in Beta 1a and Alpha, respectively.

Radionuclides are sparse in KOA crater and only common within KBZ-4. Here, they mimic the gamma-ray profile (fig. 7-20), with peak abundance in Alpha 1 and a trace at the base of Beta 1b and top of Beta 2.

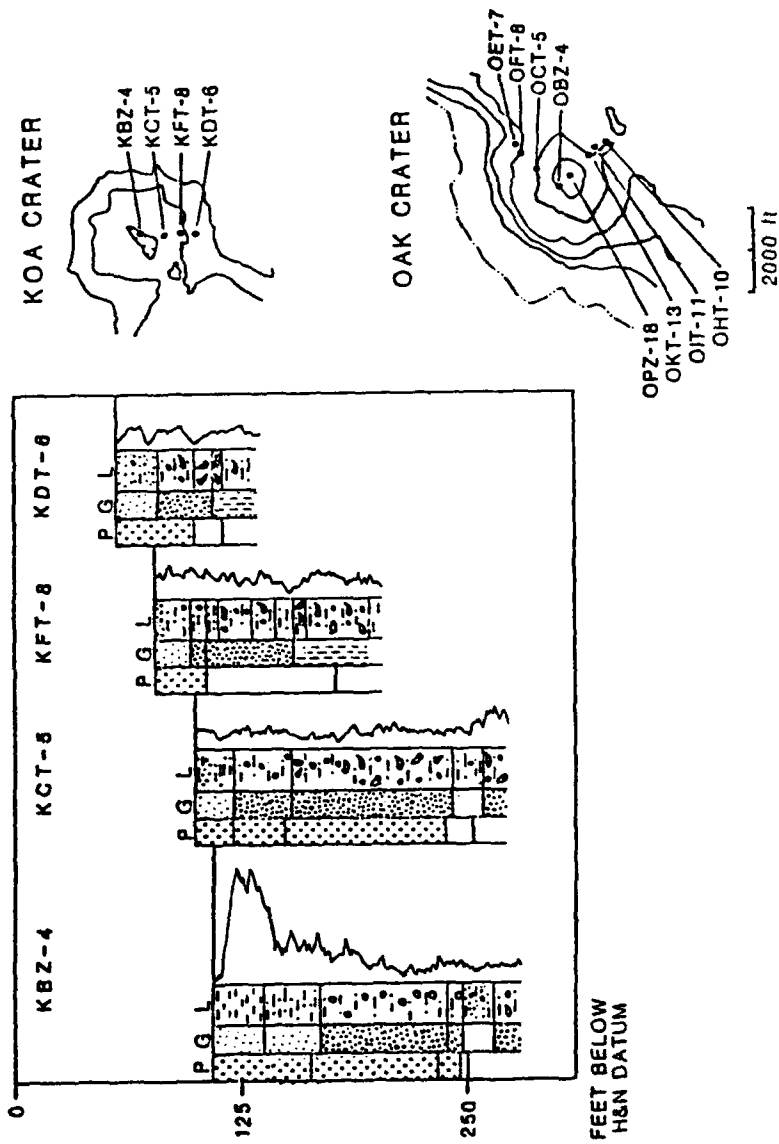


FIGURE 7-20. -- Borehole lithology (L), geologic (G) and paleontologic (P) crater zones, and gamma-ray logs for selected boreholes, KOA crater, and index maps for the KOA and OAK craters. Symbols the same as Figure 7-19.

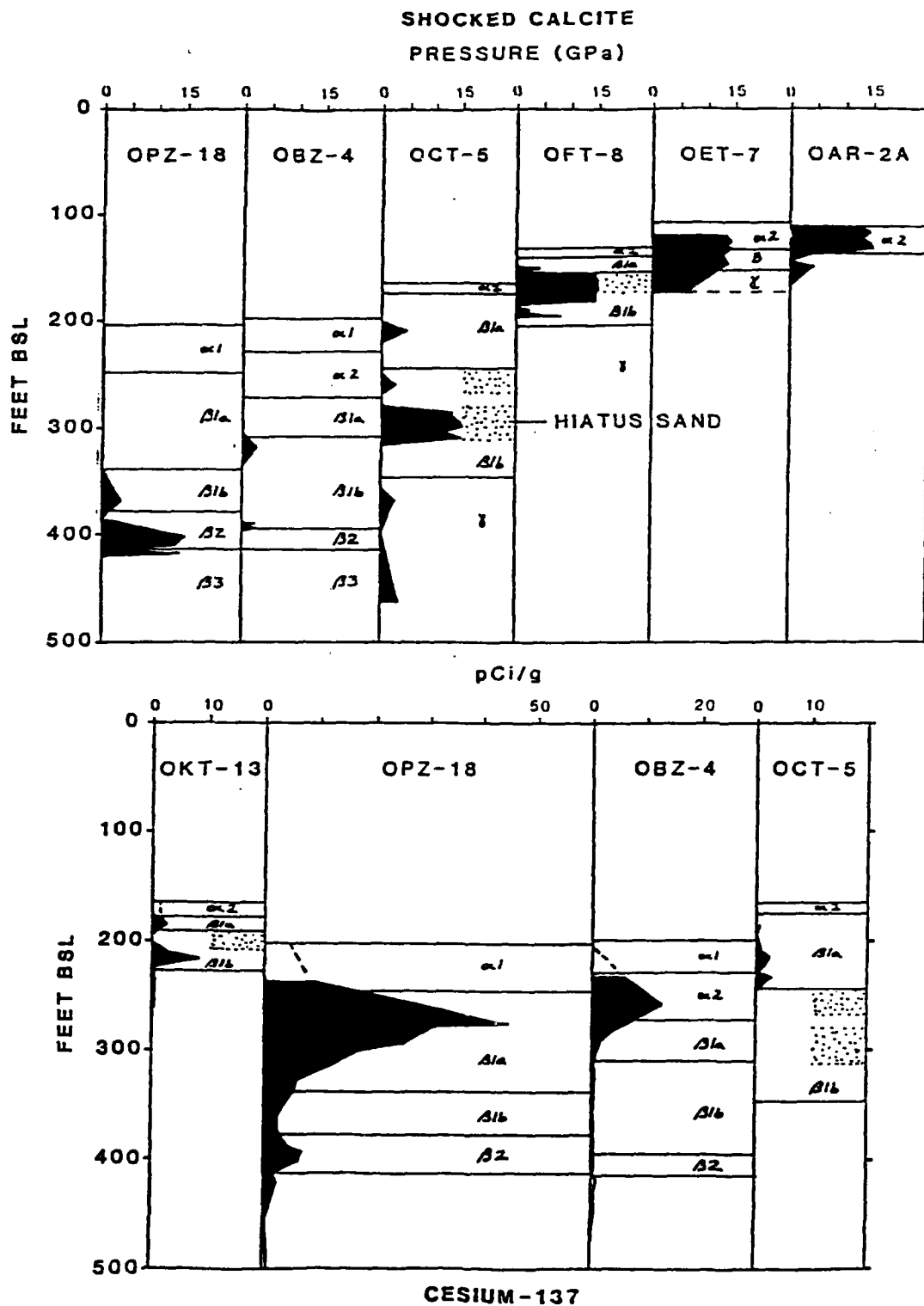


FIGURE 7-21. — Distribution of shocked calcite and Cesium-137 and relationship to crater zones in boreholes analyzed in OAK crater.

Distribution of Shocked Calcite

The distribution of shocked calcite is shown in Figure 7-21 (Polansky and Ahrens, Ch. 4 of this report). Only sparse, possibly moderately shocked calcite is present in the central crater area within Beta 1b. Highly shocked calcite is found within the injected material in OPZ-18. Under the terraces, possibly moderately shocked calcite is found in Beta 1a, Beta 1b, and Gamma with highly shocked calcite in the "hiatus" sand, Beta 1s. Outside the limits of crater-derived rubble (Beta zone), highly shocked calcite occurs in Alpha 2 and Beta in OET-7 and in Alpha 2 in OAR-2A. The material in OAR-2A represents post-event deposition of shocked calcite away from the crater, probably by the sweeping away of fine-grained ejecta from the reef tract by currents and redeposition of it in the area of OAR-2A. The material in OET-7 in graded sands (Alpha 2) seems to represent post-event deposition like that in OAR-2A. The material in OET-7 in the undifferentiated rubble apparently represents buried ejecta.

Depression and Uplift of Structural Surfaces

The surface at the top of the Pleistocene in both the OAK and KOA areas shows a pattern of central removal and lateral depression on the net-change (delta) figures (figs. 7-22A and 7-23A, respectively) derived from the pre- and post-shot surface contour maps (figs. 7-4 and 7-24). In addition, in the OAK area, two lateral depression troughs are developed along the pre-shot slope from reef to lagoon. Also, the Pleistocene surface appears to be irregularly disrupted or preserved beneath the debris blanket (dashed lines, fig. 7-22A) and irregularly uplifted near the margins of the debris blanket. The maximum current depression observed in OAK is 63 ft and in KOA is 53 ft. The maximum uplift in OAK is 14 ft. No strata in KOA are currently uplifted.

The surface at the top of the Pliocene in the OAK area (fig. 7-22B) shows central concentric depression slightly skewed toward the reef and a broad region of shallow uplift beneath both the debris blanket and the lagoon. The maximum depression is 193 ft beneath GZ. The maximum uplift appears to be about 21 ft. The Pliocene surface in the KOA area certainly was influenced by detonation of the MIKE device (fig. 7-23B). KOA shows a complicated pattern of depression with maximum depression on the lateral wings away from GZ. The pattern of depression from MIKE crater area would suggest that the area in the proximity of KOA GZ experienced 0 to 10 ft depression and the entire region from KOA GZ to MIKE experienced progressively greater depression toward MIKE. This possibly influenced the apparent lateral extension in depression roughly perpendicular to the line from KOA ground-zero to MIKE ground-zero.

COMPARISON OF OAK AND KOA CRATERS

The following comparisons and contrasts can be made between KOA and OAK craters:

- (1). The base of the zone of sonic degradation (ZSD) is similar in both craters -- 1,139 ft bsl for OAK ground-zero (GZ) and 1,101 ft bsl for KOA GZ. The ZSD appears to form a narrower cone at KOA

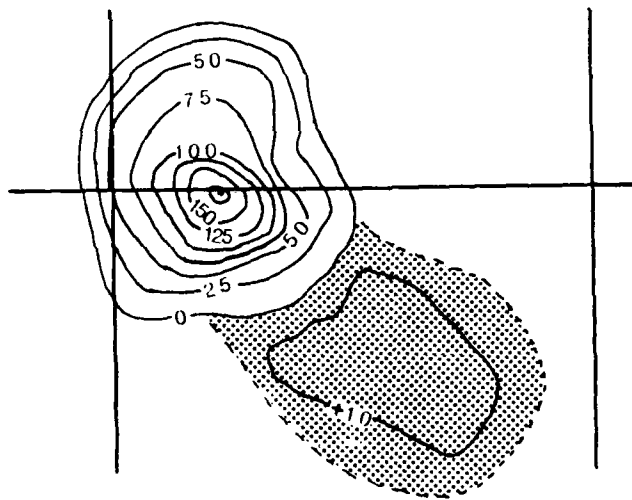
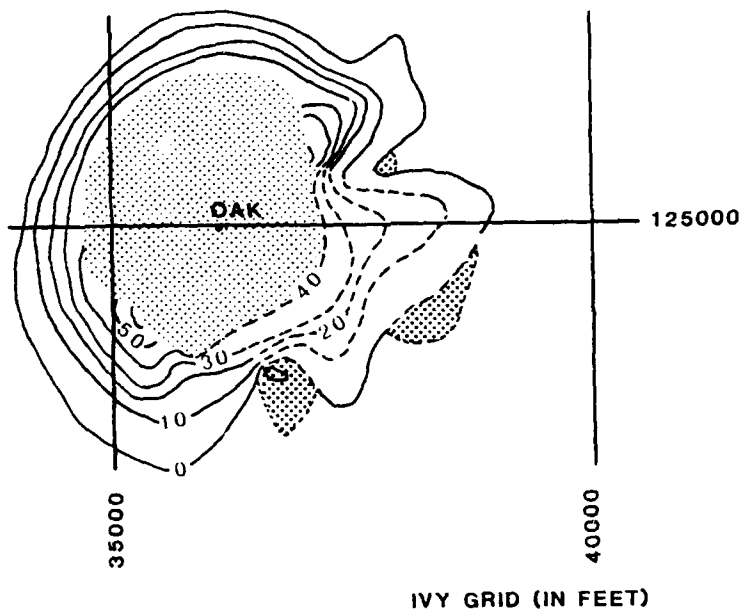


FIGURE 7-22. -- Maximum depression/uplift of Pleistocene and Pliocene surfaces, OAK crater. Pleistocene surface is projected beneath debris blanket, where it is disrupted but probably remains as several isolated outliers such as encountered in OIT-11. Surface is lightly stippled where removed, heavily stippled where uplifted.

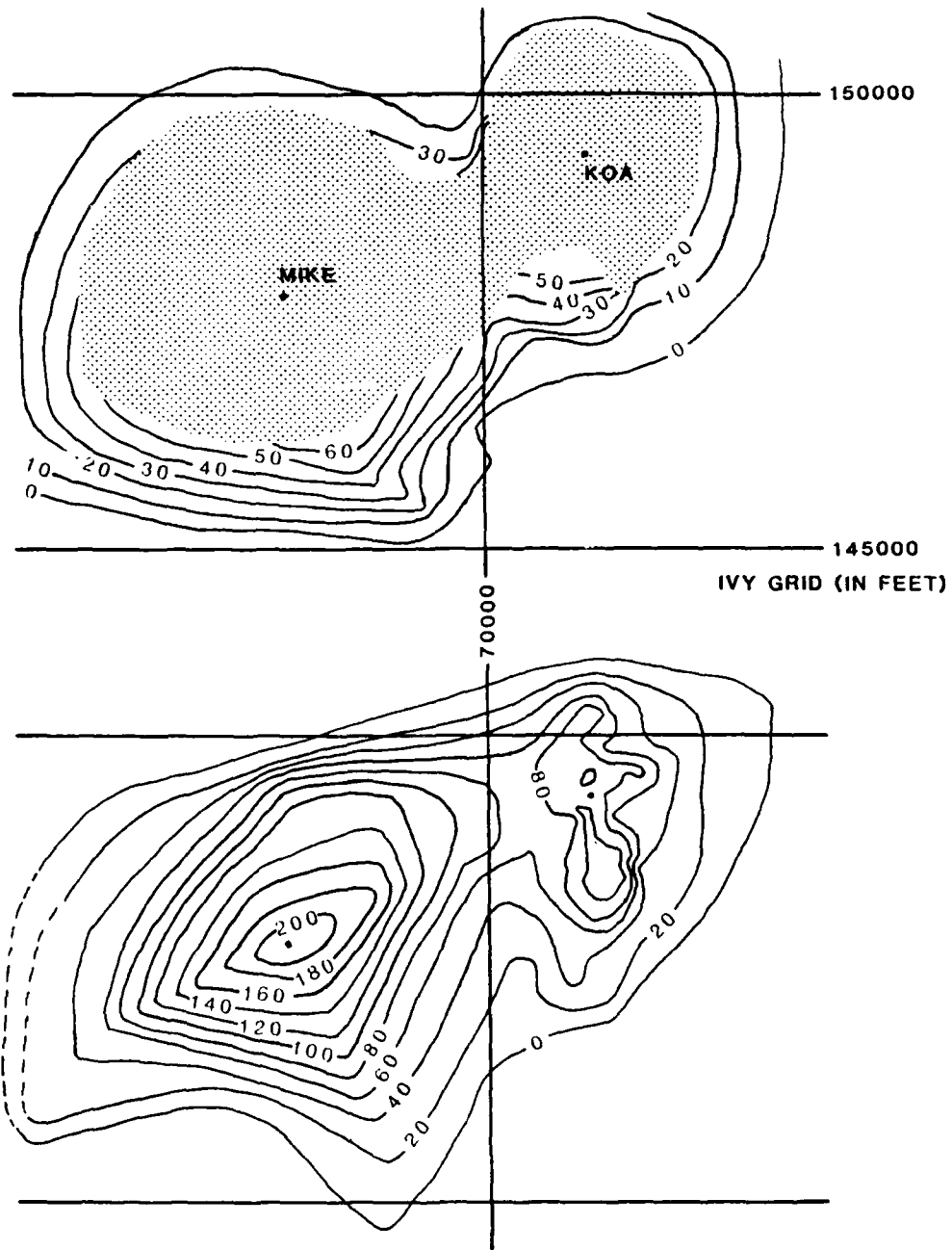


FIGURE 7-23. -- Maximum depression of Pleistocene and Pliocene surfaces, KOA crater. Surface is lightly stippled where removed.

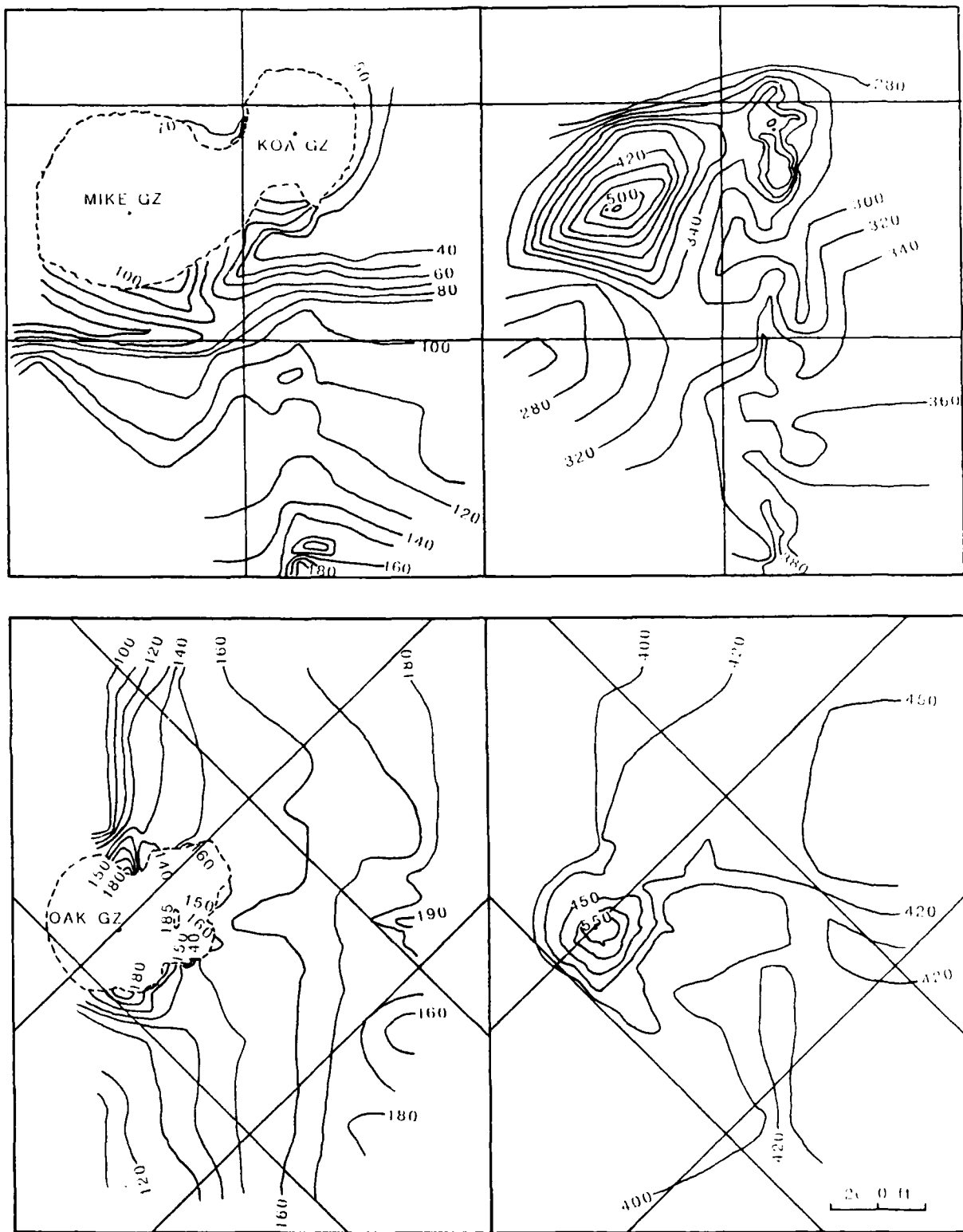


FIGURE 7-24. -- Present-day (post-shot) location of Pleistocene and Pliocene surfaces, KOA and OAK craters. Contours in ft below H&N datum (bsl).

- (2). MP-3, the significantly cemented and altered zone, was probably 246 ft thick with the top at 280 ft bsl at KOA GZ and 183 ft thick with the top at 400 ft bsl at OAK GZ.
- (3). MP-3 is depressed approximately 193 ft at OAK GZ and approximately 89 ft at KOA GZ. MP-3 shows depression and fracture at OAK and, in addition, at KOA, shows apparent rebound in the central part of the crater.
- (4). At ground-zero, the Alpha zone (mud and graded sand) is comparable between KOA and OAK; however, the Beta zone (rubble) is twice as thick at OAK. In particular, Beta 3 (rubble floatstone) is much thinner at KOA. The total lateral extent of the Beta zone is nearly the same at both craters.
- (5). The transition sand (Beta 2) is more extensive in KOA than OAK, with an average diameter of approximately 918 ft at KOA and 816 ft at OAK. The transition sand is more elongate oval at KOA than at OAK.
- (6). The collapse rubble (Beta 1b) is similar in both craters, although thicker in OAK. The Beta 1b zone thins toward the lagoon at OAK and thins toward MIKE crater at KOA.
- (7). The hiatus sand (Beta 1s) is much less extensive at KOA, presumably due to thinner and shorter-term deposition and to more extensive destruction by late-stage collapse.
- (8). The graded rubble (Beta 1a) is similar in both craters. The rubble becomes thicker and muddier in the direction of the lagoon at OAK (i.e., toward its distal margin) and in the direction of MIKE crater in KOA. For all intent and purpose, for the KOA event, MIKE served as a "lagoon" similar to the natural lagoon off OAK, but much smaller in extent.
- (9). The graded sands (Alpha 2) are similar in both craters. This zone is common throughout the KOA crater but absent near the bathymetric center (OPZ-18) of OAK crater.
- (10). Mud (Alpha 1) occupies the central region of both craters.
- (11). A debris blanket is extensive on the lagoon side of OAK; only two possible debris mounds of limited distribution exist on the MIKE-side of KOA.
- (12). Deep-piped material is common only in Alpha 2 in KOA and probably vented in a limited area at the central crater. Deep-piped material is common to Alpha 1, Alpha 2, and Beta 1a in OAK and probably vented in an extensive area of the central crater and terraces.
- (13). Shallow-piped material is common to Alpha and Beta 1a zones throughout the crater wings and found in all zones in the central crater in both craters. In KOA, it is represented by EE-GG material in the central

crater and EE material in the crater wings. In OAK, it is represented by FF/GG material throughout the crater.

- (14). KOA crater is characterized by late-time sedimentation exceeding subsidence. OAK crater, in contrast, is characterized by late-time subsidence exceeding sedimentation.
- (15). Device-produced radionuclides appear to be mostly limited to the Beta 2 and overlying zones in the craters. Radionuclides were detectable only in KBZ-4 for the KOA crater. In OAK crater, peak abundance of device-produced radionuclides progressively moves down in the crater zones away from GZ. For example, the peak abundance is in Alpha 2 in OBZ-4, at the top of Beta 1a in OPZ-18, at the bottom of Beta 1a at OCT-5, and at the bottom of Beta 1b at OKT-13.

GEOLOGIC CRATER MODEL FOR OAK AND KOA

The transition sand (Beta 2) represents the remnants of the base of the excavational crater. It is characterized by sand-sized material that is formed by fracture and pulverization, by its transitional nature from mixed paleontology to unmixed paleontology within it, and by its containing injection dikes and debris. That shocked calcite is not common within the transition sand is due to two factors: (1) the sampling technique used in which granule- and larger-sized clasts were predominantly sampled (Polansky and Ahrens, 1987, Ch. 4 of this report), and (2) the relatively low shock pressures that probably existed in this region at formation (< 15 kilobars).

The rubble floatstone (Beta 3), beneath the base of the excavational crater (Beta 2), may represent fracture and disruption of sediment and rock caused by the maximum growth of the transient crater.

The collapse rubble (Beta 1b) represents crater-sidewall and partial flap collapse. This zone reflects paleontologic mixing of zones near the base of the excavational crater. The asymmetric crater at OAK demonstrates partial sidewall and flap collapse and movement down the resulting slope away from the transient crater to form the majority of the debris blanket. The part of the flap involved in craterward collapse is that closest to the sidewall which would represent paleontologic zones contained in the sidewall itself. That the paleontologic mixing seems to reflect mixing of material from zones near the base of the crater suggests that most of this unit was deposited rapidly as a single, major, crater-wide collapse feature. This major collapse appears to have destroyed the lateral part of the excavational crater base and its sidewalls. The highly mixed material in the central crater bowl represents a variety of depositional modes that may include wash-back and piping of sufficient magnitude to keep the central bowl "boiling" (continuously mixing). This part of the unit was deposited contemporaneously with the "hiatus" sand (Beta 1s) which represents wash-back and a brief period of quasi-stabilization of the crater and deposition of post-event sediments. The "hiatus" sand is well sorted and contains the highest concentration of shocked calcite indicating deposition from wash-back and fall-back, but, curiously, contains no radionuclides. At OAK and KOA craters, the occurrences of radionuclides are spotty. The decades that have transpired since the event have allowed many radionuclides to dissipate (Ristvet and Tremba, 1986). The

remaining commonly detectable radionuclide is Cesium-137. It is associated with muddy sediments (McMurtry and others, 1985; Wardlaw and Henry, 1986b) and may have been preferentially deposited with muds, and, therefore, would not be common in well-sorted sands. Cesium-137 is involved in progressively younger and muddier deposits in the crater-fill toward ground-zero. Its absence in the "hiatus" sand probably indicates the winnowing out of silt and finer grains during the wash-back / fall-back process.

The graded rubble (Beta 1a) represents deposition probably caused by several major slumps. This indicates that subsidence significantly destabilized the existing crater margins and resulted in collapse. One such collapse in OAK appears to have originated on the reef side. Material from this collapse flowed through the crater and breached the debris blanket, leaving deposits on top of the debris blanket (OHT-10, OJT-12), and flowed out into the lagoon, as seen in the enhanced sea-floor image of OAK (fig. 7-14).

The graded sands and slumps (Alpha 2) represent late-stage, local collapse and deposition of the expanding and subsiding crater margins.

Late-stage mud (Alpha 1) represents post-event, low-energy deposition within the central crater. The differences in Alpha 1 and distal Alpha 2 sands are slight, as shown by the sediment analysis by Melzer and Patti (written communication, 1987).

The idealized distribution of these crater units is shown for a symmetric crater (KOA, fig. 7-25A) and for a asymmetric crater (OAK, fig. 7-25B). The gradational units beneath the transition sand that represent gradually less-stressed sediment and rock within the significantly fractured zone of sonic degradation are also shown.

Thinning Analysis

This analysis simply compares the pre-shot model of inferred horizon location to the measured post-shot position. The comparison of positions is shown in Figures 7-26 to 7-29 and Tables 7-5 and 7-7. The analysis is displayed graphically in Figures 7-30 and 7-31 and tabulated in Tables 7-6 and 7-8. The upper correlation line in Figures 7-30 and 7-31 correlates the pre-shot model to the probable original stratigraphic depth now preserved beneath crater-fill (where present).

Stratigraphic Density Profile

The analysis of the borehole gravity surveys (Beyer, Ristvet, and Oberste-Lehn, 1986; and Beyer, Ch. 2 of this report) provide valuable information about bulk density of the strata in the vicinity of OAK crater. By averaging the borehole-gravimetry results within stratigraphic units, the density change can be compared directly with inferred stratigraphic thinning or thickening for areas where borehole gravity surveys were taken. Figure 7-32 and Table 7-9 relate the gravimetry results to the stratigraphic units. MP-2a appears anomalously dense in the reference sections. The average of MP units 2a-c in the reference sections is utilized to compensate for this anomalous density, especially to compare to crater-fill material in the analysis.

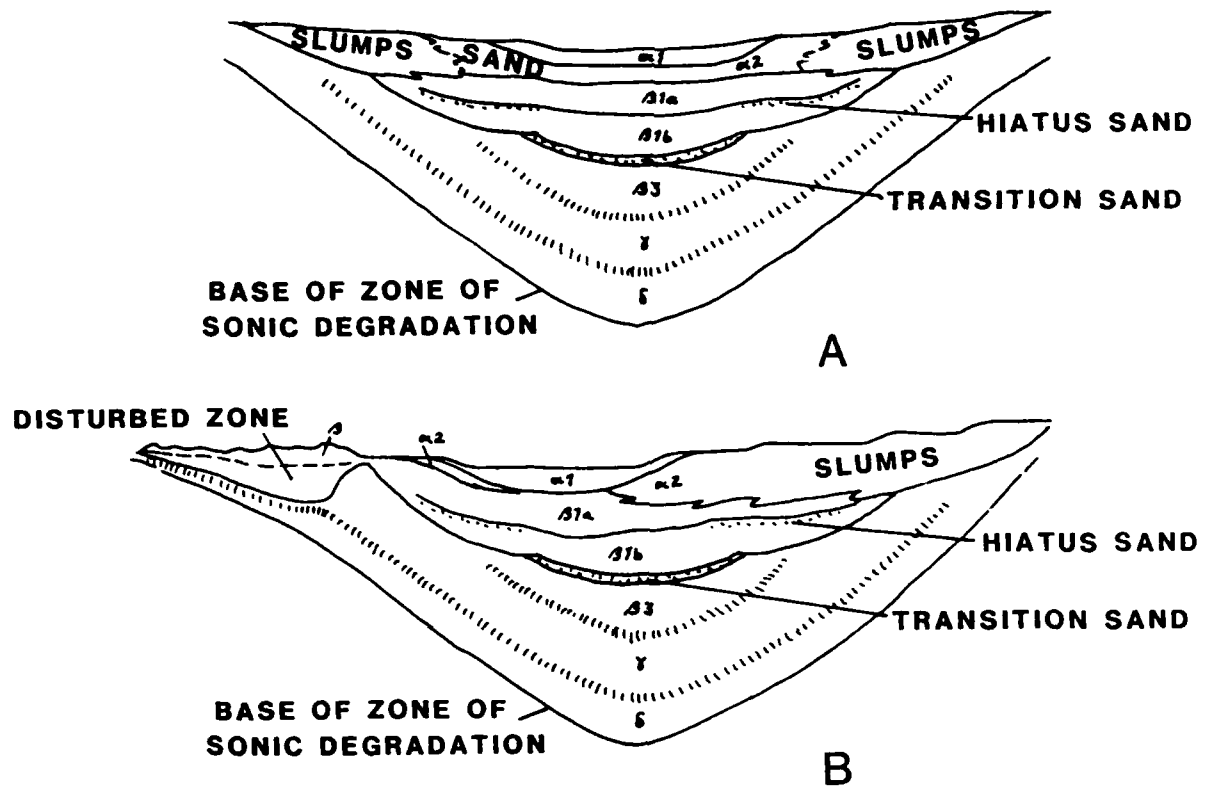


FIGURE 7-25. -- Idealized model of geologic crater for a symmetric crater (A) and an asymmetric crater developed on a significant slope (B).

TABLE 7-5. -- Depth (ft bsl) to MP unit boundaries, pre- and post-shot, OAK crater. Boreholes listed in order of increasing distance from ground zero.

UNIT	OBZ-4		OPZ-18		OCT-5		OTG-23		OUT-24	
1	14	-	47	-	16.5	-	45	-	2	-
2a	123	-	128	-	115	-	128	-	106	-
2b	165	-	166	-	155	-	168	-	145	-
2c	265	-	275	-	255	368.4	253	?	225	373.0
2d	315	-	363	568.9	305	417.9	327	434.0	276	407.0
3a	395	593.0	410	593.0	387	432.7	409	484.0	355	457.1
3b	544	701.2	555	723.5	534	572.2	544	610.0	490	592.0
4a	592	747.3	600	761.9	585	623.7	594	669.0	528	630.0
4b	775	847.7	765	809.9	785	799.7	766	787.0	784	784.0
5a	950	1013.8	956	1000.0	945	944.6	1000	1000.4	925	925.0
5b	1050	1065.1	1050	1063.0	-	-	-	-	1025	1025.0
5c	1115	1114.6	1114	1114.0	-	-	-	-	-	-

UNIT	OKT-13		OFT-8		OIT-11		OET-7		OQT-19	
1	102	-	16	-	122	-	18	-	46	-
2a	141	-	115	204.1	147	185.4	118	173.4	129	168.0
2b	170	232.9	155	223.3	209	247.4	167	220.6	195	233.9
2c	275	326.6	230	272.0	-	-	279	294.7	240	274.7
2d	362	411.6	305	344.6	345	375.0	305	320.4	330	365.3
3a	410	431.3	390	419.8	405	434.8	395	410.0	406	413.3
3b	547	564.0	535	565.0	545	562.0	540	555.0	548	548.3
4a	598	614.7	589	618.0	591	608.0	595	610.0	588	587.5
4b	766	765.8	794	794.0	758	758.0	793	793.0	767	766.5
5a	975	974.5	925	925.0	980	980.0	925	925.0	1020	1020.1
5b	1037	1036.5	-	-	-	-	-	-	-	-
5c	-	-	-	-	-	-	-	-	-	-

UNIT	OHT-10		OJT-12		ODT-6		ONT-16		ORT-20	
1	124	-	115	-	20	-	132	-	70	-
2a	152	-	149	-	116	161.5	149	-	130.5	160.6
2b	212	213.3	216	238.0	160	201.3	219	238.6	187	216.2
2c	-	-	-	-	231	231.3	-	-	243	262.7
2d	361	360.8	350	350.0	315	315.0	338	337.8	327	346.7
3a	419	403.4	405	390.3	397	397.0	407	395.2	405	411.7
3b	547	531.4	547	531.0	546	546.0	550	537.9	552	552.0
4a	600	584.0	600	584.0	594	594.0	600	588.0	586	586.4
4b	751	751.1	732	732.0	792	792.0	715	715.0	767	767.0
5a	987	987.3	991	991.0	925	925.0	994	993.8	1014	1013.5
5b	-	-	-	-	-	-	-	-	-	-
5c	-	-	-	-	-	-	-	-	-	-

(TABLE 7-5 continued on next page.)

TABLE 7-5. (continued from preceding page.)

UNIT	OMT-15		OLT-14	
1	142	-	132	-
2a	153	140.8	158	159.4
2b	225	225.0	227	227.0
2c	-	-	-	-
2d	335	334.6	341	341.1
3a	395	373.9	399	383.8
3b	551	529.7	550	534.6
4a	600	579.0	600	585.0
4b	702	701.9	700	700.0
5a	1014	1013.5	1010	1010.2

Distance of boreholes from surface ground-zero, in feet:

OBZ-4	7
OPZ-18	335
OCT-5	658
OTG-23	804
OUT-24	858
OKT-13	989
OFT-8	1129
OIT-11	1206
OET-7	1375
OQT-19	1444
OHT-10	1462
OJT-12	1696
ODT-6	1715
ONT-16	1827
ORT-20	1846
OMT-15	2204
OLT-14	2754

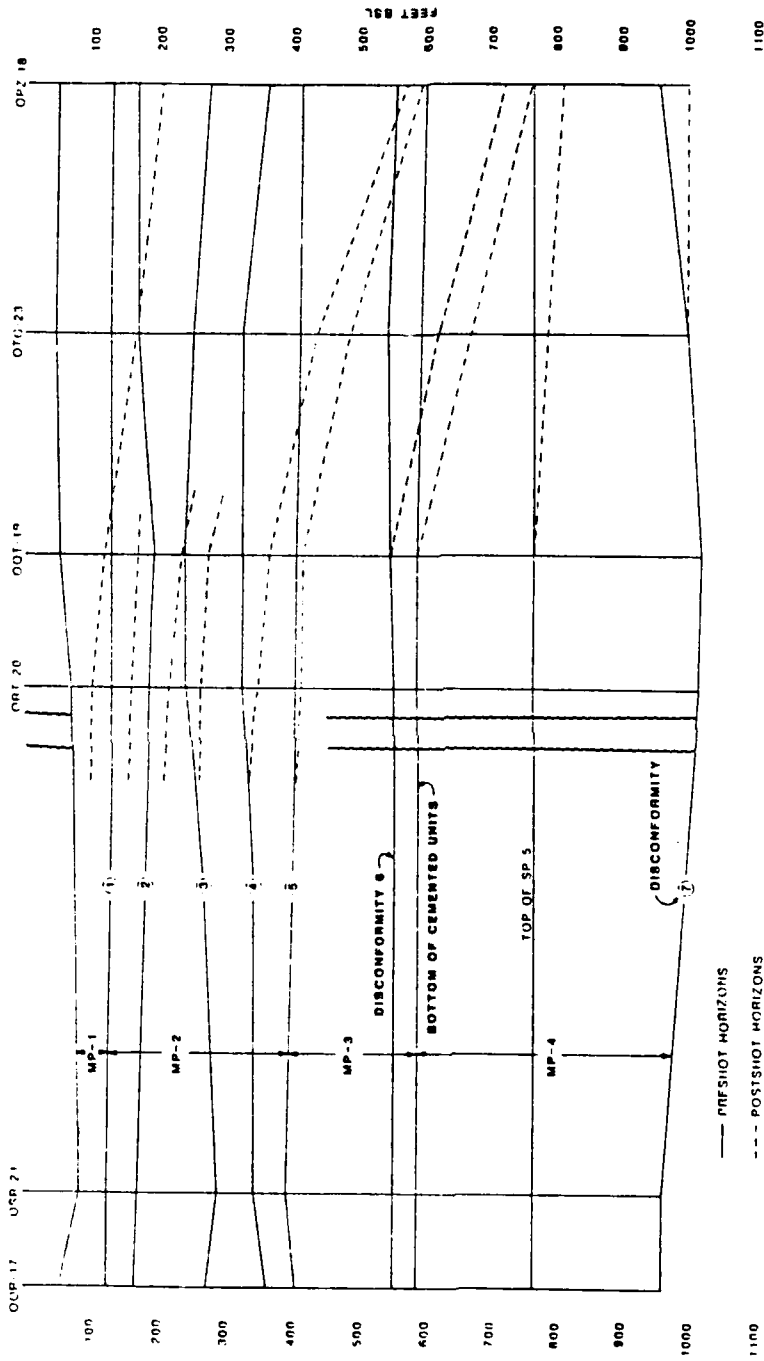


FIGURE 7-26. -- Horizon location in fence diagram from boreholes OOR-17 to OOR-18. Pre-shot location as a solid line except for unit MP-4a/4b boundary which is short dashes. Dashed line represents post-shot location where different from pre-shot location. Squiggles, breaks, and scale as in Figure 7-8.

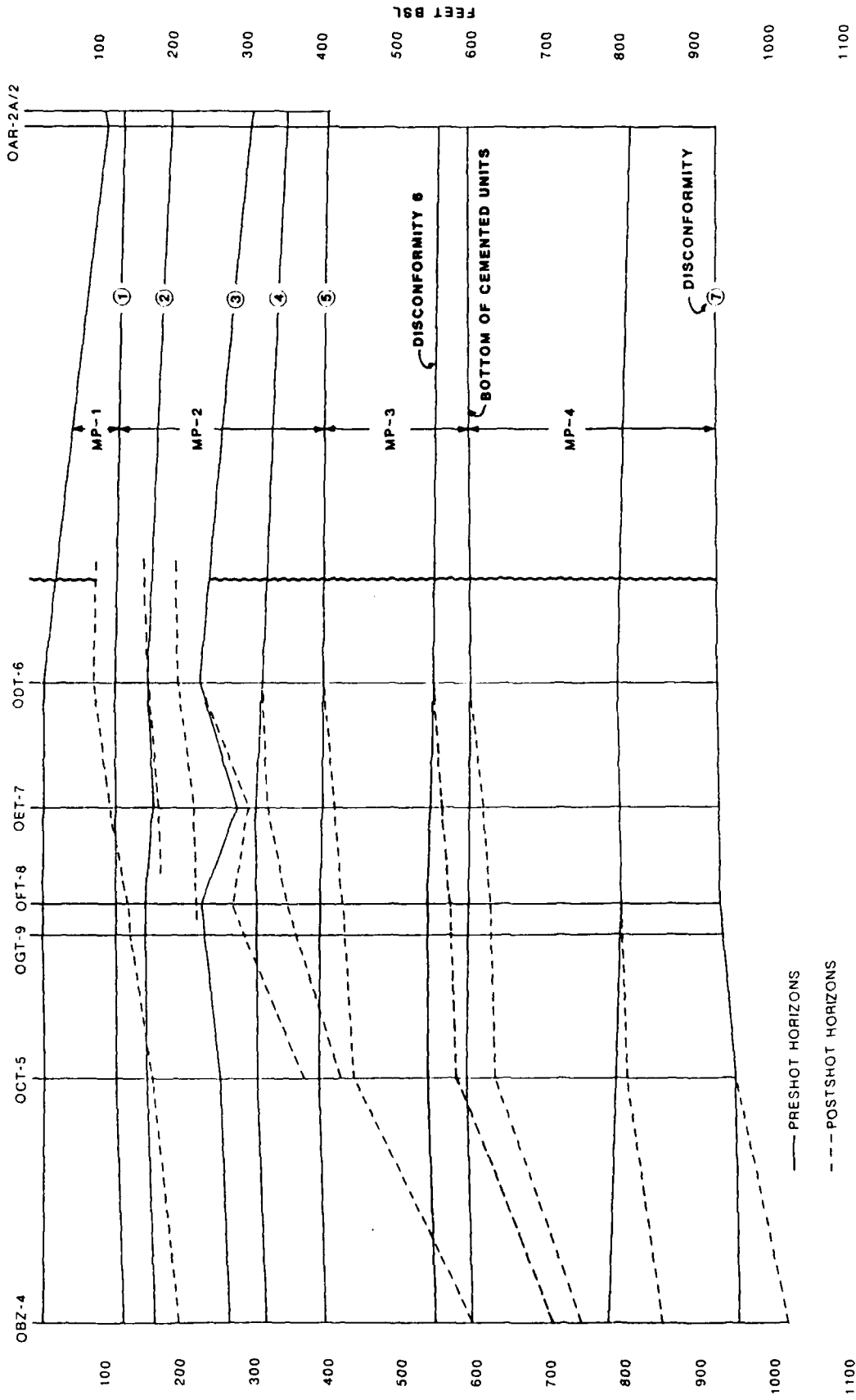


FIGURE 7-27. -- Horizon location in fence diagram from boreholes OBZ-4 to OAR-2/2A as in Figure 7-26. Squiggles, breaks, and scale as in Figure 7-9.

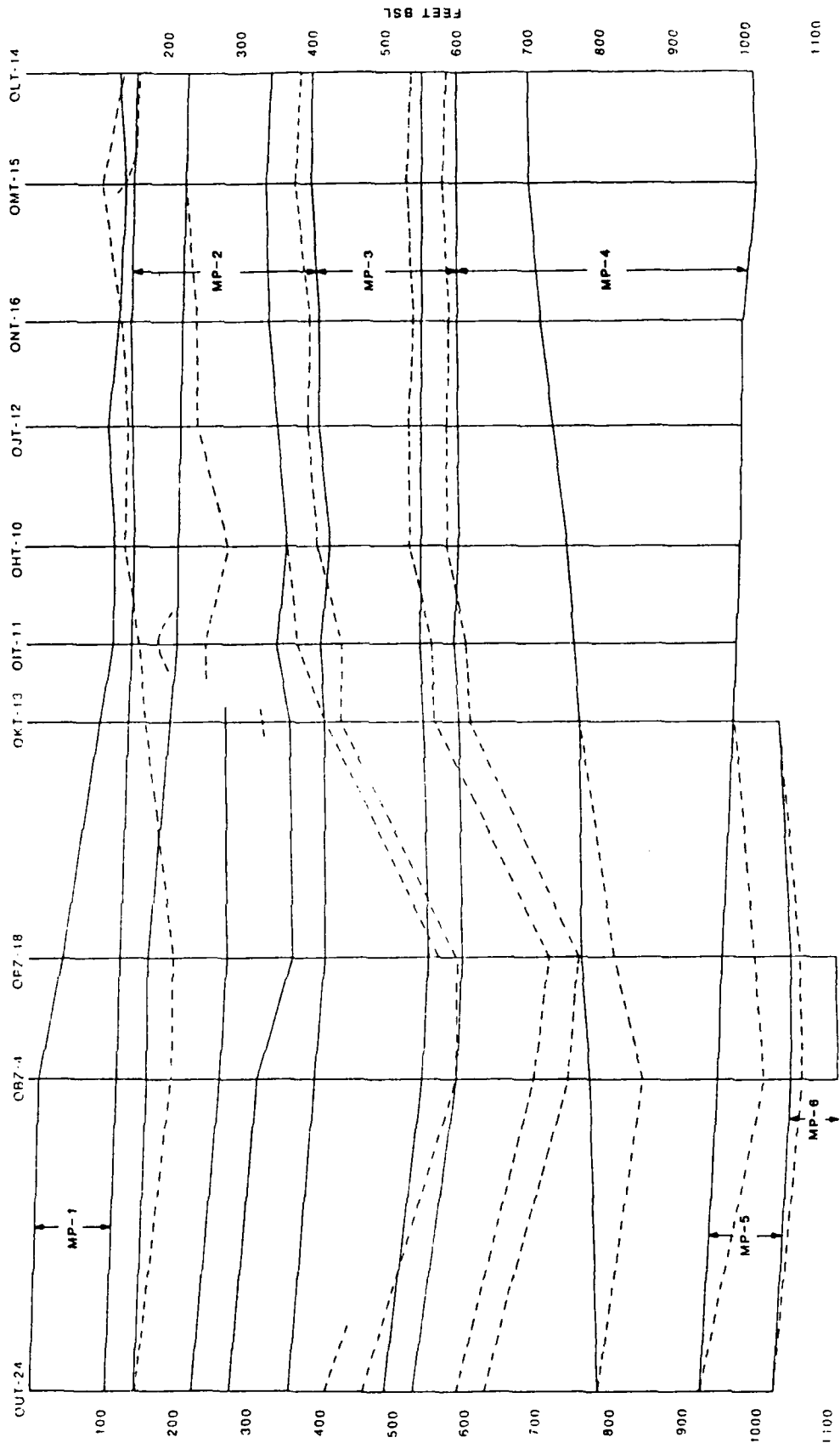


FIGURE 7-28. -- Horizon location in fence diagram from boreholes OUT-24 to OLT-14 as in Figure 7-26. Scale is vertically exaggerated 2:1.

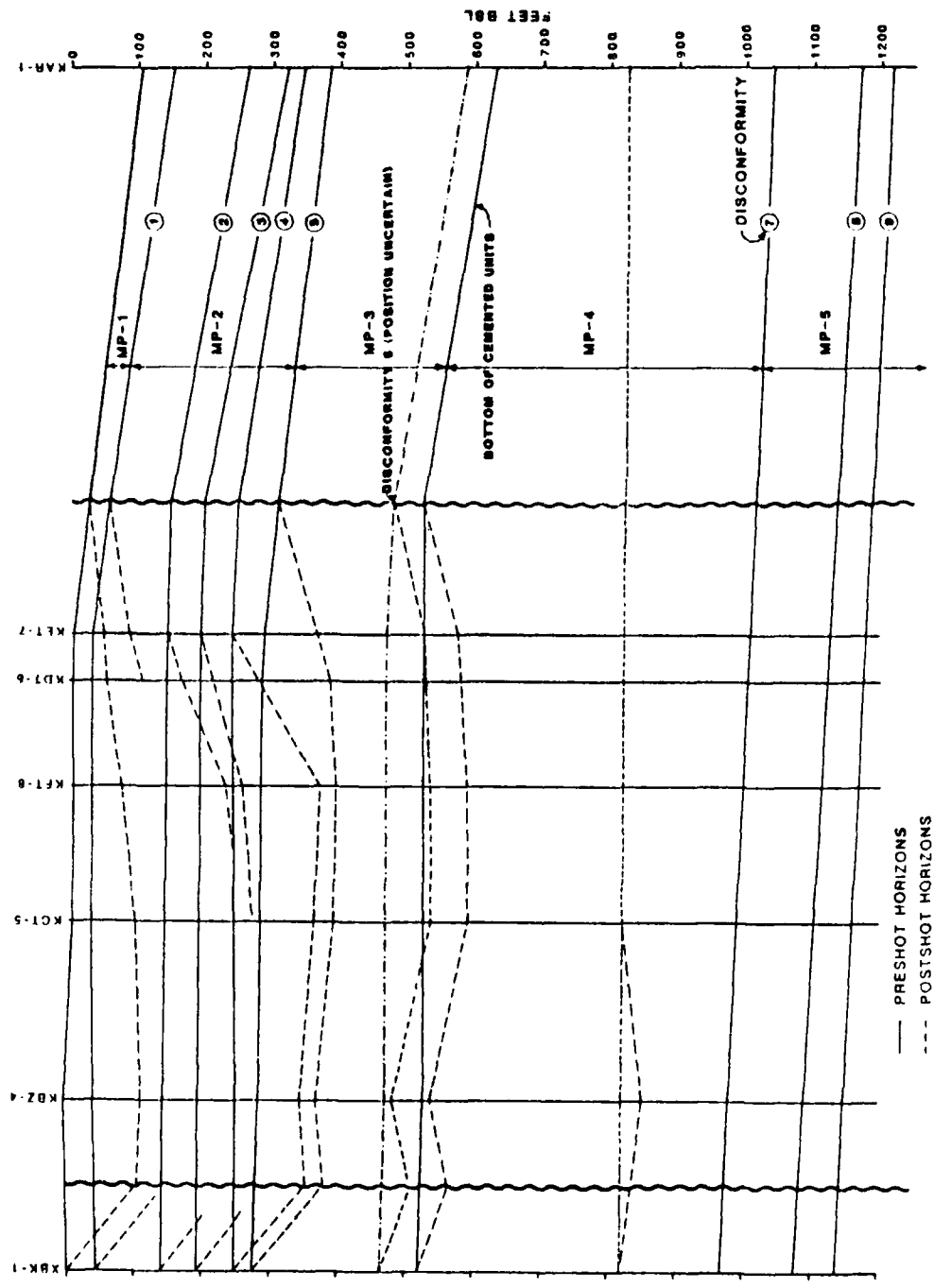


FIGURE 7-29. -- Horizon location in fence diagram from boreholes XBK-1a to KET-7 as in Figure 7-26. Squiggles, breaks, and scale as in Figure 7-7.

TABLE 7-6. -- Thinning/thickening analysis (in percent) of MP units beneath OAK crater. * = percent removed, where removal has occurred lower number indicates thinning in remaining sediments; + = percent thickened; averages indicated by brackets are weighted.

UNIT	OBZ-4	OPZ-18	OCT-5	OTG-23	OUT-24	OKT-13
1*	100	100	100	100	100	100
1	-	-	-	-	-	-
2*	28	17	40	26	28	11
2a	-	-	-	-	-	-
2b	- 02	- 08	- 47	- 19	- 30	11 15
2c	-	-	01	-	33	02
2d	-	49	69	39	37	59
3a	27 22	10 11	05 04	00 00	00 00	03 02
3b	04	15	00	00	00	01
4a	45 26	71 33	12 11	31 18	40 26	10 05
4b	05	00	09	09	00	00
5a	49 39	33 28	00	00	00	00
5b	23	20	00	00	00	00

UNIT	OFT-8	OIT-11	OET-7	OQT-19	ODT-6	ORT-20
1*	100	40	14	23	10	00
1	-	09	37	21	14	02
2*	00	00	00	00	00	00
2a	52	00	04	00	10	02
2b	35 22	06 03	34 15	09 11	68 16	17 09
2c	03	00	01	00	00	00
2d	12	00	00	37	00	17
3a	00 00	09 07	00 00	05 04	00 00	05 04
3b	00	00	00	00	00	00
4a	14 09	10 04	09 05	00	00	00
4b	00	00	00	00	00	00
5a	00	00	00	00	00	00
5b	00	00	00	00	00	00

UNIT	OHT-10	OJT-12	ONT-16	OMT-15	OLT-14
1*	100	100	100	89	53
1	-	-	-	-	-
2*	09	14	02	00	00
2a	-	-	-	+17	02
2b	- 13	16 18	17 13	00 10	00 07
2c	-	-	-	-	-
2d	27	27	17	35	18
3a	00	00	00	00	00
3b	00	00	00	00	00
4a	+11 +04	+12 +04	+10 +03	+21 +05	+15 +04
4b	00	00	00	00	00
5a	00	00	00	00	00
5b	00	00	00	00	00

TABLE 7-7. -- Depths (ft bsl) to MP unit boundaries, pre- and post-shot, KOA crater. Boreholes listed in order of increasing distance from ground-zero.

UNIT	KBZ-4		KCT-5		KFT-8		KDT-6		KET-7	
1	+7	-	7	-	6	-	5	-	5	-
2a	37	-	35	-	33	-	33	-	32	-
2b	145	(247.2)	146	(242.5)	146	233.1	147	166.8	148	148.0
2c	193	287.0	195	274.3	195	257.4	195	215.0	195	195.0
2d	250	344.0	246	365.4	244	372.0	243	282.0	242	242.0
3a	282	368.6	285	392.9	285	395.6	286	382.0	288	368.0
3b	470	480.7	470	-	470	-	470	-	470	-
4a	528	539.0	526	593.0	525	590.0	525	581.0	525	575.0
4b	820	848.1	820	820.0	820	820.0	820	820.0	820	820.0
5a	979	979.0	996	996.0	999	999.0	1005	1005.0	1008	1008.0
5b	1090	1089.6	-	-	-	-	-	-	-	-
5c	1147	1147.3	-	-	-	-	-	-	-	-

Distance of boreholes from ground-zero, in feet:

KBZ-4	12
KCT-5	645
KFT-8	870
KDT-6	1182
KET-7	1326

TABLE 7-8. -- Thinning/thickening analysis (in percent) of MP units beneath KOA crater, symbols as in Table 7-6.

UNIT	KBZ-4		KCT-5		KFT-8		KDT-6		KET-7	
1*	100		100		100		100		00	
1	-		-		-		-		+110	
2*	44		55		17		00		00	
2a	-		-		-		49		50	
2b	18	12	+64	+08	49	+16	00	+07	00	+08
2c	00		+78		+133		+39		00	
2d	24		30		57		+132		+173	
3a	41	31		17		19		17		13
3b	00									
4a	+05	03	23	15	23	14	19	12	17	11
4b	18		00		00		00		00	
5a	00		00		00		00		00	
5b	00		00		00		00		00	

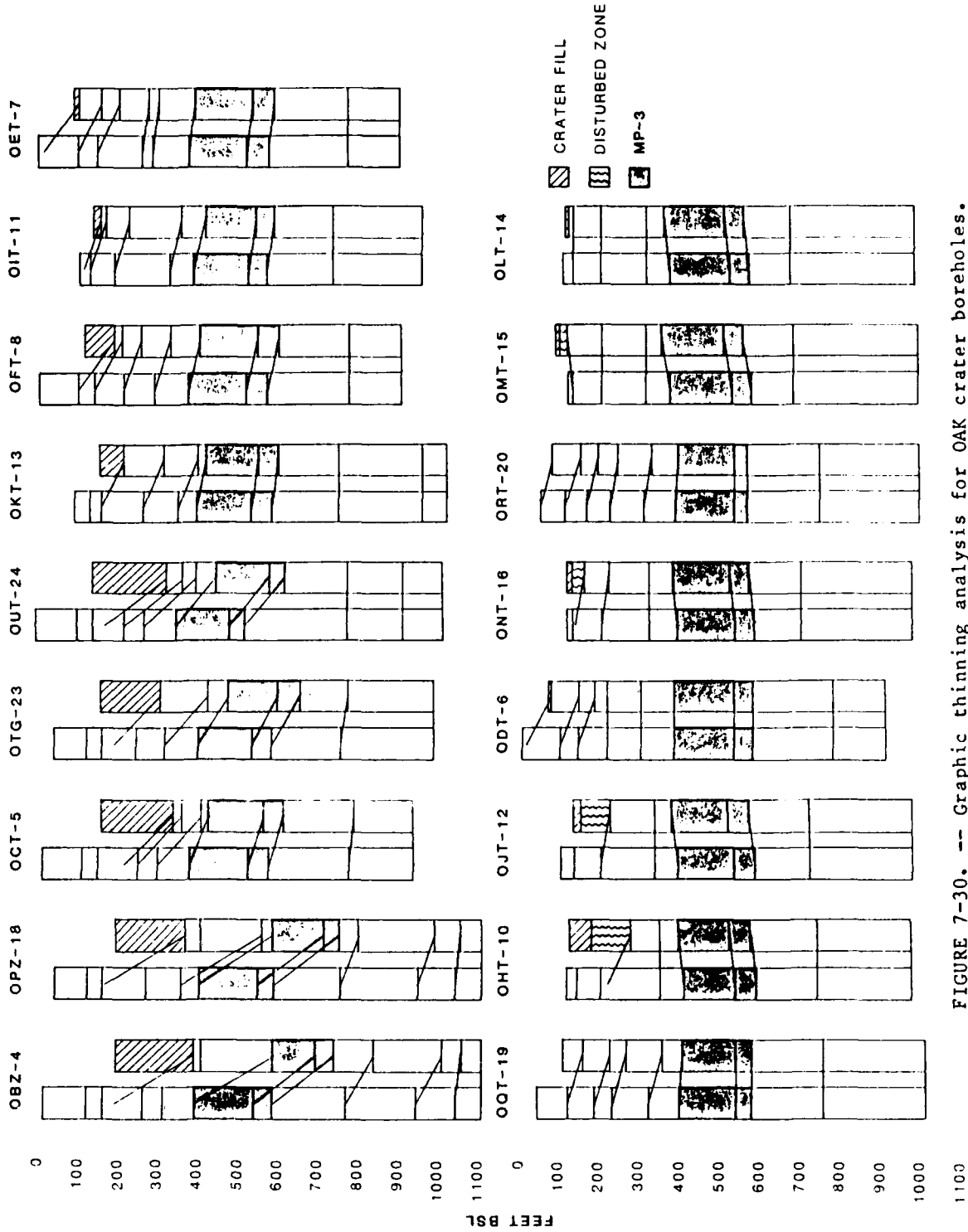


FIGURE 7-30. -- Graphic thinning analysis for OAK crater boreholes.
Correlation lines connect pre- and post-shot position of major horizons
including stratigraphic base of crater-fill.

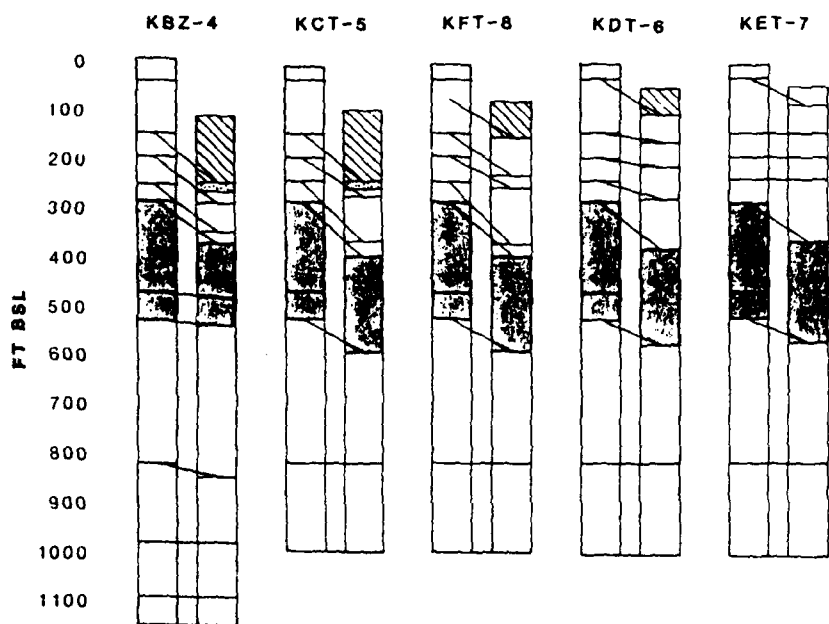


FIGURE 7-31. -- Graphic thinning analysis for KOA crater boreholes as in Figure 7-30.

TABLE 7-9. -- Stratigraphic bulk density analysis. Values in gm/cc. Change from bulk density model (the composite reference sections) is indicated in parenthesis.

AVERAGE DENSITIES FOR STRATIGRAPHIC MATERIAL PROPERTY UNITS AND CRATER ZONES						
MODEL	ORT-20	QQT-19	OTG-23	OPZ-18		
					1.812(-.06*)	α
					1.876(-.02*)	β_{1a}
1	--	1.855	1.895	--	1.982(+.03*)	β_{1b}
2a	1.965	1.923(-.02)	1.921(-.02)	--	1.967(+.03*)	β_2
2b	1.908	1.918(+.01)	1.904(-)	--	2.027(+.06*)	β_3
2c	1.919	1.923(-)	1.942(+.01)	2.017(+.05)	2.124(+.11)	2c
2d	1.920	1.985(+.03)	1.982(+.03)	2.030(+.06)	2.167(+.13)	2d
3a	1.978	1.985(-)	2.018(+.02)	2.052(+.04)	2.116(+.07)	3a
3b	1.976	--	1.950(-.01)	2.063(+.04)	2.080(+.05)	3b
4a	2.011	--	2.025(+.01)	2.150(+.07)	2.045(+.02)	4a
4b	--	--	1.959	--	1.993(+.02)	4b

The model is the average value for units in the reference boreholes OOR-17 and OSR-21, asterisk (*) indicates the difference in bulk density from average value value of normal sediments (2a-c) which is 1.919, QQT-19 is used for model density value of unit 4b.

α = Alpha β_{1a} = Beta 1a β_{1b} = Beta 1b
 β_2 = Beta 2 β_{3a} = Beta 3a

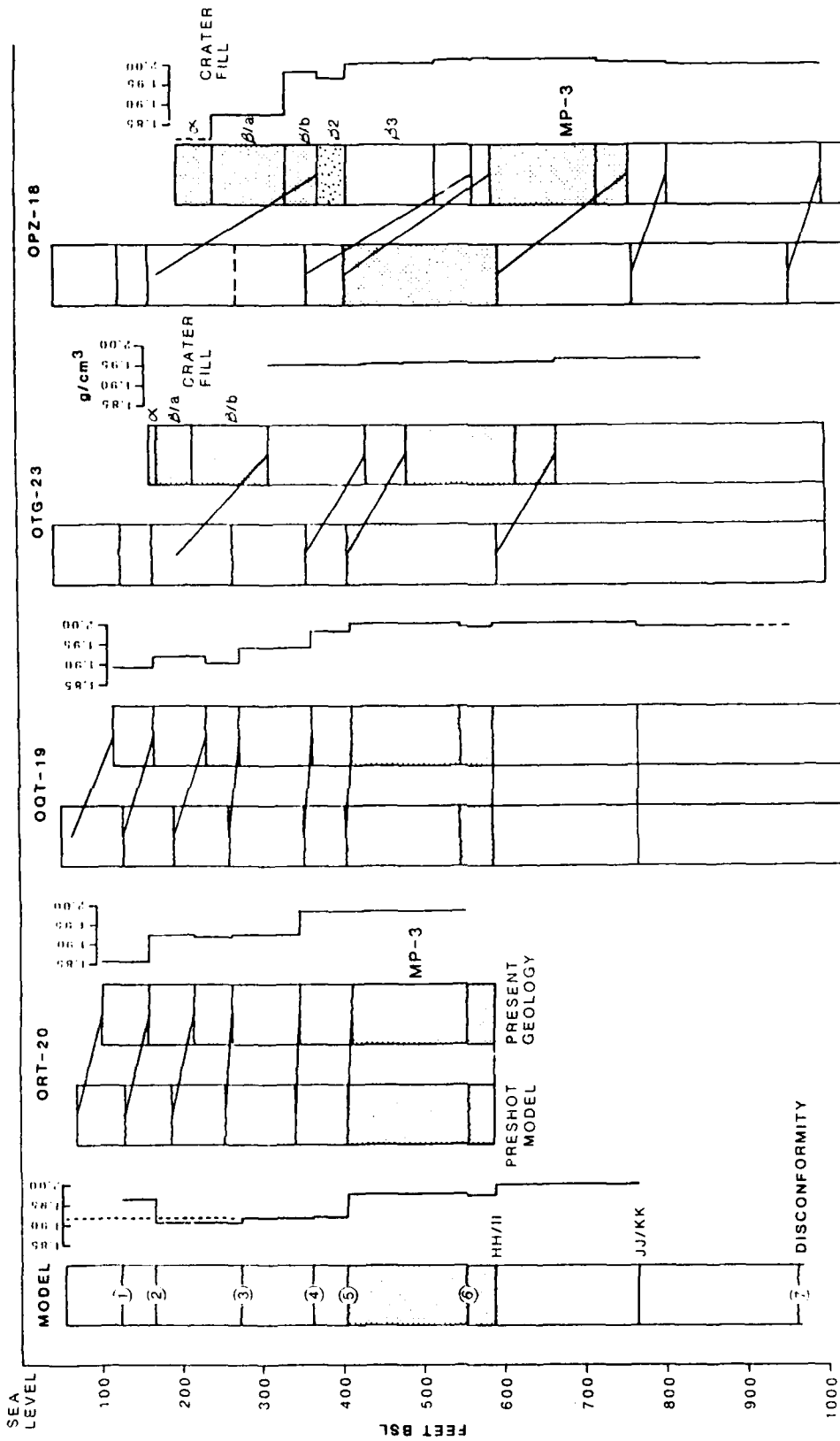


FIGURE 7-32. -- Stratigraphic density profile based on borehole gravimetry.

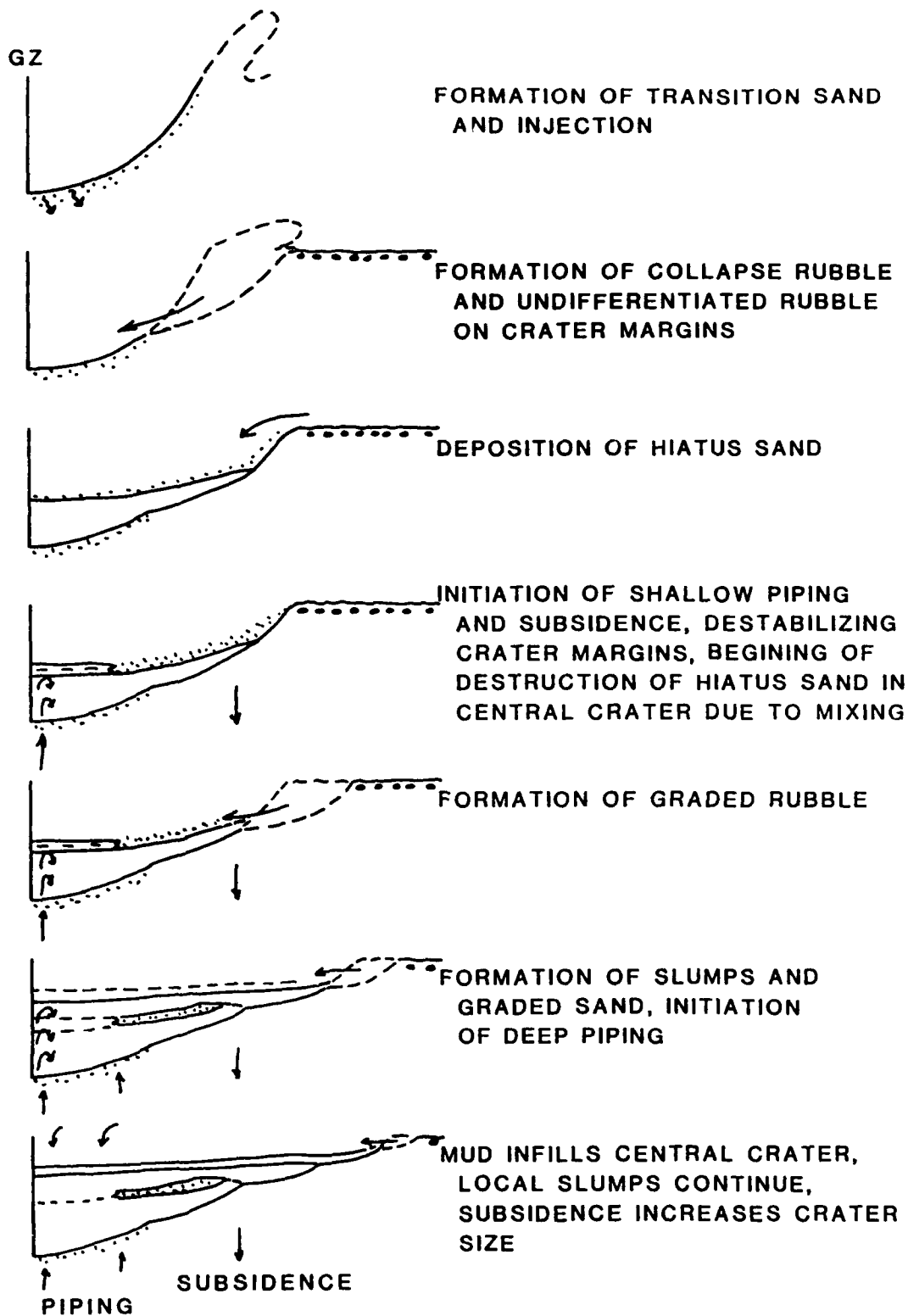


FIGURE 7-33. -- Idealized succession of major depositional events to form geologic crater. No horizontal scale is implied.

General Densification and Flow Patterns

OAK Crater.

The density values measured for the crater zones Alpha and Beta in OAK (OPZ-18) are compared to the average value of normal (undisturbed) sediments in MP-2(a-c). The author feels that the average value for MP-2a through MP-2c also adequately characterizes the upper sediments that were not measured by gamma-gamma density or borehole gravimetry (MP-1 and part of MP-2a). Material in the upper crater zones (Alpha and Beta 1a) in OAK appear to be less dense than normal sediments. Beta 1b and Beta 2 appear to be slightly more dense than normal sediments. Beta 3 has significant densification. Beneath the rubble zone (Beta), the rock and sediment occur in normal stratigraphic order, and density and thinning can be compared directly to the reference sections.

MP-2c (OPZ-18 and OTG-23) immediately subjacent to the Beta zone is moderately densified. Thinning of this unit cannot be calculated because the top of the unit is not preserved in either borehole. However, the significant densification in OPZ-18 suggests this unit behaved similar to the underlying unit, MP-2d in the area of that borehole.

MP-2d under the central crater area shows the most significant densification. However, densification cannot account entirely for the roughly 50 percent thinning of the unit over a wide area.

Densification within MP-3 accounts for most of the thinning observed within that unit except beneath the central crater. Beneath the central crater, collapse of vugs could compensate for considerable volume loss (thinning) with little observed density increase.

MP-4a shows essentially no densification under the central crater area and at least 40 percent thinning over a wide area. MP-4a and MP-4b are differentiated by organic concentration. It is probable that both units flowed and mixed obscuring their relationship in a manner so that the organics identifying MP-4b occur higher than predicted, and thinning in MP-4a is exaggerated (especially in OPZ-18). Nevertheless, the whole unit, MP-4, experienced 20 percent thinning over a wide area that is not accounted for by densification.

If the geologic pre-shot models are correct, than the stratigraphic units that show thinning is excess of that explained by densification must have been partially removed by flow. Two units under the central crater area that indicate significant flow are MP-2d and MP-4a. Material from these units previously has been shown to have been piped (vertical flow) to the surface. Material from MP-4 is involved in the majority of deep piping, but the estimated volume of that material preserved in the crater fill only accounts for a small amount of material that flowed.

It appears most of the volume lost is accounted by lateral flow. Two lines of evidence support this: (1) The density increase detected in MP-4 at the base of OTG-23 suggests lateral densification presumably from lateral

flow, and (2) The uplifted MP-3 over much of the lagoon (refer to fig. 7-21) appears to be caused by thickening of MP-4. This bulging or bulking of MP-4 clearly is visible in all the seismic-reflection survey profiles that run through the lagoon opposite the crater.

Piping (vertical flow) is clearly a post-dynamic phenomenon. The units that appear to have experienced lateral flow, also were involved with late-stage piping. These units in OAK appear to be MP-2c over a limited extent (because it was excavated in the central portion of the crater) and MP-2d, MP-4a, and MP-4b (over a wider extent). Deep piping appears to have been vented initially through the central part of the crater and subsequently through concentric fracture zones developed farther laterally (due to subsidence) represented by the piped mounds or volcanoes preserved on the terraces today. Shallow piping appears to be a more widespread phenomena over the crater area, though it too was, at least partially, vented through the central part of the crater as evidenced by the presence of shallow-piped material in all central crater zones.

KOA Crater.

By comparison with OAK crater, KOA experienced much more shallow lateral and vertical flow within its units. Thinning and bulking (thickening) is observed in MP-2b, MP-2c, and MP-2d. The thinning appears in increasing area in each lower unit and, therefore, the thickening occurs farther from ground-zero with depth. MP-3 appears more thinned than in OAK and may have experienced flow. MP-4 appears to have thinned and flowed. However, the thinning in MP-4 is complicated in its area of distribution; represented by central rebound and perhaps channeled vertical flow through the central uplift. Shallow piping appears to have been pervasive and is indicated by the common EE material in much of the mixed zone. Venting of some of the shallow-piped material in the areas of KBZ-4 and KCT-5 is suggested by the deeper mixing of this shallow-piped material in the crater fill of these boreholes.

Relative Timing of Depositional Events

The idealized succession of depositional events is shown in Figure 7-33.

For purpose of discussion, the following stages of crater development, referred to as craters, are defined:

- (1). Maximum transient crater. That crater formed when the outgoing velocity vector is zero, prior to rebound. The formation of the Beta 3 rubble beneath the excavational crater is thought to represent the maximum transient-crater growth.
- (2). Terminal transient crater. That crater formed at the end of the transient-crater phase, following rebound.
- (3). Collapse crater. That crater formed at the end of the formation of the rubble from the collapse of the sidewall/flap (early stage collapse, Beta 1b).

- (4). Initial slump crater. That crater formed at the end of the formation of late-stage collapse rubble (Beta 1a).
- (5). Apparent crater. That crater observed today, determined by extrapolation of post-shot measurements to the land or water surface at shot time (B. L. Ristvet, personal communication). This crater also has been referred to as the subsidence crater.

For OAK crater, in chronologic order from oldest to youngest, the sequence of depositional events is:

- (1). Formation of transition sand (Beta 2) at base of transient crater, dynamic lateral flow of subsurface units, air-blast deformation.
- (2). Collapse of excavational-crater wall/rim destroying lateral extent of transition sand and forming collapse rubble (Beta 1b); formation of collapse crater; initiation of liquefied (post-dynamic) flow, especially in MP-2c, MP-2d, MP-4a, and MP-4b; and initiation of subsidence.
- (3). Penecontemporaneous formation of undifferentiated rubble zone external of collapse crater by partial flap collapse in addition to prior air-blast deformation.
- (4). Penecontemporaneous formation of debris blanket by probable partial failure and movement of the excavational-crater wall/rim lagoonward.
- (5). Infilling of at least part of remaining crater bowl (collapse crater) by wash- and/or fall-back initiating deposition of "hiatus" sand (Beta 1s); and initiation of winnowing (removal in water suspension) of fine-grained sediments.
- (6). Continuation of deposition of "hiatus" sand over outer crater and contemporaneous initiation of shallow piping in the central crater; continued liquefied lateral flow and subsidence; continued winnowing.
- (7). A sequence of crater-margin collapses to form graded rubble (Beta 1a). One collapse (slump) resulted in a flow large enough to cross the crater, breach the debris blanket, and flow into the lagoon. Subsidence, piping, liquefied lateral flow, and winnowing continued. Shallow-piped material reached the surface throughout the crater before or during initiation of Beta 1a deposition.
- (8). Margin slumping and graded-sand (turbidite) deposition (Alpha 2); subsidence, piping, liquefied lateral flow, and winnowing continued. Deep-piped material reached the surface at the beginning of Alpha 2 deposition.
- (9). Late-time partial infilling of central part of the crater with mud (Alpha 1); subsidence, piping, and lateral flow continuing but progressively less. Mud deposition has continued to present. Local slumping, sand deposition, and winnowing has continued along the reef margin mainly as a consequence of natural geologic processes.

Because the OAK crater developed on a slope, the bathymetric center of the crater moved downslope at the end of early-stage collapse (generally shown as an apparent, progressively lagoonward migration of the low point of successive crater-fill units in fig. 7-25B).

For KOA crater, the events (from oldest to youngest) are:

- (1). Same as in OAK.
- (2). Same as in OAK; liquefied lateral flow especially in MP-2b, MP-2c, MP-2d, MP-4a, and MP-4b.
- (3). Penecontemporaneous formation of debris mounds by partial MIKE-ward collapse and movement of crater wall/rim.
- (4). Same as in OAK, resulting in the much-thickened section at KET-7.
- (5). Same as in OAK.
- (6). Possible deposition of a thin "hiatus" sand over outer crater (this was mostly destroyed by subsequent collapse); initiation of shallow piping; and continued liquefied lateral flow and subsidence.
- (7). A sequence of crater-margin collapse to form graded rubble; subsidence, shallow piping, and liquefied lateral flow continued.
- (8). Margin slumping and graded-sand (turbidite-flow) deposition (Alpha 2) and piping in the central part of the crater; continued but reduced subsidence and lateral flow. Deep-piped material reached the surface at the initiation of Alpha 2 deposition.
- (9). Late-time infilling of central part of the crater with mud (Alpha 1); localized slumping and sand deposition around most of crater (except near MIKE). Subsidence has lessened markedly. Deep piping has discontinued before deposition of mud (Alpha 1).

VOLUME PROBLEMS

Beyer (Ch. 2 of this report) and Trulio (Ch. 6) demonstrate that densification can only account for 8 to 15 percent of the subsidence measured in the crater wings of OAK. Yet OAK appears to be substantially a subsidence crater. Peterson and Henny (Ch. 5) show substantial late-time subsidence (post two months post-shot) by comparing the 1958 H&N post-shot map with the 1984 USGS bathymetric map. Peterson and Henny estimate an apparent (conservative) volume increase of the crater of 231 million cubic ft or 25 percent of the apparent crater volume. Piping clearly demonstrates the existence of a long-term unstable liquefied mass at depth beneath the crater.

Piping is one avenue by which this liquefied mass could achieve stability. It is the expression of liquefied flow vertically. Dikes, lagoon uplift, and densification of MP-4 laterally all demonstrate lateral flow.

Evidence for Piping and Lateral Flow

Piping is not an hypothesis but a process the results of which are observed in both OAK and KOA craters.

Surface. -- Sand volcanoes are present on the terraces of OAK crater (fig. 7-14). Their presence on the terraces indicates that deep piping persisted after the majority of Alpha deposition (slumps and sand turbidity flows) and that flow (at least vertical) is a very long-term process.

Crater-Fill. -- The volume of piped material is estimated for the crater-fill of the central bowl of OAK. Deep-piped material (biostratigraphic zones II-MM) is 4.83 million cubic ft. Shallow-piped material (biostratigraphic zones FF-GG) is 45.62 million cubic ft. Deep-piped material is only surficial outside the central bowl (i.e., on the terraces). Shallow-piped material is throughout the crater-fill above the hiatus sand (Beta 1s), so an appreciable additional volume exists but has not been calculated (further paleontologic study is needed for these estimates). Shallow piping reached the crater surface after deposition of the hiatus sand. Deep piping reached the crater surface after deposition of the graded rubble (Beta 1b). This is true for both OAK and KOA craters and suggests that shallow piping reached the surface on the order of minutes, deep piping on the order of hours, and both persisted for days. In OAK, deep- and shallow-piped material is present in the late-stage mud (Alpha 1) deposits suggesting very long-term deposition (many months). In KOA, only shallow-piped material is present in the late-stage mud (Alpha 1) deposits. Deep-piped material is present in the graded sands (Alpha 2) suggesting an ending of deep-piping at the initiation of Alpha 1 deposition in KOA (approximately 1-2 months). If the liquefied material mass exhibits vertical flow for days, why is lateral flow constrained to the dynamic phase of crater development? Material from MP-4 (deep-piped) would have an effective seal by MP-3 in most places except in the proximity of large fractures and vents. The material was depressed under the central crater and the sealed avenue of flow would be up along the lower surface of MP-3.

Subsurface. -- Unit MP-4 shows densification away from the central crater. Borehole gravimetry shows a substantial increase in density in MP-4 in OQT-23 for that part that was measured (refer to tbl. 7-9). Gamma-gamma density shows a similar substantial increase in density throughout MP-4 in OKT-13. The H&N post-shot bathymetry (Peterson and Henny, Ch. 5 of this report) shows a rise in the lagoon sea-floor depth that exceeds the thickness of the debris measured in several boreholes. This indicates uplift of the surface. As previously mentioned, MP-3 shows uplift throughout the lagoon (refer to fig. 7-22). Both these lines of evidence suggest significant lateral flow of MP-4, densifying the material laterally and uplifting the overlying sediment and rock over much of the lagoon. It appears that calculations down to the line of zero net displacement (contour D, Trulio, Ch. 6 of this report) do not adequately encompass all significant subsurface crater phenomena because much appears to happen below this line.

Loss of Material from the Crater. -- In OAK, large ejecta or debris is found entirely within the apparent crater. Halley and others (1986b) demonstrated several clasts (unspecified size, but generally cobble-sized or larger material collected by submersible) to be debris. Debris rays were observed along the reef tract, generally all within the apparent crater. The debris blanket is within the apparent crater. Where did all the material go to form the apparent crater?

Debris is indicated outside the apparent crater in three places:

- (1). In the breach and turbidite flow deposit (fig. 7-14) deposition of an unknown volume of debris is inferred from the enhanced sea-floor image.
- (2). At OAR-2A, the upper 25 ft of sediment (mostly sand) contains highly shocked material, probably ejecta swept from the reef tract and deposited at this site. This thickness could represent a substantial amount of material deposited along the toe of the slope from reef to lagoon on both the northeast and southwest sides of the crater.
- (3). In mud in the lagoon, clay-sized material is common in samples from throughout the northeastern part of the lagoon (Wardlaw and Henry, 1986b). It is probably mostly blast-derived and represents a substantial volume of fine-grained ejecta and material from the craters. Post-shot photographs show mud-laden plumes into the ocean and lagoon far beyond the apparent crater, suggesting this loss was not trivial.

The uplifted area in the lagoon near OAK (fig. 7-22) suggests that a considerable volume of material from MP-4 moved outside the apparent crater in the subsurface. If a 5-7 percent density increase accompanied this thickening it would account for an appreciable amount of the apparent crater.

SUMMARY

OAK and KOA craters are similar. They exhibit the same geologic crater zonation. The zone of sonic degradation that defines the geologic crater is very similar for both craters. OAK and KOA differ in type of device, in coupling, and in depth and radius of the various stages of crater development that are not within the scope of this paper. The KOA area was preconditioned by MIKE and possibly other devices. It contains a better, thicker cemented interval (MP-3) at shallower depths than OAK. These two factors contributed strongly to the major differences between KOA and OAK. KOA is a crater that developed early and had far less late-stage modification, as indicated by its lack of late-stage piping and diminished late-stage subsidence. OAK, on the other hand, is a crater most of which developed later and had significant late-stage subsidence and piping. It appears that as much as 66 percent of the apparent crater volume of OAK may be due to subsidence. In contrast, only about 20 percent of KOA may be due to subsidence.

Piping requires a liquefied material mass at depth. Piping lasted for months at both craters. Subsidence lasted for months at both craters. The prolonged existence of a liquefied material mass at depth is related causally to prolonged subsidence.

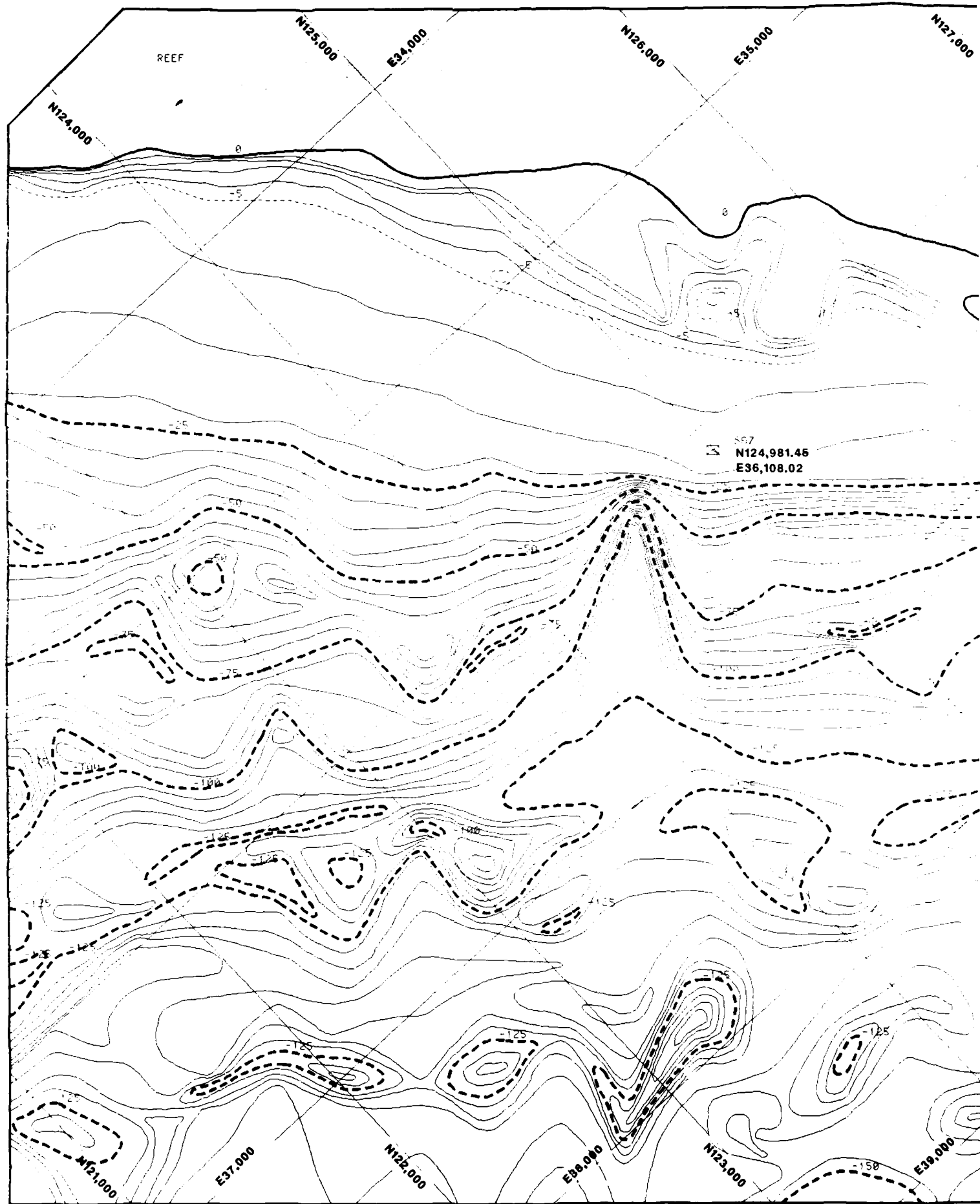
REFERENCES CITED

- Beyer, L. A., Ristvet, B. L., and Oberste-Lehn, D., 1986, Chapter 8: Preliminary density and porosity data and field techniques of borehole gravity surveys, OAK crater, in, Henry, T. W., and Wardlaw, B. R., eds., Pacific Enewetak Atoll Crater Exploration (PEACE) Program, Enewetak Atoll, Republic of the Marshall Islands; Part 3: Stratigraphic analysis and other geologic and geophysical studies in vicinity of OAK and KOA craters: U.S. Geological Survey Open-File Report 86-555, 28 p.
- Beyer, L. A., 1987, Chapter 2: Analysis of borehole gravity surveys at OAK crater, in, Henry, T. W., and Wardlaw, B. R., eds., Pacific Enewetak Crater Exploration (PEACE) Program, Enewetak Atoll, Republic of the Marshall Islands; Part 4: Additional studies of OAK and KOA craters, U.S. Geological Survey Open-File Report 87-xxx.
- Brouwers, E. M., Cronin, T. M., and Gibson, T. G., 1986, Chapter 11: Additional paleontologic studies, OAK and KOA craters, in, Henry, T. W., and Wardlaw, eds., Pacific Enewetak Atoll Crater Exploration (PEACE) Program, Enewetak Atoll, Republic of the Marshall Islands; Part 3: Stratigraphic analysis and other geologic and geophysical studies in vicinity of KOA and OAK craters: U.S. Geological Survey Open-File Report 86-555, 18 p.
- Couch, R. F., Jr., Fetzer, J. A., Goter, E. R., Ristvet, B. L., Tremba, E. L., Walter, D. R., and Wenland, V. P., 1975, Drilling operations on Eniwetok Atoll during Project EXPOE: Air Force Weapons Laboratory Technical Report AFWL-TR-75-216, Kirtland Air Force Base, New Mexico, 270 p.
- Cronin, T. M., Brouwers, E. M., Bybell, L. M., Edwards, L. E., Gibson, T. G., Margerum, R., and Poore, R. Zoro, 1986, Pacific Enewetak Crater Exploration (PEACE) Program, Enewetak Atoll, Republic of the Marshall Islands; Part 2: Paleontology and biostratigraphy application to OAK and KOA craters, U.S. Geological Survey Open-File Report 86-159, 39 p.
- Cronin, T. M., and Gibson, T. G., 1987, Chapter 3: Paleontologic evidence for sedimentary mixing at OAK crater, Enewetak Atoll, in, Henry, T. W., and Wardlaw, B. R., eds., Pacific Enewetak Crater Exploration (PEACE) Program, Enewetak Atoll, Republic of the Marshall Islands; Part 4: Additional studies of OAK and KOA craters, U.S. Geological Survey Open-File Report 87-665.
- Folger, D. W., Robb, J. M., Hampson, J. C., Davis, P. A., Bridges, P. M., and Roddy, D. J., 1986, Sidescan-sonar survey of OAK and KOA craters, in, Folger, D. W., ed., Sea-floor observations and subbottom seismic characteristics of OAK and KOA craters, Enewetak Atoll, Marshall Islands: U.S. Geological Survey Bulletin 1678, 18 p.
- Grow, J. A., Lee, M. W., Miller, J. J., Agena, W. F., Hampson, J. C., Foster, D. S., and Woellner, R. A., 1986, Multichannel seismic-reflection survey of KOA and OAK craters, in, Folger, D. W., ed., Sea-floor observations and subbottom seismic characteristics of OAK and KOA craters, Enewetak Atoll, Marshall Islands: U.S. Geological Survey Bulletin 1678, 46 p.

- Halley, R. B., Slater, R. A., Shinn, E. A., Folger, D. W., Hudson, J. H., Kindinger, J. L., and Roddy, D. J., 1986a, Observations of OAK and KOA craters from the submersible, in, Folger, D. W., ed., Sea-floor observations and subbottom seismic characteristics of OAK and KOA craters, Enewetak Atoll, Marshall Islands: U.S. Geological Survey Bulletin 1678, 32 p.
- Halley, R. B., Major, R. P., Ludwig, K. R., Peterman, Z. L., and Matthews, R. K., 1986b, Preliminary analyses of OAK debris samples, in, Folger, D. W., ed., Sea-floor observations and subbottom seismic characteristics of OAK and KOA craters, Enewetak Atoll, Marshall Islands: U.S. Geological Survey Bulletin 1678, 11 p.
- McMurtry, G. M., Schneider, R. C., Colin, P. K., Buddemeier, R. W., and Suchanek, R. H., 1985, Redistribution of fallout radionuclides in Enewetak Atoll lagoon sediments by calianassid bioturbation: *Nature*, v. 313, no. 6004, p. 674-677.
- Peterson, J. L., and Henny, R. W., 1987, Chapter 5: Bathymetric studies of OAK crater, in, Henry, T. W., and Wardlaw, B. R., eds., Pacific Enewetak Crater Exploration (PEACE) Program, Enewetak Atoll, Republic of the Marshall Islands; Part 4: Additional studies of OAK and KOA craters: U.S. Geological Survey Open-File Report 87-665.
- Polanskey, Carol, and Ahrens, T. J., 1987, Chapter 4: Shock history of PEACE samples, in, Henry, T. W., and Wardlaw, B. R., eds., Pacific Enewetak Crater Exploration (PEACE) Program, Enewetak Atoll, Republic of the Marshall Islands; Part 4: Additional studies of OAK and KOA craters: U.S. Geological Survey Open-File Report 87-665.
- Ristvet, B. L., Tremba, E. L., Couch, R. F., Jr., Fetzer, J. A., Goter, E. R., Walter, D. R., and Wendland, V. P., 1978, Geologic and geophysical investigations of the Enewetak nuclear craters: Air Force Weapons Laboratory Technical Report AFWL-TR-77-242, 300 p.
- Ristvet, B. L., and Tremba, E. L., 1986, Chapter 12: Radiation chemistry of the subsurface of OAK and KOA craters, in, Henry, T. W., and Wardlaw, B. R., eds., Pacific Enewetak Atoll Crater Exploration (PEACE) Program, Enewetak Atoll, Republic of the Marshall Islands; Part 3: Stratigraphic analysis and other geologic and geophysical studies in vicinity of OAK and KOA craters: U.S. Geological Survey Open-File Report 86-555, 15 p.
- Trulio, J. G., 1987, Chapter 6: Constraints on densification and piping in the OAK event, in, Henry, T. W., and Wardlaw, B. R., eds., Pacific Enewetak Crater Exploration (PEACE) Program, Enewetak Atoll, Republic of the Marshall Islands; Part 4: Additional studies of OAK and KOA craters: U.S. Geological Survey Open-File Report 87-665.

Wardlaw, B. R., and Henry, T. W., 1986a, Chapter 2: Physical stratigraphic framework, in, Henry, T. W., and Wardlaw, B. R., eds., Pacific Enewetak Atoll Crater Exploration (PEACE) Program, Enewetak Atoll, Republic of the Marshall Islands; Part 3: Stratigraphic analysis and other geologic and geophysical studies in vicinity of OAK and KOA craters: U.S. Geological Survey Open-File Report 86-555, 36 p.

Wardlaw, B. R., and Henry, T. W., 1986b, Chapter 14: Geological interpretation of OAK and KOA craters, in, Henry, T. W., and Wardlaw, B. R., eds., Pacific Enewetak Atoll Crater Exploration (PEACE) Program, Enewetak Atoll, Republic of the Marshall Islands; Part 3: Stratigraphic analysis and other geologic and geophysical studies in vicinity of OAK and KOA craters: U.S. Geological Survey Open-File Report 86-555, 39 p.



OAK CRATER SHOT CONTOUR MAP

OPEN-FILE REPORT 87-665
PLATE 5-1

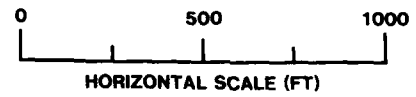
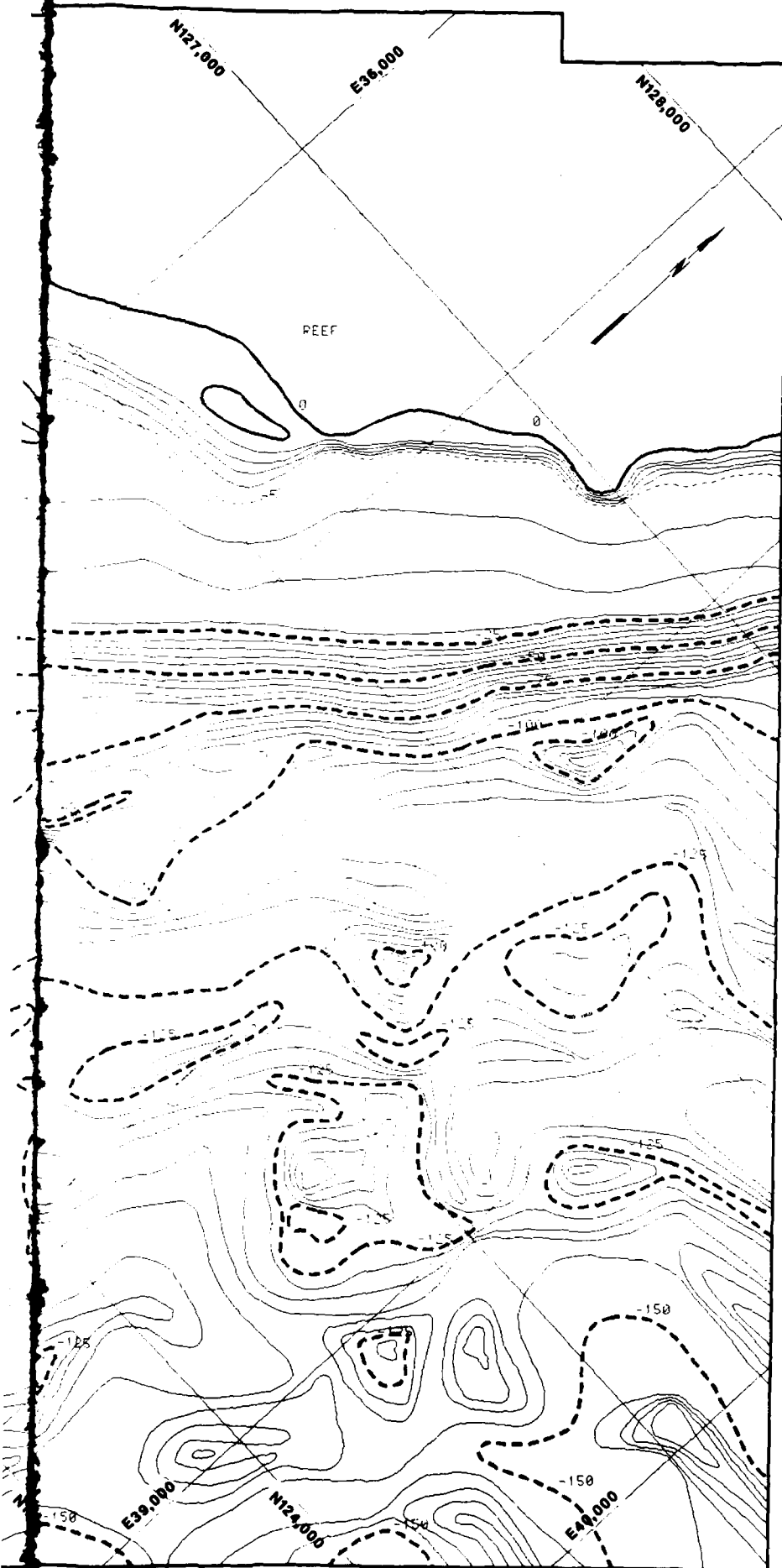


PLATE 5-1
OAK CRATER, ALICE REEF (STA. 25)
H&N (1258) PRESHOT TOPOGRAPHIC AND HYDROGRAPHIC MAP

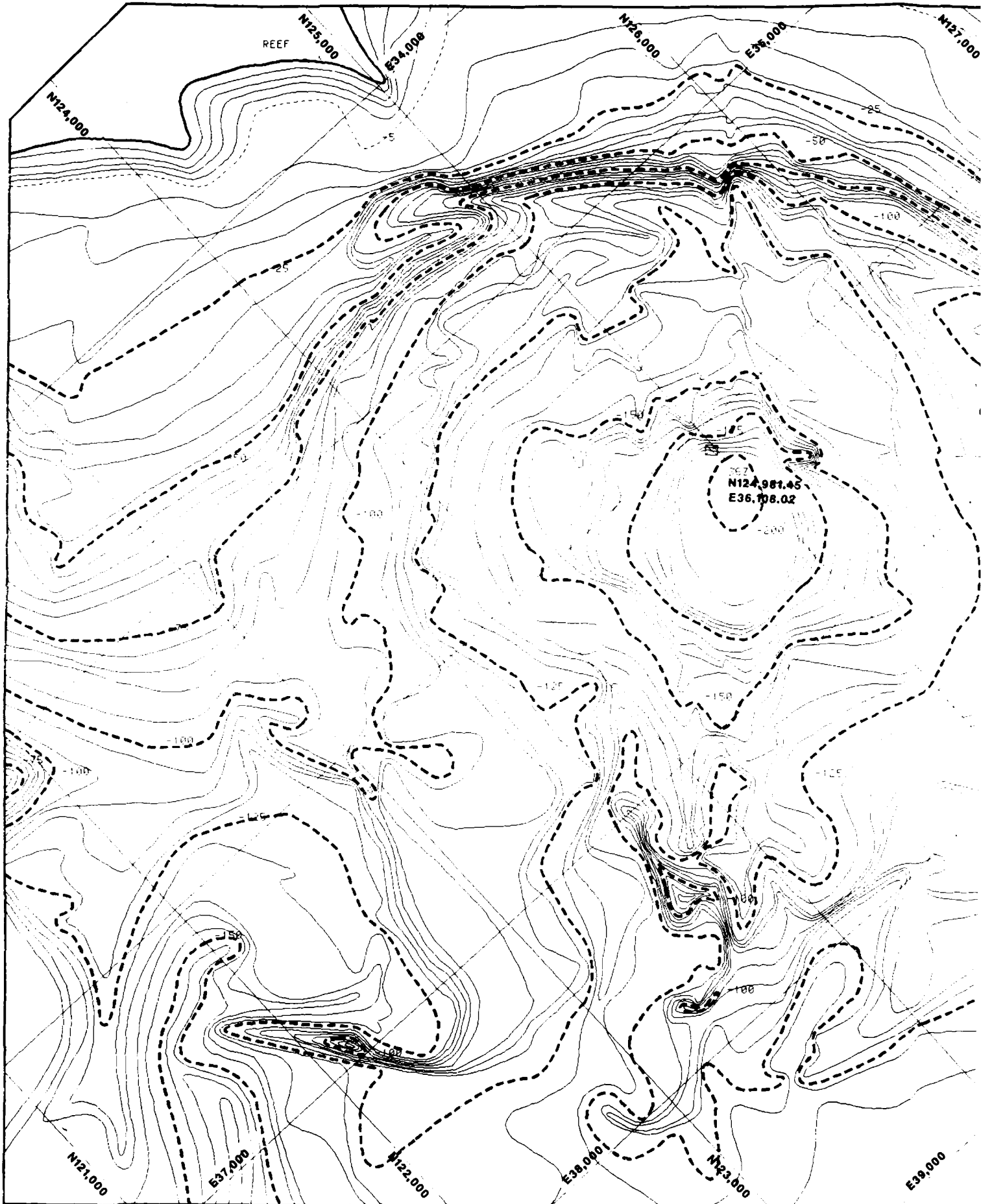
Map prepared for the PEACE Program for the Air Force Weapons Laboratory (AFWL) under the direction of the New Mexico Engineering Research Institute (NMERI) by the Technology Applications Center (TAC), December 1986.

BASE MAP:

Holmes and Narver, Inc.; Blue-line copy of "Topography & Hydrography Sta. 25, Alice Reef," June 9 through 26, 1958; Sheet No. J/S 03-001-C10; dated September 13, 1958; Survey conducted for U.S. Atomic Energy Commission (AEC).

NOTES:

- Contour interval above the minus 5 ft datum is 1 ft.
- Contour interval below the minus 5 ft datum is 5 ft.
- Dotted lines represent contours above the 0 ft datum.
- Thick solid line represents 0 ft elevation.
- Dashed-dotted line represents the minus 5 ft contour.
- Dashed lines represent 25 ft contour increments below 0 ft elevation.
- Datum is 0.5 ft below Approximate Mean Low Water Springs (AMLS).
- Datums: Survey based on the Texas State Plane North Zone system, units in ft.
- Surface: Figure 100, 1:50,000, NAD 83, 124,901,150 and 1:50,000, 124,901,150.



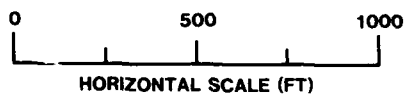
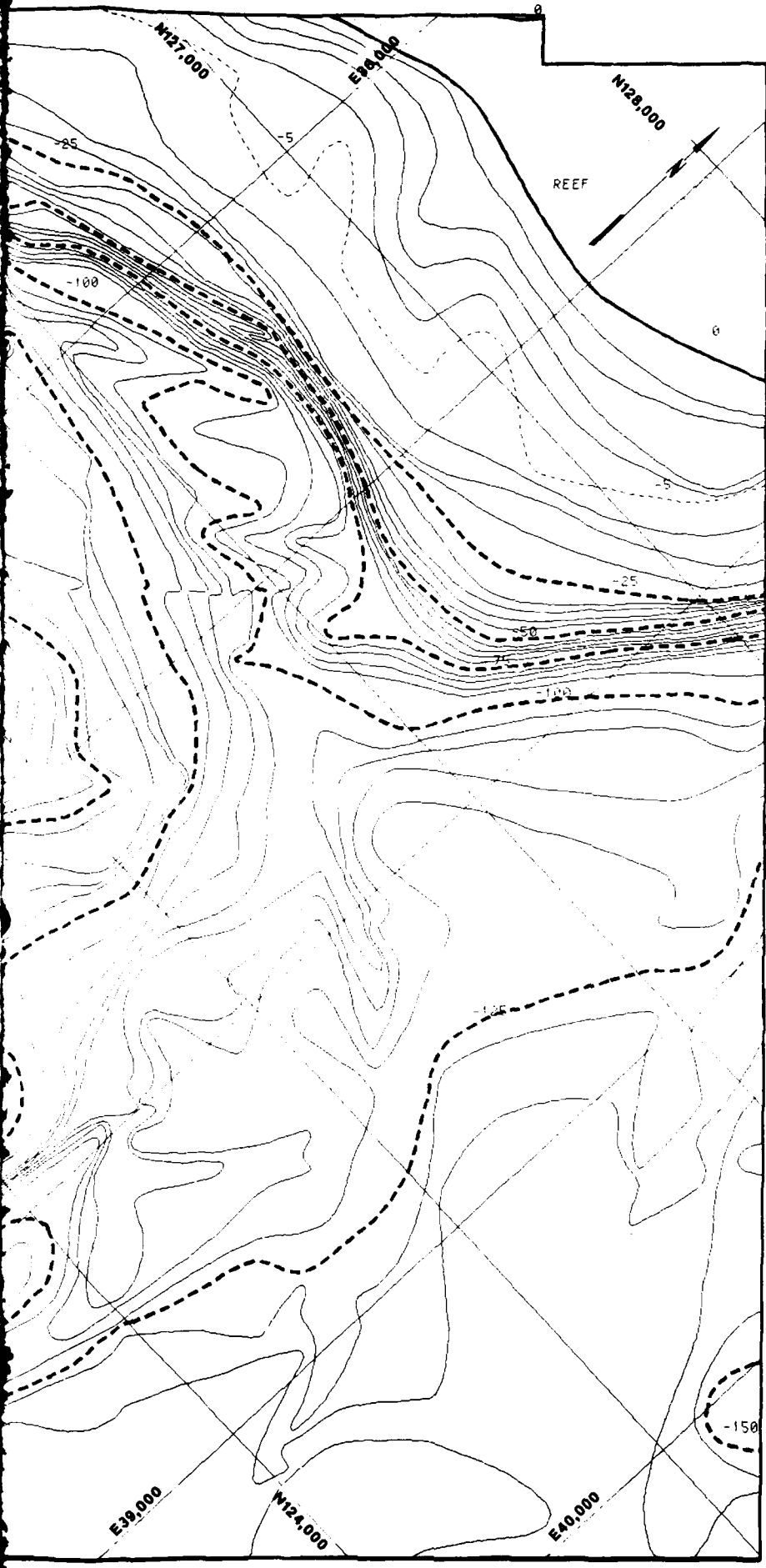


PLATE 5-2
 OAK CRATER, ALICE REEF (STA. 25)
 H&N (1958) PRESHOT TOPOGRAPHIC AND HYDROGRAPHIC MAP

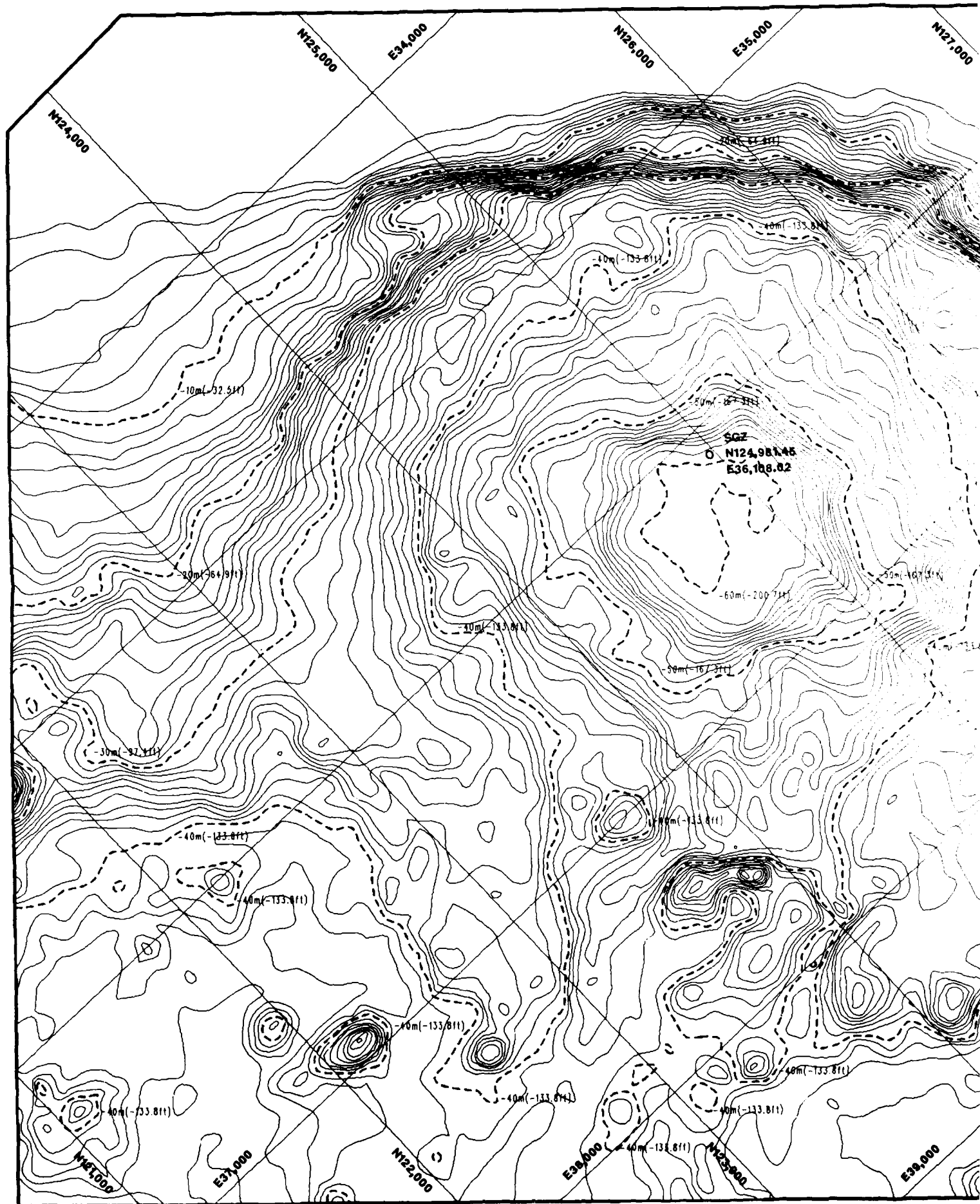
Map prepared for the PEACE Program for the Air Force Weapons Laboratory (AFWL) under the direction of the New Mexico Engineering Research Institute (NERI) by the Technology Applications Center (TAC), December 1946.

BASE MAP:

Holmes and Narver, Inc.; Blue-line copy of "Topography & Hydrography Sta. 25, Alice Reef," August 16 through September 4, 1958; Sheet No. J'S 02-001-111; dated October 1, 1958. Survey conducted for U.S. Atomic Energy Commission (AEC).

NOTES:

- Contour interval above the minus 5 ft datum is 1 ft.
- Contour interval below the minus 5 ft datum is 5 ft.
- Dotted lines represent contours above the 0 ft datum.
- Thick solid line represents 0 ft elevation.
- Dashed-dotted line represents the minus 5 ft contour.
- Dashed lines represent 25 ft contour increments below 0 ft elevation.
- Datum is 0.5 ft below Approximate Mean Low Water Spring (AMLWS).
- Celestial Survey based on the IVF Grid Coordinate System (units in ft).
- Surface Ground Zero (SGZ) coordinates: N = 124,481.45 and E = 36,108.02.



POSTSHOT CONTOUR MAP

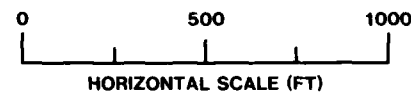
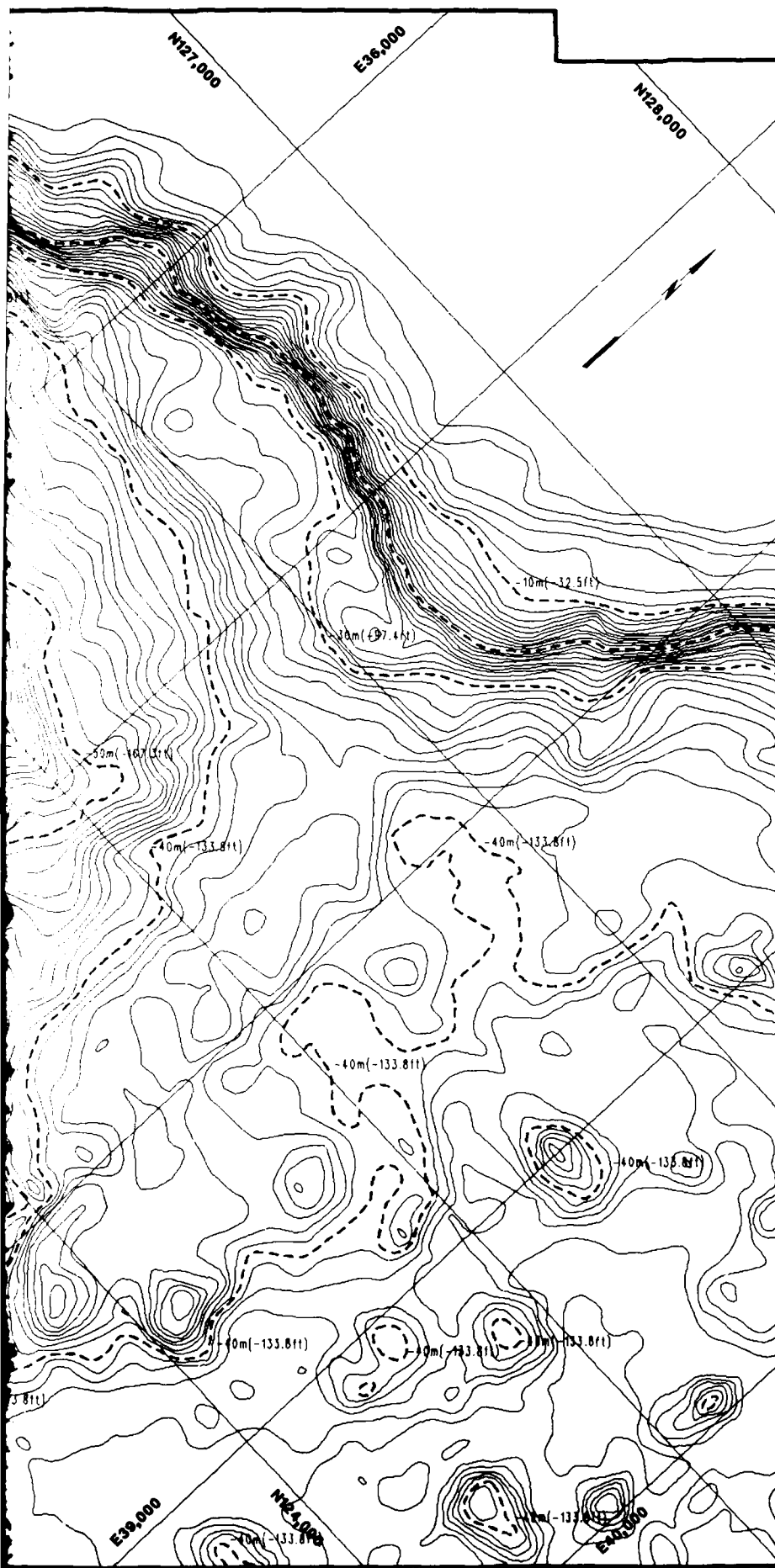


PLATE 5-3
OAK CRATER, ALICE REEF (STA. 25)
USGS (1984) POSTSHOT HYDROGRAPHIC MAP

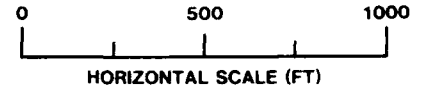
Map prepared for the PEACE program for the Office of Naval Operations, Laboratory AFM, under the direction of the Naval Weapons Engineering Research Institute (NWEI) by the Technology Applications Center (TAC), 1984.

BASE MAP:
U.S. Geological Survey (1984); "Bathymetric Map of Oak Crater Area, Eniwetok Atoll," Surveyed June 1 through September 20, 1984; compiled September 1985. The base map is a mylar working-scale copy 1:6000 of the map published in 1986 in U.S. Geological Survey Bulletin 167B as Fig. 7, D, AP. Survey conducted for Defense Nuclear Agency (DNA).

- NOTES:
- Contour interval is 1 m (approximately 3.3 ft).
 - Data incomplete above minus 4 m (minus 13.0 ft).
 - Dashed lines represent 10 m contour intervals displayed with depth corrected values in ft.
 - Data corrected for water depths as determined from Drilling Phase of PEACE Program.
 - Cadastral Survey based on the 1971 Grid Coordinate System (units in ft).
 - Surface Ground Zero (SGZ) coordinates: N = 174,981.45 and E = 37,100.00.



**OAK CRATER
SHOT ISOPACH MAP, NEGATIVE Δ -RELIEF**



LEGEND

● - BOREHOLE LOCATION WITHIN MAPPED AREA
(BOREHOLES DRILLED 1985)

[White box]	POSITIVE Δ -RELIEF
[Horizontal lines]	NO CHANGE
[Diagonal lines /]	0 - 5 FT - NEGATIVE Δ -RELIEF
[Diagonal lines \]	5 - 10 FT
[Vertical lines]	10 - 15 FT
[Horizontal lines]	15 - 20 FT
[Diagonal lines /]	20 - 30 FT
[Diagonal lines \]	30 - 40 FT
[Vertical lines]	40 - 50 FT
[Horizontal lines]	50 - 60 FT
[Diagonal lines /]	60 - 70 FT
[Diagonal lines \]	70 - 80 FT
[Vertical lines]	80 - 90 FT
[Horizontal lines]	90 - 100 FT
[Diagonal lines /]	100 - 110 FT
[Diagonal lines \]	110 - 120 FT
[Vertical lines]	120 - 130 FT
[Horizontal lines]	130 - 140 FT
[Diagonal lines /]	140 - 150 FT
[Diagonal lines \]	150 - 160 FT
[Vertical lines]	160 - 170 FT
[Horizontal lines]	170 - 180 FT
[Diagonal lines /]	180 - 190 FT

**PLATE 5-4
OAK CRATER, ALICE REEF (STA. 25)
EARLYTIME NEGATIVE Δ -RELIEF ISOPACH MAP**

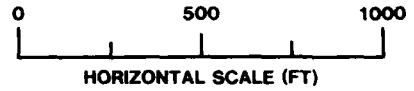
This isopach map was prepared for the U.S. Geological Survey by the U.S. Army Corps of Engineers, Hydrologic Engineering Center, Fort Belvoir, Illinois. The map shows the negative relief isopach map for the Oak Crater, Alice Reef (Sta. 25) area. The map was prepared using data from the U.S. Army Corps of Engineers, Hydrologic Engineering Center, Fort Belvoir, Illinois. The map was prepared in 1985. The map shows the negative relief isopach map for the Oak Crater, Alice Reef (Sta. 25) area. The map was prepared using data from the U.S. Army Corps of Engineers, Hydrologic Engineering Center, Fort Belvoir, Illinois. The map was prepared in 1985.



**CRATER
ISOPACH MAP, POSITIVE Δ -RELIEF**

OPEN-FILE REPORT 87-665
PLATE 5-5

MAP



LEGEND

● - BOREHOLE LOCATION WITHIN
MAPPED AREA
(BOREHOLES DRILLED 1985)

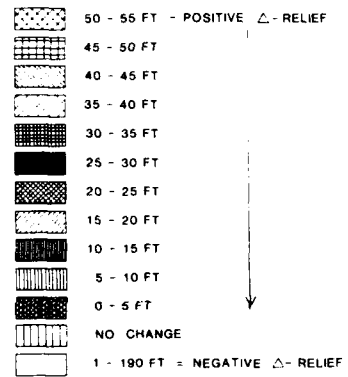


PLATE 5-5
OAK CRATER, ALICE REEF (STA 25)
EARLYTIME POSITIVE Δ -RELIEF ISOPACH MAP

Map prepared for the DEEP Program for the Alaska Division of
Laboratory, AFRL under the direction of the New York
Engineering Research Institute (NEMI) by the
Technology Applications Center (TAC), 1985.

ISOPACH MAP - Illustrating postshot distribution of
earlytime (0-100 days) positive Δ -relief at the
crater center level (2000).

BASE MAPS:

Holmes and Narver, Inc., "Well-log study of Topography &
Hydrographs (14-15, Alice Reef), June 4 through 20,
1954, Sheet No. 10-132-101011, Great Lakes Area,
1954, Survey conducted for U.S. Atomic Energy
Commission (AEC).

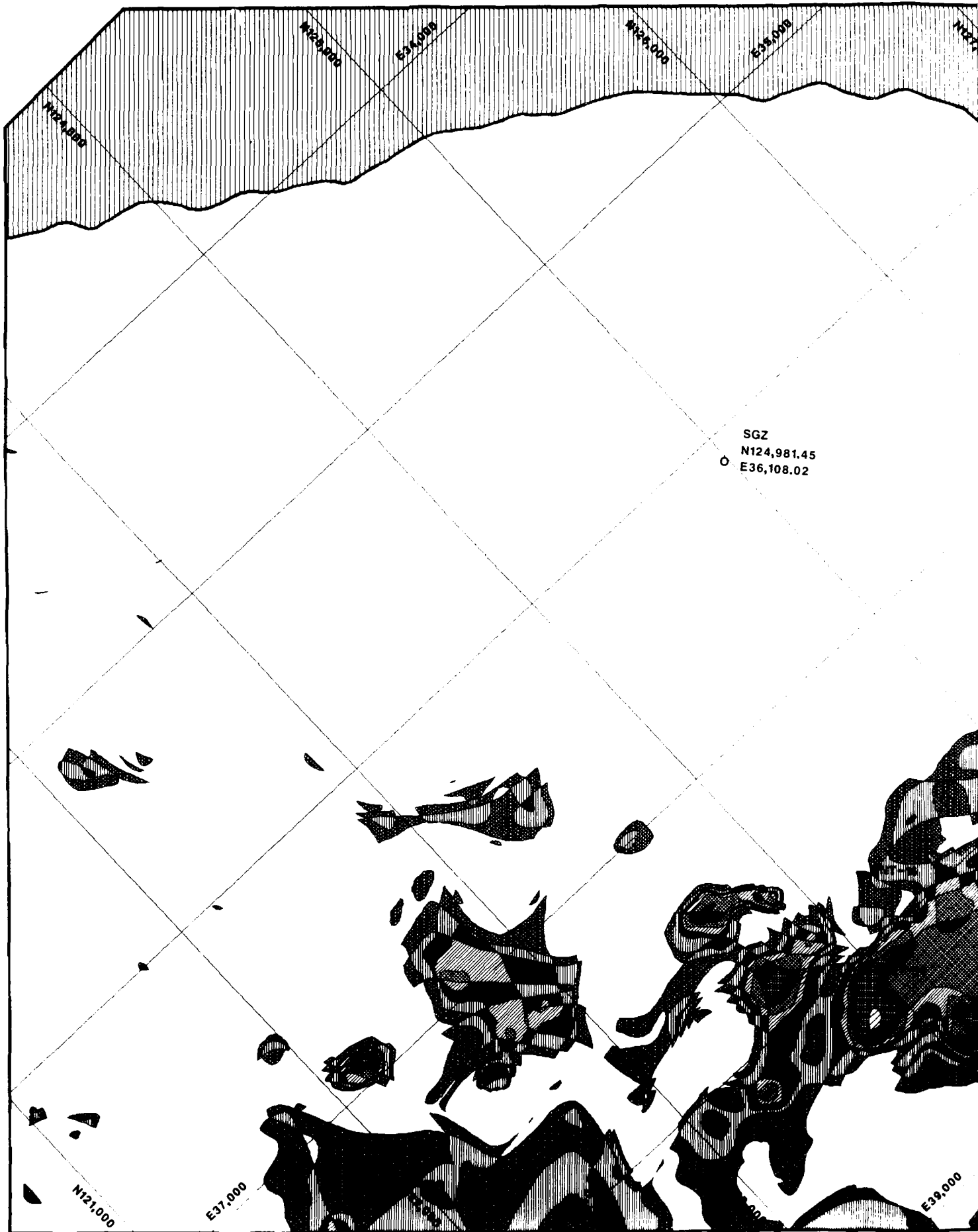
Holmes and Narver, Inc., "Well-log study of Topography &
Hydrographs (14-15, Alice Reef), August 14 through
September 4, 1954, Sheet No. 10-132-101011, Great
Lakes Area, Survey conducted for U.S. Atomic
Energy Commission (AEC).

Notes:

1. The isopach map is based on the data from the
earlytime (0-100 days) positive Δ -relief at the
crater center level (2000).
2. The isopach map is based on the data from the
earlytime (0-100 days) positive Δ -relief at the
crater center level (2000).

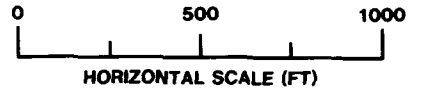






OAK CRATER
 AIR SHOT ISOPACH MAP, POSITIVE Δ -RELIEF

OPEN-FILE REPORT 87-665
 PLATE 5-7



LEGEND

● - BOREHOLE LOCATION WITHIN
 MAPPED AREA
 (BOREHOLES DRILLED 1985)

[Stippled pattern]	50 - 55 FT - POSITIVE Δ -RELIEF
[Horizontal lines]	45 - 50 FT
[Diagonal lines (top-left to bottom-right)]	40 - 45 FT
[Diagonal lines (top-right to bottom-left)]	35 - 40 FT
[Vertical lines]	30 - 35 FT
[Dotted pattern]	25 - 30 FT
[Cross-hatch pattern]	20 - 25 FT
[Horizontal lines]	15 - 20 FT
[Diagonal lines (top-left to bottom-right)]	10 - 15 FT
[Diagonal lines (top-right to bottom-left)]	5 - 10 FT
[Vertical lines]	0 - 5 FT
[White box]	NO CHANGE
[White box]	1 - 190 FT - NEGATIVE Δ -RELIEF

PLATE 5-7
 OAK CRATER, ALICE REEF (STA.25)
 LATETIME POSITIVE Δ -RELIEF ISOPACH MAP

MAP prepared for the PLACE Program for the Air Force Weapons Laboratory (AFWL) under the direction of the New Mexico Engineering Research Institute (NEMI) by the Technology Applications Center (TAC), 1985.

ISOPACH MAP illustrating latetime (0 + 27 yrs) distribution of positive Δ -relief from the preshot zero (0) level (m.s.w.).

RASE MAPS

Holmes and Narver, Inc.; Blue-line copy of "Topography & Hydrography Sta. 25, Alice Reef," June 3 through 26, 1968; Sheet No. J15 32-101-010, dated September 13, 1958; Survey conducted for U.S. Atomic Energy Commission (AEC).

U.S. Geological Survey (1994), "Mathematical Map of the Oak Crater Area, Inverness Area," Surveyed June 11 through September 20, 1984; compiled September 1985. The map is a 1:4000 scale working-scale copy of the map published in 1996 in U.S. Geological Survey Bulletin 1684 as Fig. 1, p. 84. Survey conducted for Defense Nuclear Agency (DNA).

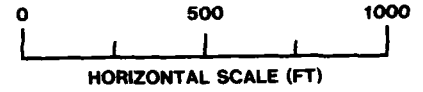
NOTES

1. All data were derived from water depths as determined from the 1958 and 1968 surveys.
2. The 1958 and 1968 surveys were conducted by the U.S. Army Corps of Engineers.
3. The 1994 survey was conducted by the U.S. Geological Survey.
4. The 1994 survey was conducted for the Defense Nuclear Agency.



**OAK CRATER
POSTSHOT ISOPACH MAP, NEGATIVE Δ -RELIEF**

OPEN-FILE REPORT 87-565
PLATE 5-8



LEGEND

● - BOREHOLE LOCATION WITHIN
MAPPED AREA
(BOREHOLES DRILLED 1985)

	POSITIVE Δ -RELIEF
	NO CHANGE
	0 - 5 FT = NEGATIVE Δ -RELIEF
	5 - 10 FT
	10 - 15 FT
	15 - 20 FT
	20 - 25 FT
	25 - 30 FT
	30 - 35 FT
	35 - 40 FT
	40 - 45 FT
	45 - 50 FT
	50 - 55 FT

PLATE 5-8
OAK CRATER, ALICE REEF (STA.25)
COMPARATIVE POSTSHOT ISOPACH MAP (NEGATIVE Δ -RELIEF)

Map prepared for the RAGE Program for the Air Force Weapons Laboratory AFEL, under the direction of the New Mexico Engineering Research Institute (NEMI), by the Technology Applications Center (TAC), December 1985.

ISOPACH MAP: Illustrating isostatic 0 - 60 days postshot Δ distribution of negative relief from the 455 postshot zero "level" datum.

RAGE MAPS:

480000 and 480000, 1:50,000 Scale, Photocopy of Hydrographic & Hydrography Map 25, Alice Reef, August 12 through September 3, 1954, Sheet No. 103-731(1), dated October 1, 1954. Survey conducted for U.S. Atomic Energy Commission (AEC).

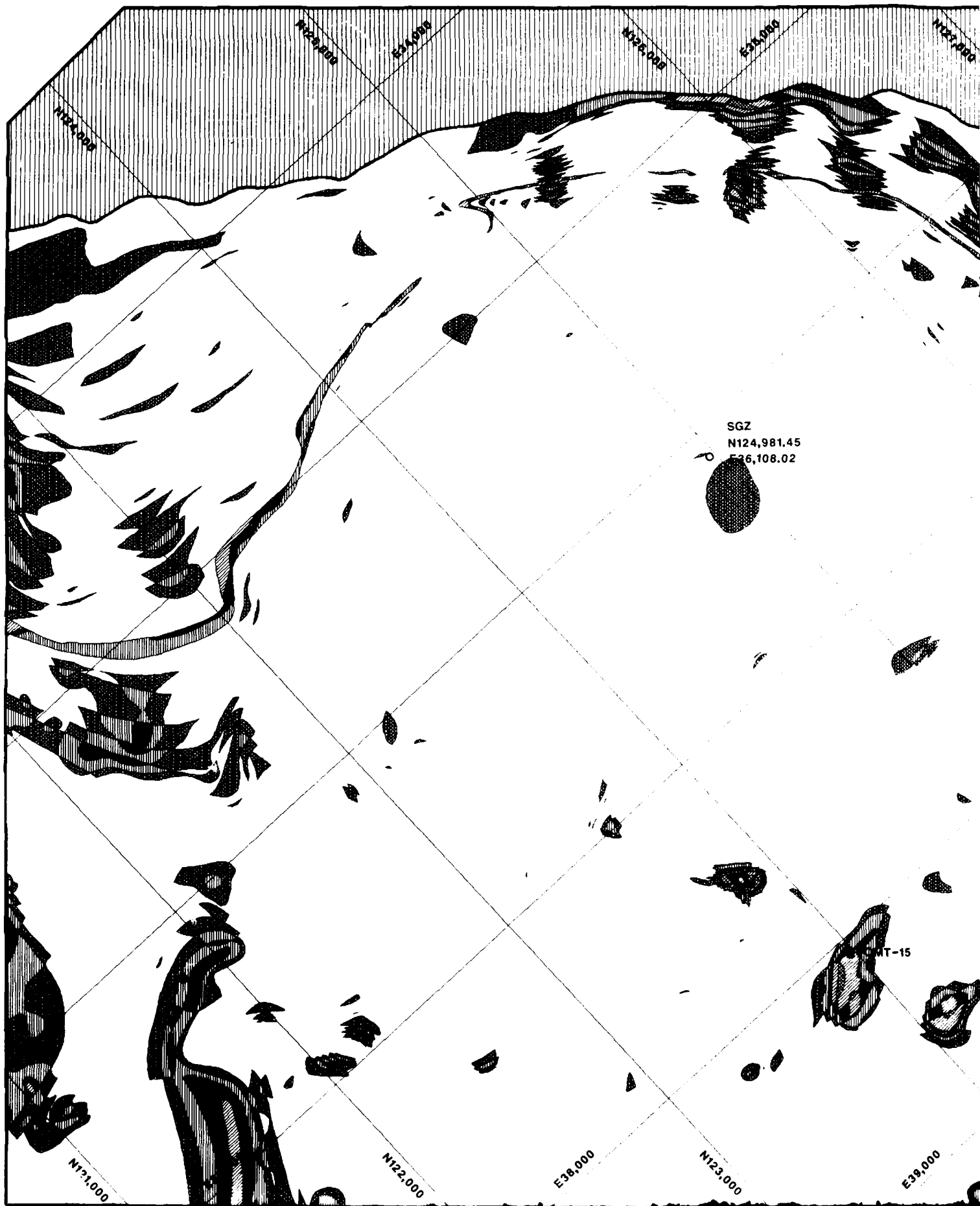
U.S. Geological Survey (1984). Bathymetric Map of Oak Crater Area, Eniwetok Atoll. Surveyed June 11 through September 27, 1984; completed September 1984. The map map is a digital working scale copy of 400' of the map published in 1976 by U.S. Geological Survey Bulletin 143K as Figure 1, p. 44. Survey conducted for Atomic Nuclear Agency (ANA).

NOTES:

1. 1954 data correction for water depth is indicated on the 480000 map as a dashed line.

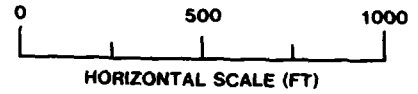
2. The 1954 data was used to generate the 1984 map.

3. The 1984 map is a digital working scale copy of 400' of the map published in 1976 by U.S. Geological Survey Bulletin 143K as Figure 1, p. 44. Survey conducted for Atomic Nuclear Agency (ANA).



**OAK CRATER
POSTSHOT ISOPACH MAP, POSITIVE Δ -RELIEF**

OPEN-FILE REPORT 87-665
PLATE 5-9



LEGEND

● - BOREHOLE LOCATION WITHIN
MAPPED AREA
(BOREHOLES DRILLED 1985)

[Stippled pattern]	50 - 55 FT	POSITIVE Δ -RELIEF
[Cross-hatched pattern]	45 - 50 FT	
[Horizontal line pattern]	40 - 45 FT	
[Vertical line pattern]	35 - 40 FT	
[Diagonal line pattern]	30 - 35 FT	
[Dotted pattern]	25 - 30 FT	
[Solid black pattern]	20 - 25 FT	
[Horizontal line pattern]	15 - 20 FT	
[Vertical line pattern]	10 - 15 FT	
[Diagonal line pattern]	5 - 10 FT	
[Dotted pattern]	0 - 5 FT	
[White pattern]	NO CHANGE	
[White pattern]	1 - 190 FT = NEGATIVE Δ -RELIEF	

PLATE 5-9
OAK CRATER, ALICE REEF (STA.25)
COMPARATIVE POSTSHOT ISOPACH MAP (POSITIVE Δ -RELIEF)

Map prepared for the National Geophysical Research Institute, Texas A&M University, Houston, Texas, by the Engineering Research Institute, NASA, Houston, Texas, under contract NAS 17-010-001.

ISOPACH MAP: This isopach map was prepared from the 1985 postshot data for the Alice Reef.

BASE MAPS:

Holmes and Narver, 1944, "Bathymetric Map of the Crater Area, Shallow Water, August to December, 1944," Survey conducted for the Atomic Energy Commission (AEC).

U.S. Geological Survey, 1944, "Bathymetric Map of the Crater Area, Shallow Water, Surveyed from 17 through 24 December 1944," Report September 1945, Report of the U.S. Geological Survey, Washington, D.C., published in 1945.

NOTES:

This map is a derivative of the 1985 postshot data for the Alice Reef. The map is a derivative of the 1985 postshot data for the Alice Reef. The map is a derivative of the 1985 postshot data for the Alice Reef.